MASARYK UNIVERSITY

Faculty of Science
Department of Experimental Biology

DEVELOPMENT OF MOLECULAR TOOLS FOR EXPERIMENTAL BIOLOGY OF PLANTS AND FUNGI

Mgr. Markéta Šámalová, Ph.D.

Habilitation Thesis

Brno 2022

ACKNOWLEDGEMENT

I would like to thank all my colleagues and friends at the Department of Plant Sciences at the University of Oxford, at the Pasteur Institute and at Masaryk University, who contribute to the excellence of science.

CONTENT

COMMENTARY

Herein, I present my scientific research conducted during my career in experimental biology. The primary goal was to develop molecular biology tools that would contribute to a fundamental understanding of nature and its principle.

Firstly, I focused on basic research and participated in the development of one of the most sensitive, fast and tightly regulated chemically inducible systems, the pOp6/LhGR system, for the model plant species *Nicotiana tobacum* and *Arabidopsis thaliana*. Further, we have expanded its use to an important crop species and genetic model for monocots, rice. In a detailed review, we have summarized its important characteristics and compared it with other available inducible systems and published step-by-step protocols for using the pOp6/LhGR system in various plant species. Next, we developed a fluorescence toolkit for quantitative and qualitative ratiometric fluorescence imaging assays for transient expression in tobacco as well as stable *Arabidopsis* transformants that were successfully used in a number of endomembrane trafficking studies.

Later, when I shifted my interest to more applied science, and through the understanding of the fundamentals of fungal infection processes, we tried to develop strategies to combat the major rice pathogen *Magnaporthe oryzea*. Application of the findings could serve for designing specifically targeted fungicides to be used rather than broadly applied chemistries. Moving to the medical science, we sought to find a putative cure for aspergillosis, a fatal human disease, and created a library of *Aspergillus fumigatus* mutants and identified a potentially suitable target candidate for immunization therapy.

Finally, after returning to plant sciences, back to my *alma mater*, Masaryk University in Brno, and combining my expertise from different scientific fields, I focused on multidisciplinary research. Together with physicists, mathematicians and material scientists we are developing new tools for imaging, probing and quantifying the biomechanical properties of plant cell walls.

In conclusion, I hope I have added a few small pieces to the mosaic of understanding of the world around us, which we as scientists are trying to decipher in order to improve the quality of our lives as well as for the future generations.

[1] Samalova, M., Brzobohaty, B. and Moore, I. (2005) pOp6/LhGR: a stringently regulated and highly responsive dexamethasone-inducible gene expression system for tobacco. *Plant J*. **41**, 919-935. (**IF=6.969**)

Experimental work (%)	Supervision (%)	Manuscript (%)	Research direction (%)
100	-	50	20

[2] Craft, J., Samalova, M., Baroux, C., Townley, H., Martinez, A., Jepson, I., Tsiantis, M. and Moore, (2005) New pOp/LhG4 vectors for stringent glucocorticoid-dependent transgene expression in *Arabidopsis. Plant J.* **41**, 899-918. (**IF=6.969**)

Experimental work (%)	Supervision (%)	Manuscript (%)	Research direction (%)
40	-	30	10

[3] Samalova, M., Kirchhelle, C. and Moore, I. (2019) Universal methods for transgene induction using dexamethasone-inducible transcription activation system pOp6/LhGR in *Arabidopsis* and other plant species. *Curr. Protocols Plant Biol.* **4**, e20089. (**IF=1.029**)

Experimental work (%)	Supervision (%)	Manuscript (%)	Research direction (%)
-	-	70	50

[4] Samalova, M. and Moore, I. (2021) The steroid-inducible pOp6/LhGR gene expression system is fast, sensitive and does not cause plant growth defects in rice (*Oryza sativa*). *BMC Plant Biol*. **21**, 461. (**IF=5.26**)

Experimental work (%)	Supervision (%)	Manuscript (%)	Research direction (%)
100	-	100	50

[5] Samalova, M., Fricker, M. and Moore, I. (2006) Ratiometric fluorescence-imaging assays of plant membrane traffic using polyproteins. *Traffic*, **7**, 1701-1723. (**IF=6.612**)

Experimental work (%)	Supervision (%)	Manuscript (%)	Research direction (%)
95	-	50	30

[6] Pinheiro, H., Samalova, M., Geldner, N., Chory, J., Martinez, A. and Moore, I. (2009) Genetic evidence that the higher plant Rab-D1 and Rab-D2 GTPases exhibit distinct but overlapping interactions in the early secretory pathway. *J. Cell Science*, **122**, 3749-3758. (**IF=6.144**)

Experimental work (%)	Supervision (%)	Manuscript (%)	Research direction (%)
30	-	20	5

[7] Gurr, S., Samalova, M. and Fisher, M. (2011) The rise and rise of emerging infectious fungi challenges food security and ecosystem health. *Fungal Biol. Rev.* **25**, 181-188. (**IF=2.6**)

Experimental work (%)	Supervision (%)	Manuscript (%)	Research direction (%)
-	-	30	20

[8] Samalova, M., Johnson, J., Illes, M., Kelly, S., Fricker, M. and Gurr, S. (2013) Nitric oxide generated by the rice blast fungus *Magnaporthe oryzae* drives plant infection. *New Phytol.*, **197**, 207-222. (**IF=6.545**)

Experimental work (%)	Supervision (%)	Manuscript (%)	Research direction (%)
50	50	30	30

[9] Samalova, M., Meyer, A., Gurr, S. and Fricker, M. (2014) Robust anti-oxidant defences in the rice blast fungus *Magnaporthe oryzae* confer tolerance to the host oxidative burst. *New Phytol.* **201**, 556-573. (**IF=7.672**)

Experimental work (%)	Supervision (%)	Manuscript (%)	Research direction (%)
80	-	40	30

[10] Samalova, M., Melida, H., Vilaplana, F., Bulone, V., Soanes, D.M., Talbot, N. J. and Gurr, S.J. (2017) The β-1,3-glucanosyltransferases (Gels) affect the structure of the rice blast fungal cell wall during appressorium-mediated plant infection.: The Gels affect fungal wall structure during infection. *Cell. Microbiol.* **19**, e12659. (**IF=4.554**)

Experimental work (%)	Supervision (%)	Manuscript (%)	Research direction (%)
70	-	50	30

[11] Samalova, M., Carr, P., Bromley, M., Blatzer, M., Moya-Nilges, M., Latge, J.-P. and Mouyna, I. (2020) GPI anchored proteins in *Aspergillus fumigatus* and cell wall morphogenesis. *Curr. Top. Microbiol. Immunol.* **425**, 167-186. (**IF=4.737**)

Experimental work (%)	Supervision (%)	Manuscript (%)	Research direction (%)
70	-	10	10

[12] Samalova, M., Gahurova, E. and Hejatko, H. (2022) Expansin-mediated developmental and adaptive responses: A matter of cell wall biomechanics? *Quantitative Plant Biology*, **3:e11**, 1-14.

Experimental work (%)	Supervision (%)	Manuscript (%)	Research direction (%)
-	70	50	50

1. Universal chemically inducible gene expression system pOp6/LhGR for transgene expression in plants

Chemically inducible systems for regulated gene expression are essential tools for basic plant biology research as well as biotechnology. Their applications are most desirable for expression of gene products that interfere with regeneration, growth or reproduction of plants; expression at different stages of plant development and for specific duration; conditional genetic complementation as well as co-suppression and overexpression studies. They can reveal a clear correlation between induction of the transgene and occurrence of an altered phenotype and allow analysis of primary effects before homeostatic mechanisms start to counteract. When combined with artificial micro-RNA (amiRNA) or novel CRISPR-Cas9 technology they create powerful tools for generation of knock-down, knock-out or chimeric plants.

However, the actual development of chemically inducible systems for tight control of plant gene expression is a challenging task. There are a number of properties that are required for an ideal system, those include minimal non-induced basal expression levels, high inducibility, specificity and a dynamic range of response with respect to an inducer. Also, fast response and induction by various methods is desirable. An ideal system should be applicable to several plant species and should not cause any adverse physiological effects in plants by itself or its inducer. The inducer is further required to show high specificity, high efficiency at low concentrations and must not be found in target plants. Therefore, the components for such systems are usually derived from non-plant sources.

The systems typically contain two transcription units. Whereas the first unit employs a constitutive or tissue-specific promoter to express a chemical-responsive transcription factor, the second unit consists of multiple copies of the transcription factor binding site linked to a minimal plant promoter, which is used to express the target gene (Figure 1).

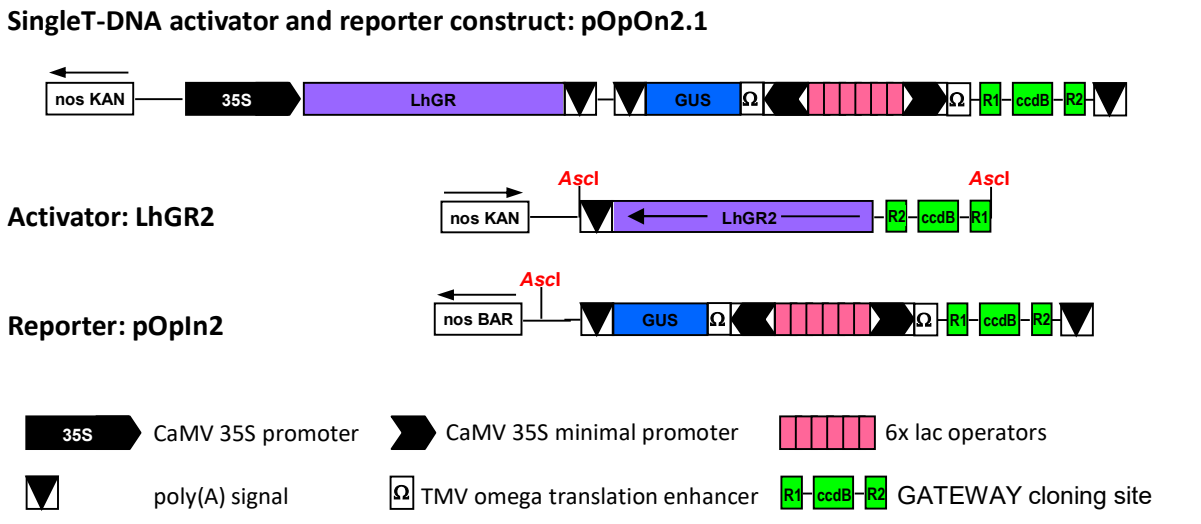

Figure 1: A schematic representation of the final pOp6/LhGR constructs. (See Samalova *et al.*, 2019 for details)**.**

Over the years we have made considerable efforts to developed one of the most widely adopted dexamethasone-inducible transcription activation systems pOp/LhGR (Craft *et al.*, 2005; Samalova *et*

al., 2005). It comprises of a transcription activator LhGR which is a fusion between a high-affinity DNA-binding mutant of *Escherichia coli lac* repressor, *lac*I^{His17}, transcription-activation-domain-II of GAL4 from *Saccharomyces cerevisiae*, creating originally the LhG4 activator, and the ligand-binding domain (LBD) of the rat glucocorticoid receptor (GR). The pOp is a chimeric promoter that consists of *lac* operators cloned upstream of a minimal CaMV 35S promoter (-50 to +8) and is apparently silent when introduced into plants. The principle of the system is that in the absence of the steroid ligand, dexamethasone (Dex), the transcription factor is trapped in an inactive complex via interaction of the GR LBD and heat-shock protein HSP90. However, upon induction with Dex, this complex is disrupted allowing the LhGR activator to bind to the pOp promotor and inducing expression of the target gene of interest. Both units can be placed either on a single T-DNA or separately on two T-DNAs (Figure 1).

We have maximised the induction levels by (i) testing three topologically different fusions between LhG4 and GR LBD; (ii) increasing the number of optimized *lac* operator sequences and (iii) optimising the methods of induction (Craft *et al*., 2005; Samalova *et al*., 2005; Samalova *et al*., 2019). During my PhD work I tested the pOp6/LhGR system in transgenic tobacco (Samalova *et al*., 2005). The system proved to be efficient, tightly regulated and has become the most sensitive system ever developed for tobacco plants as 1 nM Dex concentration was sufficient for half maximal induction of β-glucuronidase (GUS) activity. At that time, I also contributed largely to development of the system in *Arabidopsis* (Craft *et al*., 2005 shared first authorship). My latest publication on the topic describes the functionality of the system in a monocotyledonous model plant and the world`s staple diet crop, rice (Samalova and Moore, 2021). It shows the stability of the system in transgenic rice plants over several generations, the time course and dose response characteristics, optimization of induction by testing various steroids as inducers and finally methods of systemic and localised applications without causing any detrimental effects in rice even after prolonged induction. The paper discussed in details the construct design and possible reasons for toxicity, leakiness and silencing of the system in plants. Finally, the pOp6/LhGR system is compared with other chemically inducible systems tested in rice in an attempt to identify the ideal inducible system for the species.

Furthermore, we have written an extensive review (Moore *et al.*, 2006) comparing properties of the most promising inducible systems developed to date that included, apart from our pOp6/LhGR system, another dexamethasone-inducible GVG system (Aoyama and Chua, 1997), the estrogen-inducible XVE system (Zuo *et al*., 2000), the ecdysone agonist-inducible VGE system (Padidam *et al*., 2003; Koo *et al*., 2004) and ethanol-inducible *alc* systems (Caddick *et al*., 1998; Roslan *et al*., 2001; Salter *et al*., 1998). Although written in 2006, the systems characteristics are still of a great value and potential as to our knowledge, a new system of the same qualities has not been developed so far.

Lastly, we wrote detailed protocols for the pOp6/LhGR usage in *Arabidopsis* and other plant species (Samalova *et al*., 2019) that described step-by-step induction methods to reliably induce expression at different developmental stages. They included transgene induction at the seedling stage: on agar-solidified plates, in liquid medium, and in imaging chambers designed for time-lapse microscopy and furthermore two methods for later stages such as watering for systemic induction, and painting for local induction. It also introduced new, versatile, GATEWAY compatible vectors (Figure 1) that are now available and can be obtained from the NASC stock centre. The paper is dedicated to Dr. Ian Moore, the creator of the system, our colleague and friend, who passed away unexpectedly in 2018.

In conclusion, the versatility and ease of use makes the pOp6/LhGR system a valuable tool for fundamental and applied research in many laboratories. Recently, a comprehensive library of cell-type specific activator lines was created in *Arabidopsis* (Schurholz *et al*., 2018); the system was combined with artificial micro-RNA (amiRNA) to knockdown multigene expression (Goth *et al*., 2012; Samalova *et al*., 2020) and hairpin RNAi molecules to silence gene expression (Wielopolska *et al*., 2005; Liu and Yoder, 2016). Apart from *Arabidopis* (Craft *et al*., 2005) and tobacco (Samalova *et al*., 2005) the system was tested in various other species including citrus plant (Rossignol *et al*., 2014) and *Medicago truncatula* (Liu and Yoder, 2016) and most recently in rice (Vlad *et al*., 2019; Samalova and Moore, 2021). The ultimate goal is to combine the system with the CRISPR/Cas9 technology to create an inducible genome editing (IGE) system for *Arabidopsis* and other species that would enable efficient generation of target gene knockouts in desired cell types and developmental stage as it has been already demonstrated for the XVE system (Wang *et al*., 2020).

ATTACHMENTS:

[1] Samalova, M., Brzobohaty, B. and Moore, I. (2005) pOp6/LhGR: a stringently regulated and highly responsive dexamethasone-inducible gene expression system for tobacco. *Plant J*. **41**, 919-935.

[2] Craft, J., Samalova, M., Baroux, C., Townley, H., Martinez, A., Jepson, I., Tsiantis, M. and Moore, (2005) New pOp/LhG4 vectors for stringent glucocorticoid-dependent transgene expression in *Arabidopsis. Plant J.* **41**, 899-918.

[3] Samalova, M., Kirchhelle, C. and Moore, I. (2019) Universal methods for transgene induction using dexamethasone-inducible transcription activation system pOp6/LhGR in *Arabidopsis* and other plant species. *Curr. Protocols Plant Biol.* **4**, e20089.

[4] Samalova, M. and Moore, I. (2021) The steroid-inducible pOp6/LhGR gene expression system is fast, sensitive and does not cause plant growth defects in rice (*Oryza sativa*). *BMC Plant Biol*. **21**, 461.

2. Ratiometric fluorescent markers for quantitative and qualitative analysis of plant membrane traffic

The membrane traffic and endomembrane organization of the secretory pathway comprises of a number of functionally and morphologically distinct organelles including the endoplasmic reticulum (ER), Golgi apparatus and *trans*-Golgi network, endosomes, vacuoles as well as plasma membrane, that communicate together and also with the external environment via targeted vesicule fusions. Increasing use of fluorescent proteins (FPs) and their improved spectra derivatives to visualise these endomembrane organelles has had a substantial impact on plant membrane traffic investigations and revolutionized *in vivo* studies of protein localisation and complex dynamics.

A major challenge in studying such a dynamic system is the requirement for development of marker tools that can be incorporated into the membrane or lumen of any given compartment. Before genetically encoded fluorescent probes were developed, dyes such as FM4-64 were routinely used to stain membranes of live cells, however, their limitation is that they label a variety of membranes and in a time-dependent manner (Sparkes and Brandizzi, 2012).

Advanced fluorescent protein-based microscopy techniques to study the organization and dynamics of plant endomembranes have evolved alongside with the technology and include fluorescence (or Forster) resonance energy transfer (FRET), fluorescence lifetime imaging microscopy (FLIM), fluorescence recovery after photobleaching (FRAP), bimolecular fluorescence complementation (BiFC), photoactivation using photoactivable GFP (PAGFP) and ratiometric fluorescence measurements. Furthermore, live cell imaging has generated high demands on the optical imaging instrumentation based on light-sheet and confocal laser scanning microscopy (CLSM) which eliminates the out-of-focus light. The latest additions include spinning-disc confocal microscopes and Airyscan moduli that have further improved the signal-to-noise ratio, imaging resolution and time making it possible to image live cells in real-time with minimal photo-toxicity. Together with the state-of-the-art super resolution microscopy it is now possible to resolve biological structures at tens of nanometres.

We have developed a set of ratiometric fluorescent markers for the use in plant trafficking assays (Samalova *et al*., 2006) that facilitated by software packages (Samalova *et al*., 2008) greatly increase the ease and quality of fluorescence analysis of membrane traffic for transformed *Arabidopsis* seedlings as well as frequently used transient expression in tobacco leaf epidermal cells. For both quantitative and qualitative assays, it is important that the marker does not itself perturb the trafficking process. However, the expression level of a marker can influence the intracellular localisation of itself and other proteins. In practise, transient expression studies require to keep transfection rates low. However, due to the stochastic nature of the transfection process, this leads to large cell-to-cell variation in marker expression and analyses often rely on subjective scoring of individual cells in the population (Batoko *et al*., 2000; Kotzer *et al*., 2004; Zheng *et al*. 2005). Furthermore, the variability in co-expression of marker and test constructs significantly complicates the analysis and the approach cannot be applied to quantify changes in intracellular marker localisation.

A potential solution to these problems is to provide a stoichiometric baseline-reference for the expression efficiency of the marker. This approach corrects for variability in marker expression and imagining efficiency while providing a means to normalize between experiments. Ideally this should be measurable under the same conditions as the trafficked marker in either transfected protoplasts, single cells, or whole tissues and over a broad range of magnifications. With that in mind, we strived for development of a ratiometric approach utilising previously tested polyproteins based on the Foot and Mouth Disease Virus (FMDV) 'self-cleaving' 2A peptide (Halpin *et al*., 1999; Ryan *et al*., 1999). These polyproteins express the fluorescent marker and a spectrally distinct fluorescent reference marker from a single open-reading frame which is translated to generate two separate polypeptides in stoichiometric amounts (Figure 2).

The FMDV 2A peptide (referred to as 2A) is a 20 amino-acid peptide that originally promotes separation of the 2A and 2B viral translation products from a polyprotein. It disrupts the polypeptide backbone between the terminal glycine and proline residues of a highly conserved Pro-Gly-Pro motif at the carboxy-terminus of the 2A sequence. The mechanism is apparently protease independent and occurs relatively early to the emergence of the polypeptide from the ribosome exit channel (Ryan *et al*., 1999). Current models suggest that the 2A peptide acts as an esterase that hydrolyses the link between the nascent polypeptide and the t-RNA in the ribosome P-site prior to formation of the terminal Gly-Pro bond of 2A (Ryan *et al*., 1999). As translation of the remainder of the ORF can

proceed after 2A-mediated hydrolysis, sequences upstream and downstream of 2A are translated as two polypeptides from the same ORF in a fixed stoichiometry. However, it appears that the precise stoichiometry can vary between constructs depending on the sequence preceding the FMDV 2A sequence (Ryan *et al.*, 1999).

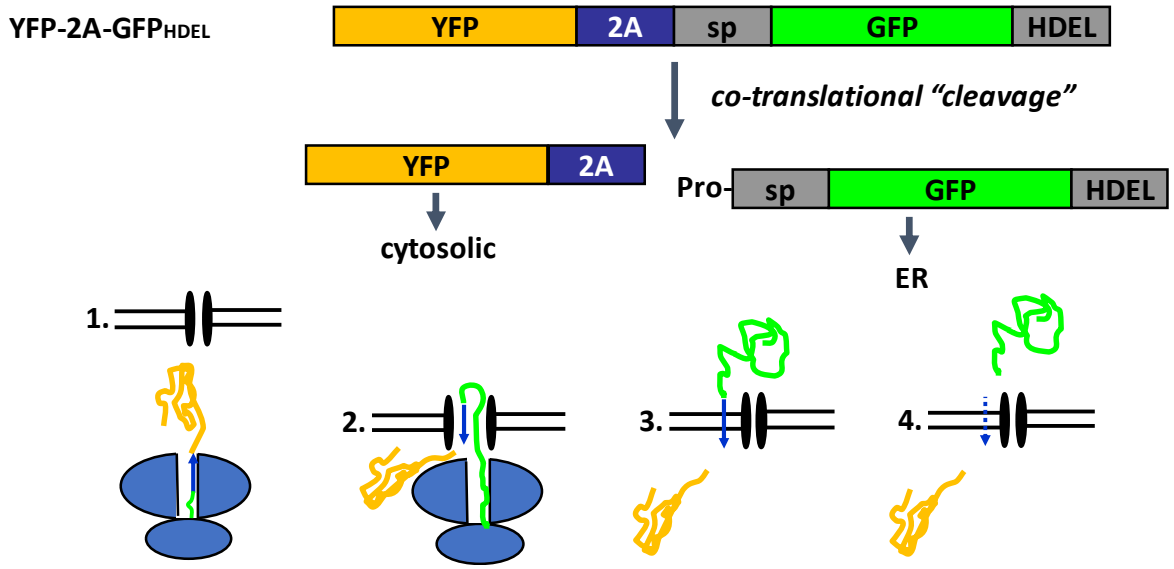

Figure 2: A schematic representation of the principle of FMDV 2A peptide function. (See Samalova *et al.*, 2006 for details).

In our experiments, we generated 2A-based polyprotein fusions in which a green fluorescent protein (GFP) molecule was targeted to the secretory pathway or ER while a co-expressed reference marker was targeted to the cytoplasm or nucleus (Samalova *et al.*, 2006). It was also possible to target two proteins to different endomembrane compartments, however, in this case we observed that upstream moiety of the polyprotein was sorted to the vacuole owing to hidden vacuolar sorting determinant within the 19-residues of 2A sequence that remain attached to carboxy-terminus of the cleavage product. Furthermore, in contrast to expectation based on the literature, we provided evidence that the 2A sequence, in a range of different fluorescent protein fusions, did not efficiently promote disruption of the polypepide backbone during translation on plant ribosomes. We proposed an alternative model and with these new findings discussed the implications for the use of 2A technology in plant cells (Samalova *et al.*, 2006).

For practical use of these constructs, we took advantage of pH sensitivity of GFP derivatives that allows secreted GFP (secGFP} molecules to be used to report on biosynthetic membrane traffic as it does not accumulate in a fluorescent form in the apoplast or vacuole (Batoko *et al.*, 2000; Zheng *et al.*, 2005). On the other hand, perturbation of the anterograde traffic can be easily visualised by the accumulation of the secGFP fluorescence in upstream compartments such as ER, Golgi apparatus or prevacuolar compartments.

We have developed two approaches based on the FMDV 2A constructs to quantify secGFP accumulation (Samalova *et al.*, 2006). The first one uses a cytoplasmic yellow fluorescent protein (YFP) as a reference and is the most suitable for the analysis of cell populations imaged at relatively low magnification when cytoplasm and ER are not well distinguished. The second approach is applicable to individual cells and uses a nuclear targeted red fluorescent protein (RFP). The single-cell

assay allows a number of data points to be extracted from a single transfection experiment, while the low background and high dynamic range allow improved estimates of secGFP accumulation. The assay has the potential to correct for variations in marker expression or imaging efficiency in various cell types of two most often used plant model organisms, tobacco and *Arabidopsis*.

We showed that the ratiometric fluorescent markers that targets proteins to distinct cellular compartments greatly improved sensitivity, objectivity, and statistical robustness of the quantitative assays of membrane traffic in plant cells (Samalova *et al*., 2006). They allowed the expression level of a trafficked marker to be inferred from the accumulation of a spectrally distinct fluorescent marker in another cellular compartment so cells could be compared. We described in details imaging protocols and analysis to quantify the marker expression in cell populations as well as individual cells of both stable transgenic *Arabidopsis* or transfected tobacco cells. Also, we provided semi-automated image analysis software packages for quantitative analyses and discussed the advantages and disadvantages of particular fluorescent protein derivatives, their photochemical and biological properties and use in various plant species and applications (Samalova *et al*., 2008).

The 2A constructs harbouring secGFP were used as a visual reporter for the endomembrane system and were coupled with several forward genetics screens. The screens were based on fluorescence microscopy analysis of mutants derived from ethyl methanesulfonate (EMS) mutagenized lines expressing the 2A-secGFP markers. The aim was to identify plants showing localization of the reporter in compartments and structures that were different from the wild-type. Although, the screens were labour intense, the use of next generation sequencing for mutation mapping led to identification of mutants of the secretory and the endocytic pathways (Teh and Moore., 2007; Au *et al*., 2012). For example, the *gnom-like1* (GNL1) allele showed that the protein, involved in vesicle coat formation and vesicle-cytoskeleton interactions, was localized to Golgi and played a role in the biosynthetic anterograde route (Teh and Moore, 2007). In another screen for seedling-lethal membrane trafficking mutants, four recessive *gsh2* alleles of *GSH2* gene encoding glutathione synthase were recovered (Au *et al*., 2012). Each allele was characterised by loss of the typical polygonal ER network and the appearance of swollen ER-derived bodies accumulating GFP. However, the *gsh2* seedlings maintained redox state in the cytoplasm but were more sensitive to oxidative stress (Au *et al*., 2012).

We also investigated whether the 2A peptide could be used to indirectly monitor the expression level of proteins such as Rab GTPases that are very sensitive to tagging at the amino-terminus. Instead, we used 2A to link a nuclear targeted RFP (nlsRFP) to the amino-terminus of the Rab protein. However, the nlsRFP-2A-Rab fusion exhibited lower activity than the untagged protein and the 2A-mediated cleavage was inefficient. These observations were similar to previously reported 2A activity in plant cells that was influenced markedly by the upstream moiety of the fusion protein (Ma and Mitra, 2002). An interesting possible solution to this problem was later demonstrated by Buren and colleagues (2012) who inserted the GUS amino-terminal sequence in front of the 2A sequence and increased the cleavage efficiency of cytosolically expressed constructs, including small GTPase proteins.

Rab GTPases are crucial determinants of membrane identity and membrane targeting essential for correct membrane trafficking. Rab GTPases undergo a regulated cycle between GDP-bound and GFP-bound forms while cycling on and off particular endomembranes, providing transient interaction

surfaces for the recruitment of effector proteins and complexes (Woollard and Moore, 2008). Genomic data have shown that higher plants have evolved a unique set of Rab proteins that perhaps reflects the specific demands of plant cell trafficking. Mammals and *Arabidopsis* each have about 60 Rab GTPases compared to only 6-10 found in yeast, but interestingly, 80% of predicted mammalian Rab subclasses are absent in *Arabidopsis*. All 57 *Arabidopsis* RAB sequences fall into 8 clades (RAB-A to RAB-H) that have diversified to such an extent that they may contain functionally distinct proteins (Rutherford and Moore, 2002).

As a member of Moore group that over the years systematically investigated each Rab clade (Batoko *et al*., 2000; Kotzer *et al*., 2004; Zheng *et al*., 2005; Chow *et al*., 2008; Camacho *et al*., 2009; Kirchhelle *et al*., 2016) I was interested in the Rab-D clade that was further divided into two subclasses Rab-D1 and Rab-D2 represented with three members (D2a, b and c). Prior work in *Arabidopsis* was performed with Rab-D2a whose role in the traffic between the ER and the Golgi apparatus was demonstrated using the dominant negative RAB-D2a[N121I] mutant (Batoko *et al*., 2000). In our research, we provided further genetic evidence that the Rab-D1 and Rab-D2 GTPases exhibited distinct but overlapping interactions in the early secretory pathway (Pinheiro *et al*., 2009). Both targeted fluorescent proteins to the same punctate structures associated with Golgi stacks and *trans*-Golgi-network. The inhibitory N121I mutants of each protein inhibited traffic of diverse cargos at the ER but appeared to act via distinct biochemical pathways. Insertional mutants confirmed that the three Rab-D2 genes were extensively redundant and performed and essential function that could not be provided by Rab-D1 that on the other hand was non-essential. Triple knock-out plants lacking *RAB-D1*, *RAB-D2b* and *RAB-D2c* were short, bushy with low fertility, indicating that the Rab-D1 and Rab-D2 subclasses have overlapping functions (Pinheiro *et al*., 2009).

ATTACHMENTS:

[5] Samalova, M., Fricker, M. and Moore, I. (2006) Ratiometric fluorescence-imaging assays of plant membrane traffic using polyproteins. *Traffic*, **7**, 1701-1723.

[6] Pinheiro, H., Samalova, M., Geldner, N., Chory, J., Martinez, A. and Moore, I. (2009) Genetic evidence that the higher plant Rab-D1 and Rab-D2 GTPases exhibit distinct but overlapping interactions in the early secretory pathway. *J. Cell Science*, **122**, 3749-3758.

3. Fluorescent marker and assay development to study *Magnaporthe oryzae*, the rice blast disease fungus

Perhaps not obvious at first, but fungi have a huge global, social and economic impact. Interestingly, only a small percentage (< 5%) of all fungi are known and only few are highly exploited as edible mushrooms, in food industry or as producers of pharmaceuticals and industrial enzymes. Importantly, fungi are intrinsic to recycling organic matter and promoting plant growth as mycorrhizal symbionts. Conversely, pathogenic fungi challenge food security due to harvest losses, threaten wildlife extinction and cause human diseases, even fatal infections, mainly in immunocompromised patients (Gurr *et al*., 2011). Alarming is the emergence of new fungal pathotypes that can “hop” plant species and spread to new hosts including food staple crops. This trend is caused partially by climate changes but largely due to modern agricultural practices and

detiorating ecosystem health (Fisher *et al*., 2012). Therefore, new improved disease surveillance and reporting are needed which goes together with the need for increased interest in fungal research and public awareness. Further combining multidisciplinary approaches to answer key plant pathology questions, how pathogens overcome plant immunity and manipulate plant processes, and how to minimize losses due to pathogens, would enhance chances in achieving global food security.

Rice is the world staple diet that feeds about half of the world`s population. The severe rice blast disease caused by Ascomycete fungus *Magnaporthe oryzae* is responsible for up to 30 % loss of harvest and can destroy an infected field completely within a couple of weeks by producing and spreading 10^{11} spores per acre in a growing season (Barksdale and Asai, 1961). *M. oryzae* was the first fungal plant pathogen genome to be sequenced (Dean *et al*., 2005) and has become a major pathosystem model to understand the mechanisms regulating the infection cycle (Figure 3).

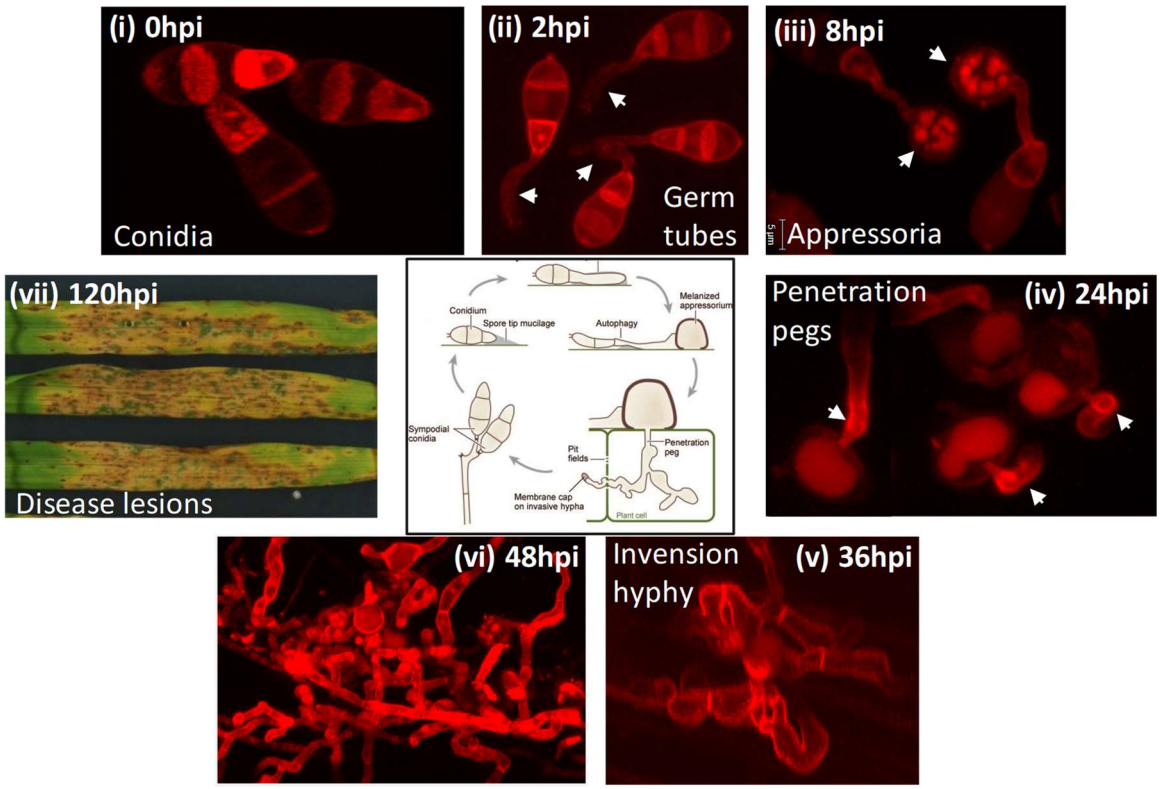

Figure 3: The infection cycle of *Magnaporthe oryzae*. *(i) The three-celled asexual conidium lands on the rice leaf surface and adheres to the hydrophobic cuticle. (ii) The perception of host cues leads to initiation of a polarized germ tube from the terminal cell. (iii) The germ tube elongates, hooks and then begins to differentiate at the tip to form a highly specialized, dome-shaped appressorium accumulating glycerol. Efflux of glycerol from the appressorium is prevented by deposition of dense melanin inner layer between the chitin-rich cell wall and plasma membrane. The re-location of storage products such as lipids to the appressorium is accompanied by autophagic cell death of the conidium. (iv) An enormous amount of turgor pressure develops in the melanised appressorium that is translated into mechanical force and rupture the plant epidermis through a penetration peg formed at the base of the appressorium. (v) Once the fungus enters rice tissue, it develops bulbous, branched hyphae that invaginate the plant plasma membrane and expand within the first occupied epidermal rice cells. (vi) The fungus then spreads to neighbouring cells and switches from the biotrophic growth – when the fungus occupies living rice cells to necrotrophic growth when rice cells lose viability,*

hence, M. oryzae *is considered a hemibiotroph. (vii) Disease lesions form on the infected leaf surface 72–96 hours post inoculation (hpi) and under humid conditions conidiophores carrying new conidia are produced. CLSM images of fluorescent conidia germinated on a glass slide (i-iii), onion peels (iv) rice sheath leaves (v-vi) and barley plants (vii) produced by M. Samalova (details in Samalova* et al*., 2017). Description based on Ebbole (2007).*

3.1. ROS are important players in plant-pathogens interactions

Reactive oxygen species (ROS) are highly reduced forms of oxygen molecules (e.g. superoxide or hydrogen peroxide) involved in many important physiological processes including growth and development of both plants and fungi. ROS are predicted to be critical components of rice – *M. oryzae* interaction, however, their regulations and pathways are largely unknown. Interestingly, in *M. oryzae*, ROS are produced by normal cell metabolism by a number of enzymes, including well described NADPH oxidases, and act as signalling molecules associated with key transitions in fungus development such conidiation, spore germination, appressorium formation and penetration, apoptosis and secondary metabolism (Kou *et al*., 2019).

However, inside the rice cells, the fungus must scavenge the host-derived ROS as often plants response to the infection is rapid production of ROS as part of the general pathogen-associated molecular pattern (PAMP)-triggered immunity or more specific effector-triggered immunity (ETI) responses (Torres, 2010; Heller and Tudzynski, 2011). Produced ROS cross-link plant wall polymers to form a barrier to pathogen penetration, attack the pathogen directly or act as diffusible signals in the plant that upregulate expression of pathogenesis-related proteins (Lamb and Dixon, 1997; Heller and Tudzynski, 2011). *M. oryzae* virulent strains are capable of suppressing ROS accumulation and attenuating rice blast resistance by the effector secretion, for example AvrPii and AvrPiz-t (Zhou *et al*., 2006). However, in resistant rice varieties, *M. oryzae* infection is halted at the penetration stage or during early colonization, and is associated with a hypersensitive response (HR) (Torres, 2010; Heller and Tudzynski, 2011).

Hence, fungi require effective anti-oxidant defence systems to operate in environments with endemic oxidative stress. A vast array of anti-oxidant genes exists in the *M. oryzea* genome (Dean *et al*., 2005), although less is known about the low-molecular-weight anti-oxidants in fungi more generally. The major cytoplasmic anti-oxidant that diminishes oxidative stress in eukaryotes is glutathione (Gessler *et al*., 2007).

We have developed a tool to investigate the fungus physiological redox state based on transgenic redox green fluorescent protein (roGFP) (Dooley *et al*., 2004; Schwarzlander *et al*., 2008; Meyer and Dick, 2010). The probe allow to quantify the glutathione concentrations and follow the electrochemical potential of the reduced glutathione: oxidized glutathione (GSH:GSSG) redox couple (E_{GSH}) and dynamics *in vivo*. Furthermore, to improve the roGFP response kinetics, we included a glutaredoxin (Grx) subunit (Gutscher *et al*., 2008) and created a Grx1-roGFP2 construct (Samalova *et al*., 2014) optimized for expression in *M. oryzae*.

The Grx1-roGFP marker is specifically sensitive to small changes in the degree of glutathione oxidation from the highly reduced level typically found *in vivo* (Meyer and Dick, 2010). We used four-dimensional (x,y,z,t) live-cell confocal imaging and a range of fluorescent reporters to determine, (i) whether there is physiological evidence for the redox control of early development in *M. oryzae*

mediated by changes in E_{GSH}; (ii) what is the relative level of endogenous ROS production during development; (iii) what is the capacity of the glutathione anti-oxidant system to deal with an inflicted oxidative burst, as might be encountered during host infection; and (iv) what impact is applied by the actual host oxidative burst on E_{GSH} *in vivo* during susceptible and resistant interactions (Samalova *et al*., 2014).

We found out that high levels of mitochondrial as well as ROS activity were localized to the growing germ tube and appressorium, but E_{GSH} was highly reduced and tightly regulated during development. Furthermore, germlings were extremely resistant to external H_2O_2 exposure *ex planta*. E_{GSH} remained highly reduced during successful infection of the susceptible rice cultivar CO39. By contrast, there was a dramatic reduction in the infection of resistant (IR68) rice, but notably the sparse hyphae that did form also maintained a similar reduced E_{GSH} (Samalova *et al*., 2014).

In conclusion, *M. oryzae* has a robust anti-oxidant defence system and maintains tight control of E_{GSH} despite substantial oxidative challenges. Furthermore, the magnitude of the host oxidative burst alone is not sufficient to stress the pathogen enough to prevent infection in this pathosystem. It seems that ROS produced by rice are not an ample toxic line of defense to *M. oryzae* even in avirulent interactions. It is possible that ROS play a dominant role in signalling, rather than in ROS toxicity.

3.2. NO is an important signalling molecule

Nitric oxide (NO) is a free radical gas able to diffuse rapidly through biological membranes thus allowing to act as a signalling molecule with multiple and crucial roles across the kingdoms. However, NO can be also damaging through its high reactivity causing protein nitrosylation, nitrosative stress and apoptosis. Hence, it is often used by higher organisms as a defence line against microbial pathogens including bacteria and fungi. In mammals, the oxidative synthesis involves the conversion of L-arginine and O_2 into citrulline and NO by up to three isoforms of nitric oxide synthase (NOS) (Alderton *et al*., 2001). Additional reductive pathways were also found in mammas that allowed the conversion of nitrite to NO with the involvement of different enzymes, e. g. cytochrome c, P450, deoxyhaemoglobin or non-enzymatic reactions under acidic conditions (Zweier *et al*., 2010).

In plants NO has been implicated in several developmental processes, as well as in abiotic stress responses and plant immunity initiating plant responses to pathogens (Delledonne *et al*., 1998; Zeier *et al*., 2004; Prats *et al*., 2005; Besson-Bard *et al*., 2008). A similar mammalian-like NOS activity in plants was reported initially, but had not been substantiated later, as the original putative NOS candidate, *Arabidopsis AtNOA1* (Guo *et al*., 2003) was shown to be only indirectly associated with NO production (Moreau *et al*., 2008) and homology with known NOS has not been demonstrated (Canovas *et al*., 2016). On the other hand, the reductive NO synthesis was shown to be widespread in plants and involved the action of the nitrate reductase at saturating nitrite concentrations under reductive conditions (Yamasaki and Sakihama, 2000).

Evidence is also emerging that NO is an important regulatory molecule in fungi, including plant pathogens. This presents a compelling challenge; fungi may use NO as a signalling molecule to control their development, but, at the same time, NO may prime the host and activate defence. The mechanism of NO synthesis has not yet been described in fungi, however, there may be a number of different routes for NO formation, including both oxidative and reductive pathways. On the oxidative

side, mNOS or NOS-like sequences have been described in *Aspergillus spp*. and *Glomerella graminicola* (Turrion-Gomez and Benito, 2011). On the reductive side, genes for nitrate reductase and nitrite reductase are present in all filamentous fungal genome analysed thus far, but their potential role in NO synthesis has not been addressed apart from a recent report in which the authors demonstrated that *Aspergillus* can synthesize NO from nitrate by means of nitrate reductase (Marcos *et al.* 2016).

We investigated the role of NO in *M. oryzae* development by optimising a novel assay for DAR-4M fluorescent dye and NO scavengers, and provided evidence for production of NO by germinating conidia and during early appressorium formation (Samalova *et al.*, 2013). Importantly NO scavengers delayed germination and early development on artificial hydrophobic surfaces and dramatically reduced lesion formation on barley (*Hordeum vulgare*). Further, we tested possible NO-generating enzymes by creating knock-out strains of candidate genes. We revealed that neither nitrate (*NIA1*) nor nitrite reductase (*NII1*) were responsible for NO generation using single and double knock-outs, and both genes were dispensable for pathogenicity on rice and barley, however they were essential for nitrate assimilation. Similarly, single and multiple knock-outs of most closely related mNOS-like gene family (nitric oxide synthase-like genes *NOL2* and *NOL3*) did not affect NO production or produce obvious defect in pathogenicity. We also provided evidence that NO was not produced by other arginine-dependent systems of polyamine oxidases in *M. oryzae* nor non-enzymatically by low pH. Finally, we concluded that NO is a critical signalling molecule in early development and has a major impact on plant-pathogen interactions but its mode of synthesis remains elusive (Samalova *et al.*, 2013).

ATTACHMENTS:

[7] Gurr, S., Samalova, M. and Fisher, M. (2011) The rise and rise of emerging infectious fungi challenges food security and ecosystem health. *Fungal Biol. Rev.* **25**, 181-188.

[8] Samalova, M., Johnson, J., Illes, M., Kelly, S., Fricker, M. and Gurr, S. (2013) Nitric oxide generated by the rice blast fungus *Magnaporthe oryzae* drives plant infection. *New Phytol.*, **197**, 207-222.

[9] Samalova, M., Meyer, A., Gurr, S. and Fricker, M. (2014) Robust anti-oxidant defences in the rice blast fungus *Magnaporthe oryzae* confer tolerance to the host oxidative burst. *New Phytol.* **201**, 556-573.

4. Deconstructing fungal cell walls to find specific targets for antifungal drugs

Fungal cell wall (CW) is indispensable for cell integrity maintenance and for protection from environmental stresses. Current research has uncovered the remarkable influence of the fungal CW on many aspects of physiology of fungi, their morphogenesis and growth, especially during interaction with the environment and host colonization (Geoghegan *et al.*, 2017). The CW is considered to be a dynamic structure that changes both form and composition rather than a simple “armour”. Perhaps it is not surprising that one-fifth of the yeast genome is devoted to the biosynthesis of the CW (de Groot *et al.*, 2001). It includes genes that encode carbohydrate active enzymes (summarized in CAZy database http://www.cazy.org) and contain multigene families of

glucan and chitin synthesis as well as an array of remodelling enzymes. Interestingly, many of the components of fungal CWs are conserved in different species while others are unique and vary not only between species but also within cell types of the same species especially when exposed to different environmental conditions (Coronado *et al.*, 2007).

Fundamentally, fungal CWs are all constructed in a similar way (Figure 4). Fibrous and gel-like carbohydrate polymers form a tensile and robust core scaffold to which a variety of proteins and other exterior components are attached, making strong, but flexible, and chemically diverse CWs. Most CWs are composed of layers, with the innermost layer comprising a relatively conserved structural part while the outer layers are more heterogeneous and customised to the physiology of particular fungi. In most fungal species the inner CW consists of a core of covalently attached branched β-(1,3)-glucan with 3-4% hydrogen bond interchains linked to chitin (Latge, 2007) that can assemble into microfibrils forming a basket-like scaffold around the cell. This exoskeleton represents the load-bearing, structural component of the wall that resists the considerable internal hydrostatic pressure exerted on the wall by the cytoplasm and membrane. To the branched β-(1,3):β-(1,6) glucan other polysaccharides and proteins are bound.

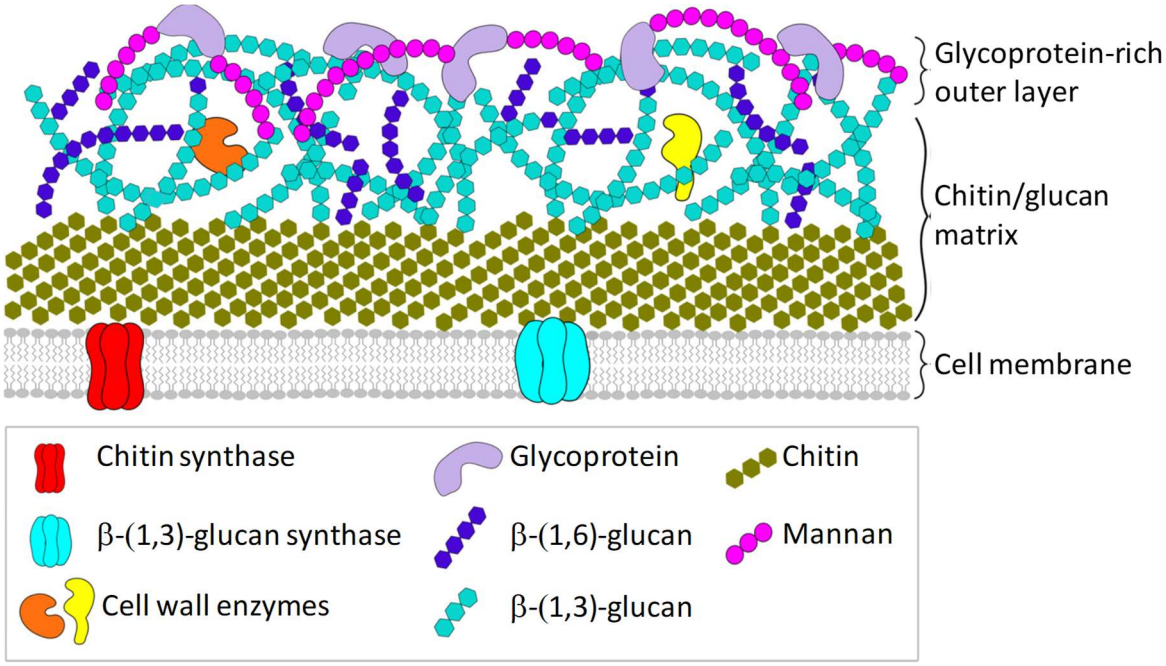

Figure 4: Basic structure of the fungal cell wall (CW). *The wall is composed of a reticulate network of stress-bearing, shape-conferring polysaccharides with non-covalently and covalently linked embedded proteins. The inner CW is a chitin–glucan-rich interconnected matrix while the outer layer is rich in mannosylated glycoproteins (Adapted from Geoghegan* et al*., 2017).*

Further, there are unique aspects of the CWs of phytopathogenic fungi compared to those with exclusively saprophytic lifestyles or opportunistic human pathogens. These include perception of host-derived developmental cues (e.g. a hard, hydrophobic surface), development of specific infection or feeding structures (e.g. appressoria and haustoria) and avoidance of plant immune recognition. The key for plant infection is that the pathogen remains initially undetected and thus it colonizes plant tissues without eliciting a plant defence response. This process in crucially dependent on the ability of the fungus to change the CW composition (Fujikawa *et al.*, 2012; Oliveira-Garcia and

Deising, 2016), as oligomers released from chitin and β-glucan by the host degradation enzymes act as pathogen-associated molecular patterns (PAMPs) triggering the plant immune responses. Those changes at the infection front include deacetylation of chitin (forming chitosan), reduction of β-glucan content, by synthesis of α(1,3)-glucan, or by effector protein secretion (Geoghegan *et al.*, 2017). Although the release of PAMPs can be avoided to some extent, the pathogen must also be able to withstand the challenge of constant surveying and the plant defences that include plant-derived secreted chitinases, glucanases, reactive oxygen and nitrogen species (as discussed in Chapter 3), toxins and antimicrobial peptides (Jones and Dangl, 2006).

Fungal CW is a complex meshwork of interlinked polysaccharides and proteins. Typically, the individual polysaccharides are synthesized at the plasma membrane, however, their structure and connectivity to other components is carried out by various carbohydrate-modifying enzymes involved in glucan chain elongation and branching, chitin deacetylation and glucan-chitin crosslinking. Interestingly, alkali-soluble fungal CW polysaccharide α-(1,3)-glucan located in the outer layers of the CW has been closely linked to the plant infection process. Specifically, mutant strains of *M. oryzae*, where the only α-(1,3)-glucan synthase (AGS1) gene has been deleted, are non-pathogenic. More importantly, transgenic rice plants expressing a bacterial α-(1,3)-glucanase are more resistant to infection by *M. oryzae* and other fungi (Fujikawa *et al*., 2012).

β-glucans are the dominant polysaccharide in the alkali-insoluble fraction of the fungal CW and are crucial for providing tensile strength to the wall thus maintaining cell shape in all fungi. The essential role of β-(1,3)-glucan was demonstrated by deletion of a single β-(1,3)-glucan synthase that was lethal in all filamentous fungi studied (Latge, 2007). Linear chains of β-(1,3)-glucan are synthesized by a membrane-localized glucan synthase and are extruded into the wall as polymerization proceeds (Latge, 2007). Simultaneously the formation and elongation of β-(1,3)-glucan branches is performed by a family of β-(1,3)-glucan glucanosyltransferase enzymes (Gels), which are themselves anchored in the plasma membrane through the glycosylphosphatidylinositol (GPI) anchor (Mouyna *et al*., 2000; Hurtado-Guerrero *et al*., 2009). Further extensive fungal CW remodelling involves formation of β-(1,6) branching points and crosslinking between β-glucans and chitin (Latge, 2007).

4.1. Identifying GPI-anchored proteins crucial for pathogenicity of *Magnaporthe oryzae*

Glycosylphosphatidylinositol (GPI) anchored proteins are a class of proteins attached to the extracellular leaflet of the plasma membrane via post-translational modification, the glycolipid anchor. GPI-anchored proteins are expressed in all eukaryotes and include enzymes such as transglycosidases, CW hydrolases and deacetylase, yapsins and adhesins. Genome-wide analyses have been performed to predict all proteins that can be modified by the addition of the GPI anchor in fungi (de Groot *et al*., 2003; Eisenhaber *et al*., 2004). While *S. cerevisiae* is predicted to have around 66 GPI proteins, many fungal pathogens have more, with some *Candida* species having over 100 predicted GPI proteins. Furthermore, many predicted GPI proteins are species-specific, with no known orthologues and many with unknown functions.

Gels (Glucan elongation proteins), are GPI-anchored proteins also known as Glycolipid anchored surface proteins (Gas), belong to a conserved family unique to fungi. They incorporate nascent β-(1,3)-glucan molecules into the existing β-glucan meshwork (Popolo and Vai, 1999). The transglycosylating mechanism shown *in vitro* involves two steps; first, a cleave of β-(1,3) glycosidic

linkage in the glucan chain, and second, subsequent reformation of a β-(1-3) linkage between the reducing end of one released chain and the nonreducing end of side branches in existent β-glucans (Hurtado-Guerrero *et al.* 2009).

In our *M. oryzae* research, we identified five putative β-(1,3)-glucan glucanosyltransferases that each carry the Glycoside hydrolase 72 domain (GH72) and a putative Carbohydrate-binding module (CBM43 in the CAZy database), that we designated as $GH72^{+}$ (those include Gel3 and Gel4 proteins) or without this motif ($GH72^{-}$) (Samalova *et al*., 2017). Subsequently, we localized the Gel3 and Gel4 proteins to the cell periphery by creating internal fusions with fluorescent proteins mCherry and GFP, respectively. We showed spatial and temporal differences in the gene expression; both *GEL3* and *GEL4* were expressed in ungerminated and germinated spores, and germ tubes, however, did not co-localise fully. Interestingly, *GEL3* was highly expressed during germling development on onion epidermis that supports penetration pegs development, and in invasive hyphae in infected rice cells (see Figure 3), but was not visibly expressed in vegetative hyphae. By contrast, *GEL4* was not expressed during plant infection but it was expressed in vegetative hyphae. Thus, *GEL3* expression was most strongly associated with the host invasion.

Interestingly, single *GEL* gene deletions of all family members did not reveal any phenotypic differences from wild-type (WT) strain apart from *gel4* mutant that had reduced growth. Double mutant *gel3gel4* was further sensitive to oxidative stress. However, both $GH72^{+}$ (*gel3gel4*) as well as $GH72^{-}$ (*gel1gel2gel5*) mutant strains proved dispensable for pathogenicity. Further systematic testing of various triple knock-out combinations revealed that the *gel1gel3gel4* mutant had a hyper-branching phenotype with shortened hyphal cells and did not form any spores. Hence the mutant could not infect intact rice leaves and was unable to cause rice blast disease! This discovery forms an attractive target for the future development of novel antifungal drugs. As Gels tethered to the plasma membrane by GPI anchors, but located in the CW, are perfectly placed to be the ideal target without the need for the antifungal drugs to cross the plasma membrane.

Further our RNA-seq analysis studies revealed an effect not only on perturbed expression of genes encoding CW-associated enzymes, but on many membrane-proteins associated with surface sensing, including G-protein-coupled receptors. Lastly, we provided the first *M. oryzae* detailed description of the CW composition in which glucosyl residues represented 75% of the monosaccharide components. The analysis revealed only minor differences in the glucose content between WT and the triple *gel1gel3gel4* mutant with only significant increase in galactose. However, detailed linkage analysis of the wall polysaccharides of *gel3gel4* and the triple knock-out revealed increased proportions of 1,3-linked glucose residues, while the proportions of terminal glucose and residues indicative of the presence of branching points (1,3,6-Glcp) were less abundant. These data suggest that the proteins function on the 1,3-glucan chains and might be involved in branching activity indirectly (Samalova *et al*., 2017).

4. 2. Dissecting the roles of GPI-anchored proteins in *Aspergillus fumigatus*, the deadly human pathogen

Aspergillus fumigatus is a saprofitic fungus that lives primarily in the soil and grows on decaying vegetation, however, it is also an opportunistic human pathogen responsible for one of the most severe lung infections that are deadly for immunocompromised patients, aspergillosis. Because of its hostile ecological niche, it has developed strategies to survive competitive environmental conditions

and by pass human host defences. To overcome the morbidity and mortality caused by *A. fumigatus* and to facilitate the design of new therapeutics, we need to understand the pathogenesis of aspergillosis first, and use the fungal CW as a valuable source for diagnostics as well as unique targets for chemotherapeutic treatments. In nature *A. fumigatus* spreads by asexual sporulation producing chains of conidia on characteristic conidiophore heads (Figure 5). Interestingly, new evidence suggested the presence of a cryptic sexual cycle induced when isolates of compatible mating types (*MAT1-1* and *MAT1-2*) were crossed and produced cleistothecia containing asci with heat-resistant ascospores (O'Gorman *et al*., 2009). However, growth conditions that are required to trigger the sexual reproduction are rarely encountered in nature (Dyer and O'Gorman, 2012).

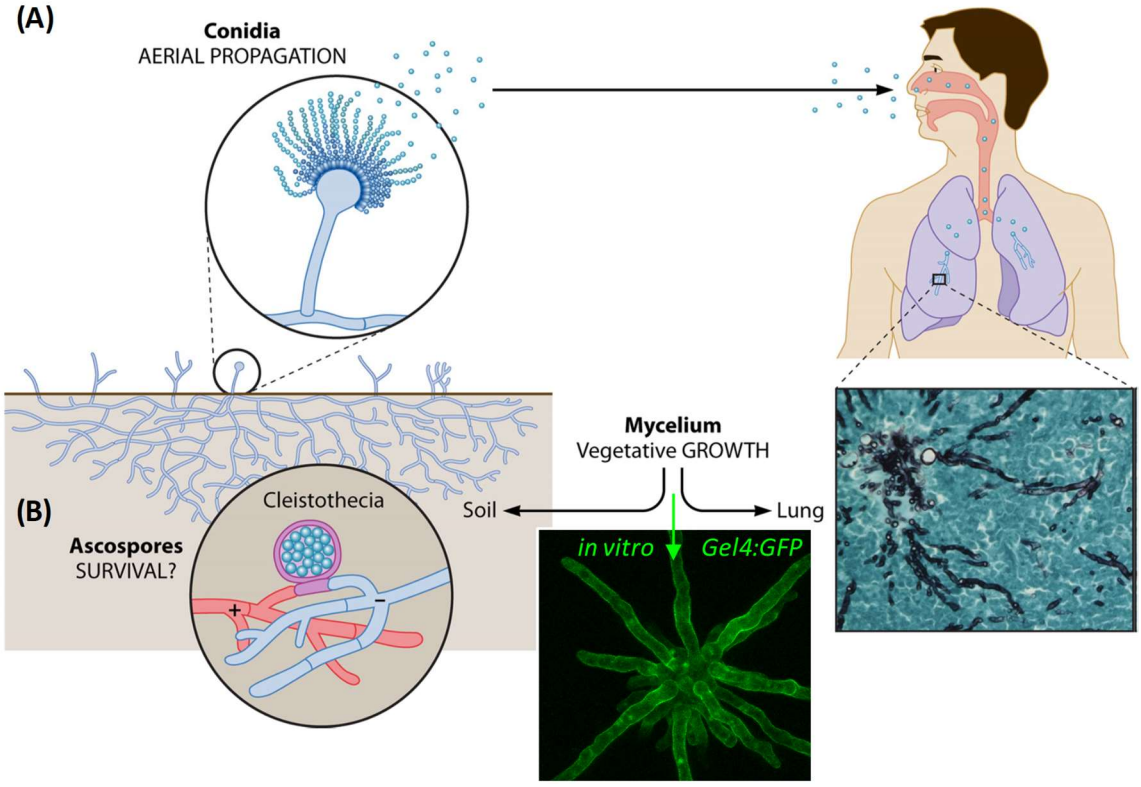

Figure 5: Cell cycle of *Aspergillus fumigatus*. A. fumigatus *is a trimorphic filamentous fungus with vegetative mycelium in nature and in patients that produce asexual conidia after mycelial starvation (A). The resting ascospores are produced from two heterothallic strains of opposite sex (B). (Adapted from Latge and Chamilos, 2019). A CLSM image of fungal colony expressing pGEL4::GEL4:GFP fusion grown* in vitro *produced by M. Samalova (unpublished).*

Aspergillus species cause a wide range of diseases in humans depending on the underlying immune status of the host. Lung infection due to *A. fumigatus* is caused by inhalation of airbone conidia present in any environment followed by *Aspergillus* colonization of lung tissue that can develop into invasive pulmonary aspergillosis. Cilia on airway epithelial cells and resident alveolar macrophages readily remove inhaled conidia, however, in individuals who are unable to clear the inhaled fungus, conidia remain in the lungs and can germinate to cause the infection. Furthermore, the physiological human body temperature of 37 °C degrees is optimal for the growth of *Aspergillus* spp. Also, *A. fumigatus* has one of the fastest growth rates among fungal species and can adapt to hypoxic conditions during growth in compost heaps or in lungs of human host by major transcriptional and

metabolic changes (Barker *et al*., 2012). Within 4–6 h, conidia can germinate into short hyphae known as germ tubes. Following germination, mycelial growth commences and the fungus creates a colony in which the hyphae are embedded in an extracellular matrix.

During the life cycle of *A. fumigatus*, the composition of the CW continuously changes with its progression and in response to environmental changes. Hence on one hand, the host immune system needs to recognize the distinct morphological forms and control fungal growth to prevent tissue invasion. On the other hand, the fungus requires nutrients and needs to adapt to the hostile environment, thus tries to escape recognition by the immune system by masking the surface molecules and modulating immune host responses (van de Veerdonk *et al*., 2017).

For human fungal pathogens, the wall induces innate and adaptive immune responses, so the fungal CW design often incorporates immune decoys and shields (Erwig and Gow, 2016). The CW of *A. fumigatus* contains the pathogen-associated molecular patterns (PAMPs) that are recognized by host pattern recognition receptors (PRRs) on innate immune cells. The cells recognize *A. fumigatus* and subsequently induce inflammatory networks to clear the pathogen. Such innate immune responses include phagocytosis and killing of the fungus by ROS production inside phagosomes by the NADPH oxidase complex (McCormick *et al*., 2010), as well as cytokine signalling that regulates the activation of adaptive immune responses and epithelial host defences (Gresnigt *et al*. 2012). The best-characterized PRR for *A. fumigatus* is the C-type lectin receptor dectin 1, which recognizes β-1,3-glucan and is crucial for early host defences in the respiratory tract (Brown and Gordon, 2001). Galactomannan can be recognized by dectin2 (Reedy *et al*., 2016), which subsequently regulates important antifungal effectors and the induction of cytokines (Taylor *et al*., 2014).

A. fumigatus uses several immune evasion and immune adaptation strategies for survival in the human host by avoiding being recognized. For example, conidial surface hydrophobin and melanin molecules not only protect conidia from oxidative stress and desiccation but also masks PAMPs present in the CW. Hydrophobins are hydrophobic proteins forming rodlets that protect the spores from enzymes, oxidants, and foraging phagocytes (Wessels, 1996), such as the conidial rodlet protein RodA. The immune response is delayed until this layer cracks upon spore swelling and germination (Paris *et al*., 2003). Once the integrity of the rodlet layer of these spores is broken, then the underlying galactosaminoglycan (GAG) and β-(1,3)-glucan layers are recognized by alveolar macrophages, enabling initiation of the innate immune response (Aimanianda *et al*., 2009). Interestingly, *A. fumigatus* during its growth produces soluble GAG together with other molecules, such as gliotoxin and fumagilin, which are toxic to host cells and induce apoptosis. Such strategies have been hypothesized to have evolved to enable *A. fumigatus* to evade predators, such as amoebae in soil (van de Veerdonk *et al*., 2017).

In our research, we investigated and generated a mutant library of all predicted GPI anchored proteins in *A. fumigatus*, in total 86 proteins, and published their complete list (Samalova *et al*., 2020). The phenotypic analysis of constructed knock-out mutants included characterisation of conidial morphology and viability, their growth, adhesion and ability to form biofilms (Beauvais *et al*., 2014). Identification of putative GPI anchored proteins in the *A. fumigatus* genome was performed using the prediction programs PredGPI (http://gpcr.biocomp.unibo.it/) and big PI (http://mendel.imp.ac.at/sat/gpi/gpi_server.html) (Eisenhaber *et al*., 2004). Comparative genomic analysis revealed that orthologues of only 28 proteins (32.5%) were common to yeasts *S. cerevisiae*

and *C. albicans* and filamentous fungi and further 38 proteins (44%) were found only in filamentous fungal species. Interestingly, 20 GPI-anchored proteins (23.5%) were present exclusively in the genomes of the *Aspergilli*.

Most GPI-anchored proteins common to yeast and filamentous fungi are acting on the CW morphogenesis or are associated with CW structures. Among them are previously well studied enzymes (e.g. Gel, Bgt2*,* Dfg, Sun, and Crh) with proven functions associated with CW polysaccharids remodelling. For example, transglycosidases, the first one identified belong to the GEL family (GH72, discussed above) in *Aspergillus* /GAS in *Saccharomyces* /PHR in *Candida* and is responsible for the elongation of β-(1,3)-glucans. Interestingly, while most of the CW biosynthetic processes occur in the Golgi and at the cell membrane, part of the fungal CW biosynthesis takes place within the wall itself. The essential role of Gel activity was demonstrated by deletion of *GEL4* in *A. fumigatus* that was lethal (Hartland *et al*. 1996; Gastebois *et al*., 2010). Only recently it was proven that some members of this family have a dual activity that allows them not only to elongate but also to branch the neo elongated β-(1,3)-glucan (Aimanianda *et al*. 2017). This branching activity was only seen in enzymes that have the CBM43 module and loss of this motif abolished the β-(1,3)-glucan branching (Aimanianda *et al*. 2017).

As most of the previously analysed GPI-anchor proteins were associated with CW construction and fungal morphogenesis, we investigated the role of newly identified GPI-anchored proteins in that and found out that ten of them showed a distinct phenotype from the parental strain, including conidial shape, hyphal growth, sensitivity to CW perturbance dyes (congo red and calcofluor white), adhesion or biofilm formation (Samalova *et al*., 2020). However, most of the proteins exclusively present in filamentous fungi genome (25 on the 38 identified) displayed unknown functions. Similarly, proteins found exclusively in *Aspergillus* species were of unknown functions. Further six proteins only present in the *Aspergillus* species were phylogenetically closed to *A. fumigatus*, however, no significant homology or domain has been found with any known proteins. Interestingly, only the deletion of *AFUA_8G01700* showed a distinct phenotype from the parental strain, including reduced growth, higher sensitivity to drugs and reduced adhesion and is a subject of further investigation (*publication in prep*.).

To summarise, we identified three different categories of GPI anchored proteins in *A. fumigatus*. The first category of proteins is highly conserved in all fungi and is essential for cell wall morphogenesis. Most of them belong to multigenic families of proteins, but curiously, only one or two genes in a family is responsible for the phenotype observed (Gastebois *et al*., 2010; Mouyna *et al*., 2005; Millet *et al*. 2018; Muszkieta *et al*. 2019). In the second category, we identified and characterized proteins present only in filamentous fungi, which are mostly involved in biofilm formation, adhesion, and virulence process. Finally, the third category is only present in *Aspergillus* species. These proteins seem to be mostly associated with the formation of the conidial stage but again their function is unknown. Our review suggests that other non-GPI-bound transglycosidases are important for the remodelling of cell wall construction and remain to be discovered (Samalova *et al*., 2020).

ATTACHMENTS:

[10] Samalova, M., Melida, H., Vilaplana, F., Bulone, V., Soanes, D.M., Talbot, N. J. and Gurr, S.J. (2017) The β-1,3-glucanosyltransferases (Gels) affect the structure of the rice blast fungal cell wall

during appressorium-mediated plant infection.: The Gels affect fungal wall structure during infection. *Cell. Microbiol.* **19**, e12659.

[11] Samalova, M., Carr, P., Bromley, M., Blatzer, M., Moya-Nilges, M., Latge, J.-P. and Mouyna, I. (2020) GPI anchored proteins in *Aspergillus fumigatus* and cell wall morphogenesis. *Curr. Top. Microbiol. Immunol.* **425**, 167-186.

5. Novel imaging tools to explore expansins as factors controlling cell wall biomechanics

Changes in CW mechanical properties are the driving force of plant growth and development as predicted by a number of biomechanical models (Braybrook and Jonsson, 2016; Geitmann and Ortega, 2009; Haas *et al*., 2020; Hamant and Traas, 2010; Sassi and Traas, 2015). However, novel technologies that can characterize those changes at the cellular or tissue level in the developing organs are sorely required. One novel approach is Brillouin spectroscopy, a powerful all optical label-free technique that, combined with confocal microscopy, allows biomechanical measurements of live cells (Scarcelli *et al*., 2015) and tissue (Elsayad *et al*., 2016) without contact or perturbation of the biological sample under study. More specifically, the measured Brillouin light scattering (BLS) is an inelastic scattering of light by inherent or stimulated high frequency acoustic vibrations (phonons) in a sample (Berne and Pecora, 2000). Their speed is directly related to the elastic modulus ("stiffness") of the material and can be monitored in 3D with a lateral resolution close to the diffraction limit (Elsayad *et al*., 2019; Prevedel *et al*., 2019).

Primary plant CW consists predominantly of the polysaccharides cellulose, hemicellulose and pectins (Wolf *et al*., 2012). CW is a layered structure in which the load-bearing cellulose microfibrils interconnected with xyloglucans are embedded into pectin matrix (Zhang *et al*., 2021). The properties of the CW are constantly being remodelled to allow developmental and adaptive responses that are necessary for plant growth and development. The CW biomechanics is regulated by a number of agents including expansins (Cosgrove, 2000; McQueen-Mason *et al*., 1992), glucanases (Zhang *et al*., 2019), pectin methylesterases (Peaucelle *et al*., 2011; Wang *et al*., 2020), calcium ions (Wang *et al*., 2020) and others. While expansins induce a creep, meaning an irreversible, time dependent CW enlargement, other enzymes are involved in the CW remodelling and those processes should be distinguished (Wang *et al*., 2020).

Expansins were discovered as plant proteins responsible for CW loosening (McQueen-Mason *et al*., 1992) during pH-dependent "acid growth" (Rayle and Cleland, 1992) as they induce stress relaxation and extension of plant CWs. Interestingly, expansins are also found in fungi and bacteria (Georgelis *et al*., 2015) and those have been often utilised in industrial applications to facilitate degradation of lignocellulose material used further for biomass conversion into biofuels (Liu *et al*., 2015). To fully comprehend the well-studied field, we wrote a review on expansins focused on the role of biomechanics in the expansin-mediated developmental and adaptive responses of plants (Samalova *et al*., 2022). In this review we summarised current knowledge of expansin structure, function and a mode of action as well as the past and modern models of the plant CW. Interestingly, expansins do not act as enzymes, as they lack the hydrolytic activity, but they disrupt non-covalent bonds between the cellulose microfibrils, xyloglucans and other CW components (Cosgrove, 2018). Measurements of expansin activity were typically performed by clamping the samples in a custom-made mechanical

extensometer and to avoid the complexities of growing plant tissues, onion epidermal wall strips were used instead (Cosgrove, 1989; Durachko *et al*., 2017; Zhang *et al*., 2019; Wang *et al*., 2020). However, there are 36 expansins in *Arabidopsis* (Sampedro and Cosgrove, 2005) that promote CW loosening and are related to growth of specific cell types.

In our current investigations we focus on a small group of expansins that were predicted to be the direct targets of cytokinin signalling in *Arabidopsis* (Lee *et al*., 2007; Pacifici *et al*., 2018). We determined their hormonal responsiveness and specificity of expression and localization in roots using both transcriptional (*pEXPA1::nls:3xGFP*) as well as translational (*pEXPA1::EXPA1:mCherry*) fusions and localised them, for the first time *in vivo*, to the CWs (Samalova *et al*., 2020). We found EXPA1 localised dominantly in the epidermis of lateral root cap. However, the response to exogenously applied plant hormone cytokinins was moderate unlike the robust response to auxins. Further, we found EXPA10 and EXPA14 localised predominantly at the three-cell boundaries of epidermis/cortex in various root zones. Interestingly, cell type-specific localisation of EXPA15 overlapped with higher CW stiffness measured via fluorescence emission - Brillouin imaging (FBi) correlative microscopy (Elsayad *et al*., 2016), implying a possible role of expansins in the control of biomechanical CW properties.

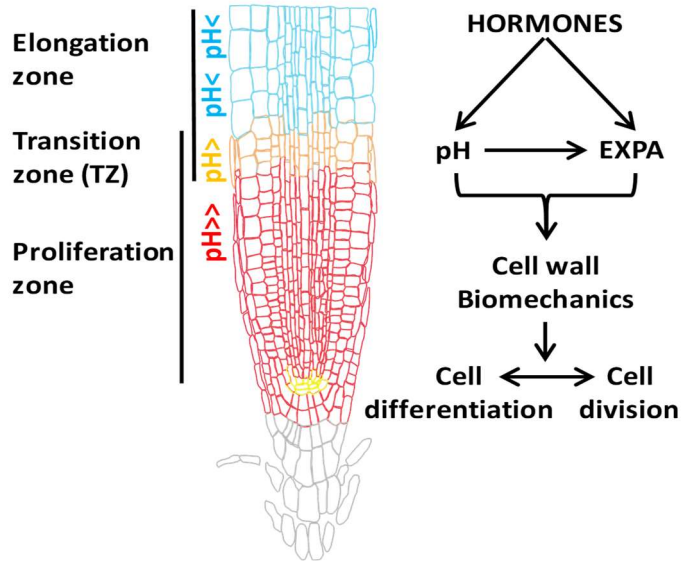

Figure 6: An integrative model of hormone-driven expansin role in root apical meristem. *The model proposes that hormone-mediated pH distribution within the root apoplast, together with tightly controlled spatiotemporal specificity of expansin expression, plays an important regulatory role controlling the CW biomechanics and thus root growth and development in* Arabidopsis.

We confirmed the ability of expansin to increase the CW stiffness in stable transgenic lines following dexamethasone-induced *EXPA1* overexpression that was indicated by higher Brillouin frequency shift (BFS). The unexpected finding was substantiated by increase of the apparent Young modulus (Peaucelle, 2014) measured via atomic force microscopy (AFM) that is considered as the gold standard for biomechanical studies. Further *in situ* measurement of the refraction index in living cells using a holotomographic microscope excluded the possibility that the observed EXPA1-induced increase of BFS was due to changes in the CW mass density. Surprisingly, the *EXPA1* overexpression resulted in a root growth arrest phenotype, associated with shortening of the root apical meristem,

severity of which was enhanced by lower pH. We proposed that tightly controlled spatiotemporal specificity of expansin expression in a combination with localisation of their protein products into distinct extracellular matrix domains, and hormonal-mediated pH distribution within the root apoplast, plays an important regulatory role controlling the *Arabidopsis* root growth and development (Figure 6). Disturbing the delicate balance of biomechanical CW properties has severe consequences for the plant growth (Samalova *et al*., 2020).

In our ongoing research, we aim to determine the apoplastic pH of individual tissues of *Arabidopsis* roots and correlate growth changes triggered by expansin cell-specific overexpression with pH of CW in order to elucidate the role of expansins in the control of CW biomechanical properties that are driving root growth and development. We plan to use the improved, genetically encoded apoplastic pH sensor pH_{apo} (Kesten *et al*., 2019), to map the pH of CWs (apoplast) of the various root tissues in *Arabidopsis* seedlings, and also utilise a novel fluorescent dye 8-hydroxypyrene-1,3,6-trisulfonic acid trisodium salt (HPTS) that was described as a suitable fluorescent pH indicator for assessing apoplastic pH at a cellular resolution in *Arabidopsis* roots (Barbez *et al*., 2017). Further, we activate CW loosening in individual cell types of the root by employing the DEX-inducible transcription activation system pOp6/LhGR (Craft *et al*., 2005). We take advantage of already generated activator lines (Schurholz *et al*., 2018) that drive the cell type-specific expression of the LhGR activator by specific promoters, and prepare additional LhGR lines to cover all root cell types.

After applying a fungal toxin fusicoccin (Ballio *et al*., 1964) that can trigger immediate apoplast acidification (Fendrych *et al*., 2016) and/or after exogenous application of hormones (auxins and CKs) we plan to follow *in vivo* growth changes measured on the transition/elongation zone boundaries corresponding to the activator line used. Alternatively, rather than global, external pH changes of the whole root we can also try to induce internal, tissue specific changes by re-transforming the selected lines with a proton pump (pOp6:H^+-ATPase). After its activation in the same tissue as the expansin, it will acidify the specific cell type by pumping H^+ into the apoplast. That gives us control over the pH changes with cell-type resolution and allows us to investigate the role of cell type-specific expansin expression in the control of CW biomechanics that drives the root growth and development. Together with mathematicians, physicists and material scientists we aim to build a model that will describe the mechanics beyond the root growth, and further develop those unique biomechanical imaging techniques mentioned above.

ATTACHMENTS:

[12] Samalova, M., Gahurova, E. and Hejatko, H. (2022) Expansin-mediated developmental and adaptive responses: A matter of cell wall biomechanics? *Quantitative Plant Biology*, **3:e11**, 1-14.

REFERENCES

Aimanianda, V., Bayry, J., Bozza, S., Kniemeyer, O., Perruccio, K., Elluru, S.R., Clavaud, C., Paris, S., Brakhage, A.A., Kaveri, S.V., Romani, L. and Latge, J.P. (2009) Surface hydrophobin prevents immune recognition of airborne fungal spores. *Nature*, **460**, 1117–1121.

Aimanianda, V., Simenel, C., Garnaud, C., Clavaud, C., Tada, R., Barbin, L., Mouyna, I., Heddergott, C., Popolo, L., Ohya, Y., Delepierre, M. and Latge, J.P. (2017) The dual activity responsible for the elongation and branching of β-(1,3)-glucan in the fungal cell wall. *mBio*, **8**, e00619–17.

Alderton, W.K., Cooper, C.E. and Knowles, R.G. (2001) Nitric oxide synthases: structure, function and inhibition. *Biochem. J*. **357**, 593–615.

Aoyama, T. and Chua, N.-H. (1997) A glucocorticoid-mediated transcriptional induction system in transgenic plants. *Plant J*. **11**, 605-612.

Au, K. K. C., Perez-Gomez, J., Neta, H., Muller, C., Meyer, A. J., Fricker, M. D. and Moore, I. (2012) A perturbation in glutathione biosynthesis disrupts endoplasmic reticulum morphology and secretory membrane traffic in *Arabidopsis thaliana*. *Plant J*. **71**, 881-89.

Ballio, A., Chain, E.B., De Leo, P., Erlanger, B.F., Mauri, M. and Tonolo A. (1964) Fusicoccin: a new wilting toxin produced by *Fusicoccum amygdali* Del. *Nature* **203**, 297

Barbez, E., Dunser, K., Gaidora, A., Lendl, T. and Busch, W. (2017) Auxin steers root cell expansion via apoplastic pH regulation in *Arabidopsis thaliana*. *Proc. Natl. Acad. Sci.* **114**, E4884-E4893.

Barker, B. M., Kroll, K., Vödisch, M., Mazurie, A., Kniemeyer, O. and Cramer, R.A. (2012) Transcriptomic and proteomic analyses of the *Aspergillus fumigatus* hypoxia response using an oxygen-controlled fermenter. *BMC Genomics*, **13**, 62.

Barksdale, T.H. and Asai, G.N. (1961) Diurnal spore release of *Pyricularia oryzae* (*Magnaporthe oryzae*) from rice leaves. *Phytopathol.* **51**, 313-317.

Batoko, H., Zheng, H.Q., Hawes, C. and Moore, I. (2000) A Rab1 GTPase is required for transport between the endoplasmic reticulum and Golgi apparatus for normal Golgi movement in plants. *Plant Cell*, **12**, 2201–2217

Beauvais, A., Fontaine, T., Aimanianda, V. and Latge, J. P. (2014) *Aspergillus* cell wall and biofilm. *Mycopathologia*, **178**, 371–377.

Berne, B.J. and Pecora, R. eds. (2000) Dynamic light scattering, with applications to chemistry, biology, and physics. *New York*, NY: Dover Publications.

Besson-Bard, A., Pugin, A. and Wendehenne, D. (2008) New insights into nitric oxide signaling in plants. *Ann. Rev. Plant Biol.* **59**, 21–39.

Braybrook, S. and Jönsson, H. (2016) Shifting foundations: the mechanical cell wall and development. *Curr. Opin. Plant Biol.* **29**, 115-120.

Brown, G. D. and Gordon, S. (2001) Immune recognition: A new receptor for β-glucans. *Nature* **413**, 36–37.

Buren, S., Ortega-Villasante, C., Otvos, K., Samuelsson, G., Bako, L. and Villarejo, A. (2012) Use of foot-and mouth disease virus 2A peptide co-expression system to study intracellular protein trafficking in *Arabidopsis. Plos One*, **12**, e51973.

Caddick, M.X., Greenland, A.J., Jepson, I., Krause, K.-P., Qu, N., Riddell, K.V., Salter, M.G., Schuch, W., Sonnewald, U. and Tomsett, A.B. (1998) An ethanol inducible gene switch for plants used to manipulate carbon metabolism. *Nat. Biotechnol.* **16**, 177-180.

Camacho, L., Smertenko, A.P., Perez-Gomez, J., Hussey, P.J. and Moore, I. (2009) *Arabidopsis* Rab-E GTPases exhibit a novel interaction with a plasma-membrane phosphatidylinositol-4-phosphate 5-kinase. *J. Cell Sci.* **122**, 4383-4392.

Canovas, D., Marcos, J.F., Marcos, A.T. and Strauss, J. (2016) Nitric oxide in fungi: is there NO light at the end of the tunnel? *Curr. Genet*. **62**, 513–518.

Chow, C.M., Neto, H., Foucart, C. and Moore, I. (2008) Rab-A2 and Rab-A3 GTPases define a *trans*-Golgi endosomal membrane domain in *Arabidopsis* that contributes substantially to the cell plate. *Plant Cell*, **20**, 101-123.

Coronado, J.E., Mneimneh, S., Epstein, S.L., Qiu, W.G. and Lipke, P.N. (2007) Conserved processes and lineage-specific proteins in fungal cell wall evolution. *Eukaryot Cell*, **6**, 2269–2277.

Cosgrove, D. J. (1989) Characterization of long-term extension of isolated cell-walls from growing cucumber hypocotyls. *Planta*, **177**, 121–130.

Cosgrove, D. J. (2000) Loosening of plant cell walls by expansins. *Nature*, ***407***, 321-326.

Cosgrove, D. J. (2018) Nanoscale structure mechanics and growth of epidermal cell walls. *Curr. Opin. Plant Biol*. **46**, 77-86.

Craft, J., Samalova, M., Baroux, C., Townley, H., Martinez, A., Jepson, I., Tsiantis, M. and Moore, I. (2005) New pOp/LhG4 vectors for stringent glucocorticoid-dependent transgene expression in *Arabidopsis. Plant J.* **41**, 899-918.

Dean, R., Talbot, N., Ebbole, D. *et al*. (2005) The genome sequence of the rice blast fungus *Magnaporthe grisea*. *Nature*, **434**, 980–986.

de Groot, P.W., Hellingwerf, K.J. and Klis, F.M. (2003) Genome-wide identification of fungal GPI proteins. *Yeast*, **20**, 781–796.

de Groot, P.W., Ruiz, C., Vazquez de Aldana, C.R., Duenas, E., Cid, V.J., Del Rey, F., Rodriquez-Pena, J.M., et al. (2001) A genomic approach for the identification and classification of genes involved in cell wall formation and its regulation in Saccharomyces cerevisiae. *Comp. Funct. Genom.* **2**, 124–142.

Delledonne, M., Xia, Y.J., Dixon, R.A., and Lamb, C. (1998) Nitric oxide functions as a signal in plant disease resistance. *Nature*, **394**, 585–588.

Dooley, C.T., Dore, T.M., Hanson, G.T., Jackson, W.C., Remington, S.J. and Tsien, R.Y. (2004) Imaging dynamic redox changes in mammalian cells with green fluorescent protein indicators. *J. Biol. Chem.* **279**, 22284–22293.

Durachko, D., Park, Y. B., Zhang, T. and Cosgrove, D. J. (2017) Biomechanical characterization of onion epidermal cell walls. *Bio-Protocol*, **7**, https://doi. org/10.21769/BioProtoc.22662.

Dyer, P.S. and O'Gorman, C.M. (2012) Sexual development and cryptic sexuality in fungi: insights from *Aspergillus* species. *FEMS Microbiol. Rev.* **36**, 165–192.

Ebbole, D.J. (2007) *Magnaporthe* as a model for understanding host–pathogen interactions. *Ann.l Rev. Phytopathol*. **45**, 437–456.

Eisenhaber, B., Schneider, G., Wildpaner, M. and Eisenhaber, F. (2004) A sensitive predictor for potential GPI lipid modification sites in fungal protein sequences and its application to genome-wide studies for *Aspergillus nidulans*, *Candida albicans*, *Neurospora crassa*, *Saccharomyces cerevisiae* and *Schizosaccharomyces pombe*. *J. Mol. Biol.* **337**, 243–253.

Elsayad, K., Werner, S., Gallemí, M., Kong, J., Sanchez Guajardo, E. R., Zhang, L., Jaillais, Y., Greb, T. and Belkhadir, Y. (2016) Mapping the subcellular mechanical properties of live cells in tissues with fluorescence emission–Brillouin imaging. *Science Signaling*, ***9***, rs5.

Elsayad, K., Polakova, S. and Gregan, J. (2019) Probing mechanical properties in biology using Brillouin microscopy. *Trends in Cell Biol.* **8**, 608-611.

Erwig, L.P. and Gow, N.A.R. (2016) Interactions of fungal pathogens with phagocytes. *Nat. Rev. Microbiol*. **14**, 163–176.

Fendrych, M., Leung, J., and Friml, J. (2016) TIR1/AFB-Aux/IAA auxin perception mediates rapid cell wall acidification and growth of *Arabidopsis* hypocotyls. *eLife* **5**, e19048.

Fisher, M.C., Henk, D.A., Briggs, C.J., Brownstein, J.S., Madoff, L.C., McCraw, S.L. and Gurr, S.J. (2012) Emerging fungal threats to animal, plant and ecosystem health. *Nature*, **484**, 186–194.

Fujikawa, T., Sakaguchi, A., Nishizawa, Y., Kouzai, Y., Minami, E., Yano, S. *et al*. (2012) Surface alpha-1,3-glucan facilitates fungal stealth infection by interfering with innate immunity in plants. *PLoS Pathog*. **8**, 16.

Gastebois, A., Fontaine, T., Latge, J.P. and Mouyna I (2010) β(1-3)-Glucanosyltransferase Gel4p is essential for *Aspergillus fumigatus*. *Eukaryot Cell*, **9**, 1294–1298.

Geitmann, A. and Ortega, J.K.E. (2009) Mechanics and modeling of plant cell growth. *Trends Plant Sci.* **14**, 467-478.

Geoghegan, I., Steinberg, G. and Gurr, J. (2017) The role of the fungal cell wall in the infection of plants. *Trends Microbiol*. **25**, 957-967.

Georgelis, N., Nikolaidis, N. and Cosgrove, D. J. (2015) Bacterial expansins and related proteins from the world of microbes. *App. Microbiol. Biotechnol.* **99,** 3807–3823.

Gessler, N.N., Averyanov, A.A. and Belozerskaya, T.A. (2007) Reactive oxygen species in regulation of fungal development. *Biochemistry-Moscow*, **72**, 1091–1109.

Goh, H.-H., Sloan, J., Dorca-Fornell, C. and Fleming, A. (2012) Inducible repression of multiple expansin genes leads to growth suppression during leaf development. *Plant Physiol*. **159**, 1759-1770.

Gresnigt, M. S., Netea, M. G. and van de Veerdonk, F. L. (2012) Pattern recognition receptors and their role in invasive aspergillosis. *Ann. NY Acad. Sci.* **1273**, 60–67.

Guo, F.Q., Okamoto, M. and Crawford, N.M. (2003) Identification of a plant nitric oxide synthase gene involved in hormonal signaling. *Science,* **302**, 100–103.

Gurr, S., Samalova, M. and Fisher, M. (2011) The rise and rise of emerging infectious fungi challenges food security and ecosystem health. *Fungal Biol. Rev*. **25**, 181-188.

Gutscher, M., Pauleau, A.L., Marty, L., Brach, T., Wabnitz, G.H., Samstag, Y., Meyer, A.J. and Dick, T.P. (2008) Real-time imaging of the intracellular glutathione redox potential. *Nat. Met.* **5**, 553–559.

Haas, K.T., Wightman, R., Meyerowitz, E.M. and Peaucelle, A. (2020) Pectin homogalacturonan nanofilament expansion drives morphogenesis in plant epidermal cells. *Science,* **367**, 1003-1007.

Halpin, C., Cooke. S.E., Barakate. A., El Amrani, A. and Ryan, M.D. (1999) Self-processing 2A-polyproteins – a system for co-ordinate expression of multiple proteins in transgenic plants. *Plant J*. **17**, 453–459.

Hamant, O. and Traas, J. (2010) The mechanics behind plant development. *New Phytol.* **185**, 369-385.

Hartland, R.P., Fontaine, T., Debeaupuis, J.P., Simenel, C., Delepierre, M. and Latge, J.P. (1996) A novel β-(1-3)-glucanosyltransferase from the cell wall of *Aspergillus fumigatus*. *J. Biol. Chem.* **271**, 26843–26849.

Heller, J. and Tudzynski, P. (2011) Reactive oxygen species in phytopathogenic fungi: signaling, development, and disease. *Ann. Rev. Phytopathol*. **49**, 369-390.

Hurtado-Guerrero, R., Schuttelkopf, A. W., Mouyna, I., Ibrahim, A. F., Shepherd, S., Fontaine, T. *et al*., (2009) Molecular mechanisms of yeast cell wall glucan remodelling. *J. Biol. Chem*. **284**, 8461–69.

Jones, J.D.G. and Dangl, J.L. (2006) The plant immune system. *Nature*, **444**, 323–329.

Kesten, C., Gamez-Arjona, F.M., Menna, A., Scholl, S., Dora, S., Huerta, A.I., Huang, H.Y., Tintor, N., Kinoshita, T., Rep, M., Krebs, M., Schumacher, K. and Sanchez-Rodríguez, C. (2019) Pathogen-induced pH changes regulate the growth-defense balance in plants. *EMBO J.* e101822.

Kirchhelle, C., Chow, C.M., Foucart, C., Neto, H., Stierhof, Y.D., Kalde, M., Walton, C., Fricker, M., Smith, R.S., Jerusalem, A., Irani, N. and Moore, I. (2016) The specification of geometric edges by a plant Rab GTPase is an essential cell-patterning principle during organogenesis in *Arabidopsis*. *Develop. Cell*, **36**, 386-400.

Koo, J.C., Asurmendi, S., Bick, J., Woodford-Thomas, T. and Beachy, R.N. (2004) Ecdysone agonist-inducible expression of a coat protein gene from tobacco mosaic virus confers viral resistance in transgenic *Arabidopsis*. *Plant J*. **37**, 439–448.

Kotzer, A.M., Brandizzi, F., Neumann, U., Paris, N., Moore, I. and Hawes, C. (2004) AtRabF2b (Ara7) acts on the vacuolar trafficking pathway in tobacco leaf epidermal cells. *J. Cell Sci*. **117**, 6377–6389.

Kou, Y.J., Qiu, J.H. and Tao, Z. (2019) Every coin has two sides: reactive oxygen species during rice–*Magnaporthe oryzae* interaction. *Int. J. Mol. Sci.* **20**, 1191.

Lamb, C. and Dixon, R.A. (1997) The oxidative burst in plant disease resistance. *Ann. Rev. Plant Physiol. Plant Molec. Biol.* **48**, 251–275.

Latge, J.P. (2007) The cell wall: a carbohydrate armour for the fungal cell. *Mol. Microbiol*. **66**, 279–290.

Latge, J.P. and Chamilos, G. (2019) *Aspergillus fumigatus* and aspergillosis in 2019. *Clin. Microbiol. Rev*. **33**, e00140-18.

Lee, D.J., Park, J.Y., Ku, S.J., Ha, Y.M., Kim, S., Kim, M.D., Oh, M.H. and Kim. J. (2007) Genome-wide expression profiling of *ARABIDOPSIS RESPONSE REGULATOR 7*(*ARR7*) overexpression in cytokinin response. *Mol. Genet. Genom.* **277**, 115-137.

Liu, S.M. and Yoder, J.I. (2016) Chemical induction of hairpin RNAi molecules to silence vital genes in plant roots. *Sci. Rep.* **6**, 37711.

Liu, X., Ma, Y. and Zhang, M. (2015) Research advances in expansins and expansion-like proteins involved in lignocellulose degradation. *Biotechnol. Letters*, **37**, 1541-1551.

Ma, C.L. and Mitra, A. (2002) Expressing multiple genes in a single open reading frame with the 2A region of foot-and-mouth disease virus as a linker. *Mol. Breed.* **9**, 191–199.

Marcos, A.T., Ramos, M.S., Marcos, J.F., Carmona, L., Strauss J. and Canovas, D. (2016) Nitric oxide synthesis by nitrate reductase is regulated during development in *Aspergillus*. *Mol. Biol*. **99**, 15-33.

McCormick, A., Heesemann, L., Wagener, J., Marcos, V., Hartl, D., Loeffler, J., Heesemann, J. and Ebel, F. (2010) NETs formed by human neutrophils inhibit growth of the pathogenic mold *Aspergillus fumigatus*. *Microbes Infect*. **12**, 928–936.

McQueen-Mason, S., Durachko, D. M. and Cosgrove, D. J. (1992) Two endogenous proteins that induce cell wall extension in plants. *Plant Cell*, **4**, 1425–1433.

Meyer, A.J. and Dick, T.P. (2010) Fluorescent protein-based redox probes. *Antioxidants & Redox Signaling*, **13**, 621–650.

Millet, N., Latge, J.P. and Mouyna, I. (2018) Members of glycosyl-hydrolase family 17 of *A. fumigatus* differentially affect morphogenesis. *J. Fungi Basel*. 4.

Moore, I., Samalova, M. and Kurup, S. (2006) Transactivated and chemically inducible gene expression in plants. *Plant J*. **45**, 651-683.

Moreau, M., Lee, G.I., Wang, Y., Crane, B.R. and Klessig, D.F. (2008) *AtNOS*/*AtNOA1* is a functional *Arabidopsis thaliana* cGTPase and not a nitric-oxide synthase. *J. Biol. Chem*. **283**, 32957–32967.

Mouyna, I., Monod, M., Fontaine, T., Henrissat, B., Lechenne, B. and Latge, J. P. (2000) Identification of the catalytic residues of the first family of beta-(1,3) glucanosyltransferases identified in fungi. *Biochem. J.* **347**, 741–747.

Mouyna, I., Morelle, W., Vai, M., Monod, M., Lechenne, B., Fontaine, T., Beauvais, A., Sarfati, J., Prevost, M.C., Henry, C. and Latge, J.P. (2005) Deletion of *GEL2* encoding for a β(1–3)-glucanosyltransferase affects morphogenesis and virulence in *Aspergillus fumigatus*. *Mol. Microbiol*. **56**, 1675–1688.

Muszkieta, L., Fontaine, T., Beau, R., Mouyna, I., Vogt, M.S., Trow, J., Cormack, B.P., Essen, L.O., Jouvion, G., and Latge, J.P. (2019) The glycosylphosphatidylinositol-anchored DFG family is essential for the insertion of galactomannan into the β-(1,3)-glucan-chitin core of the cell wall of *Aspergillus fumigatus*. *mSphere*, **4**, e00397–19.

O'Gorman, C.M., Fuller, H.T. and Dyer, P.S. (2009) Discovery of a sexual cycle in the opportunistic fungal pathogen *Aspergillus fumigatus*. *Nature*, **457**, 471–474.

Oliveira-Garcia, E. and Deising, H.B. (2016) Attenuation of PAMP triggered immunity in maize requires down-regulation of the key beta-1,6-glucan synthesis genes *KRE5* and *KRE6* in biotrophic hyphae of *Colletotrichum graminicola*. *Plant J*. **87**, 355–375.

Pacifici, E., Di Mambro, R., Dello Ioio, R., Costantino, P. and Sabatini, S. (2018) Acidic cell elongation drives cell differentiation in the *Arabidopsis* root. *EMBO J*. **37**, e99134.

Padidam, M., Gore, M., Lu, D.L. and Smirnova, O. (2003) Chemical-inducible, ecdysone receptor-based gene expression system for plants. *Trans. Res*. **12**, 101–109.

Paris, S., Debeaupuis, J.P., Crameri ,R., Carey, M., Charles, F., Prevost, M.C., Schmitt, C., *et al*. (2003) Conidial hydrophobins of *Aspergillus fumigatus*. *Appl. Environ. Microbiol.* **69**, 1581–1588.

Peaucelle, A. (2014) AFM-based mapping of the elastic properties of cell walls: at tissue, cellular, and subcellular resolutions. *J. Vis. Exp.* **89**, 51317.

Peaucelle, A., Braybrook, S.A., Le Guillou, L., Bron, E., Kuhlemeier, C. and Höfte, H. (2011) Pectin-induced changes in cell wall mechanics underlie organ initiation in *Arabidopsis*. *Curr. Biol.* **21**, 172026.

Pinheiro, H., Samalova, M., Geldner, N., Chory, J., Martinez, A. and Moore, I. (2009) Genetic evidence that the higher plant Rab-D1 and Rab-D2 GTPases exhibit distinct but overlapping interactions in the early secretory pathway. *J. Cell Sci*. **122**, 3749-3758.

Popolo, L. and Vai, M. (1999) The Gas1 glycoprotein, a putative wall polymer cross-linker. *Biochim et Biophys Acta – General Subjects*, **1426**, 385–400.

Prats, E., Mur, L.A.J., Sanderson, R. and Carver, T.L.W. (2005) Nitric oxide contributes both to papilla-based resistance and the hypersensitive response in barley attacked by *Blumeria graminis* f. sp *hordei*. *Mol. Plant Pathol.* **6**, 65–78.

Prevedel, R., Diz-Munoz, A., Ruocco, G. and Antonacci, G. (2019) Brillouin microscopy: an emerging tool for mechanobiology. *Nat. Methods*, **16**, 969-977.

Rayle, D. L. and Cleland, R. E. (1992) The Acid Growth Theory of auxin-induced cell elongation is alive and well. *Plant Physiol*. **99**, 1271–1274.

Reedy, J. L., Wuethrich, M. A., Latge, J. P. and Vyas, J. M. (2016) Dectin-2 is a receptor for galactomannan. The Aspergillus Website http://www.aspergillus.org.uk/content/dectin-2-receptor-galactomannan.

Roslan, H.A., Salter, M.G., Wood, C.D., White, M.R.H., Croft, K.P., Robson, F., Coupland, G., Doonan, J., Laufs, P., Tomsett, A.B. and Caddick, M.X. (2001) Characterization of the ethanol-inducible *alc* gene-expression system in *Arabidopsis thaliana*. *Plant J.* **28**, 225–235.

Rossignol, P., Orbovic, V. and Irish, V.F. (2014) A dexamethasone-inducible gene expression system is active in citrus plants. *Sci. Hortic.* **172**, 47-53.

Rutherford, S. and Moore, I. (2002) The *Arabidopsis* Rab GTPases family: another enigma variation. *Curr. Opin. Plant Biol.* **5**, 518-528.

Ryan, M.D., Donnelly, M., Lewis, A., Mehrotra, A.P, Wilkie, J. and Gani, D. (1999) A model for nonstoichiometric, cotranslational protein scission in eukaryotic ribosomes. *Bioorg. Chem.* **27**, 55–79.

Salter, M.G., Paine, J.A., Riddell, K.V., Jepson, I., Greenland, A.J., Caddick, M. and Tomsett, A.B. (1998) Characterisation of the ethanol-inducible alc gene expression system for transgenic plants. *Plant J*. **16**, 127–132.

Samalova, M. and Moore, I. (2021) The steroid-inducible pOp6/LhGR gene expression system is fast, sensitive and does not cause plant growth defects in rice (*Oryza sativa*). *BMC Plant Biol*. **21**, 461.

Samalova, M., Brzobohaty, B. and Moore, I. (2005) pOp6/LhGR: a stringently regulated and highly responsive dexamethasone-inducible gene expression system for tobacco. *Plant J*. **41**, 919-935.

Samalova, M., Fricker, M. and Moore, I. (2006) Ratiometric fluorescence-imaging assays of plant membrane traffic using polyproteins. *Traffic*, **7**, 1701-1723.

Samalova, M., Fricker, M. and Moore, I. (2008) Quantitative and qualitative analysis of plant membrane traffic using fluorescent proteins. *In* Methods in Cell Biology, Fluorescent Proteins, 2nd Edition, K.F. Sullivan (ed.), Academic Press, **85**, 353-380.

Samalova, M., Johnson, J., Illes, M., Kelly, S., Fricker, M. and Gurr, S. (2013) Nitric oxide generated by the rice blast fungus *Magnaporthe oryzae* drives plant infection. *New Phytol.* **197**, 207-222.

Samalova, M., Meyer, A., Gurr, S. and Fricker, M. (2014) Robust anti-oxidant defences in the rice blast fungus *Magnaporthe oryzae* confer tolerance to the host oxidative burst. *New Phytol.* **201**, 556-573.

Samalova, M., Melida, H., Vilaplana, F., Bulone, V., Soanes, D.M., Talbot, N. J. and Gurr, S.J. (2017) The β-1,3-glucanosyltransferases (Gels) affect the structure of the rice blast fungal cell wall during

appressorium-mediated plant infection.: The Gels affect fungal wall structure during infection. *Cell. Microbiol.* **19**, e12659.

Samalova, M., Kirchhelle, C. and Moore, I. (2019) Universal methods for transgene induction using the dexamethasone-inducible transcription activation system pOp6/LhGR in *Arabidopsis* and other plant species. *Curr. Protoc. Plant Biol.*, e20089.

Samalova, M., Carr, P., Bromley, M., Blatzer, M., Moya-Nilges, M., Latge, J.-P. and Mouyna, I. (2020) GPI anchored proteins in *Aspergillus fumigatus* and cell wall morphogenesis. *Curr. Top. Microbiol. Immunol.* **425**, 167-186.

Samalova, M., Elsayad, K., Melnikava, A., Peaucelle, A., Gahurova, E., Gumulec, J., Spyroglou, I., Zemlyanskaya, E.V., Ubogoeva, E.V. and Hejatko, J. (2020) Expansin-controlled cell wall stiffness regulates root growth in *Arabidopsis*. *bioRxiv* 2020.06.25.170969.

Samalova, M., Gahurova, E. and Hejatko, H. (2022) Expansin-mediated developmental and adaptive responses: A matter of cell wall biomechanics? *Quantitative Plant Biology*, **3:e11**, 1-14.

Sampedro, J. and Cosgrove, D. J. (2005) The expansin superfamily. *Genome Biol*ogy, **6**, 242.

Sassi, M. and Trass, J. (2015) When biochemistry meets mechanics: a systems view of growth control in plants. *Curr. Opin. Plant Biol.* **28**, 137-143.

Scarcelli, G., Polacheck, W.J., Nia, H.T., Patel., K., Grodzinsky, A.J., Kamm, R.D. and Yun, S.H. (2015) Noncontact three-dimensional mapping of intracellular hydromechanical properties by Brillouin microscopy. *Nat. Methods*, 1132-1134.

Schurholz, A.K., Lopez-Salmeron, V., Li, Z.N., Forner, J., Wenzl, C., Gaillochet, C., Augustin, S., Barro, A.V., Fuchs, M., Gebert, M., Lohmann, J.U., Greb, T. and Wolf, S. (2018) A comprehensive toolkit for inducible, cell type-specific gene expression in *Arabidopsis*. *Plant Physiol*. **178**, 40-53.

Schwarzlander, M., Fricker, M.D., Muller, C., Marty, L., Brach, T., Novak, J., Sweetlove, L.J., Hell, R. and Meyer, A.J. (2008) Confocal imaging of glutathione redox potential in living plant cells. *J. Microsc*opy, **231**, 299–316.

Sparkes, I. and Brandizzi, F. (2012) Fluorescent protein-based technologies: shedding new light on the plant endomembrane system. *Plant J*. **70**, 96-107.

Taylor, P. R. Roy, S., Leal Jr., S.M., Sun, Y., Howell, S.J., Cobb, B.A., Li, X. and Pearlman, E. (2014) Activation of neutrophils by autocrine IL-17A–IL-17RC interactions during fungal infection is regulated by IL-6, IL-23, RORγt and dectin-2. *Nat. Immunol*. **15**, 143–151.

Teh, O.K. and Moore, I. (2007) An ARF-GEF acting at the Golgi and in selective endocytosis in polarized plant cells. *Nature*, **448**, 493-496.

Torres, M.A. (2010) ROS in biotic interactions. *Physiolog. Planta.* **138**, 414–429.

Turrion-Gomez, J.L. and Benito, E.P. (2011) Flux of nitric oxide between the necrotrophic pathogen *Botrytis cinerea* and the host plant. *Mol. Plant Pathol*. **12**, 606-616.

van de Veerdonk, F.L., Gresnigt, M. S., Romani, L., Netea, M.G. and Latge, J.P. (2017) *Aspergillus fumigatus* morphology and dynamic host interactions. *Nat. Rev. Microbiol.* **15**, 661-674.

Vlad, D., Abu-Jamous, B., Wang, P. and Langdale, J. (2019) A modular steroid-inducible gene expression system for use in rice. *BMC Plant Biol*. **19**, 426.

Wang, X., Wilson, L. and Cosgrove, D. J. (2020) Pectin methylesterase selectively softens the onion epidermal wall yet reduces acid-induced creep. *J. Exp. Bot*. **71**, 2629–2640.

Wang, X., Ye, L., Lyu, M., Ursache, R., Loytynoja, A. and Mahonen, A.P. (2020) Aa inducible genome editing system for plants. *Nat. Plants*, **6**, 766-772.

Wessels, J.G.H. (1996) Hydrophobins: proteins that change the nature of the fungal surface. *Adv. Microb. Physiol.* **38**, 1–45.

Wielopolska, A., Townley, H., Moore, I., Waterhouse, P. and Helliwell, C. (2005) A high-throughput inducible RNAi vector for plants. *Plant Biotechnol. J.* **3**, 583-590.

Wolf, S., Hematy, K. and Hofte, H. (2012) Growth control and cell wall signaling in plants. *Annu. Rev. Plant Biol.* **63**, 381-407.

Woollard, A.D. and Moore, I. (2008) The function of Rab GTPases in plant membrane traffic. *Curr. Opin. Plant Biol.* **11**, 610-619.

Yamasaki, H. and Sakihama, Y. (2000) Simultaneous production of nitric oxide and peroxynitrite by plant nitrate reductase: *in vitro* evidence for the NR-dependent formation of active nitrogen species. *FEBS Lett*. **468**, 89–92.

Zeier, J., Delledonne, M., Mishina, T., Severi, E., Sonoda, M. and Lamb, C. (2004) Genetic elucidation of nitric oxide signaling in incompatible plant-pathogen interactions. *Plant Physiol*. **136**, 2875–2886.

Zhang, T., Tang, H., Vavylonis, D. and Cosgrove, D. J. (2019) Disentangling loosening from softening: insights into primary cell wall structure. *Plant J*. **100**, 1101–1117.

Zhang, Y., Yu, J., Wang, X., Durachko, D.M., Zhang, S. and Cosgrove, D.J. (2021) Molecular insights into the complex mechanics of plant epidermal cell walls. *Science*, **372**, 706-711.

Zheng, H.Q., Camacho, L., Wee, E., Henri, B.A., Legend, J., Leaver, C.J., Malho, R., Hussey, P.J. and Moore I. (2005) A Rab-E GTPase mutant acts downstream of the Rab-D subclass in biosynthetic membrane traffic to the plasma membrane in tobacco leaf epidermis. *Plant Cell*, **17**, 2020–2036.

Zhou, B., Qu, S., Liu, G., Dolan, M., Sakai, H., Lu, G., Bellizzi, M. and Wang, G.L. (2006) The eight amino-acid differences within three leucine-rich repeats between Pi2 and Piz-t resistance proteins determine the resistance specificity to *M. grisea*. *Mol. Plant-Microbe Interact.* **19**, 1216–1228.

Zuo, J., Niu, Q.-W. and Chua, N.-H. (2000) An estrogen receptor-based transactivator XVE mediates highly inducible gene expression in transgenic plants. *Plant J*. **24**, 265-273.

Zweier, J.L., Li, H., Samouilov, A. and Liu, X. (2010) Mechanisms of nitrite reduction to nitric oxide in the heart and vessel wall. *Nitric Oxide Biol. Chem.* **22**, 83–90.

LIST OF FIGURES

LIST OF ATTACHMENTS

[1] Samalova, M., Brzobohaty, B. and Moore, I. (2005) pOp6/LhGR: a stringently regulated and highly responsive dexamethasone-inducible gene expression system for tobacco. *Plant J*. **41**, 919-935. (**IF=6.969**)

[2] Craft, J., Samalova, M., Baroux, C., Townley, H., Martinez, A., Jepson, I., Tsiantis, M. and Moore, (2005) New pOp/LhG4 vectors for stringent glucocorticoid-dependent transgene expression in *Arabidopsis. Plant J.* **41**, 899-918. (**IF=6.969**)

[3] Samalova, M., Kirchhelle, C. and Moore, I. (2019) Universal methods for transgene induction using dexamethasone-inducible transcription activation system pOp6/LhGR in *Arabidopsis* and other plant species. *Curr. Protocols Plant Biol.* **4**, e20089. (**IF=1.029**)

[4] Samalova, M. and Moore, I. (2021) The steroid-inducible pOp6/LhGR gene expression system is fast, sensitive and does not cause plant growth defects in rice (*Oryza sativa*). *BMC Plant Biol*. **21**, 461. (**IF=5.26**)

[5] Samalova, M., Fricker, M. and Moore, I. (2006) Ratiometric fluorescence-imaging assays of plant membrane traffic using polyproteins. *Traffic*, **7**, 1701-1723. (**IF=6.612**)

[6] Pinheiro, H., Samalova, M., Geldner, N., Chory, J., Martinez, A. and Moore, I. (2009) Genetic evidence that the higher plant Rab-D1 and Rab-D2 GTPases exhibit distinct but overlapping interactions in the early secretory pathway. *J. Cell Science*, **122**, 3749-3758. (**IF=6.144**)

[7] Gurr, S., Samalova, M. and Fisher, M. (2011) The rise and rise of emerging infectious fungi challenges food security and ecosystem health. *Fungal Biol. Rev.* **25**, 181-188. (**IF=2.6**)

[8] Samalova, M., Johnson, J., Illes, M., Kelly, S., Fricker, M. and Gurr, S. (2013) Nitric oxide generated by the rice blast fungus *Magnaporthe oryzae* drives plant infection. *New Phytol.*, **197**, 207-222. (**IF=6.545**)

[9] Samalova, M., Meyer, A., Gurr, S. and Fricker, M. (2014) Robust anti-oxidant defences in the rice blast fungus *Magnaporthe oryzae* confer tolerance to the host oxidative burst. *New Phytol.* **201**, 556-573. (**IF=7.672**)

[10] Samalova, M., Melida, H., Vilaplana, F., Bulone, V., Soanes, D.M., Talbot, N. J. and Gurr, S.J. (2017) The β-1,3-glucanosyltransferases (Gels) affect the structure of the rice blast fungal cell wall during appressorium-mediated plant infection.: The Gels affect fungal wall structure during infection. *Cell. Microbiol.* **19**, e12659. (**IF=4.554**)

[11] Samalova, M., Carr, P., Bromley, M., Blatzer, M., Moya-Nilges, M., Latge, J.-P. and Mouyna, I. (2020) GPI anchored proteins in *Aspergillus fumigatus* and cell wall morphogenesis. *Curr. Top. Microbiol. Immunol.* **425**, 167-186. (**IF=4.737**)

[12] Samalova, M., Gahurova, E. and Hejatko, H. (2022) Expansin-mediated developmental and adaptive responses: A matter of cell wall biomechanics? *Quantitative Plant Biology*, **3:e11**, 1-14.

The Plant Journal (2005) **41**, 919–935 doi: 10.1111/j.1365-313X.2005.02341.x

TECHNICAL ADVANCE

pOp6/LhGR: a stringently regulated and highly responsive dexamethasone-inducible gene expression system for tobacco

Marketa Samalova[1,2,3], Bretislav Brzobohaty[3,4] and Ian Moore[1,*]
[1]*Department of Plant Sciences, University of Oxford, South Parks Rd, Oxford OX1 3RB, UK,*
[2]*Department of Plant Physiology and Anatomy, Faculty of Science, Masaryk University, Kotlarska 2, CZ-61265 Brno, Czech Republic,*
[3]*Institute of Biophysics AS CR, Kralovopolska 135, CZ-61265 Brno, Czech Republic, and*
[4]*Department of Functional Genomics and Proteomics, Faculty of Science, Masaryk University, Kotlarska 2, CZ-61265 Brno, Czech Republic*

Received 6 August 2004; revised 1 December 2004; accepted 14 December 2004.
*For correspondence (fax +44 0 1865 275074; e-mail ian.moore@plants.ox.ac.uk).

Summary

We describe pOp/LhGR, a dexamethasone-inducible derivative of the pOp/LhG4 transcription activation system, and its use in tobacco to regulate expression of *uidA* (encoding β-glucuronidase; GUS) and the cytokinin-biosnythetic gene *ipt*. The pOp/LhGR system exhibited stringent regulation and strong induced phenotypes in soil and tissue culture. In conjunction with an improved target promoter, pOp6, that carries six copies of an optimized *lac* operator sequence the pOp6/LhGR system directed induced GUS activities that exceeded those obtained with pOp/LhG4 or the CaMV 35S promoter but without increased uninduced activity. A single dose of dexamethasone was sufficient to direct cytotoxic levels of *ipt* expression in soil-grown plants although uninduced plants grew normally throughout a complete life cycle. *In vitro*, induced transcripts were detectable within an hour of dexamethasone application and 1 nM dexamethasone was sufficient for half maximal induction of GUS activity. Various methods of dexamethasone application were successfully applied under tissue culture and greenhouse conditions. We observed no inhibitory effects of dexamethasone or LhGR on plant development even with the highest concentrations of inducer, although tobacco seedlings were adversely affected by ethanol used as a solvent for dexamethasone stock solutions. The pOp/LhGR system provides a highly sensitive, efficient, and tightly regulated chemically inducible transgene expression system for tobacco plants.

Keywords: chemically inducible gene expression, glucocorticoid, dexamethasone, *ipt*, cytokinin, tobacco.

Introduction

Technologies that offer control over temporal and spatial aspects of transgene expression have several potential applications in basic plant biology research and in biotechnology (Gatz and Lenk, 1998; Padidam, 2003; Zuo and Chua, 2000). In most organisms, including plants, temporal control of transgene expression is commonly achieved through use of an inducible promoter that specifically expresses a transgene in response to an exogenous inducer. Such systems offer the possibility of restricting transgene expression to a particular developmental stage or generation. This is particularly valuable when using transgenes whose constitutive expression is detrimental or even lethal to the host plants. Each of the chemically inducible systems described to date (for reviews see Gatz and Lenk, 1998; Padidam, 2003; Zuo and Chua, 2000) is based on the introduction of a chemically responsive transcriptional activator or repressor that interacts with specific sequences in a target promoter. Many of these inducible systems have been successfully

employed in particular species (Bruce *et al.*, 2000; Chen *et al.*, 2003; Faiss *et al.*, 1997; Laufs *et al.*, 2003; Unger *et al.*, 2002; Zuo *et al.*, 2001), yet it has proved difficult to develop a chemically inducible system that is highly specific, is silent in the absence of inducer, displays strong activation upon induction, and is applicable to several plant species (Andersen *et al.*, 2003; Corlett *et al.*, 1996; Gatz, 1996; Kang *et al.*, 1999; Lloyd *et al.*, 1994; Ouwerkerk *et al.*, 2001; Tang and Newton, 2004; Zuo and Chua, 2000). The latter criterion is likely to become increasingly relevant with the increasing number of species subjected to large-scale sequencing projects (e.g. Andersen *et al.*, 2003; Ouwerkerk *et al.*, 2001) and the growing interest in comparative development and physiology (e.g. Tsiantis and Hay, 2003).

We have previously reported a transcription activation system, pOp/LhG4, that allows a transgene to be expressed following a cross to a specific activator line (Moore *et al.*, 1998). By using activator lines that direct expression either constitutively or in specific tissues, this system has been used to investigate various aspects of development in Arabidopsis, tobacco, and maize (An *et al.*, 2004; Baroux *et al.*, 2001a,b, 2005; Brewer *et al.*, 2004; Emery *et al.*, 2003; Eshed *et al.*, 2001; Gross-Hardt *et al.*, 2002; Hudson *et al.*, 2003; Lenhard and Laux, 2003; Lenhard *et al.*, 2001, 2002; Lexa *et al.*, 2002; Ohno *et al.*, 2004; Schoof *et al.*, 2000; Segal *et al.*, 2003). The pOp/LhG4 system comprises (1) a chimeric promoter pOp that consists of *lac* operators cloned upstream of a minimal CaMV promoter (−50 to +8) and (2) a transcription activator LhG4 which is a fusion between a high-affinity DNA-binding mutant of *lac* repressor, *lacI*^{His17}, and transcription-activation-domain-II of *GAL4* from *Saccharomyces cerevisiae*. The pOp promoter is apparently silent when introduced into reporter lines that lack LhG4 but is activated in specific cells of F_1 plants when reporter lines are crossed with activator lines that express LhG4 from appropriate tissue-specific promoters.

Although the pOp/LhG4 system offers tissue-specific control over transgene expression through use of tissue-specific promoters, it provides minimal temporal control. To increase the versatility of this system we brought the existing pOp/LhG4 system under chemical control by adding the ligand-binding domain (LBD) of the rat glucocorticoid receptor (GR) to LhG4 creating a glucocorticoid-dependent transcription factor LhGR. The activity of many intracellular proteins can be hormonally regulated post-translationally when they are fused to the LBD of steroid receptors (Picard *et al.*, 1988). This approach has been successfully applied to plant transcription factors by exploiting the LBD of glucocorticoid or oestrogen receptors (Aoyama *et al.*, 1995; Lloyd *et al.*, 1994; Sablowski and Meyerowitz, 1998; Simon *et al.*, 1996). Neither GR LBD nor the commonly used inducing ligands such as dexamethasone have any reported detrimental consequences for plant development, although a synthetic transcription factor that incorporates the GR LBD can be detrimental when activated in Arabidopsis (Kang *et al.*, 1999) and other species (Andersen *et al.*, 2003; Ouwerkerk *et al.*, 2001).

The principle of GR-based transcriptional systems is that in the absence of the steroid ligand, a transcription factor is trapped in an inactive complex via interaction between the GR LBD and heat-shock protein HSP90. This complex is believed to interfere with the function of the bound fusion protein by steric hindrance, blocking interactions with other proteins or with DNA target sites (Picard, 1993). The binding of dexamethasone to the LBD mediates dissociation of the fusion protein from HSP90. This model predicts that the effectiveness of the control exerted by GR LBD on a heterologous protein depends on how components of the HSP90 complex are positioned relative to at least one critical functional domain in the heterologous moiety. Domains that either face away from the HSP90 complex or are too distant would not be regulated (Picard, 1993). As hormone-binding domains form the C-terminus of steroid receptors, hormone-binding domains have usually been fused to the C-terminus of heterologous proteins, however the hormone-binding domain works at other positions (Böhner *et al.*, 1999; Braselmann *et al.*, 1993; Bruce *et al.*, 2000; Eilers *et al.*, 1989).

In the accompanying paper we describe the properties of three topologically different fusions between LhG4 and GR LBD in Arabidopsis (Craft *et al.*, 2005). In this report we show that these components can be combined with improved target promoters (Craft *et al.*, 2005) to provide a tightly regulated and efficient transcriptional activation system for tobacco. As reporter genes we used *Escherichia coli uidA*, encoding β-glucuronidase (GUS), and the Ti-plasmid derived *ipt* gene encoding isopentenyltransferase which catalyses an early step in cytokinin synthesis (Heidekamp *et al.*, 1983). The GUS reporter provides a quantitative assay of gene expression while the *ipt* gene, which is active at very low expression levels (Böhner and Gatz, 2001; Gatz and Lenk, 1998), allowed us to determine whether the GR LBD is sufficient for practically complete inhibition of the transcriptional activity of LhGR in the absence of dexamethasone.

Results

To determine the effectiveness of the pOp/LhGR system in tobacco we tested three different fusions between LhG4 and the LBD of a rat GR. These fusions differed in the position of the GR domain relative to the DNA-binding and activation domains of LhG4 (Craft *et al.*, 2005). The GR domain was fused either at the N-terminus (LhGR-N), the C-terminus (LhGR-C) or internally, between the DNA-binding and transcription activation domains (LhGR-I) of LhG4. All constructs were placed under control of the CaMV 35S promoter (Figure 1a).

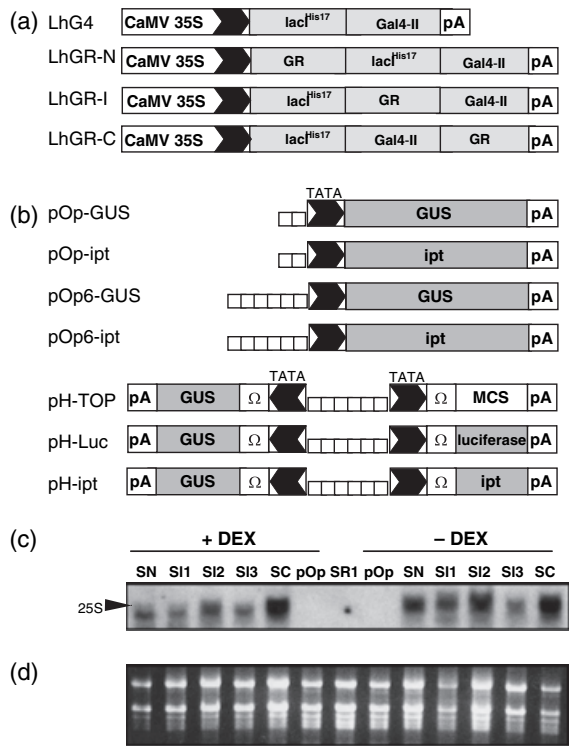

Figure 1. The pOp/LhGR system in tobacco.
Schematic representations of activator (a) and reporter (b) constructs. All activator constructs are expressed from the CaMV 35S promoter. Transcription activator LhG4 comprises a high-affinity DNA-binding *lac* repressor mutant (lacI^{His17}, residues 1–330) and yeast *GAL4* transcription-activation-domain-II (residues 768–881). The steroid-binding domain (residues 508–795) of a rat glucocorticoid receptor (GR) was added in different positions with respect to LhG4 creating N-terminal fusion (LhGR-N), C-terminal fusion (LhGR-C) and internal fusion (LhGR-I) as indicated.
(b) In pOp and pOp6 reporter constructs reporter genes (*GUS*, *ipt*) are expressed under the control of chimeric promoters that consist of either two or six *lac* operators (open boxes) cloned upstream of a minimal CaMV 35S promoter (−50 to +8 relative to the initiation of transcription). pH-TOP reporter construct contains two divergent minimal promoters with a central array of six operators and TMV omega translation enhancers, enabling simultaneous expression of a *GUS* reporter gene as well as a second gene cloned into multiple cloning site (MCS). In pOp6 and pH-TOP the *lac* operator sequences form part of a 52-bp direct repeat.
(c) RNA gel blot analysis of total RNA from pOp-ipt-S/LhGR and control lines. Tissue was taken from seedlings of the T_1 generation grown on MS media with or without 20 μM dexamethasone. The blot was hybridized with a 32P-labelled probe comprising the LhG4 coding sequence.
(d) Photograph of the ethidium bromide-stained RNA gel used in (c).

The pOp/LhGR system induces ipt *phenotypes only in the presence of inducer*

To test the activity of the three LhGR fusions, we used transgenic line pOp-ipt-S which carries the *ipt* gene of *Agrobacterium tumefaciens* under control of the pOp promoter (Lexa *et al.*, 2002). The *ipt* gene encodes isopentenyl transferase which catalyses the first committed step in cytokinin biosynthesis (Åstot *et al.*, 2000; Heidekamp *et al.*, 1983). *ipt* expression results in a range of cytokinin-related phenotypes depending on its expression level (Böhner and Gatz, 2001; Estruch *et al.*, 1991; Faiss *et al.*, 1997; Gan and Amasino, 1995; van Loven *et al.*, 1993; McKenzie *et al.*, 1998; Medford *et al.*, 1989; Schmülling *et al.*, 1989; Smart *et al.*, 1991; Smigocki, 1991) providing a sensitive assay of uninduced 'leaky' expression and an indicator of induced expression efficiencies. To confirm the utility of the pOp-ipt-S line, it was retransformed with the activator construct pBIN-35S-LhG4 which expresses the LhG4 transcription factor (Moore *et al.*, 1998), and 25 of 26 transgenic shoots recovered turned into teratomas unable to form roots (data not shown). In parallel, the three LhGR constructs were transformed into the same reporter line and seedlings of the T_1 generation germinated on kanamycin were screened for dexamethasone-inducible *ipt* expression. After 4 weeks growth on medium containing 20 μM dexamethasone, cytokinin-related phenotypes were observed in five of the 36 pOp-ipt-S/LhGR lines (these were 1 of 14 LhGR-N lines, 3 of 12 LhGR-I lines, and one of 10 LhGR-C lines; these five lines were named S/N, S/I1, S/I2, S/I3, and S/C respectively; Figure 2a, pOp-ipt-S). The morphological alterations in these lines included inhibition of root growth, thickening of the hypocotyl, reduced cotyledon area and formation of shoots in axils of the cotyledons. No such phenotypes were observed in seedlings grown without dexamethasone or in control seedlings (pOp-ipt-S and SR1) with or without dexamethasone (Figure 2a, pOp-ipt-S). Northern analysis performed on seedlings of the five inducible lines (S/N, S/I1, S/I2, S/I3, S/C) showed that LhGR transcripts of the expected size could be detected in all cases (Figure 1c,d).

To monitor the subsequent development of the *ipt* phenotype, six plants from lines S/N, S/I3, and S/C lines were maintained on media with dexamethasone. After a further 2-week growth, the plants on dexamethasone exhibited reductions in stem elongation, leaf expansion, and apical dominance, while root development was arrested (Figure 2b,c,e). After a further 6 weeks growth most of the induced plants developed teratomas at the base of the stem (Figure 2b,d). To establish the ability of each line to develop roots, 6-week-old plants were cut at the base of the stem and transferred onto fresh media (with or without 20 μM dexamethasone). S/N, S/I3, and S/C plants grown on dexamethasone produced no roots even after 12 days whereas the average number of roots on control plants was at least 18.0 ± 5.0 and 27.3 ± 5.6 after 6 and 12 days respectively. When maintained in the absence of dexamethasone, the pOp-ipt-S/LhGR plants were indistinguishable from controls in all of the parameters described above, although one of the three S/C plants produced an axillary shoot at the base of the stem in the absence of inducer (Figure 2b,e and Table S1a).

Several plants of lines S/N, S/I1, S/I2, S/I3, and S/C germinated on dexamethasone-free medium were transferred to soil and their development in the greenhouse was monitored over the entire growth cycle to allow time for the

cumulative effects of any leaky pOp activation to become apparent. Based on a number of morphological and temporal indicators of development, we were unable to identify any significant differences between the development of pOp-ipt-S/LhGR plants (Table S1b). In contrast, cytokinin-related phenotypes were observed in the inducible *ipt* lines

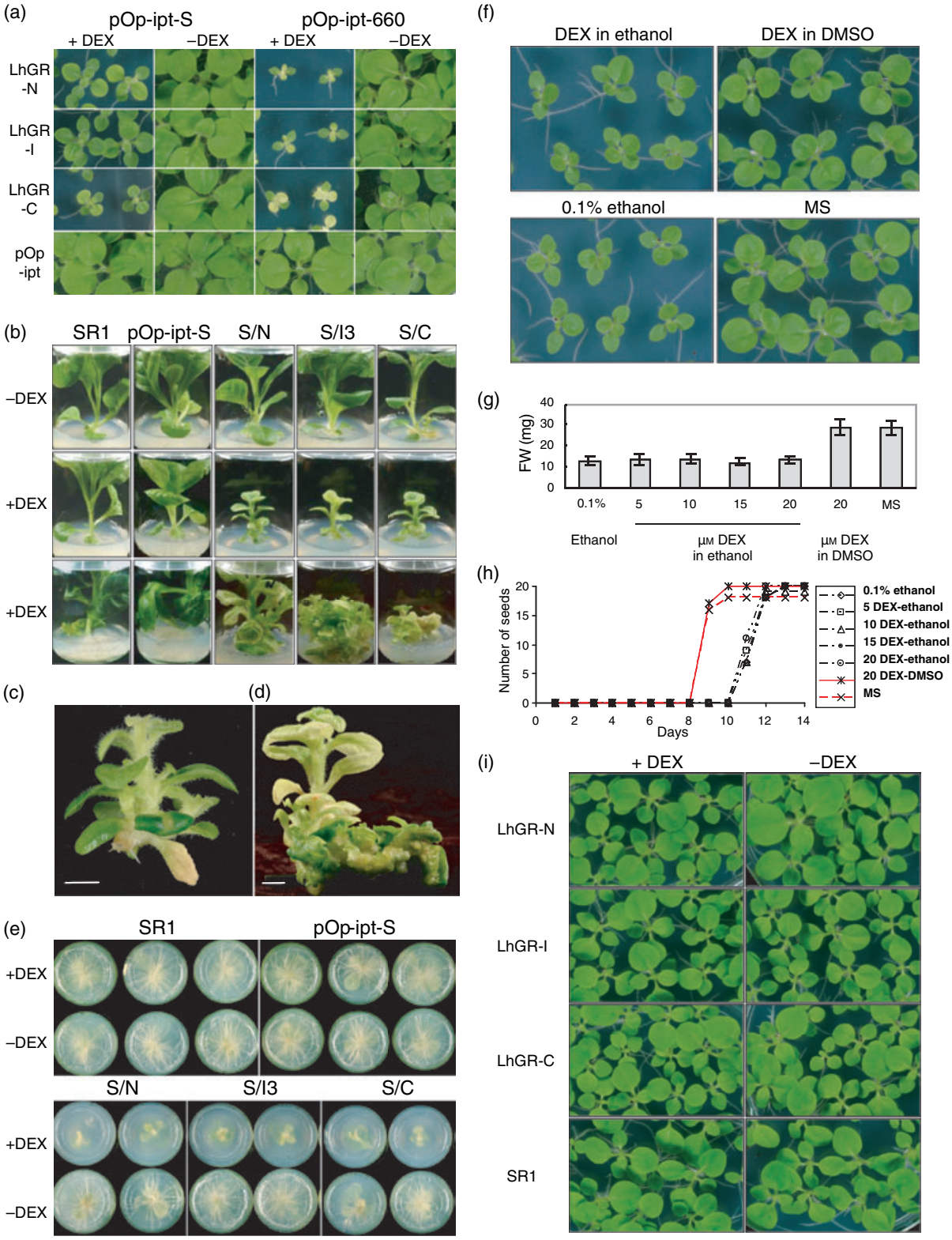

after the application of dexamethasone to soil-grown plants at various stages of development (see below). To confirm these findings, activator lines derived by segregation from S/N, S/I3, and S/C (see Experimental procedures) were crossed with pOp-ipt-660 (Lexa *et al.*, 2002), that elicits stronger induced phenotypes than pOp-ipt-S. As shown in Figure 2(a), induced phenotypes were indeed stronger with pOp-ipt-660, although uninduced seedlings again developed normally. Furthermore, when pOp-ipt-660/LhGR-N plants were allowed to complete a life cycle under growth room conditions no evidence of leaky *ipt* expression was obtained (Table S1c).

We concluded that all three LhGR fusions were capable of activating the pOp promoter in a dexamethasone-dependent fashion in tobacco though the frequency was apparently lower than with LhG4. T_2 families of all five lines exhibited quantitatively and qualitatively similar phenotypes on dexamethasone containing medium indicating that the inducible pOp activation phenotype is inherited and stable over at least three generations.

Effect of different concentrations of dexamethasone

To investigate the dose–response characteristics of the pOp/LhGR system we chose to work with the LhGR-I activator line S/I1 which was generated with the weaker of the two pOp-ipt reporter lines described above. A double homozygous T_2 line, S/I1-1, was identified and used for all subsequent experiments. Seeds were sown on MS media containing 0.625, 1.25, 2.5, 5, 10, 20, 30 μM dexamethasone to which ethanol was added to final concentration of 0.1% and on control medium containing only 0.1% ethanol. Figure 3(a) shows that even 0.625 μM dexamethasone almost completely induced the *ipt* phenotype.

A similar experiment was conducted on soil-grown plants. Three weeks after transfer to soil, plants were watered with 50 ml of either 5, 10, 20, 40, or 60 μM dexamethasone (all with ethanol at 0.2% v/v) or with a control solution containing only ethanol. This treatment was repeated three times per week for 4 weeks and the resulting phenotypes are shown in Figure 3(b). The plants exhibited all the typical signs of cytokinin overproduction in a concentration-dependent manner. Their height was reduced, although the number of leaves on the main stem was not, indicating that the reduced height was attributable to shortening of the internodes. The plants showed early release of axillary buds from dormancy, delayed flowering, and a reduced number of fruits as flower buds fell off at an early stage. The senescence of the plants was delayed but leaves were wrinkled and chlorotic, with necrotic regions developing mainly at the margins, and the root system was reduced greatly (Figure 3c). In subsequent experiments we found that a single dexamethasone treatment was sufficient to induce the full phenotype (see below).

Different methods of dexamethasone application can result in different phenotypes

To determine whether dexamethasone would induce different phenotypes when applied generally or locally, plants of line S/I1-1 were either watered or painted with a 20 μM dexamethasone solution or the dexamethasone solution was applied to the axillary buds only (see Experimental procedures). The treatment was performed three times per week for 4 weeks. Painting leaves with dexamethasone induced the full range of phenotypes observed with soil watering suggesting that application via the roots and leaves resulted in similar levels and distribution of cytokinins (Figure 3d). In contrast, local application of dexamethasone to axillary buds resulted in a higher incidence of release from dormancy but with little influence on the height, flowering time, or fertility of the plants (Figure 3d). Nevertheless, the root system was still reduced and necrotic patches were observed on some leaves (not shown) suggesting that either dexamethasone or cytokinin was transported to other regions of the plant. S/I1-1 plants treated with the control solution were comparable to SR1 plants and displayed no sign of cytokinin overproduction (Figure 3d).

Figure 2. Phenotypes of pOp-ipt/LhGR and control lines grown with or without dexamethasone.
(a) Four-week-old tobacco seedlings of reporter lines pOp-ipt-S and pOp-ipt-660 either re-transformed (pOp-ipt-S) or crossed (pOp-ipt-660) with activator fusions LhGR-N, LhGR-I and LhGR-C grown on media containing 20 μM dexamethasone or 0.1% ethanol. Seedlings from self-pollinated reporters were used as a control.
(b) Six-week (upper and middle row) and 12-week (bottom row) old tobacco plants of wild type (SR1), reporter line pOp-ipt-S and pOp-ipt-S re-transformed with LhGR-N (line S/N), LhGR-I (line S/I3) or LhGR-C (line S/C) activator fusion grown on media with or without 20 μM dexamethasone.
(c) Details of 6- and (d) 12-week-old tobacco plants (line S/N) grown on media containing 20 μM dexamethasone. Bars = 1 cm.
(e) Root system of 6-week-old tobacco plants of wild type (SR1), reporter line pOp-ipt-S (upper rows) and S/N, S/I3 and S/C plants (lower rows) grown on media with or without 20 μM dexamethasone.
(f) The effect of dexamethasone and ethanol on growth and development of wild-type tobacco seedlings. The seedlings were grown on MS media containing 20 μM dexamethasone dissolved either in ethanol or DMSO and control media containing 0.1% ethanol or any supplements.
(g) Fresh weight of wild-type tobacco shoots grown on media containing 0.1% ethanol, different concentrations of dexamethasone (5, 10, 15, 20 μM) to which ethanol was added to a final concentration of 0.1%, media containing 20 μM dexamethasone dissolved in DMSO and MS medium alone. Dexamethasone application has no significant effect on tobacco development ($P < 0.05$).
(h) Germination of wild-type tobacco seedlings on the media described above (in g) was delayed owing to ethanol used as a solvent for dexamethasone.
(i) Four-week-old tobacco seedlings of activator lines LhGR-N, LhGR-I, LhGR-C and a wild-type control (SR1) grown on media containing 20 μM dexamethasone or 0.1% ethanol. Neither LhGR nor dexamethasone had inhibitory effects on seedling development.

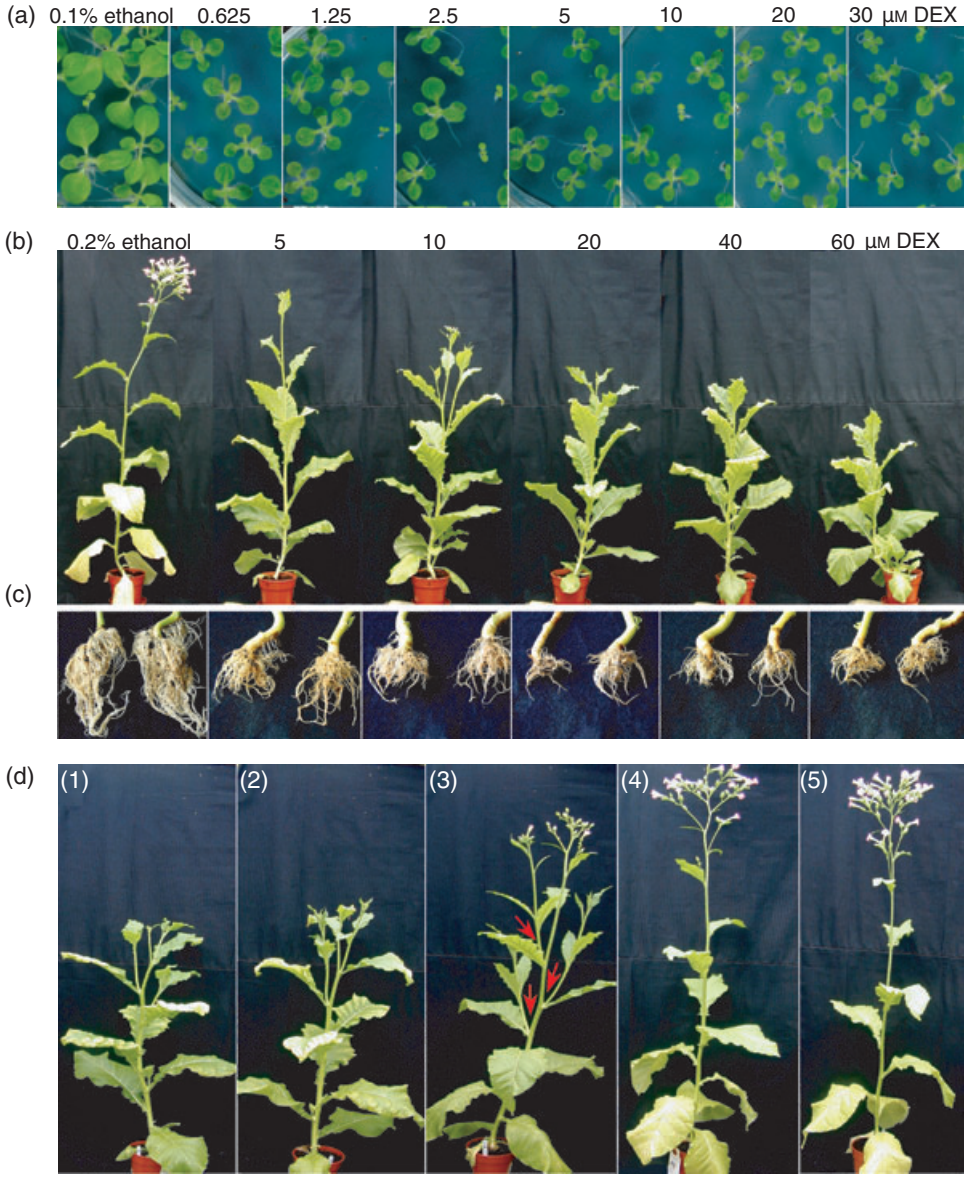

Figure 3. Effect of different dexamethasone concentrations and different methods of dexamethasone treatment.
(a) Seeds of double homozygous line pOp-ipt-S/LhGR-I (S/I1-1) were sown on media containing 0.1% ethanol or dexamethasone at the concentrations indicated to which ethanol was added to final concentration of 0.1%. The plants were grown for 4 weeks *in vitro*.
(b) Tobacco plants pOp-ipt-S/LhGR-I (line S/I1-1) were watered with a control solution without dexamethasone or with 5, 10, 20, 40, 60 μM dexamethasone solution (50 ml) three times per week. Shown are plants and their root system (c) after 4 weeks of treatment.
(d) Tobacco plants pOp-ipt-S/LhGR-I (line S/I1-1) were treated with a dexamethasone-containing solution (20 μM) or a control solution three times per week for 4 weeks. Different methods of dexamethasone treatment were used: (1) watering plants with the solution (50 ml), (2) painting of all leaves with the solution and (3) application of the solution on axillary buds. Local application of dexamethasone resulted in early release of axillary buds, however, had less effect on leaf appearance and plant height. (4) Plant watered with 0.1% ethanol is shown as a control. (5) Wild-type tobacco plant (SR1) watered with 0.1% ethanol.

Testing for inhibitory influences of LhGR, dexamethasone, and ethanol on plant development

The inducing chemical or the chemically responsive transcription factor used in some other inducible expression systems can adversely affect plant function (Andersen *et al.*, 2003; Corlett *et al.*, 1996; Gatz, 1996; Kang *et al.*, 1999; Ouwerkerk *et al.*, 2001). To determine whether dexamethasone itself affects plant development, wild-type tobacco seeds were sown on media containing 5, 10, 15, or 20 μM dexamethasone to which ethanol was added to a final concentration of 0.1%. Control media contained either 0.1% v/v ethanol, 20 μM dexamethasone from a stock dissolved in DMSO (0.1% v/v final concentration), or no

supplements. Seedling development was not influenced by even the highest concentrations of dexamethasone used, however 0.1% ethanol markedly inhibited seedling development (Figure 2f) as exemplified by shoot fresh weight of 2-week-old seedlings (Figure 2g). Monitoring seedling development over the first 2 weeks indicated that much of this reduction could be attributed to an approximately 2-day delay in germination (Figure 2h) followed by further delays in the subsequent rate of seedling development (not shown). To establish whether LhGR inhibits seedling development before or after activation with dexamethasone, untransformed seedlings and LhGR-N, -I, and -C activator lines derived by segregation from the five original pOp-ipt-S/LhGR transformants (see Experimental procedures) were sown on media containing either 20 μM dexamethasone and 0.1% v/v ethanol or ethanol alone. As before no effect of dexamethasone could be seen, although ethanol was again inhibitory and on each medium the LhGR activator lines were indistinguishable from the untransformed controls (Figure 2i).

Improved reporters pOp6 and pH-TOP

The data above show that the LhGR system is capable of inducing the pOp-promoter to generate strong cytokinin-overproduction phenotypes when used to express an *ipt* gene. However, when we tested LhGR-N, -I, or -C with pOp-GUS reporter lines (Moore *et al.*, 1998), we found that induced GUS expression was barely detectable even in the best lines selected from a population of 52 primary transformants. Such low levels of induced activity would severely restrict the useful applications of the pOp/LhGR system, so we attempted to improve the transcriptional efficiency of the system. We have found that the efficiency of the pOp promoter in Arabidopsis can be improved by increasing the number of *lac* operator binding sites from two to six and spacing them to allow simultaneous occupancy by LhG4 or LhGR (Craft *et al.*, 2005). Therefore, we tested the performance of plasmids carrying the improved operator array (Figure 1b) in conjunction with LhGR in tobacco. Plasmid pOp6-GUS was derived from pOp-GUS (Moore *et al.*, 1998) by exchanging the two operators of pOp with the six-operator array. Plasmid pH-TOP carries two divergent minimal promoters flanking the array of six *lac* operators. One of these promoters drives expression of GUS while the other carries multiple cloning sites for insertion of genes of interest. In this way, GUS provides a simple screen for functional T-DNA insertions and for the efficiency of dexamethasone-induced gene expression. To test whether GUS activity also provides a quantitative indicator of the expression efficiency of a gene cloned in the multiple cloning site, we used a pH-TOP derivative, pH-Luc, carrying a luciferase reporter in this site (Craft *et al.*, 2005).

Expression characteristics of pOp6-GUS/LhGR and pH-Luc/LhGR lines

To test the effectiveness of the new reporter constructs we transformed them into the activator lines that were generated by segregation from the original pOp-ipt-S/LhGR lines S/N, S/I3 and S/C described above. The majority of T_0 plants exhibited dexamethasone-inducible GUS expression in

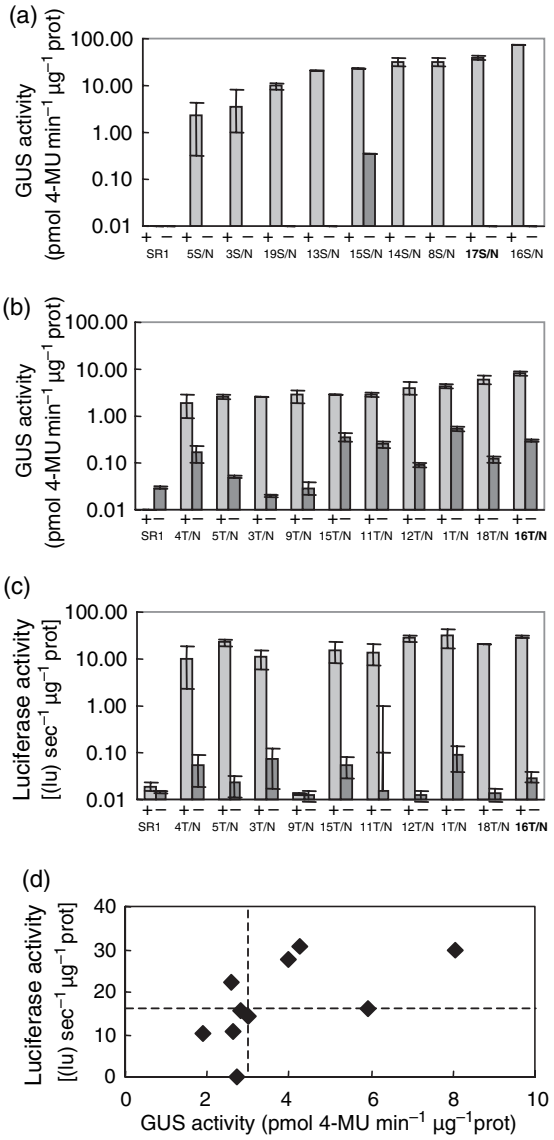

Figure 4. Expression characteristics of pOp6-GUS/LhGR-N and pH-Luc/LhGR-N lines.

(a) GUS activity in seedlings of nine independent pOp6-GUS/LhGR-N lines grown on media containing 20 μM dexamethasone (+) or on control media (−) for 3 weeks. Wild-type tobacco plants (SR1) are included as a negative control.

(b) GUS and (c) luciferase activity in seedlings of 10 independent pH-Luc/LhGR-N lines grown on media containing 20 μM dexamethasone (+) or on control media (−) for 3 weeks. Wild-type tobacco plants (SR1) are included as a negative control.

(d) GUS and luciferase activities in 10 independent pH-Luc/LhGR-N lines. Error bars show standard deviations.

infiltrated leaf tissue, so T_1 seeds from 23 selected pOp6-GUS/LhGR lines and 16 pH-Luc/LhGR lines were grown on selective media with or without 20 μM dexamethasone. Strongly inducible GUS expression was detected by histochemical staining in 38 of these lines. After 3 weeks of growth in Petri dishes, seedlings were assayed histochemically for GUS activity. Extractable GUS activity was determined in seedlings of nine selected pOp6-GUS/LhGR-N lines

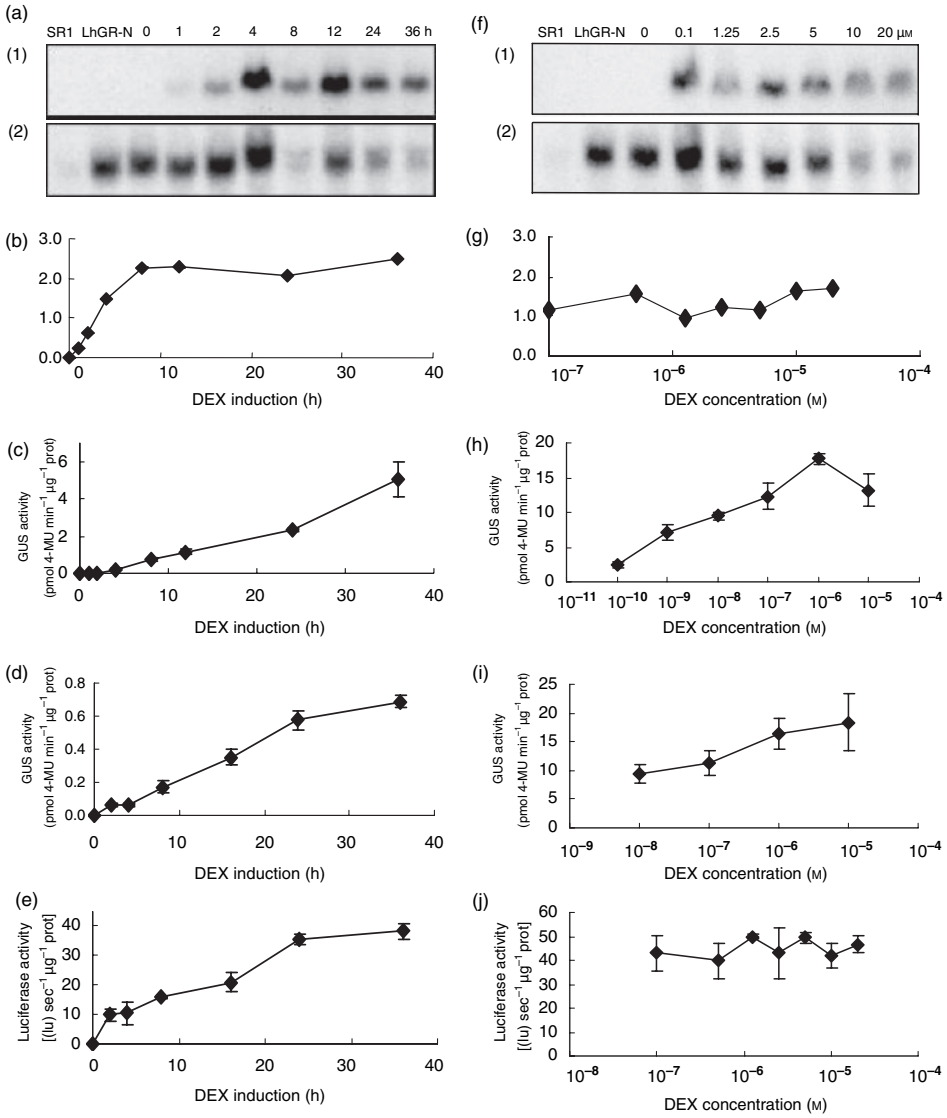

Figure 5. Time course of accumulation of induced GUS and luciferase activities and dose–response characteristics of pOp6-GUS/LhGR-N and pH-Luc/LhGR-N lines.
(a) Three-week-old seedlings pOp6-GUS/LhGR-N (line 17S/N) were induced in liquid medium with 20 μM dexamethasone for 0, 1, 2, 4, 8, 12, 24 and 36 h. Total RNA was blotted and hybridized to a 32P-labelled probe. Sequences used were (1) GUS and (2) actin (as a loading control). GUS transcript levels were normalized to those of the actin control and are plotted in (b).
(c) Seedlings pOp6-GUS/LhGR-N (line 17S/N) were induced in liquid medium with 20 μM dexamethasone for 0, 1, 2, 4, 8, 12, 24 and 36 h. The samples were prepared in CCLR buffer (see Experimental procedures) to allow comparison with pH-Luc/LhGR-N line (d). Seedlings pH-Luc/LhGR-N (line 16T/N) were induced in liquid medium with 20 μM dexamethasone for 0, 2, 4, 8, 16, 24 and 36 h. The samples were prepared in CCLR buffer, so that (d) GUS and (e) luciferase activity could be measured in the same sample.
(f) Three-week-old seedlings pOp6-GUS/LhGR-N (line 17S/N) were induced in liquid medium with dexamethasone at the concentrations indicated for 24 h. Total RNA was blotted and hybridized to a 32P-labelled probe. Sequences used were (1) GUS and (2) actin (as a loading control). GUS transcript levels were normalized to those of the actin control and are plotted in (g).
(h) Seedlings pOp6-GUS/LhGR-N (line 17S/N) were induced in liquid medium with 0.1, 1, 10 nM and 0.1, 1 and 10 μM dexamethasone for 48 h, then GUS activity was determined fluorimetrically.
(i) Seedlings pH-Luc/LhGR-N (line 16T/N) were induced in liquid medium with 0.01, 0.1, 1 and 10 μM dexamethasone for 24 h, then GUS activity was determined fluorimetrically.
(j) Seedlings pH-Luc/LhGR-N (line 16T/N) were induced in liquid medium with 0, 0.1, 0.5, 1.25, 2.5, 5, 10 and 20 μM dexamethasone for 24 h, then luciferase activity was determined.

grown for 3 weeks on inducing or control media and induced activities ranged from 2 to 72 pmol 4-MU min^{-1} μg^{-1} protein (an average of 26 pmol 4-MU min^{-1} μg^{-1} protein; Figure 4a). In many cases, the GUS activity reached or exceeded levels comparable to those obtained with the CaMV 35S promoter (typically 10–30 pmol 4-MU min^{-1} μg^{-1} protein; Moore *et al.*, 1998; Weinmann *et al.*, 1994). The background activity (average 0.006 $\pm$ 0.006 pmol 4-MU min^{-1} μg^{-1} protein) was comparable to the controls (average of 0.009 $\pm$ 0.001 pmol 4-MU min^{-1} μg^{-1} protein) in all cases but one (line 15S/N, 0.34 $\pm$ 0.01 pmol 4-MU min^{-1} μg^{-1} protein). This represents an average 4300-fold induction for the eight most inducible lines.

The GUS activity detected in 10 selected pH-Luc/LhGR-N lines (Figure 4b) was significantly lower than in pOp6-GUS/LhGR-N lines (average of four compared with 26pmol 4-MU min^{-1} μg^{-1} protein) and the average background activity was 10-fold higher than untransformed controls. Consequently, the average induction of GUS activity in the pH-Luc/LhGR-N lines was 20-fold. These seedlings were also used for determining extractable luciferase activity (Figure 4c). The background activity was comparable to control SR1 plants in most cases and the average induction of luciferase activity by dexamethasone in the nine best lines was 500-fold. Surprisingly, plotting induced GUS and luciferase activities for 10 independent pH-Luc/LhGR-N lines (Figure 4d) showed that the correlation was poor. Nevertheless, the best five GUS-expressing lines included four of the five best luciferase expressers.

Time course of dexamethasone-induced gene expression

To establish the rate of pOp6-GUS/LhGR-N activation under optimal conditions seedlings were transferred into liquid medium and induced with 20 μM dexamethasone for various times before being assayed by Northern blot of total RNA. GUS transcripts could not be detected in the absence of dexamethasone but were detectable 1 h after its addition and increased in abundance reaching a steady-state during the subsequent 7 h (Figure 5a,b). When extractable GUS activity was determined, increases were detected 2 h after application of dexamethasone and activity had not reached a steady-state even 34 h later (Figure 5c). In similar experiments with pH-Luc/LhGR-N, both GUS and luciferase activities were induced rapidly after addition of dexamethasone and the proteins accumulated but did not reach their maximum even 36 h after induction (Figure 5d,e).

Dose–response characteristics of dexamethasone-induced gene expression

To establish the dose–response curve for activation of pOp6-GUS/LhGR-N under optimal conditions, dexamethasone was added to seedlings in liquid medium at final concentrations between 0.1 and 20 μM as these concentrations spanned the range of inducing concentrations reported for other dexamethasone-inducible systems. Surprisingly, analysis of total RNA extracted 24 h after induction showed that the lowest concentration tested (0.1 μM) was sufficient to induce GUS transcripts to their maximum abundance (Figure 5f,g). When extractable GUS activity was determined 48 h after application of dexamethasone at concentrations ranging from 0.1 nM to 10 μM maximum activity was reached at about 0.1 μM (Figure 5h and data not shown). Remarkably, 20% of maximum activity was measured even with a dexamethasone concentration of 0.1 nM. Furthermore, the non-induced activity was not significantly different from the control SR1 line alone. Similar experiments with a pH-Luc/LhGR-N line also showed that there was no significant difference in GUS and luciferase activities induced with 0.1 and 10 μM dexamethasone (Figure 5i,j).

Expression characteristics of pOp6-GUS/LhGR plants in soil

We next investigated the induction characteristics of the pOp6-GUS promoter with LhGR-N under greenhouse conditions. Three 8-week-old plants of line 17S/N were watered with 50 ml of 20 μM dexamethasone on two consecutive days and samples were taken from the third oldest leaf at the time of the first dexamethasone treatment and on several subsequent occasions over an 8-week period. Induced GUS activity was detectable within 24 h of induction and peaked after 3 weeks (Figure S1a). Histochemical staining of leaf samples indicated that after 1 week, GUS activity was predominantly confined to the vascular tissues. In contrast, when leaves were painted with a 20 μM solution of dexamethasone, GUS staining was observed in both the vascular tissues and the lamina (data not shown). To determine the distribution of GUS activity throughout the plant following induction via the soil, plants were induced as above and 10 days after the first dexamethasone treatment GUS activity was measured in each leaf. Highest GUS activities were recorded in the fifth oldest leaf with substantially less activity being found in the youngest and oldest leaves (Figure S1b). To establish whether localized induction could be achieved by painting individual leaves with a dexamethasone solution, young growing leaves or older fully expanded leaves were painted on one side of the mid-vein and GUS activity in the painted and non-painted halves was determined 1, 3, and 7 days later. There was apparently a small amount of transport of dexamethasone into the non-painted areas where the appearance of GUS activity paralleled that in the painted areas (Figure S1c,d). When a leaf in the middle of the plant was painted with dexamethasone and GUS activity was measured in this and the two adjacent leaves, there was no induction of GUS activity in the lower leaf over 7 days but there was some

weak induction in the upper leaf in one of the three plants tested (Figure S1e). We conclude that the pOp6/LhGR system functions efficiently in soil-grown plants allowing systemic induction of the promoter in the shoot by application of dexamethasone to the soil and localized induction in individual leaves by leaf painting.

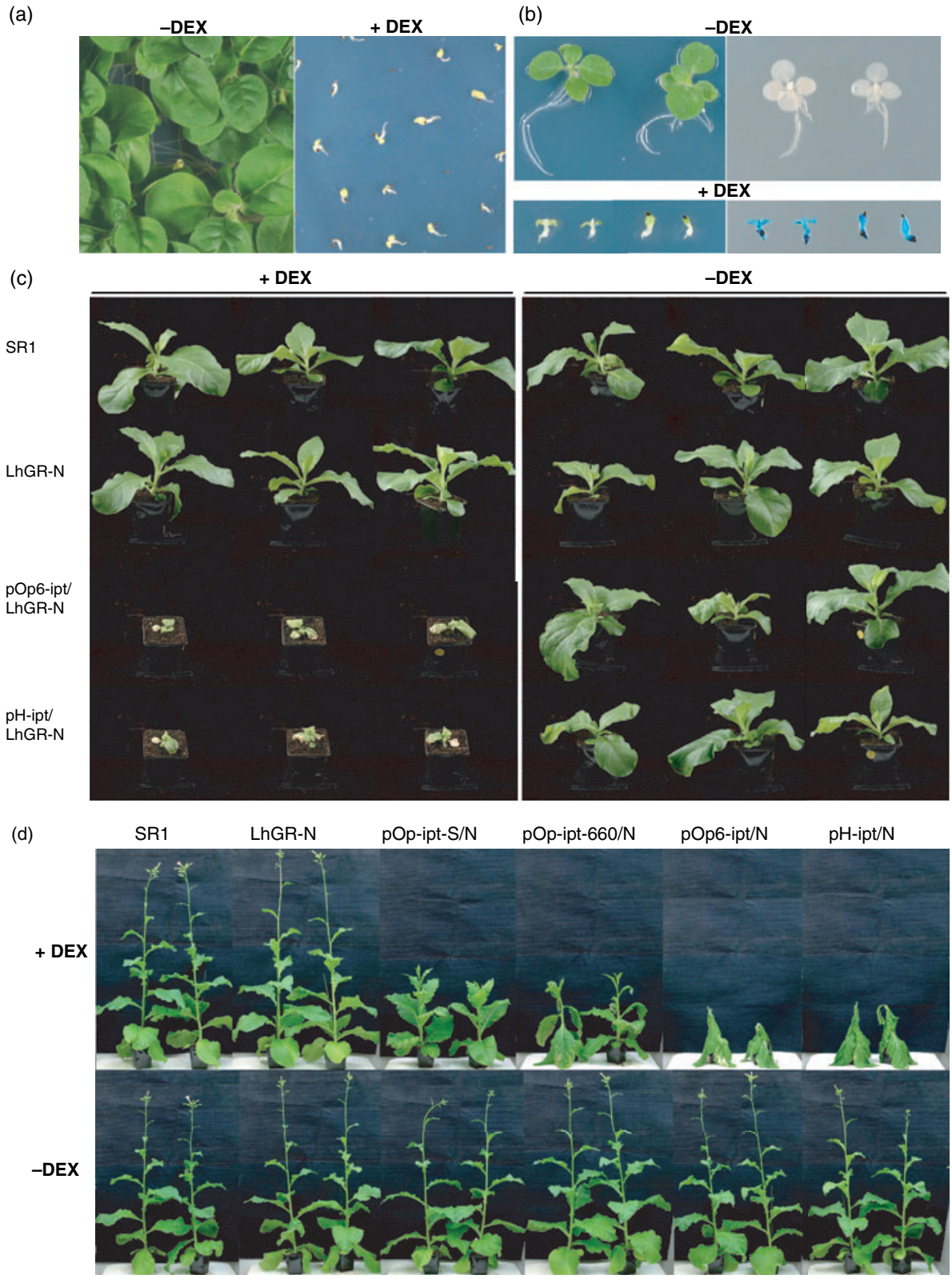

Expression characteristics of pOp6 with the ipt *reporter gene*

The data reported above indicate that the improved promoters in pOp6-GUS and pH-Luc provide high levels of inducible expression using GUS or luciferase reporters. However, we wanted to ensure that this improved efficiency had not been achieved at the expense of increased uninduced expression that might preclude the use of these promoters with deleterious genes. For this reason the *ipt* coding sequence (Heidekamp *et al.*, 1983) used previously with pOp was used to replace GUS in pOp6-GUS and luciferase in pH-Luc to generate pOp6-ipt and pH-ipt. We then asked whether we could recover phenotypically normal plants that exhibited strong inducible *ipt*-related phenotypes. The homozygous activator line LhGR-N was retransformed with pOp6-ipt and pH-ipt. Although some primary transformants failed to root, we recovered six pOp6-ipt/LhGR-N and 23 pH-ipt/LhGR-N lines that formed roots and grew normally after transfer to the greenhouse. T_1 seeds from these 29 lines were plated with and without dexamethasone to screen for induced and uninduced phenotypes.

Five of the six pOp6-ip/LhGR-N lines and all 23 of the pH-ipt/LhGR-N lines exhibited strong inducible phenotypes that were more severe than those observed with pOp-ipt. In most cases seedlings plated on dexamethasone-containing medium failed to develop beyond the cotyledon stage and seedlings of some lines were killed upon induction (Figure 6a,b). Three-week-old plants from representative pOp6-ipt/LhGR-N and pH-ipt/LhGR-N lines were transferred into soil along with control plants and pOp-ipt lines that carried the same LhGR-N activator locus. Either 10 or 21 days later, these plants were induced by watering once with 50 ml of 20 μM dexamethasone. In each case, within 3 days of induction, necrotic lesions were observed on the leaves of pOp6-ipt/LhGR-N and pH-ipt/LhGR-N plants but not on any of the pOp-ipt/LhGR-N or control plants. Photographs taken about 2 weeks after induction reveal that the pOp6-ipt/LhGR-N and pH-ipt/LhGR-N plants had ceased to develop further and, in the case of the older plants, severe wilting had occurred (Figure 6c,d). The pOp-ipt/LhGR-N lines developed typical cytokinin-related phenotypes as reported above but their response was weaker than that of the pOp6-ipt/LhGR-N and pH-ipt/LhGR-N plants. In contrast, we noted no abnormalities in the growth or appearance of uninduced lines either as seedlings on plates or in the growth room in soil. To verify that non-induced pOp6-ipt/LhGR-N and pH-ipt/LhGR-N plants exhibited no measurable alteration in development we measured a number of developmental parameters in 7- and 9-week-old plants (Table S1c). There was no significant difference between the height, leaf number, flowering time, or fruit set of the pOp6-ipt/LhGR-N or pH-ipt/LhGR-N plants and the control plants in this population.

We conclude that the improved promoter can be used to generate plants that exhibit extreme cytokinin-related phenotypes and that any uninduced expression in these plants is so low that it was unable to alter plant development during the entire growth cycle.

Discussion

In the last decade several chemically inducible gene expression systems have been reported for plants (reviewed in Gatz and Lenk, 1998; Padidam, 2003; Zuo and Chua, 2000). The utility of any such system is determined in the main by its uninduced expression levels and its fold induction. The ideal system will deliver undetectable expression in the uninduced state but induced levels should be comparable to strong constitutive promoters such as CaMV 35S. In practice this requires the dynamic range to be 1000-fold or higher (Böhner *et al.*, 1999; Padidam *et al.*, 2003; Roslan *et al.*, 2001; Zuo *et al.*, 2000). It is also important that the inducing chemical can be applied systemically and that the concentrations required for full induction are substantially lower than those that interfere with plant physiology or development. Furthermore, the chemically responsive transcription factor should not cause any undesirable effects in the induced or uninduced state and the system should operate in several plant species including the common experimental species Arabidopsis and tobacco. Each of the systems reported to date satisfies several of these criteria but only one system appears to satisfy all (Padidam *et al.*, 2003), although the system has yet to be tested with a physiologically active transgene. This paper together with an accompanying report (Craft *et al.*, 2005) describes a new system, derived from the previously published pOp/LhG4 system (Moore *et al.*, 1998) that satisfies the criteria outlined above. In combination with improved pOp promoters this modified transcription factor, LhGR, facilitates highly inducible and tightly regulated transgene expression in tobacco in response to nanomolar concentrations of dexamethasone. The system has been

Figure 6. Phenotypes of various *ipt* lines after treatment with dexamethasone.
(a) Four-week-old tobacco seedlings pOp6-ipt/LhGR-N (line 303/N) grown on hygromycin-containing media with either 0.1% ethanol or 20 μM dexamethasone.
(b) Three-week old tobacco seedlings pH-ipt/LhGR-N (line 171/N) grown on hygromycin-containing media with either 0.1% ethanol or 20 μM dexamethasone. Seedlings grown similarly but histochemically stained for GUS activity. The reaction was stopped after 4 h of incubation with the substrate.
(c) Wild type (SR1), LhGR-N, pOp6-ipt/LhGR-N (line 303/N), and pH-ipt/LhGR-N (line 171/N) plants after 12 days of treatment with 50 ml of 20 μM dexamethasone solution (left) or with 0.1% ethanol (right). The plants were induced at an early stage of development (after 3 weeks of growth in tissue culture and 10 days in soil).
(d) Wild type (SR1), LhGR-N, pOp-ipt-S/LhGR-N (line S/N), pOp-ipt-660/LhGR-N (line 660/N), pOp6-ipt/LhGR-N (line 303/N), and pH-ipt/LhGR-N (line 171/N) plants after 4 weeks of treatment with 50 ml of 20 μM dexamethasone solution (upper row) or 0.1% ethanol (lower row). Plants were induced at a later stage of development than in (c) (after 3 weeks of growth in tissue culture and 3 weeks in soil).

tested with the reporters GUS and luciferase as well as the physiologically active *ipt* sequence from *A. tumefaciens* (Heidekamp *et al.*, 1983).

In the native GR, the LBD is situated at the caroboxy terminus of the protein, but we found that it worked effectively at all three positions in LhG4. This contrasted with our experience of the identical constructs in Arabidopsis where LhGR-N provided the best expression characteristics while LhGR-I proved ineffective and LhGR-C was leaky (Craft *et al.*, 2005). Work is underway to investigate why these constructs behave differently in these two species. LhGR-N proved to be stringently repressed and highly inducible in both species.

When *ipt* was introduced into an LhGR-N activator line under control of the improved promoters, we found that in most cases induced *ipt* expression was so high that seedlings failed even to expand their cotyledons and eventually died. Plants treated with dexamethasone via the soil developed necrotic lesions and severely wilted within a week of treatment and also eventually died. Despite the severity of the induced *ipt* phenotypes we did not observe or measure any difference between the development or appearance of uninduced plants and controls. The *ipt* gene has been chosen for this type of analysis in part because plants are sensitive to low levels of expression that can be difficult to measure with conventional reporters such as GUS (Schmülling, 2002). This gene has been effectively regulated by the GVG and pOp/LhGR systems in Arabidopsis (Åstot *et al.*, 2000; Craft *et al.*, 2005) and by GVG in tobacco and lettuce (Kunkel *et al.*, 1999) but has been used most extensively in tobacco in conjunction with inducible systems based on the *Tn*10-encoded tetracycline repressor (Gatz *et al.*, 1992). The tetracycline-derepression system reported by Faiss *et al.* (1997) generated weaker phenotypes than those reported here, yet even the uninduced plants exhibited marked stunting indicating that the system was leaky (Böhner and Gatz, 2001). This problem was overcome by adding the GR domain and a transcriptional activation domain to the *tet*-repressor to generate a dexamethasone-inducible factor (Böhner *et al.*, 1999). However in this system the *ipt* phenotypes induced by application of dexamethasone were even weaker than those obtained with the leaky tetracycline-derepression system (Böhner and Gatz, 2001). In comparison, the LhGR system appears to offer advantages: the original pOp promoter delivers phenotypes that appear to be of similar severity to those reported with the *tet*-repressor-based systems while the newer promoters exceed these levels, yet neither produces detectable uninduced activity in conjunction with the *ipt* sequence.

The XVE system has been characterized principally by Northern blot and assays based on expression of GFP or Cre recombinase (Guo *et al.*, 2003; Zuo *et al.*, 2000, 2001). The ethanol system has been used to direct expression of reporter proteins, yeast cytosolic invertase, UNUSUAL FLORAL ORGANS, RNAi, and tissue-specific gene induction during plant development in tobacco or Arabidopsis (Caddick *et al.*, 1998; Chen *et al.*, 2003; Deveaux *et al.*, 2003; Laufs *et al.*, 2003; Roslan *et al.*, 2001; Salter *et al.*, 1998). Although highly inducible in soil, it exhibits significant uninduced activity in tissues or seedlings growing on agar medium owing perhaps to the accumulation of endogenous alcohols in such conditions (Roslan *et al.*, 2001; Salter *et al.*, 1998).

When dexamethasone was applied via the growth medium to plants in sterile culture or in soil, GUS activities reached 70 pmol 4-MU min^{-1} μg^{-1} protein. The average induced GUS activity measured in the population of plants generated with pOp6-GUS/LhGR-N was 26 pmol 4-MU min^{-1} μg^{-1} protein while the average uninduced activity was 0.006 pmol 4-MU min^{-1} μg^{-1} protein. This corresponds to an average fold induction of 4300 and compares favourably with the average fold induction of other inducible systems (Böhner *et al.*, 1999; Padidam *et al.*, 2003; Roslan *et al.*, 2001; Zuo *et al.*, 2000). In some reports the fold inductions measured for individual plants were reported to exceed these values (up to 63 000-fold in one case; Böhner and Gatz, 2001). Similarly, individual plants within our population also appeared to exhibit substantially more than 4300-fold induction (up to 12 000-fold). However, such estimates are of questionable significance as they are highly sensitive to the estimate of uninduced activity and this is very difficult to make for a non-leaky system. Of more significance is the demonstration that the average induced activity in the pOp6/LhGR-N plants exceeds that previously reported for the pOp/LhG4 system in tobacco (Moore *et al.*, 1998) and is similar to that reported for 35S-GUS (Moore *et al.*, 1998; Weinmann *et al.*, 1994). These high levels of induced GUS expression are consistent with the extreme severity of the *ipt* phenotypes we observed. The best lines exceeded the 35S-GUS levels several fold. In this respect the LhGR system is similar to the ecdysone-receptor-based systems (Martinez *et al.*, 1999; Padidam *et al.*, 2003). The XVE oestrogen-based system was also reported to direct expression levels that exceed those of CaMV 35S but this observation is difficult to compare with other studies because the XVE protein was expressed from the synthetic G10-90 promoter that is itself several fold more active than the CaMV 35S promoter (Zuo *et al.*, 2000).

The kinetics of transcript accumulation in the pOp6/LhGR-N system are similar to those reported for other systems (Aoyama and Chua, 1997; Böhner *et al.*, 1999; Roslan *et al.*, 2001; Salter *et al.*, 1998; Zuo *et al.*, 2000). It is also potentially of value to be able to modulate gene expression by varying the dose of inducer and this requires a shallow dose–response curve. In the pOp6/LhGR-N system we found that induced GUS activity in seedlings reached its maximum with 0.1 μM dexamethasone and was induced to 50% by 1 nM dexamethasone. The pOp6/LhGR-N system in tobacco responds more sensitively than the dexamethasone-inducible GVG system which requires 10 μM for full induction in

tobacco seedlings and 3 μM for induction to 50% (Aoyama and Chua, 1997). In fact, pOp6/LhGR-N in tobacco exhibits the most sensitive induction kinetics of any published system.

In agreement with other workers (Aoyama and Chua, 1997; Böhner *et al.*, 1999), we found that seedlings developed normally at up to 30 μM dexamethasone which is 300-fold higher than the concentration required to saturate the response with pOp6/LhGR-N. Tobacco seedling development was sensitive to ethanol used to dissolve dexamethasone, so the use of alternative solvents or water-soluble dexamethasone formulations is advisable. Significantly, the concentration of ethanol that was sufficient to impair seedling development *in vitro* (0.1% v/v) was similar to that reported to be necessary for full induction of the AlcR-based ethanol-inducible system in seedlings (Salter *et al.*, 1998). We did not observe any alterations in the development or appearance of tobacco plants carrying the LhGR fusions either with or without induction suggesting that, like LhG4, LhGR is not intrinsically inhibitory. This is also the case with the dexamethasone-inducible GVG and TGV systems in tobacco, although the GVG system induces growth abnormalities following induction by dexamethasone in Arabidopsis (Kang *et al.*, 1999) and other species (Andersen *et al.*, 2003; Ouwerkerk *et al.*, 2001).

Dexamethasone can be applied to plant tissues at many stages using a variety of application procedures. We found that seedlings germinated on or transferred onto dexamethasone containing medium *in vitro* exhibited activation of pOp6/LhGR throughout the seedling, although transpiration is likely to be minimal under these conditions. Dexamethasone delivered through the roots in older plants in soil resulted in activation of pOp6/LhGR throughout the plant but principally in the vascular tissues whereas painting with dexamethasone solution resulted in induction throughout the leaf. Transport of dexamethasone from leaf to leaf is minimal allowing localized induction of individual leaves. In this respect dexamethasone is perhaps more versatile than ethanol, which is volatile and efficiently transported even between plants (Roslan *et al.*, 2001). Indeed with pOp-ipt/LhGR we found that localized application of dexamethasone to leaf axils produced a different growth phenotype than widespread application via the soil or leaf painting. Similar observations have been made with the TGV system and with tetracycline (Böhner and Gatz, 2001; Faiss *et al.*, 1997). The distribution of induced expression in tissues of soil-grown plants carrying the recent ecdysone-receptor-based system (Padidam *et al.*, 2003) has not been reported but foliar application is apparently inefficient for this and another ecdysone-receptor-based system (Padidam, 2003). Finally there is no evidence of endogenous ligands for GR in plants which makes GR-based systems more attractive and versatile than ethanol and oestrogen-based systems for which endogenous ligands can exist in certain species or growth conditions (Salter *et al.*, 1998; Zuo and Chua, 2000).

The strategy of using an increased number of operators when designing inducible systems has been successfully used several times (Aoyama and Chua, 1997; Böhner *et al.*, 1999; Martinez *et al.*, 1999; Padidam *et al.*, 2003; Weinmann *et al.*, 1994; Zuo *et al.*, 2000). Although the pOp promoter was suitable for inducing cytokinin-related phenotypes in tobacco, LhGR directed very little dexamethasone-inducible GUS expression from pOp-GUS lines that were competent to respond efficiently to LhG4 (data not shown). The high sensitivity of the pOp6 promoter to LhGR-N may account for its efficient induction using a variety of dexamethasone application procedures with seedlings and mature plants. The proximity of the regulatory GR domain to the DNA-binding helices of LhGR may contribute to the efficient repression of transcriptional activity in the absence of inducer, providing tight regulation of even the pOp6 promoter in conjunction with the *ipt* reporter.

In an attempt to provide an easily scored marker of functional T-DNA integrations and of induction efficiency, we tested pH-TOP which drives transcription of a GUS reporter and a second gene-of-interest from the same pOp6 operator array (Craft *et al.*, 2005). Transcription from minimal promoters flanking an enhancer element are correlated in individual transformants, although absolute expression levels can vary substantially between individuals (Ott *et al.*, 1990). Surprisingly we found that GUS and luciferase activities driven from the same operator array in pH-Luc/LhGR-N transformants were poorly correlated. We have made similar observations with pH-TOP derivatives in Arabidopsis (Craft *et al.*, 2005). This suggests that the principal determinants of position-dependent expression efficiency in pOp6 reporter constructs probably lie in regions outside the *lac* operator array. Modifying the minimal promoter sequence or length can significantly alter the efficiency of inducible gene expression (Martinez *et al.*, 1999; Weinmann *et al.*, 1994), so the two minimal promoters might be a source of variability in expression level between genes cloned in the pH-TOP vector. Alternatively, sequence-specific PTGS thresholds may independently affect the relative levels of each marker as described recently for Arabidopsis (Schubert *et al.*, 2004). Nevertheless, pH-TOP may still be of some practical value because pre-screening pH-TOP transformants for high inducible GUS activities is likely to identify most of the lines that exhibit efficient inducible expression of the gene-of-interest. Furthermore, pH-TOP-driven expression in tobacco is mitotically stable, so it can be used to monitor the efficiency with which the reporter locus has been activated in any particular experiment.

In conclusion, we show that the pOp6/LhGR system provides a highly sensitive, efficient, and tightly regulated chemically inducible transgene expression system for tobacco. We have made similar observations with these constructs in Arabidopsis suggesting that this system

might be applicable to a variety of plant species. Furthermore, the system described here is compatible with the previously reported LhG4 system for which a large number of tissue-specific activator constructs are available. Genes of interest introduced into tobacco under control of the pOp6 promoter could thus be activated in precise temporal or spatial domains after crossing with the appropriate LhGR or LhG4 activator line.

Experimental procedures

Construct preparation

Standard procedures were used for DNA cloning and analysis (Ausubel *et al.*, 1993). Kanamycin-resistant pBINPLUS (van Engelen *et al.*, 1995) and pGreen (Hellens *et al.*, 2000) and hygromycin-resistant pVKH18 (a derivative of pOp-GUS in which the pOp-GUS cassette was replaced by a polylinker; Moore *et al.*, 1998) binary vectors for *Agrobacterium*-mediated plant transformation were used. pBIN-LhGR-N, -I, -C and pBIN-LhG4 have been described (Craft *et al.*, 2005). The DNA sequence encoding the *ipt* gene was amplified from a cloned sequence kindly provided by Dr Csaba Koncz, Max-Planck-Institut fuer Zuechtungsforschung, Cologne, Germany, using forward 5′-AAAAAAGTCGACATGGACCTG-CATCTAATTTTCGGTCCAAC-3′ and reverse 5′-AAAAACCCGGGC-TAATACATTCCGAACGGATGACCTTCGAATC-3′ primers and cloned as an *Sal*I/*Sma*I fragment into multiple cloning site of pU-BOP (see below) downstream of a modified pOp promoter. An *Sac*I/*Hin*dIII fragment containing the two *lac* operators, the minimal CaMV 35S promoter, *ipt* coding sequence and polyadenylation signal was isolated from this clone and inserted into pVKH18 vector to generate pOp^{BK}-ipt. Second, a fragment containing the pOp6 promoter (Craft *et al.*, 2005) was isolated as an *Sac*I/*Sal*I fragment and cloned into the *Sac*I and *Sal*I sites of pOp^{BK}-ipt thereby replacing the pOp promoter with pOp6. pH-ipt was prepared by cloning the DNA sequence encoding the *ipt* coding sequence as a *Sal*I/*Sma*I fragment into the *Sal*I and *Sma*I sites of pH-TOP (Craft *et al.*, 2005).

Construction of pU-BOP pOp^{BK} a modified pOp promoter from which several restriction sites had been removed (Baroux *et al.*, 2005), was isolated from pOp^{BK}-GUS as an *Ecl*136II- *Hin*dIII fragment and inserted into the corresponding sites of pBluescript SKII (Stratagene, La Jolla, CA, USA). The *Hin*dIII site was digested and converted to an *Nhe*I site by treatment with Klenow fragment of DNA polymerase I and religation. An *Ecl*136II*Kpn*I fragment was then isolated and inserted into the corresponding sites of the pK18 polylinker followed by the polyA signal from pRT101 (Töpfer *et al.*, 1987) isolated and inserted using *Bam*HI and *Hin*dIII to generate pK-BOP. pU-BOP was constructed by transferring the pOp^{BK}-polylinker-polyA cassette from pK-BOP into pUC19 using *Ecl*136II and *Hin*dIII.

Plant transformation and maintenance

The reporter lines pOp-ipt-S and pOp-ipt-660 were generated in *Nicotiana tabacum* cv. SR1 Petit Havana as described previously (Lexa *et al.*, 2002). The binary vectors were transformed into *A. tumefaciens* strain GV3101::pMP90 (Koncz and Schell, 1986). Leaf disc transformation of activator lines and reporter lines was used to generate primary transformants that were selected either on kanamycin or hygromycin at 50 and 20 $\mu g\ ml^{-1}$ respectively. In tissue culture, plants were grown on MS medium (Murashige and Skoog, 1962) supplemented with 3% (w/v) sucrose and 0.8% agar. Plants were grown with 16 h light/8 h dark at a daytime temperature of 25°C.

Selection of activator lines LhGR-N, -I and -C

LhGR-N, -I and -C activator lines were selected from T_1 populations of lines S/N, S/I3 and S/C generated with the weak reporter line pOp-ipt-S. These lines were heterozygous for the pOp-ipt T-DNA at a single Mendelian locus. Segregating T_1 progeny were selected on kanamycin (to select for LhGR) and 20 μM dexamethasone. Plants that exhibited no cytokinin-related phenotypes were transferred to the greenhouse and their pollen was used for pollination of reporter line pOp-ipt-660. The activator plants were also used for re-transformation with pOp6-GUS, pOp6-ipt and pH-Luc, and pH-ipt all of which encode hygromycin resistance in tobacco.

Methods of dexamethasone application

Dexamethasone (Sigma, Dorset, UK) was dissolved in ethanol and kept as 20 mM stock at −20°C. Unless otherwise stated 20 μM dexamethasone was used. Dexamethasone was added to MS media to achieve induction during seed germination or after seedling transfer in sterile conditions. Induction in liquid media was performed in conical flasks (250 ml) containing 100 ml MS media. Typically 2–3-week-old seedlings (20–40 individuals) were transferred into the flasks and kept on an orbital shaker (approximately 80 rpm) in a plant growth chamber. Two days later dexamethasone at the appropriate concentration was added. The seedlings were harvested after the required period, blotted dry, and freezed in liquid nitrogen. Tobacco plants grown in soil were watered with 50 ml of a solution containing dexamethasone. The treatment was performed either once or repeatedly as stated; in the meantime the plants were watered as required without any supplements. Tobacco leaves were painted using a paintbrush with a dexamethasone solution containing 0.02% Silwet L-77. Approximately 5–10 ml of the solution was used for a single treatment of all leaves, depending on the size of the plant. Approximately 1 ml was used for a single treatment of a single leaf. Approximately 0.5 ml of the solution was applied to the leaf axils temporarily covered with parafilm to prevent the solution from running down the stem.

Analysis of β-glucuronidase and luciferase reporter activity

Histochemical GUS staining and fluorometric GUS assay was performed according to Jefferson (1987). Extraction of luciferase and assays for relative light units (lu) were performed as described by Luehrsen and Walbot (1993). We found that CCLR extraction buffer used in this assay inhibited GUS activity by five- to 15-fold, so separate extracts were made according to Jefferson (1987) for comparison with GUS activities in other samples. The protein content of all extracts was determined spectrophotometrically using Bio-Rad Protein Assay Reagent (Bio-Rad laboratories, Hemel Hempsted, UK).

RNA gel blot analysis

Total RNA was extracted from plant tissue, dissolved in formamide, and 10 μg of each RNA sample was electrophoresed, blotted onto Hybond N^+ membranes (Amersham, Cardiff, UK), hybridized with

^{32}P-labelled probes, and analysed by autoradiography using Kodak X-AR film (Rochester, NY, USA), all as described in Moore *et al.* (1997). To detect the LhGR transcripts, the LhG4 sequence was isolated from pLhG4 (Moore *et al.*, 1998) as an *Xba*I fragment. To detect the GUS transcript, the sequence was isolated from pRT103GUS (Töpfer *et al.*, 1987) as an *Xho*I/*Ssp*I fragment. The film was developed using an AGFA Curix 60 X-ray film developer (AGFA, Herts., UK). In some cases the hybridizing radioactivity was quantified using a Bio-Rad Molecular Imager FX and Bio-Rad Multi-Analyst^{TM}/PC Version 1.1 software. Hybridized probes were removed from filters by subjecting them to three washes with boiling strip solution (0.1 × SSC, 0.1% w/v SDS) and were hybridized with a sequence encoding a 571-bp fragment of a tobacco actin gene that had been amplified from genomic DNA using primers Nt-Act-3′a (5′-ATCCAGACACTRTACTTYCTCTC-3′) and Nt-Act-3′b (5′-TCCARACRCTGTAYTTCCTCTC-3′).

Acknowledgements

We are indebted to Prof. Peter Meyer, University of Leeds, for use of plant cultivation facilities during part of this work and to Rudolf Kalab for financial support. We are grateful to Csaba Koncz and Debora Grosskopf for providing the cloned *ipt* sequence, to Andrew Millar for providing the pLuc plasmid, to Helen Townley, Judith Craft, and Hazel Betts for the pOp6 promoter and pH-TOP. We thank John Baker for the photographic work. This work was supported by a Royal Society Joint Project Grant to IM and BB; by GA AS CR Grant No. IAA5004001; Ministry of Education of the Czech Republic Grant No. MSM143100008; AS CR Grant No. KSK5052113 to BB; and a Marie Curie PhD fellowship to MS.

Supplementary Material

The following material is available from http://www.blackwellpublishing.com/products/journals/suppmat/TPJ/TPJ2341/TPJ2341sm.htm

Figure S1. Induction characteristics of pOp6-GUS/LhGR-N plants in soil.

Table S1 Growth characteristics of various *ipt*-containing lines in the absence of dexamethasone.

References

An, H., Roussot, C., Suarez-Lopez, P. *et al.* (2004) CONSTANS acts in the phloem to regulate a systemic signal that induces photoperiodic flowering in Arabidopsis. *Development*, **131**, 3615–3626.

Andersen, S.U., Cvitanich, C., Hougaard, B.K., Roussis, A., Gronlund, M., Jensen, D.B., Frokjaer, L.A. and Jensen, E.O. (2003) The glucocorticoid-inducible GVG system causes severe growth defects in both root and shoot of the model legume *Lotus japonicus*. *Mol. Plant Microbe Interact.* **16**, 1069–1076.

Aoyama, T. and Chua, N.-H. (1997) A glucocorticoid-mediated transcriptional induction system in transgenic plants. *Plant J.* **11**, 605–612.

Aoyama, T., Dong, C.H., Wu, Y., Carabelli, M., Sessa, G., Ruberti, I., Morelli, G. and Chua, N.-H. (1995) Ectopic expression of the Arabidopsis transcriptional activator *At*HB-1 alters leaf cell fate in tobacco. *Plant Cell*, **7**, 1773–1785.

Åstot, C., Dolezal, K., Nordstrom, A., Wang, Q., Kunkel, T., Moritz, T., Chua, N. and Sandberg, G. (2000) An alternative cytokinin biosynthesis pathway. *Proc. Natl Acad. Sci. USA*, **97**, 14778–14783.

Ausubel, F.M., Brent, R., Kingston, R.E., Moore, D.D., Seidman, J.G., Smith, J.A. and Struhl, K. (eds) (1993) *Current Protocols in Molecular Biology*. New York: Wiley.

Baroux, C., Blanvillain, R. and Gallois, P. (2001a) Paternally inherited transgenes are down-regulated but retain low activity during early embryogenesis in Arabidopsis. *FEBS Lett.* **509**, 11–16.

Baroux, C., Blanvillain, R., Moore, I.R. and Gallois, P. (2001b) Transactivation of *BARNASE* under the *AtLTP1* promoter affects the basal pole of the embryo and shoot development of the adult plant in Arabidopsis. *Plant J.* **28**, 503–515.

Baroux, C., Blanvillain, R., Betts, H., Batoko, H., Craft, C., Martinez, A., Gallois, P. and Moore, I. (2005) Predictable activation of tissue-specific expression from a single transgene locus using the pOp/LhG4 transactivation system in Arabidopsis. *Plant Biotech. J.* **3**, 91–101.

Böhner, S. and Gatz, C. (2001) Characterization of novel target promoters for the dexamethasone-inducible/tetracycline-repressible regulator TGV using luciferase and isopentenyl transferase as sensitive reporter genes. *Mol. Gen. Genet.* **264**, 860–870.

Böhner, S., Lenk, I., Rieping, M., Herold, M. and Gatz, C. (1999) Transcriptional activator TGV mediates dexamethasone-inducible and tetracycline-inactivable gene expression. *Plant J.* **19**, 87–95.

Braselmann, S., Graninger, P. and Busslinger, M. (1993) A selective transcriptional induction system for mammalian cells based on Gal4-estrogen receptor fusion proteins. *Proc. Natl Acad. Sci. USA*, **90**, 1657–1661.

Brewer, P.B., Howles, P.A, Dorian, K., Griffith, M.E., Ishida, T., Kaplan-Levy, R.N., Kilinc, A. and Smyth, D.R. (2004) PETAL LOSS, a trihelix transcription factor gene, regulates perianth architecture in the Arabidopsis flower. *Development*, **131**, 4035–4045.

Bruce, W., Folkerts, O., Garnaat, C., Crasta, O., Roth, B. and Bowen, B. (2000) Expression profiling of the maize flavonoid pathway genes controlled by estradiol-inducible transcription factors CRC and P. *Plant Cell*, **12**, 65–80.

Caddick, M.X., Greenland, A.J., Jepson, I., Krause, K.-P., Qu, N., Riddell, K.V., Salter, M.G., Schuch, W., Sonnewald, U. and Tomsett, A.B. (1998) An ethanol inducible gene switch for plants used to manipulate carbon metabolism. *Nat. Biotechnol.* **16**, 177–180.

Chen, S., Hofius, D., Sonnewald, U. and Bornke, F. (2003) Temporal and spatial control of gene silencing in transgenic plants by inducible expression of double-stranded RNA. *Plant J.* **36**, 731–740.

Corlett, J.E., Myatt, S.C. and Thompson, A.J. (1996) Toxicity symptoms caused by high expression of Tet repressor in tomato (*Lycopersicon esculentum* Mill. L.) are alleviated by tetracycline. *Plant Cell Environ.* **19**, 447–454.

Craft, J., Samalova, M., Baroux, C., Townley, H., Martinez, A., Jepson, I., Tsiantis, M. and Moore, I. (2005) New pOp/LhG4 vectors for stringent glucocorticoid-dependent transgene expression in Arabidopsis. *Plant J.* In press.

Deveaux, Y., Peaucelle, A., Roberts, G.R., Coen, E., Simon, R., Mizukami, Y., Traas, J., Murray, J.A.H., Doonan, J.H. and Laufs, P. (2003) The ethanol switch: a tool for tissue-specific gene induction during plant development. *Plant J.* **36**, 818–930.

Eilers, M., Picard, D., Yamamoto, K.R. and Bishop, J.M. (1989) Chimeras of myc oncoprotein and steroid receptors cause hormone and steroid dependent transformation of cells. *Nature*, **340**, 66–68.

Emery, J.F., Floyd, S.K., Alvarez, J., Eshed, Y., Hawker, N.P., Izhaki, A., Baum, S.F. and Bowman, J.L. (2003) Radial patterning of Arabidopsis shoots by class *IIIHD-ZIP* and *KANADI* genes. *Curr. Biol.* **13**, 1768–1774.

van Engelen, F.A., Molthoff, J.W., Conner, A.J., Nap, J.P., Pereira, A. and Steikma, W.J. (1995) pBinPlus: an improved plant transformation vector based on pBin19. *Transgenic Res.* **4**, 288–290.

Eshed, Y., Baum, S.F., Perea, J.V. and Bowman, J.L. (2001) Establishment of polarity in lateral organs of plants. *Curr. Biol.* **11**, 1251–1260.

Estruch, J.J., Prinsen, E., van Onckelen, H., Schell, J. and Spena, A. (1991) Viviparous leaves produced by somatic activation of an inactive cytokinin-synthesizing gene. *Science*, **254**, 1364–1367.

Faiss, M., Zalubilová, J., Strnad, M. and Schmülling, T. (1997) Conditional transgenic expression of the *ipt* gene indicates a function for cytokinins in paracrine signaling in whole tobacco plants. *Plant J.* **12**, 401–415.

Gan, S. and Amasino, R.M. (1995) Inhibition of leaf senescene by autoregulated production of cytokinin. *Science*, **270**, 1986–1988.

Gatz, C. (1996) Chemically inducible promoters in transgenic plants. *Curr. Opin. Biotechnol.* **7**, 168–172.

Gatz, C. and Lenk, I. (1998) Promoters that respond to chemical inducers. *Trends Plant Sci.* **3**, 352–358.

Gatz, C., Frohberg, C. and Wendenburg, R. (1992) Stringent repression and homogeneous de-repression by tetracycline of a modified CaMV35S promoter in intact transgenic tobacco plants. *Plant J.* **2**, 397–404.

Gross-Hardt, R., Lenhard, M. and Laux, T. (2002) *WUSCHEL* signaling functions in interregional communication during Arabidopsis ovule development. *Genes Dev.* **16**, 1129–1138.

Guo, H.-S., Fei, J.-F., Xie, Q. and Chua, N.-H. (2003) A chemical-regulated inducible RNAi system in plants. *Plant J.* **34**, 383–392.

Heidekamp, F., Dirkse, W.G., Hille, J. and van Ormondt, H. (1983) Nucleotide sequence of the *Agrobacterium tumefaciens* octopine Ti plasmid-encoded *tmr* gene. *Nucleic Acids Res.* **11**, 6211–6223.

Hellens, R.P., Edwards, E.A., Leyland, N.R., Bean, S. and Mullineaux, P.M. (2000) pGreen: a versatile and flexible binary Ti vector for *Agrobacterium*-mediated plant transformation. *Plant Mol. Biol.* **42**, 819–832.

Hudson, M.E., Lisch, D.R. and Quail, P.H. (2003) The *FHY3* and *FAR1* genes encode transposase-related proteins involved in regulation of gene expression by the phytochrome A-signaling pathway. *Plant J.* **34**, 453–471.

Jefferson, R.A. (1987) Assaying chimeric genes in plants: the GUS gene fusion system. *Plant Mol. Biol. Rep.* **5**, 387–405.

Kang, H.-G., Fang, Y. and Singh, K.B. (1999) A glucocorticoid-inducible transcription system causes severe growth defects in Arabidopsis and induces defence-related genes. *Plant J.* **20**, 127–133.

Koncz, C. and Schell, J. (1986) The promoter of TL-DNA controls the tissue specific expression of chimeric genes carried by a novel type of *Agrobacterium* binary vector. *Mol. Gen. Genet.* **204**, 383–396.

Kunkel, T., Niu, Q.-W., Chan, S.-Y. and Chua, N.-H. (1999) Inducible isopentenyl transferase as a high-efficiency marker for plant transformation. *Nat. Biotechnol.* **17**, 916–919.

Laufs, P., Coen, E., Kronenberger, J., Traas, J. and Doonan, J. (2003) Separable roles of *UFO* during floral development revealed by conditional restoration of gene function. *Development*, **130**, 785–796.

Lenhard, M. and Laux, T. (2003) Stem cell homeostasis in the Arabidopsis shoot meristem is regulated by intercellular movement of CLAVATA3 and its sequestration by CLAVATA1. *Development*, **130**, 3163–3173.

Lenhard, M., Bohnert, A., Jurgens, G. and Laux, T. (2001) Termination of stem cell maintenance in Arabidopsis floral meristems by interactions between *WUSCHEL* and *AGAMOUS*. *Cell*, **105**, 805–814.

Lenhard, M., Jurgens, G. and Laux, T. (2002) The *WUSCHEL* and *SHOOTMERISTEMLESS* genes fulfil complementary roles in Arabidopsis shoot meristem regulation. *Development*, **129**, 3195–3206.

Lexa, M., Genkov, T. and Brzobohaty, B. (2002) Inhibitory effects of elevated endogenous cytokinins on nitrate reductase in *ipt*-expressing tobacco are eliminated by short-term exposure to benzyladenine. *Physiol. Plant.* **115**, 284–290.

Lloyd, A.M., Schena, M., Walbot, V. and Davis, R.W. (1994) Epidermal cell fate determination in Arabidopsis: patterns defined by a steroid-inducible regulator. *Science*, **266**, 436–439.

van Loven, K., Beinsberger, S.E.I., Valcke, R.L.M, van Onckelen, H.A. and Clijsters, H.M.M. (1993) Morphometric analysis of the growth of *Phsp70-ipt* transgenic tobacco plants. *J Exp. Bot.* **44**, 1671–1678.

Luehrsen, K.R. and Walbot, W. (1993) Firefly luciferase as a reporter for plant gene expression studies. *Promega Notes Mag.* **44**, 24.

Martinez, A., Sparks, C., Hart, C.A., Thompson, J. and Jepson, I. (1999) Ecdysone agonist-inducible transcription in transgenic tobacco plants. *Plant J.* **5**, 559–569.

McKenzie, M.J., Mett, V., Reynolds, P.H.S. and Jameson, P.E. (1998) Controlled cytokinin production in transgenic tobacco using a copper-inducible promoter. *Plant Physiol.* **116**, 969–977.

Medford, J.L., Horgan, R., El-Sawi, Z. and Klee, H.J. (1989) Alteration of endogenous cytokinins in transgenic plants using chimeric isopentenyl transferase gene. *Plant Cell*, **1**, 403–413.

Moore, I., Diefenthal, T., Zarsky, V., Schell, J. and Palme, K. (1997) A homolog of mammalian GTPase Rab2 is present in Arabidopsis and is expressed predominantly in pollen grains and seedlings. *Proc. Natl Acad. Sci. USA*, **94**, 762–767.

Moore, I., Gälweiler, L., Grosskopf, D., Schell, J. and Palme, K. (1998) A transcription activation system for regulated gene expression in transgenic plants. *Proc. Natl Acad. Sci. USA*, **95**, 376–381.

Murashige, T. and Skoog, F. (1962) A revised medium for rapid growth and bioassays with tobacco tissue. *Physiol. Plant.* **15**, 493–497.

Ohno, C.K., Reddy, G.V., Heisler, M.G.B. and Meyerowitz, E.M. (2004) The Arabidopsis *JAGGED* gene encodes a zinc finger protein that promotes leaf tissue development. *Development*, **131**, 1111–1122.

Ott, R., Ren, L. and Chua, N.-H. (1990) A bidirectional enhancer cloning vehicle for higher plants. *Mol. Gen. Genet.* **221**, 121–124.

Ouwerkerk, P.B.F., de Kam, R.J., Hodge, J.H.C. and Meijer, A.H. (2001) Glucocorticoid-inducible gene expression in rice. *Planta*, **213**, 370–378.

Padidam, M. (2003) Chemically regulated gene expression in plants. *Curr. Opin. Plant Biol.* **6**, 169–177.

Padidam, M., Gore, M., Lu, D.L. and Smirnova, O. (2003) Chemical-inducible, ecdysone receptor-based gene expression system for plants. *Transgenic Res.* **12**, 101–109.

Picard, D. (1993) Steroid-binding domains for regulating the functions of heterologous proteins in cis. *Trends Cell Biol.* **3**, 278–280.

Picard, D., Salser, S.J. and Yamamoto, K.R. (1988) A movable and regulable inactivation function within the steroid binding domain of the glucocorticoid receptor. *Cell*, **54**, 1073–1080.

Roslan, H.A., Salter, M.G., Wood, C.D. *et al.* (2001) Characterization of the ethanol-inducible *alc* gene-expression system in *Arabidopsis thaliana*. *Plant J.* **28**, 225–235.

Sablowski, R.W.M. and Meyerowitz, E.M. (1998) A homolog of *NO APICAL MERISTEM* is an immediate target of the floral homeotic genes *APETALA3*/*PISTILLATA*. *Cell*, **92**, 93–103.

Salter, M.G., Paine, J.A., Riddell, K.V., Jepson, I., Greenland, A.J., Caddick, M. and Tomsett, A.B. (1998) Characterisation of the ethanol-inducible *alc* gene-expression system for transgenic plants. *Plant J.* **16**, 127–132.

Schmülling, T. (2002) New insights into the functions of cytokinins in plant development. *J. Plant Growth Regul.* **21**, 40–49.

Schmülling, T., Beinsberger, S., De Greef, J., Schell, J., van Onckelen, H. and Spena, A. (1989) Construction of a heat-inducible chimeric gene to increase the cytokinin content in transgenic plant tissue. *FEBS Lett.* **289**, 401–406.

Schoof, H., Lenhard, M., Haecker, A., Mayer, K.F.X., Jurgens, G. and Laux, T. (2000) The stem cell population of Arabidopsis shoot meristem is maintained by a regulatory loop between the *CLAVATA* and *WUSCHEL* genes. *Cell*, **100**, 635–644.

Schubert, D., Lechtenberg, B., Forsbach, A., Gils, M., Bahadur, S. and Schmidt, R. (2004) Silencing in Arabidopsis T-DNA transformants: the predominant role of a gene-specific RNA sensing mechanism versus position effects. *Plant Cell*, **16**, 2561–2572.

Segal, G., Song, R. and Messing, J. (2003) A new *opaque* variant maize by a single dominant RNA-interference-inducing transgene. *Genetics*, **165**, 387–397.

Simon, R., Igeno, M. and Coupland, G. (1996) Activation of floral meristem identity genes in Arabidopsis. *Nature*, **384**, 59–62.

Smart, C.M., Scofield, S.R., Beven, M.W. and Dyer, T.A. (1991) Delayed leaf senescence in tobacco plants transformed with *tmr*, a gene for cytokinin production in *Agrobacterium*. *Plant Cell*, **3**, 647–656.

Smigocki, A.C. (1991) Cytokinin content and tissue distribution in plants transformed by a reconstructed isopentenyl transferase gene. *Plant Mol. Biol.* **16**, 105–115.

Tang, W. and Newton, R.J. (2004) Glucocorticoid-inducible transgene expression in loblolly pine (*Pinus taeda* L.) cell suspension cultures. *Plant Sci.* **166**, 1351–1358.

Töpfer, R., Matzeit, V., Gronenborn, B., Schell, J. and Steinbiss, H.-H. (1987) A set of plant expression vectors for transcriptional and translational fusions. *Nucleic Acids Res.* **15**, 5890.

Tsiantis, M. and Hay, A. (2003) Comparative plant development: the time of the leaf? *Nat. Rev. Genet.* **4**, 169–180.

Unger, E., Cigan, A.M., Trimnell, M., Xu, R.J., Kendall, T., Roth, B. and Albertsen, M. (2002) A chimeric ecdysone receptor facilitates methoxyfenozide-dependent restoration of male sterility in *ms45* maize. *Transgenic Res.* **11**, 455–465.

Weinmann, P., Gossen, M., Hillen, W., Bujard, H. and Gatz, C. (1994) A chimeric transactivator allows tetracycline-responsive gene expression in whole plants. *Plant J.* **5**, 559–569.

Zuo, J. and Chua, N.-H. (2000) Chemical-inducible systems for regulated expression of plant genes. *Curr. Opin. Biotechnol.* **11**, 146–151.

Zuo, J., Niu, Q.-W. and Chua, N.-H. (2000) An estrogen receptor-based transactivator XVE mediates highly inducible gene expression in transgenic plants. *Plant J.* **24**, 265–273.

Zuo, J., Niu, Q.-W., Moller, S.G. and Chua, N.-H. (2001) Chemical-regulated, site-specific DNA excision in transgenic plants. *Nat. Biotechnol.* **19**, 157–161.

The Plant Journal (2005) **41**, 899–918 doi: 10.1111/j.1365-313X.2005.02342.x

TECHNICAL ADVANCE

New pOp/LhG4 vectors for stringent glucocorticoid-dependent transgene expression in Arabidopsis

Judith Craft[1,‡], Marketa Samalova[1,‡], Celia Baroux[1,†,§], Helen Townley[1,§], Alberto Martinez[2], Ian Jepson[2], Miltos Tsiantis[1] and Ian Moore[1,*]

[1]*Department of Plant Sciences, University of Oxford, South Parks Rd, Oxford, OX1 3RB, UK, and*

[2]*Syngenta Ltd, Jealott's Hill Research Station, Bracknell, Berks. RG42 6ET, UK*

Received 6 August 2004; revised 1 December 2004; accepted 14 December 2004.

[*]For correspondence (fax +44 0 1865 275074; e-mail ian.moore@plants.ox.ac.uk).

[†]Present address: Institute of Plant Biology, University of Zürich, Zollikerstrasse 107, 8008 Zürich, Switzerland.

[‡,§]These authors contributed equally to this work.

Summary

To facilitate glucocorticoid-inducible transgene expression from the pOp promoter in Arabidopsis the ligand-binding domain of a rat glucocorticoid receptor (GR LBD) was fused to the amino terminus of the synthetic transcription factor LhG4 to generate LhGR-N. Fusions bearing the GR LBD at other positions in LhG4 exhibited incomplete repression or inefficient induction. LhGR-N was stringently repressed in the absence of exogenous glucocorticoid but was fully activated by addition of 2 μM dexamethasone which resulted in 1000-fold increase in GUS reporter activity. Half maximal induction was achieved with 0.2 μM dexamethasone. Reporter transcripts were detectable within 2 h of dexamethasone application and peaked 4–10 h later. Neither LhGR-N nor dexamethasone affected seedling development although ethanol retarded development when used as a solvent for dexamethasone. The efficiency of the pOp target promoter was improved 10- to 20-fold by incorporating six copies of the ideal *lac* operator with sufficient inter-operator spacing to allow simultaneous occupancy. Introduction of the TMV Ω sequence into the 5′UTR resulted in a further 10-fold increase in dexamethasone-inducible reporter activity and an increase in the induction factor to 10^4. Although promoters containing the TMV Ω sequence exhibited slightly increased basal expression levels in the absence of dexamethasone, stringent regulation of the cytokinin biosynthetic gene *ipt* was achieved with all promoters. Despite the severity of the induced *ipt* phenotypes, transcripts for the KNOX homoeodomain transcription factors *BREVIPEDICELLUS* and *SHOOTMERISTEMLESS* were not significantly increased within 48 h of dexamethasone application to seedlings.

Keywords: steric hindrance, homoeobox, isopentenyl transferase, transgenic plant, translation enhancer.

Introduction

Transgenes are central to the elucidation of gene function. However, the expression of transgenes from constitutive and broadly expressed promoters such as CaMV 35S is problematic if the transgene compromises plant viability or fertility. Moreover, the ability to temporally modulate transgene activity is essential in some physiological and developmental studies. For these reasons, considerable effort has been made to establish chemically inducible promoters for transgene expression in plants (for reviews see Gatz and Lenk, 1998; Padidam, 2003; Zuo and Chua, 2000).

Of the systems developed to date, the majority contain two transcription units. The first consists typically of a target promoter comprising multiple copies of a specific transcription factor binding site linked to a minimal promoter, typically a truncated 35S promoter, which drives the target gene; the second employs a constitutive promoter to express a chemically responsive transcription factor that specifically recognizes the first component. Numerous systems have been developed, founded on a diverse collection of non-plant regulatory elements and responsive to a variety

of chemicals including tetracycline (Gatz *et al.*, 1992; Weinmann *et al.*, 1994), copper (Mett *et al.*, 1993), ethanol (Caddick *et al.*, 1998; Deveaux *et al.*, 2003), and steroids or steroid mimics (Aoyama and Chua, 1997; Böhner *et al.*, 1999; Bruce *et al.*, 2000; Martinez *et al.*, 1999; Padidam *et al.*, 2003; Zuo *et al.*, 2000). In this and the accompanying article we describe a new steroid-inducible transgene expression system based on the widely used pOp/LhG4 transcription activation system (Moore *et al.*, 1998).

The pOp/LhG4 system comprises (i) a chimeric promoter pOp that consists of two ideal *lac* operators cloned upstream of a minimal CaMV 35S promoter and (ii) a transcription activator LhG4 which is a fusion between a high-affinity DNA-binding mutant of *lac* repressor, and transcription-activation-domain-II of *GAL4* from *Saccharomyces cerevisiae* (Moore *et al.*, 1998). The pOp promoter is silent when introduced into reporter lines that lack LhG4 but can be activated in specific cells of the F_1 when reporter lines are crossed with activator lines that express LhG4 from appropriate promoters (Baroux *et al.*, 2001a,b, 2005; Lexa *et al.*, 2002; Moore *et al.*, 1998; Schoof *et al.*, 2000). By using activator lines that direct expression either constitutively or in specific tissues, this system has been used to investigate various aspects of development in Arabidopsis, tobacco, and maize (An *et al.*, 2004; Baroux *et al.*, 2001a,b; Brewer *et al.*, 2004; Emery *et al.*, 2003; Eshed *et al.*, 2001; Gross-Hardt *et al.*, 2002; Hudson *et al.*, 2003; Lenhard and Laux, 2003; Lenhard *et al.*, 2001, 2002; Lexa *et al.*, 2002; Ohno *et al.*, 2004; Schoof *et al.*, 2000; Segal *et al.*, 2003).

Although the pOp/LhG4 system offers tissue-specific control over transgene expression through use of tissue-specific promoters, it provides minimal temporal control. The activity of several native and artificial plant transcription factors has been made conditional on the presence of steroid ligands by fusion to the LBD of GR or oestrogen receptors (Aoyama *et al.*, 1995; Lloyd *et al.*, 1994; Sablowski and Meyerowitz, 1998; Simon *et al.*, 1996). The principle of GR-based transcriptional systems is that in the absence of the steroid ligand, a transcription factor is trapped in an inactive complex via interaction between the GR LBD and heat-shock protein HSP90 (Picard, 1993). This complex is believed to interfere with the function of the bound fusion protein by steric hindrance, blocking interactions with other proteins or with DNA target sites (Picard, 1993). The binding of dexamethasone to the LBD mediates dissociation of the fusion protein from HSP90. This model predicts that the effectiveness of the control exerted by GR LBD on a heterologous protein depends on how components of the HSP90 complex are positioned relative to at least one critical functional domain in the heterologous moiety. Domains that either face away from the HSP90 complex or are too distant would not be regulated (Picard, 1993).

Here we describe the properties of three topologically different fusions between LhG4 and GR LBD in Arabidopsis and show that an amino terminal fusion exhibits highly inducible and stringently regulated transcriptional activity. To demonstrate the utility of the system, glucocorticoid-inducible *ipt* expression was used to regulate bacterial *ipt* expression and to resolve whether cytokinins act as positive regulators of class-I KNOX transcription factor expression.

Despite its successful use in numerous studies, the pOp/LhG4 system does not appear to result in amplification of expression levels; that is, if a promoter is used to drive LhG4 expression which then activates a pOp-GUS reporter, the induced reporter activity is not greater than a direct promoter-GUS fusion (Baroux *et al.*, 2005; Moore *et al.*, 1998). In the cases we have examined, expression levels achieved with the pOp/LhG4 system are typically 30–100% of the levels obtained with the best transformants carrying direct promoter-GUS fusions (Baroux *et al.*, 2005). Amplification of expression levels has been reported with other expression systems (Weijers *et al.*, 2003) which typically incorporate between four and 10 binding sites in the target promoter (Böhner *et al.*, 1999; Martinez *et al.*, 1999; Padidam *et al.*, 2003; Schwechheimer *et al.*, 1998; Weijers *et al.*, 2003; Weinmann *et al.*, 1994; Zuo *et al.*, 2000). Similarly, transcription from native eukaryotic promoters is achieved through a series of co-operative interactions between multiple transcription factor binding sites within enhancer elements (Blackwood and Kadonaga, 1998; Blair *et al.*, 1994; Kadonaga, 2004). The pOp promoter caries two ideal *lac* operators but these are positioned only 6 bp apart and the structure of DNA-bound *lac* repressor (Lewis *et al.*, 1996) predicts that steric constraints will prevent these two sites from being simultaneously occupied. Thus the pOp promoter operationally comprises a single LhG4 or LhGR binding site. Although this is clearly sufficient for CaMV35S::LhG4 and LhGR to activate the pOp promoter with an efficiency approaching that of CaMV35S (Moore *et al.*, 1998), multimerizing the *lac* operators in the pOp promoter would be expected to increase its efficiency. However initial attempts to do this were thwarted by the recombinational instability of contiguous *lac* operator arrays. Here we show that four or six copies of the *lac* operator sequence are stable when part of a 52-bp direct repeat and substantially improve the expression characteristics of the pOp promoter with both LhG4 and LhGR.

Results

N-terminal, C-terminal and internal LhGR fusions exhibit distinct properties

To bring LhG4 under control of glucocorticoid ligands, we tested three different constructs in which the GR LBD (residues 508–795, including the NLS; Picard and Yamamoto, 1987) was present at the carboxy terminus (LhGR-C), the amino terminus (LhGR-N), or internally (LhGR-I) between

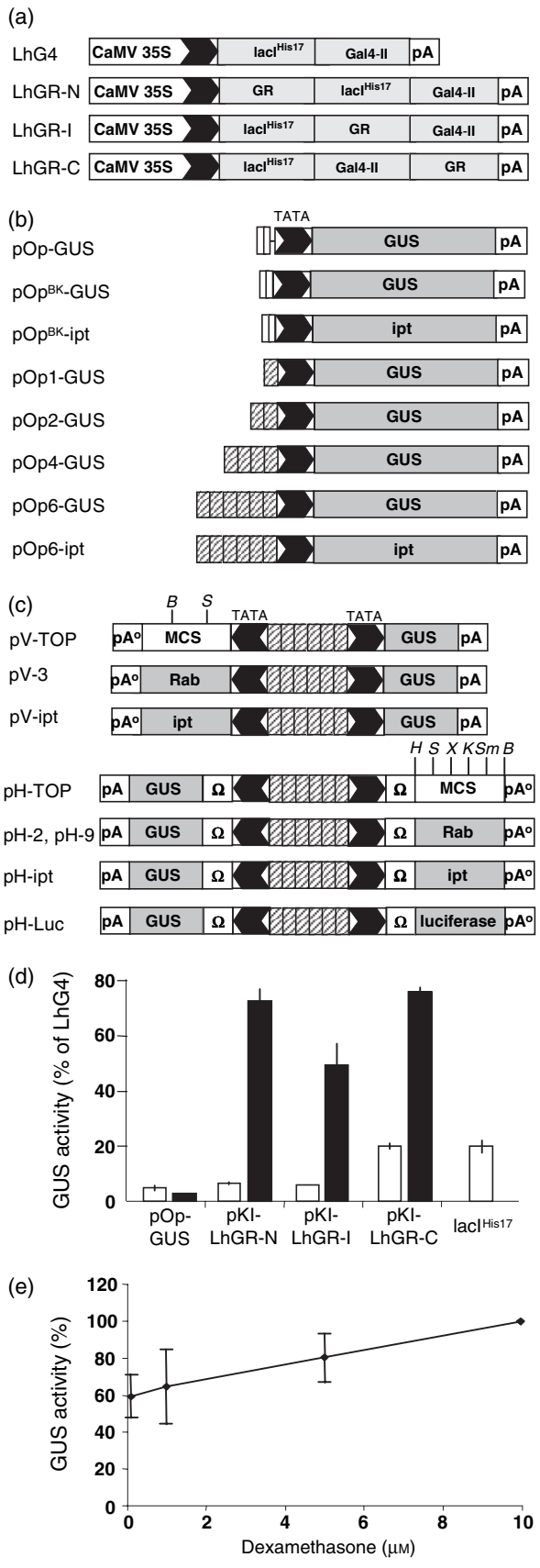

Figure 1. Schematic diagrams of DNA constructs.
Relevant expression cassettes only are shown. All constructs represent binary T-DNA vectors with the right T-DNA border located to the right of the diagram. All reporter constructs carry a Pnos::HPT selectable marker at the left border and activator constructs carry either methotrexate resistance (LhG4) or kanamycin resistance (LhGR) markers at the left border (Moore *et al.*, 1998).
(a) Activator constructs express LhG4 or LhGR from the CaMV35S promoter (Moore *et al.*, 1998). LacI^{His17} indicates residues 1–330 of the Y17H mutant of *lac* repressor (Lehming *et al.*, 1987); Gal4-II indicates transcription activation-domain-II (residues 768–881) of *Saccharomyces cerevisiae* Gal4p; GR indicates the LBD (residues 508–795) of a rat glucocorticoid receptor at the amino terminus (LhGR-N), the carboxy terminus (LhGR-C), or between the *lacI* and *GAL4* domains (LhGR-I). pA indicates the CaMV35S polyadenylation signal.
(b) Reporter construct pOp-GUS (Moore *et al.*, 1998) and its derivative pOp^{BK}-GUS (Baroux *et al.*, 2005) carry two closely spaced *lac* operators and differ only by deletion of 40 bp between the operators (open rectangles) and the minimal CaMV promoter (TATA). pOp1-GUS to pOp6-GUS carry one, two, four or six copies of a 52-bp repeat that contains an ideal *lac* operator (hatched rectangles). GUS and ipt indicate the coding sequences of the *Escherichia coli uid*A and *Agrobacterium tumefaciens ipt* coding regions respectively. pA, CaMV35S polyadenylation signal.
(c) pV-TOP and pH-TOP and their derivatives used in this work. Rab and luciferase indicate the coding regions of Arabidopsis Rab GTPase RabD1 (Rutherford and Moore, 2002) and firefly luciferase respectively. Ω, TMV Ω translation enhancer; pA°, octopine synthase polyadenylation signal; MCS, multiple cloning site/polylinker; *B, S, H, X, K,* and *Sm* represent unique recognitions sites for *Bam*HI, *Sal*I, *Hin*dIII, *Xho*I, *Kpn*I, and *Sma*I, respectively, within the MCS of pV-TOP and pH-TOP; other symbols as in (b). The selectable marker cassettes in pV-TOP and pH-TOP have polyadenylation signals from T-DNA genes 7 and nopaline synthase, respectively, and thus have no elements in common with the cassettes shown here.
(d) GUS activity in Arabidopsis protoplasts incubated in the presence of either 10 μM dexamethasone (black bars) or 0.1% ethanol (white bars) following transfection with the reporter plasmid alone (pOp^{BK}-GUS), reporter plasmid plus the activator plasmids pKI-LhGR-N, -I, or -C (as indicated), or reporter plus pKI-HisA0 (Moore *et al.*, 1998) which expresses the Y17H mutant of *lac* repressor without an activation domain (lacI^{His17}). Activity is expressed as a percentage of the activity obtained in control transfections with reporter plus pKI-HisA-Gal4 which expresses LhG4 (Moore *et al.*, 1998); data derived from two independent sets of transfections each with six to eight replicates, except for lacI^{His17} where data are derived from two transfection experiments.
(e) GUS activity induced by various dexamethasone concentrations in Arabidopsis protoplasts transfected with pOp^{BK}-GUS and pKI-LhGR-N. Data from four independent replicates plus standard deviation expressed as percentage of the activity obtained with 10 μM dexamethasone.

the *lac* repressor and Gal4 activation domains of LhG4 (Figure 1a). These constructs were cloned under control of CaMV 35S transcription signals, yielding plasmids pKI-LhGR-N, -I, and -C, and their ability to activate pOp-GUS (Figure 1b) expression in a dexamethasone-dependent fashion was tested by transient expression in Arabidopsis protoplasts. As shown in Figure 1(d) all three fusions directed dexamethasone-inducible GUS activity but LhGR-I was substantially less active than LhGR-N or LhGR-C while LhGR-C exhibited considerable uninduced activity. In contrast, LhGR-N was efficiently repressed in the absence of dexamethasone and was effectively induced in the presence of this compound (Figure 1d). LhGR-N exhibited a flat dose–response curve in the micromolar range such that 0.1 μM dexamethasone was sufficient to achieve 50% of the activity obtained with 10 μM (Figure 1e).

LhG4 and LhGR-N, -I and -C were cloned under CaMV 35S control in a binary vector (yielding plasmids pBIN-LhG4 and

pBIN-LhGR-N, -I, and -C) and used to super-transform Arabidopsis reporter line pOp-GUS(g2) which is homozygous for a pOp-GUS transgene (Baroux *et al.*, 2005). For each construct, a rosette leaf was detached from 11 or 12 primary transformants, incubated for 48 h in 10 μM dexamethasone, and stained for GUS activity. All of the LhGR-C plants and 11 of the 12 LhGR-N plants exhibited staining intensities similar to those achieved with LhG4. In contrast, only one of the 11 LhGR-I plants exhibited strong inducible GUS activity (LhGR-I 3c) and two lines exhibited significant uninduced activity (examples are shown in Figure S1a). In the absence of dexamethasone, GUS activity was not detected in any of the LhGR-N plants whereas all the LhGR-C plants showed low but detectable uninduced GUS activity (Figure S1a). Thus the poor inducibility and the leakiness that characterized LhGR-I and LhGR-C, respectively, in transient expression were recapitulated in the T_1 population while LhGR-N again exhibited promising induction characteristics. These characteristics were maintained into the T_3 generation (Figure S1b). Quantitative GUS assays confirmed the superior induction characteristics of LhGR-N lines and LhGR-N(4c) was selected for detailed characterization.

Induction of LhGR-N with dexamethasone is rapid, stable, uniform and does not affect plant growth in vitro

Seedlings of LhGR-N(4c) exhibited no staining (after 16 h incubation) when grown on medium lacking dexamethasone but GUS activity was induced throughout seedlings germinated and grown on medium supplemented with 10 μM dexamethasone (Figure 2a and Figure S1b).

To establish the characteristics of LhGR-N under conditions that are likely to be optimal for application of the inducing chemical, seedlings grown in liquid medium were supplied with 10 μM dexamethasone. After 48 h, extractable GUS activity measured in LhGR-N(4c) exceeded the activities detected in LhG4 lines (Figure 2b). In the absence of dexamethasone, LhGR-N(4c) exhibited no GUS activity above background levels (Table S1) indicating that LhGR-N can induce GUS activity by more than 1000-fold.

Figure 2(c) shows that 2 μM dexamethasone was sufficient to induce maximum GUS activity in LhGR-N(4c) while 50% of maximum activity was obtained with 0.2 μM dexamethasone in agreement with the data obtained from transient expression in protoplasts. Induced GUS activity was undetectable with 0.01 μM dexamethasone so the dynamic range of inducer concentrations spans 2 orders of magnitude and should allow for quantitative control over induced expression. Furthermore LhGR-N directs 5- to 10-fold less GUS activity in the presence of IPTG (Figure S2), providing additional opportunities for modulation of pOp/LhGR-mediated expression.

Analysis of GUS transcript abundance by RNA gel blot indicated that transcripts were first detected in seedlings 2 h after addition of dexamethasone (Figure 2d). GUS transcripts were maximally abundant at about 6 h and remained at this level for at least 3 days (Figure 2d).

To examine whether activation of the LhGR-N protein interferes with plant development we examined growth of seedlings on dexamethasone. As shown in Figure 2(a,e) and in Figure S3, neither wild type nor LhGR-N(4c) seedlings were affected by dexamethasone but we did observe a significant reduction in fresh weight and in the rate of seedling development if ethanol was used as a solvent for the dexamethasone (0.1% v/v final concentration). These effects were attributable to ethanol and were eliminated when dexamethasone was dissolved in dimethyl sulfoxide (DMSO). We conclude that neither dexamethasone nor activated LhGR-N adversely affects Arabidopsis seedling development.

Improved pOp reporters for use with LhG4 and LhGR

Although the pOp/LhGR-N constructs provided a tightly regulated gene expression system with a high dynamic range in Arabidopsis seedlings, the GUS activities induced in soil-grown plants were disappointingly low even after 7 days (data not shown). Furthermore, despite the demonstrated utility of the pOp/LhG4 system in diverse experimental studies, it was apparent that amplification of gene expression was not generally achieved with these constructs. Consequently we sought to improve the efficiency of the pOp promoter by multimerization of the *lac* operators.

Initial attempts at multimerizing or even dimerizing the two *lac* operator sequences of the pOp promoter were unsuccessful owing to their recombinational instability in *Escherichia coli*. Multimerized *lac* operator sequences represent a series of overlapping inverted repeats which can be particularly unstable in plasmids, even in *recA*$^-$ *E. coli* strains (Glass, 1982). In contrast multiple copies of a direct repeat such as the Gal4 UAS and the CaMV 35S enhancer are comparatively stable in standard laboratory strains of both *E. coli* and *Agrobacterium tumefaciens* (Gälweiler *et al.*, 2000; Glass, 1982; Mitsuhara *et al.*, 1996). Therefore we designed a 52-bp direct repeat in which the 18 bp ideal *lac* operator was embedded. This spacing is sufficient to allow simultaneous occupancy of adjacent operators by *lac* repressor and, based on a periodicity of 10.4 bp, corresponds to five turns of the DNA helix. However, the binding sites may be slightly out of phase *in vivo* where the average helical periodicity of DNA may be closer to 11.1 bp and may exhibit local variation (Müller *et al.*, 1996). The 52 bp sequence was cloned as a single copy or in two, four or six directly repeated copies in place of the *lac* operators in pOp^{BK}-GUS (Figure 1b; Baroux *et al.*, 2005) generating pOp1-GUS to pOp6-GUS. We found that even six copies of the 52 bp *lac* operator repeat in pOp6 were completely stable in high- and low-copy number plasmids in *E. coli* DH5α and

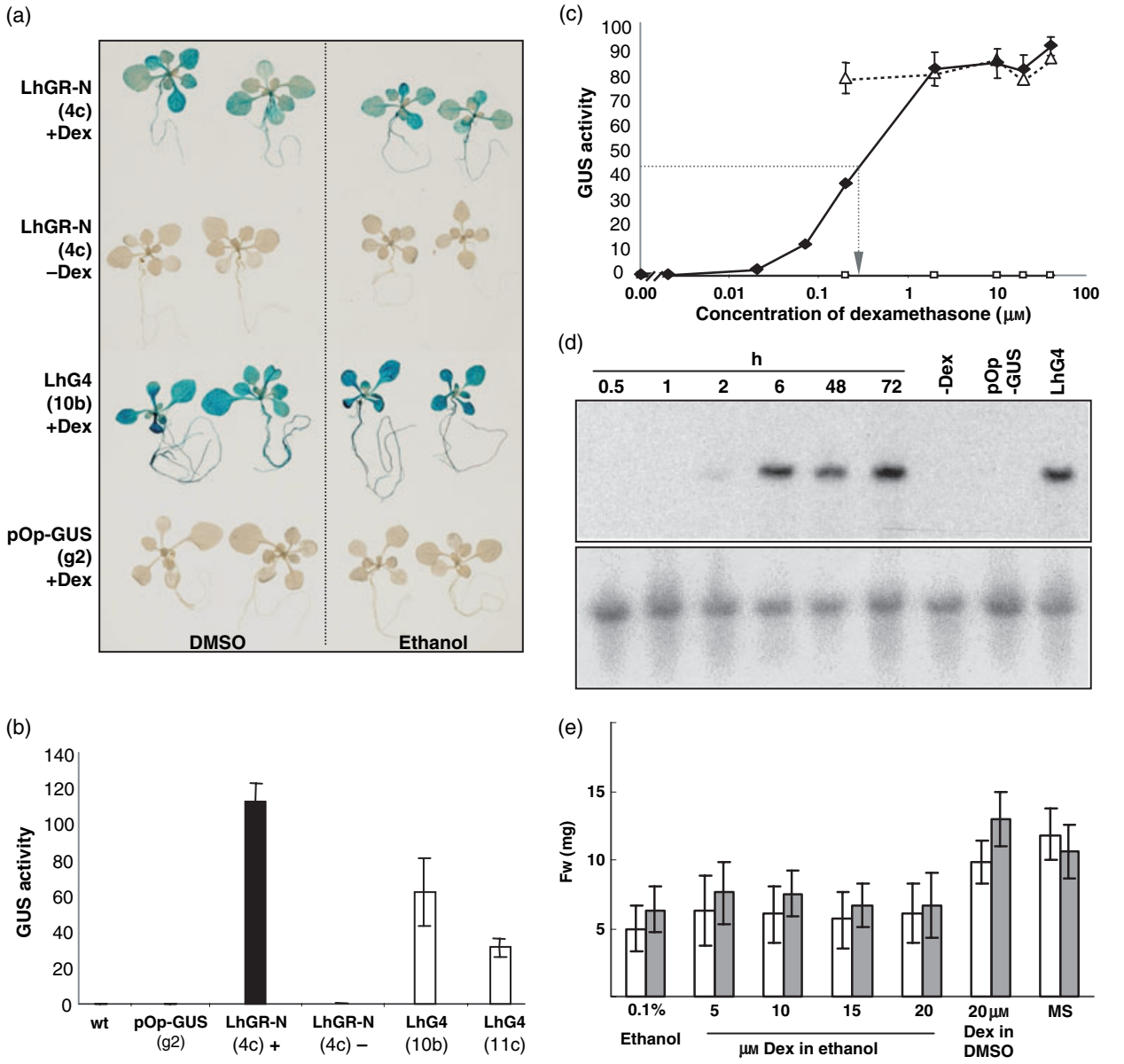

Figure 2. Induction characteristics of LhGR-N.

(a) Dexamethasone-induced GUS expression in seedlings grown on medium supplemented either with 10 μM dexamethasone (+Dex) from 10 mM stock solutions prepared in either dimethyl sulfoxide (DMSO) or ethanol, or with solvent at 0.1% as indicated. Ethanol results in a noticeable reduction in seedling size. The lines presented are indicated in brackets.

(b) Extractable GUS activity (pmol 4-MU min^{-1} μg^{-1} protein) in seedlings of untransformed Arabidopsis (wt), reporter line pOp-GUS(g2), or super-transformed lines of pOp-GUS(g2) expressing LhGR-N or LhG4 as indicated; the name of each line is indicated in brackets. Seedlings were grown in liquid medium with (+) or without (–) 10 μM dexamethasone. Error bars indicate standard deviation of between three and six measurements.

(c) GUS activity (pmol 4-MU min^{-1} μg^{-1} protein) in liquid-grown seedlings 48 h after addition of various concentrations of dexamethasone. Squares = reporter line pOp-GUS(g2); diamonds = LhGR-N(4c); triangles = pBIN-LhG4 line 10b. Bars = S.D. The concentration of dexamethasone evoking 50% of maximum GUS activity in line 4c is indicated by the dashed arrow.

(d) RNA gel blot analysis of GUS mRNA in total RNA extracted from: seedlings of LhGR-N(4c) grown in liquid culture medium at the indicated number of hours after addition of 10 μM dexamethasone; seedlings of the same line grown in the presence of 0.1% ethanol for 72 h (–Dex); seedlings of reporter line pOp-GUS(g2) (pOp-GUS) and control line 10b super-transformed with pBIN-LhG4 grown in the presence of 10 μM dexamethasone (LhG4). The lower panel shows the same blot reprobed for eIF-4A as a normalization control.

(e) Fresh weight of seedlings of LhGR-N(4c) germinated and grown for 2 weeks on unsupplemented growth medium (MS) or on medium containing either 0.1% ethanol, various concentrations of Dex plus 0.1% ethanol, or 20 μM Dex from a 20 mM stock dissolved in DMSO.

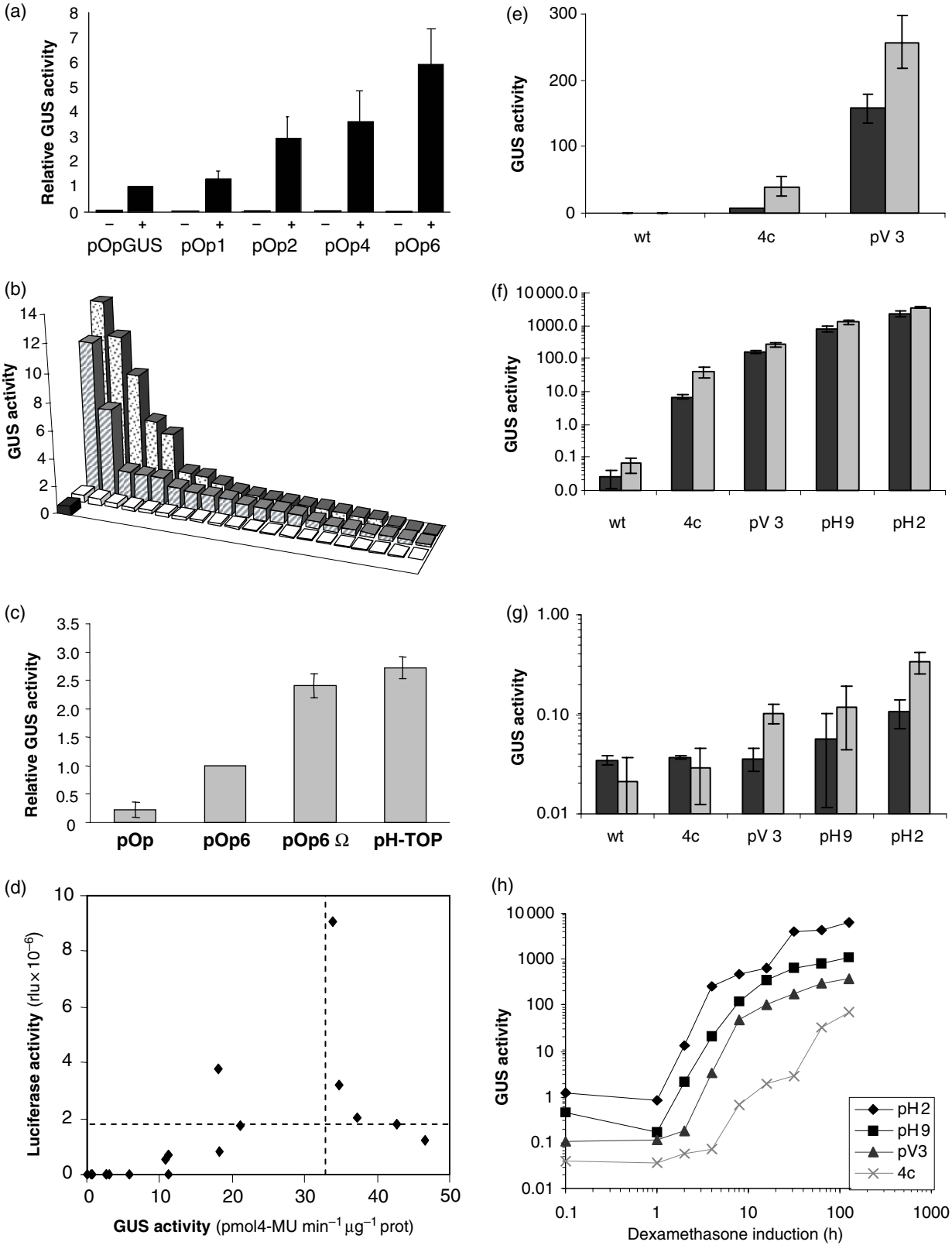
(a)
Relative GUS activity
pOpGUS
pOp1
pOp2
pOp4
pOp6
(b)
GUS activity
(c)
Relative GUS activity
pOp
pOp6
pOp6 Ω
pH-TOP
(d)
Luciferase activity (rlu×10⁻⁶)
GUS activity (pmol4-MU min⁻¹ µg⁻¹ prot)
(e)
GUS activity
wt
4c
pV 3
(f)
GUS activity
wt
4c
pV 3
pH9
pH2
(g)
GUS activity
wt
4c
pV 3
pH9
pH2
(h)
GUS activity
pH2
pH9
pV3
4c
Dexamethasone induction (h)

in *A. tumefaciens* GV3101::pMP90 (Figure S4). We have so far received only one report of recombinational instability in the 6xOp array from other laboratories to which we have distributed the plasmids.

Transient expression in Arabidopsis protoplasts showed that LhG4 directed increased GUS activity from the multimerized *lac* operators without increased background expression in the absence of LhG4 (Figure 3a). pOp-GUS, pOp4-GUS and pOp6-GUS were introduced into a CaMV35S::LhG4 activator line. GUS activities in aerial tissues of 20 T_1 seedlings were compared with those measured in F_2 seedlings from a cross between this activator line and pOp-GUS(g2) which is the most efficient pOp-GUS reporter line that we have so far identified (Baroux *et al.*, 2005). As shown in Figure 3(b), most of the pOp4-GUS and pOp6-GUS transformants exhibited higher GUS activity than the best of the pOp-GUS transformants or pOp-GUS(g2). Similar observations were made in an independent set of transformations with a second activator line (Figure S5). In the best cases GUS activities in pOp4-GUS and pOp6-GUS were more than 20-fold higher. We concluded that pOp4 and pOp6 are more efficiently activated than pOp. Nevertheless, as with the pOp promoter (Baroux *et al.*, 2005), it still advisable to screen a population of 20 or more pOp4 or pOp6 lines to identify those with the best performance.

pH-TOP and pV-TOP

When generating reporter lines with a gene of interest, it would be an advantage to have an easily scored reporter construct on the same T-DNA to report on the efficiency and pattern of pOp activation in each transgenic line. As the operator array is expected to function as an orientation-independent enhancer element we tested whether it would direct efficient and co-ordinate expression of a GUS reporter construct and a test construct when these were transcribed from divergent minimal promoters in Arabidopsis. To do this we cloned an expression cassette comprising a minimal promoter, polylinker, and polyadenylation signal upstream of the *lac* operator array in pOp6-GUS to generate the plasmid pV-TOP (Figure 1c). The pV-TOP polylinker has only two unique restriction sites so we assembled a similar divergent expression cassette in the pGREEN-II vector backbone (Hellens *et al.*, 2000) generating pH-TOP which has six unique cloning sites. During construction of pH-TOP, the TMV Ω translational enhancer sequence (Gallie *et al.*, 1987) was introduced into the 5′UTR of the GUS reporter and the multiple cloning site to increase the translational efficiency of the induced transcripts. Transient expression in Arabidopsis protoplasts confirmed that the incorporation of the TMV Ω sequence increased the LhG4-induced GUS activity two to threefold (Figure 3c), similar to the effect reported previously for TMV Ω in transgenic Arabidopsis (Holtorf *et al.*, 1995).

To test the induction characteristics of pV-TOP and pH-TOP, we and others have introduced various coding sequences into their polylinkers and tested for dexamethasone-inducible expression of each sequence after transformation into the CaMV 35S::LhGR activator line 4c-S5/7 [derived from LhGR-N(4c), as described in Experimental procedures]. Effective inducible expression was observed in all cases and data obtained with *ipt* and a benign Arabidopsis Rab GTPase (At3g11730, Rutherford and Moore, 2002) are presented here.

We first established the induction characteristics of the GUS reporter in pV-TOP and pH-TOP lines in comparison with pOp-GUS. For this we chose the pV-TOP line pV3 and the pH-TOP lines pH2 and pH9 all of which express the Rab GTPase coding region but, unlike the *ipt* lines, develop normally upon induction with dexamethasone. These lines were compared with line LhGR-N(4c) which carries the same CaMV35S::LhGR-N activator locus and our best pOp-GUS reporter locus, pOp-GUS(g2). When seedlings were induced in liquid medium we found that pV-TOP line pV3 exhibited approximately sixfold more GUS activity than pOp-GUS(g2)

Figure 3. Comparison of pOp with promoters containing multimerized *lac* operators in cultured seedlings.
(a) Transient expression in Arabidopsis protoplasts of pOp-GUS and pOp1- to pOp6-GUS either with (+) or without (–) a plasmid expressing LhG4. GUS activities (±SD) are expressed relative to the activity directed by pOp-GUS + LhG4 in four independent assays.
(b) GUS activity (pmol 4-MU min^{-1} μg^{-1} protein) in leaf tissue of 20 independent transformants generated by retransformation of CaMV35S::LhG4 line 14/1 with pOp-GUS (white bars), pOp4-GUS (hatched bars) or pOp6-GUS (stippled bars). Transformants are ordered left to right from the highest to the lowest GUS activity. The black bar indicates the GUS activity in leaf tissue of activator line 14/1 crossed with pOp-GUS(g2) which is the most efficient pOp-GUS reporter line we have identified.
(c) GUS activity relative to pOp6-GUS induced in Arabidopsis protoplasts by transient co-expression of a CaMV35S::LhG4 plasmid with the TMVΩ–containing reporter plasmids pOp6Ω -GUS (pOp6Ω) and pH-TOP, or with the pOp-GUS-derivative pOp^{BK}-GUS (Baroux *et al.*, 2005) (pOp). Data for pH-TOP are combined from three independently constructed plasmids pH-TOP-A, -E, and -K (see Experimental procedures).
(d) The GUS activities directed by CaMV35S::LhG4 in leaf tissue of individual pH-Luc transformants are plotted against their corresponding luciferase activities. The dashed lines demark those points that are within the highest 30% of the population for each.
(e, f) Seeds of inducible lines pH2, pH9, pV3, 4c and wild-type (wt) *Columbia* were germinated and grown in closed Petri dishes containing MS medium either with 10 μM dexamethasone for 12 days (black bars) or without dexamethasone for 7 days followed by transfer to liquid MS medium for 2 days and induction with 10 μM dexamethasone for 3 days (grey bars). GUS activity was then measured in three replicate pools of eight to 10 seedlings in each case. (e) Comparison of pOp-GUS(g2) line 4c with pV-TOP line pV3. (f) Comparison of the same pOp-GUS and pV-TOP lines with pH-TOP lines pH2 and pH9.
(g) Uninduced activity in seedlings grown as in (e) and (f) but with addition of DMSO in place of dexamethasone.
(h) Time course of induction. Nine-day-old seedlings of lines pH2, pH9, pV3, 4c and control wt *Columbia* were transferred from Petri dishes into liquid MS medium and incubated for 3 days before dexamethasone was added to 20 μM. Immediately prior to addition of dexamethasone and 1, 2, 4, 8, 16, 32, 64 and 128 h later, 10–12 seedlings were pooled and extractable GUS activity was determined. All GUS activities are expressed as pmol 4-MU min^{-1} μg^{-1} protein and error bars show standard deviations.

line LhGR-N(4c) while the pH-TOP lines exhibited 30- and 90-fold higher activities. The higher activities obtained with the pH-TOP lines are most probably attributable to the presence of the TMV Ω sequence.

The uptake of inducing chemicals can be poor in plants grown in closed culture vessels such as Petri dishes (Aoyama and Chua, 1997; Åstot *et al.*, 2000; Gatz *et al.*, 1992). Similar observations were made with pOp/LhGR-N but Figure 3(e,f) shows that this effect was significantly reduced with the pV-TOP and pH-TOP lines.

The uninduced activity in the pV-TOP and pH-TOP lines was generally higher than that observed with pOp-GUS(g2), particularly in liquid-grown seedlings (Figure 3g). Nevertheless, even in the worst case, pH2, addition of dexamethasone resulted in more than 10 000-fold induction of GUS activity compared with 1000-fold with pOp-GUS(g2) in line 4c. Thus the new reporters offer higher fold induction and higher absolute expression levels and are likely to be of advantage over pOp unless the critical parameter in the experiment is minimal uninduced expression (but see the discussion of pH-ipt below).

We next determined the induction kinetics of pV-TOP and pH-TOP by measuring the accumulation of GUS activity in liquid-grown seedlings following dexamethasone application. As shown in Figure 3(h), increased GUS activity was evident within 2 h of induction with pH-TOP and within 4 h with pV-TOP whereas no significant increase was detected with pOp-GUS before 8 h. In all cases GUS activity continued to increase for the next 5 days, owing probably to the stability of this enzyme (Jefferson, 1987).

We next asked whether pV-TOP and pH-TOP exhibited improved GUS induction characteristics in the greenhouse. A 20-μM dexamethasone solution was poured into trays on which pots containing flowering plants were standing. Samples were taken from rosette leaves at various time points up to 128 h after induction and were assayed for GUS activity. At the final time point, GUS activity induced from pOp-GUS(g2) in line 4c was only 7 pmol 4-MU min^{-1} μg^{-1} protein, approximately 10-fold lower than the activity typically observed *in vitro*, whereas GUS activity in pV3 was 165 pmol 4-MU min^{-1} μg^{-1} protein, 20-fold higher than 4c, and in the pH-TOP lines it was an order of magnitude higher still (Figure 4a). In the pV-TOP and pH-TOP lines, GUS activity in rosette leaves was induced approximately 8 h after dexamethasone application below the soil and continued to increase for 128 h (Figure 4b). The relative activities of pV3, pH2 and pH9 in rosette leaves were reproduced in all other organs indicating that dexamethasone is transported to most parts of the plant (Figure 4c,d). Uninduced activities in these tissues were barely above background in any case (Figure 4e). Histochemical staining of rosette leaves of pV-TOP and pH-TOP lines confirmed (i) the absence of detectable GUS activity prior to induction, (ii) the induction of GUS activity within a few hours of dexamethasone application, and (iii) the increased GUS activity relative to pOp-GUS (Figure 5). When dexamethasone was applied via the soil, GUS activity appeared first in the vascular system and only later in other tissues, whereas painting leaves with dexamethasone resulted in homogeneous induction of GUS activity across the leaf within 6 h. When only one half of the leaf was painted and tested 24 h later for GUS activity, staining was confined to the painted area indicating that diffusion or lateral transport of dexamethasone within the leaf is limited over this period. Nevertheless most tissues can receive dexamethasone via the vascular system as GUS staining of diverse organs 24 h after dexamethasone application to the soil resulted in a GUS staining pattern that resembled that of the CaMV35S>>GUS plants (Figure 5f).

We next asked whether the induced GUS activity observed in individual pH-TOP transformants was indicative of the expression level of a divergently transcribed gene cloned in the polylinker. To do this we used a pH-TOP derivative, pH-Luc that carries a luciferase coding sequence in its polylinker. pH-Luc was introduced into CaMV35S::LhG4 activator line 47/6 and the GUS and luciferase activities in leaf tissues were determined in T_2 seedlings of 17 randomly selected lines. As shown in Figure 3(d), the luciferase activity correlated rather poorly with the GUS activity which consequently had little predictive value in any individual line. Similar observations were made with pH-Luc in tobacco (Samalova *et al.*, 2005), indicating that in each species, sequence-specific factors can significantly influence the accumulation of each gene product in individual transgenic lines.

Expression of the ipt *gene can be effectively controlled by the pOp/LhGR system in Arabidopsis*

To confirm that LhGR could regulate pOp6, pV-TOP, and pH-TOP as stringently as pOp^{BK} (Figure 1; Baroux *et al.*, 2005; Lexa *et al.*, 2002) we placed the *A. tumefaciens ipt* gene (Heidekamp *et al.*, 1983) under the control of each promoter. The *ipt* gene catalyses cytokinin biosynthesis in plant cells and evokes phenotypic abnormalities at very low expression levels (Böhner and Gatz, 2001; Medford *et al.*, 1989). These constructs were introduced into the CaMV35S::LhGR activator line 4c-S5/7 (Experimental procedures). For the pH-TOP derivative, pH-ipt, only five transformants were recovered reflecting the generally low transformation rate obtained with this vector backbone.

T_1 plants and T_2 seedlings obtained with each plasmid were first scored for *ipt*-related phenotypes in the absence of dexamethasone. As shown in Table 1, the great majority of T_2 lines were phenotypically normal in the absence of dexamethasone. We confirmed this observation using growth medium containing 3% sucrose which we have found to enhance weak *ipt*-related growth phenotypes (data not shown). T_2 seedlings germinated and grown in the

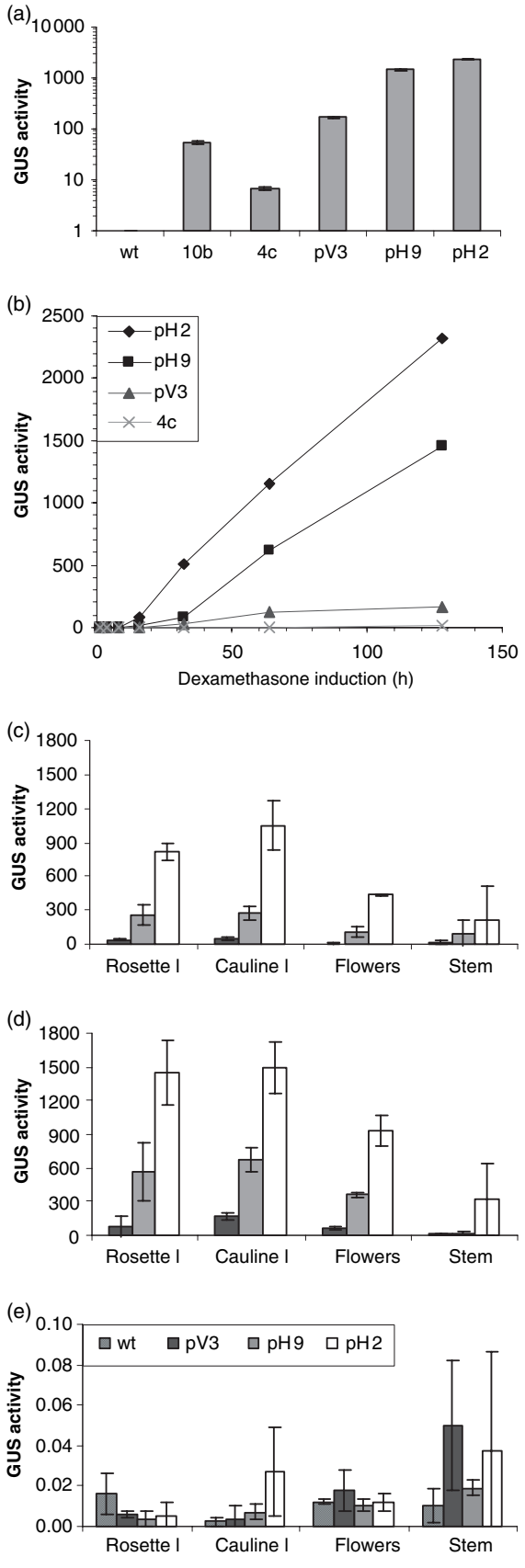

presence of dexamethasone were scored for induced *ipt* phenotypes which were categorized as weak, intermediate, or strong (examples for pOp^{BK}-ipt are shown in Figure 6a). Table 1 shows that 90–100% of T2 families exhibited inducible *ipt* phenotypes and that most pOp6-ipt, pV-ipt, and pH-ipt lines were categorized as strong whereas the pOp^{BK}-ipt families exhibited a range of weak to strong phenotypes. Some pOp6-ipt families exhibited an extreme phenotype not observed amongst the other families (Figure 6b–e). We concluded that although a slightly higher proportion of the pOp6 and pV-TOP lines exhibit weak uninduced *ipt* phenotypes, the improved reporters were as stringently regulated as the original pOp promoter in most transgenic lines.

To test this conclusion we measured root growth rate, a sensitive indicator of weak *ipt* expression, on dexamethasone-free medium. Lines that exhibited strong or extreme induced phenotypes had root growth rates that were indistinguishable from the pOp-GUS controls in the absence of inducer (Figure 6f). This confirmed that the improved promoters exhibit undetectable basal activity and that LhGR is subject to stringent repression in the absence of exogenous inducer.

When 16 T_3 seedlings from three independent homozygous pOp6-ipt and pV-ipt lines were germinated on dexamethasone-containing medium, the *ipt* phenotype was observed in all cases indicating that improved promoters provide stable and reliable expression into the T_3 generation (for examples see Figure 6g,h).

Full induction of the pOp6-ipt and pV-ipt phenotypes was achieved with a 10-fold lower concentration of dexamethasone than was necessary with pOp^{BK}-ipt (Figure 6g–i). In contrast, when GUS activity was measured in pV-ipt seedlings that had been germinated on dexamethasone-containing medium (data not shown) or induced for 48 h in liquid medium (Figure 6j) the dose–response curve was similar to that for pOp-GUS with 50% induction requiring approximately 0.2 μM dexamethasone. The apparent discrepancy in the relative GUS and *ipt* responses may reflect a threshold for full expression of the *ipt* phenotype and it may be that

Figure 4. Induction of GUS activity in greenhouse-grown plants.
(a, b) Four-week-old greenhouse-grown plants of lines pH2, pH9, pV3, and 4c were treated once by subterraneous irrigation with 900 ml of 20 μM dexamethasone as described in Experimental procedures.
(a) GUS activity in each line 128 h after dexamethasone treatment compared with wild-type (wt) *Columbia* plants and the CaMV35S>>GUS line 10b.
(b) Time course of accumulation of GUS activity in lines pH2, pH9, pV3, 4c between 0 and 128 h after dexamethasone treatment.
(c–e) Two-week-old seedlings of lines pH2, pH9, pV3 grown on MS medium lacking dexamethasone were transferred into soil and were either watered with 300 ml of 20 μM dexamethasone every 2–3 days for 3 weeks (d), or grown for 2 weeks without dexamethasone before treatment with the inducing solution for 1 week (c), or grown for 3 weeks without addition of dexamethasone (e). GUS activity was then determined in rosette leaves, cauline leaves, inflorescences, and stems (from the base of the inflorescence) in three replicate samples each comprising tissue from three independent plants. All GUS activities are expressed as pmol 4-MU min^{-1} μg^{-1} protein and error bars show standard deviations.

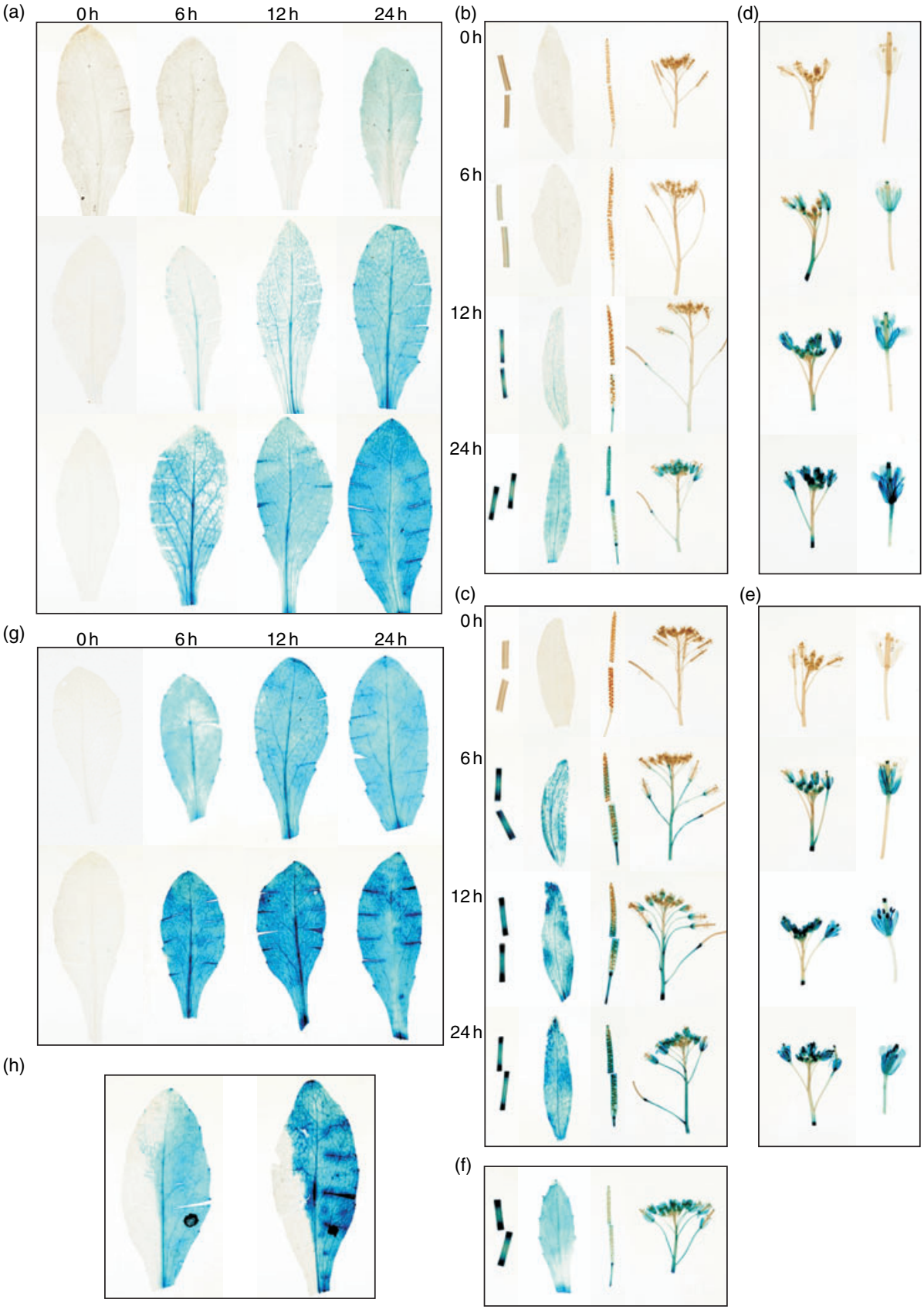
(a)
0 h
6 h
12 h
24 h
(b)
0 h
6 h
12 h
24 h
(d)
(c)
0 h
6 h
12 h
24 h
(e)
(f)
(g)
0 h
6 h
12 h
24 h
(h)

Table 1 Incidence and severity of *ipt*-related phenotypes in induced and uninduced Arabidopsis plants

	–Dex (T_1 and T_2)			+Dex (T_2)						
	No. lines	No. leaky lines	%	++++	+++	++	+	–	No. induced lines	%
pOp^{BK}-ipt	31	1	3	0	6	13	8	4	27	87
pOp6-ipt	43	9	21	4	14	0	0	2	18	90
pV-ipt	38	4	11	0	14	0	0	0	14	100
pH-ipt	5	1*	20	0	4	0	0	0	4	100

For each of the plasmids indicated, the left-hand side of the Table indicates the total number of lines studied in either the T_1 or T_2 generation (no. lines) in the absence of dexamethasone treatment (–Dex); the number of leaky lines and the percentage of the total (%) are shown in subsequent columns. The leaky lines all exhibited uninduced *ipt* phenotypes similar to the weak category described below except for one plant (*) whose phenotype was sufficiently severe that it died in the greenhouse. The right-hand side of the Table indicates the percentage (%) of T_2 lines that exhibited inducible *ipt* phenotypes when seedlings were germinated on dexamethasone-containing MS medium together with the number classified as strong (+++, retarded and aberrant growth of all organs, e.g. Figure 6c,d), intermediate (++, plants yellow with increase anthocyanin pigmentation and wrinkled leaves), or weak (+, plants pale green with serrated leaves). (–) indicates no visible *ipt* phenotype and (++++) indicates an extreme phenotype in which seedlings cease to develop before cotyledons are fully expanded (Figure 6b).

this is achieved with sub-saturating dexamethasone concentrations in the best pOp6- and pV-ipt lines.

Induction of ipt *expression does not result in increased steady-state* KNOX *transcript abundance in young seedlings*

Having established that LhGR-N is an effective tool for regulating *ipt* expression in *vivo*, we used it to ask whether class I KNOX (Knotted1 type homoeobox) expression lies downstream of cytokinin biosynthesis. It has been shown in a number of studies that ectopic KNOX expression results in increased cytokinin levels (Hewelt *et al.*, 2000; Kusaba *et al.*, 1998; Ori *et al.*, 1999; Tamaoki *et al.*, 1997). However, Arabidopsis seedlings carrying a heat-shock-inducible *ipt* gene contain markedly increased steady-state transcript levels of two class I KNOX genes, *BP/KNAT1* and *STM*, after 14 days of daily heat-shock treatment (Rupp *et al.*, 1999). This raises the possibility that cytokinin activates KNOX gene expression. We used pOp^{BK}-ipt lines that exhibited a range of *ipt* phenotypes to test whether KNOX expression is indeed sensitive to induced cytokinin levels.

When RT-PCR was performed 48 h after addition of dexamethasone to 14-day-old seedlings no pronounced or reproducible increase in *BP* transcript abundance was detected in dexamethasone-treated seedlings, even in lines that exhibited strong *ipt* phenotypes (Figure 6k). Similar results were obtained when *STM* transcripts were analysed in seedlings (data not shown). Expression of *BP* and *STM* was also assayed in leaf tissue to determine whether *ipt* expression is sufficient to activate KNOX expression in tissues where their expression is normally repressed (Figure 6l). In agreement with Figure 6(k) and previous observations (Rupp *et al.*, 1999) dexamethasone did not elevate steady-state transcript abundance for either gene. Dexamethasone application did however increase the abundance of the rapidly cytokinin-induced (D'Agostino *et al.*, 2000; Hoth *et al.*, 2003) *ARR5* transcript in leaf tissue (Figure 6l) and in seedlings of lines that exhibited strong or intermediate *ipt* phenotypes but not in a line which exhibited only weak *ipt* phenotypes, nor in the 4c-S7 activator line (Figure 6k). The *ipt*-induced increases in *ARR5* transcript abundance in lines 13, 14, 22, and 25, although small, were reproducible and similar in magnitude to those observed 24 h after induction of *ipt* expression by (Hoth *et al.*, 2003). We concluded that induction of *ipt* transcription in these seedlings resulted in increased cytokinin activity (as indicated by increased *ARR5* transcript abundance), but did not increase *KNOX* transcript abundance under these conditions.

Discussion

LhGR as a regulated transgene expression system for Arabidopsis

We show that the synthetic transcription factor LhG4 (Moore *et al.*, 1998) can be brought under stringent glucocorticoid control by fusion of a rat GR LBD to its amino terminus. This

Figure 5. Distribution of induced GUS activity in greenhouse-grown plants.
(a–c) Five-week-old greenhouse-grown plants were treated by subterraneous irrigation with 300 ml of 20 μM dexamethasone and samples were collected for histochemical GUS staining 0, 6, 12 and 24 h later.
(a) Rosette leaves of lines 4c (upper row), pV3 (middle row) and pH2 (lower row).
(b, c) Stems, cauline leaves, siliques, and inflorescences of pV3 and pH2 respectively.
(d, e) Inflorescences of pV3 and pH2 plants, respectively, were cut and stood in a 20-μM dexamethasone solution for the indicated times then stained for GUS activity. Young inflorescence tissue and a single flower are pictured for each time point.
(f) CaMV35S>>GUS control line 10b indicating the pattern of expression directed by CaMV35S.
(g) Rosette leaves of 5-week-old plants of lines pV3 (upper row) and pH2 (lower row) were painted with a 20-μM dexamethasone solution and stained for GUS activity as in (a).
(h) One half of a rosette leaf of 5-week-old plants of lines pV3 (left) and pH2 (right) was painted with a 20-μM dexamethasone solution and stained for GUS activity 24 h later as in (a). The painted half was marked with an indelible black dot. In (a) to (h), incisions were made in the leaves and siliques and samples were incubated at 28°C to improve the access of the GUS staining solution to internal tissues.

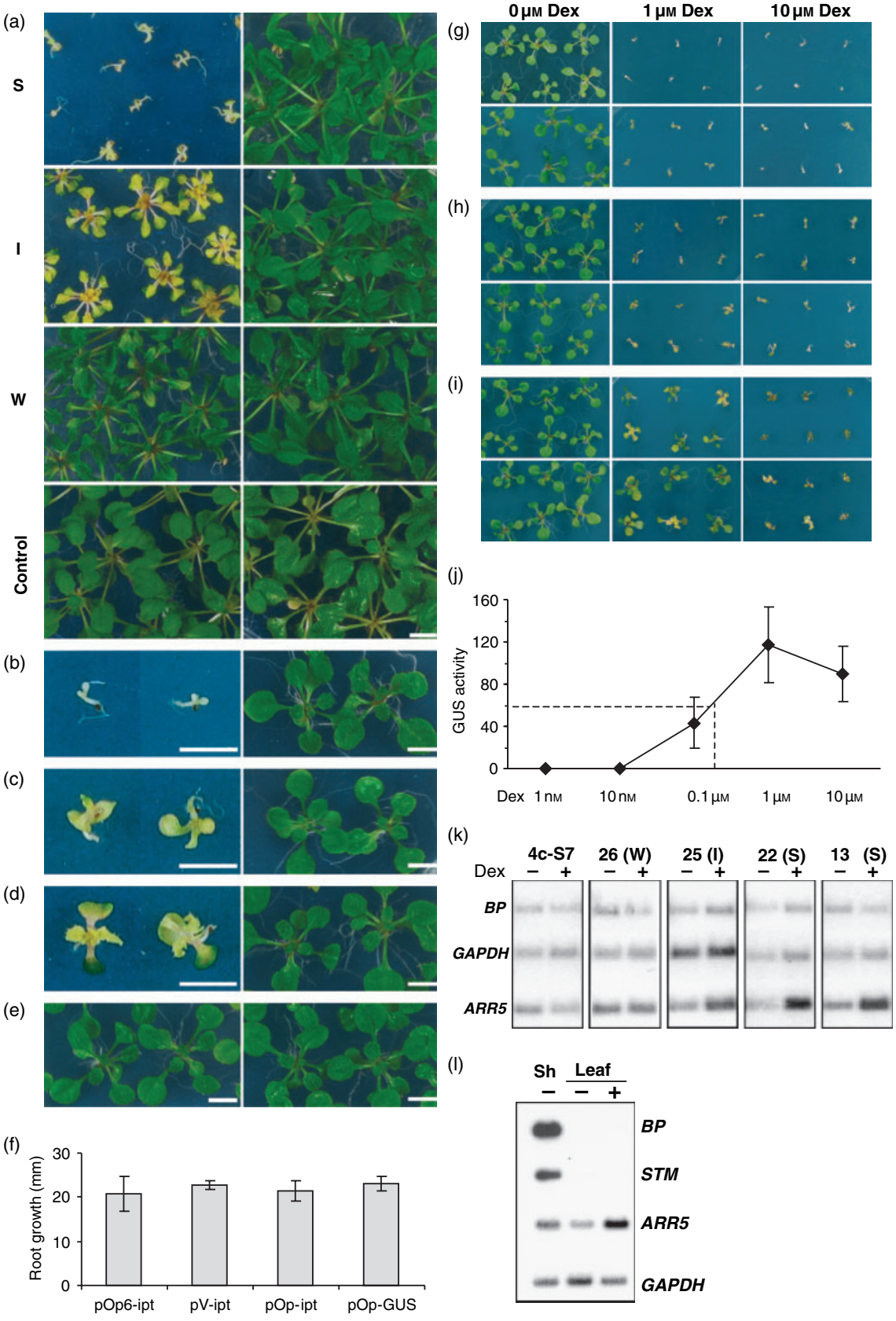
(a)
S
I
W
Control
(b)
(c)
(d)
(e)
(f)
Root growth (mm)
30
20
10
0
pOp6-ipt
pV-ipt
pOp-ipt
pOp-GUS
(g)
0 µM Dex
1 µM Dex
10 µM Dex
(h)
(i)
(j)
GUS activity
160
120
80
40
0
Dex 1 nM
10 nM
0.1 µM
1 µM
10 µM
(k)
4c-S7
26 (W)
25 (I)
22 (S)
13 (S)
Dex
− + − + − + − + − +
BP
GAPDH
ARR5
(l)
Sh
Leaf
− − +
BP
STM
ARR5
GAPDH

modified transcription factor, LhGR, can activate the pOp-GUS(g2) reporter line as efficiently as LhG4 indicating that the *lac* repressor moiety of LhG4 can accept substantial additional protein sequence at its amino terminus despite its proximity to the DNA-binding helices (residues 6–25). The close proximity of the GR LBD to the DNA-binding helices of LhGR may account for its efficient repression by steric hindrance when bound to the HSP90 complex (Picard, 1993, 2002). The stringency of repression that is mediated by GR LBD was demonstrated by use of LhGR and improved target promoters to control expression of the *A. tumefaciens ipt* gene (Heidekamp *et al.*, 1983) which alters plant development at relatively low expression levels (Böhner and Gatz, 2001; Schmülling, 2002). Even in conjunction with the original pOp promoter, induced phenotypes were more severe than those previously reported for Arabidopsis seedlings expressing *ipt* from heat shock promoters but without the adverse consequences of heat shock treatment on Arabidopsis growth (Medford *et al.*, 1989; Rupp *et al.*, 1999).

Consistent with the reports of Kang *et al.* (1999), Zuo *et al.* (2000), and others, we found that dexamethasone does not interfere with Arabidopsis development, although ethanol should be avoided as a solvent for dexamethasone as it is inhibitory even at 0.1% v/v in sterile culture media. In our experience DMSO is a benign solvent even at a final concentration of 0.1% v/v and in practice final concentrations below 0.02% v/v can be used. The adverse developmental consequences associated with activation of the dexamethasone-inducible GVG system in Arabidopsis, *Lotus japonicus*, and rice (Andersen *et al.*, 2003; Kang *et al.*, 1999; Ouwerkerk *et al.*, 2001; Zuo and Chua, 2000) can be attributed most probably to the properties of its Gal4 DNA-binding domain or its activation domain (VP16 from *Herpes simplex* virus) rather than GR LBD or dexamethasone (Gälweiler *et al.*, 2000; Kang *et al.*, 1999; Zuo and Chua, 2000; Zuo *et al.*, 2000).

Eshed *et al.* (2001) introduced the convention *PROMOTER* >>*TARGET* to denote the use of the two-component pOp/LhG4 system to express a gene of interest under control of a particular promoter (i.e. *PROMOTER::LhG4* + *pOp::TARGET*). We propose the convention *PROMOTER*>GR>*TARGET* to denote the use of LhGR to achieve inducible expression of a gene of interest (in this case *CaMV35S*>GR>*uidA* and *CaMV35S*>GR>*ipt*).

LhGR-mediated expression showed stable inheritance into the T_3 in all pOp-GUS and pOp-ipt lines tested. Furthermore, line LhGR-N(4c) that we chose for most of our subsequent work was first generated in 1998 and, after crossing to wild-type and elimination of the pOp-GUS(g2) reporter locus by segregation in F_2 progeny, it has been continuously used for crossing or retransformation work with other pOp-derivatives up to the T_8 generation.

The pOp/LhGR system can be maximally induced with approximately 1 μM dexamethasone and induction to 50% of maximum requires about 0.2 μM. Thus it is roughly 10-fold more sensitive than the previously reported GVG system in tobacco which required 10 and 3 μM for full and 50% induction respectively (Aoyama and Chua, 1997). This difference is unlikely to reflect differences in the susceptibility of these two species to dexamethasone treatment as the concentration of dexamethasone required for 50% induction of the pOp/LhGR system in tobacco is only 2 nM (Samalova *et al.*, 2005), approximately 100-times lower than that required in Arabidopsis.

We show that improved pOp promoters carrying six copies of an ideal *lac* operator positioned to facilitate simultaneous occupancy can be stably maintained in *E. coli* and exhibit improved expression characteristics in conjunction with LhG4 and LhGR. The new promoters are typically 10- to 20-fold more efficient than pOp in transgenic Arabidopsis and a further 10-fold increase in induced expression levels can be achieved by using pH-TOP which incorporates the TMV Ω translational enhancer. The improvement in the level of induced gene expression is not accompanied by loss of dynamic range and the induction factor of 10^4 obtained with pH-TOP lines compares favourably with other inducible systems in Arabidopsis and other species (Aoyama and

Figure 6. Dexamethasone-inducible *ipt* expression.

(a) Phenotypes of seedlings grown in the presence (left-hand panels) or absence (right-hand panels) of 20 μM dexamethasone. pOp^{BK}-ipt lines were chosen to represent strong (S), intermediate (I) and weak (W) phenotypes; control seedlings contain pH-Luc in the 4c-S5 background and express GUS and luciferase rather than *ipt* in response to dexamethasone application.

(b–e) Detail of 17-day-old T_2 seedlings of pOp6-ipt line 16 (b), pV-ipt line 23 (c), pOp^{BK}-ipt line 13 (d) and control line pH-Luc (e) grown on MS plates containing hygromycin and either 10 μM dexamethasone (left panels) or DMSO (right panels). The most strongly activated lines are shown. Bars = 0.5 cm.

(f) Average primary root growth ±SD (mm) over 3 days in seedlings of the pOp6-ipt, pV-ipt, and pOp^{BK}-ipt lines shown in (b)–(d) compared with pOp-GUS line 4c in the absence of dexamethasone.

(g–i) T_3 seedlings of pOp6-ipt lines 4-3 and 16-1 (g), pV-ipt lines 10-1 and 5-3 (h), and pOp^{BK}-ipt lines 11-2 and 13-1 (i) all of which are homozygous for the reporter loci were germinated and grown on MS plates containing either 0, 0.1, or 10 μM dexamethasone for 14 days, then photographed.

(j) Twelve-day-old seedlings of pV-ipt line 23 were incubated for 48 h in liquid medium and then induced with dexamethasone at the concentrations indicated for 48 h before being assayed for GUS activity. Activities (pmol 4-MU min^{-1} μg^{-1} protein ±SD) were measured in three independent samples of eight to 10 seedlings for each concentration of dexamethasone. The dotted line indicates the dexamethasone concentration that induces half-maximal GUS activity.

(k) RT-PCR analysis of *BP*, *GAPDH*, and *ARR5* transcripts in 14-day-old seedlings of pBIN-LhGR-N activator line 4c-S7 (4c-S7) and pOp^{BK}-ipt lines 26, 25, 22, and 13 incubated for 48 h in liquid medium containing 10 μM dexamethasone (+) or 0.1% DMSO (–); (S), (I), and (W) indicate the severity of the *ipt* phenotype exhibited by each line when grown on dexamethasone-containing medium as illustrated in (a).

(l) RT-PCR analysis of *BP*, *STM*, *ARR5*, and *GAPDH* transcript abundance in plants of pOp^{BK}-ipt line 14 (intermediate phenotype) grown for 7 days on MS medium then transferred to medium with (+) or without (–) dexamethasone for 14 days prior to analysis of total shoot tissue (Sh) or expanded leaves (leaf). At the time of harvesting, plants on dexamethasone exhibited clear cytokinin-overexpression phenotypes.

Chua, 1997; Böhner *et al.*, 1999; Martinez *et al.*, 1999; Padidam *et al.*, 2003; Roslan *et al.*, 2001; Zuo *et al.*, 2000). Although pH-TOP transformants exhibited marginally higher uninduced GUS activities, it was possible to obtain phenotypically normal pH-ipt lines that were strongly inducible. Indeed the induced phenotypes observed with pV-ipt and pH-ipt were stronger than those previously described in Arabidopsis (Medford *et al.*, 1989; Rupp *et al.*, 1999). GUS and *ipt* expression from pH-TOP or pV-TOP were stably inherited into the T_3 generation and beyond.

Surprisingly, GUS and Luc activities in pH-Luc transformants were poorly correlated indicating that factors acting outside the operator array can influence the expression of individual genes, some of which may be more prone to silencing. This is consistent with recent data indicating that 'position effects' on strong transgene promoters in Arabidopsis are predominantly attributable to sequence-specific thresholds of mRNA accumulation that trigger post-transcriptional gene silencing (Butaye *et al.*, 2004; Schubert *et al.*, 2004). These data also highlight the importance of maximizing translation efficiency to achieve stable high-level accumulation of gene product and in this respect the TMV Ω sequences in pH-TOP may prove advantageous. Despite the poor correlation between LhG4-mediated GUS and Luc activities in pH-Luc transformants, we believe that the pV-TOP and pH-TOP arrangement still offers some advantages over pOp6. The best 30–50% of the pH-Luc population with respect to GUS activity also included the best 30–50% with respect to luciferase expression so the number of lines to be screened for expression of the gene of interest can be reduced at least twofold if plants are first tested for inducible GUS activity. Furthermore, when working with individual pV-TOP or pH-TOP, lines the divergent GUS reporter provided confirmation that dexamethasone had been applied effectively to the tissue of interest and proved useful in correlating phenotype with genotype in populations of seedlings segregating activator or reporter loci.

The improved promoters offered a particular advantage in closed culture vessels and soil-grown plants where dexamethasone-induced GUS activities were up to 200 times higher than with pOp and substantially exceeded those reported for other inducible systems in Arabidopsis (Roslan *et al.*, 2001). Maximum activation was achieved in liquid culture, but other methods such as germination on or transfer to inductive solidified medium led to widespread and homogeneous distribution of dexamethasone. Difficulties have been reported in sustaining 17-β-estradiol application to Arabidopsis seedlings prompting the incorporation of a Cre-*lox* switch into the XVE system to generate sectors with constitutive expression following inducer application (Chen *et al.*, 2003). The lack of transpiration in closed culture vessels has previously been reported to be a limiting factor in other inducible systems (Aoyama and Chua, 1997; Åstot *et al.*, 2000; Gatz *et al.*, 1992) and we found that induced levels of GUS expression in pV-TOP and pH-TOP seedlings were roughly twofold lower in closed Petri dishes than in liquid medium. As with ethanol and estradiol, foliar application of dexamethasone was effective (Roslan *et al.*, 2001; Zuo *et al.*, 2001) but it appears that ecdysone analogues cannot be effectively applied this way (Padidam *et al.*, 2003).

The original pOp promoter has been used already in a number of significant developmental studies (Baroux *et al.*, 2001a,b; Brewer *et al.*, 2004; Lenhard and Laux, 2003; Lenhard *et al.*, 2001, 2002; Lexa *et al.*, 2002; Schoof *et al.*, 2000; Segal *et al.*, 2003) and we envisage that the improved promoters will increase the number of applications for which the pOp/LhG4 and pOp/LhGR systems are suitable. For example in the accompanying article we show that the improved promoters provide effective dexamethasone-inducible expression with LhGR in tobacco whereas the original pOp promoter did not (Samalova *et al.*, 2005). The improved promoters may prove beneficial in other crop and model species, including perhaps monocots where the pOp/LhG4 system has already been applied (Segal *et al.*, 2003). It is also likely that weaker promoters can now be used in conjunction with LhG4 and LhGR to direct practically useful tissue-specific expression of transgenes of interest (Baroux *et al.*, 2005). We expect also that the improved pOp promoters will result in amplification of expression levels. Indeed our experience to date indicates that pOp6, pV-TOP, and pH-TOP are most beneficial in conjunction with weaker activator lines. For example when using LhG4 constructs as enhancer traps, we have found that pOp4-GUS and pOp6-GUS lines detect enhancer traps at higher frequencies than the best pOp-GUS lines
(S. Rutherford, H. Townley, F. Brandizzi, J. Craft, Y. Wang, I. Jepson, A. Martinez, I. Moore, Oxford University, Oxford, UK, unpublished data).

It is worth noting that when we used the pGREEN-based pH-TOP vector we observed transformation efficiencies that were approximately 2 orders of magnitude lower than those obtained with pV-TOP and that many of the lines we did recover exhibited incomplete resistance to antibiotic. Nevertheless by screening sufficient seed we were able to recover useful transformants with all the pH-TOP derivatives we have tested.

ipt *expression does not induce KNOX-gene expression in young Arabidopsis seedlings*

The existence of functional links between cytokinin and KNOX activity was first indicated by the fact that *ipt* overexpression phenotypes mirror aspects of KNOX misexpression phenotypes including leaf serration and the presence of ectopic meristematic activity on leaves (Sinha *et al.*, 1993; discussed in Hay *et al.*, 2004). However subsequent work to establish whether cytokinins lie upstream or downstream of *KNOX* activity has led to conflicting findings

(Hay *et al.*, 2004). While several studies indicate that increased KNOX expression can elevate cytokinin levels (e.g. Ori *et al.*, 1999), evidence that the converse may be true comes from the observation that Arabidopsis plants subjected to daily heat-shock-inducible *ipt* expression for 14 days exhibited substantial increases in the steady-state abundance of mRNA for the class-I KNOX genes *STM* and *BP* (Rupp *et al.*, 1999). To account for these observations it has been proposed that KNOX protein activity and cytokinin action may form a feed-forward loop or that elevated cytokinin levels may increase the size of the apical meristem and thus the proportion of meristematic transcripts in the sample (Hay *et al.*, 2004). However we detected no significant increase in transcript levels for BP or STM in *CaMV35S*>GR>*ipt* seedlings or leaf tissues treated with dexamethasone. In contrast under the same conditions we did observe elevated transcript levels for the cytokinin-responsive gene ARR5 indicating that this mode of dexamethasone treatment was effective in elevating cytokinin activity. Our results are in good agreement with genome-wide expression data which indicate that neither *STM* nor *BP* are induced in young seedlings expressing *ipt* (Hoth *et al.*, 2003) or treated with exogenous cytokinin for 24 h (Rashotte *et al.*, 2003) although a transient increase was observed for *BP* at 6 h (Hoth *et al.*, 2003).

The markedly contrasting observations of Rupp *et al.* (1999) may reflect technical differences in experimental procedure, for example the specific properties of the promoters used (*Drosophila melanogaster* HSP70 versus CaMV35S) or differences in culture conditions. However, a plausible explanation for the dramatically increased steady state KNOX mRNA levels detected by Rupp *et al.* (1999) lies with the age of the plant material they analysed. Rupp *et al.* (1999) initiated their heat-shock treatment on 14-day-old seedlings and assayed transcript levels after a further 2 weeks of daily treatment. This overlaps the stage at which Arabidopsis forms its axillary meristems (Stirnberg *et al.*, 1999). Outgrowth of the axillary meristems is normally inhibited by apical dominance which is then released progressively following the transition to flowering (Stirnberg *et al.*, 1999). As apical dominance can be suppressed by *ipt* over-expression (Böhner and Gatz, 2001; Faiss *et al.*, 1997; McKenzie *et al.*, 1998; Medford *et al.*, 1989; Rupp *et al.*, 1999) we suggest that the heat-treated 4-week-old seedlings studied by Rupp *et al.* (1999) may have possessed substantially more active axillary meristems than the controls thus increasing the amount of meristem tissue in the samples. Consistent with this interpretation, Rupp *et al.* (1999) found that the increase in *KNOX* gene transcript abundance was confined to portions of the plant that included the stem and the young leaves and thus presumably also the axillary meristems. In contrast, the 10- to 16-day-old seedlings used in this and other studies (Hoth *et al.*, 2003; Rashotte *et al.*, 2003) were probably too young to possess apically inhibited axillary meristems (Stirnberg *et al.*, 1999). Indeed, we found that *CaMV*>GR>*ipt* lines germinated and grown on dexamethasone did not exhibit precocious release of axillary meristems within the first 3 weeks despite clear evidence of cytokinin overproduction (Figure 6a), although subsequently they developed the typical bushy phenotype (not shown).

The position of the GR LBD domain influences the expression characteristics of LhGR

In contrast to LhGR-N, fusions carrying GR LBD at other positions in the LhG4 molecule exhibited poor dexamethasone induction characteristics. Notably, LhGR-C which carried GR LBD at the C-terminus of LhG4 exhibited significant transcriptional activity in the absence of inducer. The leakiness of LhGR-C was most pronounced in transient expression assays but was also observed in transgenic seedlings. This was surprising as the LBD is carboxy terminal in GR and in the majority of artificial fusions, most of which exhibit tight regulation of their target promoter. However, there has been a report of leaky expression from such a fusion in Arabidopsis (Lloyd *et al.*, 1994).

One possible explanation for the leakiness of LhGR-C is that in this configuration a transcription activation domain lies too distant from GR LBD to be repressed by steric hindrance in the HSP90 complex (Picard, 1993). Such a domain would not be expected to affect the regulation of LhGR-N which is unlikely to bind DNA when complexed with HSP90. Any such domain is unlikely to be part of the Gal4 moiety of LhGR as mutational analysis of this activation domain indicates that sequences essential for its transcriptional activity in Arabidopsis reside near its carboxy terminus (Rutherford *et al.*, unpublished data) which lies close to the GR LBD in LhGR-C. However, we found that *lacI*^{His17} alone has some intrinsic transcriptional activity in transient expression and that this activity is quantitatively similar to the uninduced activity observed with LhGR-C (Figure 1d, lacI^{His17}). Thus *lacI*^{His17} may possess a weak activation domain that is not subject to repression by the interaction of GR LBD with HSP90 in LhGR-C. LhGR-C is not leaky in tobacco however (Samalova *et al.*, 2005), so it must be hypothesized that this domain is inactive in this species. Interestingly, we have also observed that the rat GR LBD sequence is subject to premature polyadenylation in Arabidopsis but not in tobacco (data not shown) and work is underway to establish whether this may account for the leakiness of LhGR-C in Arabidopsis.

In conclusion, the pOp/LhGR system provides a stringent dexamethasone-inducible system for Arabidopsis, complementing other alcohol- and estradiol-inducible systems that have been used successfully (Guo *et al.*, 2003; Laufs *et al.*, 2003; Roslan *et al.*, 2001; Zuo *et al.*, 2001) as discussed in the accompanying article (Samalova *et al.*, 2005). One

advantage of the pOp/LhGR system is that reporter plasmids are compatible with the increasing number of tissue-specific LhG4 and LhGR driver lines that have been constructed (Baroux *et al.*, 2005; Eshed *et al.*, 2001; Schoof *et al.*, 2000) or identified by enhancer trapping (Rutherford *et al.*, unpublished data; H. Townley, Y. Wang, I. Moore, Oxford University, Oxford, UK, unpublished data). Furthermore, LhGR is effective in tobacco (Samalova *et al.*, 2005) and LhG4 has been used successfully in maize (Segal *et al.*, 2003) so it is possible that these constructs may be useful in the study of other model and crop species.

Experimental procedures

Bacteria and plant material

Escherichia coli strain DH5α and *A. tumefaciens* strain GV3101::pMP90 (Koncz and Schell, 1986) were used throughout. *Arabidopsis thaliana* plants were of the Columbia ecotype. Unless otherwise specified, plants were grown with 16 h light, 8 h dark at 21–22°C either on a 3:1 soil:vermiculite mixture or on Murashige and Skoog (1962) medium (Sigma-Aldrich, Poole, UK) solidified with 0.8 or 0.9 % Bacto Agar (DIFCO, Le Pont de Claix, France) supplemented with 1.5% sucrose and the appropriate antibiotics or inducers. Plants were transformed using the vacuum infiltration method described by Bechtold *et al.* (1993). Transformants were selected by the addition of hygromycin or kanamycin (Melford Ltd, Ipswich, UK) to plant culture media at concentrations of 15 and 50 μg ml^{-1} respectively.

The CaMV35S::LhGR activator lines 4c-S5 and 4c-S7 used in this work were derived from CaMV35S::LhGR/pOp-GUS(g2) line 4c by crossing to wild-type and selecting for F_3 families that had lost pOp-GUS(g2) locus but were homozygous for the CaMV35S::LhGR locus. The two homozygous lines 4c-S5 and 4c-S7 were used interchangeably and are denoted here by 4c-S5/7. The CaMV::LhG4 activator lines 14/1 and 47/6 were a kind gift of Dr D. Grosskopf and Prof. K. Palme, MPI fuer Zuechtungsforschung and University of Freiburg, Germany.

Plasmid construction

DNA cloning, manipulation and analyses were all performed according to standard procedures (Ausubel *et al.*, 1993). Details of the cloning steps are provided in Supplementary Material, but are summarized here.

Construction of LhGR-N, -I, -C. The LBD of the glucocorticoid receptor (residues 508–795) (EMBL accession number: M14053.Emrod) was amplified from pBIΔGR (Lloyd *et al.*, 1994) by polymerase chain reaction (PCR) using primers that introduced *Spe*I restriction sites at each end (forward primer: 5′-AGACTAGTGAAGCTCGAAAAACAAAG-3′; reverse primer: 5′-GTACTAGTAGATTTTTGATGAAACAGAAG-3′; *Spe*I sites underlined). To construct pKI-LhGR-I this fragment was inserted into the *Spe*I site that separates the *lac* repressor and *GAL4* domains of LhG4 in pKI-HisAGal4 (Moore *et al.*, 1998). To construct LhGR-N and -C, the GR domain was inserted at *Nhe*I sites that had been introduced either immediately after the ATG codon or before the stop codon of LhG4 using primers 5′-ATCCTCGAGAACAATGGCTAGCAAACCGGTAACGTTATA-3′; reverse primer: TCACTAGTCTAGCTAGCCTCTTTTTTTGGGTTTGGTG-3′ (*Nhe*I sites underlined) respectively. LhGR-N, -I, and -C were expressed under control of CaMV 35S expression signals in plasmids pKI102 (Moore *et al.*, 1998) and pBINPLUS (van Engelen *et al.*, 1995).

Construction of pOp1-pOp6. To generate a 52-bp repeat carrying an ideal *lac* operator sequence (underlined) and an *Xba*I site (double underlined) the following oligonucleotides were annealed: NOP1: 5′CAAGAAATCTAGAAAGAAGAAAGGGAAGAGAAAGAATTGTGAGCGCTCACAATTGAAAGA3′; NOP2: 5′CTAGTCTTTCAATTGTGAGCGCTCACAATTCTTTCTCTTCCCTTTCTTCTTTCTAGATTTCTTGAGCT3′. The annealed sequence carried *Sac*I- and *Spe*I-compatible cohesive ends and was ligated into the corresponding sites of pBluescript SK-II to generate pNOP1. The *Sac*I-*Spe*I fragment was reisolated from this vector and repeatedly inserted into the compatible *Sac*I and *Xba*I sites of the same vector to generate multimers of the 52 bp repeat which were then used to replace the operators of pOp-GUS derivative pOp^{BK}-GUS (Baroux *et al.*, 2005) to generate pOp1-GUS to pOp6-GUS. The position relative to the minimal promoter of the most proximal operator in pOp^{BK}-GUS and pOp1-GUS to pOp6-GUS is identical.

The construction of pH-TOP and pV-TOP involved numerous cloning steps outlined in Supplementary Material. pH-TOP is based on the pGREEN vector system (Hellens *et al.*, 2000) while pV-TOP is based on pVKH18 and pOp^{BK}-GUS (Baroux *et al.*, 2005). pOp^{BK}-ipt, pOp6-ipt, and pH-ipt were all constructed as described in Samalova *et al.* (2005). pV-ipt was constructed by isolating the *ipt* coding region from pH-ipt as a *Sal*I-*Sma*I fragment and inserting it into the *Sal*I and Klenow-treated *Bam*HI sites of pV-TOP.

RNA gel blot analysis

Total RNA was isolated from plant tissues based on the method described by Chomczynski and Sacchi (1987), and was dissolved in formamide. Total RNA (10 μg) was used for RNA gel blot analysis as previously described (Moore *et al.*, 1997). For hybridization, a GUS probe was isolated from pRT103GUS (Töpfer *et al.*, 1987) as an *Xho*I/*Hin*dIII fragment. A fragment derived from an Arabidopsis eIF-4A cDNA was used as a loading control as described (Moore *et al.*, 1997).

RT-PCR

For RT-PCR analysis of CaMV35S>GR>*ipt* seedlings, 1 μg of total RNA that had been extracted from seedlings using RNeasy (Qiagen, Crawley, UK) was used for cDNA synthesis with an oligo dT primer and Superscript II RT (Invitrogen, Paisley, UK). PCR primers specific for *BP* /*KNAT1*, *STM*, *ARR5* and *GAPDH* were used in separate reactions over 25 cycles. The specific annealing temperatures used were 55, 59 and 53°C for *KNAT1*, *ARR5* and *GAPDH* respectively. The products were detected by Southern hybridization with gene-specific probes. Primers were as follows: *BP*, KNAT1-F, TGACAACAGCACCACTCCTC, KNAT1-R GTTTCCCCTCCGCTGTTATT (Hay *et al.*, 2002); *ARR5*, ARR5-F, TGCGTCCCGAGATGTTAGAT, ARR5-R, AAGCCGAAAGAATCAGGACA; *GAPDH* GAPDH-F, CACTTGAAGGGTGGTGCCAAG, GAPDH-R, CCTGTTGTCGCCAACGAAGTC; *STM* STM-F, 5′ ATG GAG AGT GGT TCC AAC AG 3′; STM-R 5′ CCC TAA CAT TAA CTG TGA GC 3′.

Transient expression

The transient expression protocol was adapted from previous procedures (Abel and Theologis, 1994; Mass and Werr, 1989) for use

with protoplasts derived from a suspension culture of *A. thaliana* L*er* (gift of M. May, University of Oxford) as described in Supplementary Material. When testing LhGR-N, -I, and -C, 10 μg of reporter plasmid, and 20 μg of each activator plasmid were used. When testing pOp1-GUS to pOp6-GUS, 10 μg of each reporter plasmid was transfected either alone or with 10 μg of activator construct pKI-HisA-Gal4 (Moore *et al.*, 1998). For testing the GUS activity driven by pH-TOP and its precursors, 1 pmol of reporter plasmid was used with 5 μg of pKI-HisA-Gal4.

Dexamethasone treatments

Dexamethasone (Sigma-Aldrich) was dissolved at 20 or 30 mM in ethanol or 100 mM in dimethylsufoxide and kept at −20°C. Typically 10 or 20 μM dexamethasone was used for induction. For treatment of soil-grown plants with dexamethasone throughout their life cycle we have successfully used 20 μM dexamethasone diluted from a 30-mM stock in ethanol to prevent accumulation of DMSO in the soil but ethanol is avoided as solvent *in vitro* owing to its detrimental effects on plant growth. Plants were germinated and grown on plates containing Murashige and Skoog (1962) salts and minimal organic supplements (Sigma) with 1.5% v/v sucrose (MS medium) unless otherwise stated. MS was supplemented with dexamethasone solution or an equivalent volume of DMSO. For induction in liquid medium, up to 120 12-day-old seedlings were transferred from solidified medium to conical flasks (250 ml) containing 100 ml MS medium. The flasks were kept on an orbital shaker (110 rpm) in an incubator with a 16-h photoperiod at 21°C for 2–3 days prior to addition of dexamethasone or DMSO at the appropriate concentration. After the appropriate period of incubation, the seedlings were harvested, blotted dry, and frozen in liquid nitrogen prior to the GUS assay. In the greenhouse, Arabidopsis plants grown in 22 cm × 35 cm trays with 24-cell inserts filled with a commercial peat compost (Horticultural Trade Association, Emerald Range Universal Compost, Goundrey's Ltd, Oxfordshire, UK) mixed 3:1 with vermiculite. Tap water containing the desired concentration of dexamethasone was poured into the bottom of each tray. Trays were either irrigated once with 900 ml of dexamethasone solution or irrigated every 2–3 days with 300 ml of solution as the plants required water. For fluorimetric GUS assays a transverse strip of leaf tissue was taken from the three oldest healthy leaves of four independent plants of each genotype. For leaf painting, a fine paintbrush was dipped into a 20-μM dexamethasone solution containing 0.02 % Silwet L-77 and brushed over one side of each treated leaf.

GUS, luciferase, and root growth assays

Fluorimetric and histochemical GUS assays were performed as described in Jefferson (1987) except that incubations were at 28°C with 0.5 mM potassium ferricyanide/ferrocynaide and repeated vacuum infiltration (up to 5×) which resulted in more even staining of internal mature leaf tissues. Incubations at this temperature proceeded for 24 h. Stained tissues were imaged using a Leica MZFLIII microscope (Leica Microsystems, Milton Keynes, UK) and CoolSNAP digital camera (Roper Scientific Ltd, Universal Imaging Corporation, Marlow, UK). For screening GUS positive seedlings, dexamethasone-induced histochemical staining with pH-TOP lines was usually evident within 10–20 min at room temperature. For the comparison of GUS and luciferase activities in pH-Luc transformants, two leaves were dissected from young Arabidopsis plants and used for a GUS assay and two for a luciferase assay. For each plant line, three seedlings were assayed independently. Luciferase was assayed using the 'Luciferase Assay System' from Promega (Promega Corporation, Madison, WI, USA) according to the manufacturer's instructions. Briefly, tissue was quick-frozen in liquid nitrogen and ground to a powder. Tissue was then resuspended at room temperature in 1x CCLR buffer with further homogenization. The sample was centrifuged in order to pellet tissue debris, and the supernatant retained for assay. Protein concentration was determined using the Bio-Rad Protein Assay Reagent (Bio-Rad Ltd, Hemel, Hempsted, UK), using bovine serum albumen as a standard. For each sample 10 μg of cell lysate was added to 100 μl of Luciferase Assay Reagent in a multi-well plate and assayed using a plate reading luminometer. For root growth assays plants were germinated on selective medium and after 10 days, hygromycin-resistant seedlings were transferred to fresh MS plates that were placed vertically in the growth room and the growth of the primary root was measured over a period of 3 days. Nine to 10 seedlings were used for each measurement.

Acknowledgements

We are grateful to Csaba Koncz for plasmids, to Patrick Gallois and Robert Blanvillain for seed of pOpGUS(g2), to Deborah Grosskopf and Klaus Palme for seeds of 35S::LhG4 activator lines, to Hazel Betts for seed of pV3, pH2 and pH9, and to Anthony Hall and Andrew Millar for providing a luciferase clone. We are grateful to Dr H. Batoko for providing the initial pNOP1 plasmid. This work was supported by BBSRC research grants to IM and MT and by a BBSRC Industrial CASE Studentship to JC.

Supplementary Material

The following material is available from http://www.blackwellpublishing.com/products/journals/suppmat/TPJ/TPJ2342/TPJ2342sm.htm

Figure S1. Dexamethasone-inducible GUS activity in primary transformants and characteristics of typical LhGR-N, -I, and -C transformants.

Figure S2. IPTG can reduce LhGR-mediated activation of pOp-GUS.

Figure S3. Ethanol but not dexamethasone retards seedling development *in vitro*.

Figure S4. The pOp6 operator array is stable in *Escherichia coli*.

Figure S5. LhG4-mediated GUS activity in individual pOp4-GUS and pOp6-GUS transformants.

Table S1 GUS activity in 10-day-old seedlings grown in liquid medium with or without dexamethasone

Supplementary Experimental Procedures: plasmid construction; transient expression.

Supplementary References

References

Abel, S. and Theologis, A. (1994) Transient transformation of Arabidopsis leaf protoplasts: a versatile experimental system to study gene expression. *Plant J*, **5**, 421–427.

An, H., Roussot, C., Suarez-Lopez, P. *et al.* (2004) CONSTANS acts in the phloem to regulate a systemic signal that induces photoperiodic flowering in Arabidopsis. *Development*, **131**, 3615–3626.

Andersen, S.U., Cvitanich, C., Hougaard, B.K., Roussis, A., Gronlund, M., Jensen, D.B., Frokjaer, L.A. and Jensen, E.O. (2003) The glucocorticoid-inducible GVG system causes severe growth defects in both root and shoot of the model legume *Lotus japonicus*. *Mol. Plant Microbe Interact.* **16**, 1069–1076.

Aoyama, T. and Chua, N.-H. (1997) A glucocorticoid-mediated transcriptional induction system in transgenic plants. *Plant J.* **11**, 605–612.

Aoyama, T., Dong, C.H., Wu, Y., Carabelli, M., Sessa, G., Ruberti, I., Morelli, G. and Chua, N.-H. (1995) Ectopic expression of the Arabidopsis transcriptional activator *At*HB-1 alters leaf cell fate in tobacco. *Plant Cell*, **7**, 1773–1785.

Åstot, C., Dolezal, K., Nordstrom, A., Wang, Q., Kunkel, T., Moritz, T., Chua, N. and Sandberg, G. (2000) An alternative cytokinin biosynthesis pathway. *Proc. Natl Acad. Sci. USA*, **97**, 14778–14783.

Ausubel, F.M., Brent, R., Kingston, R.E., Moore, D.D., Seidman, J.G., Smith, J.A. and Struhl, K. (eds) (1993) *Current Protocols in Molecular Biology*. New York: Wiley.

Baroux, C., Blanvillain, R. and Gallois, P. (2001a) Paternally inherited transgenes are down-regulated but retain low activity during early embryogenesis in Arabidopsis. *FEBS Lett.* **509**, 11–16.

Baroux, C., Blanvillain, R., Moore, I.R. and Gallois, P. (2001b) Transactivation of *BARNASE* under the AtLTP1 promoter affects the basal pole of the embryo and shoot development of the adult plant in Arabidopsis. *Plant J.* **28**, 503–515.

Baroux, C., Blanvillain, R., Betts, H., Batoko, H., Craft, C., Martinez, A., Gallois, P. and Moore, I. (2005) Predictable activation of tissue-specific expression from a single transgene locus using the pOp/LhG4 transactivation system in Arabidopsis. *Plant Biotech. J.* **3**, 91–101.

Bechtold, N., Ellis, J. and Pelletier, G. (1993) *In planta* agrobacterium-mediated gene-transfer by infiltration of adult *Arabidopsis thaliana* plants. *CR. Acad. Sci. III-VIE*, **316**, 1194–1199.

Blackwood, E.M. and Kadonaga, J.T. (1998) Going the distance: a current view of enhancer action. *Science*, **281**, 60–63.

Blair, W.S., Bogerd, H.P., Madore, S.J. and Cullen, B.R. (1994) Mutational analysis of the transcription activation domain of RelA: identification of a highly synergistic minimal acidic activation module. *Mol. Cell. Biol.* **14**, 7226–7234.

Böhner, S. and Gatz, C. (2001) Characterization of novel target promoters for the dexamethasone-inducible/tetracycline-repressible regulator TGV using luciferase and isopentenyl transferase as sensitive reporter genes. *Mol. Gen. Genet.* **264**, 860–870.

Böhner, S., Lenk, I., Rieping, M., Herold, M. and Gatz, C. (1999) Transcriptional activator TGV mediates dexamethasone-inducible and tetracycline-inactivable gene expression. *Plant J.* **19**, 87–95.

Brewer, P.B., Howles, P.A, Dorian, K., Griffith, M.E., Ishida, T., Kaplan-Levy, R.N., Kilinc, A. and Smyth, D.R. (2004) *PETAL LOSS*, a trihelix transcription factor gene, regulates perianth architecture in the Arabidopsis flower. *Development*, **131**, 4035–4045.

Bruce, W., Folkerts, O., Garnaat, C., Crasta, O., Roth, B. and Bowen, B. (2000) Expression profiling of the maize flavonoid pathway genes controlled by estradiol-inducible transcription factors CRC and P. *Plant Cell*, **12**, 65–80.

Butaye, K.M.J., Goderis, I.J.W.M., Wouters, P.F.J., Pues, J.M.T.G., Delaure, S.L., Brokaert, W.F., Depicker, A., Cammue, B.P.A. and De Bolle, M.F.C. (2004) Stable high-level gene expression in *Arabidopsis thaliana* using gene silencing mutants and matrix attachment regions. *Plant J.* **39**, 440–449.

Caddick, M.X., Greenland, A.J., Jepson, I., Krause, K.-P., Qu, N., Riddell, K.V., Salter, M.G., Schuch, W., Sonnewald, U. and Tomsett, A.B. (1998) An ethanol inducible gene switch for plants used to manipulate carbon metabolism. *Nat. Biotechnol.* **16**, 177–180.

Chen, S., Hofius, D., Sonnewald, U. and Bornke, F. (2003) Temporal and spatial control of gene silencing in transgenic plants by inducible expression of double-stranded RNA. *Plant J.* **36**, 731–740.

Chomczynski, P. and Sacchi, N. (1987) Single step method of RNA isolation by acid guadinium thiocyanate phenol chloroform extraction. *Anal. Biochem.* **162**, 156–159.

D'Agostino, I.B., Deruere, J. and Kieber, J.J. (2000) Characterization of the response of the Arabidopsis response regulator gene family to cytokinin. *Plant Physiol.* **124**, 1076–1717.

Deveaux, Y., Peaucelle, A., Roberts, G.R., Coen, E., Simon, R., Mizukami, Y., Traas, J., Murray, J.A.H., Doonan, J.H. and Laufs, P. (2003) The ethanol switch: a tool for tissue-specific gene induction during plant development. *Plant J.* **36**, 818–930.

Emery, J.F., Floyd, S.K., Alvarez, J., Eshed, Y., Hawker, N.P., Izhaki, A., Baum, S.F. and Bowman, J.L. (2003) Radial patterning of Arabidopsis shoots by class *IIIHD-ZIP* and *KANADI* genes. *Curr. Biol.* **13**, 1768–1774.

van Engelen, F.A., Molthoff, J.W., Connor, A.J., Nap, J.P., Pereira, A. and Stiekema, W.J. (1995) pBINPLUS: an improved plant transformation vector based on pBIN19. *Transgenic. Res.* **4**, 288–290.

Eshed, Y., Baum, S.F., Perea, J.V. and Bowman, J.L. (2001) Establishment of polarity in lateral organs of plants. *Curr. Biol.* **11**, 1251–1260.

Faiss, M., Zalubilová, J., Strnad, M. and Schmülling, T. (1997) Conditional transgenic expression of the *ipt* gene indicates a function for cytokinins in paracrine signaling in whole tobacco plants. *Plant J.* **12**, 401–415.

Gallie, D.R., Sleat, D.E., Watts, J.W., Turner, P.C. and Wilson, T.M.A. (1987) A comparison of eukaryotic viral 5′-leader sequences as enhancers of mRNA expression *in vivo*. *Nucleic Acids Res.* **15**, 8693–8711.

Gälweiler, L., Conlan, R.S., Mader, P., Palme, K. and Moore, I. (2000) The DNA-binding activity of Gal4 is inhibited by methylation of the Gal4 binding site in plant chromatin. *Plant J.* **23**, 143–157.

Gatz, C. and Lenk, I. (1998) Promoters that respond to chemical inducers. *Trends Plant Sci.* **3**, 352–358.

Gatz, C., Frohberg, C. and Wendenburg, R. (1992) Stringent repression and homogeneous de-repression by tetracycline of a modified CaMV35S promoter in intact transgenic tobacco plants. *Plant J.* **2**, 397–404.

Glass, R.E. (1982) *Gene Function: E. coli and its Heritable Elements*. London: Croom Helm Ltd.

Gross-Hardt, R., Lenhard, M. and Laux, T. (2002) *WUSCHEL* signaling functions in interregional communication during Arabidopsis ovule development. *Genes Dev.* **16**, 1129–1138.

Guo, H.-S., Fei, J.-F., Xie, Q. and Chua, N.-H. (2003) A chemical-regulated inducible RNAi system in plants. *Plant J.* **34**, 383–392.

Hay, A., Kaur, H., Phillips, A., Hedden, P., Hake, S. and Tsiantis, M. (2002) The gibberellin pathway mediates KNOTTED1-type homeobox function in plants with different body plans. *Curr. Biol.* **12**, 1557–1565.

Hay, A., Craft, J. and Tsiantis, M. (2004) Plant hormones and homeoboxes: bridging the gap? *Bioessays*, **26**, 395–404.

Heidekamp, F., Dirkse, W.G., Hille, J. and van Ormondt, H. (1983) Nucleotide sequence of the *Agrobacterium tumefaciens* octopine Ti plasmid-encoded *tmr* gene. *Nucleic Acids Res.* **11**, 6211–6223.

Hellens, R.P., Edwards, E.A., Leyland, N.R., Bean, S. and Mullineaux, P.M. (2000) pGreen: a versatile and flexible binary Ti vector for *Agrobacterium*-mediated plant transformation. *Plant Mol. Biol.* **42**, 819–832.

Hewelt, A., Prinsen, E., Thomas, M., van Onckelen, H. and Meins, F., Jr. (2000) Ectopic expression of maize *knotted1* results in the cytokinin-autotrophic growth of cultured tobacco tissues. *Planta*, **210**, 884–889.

Holtorf, S., Apel, K. and Bohlmann, H. (1995) Comparison of different constitutive and inducible promoters for the overexpression of transgenes in *Arabidopsis thaliana*. *Plant Mol. Biol.* **29**, 637–646.

Hoth, S., Ikeda, Y., Morgante, M., Wang, X., Zuo, J., Hanafey, M.K., Gaasterland, T., Tingey, S.V. and Chua, N.-H. (2003) Monitoring genome-wide changes in gene expression in response to endogenous cytokinin reveals targets in *Arabidopsis thaliana*. *FEBS Lett.* **555**, 373–380.

Hudson, M.E., Lisch, D.R. and Quail, P.H. (2003) The *FHY3* and *FAR1* genes encode transposase-related proteins involved in regulation of gene expression by the phytochrome A-signaling pathway. *Plant J.* **34**, 453–471.

Jefferson, R.A. (1987) Assaying chimeric genes in plants: the GUS gene fusion system. *Plant Mol. Biol. Rep.* **5**, 387–405.

Kadonaga, J.T. (2004) Regulation of RNA polymerase II transcription by sequence-specific DNA binding factors. *Cell*, **116**, 247–257.

Kang, H.-G., Fang, Y. and Singh, K.B. (1999) A glucocorticoid-inducible transcription system causes severe growth defects in Arabidopsis and induces defence-related genes. *Plant J.* **20**, 127–133.

Koncz, C. and Schell, J. (1986) The promoter of TL-DNA controls the tissue specific expression of chimaeric genes carried by a novel type of *Agrobacterium* binary vector. *Mol. Gen. Genet.* **204**, 383–396.

Kusaba, S., Kano-Murakami, Y., Matsuoka, M., Tamaoki, M., Sakamoto, T., Yamaguchi, I. and Fukumoto, M. (1998) Alteration of hormone levels in transgenic tobacco plants overexpressing the rice homeobox gene OSH1. *Plant Physiol.* **116**, 471–476.

Laufs, P., Coen, E., Kronenberger, J., Traas, J. and Doonan, J. (2003) Separable roles of *UFO* during floral development revealed by conditional restoration of gene function. *Development*, **130**, 785–796.

Lehming, N., Sartorius, J., Niemoller, M., Genenger, G., v Wilcken-Bergmann, B. and Muller-Hill, B. (1987) The interaction of the recognition helix of lac repressor with lac operator. *EMBO J.* **6**, 3145–3153.

Lenhard, M. and Laux, T. (2003) Stem cell homeostasis in the Arabidopsis shoot meristem is regulated by intercellular movement of CLAVATA3 and its sequestration by CLAVATA1. *Development*, **130**, 3163–3173.

Lenhard, M., Bohnert, A., Jurgens, G. and Laux, T. (2001) Termination of stem cell maintenance in Arabidopsis floral meristems by interactions between *WUSCHEL* and *AGAMOUS*. *Cell*, **105**, 805–814.

Lenhard, M., Jurgens, G. and Laux, T. (2002) The *WUSCHEL* and *SHOOTMERISTEMLESS* genes fulfil complementary roles in Arabidopsis shoot meristem regulation. *Development*, **129**, 3195–3206.

Lewis, M., Chang, G., Horton, N.C., Kercher, M.A., Pace, H.C., Schumacher, M.A., Brennan, R.G. and Lu, P. (1996) Crystal structure of the lactose operon repressor and its complexes with DNA and inducer. *Science*, **271**, 1247–1254.

Lexa, M., Genkov, T. and Brzobohaty, B. (2002) Inhibitory effects of elevated endogenous cytokinins on nitrate reductase in *ipt*-expressing tobacco are eliminated by short-term exposure to benzyladenine. *Physiol. Plant.* **115**, 284–290.

Lloyd, A.M., Schena, M., Walbot, V. and Davis, R.W. (1994) Epidermal cell fate determination in Arabidopsis: patterns defined by a steroid-inducible regulator. *Science*, **266**, 436–439.

Martinez, A., Sparks, C., Hart, C.A., Thompson, J. and Jepson, I. (1999) Ecdysone agonist-inducible transcription in transgenic tobacco plants. *Plant J.* **5**, 559–569.

Mass, C. and Werr, W. (1989) Mechanism and optimised conditions for PEG mediated DNA transformation transfection into plant protoplasts. *Plant Cell Rep.* **8**, 148–151.

McKenzie, M.J., Mett, V., Reynolds, P.H.S. and Jameson, P.E. (1998) Controlled cytokinin production in transgenic tobacco using a copper-inducible promoter. *Plant Physiol.* **116**, 969–977.

Medford, J.L., Horgan, R., El-Sawi, Z. and Klee, H.J. (1989) Alteration of endogenous cytokinins in transgenic plants using chimeric isopentenyl transferase gene. *Plant Cell*, **1**, 403–413.

Mett, V.L., Lochhead, L.P. and Reynolds, P.H.S. (1993) Copper-controllable gene expression system for whole plants. *Proc. Natl Acad. Sci. USA*, **90**, 4567–4571.

Mitsuhara, I., Ugaki, M., Hirochika, H. *et al.* (1996) Efficient promoter cassettes for enhanced expression of foreign genes in dicotyledonous and monocotyledonous plants. *Plant Cell Physiol.* **37**, 49–59.

Moore, I., Diefenthal, T., Zarsky, V., Schell, J. and Palme, K. (1997) A homolog of mammalian GTPase Rab2 is present in Arabidopsis and is expressed predominantly in pollen grains and seedlings. *Proc. Natl Acad. Sci. USA*, **94**, 762–767.

Moore, I., Gälweiler, L., Grosskopf, D., Schell, J. and Palme, K. (1998) A transcription activation system for regulated gene expression in transgenic plants. *Proc. Natl Acad. Sci. USA*, **95**, 376–381.

Müller, J., Oehler, S. and Müller-Hill, B. (1996) Repression of *lac* promoter as a function of distance, phase and quality of an auxiliary *lac* operator. *J. Mol. Biol.* **257**, 21–29.

Murashige, T. and Skoog, F. (1962) A revised medium for rapid growth and bioassays with tobacco tissue. *Physiol. Plant.* **15**, 493–497.

Ohno, C.K., Reddy, G.V., Heisler, M.G.B. and Meyerowitz, E.M. (2004) The Arabidopsis *JAGGED* gene encodes a zinc finger protein that promotes leaf tissue development. *Development*, **131**, 1111–1122.

Ori, N., Juarez, M.T., Jackson, D., Yamaguchi, J., Banowetz, G.M. and Hake, S. (1999) Leaf senescence is delayed in tobacco plants expressing the maize homeobox gene *knotted1* under the control of a senescence-activated promoter. *Plant Cell*, **11**, 1073–1080.

Ouwerkerk, P.B.F., de Kam, R.J., Hodge, J.H.C. and Meijer, A.H. (2001) Glucocorticoid-inducible gene expression in rice. *Planta*, **213**, 370–378.

Padidam, M. (2003) Chemically regulated gene expression in plants. *Curr. Opin. Plant Biol.* **6**, 169–177.

Padidam, M., Gore, M., Lu, D.L. and Smirnova, O. (2003) Chemical-inducible, ecdysone receptor-based gene expression system for plants. *Transgenic Res.* **12**, 101–109.

Picard, D. (1993) Steroid-binding domains for regulating the functions of heterologous proteins *in cis*. *Trends Cell Biol.* **3**, 278–280.

Picard, D. (2002) Heat-shock protein 90, a chaperone for folding and regulation. *Cell. Mol. Life Sci.* **59**, 1640–1648.

Picard, D. and Yamamoto, K.R. (1987) Two signals mediate hormone-dependent nuclear localisation of the glucocorticoid receptor. *EMBO J.* **6**, 3333–3340.

Rashotte, A.M., Carson, S.D.B., To, J.P.C. and Kieber, J.J. (2003) Expressing profiling of cytokinin action in Arabidopsis. *Plant Physiol.* **132**, 1998–2011.

Roslan, H.A., Salter, M.G., Wood, C.D. *et al.* (2001) Characterization of the ethanol-inducible *alc* gene-expression system in*Arabidopsis thaliana*. *Plant J.* **28**, 225–235.

Rupp, H.M., Frank, M., Werner, T., Strnad, M. and Schmülling, T. (1999) Increased steady state mRNA levels of the *STM* and *KNAT1* homeobox genes in cytokinins overproducing *Arabidopsis thaliana* indicate a role for cytokinins in the shoot apical meristem. *Plant J.* **18**, 557–563.

Rutherford, S. and Moore, I. (2002) The Arabidopsis Rab GTPase family: another enigma variation. *Curr. Opin. Plant Biol.* **5**, 518–528.

Sablowski, R.W.M. and Meyerowitz, E.M. (1998) A homolog of *NO APICAL MERISTEM* is an immediate target of the floral homeotic genes *APETALA3/ PISTILLATA*. *Cell*, **92**, 93–103.

Samalova, M., Brzobohaty, B. and Moore, I. (2005) pOp6/lhGR: a stringently regulated and highly responsive dexamethasone-inducible gene expression system for tobacco. *Plant J.* In press.

Schmülling, T. (2002) New insights into the functions of cytokinins in plant development. *J. Plant Growth Regul.* **21**, 40–49.

Schoof, H., Lenhard, M., Haecker, A., Mayer, K.F.X., Jurgens, G. and Laux, T. (2000) The stem cell population of Arabidopsis shoot meristem is maintained by a regulatory loop between the *CLAVATA* and *WUSCHEL* genes. *Cell*, **100**, 635–644.

Schubert, D., Lechtenberg, B., Forsbach, A., Gils, M., Bahadur, S. and Schmidt, R. (2004) Silencing in Arabidopsis T-DNA transformants: the predominant role of a gene specific RNA-sensing mechanism versus position effects. *Plant Cell*, **16**, 2561–2572.

Schwechheimer, C., Smith, C. and Bevan, M.W. (1998) The activities of acidic and glutamine-rich transcriptional activation domains in plant cells: design of modular transcription factors for high-level expression. *Plant Mol. Biol.* **36**, 195–204.

Segal, G., Song, R. and Messing, J. (2003) A new *opaque* variant maize by a single dominant RNA-interference-inducing transgene. *Genetics*, **165**, 387–397.

Simon, R., Igeno, M. and Coupland, G. (1996) Activation of floral meristem identity genes in Arabidopsis. *Nature*, **384**, 59–62.

Sinha, N.R., Williams, R.E., and Hake, S. (1993) Overexpression of the maize homeobox gene, *KNOTTED-1*, causes a switch from determinate to indeterminate cell fates. *Genes Dev.* **7**, 787–795.

Stirnberg, P., Chatfield, S.P. and Leyser, O.H.M. (1999) *AXR1* acts after lateral bud formation to inhibit lateral bud growth in Arabidopsis. *Plant Physiol.* **121**, 839–847.

Tamaoki, M., Kusaba, S., Kano-Murakami, Y. and Matsuoka, M. (1997) Ectopic expression of a tobacco homeobox gene, *NTH 15*, dramatically alters leaf morphology and hormone levels in transgenic tobacco. *Plant Cell Physiol.* **38**, 917–927.

Töpfer, R., Matzeit, V., Gronenborn, B., Schell, J. and Steinbiss, H.-H. (1987) A set of plant expression vectors for transcriptional and translational fusions. *Nucleic Acids Res.* **15**, 5890.

Weijers, D., van Hamburg, J.P., van Rijn, E., Hooykaas, P.J.J. and Offringa, R. (2003) Diphtheria toxin-mediated interregional communication seed development. *Plant Physiol.* **133**, 1882–1892.

Weinmann, P., Gossen, M., Hillen, W., Bujard, H. and Gatz, C. (1994) A chimeric transactivator allows tetracycline-responsive gene expression in whole plants. *Plant J.* **5**, 559–569.

Zuo, J. and Chua, N.-H. (2000) Chemical-inducible systems for regulated expression of plant genes. *Curr. Opin. Biotechnol.* **11**, 146–151.

Zuo, J., Niu, Q.-W. and Chua, N.-H. (2000) An estrogen receptor-based transactivator XVE mediates highly inducible gene expression in transgenic plants. *Plant J.* **24**, 265–273.

Zuo, J., Niu, Q.-W., Moller, S.G. and Chua, N.-H. (2001) Chemical-regulated, site-specific DNA excision in transgenic plants. *Nat. Biotechnol.* **19**, 157–161.

Universal Methods for Transgene Induction Using the Dexamethasone-Inducible Transcription Activation System pOp6/LhGR in *Arabidopsis* and Other Plant Species

Marketa Samalova,[1,2,3] Charlotte Kirchhelle,[2] and Ian Moore[2]

[1]CEITEC MU, Masaryk University, Brno, Czech Republic
[2]Department of Plant Sciences, University of Oxford, Oxford, United Kingdom
[3]Corresponding author: *marketa.samalova@ceitec.muni.cz*

Use of chemically inducible systems for transgene expression is a crucial requirement for modern plant biology research, as it allows (1) expression of transgenes that compromise plant viability or fertility when constitutively expressed and (2) spatiotemporal control of transgene expression levels. We describe the stringently regulated and highly responsive dexamethasone-inducible gene expression system pOp6/LhGR, which comprises the chimeric transcription activator LhGR and the corresponding pOp6 promoter. Upon induction, the LhGR activator binds to the pOp6 promoter and induces expression of the target gene of interest. We provide detailed protocols for inducing transgene expression at different developmental stages and in different plant species and discuss dexamethasone stability and use of its analogs. We also introduce new, versatile, GATEWAY-compatible binary vectors that are now available for the pOp6/LhGR system. © 2019 by John Wiley & Sons, Inc.

Keywords: chemically inducible gene expression • dexamethasone • glucocorticoid

How to cite this article:
Samalova, M., Kirchhelle, C., & Moore, I. (2019). Universal methods for transgene induction using the dexamethasone-inducible transcription activation system pOp6/LhGR in *Arabidopsis* and other plant species. *Current Protocols in Plant Biology*, e20089. doi: 10.1002/cppb.20089

INTRODUCTION

Chemically inducible systems for regulated gene expression are extremely useful for basic plant biology research as well as biotechnology applications. These systems are especially required for expression of gene products that interfere with regeneration, growth, or reproduction; for expression at different stages of plant development and for a specific duration; for conditional genetic complementation; and for co-suppression or overexpression studies. Temporal control can be particularly useful to de-convolve complex phenotypes related to transgene expression, as it allows monitoring of the progressive development of phenotype and may thus reveal primary effects before homeostatic mechanisms start to counteract them (e.g., Kirchhelle et al., 2016). Furthermore, use of an appropriate promoter can restrict target transgene expression to specific organs, tissues, or even cell types. Inducible expression systems like pOp6/LhGR, with their ability to control expression levels spatially and temporally, complement other technologies, like

CURRENT PROTOCOLS
A Wiley Brand

Current Protocols in Plant Biology e20089
Published in Wiley Online Library (wileyonlinelibrary.com).
doi: 10.1002/cppb.20089

amiRNA or the recent CRISPR-Cas9, creating a powerful set of tools for the generation of knock-down, knock-out, or chimeric plants.

The development of chemical-inducible systems for tight control of plant gene expression is a challenging task and an ongoing effort. A number of properties are required for an ideal system, such as very low basal expression levels, high inducibility, specificity, and a dynamic range of response with respect to an inducer. Additionally, both fast response and induction through various methods are desirable. An ideal system should work in several plant species and should not cause any adverse physiological effects in plants, nor should its inducer. The inducer is further required to show high specificity for the transgene and high efficiency at low concentrations and must not be found in target plants. Therefore, the components of such systems are usually derived from non-plant sources.

Inducible expression systems typically contain two transcription units: whereas the first unit employs a constitutive or tissue-specific promoter to express a chemical-responsive transcription factor, the second unit consists of multiple copies of the transcription factor–binding site linked to a minimal plant promoter, which is used to express the target gene. Over the years, we have invested considerable effort in developing the dexamethasone (Dex)-inducible transcription activation system pOp6/LhGR, which meets all the criteria outlined above (Craft et al., 2005; Samalova, Brzobohaty, & Moore, 2005). It comprises pOp6, a chimeric promoter that consists of *lac* operators (typically six copies, hence pOp6) cloned upstream of a minimal CaMV 35S promoter (–50 to +8). On its own, pOp6 does not produce detectable levels of transcript in plants (Craft et al., 2005). The chimeric transcription activator LhGR is a fusion between a high-affinity DNA-binding mutant of the *Escherichia coli lac* repressor *lacI*^{His17}, the transcription-activation-domain-II of *GAL4* from *Saccharomyces cerevisiae*, and the ligand-binding domain (LBD) of the rat glucocorticoid receptor (GR). In the absence of the steroid ligand Dex, the transcription factor LhGR is trapped in an inactive complex via interaction of the GR LBD and the heat-shock protein HSP90. However, upon induction with Dex, this complex is disrupted, and the LhGR activator binds to the pOp6 promoter and induces expression of the target gene of interest. The activator LhGR and the reporter comprising pOp6 and the gene of interest can be introduced into plants either on two separate T-DNAs or on a single T-DNA. We discuss advantages of these strategies and present a new set of binary GATEWAY-compatible vectors for LhGR expression.

The protocols in this unit describe use of the inducible pOp6/LhGR transgene expression system at different stages of plant development and in a range of plant species. Basic Protocol 1 provides instructions for use of the system in *Arabidopsis* seedlings under multiple conditions, such as on agar-solidified plates and in liquid medium. The Alternate Protocol provides an alternative method of use suited for time-lapse microscopy during the entire induction period through implementation of imaging chambers. Basic Protocol 2 describes two methods of use of the system in later developmental stages through watering or painting of soil-grown *Arabidopsis*. Basic Protocol 3 focuses on use of the pOp6/LhGR system in tobacco and other plant species.

STRATEGIC PLANNING

A number of vectors for transgene expression using the pOp6/LhGR system are already available (for details, see Craft et al., 2005; Moore, Samalova, & Kurup, 2006). Furthermore, a new set of versatile, GATEWAY-compatible plasmids are described later in this unit (see Commentary). These plasmids contain the activator (e.g., pBIN-LR-LhGR) and reporter (e.g., pOp6-GUS) on either two separate T-DNAs or a single T-DNA (e.g., pOpON2.1). Which one to choose depends on the type of application for which the system is used. In more complex genetic backgrounds (e.g., backgrounds with several recessive mutations), it is advantageous to use a construct that carries both the activator

and the reporter on a single T-DNA so that they can be introduced simultaneously. However, when such a vector is constructed, care must be taken to ensure that enhancers in the promoter that drive the activator do not activate the target promoter. Alternatively, separating the target promoter and the activator provides greater versatility. For example, when a gene is to be expressed in diverse patterns or at different developmental stages, a single reporter line can be activated in the desired pattern simply by re-transforming with activator constructs or by crossing into pre-existing activator lines (Baroux et al., 2005; Moore et al., 2006). Recently, a comprehensive tool set of inducible activator/driver lines targeting most cell types in *Arabidopsis*, with the focus on the three main meristems (RAM, SAM and the cambium), was created by Schurholz et al. (2018).

CAUTION: Dex is classified as a dangerous chemical (H360D, reproductive toxicity); therefore, personal protective equipment (PPE) such as protective gloves and clothing and eye/face protection is recommended while working.

CAUTION: Dimethyl sulfoxide (DMSO) is not a hazardous substance; however, PPE is also recommended (to avoid inhalation of vapor or mist).

DEXAMETHASONE-INDUCIBLE EXPRESSION OF TRANSGENES IN *ARABIDOPSIS* SEEDLINGS

BASIC PROTOCOL 1

This protocol describes how to effectively induce transgene expression in *Arabidopsis* seedlings using two different setups: either on agar-solidified plates or in liquid growth medium. Induction on plates containing agar-solidified medium (Figure 1A) has the advantage that the macroscopic phenotype (e.g., root length) can be observed directly and repeatedly throughout the induction period. In liquid medium (Figure 1B), maximum efficiency of induction can be achieved, but the phenotype can be distorted due to the growth conditions. Timing of the induction is flexible: the plants can be planted on Dex-containing medium for continuous induction from germination or transferred to Dex-containing medium at later developmental stages, depending on the experimental requirements. The methods are medium to high throughput and best suited for end-point studies.

Materials

Half-strength (½) MS (Murashige & Skoog, 1962) plates supplemented with or without Dex or DMSO (see recipe)
80% (v/v) ethanol (Sigma-Aldrich)
Arabidopsis thaliana transgenic seeds containing reporter and activator constructs (transformed using floral-dip method of Clough & Bent, 1998)
Liquid ½ MS medium supplemented with Dex or DMSO (see recipe)

Whatman filter paper (Sigma-Aldrich), cut into 5 × 5–cm squares
Laminar flow hood
1.5-ml microcentrifuge tube
1-ml Gilson pipet and sterile tip
Sterile toothpick
Micropore surgical tape (3M)
Plant growth cabinet (20°C, 16 hr light/8 hr dark)
Sterile forceps
6-well plates
Orbital shaker

Germination of Arabidopsis seedlings under sterile conditions

1. Prepare ½ MS plates supplemented with or without Dex or DMSO (as a control).

   If continuous transgene induction from germination is desired, seeds need to be plated on ½ MS supplemented with either an appropriate concentration of Dex or an equivalent

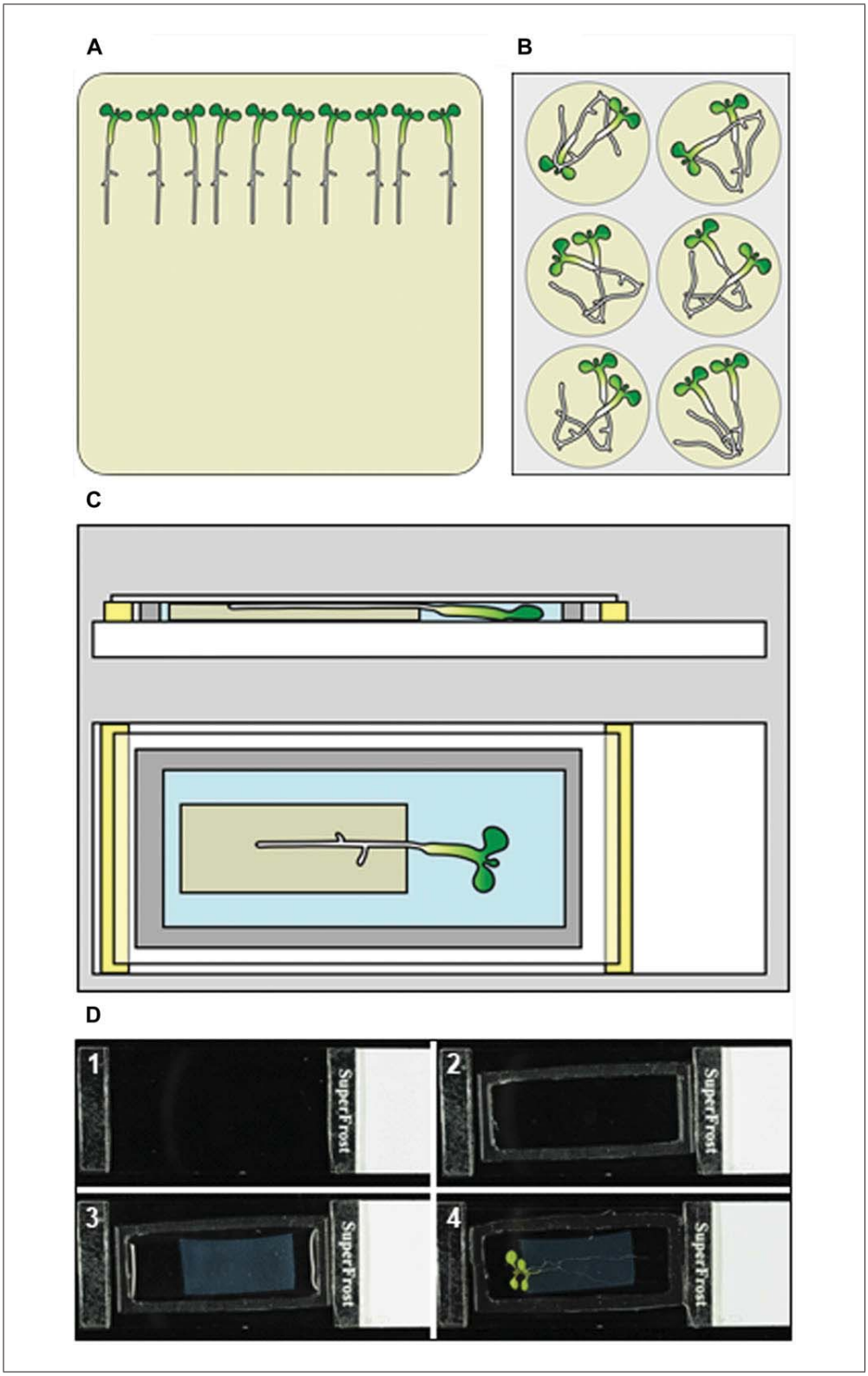

Figure 1 Induction of *Arabidopsis* seedlings. (**A**) Induction on agar-solidified growth medium. (**B**) Induction in liquid growth medium. (**C**) Induction in an imaging chamber. (**D**) Step-wise guide to imaging-chamber assembly. (1) Glass strips glued into place on a microscope slide. (2) Carolina Observation Gel gasket manufactured onto the slide. (3) Agar slab positioned and chamber filled with perfluorodecalin. (4) Seedlings placed onto the agar slab and imaging chamber closed with a coverslip. Reproduced in modified form from (Kirchhelle & Moore, 2017), with permission of the *Journal of Visualized Experiments: JoVE*.

volume of DMSO (see steps 7a and 7b). If plants will be transferred to Dex-containing medium at a later stage of development (see step 7a), prepare plain ½ MS plates.

2. Sterilize Whatman filter paper with 80% ethanol and leave to dry in a laminar flow hood.
3. Mix *Arabidopsis thaliana* transgenic seeds containing reporter and activator constructs with 1 ml of 80% ethanol in a 1.5-ml microcentrifuge tube by inversion, incubate for 5 min, pipet seeds onto the sterilized Whatman filter paper from step 2 using a 1-ml Gilson pipet with a sterile tip, and let seeds dry completely.
4. Wet tip of a sterile toothpick slightly by tapping it on a plate containing solidified ½ MS medium (see step 1). Pick seeds up individually with toothpick and place them onto plate in a straight line, 5 to 8 mm apart, leaving a distance of ≥1 cm from the top rim of the plate. Close plate with Micropore surgical tape.
5. Stratify seeds for ≥2 days at 4°C before transferring the plate to a plant growth cabinet (20°C, 16 hr light/8 hr dark) in vertical orientation.

   Stratification denotes short exposure of imbibed seeds to cold temperature to breach seed dormancy and synchronize germination.

   When we refer to seedling age throughout this unit, we mean the number of days after transfer into the plant growth cabinet.

Dexamethasone-inducible expression of transgenes on agar plates

6a. Prepare ½ MS plates supplemented with Dex or DMSO (as a control).

   Note that the appropriate concentration of Dex will vary. Maximum induction of the pOp6/LhGR system can be achieved with ~1 µM Dex (Craft et al., 2005), although depending on the transgene of interest, lower transgene expression levels may be desirable. Through application of sub-saturating concentrations of Dex, transgene expression can be titrated to desired levels (Craft et al., 2005).

7a. For transgene expression from germination, plate seeds as described in steps 3 to 5 onto a plate containing Dex and a second plate containing DMSO (as control). For transgene expression in older seedlings, germinate seedlings (see step 5) on plain ½ MS plates, grow for desired period of time, and then transfer seedlings onto a plate containing Dex and second plate containing DMSO (as a control) using sterile forceps.

Dexamethasone-inducible expression of transgenes in liquid medium

6b. Prepare liquid ½ MS medium supplemented with Dex (see step 6a) or DMSO (as a control) and aliquot into 6-well plates (5 ml per well).

7b. Using sterile forceps, transfer seedlings pre-grown on plates (see step 5) into liquid medium, taking care that the roots are fully submerged, and place them onto an orbital shaker in a plant growth cabinet (~80 rpm, 20°C, 16 hr light/8 hr dark).

   This protocol has been extensively tested for seedlings aged 5 to 12 days at the point of transfer and can be used for plants up to 4 weeks old. For practical reasons, we recommend using Basic Protocol 2 for older plants.

DEXAMETHASONE-INDUCIBLE EXPRESSION OF TRANSGENES IN IMAGING CHAMBERS

ALTERNATE PROTOCOL

This protocol describes how to induce transgene expression in *Arabidopsis* seedlings in imaging chambers (Figure 1C), rather than on agar-solidified plates or in liquid growth medium (Basic Protocol 1). The strategy is low to medium throughput and well suited for time-lapse studies involving repeated imaging using confocal laser scanning microscopy

(CLSM) throughout the induction period (Kirchhelle & Moore, 2017). Imaging chambers are manufactured directly on microscope slides using simple tools. In the imaging chambers, seedlings rest on an agar slab and are submerged in perfluorodecalin (PFD), maintaining physiological growth conditions for ≥48 hr (Kirchhelle & Moore, 2017).

Materials

Carolina Observation Gel (poly(dimethylsiloxane) gum, Carolina Biological Supply)
100% ethanol
Liquid ½ MS medium supplemented with Dex or DMSO (see recipe)
Difco Bacto agar
100 mM Dex stock solution
DMSO
Perfluorodecalin (PFD; F2 Chemicals)
Arabidopsis seedling(s) pre-grown on plain ½ MS plate(s) (see Basic Protocol 1)

Glass microscope slides (1-mm thickness, VWR International)
Glass cutter
Double-sided tape
Razor blades
Coverslips (22 × 50 mm)
50-ml Falcon tube
CLSM system

Creation of a Carolina Observation Gel gasket

1. Cut 2- to 3-mm-wide strips from the end of a glass microscope slide using a glass cutter and affix two glass strips to a second microscope slide ∼45 mm apart using double-sided tape (Figure 1D.1). Prepare ≥2 slides like this (with one imaging chamber for Dex induction and one as a DMSO control).

2. Place a ball of Carolina Observation Gel (∼2 cm in diameter) between the glass strips on a slide. Wet a second, unmodified slide with 100% ethanol and use this slide to flatten ball to the height of the glass strips. If necessary, trim excess gel with a razor blade wetted with 100% ethanol and repeat flattening.

3. Wet a razor blade with 100% ethanol. Remove part of gel to create a central chamber. Carefully trim remaining gel around the outside with a razor blade to create a gasket with a final wall thickness of approximately 1 to 2 mm (Figure 1D.2).

   The Carolina Observation Gel gasket prevents evaporation of PFD from the imaging chamber while allowing gas exchange. Use of glass strips ensures uniform height of the chamber, allowing precise horizontal orientation of the coverslip required for downstream microscopy.

Creation of an agar slab

4. Prepare liquid ½ MS medium, adding 1.5% (w/v) Difco Bacto agar before autoclaving .

5. Affix two glass strips to a microscope slide as described in step 1 and place a coverslip on slide so that it rests on both glass strips. Prepare two slides like this (to prepare one agar slab containing Dex and one containing DMSO).

6. Supplement liquid ½ MS medium from step 4 with either an appropriate concentration of Dex (from 100 mM Dex stock solution; see Reagents and Solutions and Basic Protocol 1, step 6a) or an equivalent volume of DMSO (as a control) and mix thoroughly by pipetting up and down. Pipet liquid medium into the space below the

coverslip on the microscope slide until the space is completely filled. Leave until agar is set (2 to 5 min).

The surface tension of the medium is sufficient to prevent any leaks.

The agar slab fulfills multiple functions: it provides the seedling with water and nutrients; it is used to supply Dex; and it keeps the seedling in position, allowing repeated imaging of plant organs over several days. To ensure sufficient mechanical integrity for the third purpose, the slab is solidified with 1.5% Difco Bacto agar instead of 0.8%.

Completion of the chamber setup

7. Shake a small volume (e.g., 10 ml) of PFD in a 50-ml Falcon tube to air-equilibrate it.
8. Add a sufficient amount of air-equilibrated PFD to chamber of the gel gasket from step 3 to cover the bottom surface, but do not fill chamber completely.

   This is done to avoid trapping air bubbles under the agar slab as it is placed into the chamber.
9. Remove coverslip from the agar slab prepared in step 6, cut off a piece of desired size and shape, and place piece into the chamber of the gasket, leaving a gap of 2 to 4 mm between the agar slab and the gasket (Figure 1D.3).
10. Fill chamber completely with air-equilibrated PFD from step 7.
11. Place ≥1 *Arabidopsis* seedling pre-grown on a plain ½ MS plate onto agar slab, with the cotyledons and hypocotyl hanging over the edge and floating in the PFD.

    We have successfully tested this protocol with seedlings aged 3 to 10 days at the point of transfer into the imaging chamber. Due to their size, it is difficult to accommodate older plants in imaging chambers.
12. Apply a coverslip to close chamber, gently pressing it down with the edge of a microscope slide until the coverslip rests on both glass strips (Figure 1D.4). Then, image plants either continuously or at regular intervals using a CLSM system.

    If the plants are not imaged continuously, we recommend storing the imaging chambers horizontally in a plant growth cabinet (20°C, 16 hr light/8 hr dark) to maintain physiological growth conditions.

    In contrast to water, PFD readily allows the submerged plant tissue to undergo gas exchange due to its high capacity for dissolving CO_2 and O_2 (1.9 g/ml for O_2 in PFD compared to 0.04 mg/ml in water) (Dias, Freire, Coutinho, & Marrucho, 2004) while having minimal physiological effects on a variety of plants and plant tissues (Littlejohn, Gouveia, Edner, Smirnoff, & Love, 2010; Sukumaran, Weiser, & Quamme, 1972).

DEXAMETHASONE-INDUCIBLE EXPRESSION OF TRANSGENES IN SOIL-GROWN *ARABIDOPSIS*

BASIC PROTOCOL 2

The protocol below describes how to effectively induce transgene expression in *Arabidopsis* plants grown in soil. Whereas Basic Protocol 1 is best suited to plants aged ≤4 weeks, Basic Protocol 2 can be used for plants at any stage during their life cycle. We present two methods here: soil drenching and painting. Whereas soil drenching can be used for systemic induction of transgene expression, painting allows local induction of the transgene in aerial tissues like leaves or inflorescences.

Materials

Commercial peat compost (Emerald Range Universal Compost, Goundrey's)
Vermiculite

Arabidopsis seedlings pre-germinated on ½ MS medium for 7 to 10 days (see Basic Protocol 1)
Dex (Sigma-Aldrich)
Ethanol (Sigma-Aldrich)
Silwet L-77 (Fisher Scientific)

24-cell inserts placed in plant tray (22 × 35 cm)
Forceps
Greenhouse or plant growth cabinet (20°C, 16 hr light/8 hr dark)
1000-ml plastic beakers
Fine paintbrush

Dexamethasone-inducible expression of transgenes in soil by watering

1a. Prepare ~1200 g of a mixture of peat compost and vermiculite at a 3:1 ratio and fill 24-cell inserts placed in a plant tray.

2a. Using forceps, carefully transfer an *Arabidopsis* seedling pre-germinated on ½ MS medium for 7 to 10 days into each compartment and cultivate seedlings in a greenhouse or plant growth cabinet (20°C, 16 hr light/8 hr dark).

3a. Let plants grow until the first inflorescence stem appears (or until the desired stage).

4a. Prepare 30 mM Dex stock solution in ethanol.

For treatment of soil-grown plants throughout their life cycle, use ethanol as the solvent for Dex to prevent accumulation of DMSO in the soil.

5a. Dilute Dex stock solution to the desired concentration (typically 10 to 20 μM, but also note the comments in Basic Protocol 1, step 6a) or an equivalent volume of ethanol with tap water in separate 1000-ml plastic beakers.

6a. For single treatment, pour 900 ml diluted Dex solution into bottom of the tray. For continuous induction, use repeated treatment, irrigating every 2 to 4 days with 300 ml diluted Dex solution, depending on when the plants require water.

Dexamethasone-inducible expression of transgenes in soil by painting

1b. Prepare plants and 30 mM Dex stock solution as described in steps 1a to 4a.

2b. Dilute Dex stock solution to the desired concentration (typically 10 to 20 μM, but also note the comments in Basic Protocol 1, step 6a) or an equivalent volume of ethanol in tap water and add 0.02% (w/v) Silwet L-77.

3b. For leaf induction, dip a fine paintbrush into diluted Dex solution and carefully brush it over both sides of each treated leaf, avoiding dripping into the soil. For flower induction, dip a fine paintbrush into diluted Dex solution and brush it over inflorescence.

Alternatively, for rapid induction in inflorescent tissues, cut the stems and stand them in the Dex solution directly.

BASIC PROTOCOL 3

DEXAMETHASONE-INDUCIBLE EXPRESSION OF TRANSGENES IN TOBACCO AND OTHER PLANT SPECIES

Basic Protocols 1 and 2 can be easily applied to different species of plants. The pOp6/LhGR system effectively induces transgene expression in tobacco (*Nicotiana tabacum* cv. SR1 Petit Havana) and other plant species (e.g., *Oryza sativa*) grown *in vitro* or in soil using following methods: induction on agar-solidified medium (Basic Protocol 1), in liquid medium (Basic Protocol 1), or by soil drenching (Basic Protocol 2) or local induction by painting (Basic Protocol 2) (Samalova et al., 2005, and unpub. observ.).

Table 1 Summary of Changes to Adapt Growth Conditions and Dexamethasone Induction from *Arabidopsis thaliana* to Other Plant Species

	Arabidopsis	Tobacco/rice
CULTIVATION CONDITIONS		
Strength of MS medium	½ MS	MS (full)
Sucrose content of MS medium	1% (w/v)	3% (w/v)
Size of pots (diameter)	5-6 cm	10-12 cm
Soil composition	Peat compost mixed with vermiculite at 3:1	Peat compost mixed with sand at 10:1
Stratification of seeds	Yes	No
Growth conditions	20°C, 16 hr light/8 hr dark	24°C, 16 hr light/8 hr dark
DEX INDUCTION		
Dex concentration *in vitro*	1-10 μM	Typically 20 μM
Dex concentration in soil	10-20 μM	Typically 20 μM
Single soil drenching	900 ml/tray	50 ml/pot
Repeated soil drenching	300 ml/tray every 2-4 days, with no further watering necessary	50 ml/pot every 2-4 days, with additional watering if necessary
Local induction	1-2 ml Dex solution	5-10 ml Dex solution
Additional local induction	Not applicable	Leaf axils treated with ~0.5 ml Dex solution and covered with Parafilm

Depending on the overall efficiency of the pOp6/LhGR system within individual species as well as on the size of the plant, the concentration and amount of Dex used may vary. Furthermore, depending on the morphological and physiological characteristics of the plant species used, local-induction protocols can be optimized through minor modifications. For example, in tobacco, it is possible to apply Dex to the leaf axils, which are then covered temporarily with Parafilm to prevent the solution from running down the stem. For local induction in plants with a thicker cuticle (e.g., rice), induction is more efficient when 0.1% (v/v) Tween is used instead of Silwet L-77 as the surfactant.

As an illustration, in Table 1, we summarize the main changes in growth conditions and Dex induction required to adapt use of Basic Protocols 1 and 2 from *Arabidopsis* to tobacco and rice plants.

REAGENTS AND SOLUTIONS

½ MS plates supplemented with or without Dex or DMSO

Dissolve 2.2 g MS salts (Sigma-Aldrich) in 1 L distilled water. Add 10 g [1% (w/v)] sucrose. Adjust the pH to 5.7 with 1 M KOH. Add 8 g [0.8% (w/v)] Difco Bacto agar. Sterilize the medium through autoclaving for 15 to 20 min and let it cool (50° to 55°C).

Prepare 100 mM Dex (Sigma-Aldrich) stock solution in DMSO (Sigma-Aldrich) (store at −20°C). Add either Dex to the desired concentration from the stock solution or an equivalent volume of DMSO (as a control) to the pre-cooled medium, mix thoroughly by swirling, and pour the medium into round (~20-ml) or square (~50-ml) Petri dishes; it should set within ~20 min. To prepare plain MS plates, do not supplement the medium. Store ≤1 week at 4°C.

Liquid ½ MS medium with Dex or DMSO

Dissolve 2.2 g MS salts (Sigma-Aldrich) in 1 L distilled water. Add 10 g [1% (w/v)] sucrose. Adjust the pH to 5.7 with 1 M KOH. Sterilize the medium through autoclaving for 15 to 20 min and let it cool (50° to 55°C).

Prepare 100 mM Dex (Sigma-Aldrich) stock solution in DMSO (Sigma-Aldrich) (store at −20°C). Add either Dex to the desired concentration from the stock solution or an equivalent volume of DMSO (as a control) to the pre-cooled medium and mix thoroughly by swirling. Store ≤1 week at 4°C.

COMMENTARY

Background Information

In this unit, we introduce new, versatile, GATEWAY-compatible plasmids that are available for the pOp6/LhGR system (Figure 2). These plasmids can be obtained from the Nottingham Arabidopsis Stock Centre, and their sequences can be obtained from the corresponding author upon request.

pOpOn2.1

This binary vector (Figure 2A) carries 35S-LhGR and the reporter cassette of pH-TOP (Craft et al., 2005) on the same T-DNA with a GATEWAY destination cassette downstream of pOp6Ω. This plasmid can be introduced into any genetic background to achieve inducible expression of a gene of interest in the CaMV 35S pattern. Note that the presence of the CaMV 35S promoter downstream of the pOp6 promoter may increase uninduced expression levels even though the two promoters are separated by 6 kb. This plasmid was derived from the inducible RNAi vector pOpOff2 (Wielopolska, Townley, Moore, Waterhouse, & Helliwell, 2005) by digestion with *Kpn*I and *Pme*I (to release the introns, antisense GATEWAY cassette, and OCS polyadenylation sequence) and insertion of the OCS polyadenylation sequence from pV-TOP (Craft et al., 2005) as a *Kpn*I-*Ecl*136II (*Sac*I) fragment. Current data with pOpOn2.1 suggest that expression is more efficient than with pH-TOP (in the LhGR-4C S5/S7 activator background), but pOpOn2.1 has yet to be as thoroughly tested with highly toxic transgenes. The plasmid is spectinomycin resistant in bacteria and must be propagated in GATEWAY-compatible strains such as DB3.1. Please note too that the GATEWAY cassette *does not* contain the Cm^r marker.

pBIN-LR-LhGR2

This vector (Figure 2B) consists of a promoterless optimized LhGR with an upstream GATEWAY destination cassette for insertion of promoters. To test its functionality, we inserted the CaMV 35S promoter and created the pBL-35S::LhGR2 plasmid. The LhGR sequence incorporates the codon-optimized Gal4 sequence of $LhG4^{AtO}$ (Rutherford et al., 2005). Promoter-LhGR2-pA cassettes can be removed by digestion with *Asc*I and inserted into the reporter plasmid pOpIn2 (see below) to generate single-T-DNA vectors for tissue-specific inducible expression. Based on the binary vector pBINPLUS, the plasmid is kanamycin resistant in bacteria and must be propagated in GATEWAY-compatible strains such as DB3.1.

pOpIn1

This reporter plasmid (Figure 2C) was derived from pOpOn2.1 by deletion of the LhGR cassette and a downstream remnant of the 35S enhancer (present in the original pOpOff2 plasmid), and it is suitable for insertion of target genes at GATEWAY sites. The plasmid is kanamycin resistant in plants and so is compatible with BASTA- and hygromycin-resistant enhancer trap lines (Moore et al., 2006; Rutherford et al., 2005). It is spectinomycin resistant in bacteria and must be propagated in GATEWAY-compatible strains such as DB3.1. Please note that the GATEWAY cassette *does not* contain the Cm^r marker.

pOpIn2

This is another reporter plasmid (Figure 2C) derived from pOpIn1 by deletion of the plant kanamycin-resistance marker and replacement with a BASTA-resistance marker. It is suitable for insertion of target genes at GATEWAY sites and, unlike pOpIn1, carries a unique *Asc*I site for insertion of promoter::LhGR fusions generated in pBIN-LR-LhGR (see above) to generate single-T-DNA vectors with a variety of tissue-specific inducible expression patterns. As a proof of concept, we inserted the LhGR2 driven by the *AtRPS5A* promoter in this way and created the pOpIn2-RPS5A plasmid. The plasmid is BASTA resistant in plants and so is compatible with kanamycin- and hygromycin-resistant

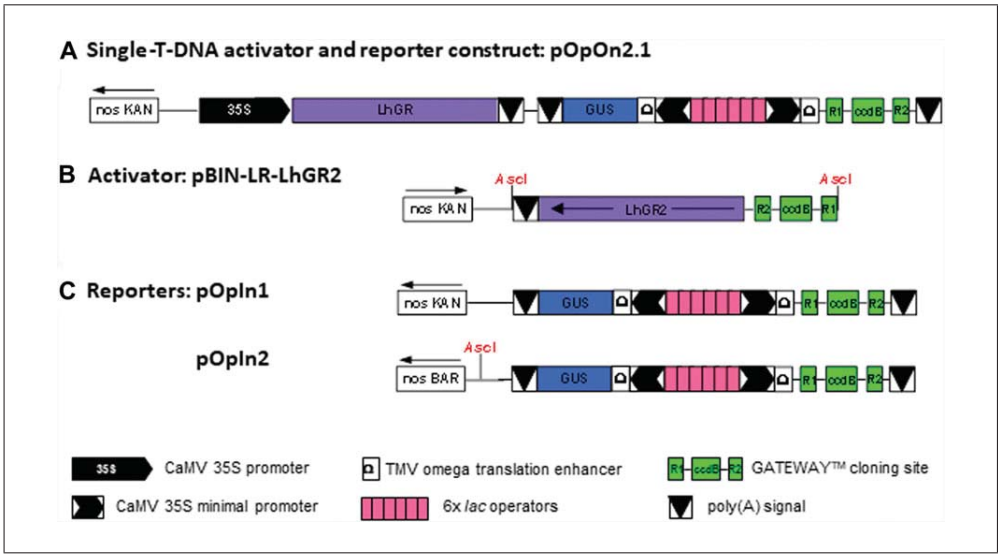

Figure 2 New, versatile, GATEWAY-compatible plasmids available for use with the pOp6/LhGR system. (**A**) Schematic representation of the single-T-DNA activator and reporter construct pOpOn2.1. (**B**) Schematic representation of the activator construct pBIN-LR-LhGR2. Note that promoter fusions can be isolated as an *Asc*I fragment for insertion into the pOpIn2 reporter plasmid (see below). (**C**) Schematic representations of the reporter constructs pOpIn1 and pOpIn2. Note the unique *Asc*I site in pOpIn2 for insertion of promoter::LhGR fusions generated in pBIN-LR-LhGR2 (see above).

driver lines (Moore et al., 2006; Rutherford et al., 2005). It is spectinomycin resistant in bacteria and must be propagated in GATEWAY-compatible strains such as DB3.1. Please note that the GATEWAY cassette *does not* contain the Cm^r marker.

Critical Parameters and Troubleshooting

Dexamethasone stability in vitro and in vivo

Under culture conditions, it is necessary to replace Dex at 10 μM every 5 to 7 days to sustain maximum rates of transcription, suggesting that Dex is stable *in vitro* for 3 to 5 days. In *Arabidopsis*, the time required for labile transcripts or proteins to return to uninduced levels after removal of the inducer ranged from 6 to 24 hr for the gene products that we tested. This time is critically dependent on transcript and protein stability and has to be established individually for every gene of interest. Transfer from Dex- to IPTG-containing medium may further increase the rate at which the system is switched off.

Under greenhouse conditions, Dex is added whenever the plants are watered, typically every 2 to 4 days, though a single application can be sufficient to sustain activities of a stable protein like GUS for several weeks. In greenhouse studies involving long-term induction, it is preferable to use ethanol as a solvent despite its increased toxicity because it is more volatile than DMSO, which accumulates in the soil over several weeks of watering.

Due to differences in solubility, Dex stock concentrations can be much higher in DMSO (≥100 mM) than in ethanol (30 mM). Caution should be taken because the solvents can interfere with plant development (Craft et al., 2005). In routine practice, fresh stocks of Dex should be made every 2 weeks or so and stored at −20°C.

Dex analogs

Dex is differentially taken up, metabolized, or compartmentalized by different plant species and therefore exhibits variability in induction efficiency and turnover or half-life. If a new plant species is tested, it is recommended to try other steroid hormone inducers, such as deoxycorticosterone (DOC) or triamcinolone acetonide (TA), at concentrations comparable to Dex. For example, TA can be used as a more efficient inducer in rice (M. Samalova and I. Moore, unpub. observ.).

Lack of transgene expression

In rare cases where the transgene is not expressed, it is advised to maximize the translation efficiency by ensuring that the initiation codon conforms to the consensus for efficient initiation in plants (Koziel, Carozzi, & Desai, 1996) as well as to codon-optimize the sequence for the species in which the transgene is to be expressed. However, it must also

be recognized that any transgene may be susceptible to post-transcriptional gene silencing (PTGS) if its transcripts accumulate to sufficient levels. In this case, selecting lines with only a single-copy T-DNA integration event for the transgene might help to mitigate the effects.

Anticipated Results

In our hands, ~90% of primary transformants recovered based on antibiotic resistance that contain both the activator and the gene of interest are inducible. Induction levels are variable in different independent lines, and to obtain the best-performing lines, 20 to 40 independent transgenic lines should be screened (Moore et al., 2006). There are several possibilities for examining induction levels: (1) observing the phenotype associated with expression of the gene of interest, (2) performing Western blots for the target protein, (3) using the GUS reporter (*uidA* gene) incorporated in most plasmids, and (4) performing quantitative real-time PCR for the gene of interest. Each of these strategies has advantages and disadvantages and thus may be more or less appropriate in any given situation. Whereas the third and fourth are relatively straightforward to implement, they both suffer from inaccuracies: the correlation of GUS and reporter gene expression is relatively poor, although the best one-third of GUS lines includes the best lines for reporter gene expression in previous tests (Moore et al., 2006). Similarly, qRT-PCR monitors mRNA levels, which may not accurately reflect the protein levels present. Conversely, the first two methods are more difficult to implement, as they depend on a quantifiable readout of a phenotype associated with expression of the transgene or the availability of an antibody against the protein of interest, respectively. However, if they can be implemented, they are likely more informative, as they interrogate functionally relevant parameters.

Time Considerations

There are several aspects to consider when using the transgene expression system in plants. The most critical is the time that it takes to generate the transgenic plants, which depends on the plant species. For example, *Arabidopsis* transgenic plants carrying a single construct with both activator and reporter sequences can be generated in 3 to 4 months, whereas tobacco transgenic plants take 6 to 9 months to generate. The timeframe may be longer for systems in which the reporter and activator are situated on separate constructs, which necessitates either crossing of separately transformed activator and reporter lines or re-transformation of pre-existing activator lines with reporter constructs (or vice versa). In many cases, is advantageous to work with homozygous lines (typically T3), which further extends the timeframe for generating suitable plant material.

The time required for Dex induction depends again on the plant species used and on the type of experiment performed. For example, *Arabidopsis* seedlings can be induced *in vitro* (Basic Protocol 1) from germination to ~4 weeks old. In soil (Basic Protocol 2), they can be induced from 1 to 12 weeks or until they reach the end of their life cycle. Induction of tobacco *in vitro* (Basic Protocol 3) can be performed from germination to several months, as tobacco is well adapted for growth under these conditions, and induction in soil is possible from 1 week to several months if necessary. In practice, how long a transgene will be induced in any given experiment heavily depends on the research question asked and may span much shorter periods of time.

Basic Protocols 1, 2, and 3 should take 1 day to 4 weeks, 1 to 12 weeks, and 1 day to 6 months, respectively, to complete. The Alternate Protocol should take 1 to 14 days.

Acknowledgements

To our great sadness, Ian Moore passed away during the preparation of this manuscript, which we dedicate to his memory. We want to thank all former members of Ian Moore's laboratory who contributed to the development of the pOp6/LhGR system over the years, especially Luisa Camacho (for pOpON 2.1), Helen Townley (for pBIN-LR-LhGR2), Matthew Spencer and Audrey Gilson (for pOpIn2 and pBL-35S::LhGR2), Astrid Woollard (for pOpIn1), and Claudia Holzeiss-Canales (for pOpIn2-RPS5A). MS has received funding from the European Union's Horizon 2020 research and innovation program under the Marie Skłodowska-Curie actions and is co-financed by the South Moravian Region under grant agreement No. 665860. This paper reflects only the author's view, and the EU is not responsible for any use that may be made of the information that it contains. This work was further supported by John Fell Fund Award 153/131 and BBSRC research grant BB/P01979X/1 to IM and CK and Leverhulme Early Career Fellowship ECF-2017-483 to CK.

Literature Cited

Baroux, C., Blanvillainh, R., Betts, H., Batoko, H., Craft, J., Martinez, A., ... Moore, I. (2005). Predictable activation of tissue-specific expression from a single gene locus using the pOp/LhG4 transactivation system in *Arabidopsis*. *Plant Biotechnology Journal*, *3*, 91–101. doi: 10.1111/j.1467-7652.2004.00104.x.

Clough, S. J., & Bent, A. F. (1998). Floral dip: A simplified method for Agrobacterium-mediated transformation of *Arabidopsis thaliana*. *The Plant Journal: For Cell and Molecular Biology*, *16*, 735–743. doi: 10.1046/j.1365-313x.1998.00343.x.

Craft, J., Samalova, M., Baroux, C., Townley, H., Martinez, A., Jepson, I., ... Moore, I. (2005). New pOp/LhG4 vectors for stringent glucocorticoid-dependent transgene expression in *Arabidopsis*. *The Plant Journal: For Cell and Molecular Biology*, *41*, 899–918. doi: 10.1111/j.1365-313X.2005.02342.x.

Dias, A., Freire, M., Coutinho, J. A., & Marrucho, I. (2004). Solubility of oxygen in liquid perfluorocarbons. *Fluid Phase Equilibria*, *222*, 325–330. doi: 10.1016/j.fluid.2004.06.037.

Kirchhelle, C., Chow, C.-M., Foucart, C., Neto, H., Stierhof, Y.-D., Kalde, M., ... Moore I. (2016). The specification of geometric edges by a plant Rab GTPase Is an essential cell-patterning principle during organogenesis in *Arabidopsis*. *Developmental Cell*, *36*, 386–400. doi: 10.1016/j.devcel.2016.01.020.

Kirchhelle, C., & Moore, I. (2017). A simple chamber for long-term confocal imaging of root and hypocotyl development. *Journal of Visualized Experiments: JoVE*, e55331–e55331. doi: 10.3791/55331.

Koziel, M. G., Carozzi, N. B., & Desai, N. (1996). Optimizing expression of transgenes with emphasis on post-transcriptional events. *Plant Molecular Biology*, *32*, 392–405. doi: 10.1007/BF00039392.

Littlejohn, G. R., Gouveia, J. D., Edner, C., Smirnoff, N., & Love, J. (2010). Perfluorodecalin enhances *in vivo* confocal microscopy resolution of *Arabidopsis thaliana* mesophyll. *The New Phytologist*, *186*, 1018–1025. doi: 10.1111/j.1469-8137.2010.03244.x.

Moore, I., Samalova, M., & Kurup, S. (2006). Transactivated and chemically inducible gene expression in plants. *The Plant Journal: For Cell and Molecular Biology*, *45*, 651–683. doi: 10.1111/j.1365-313X.2006.02660.x.

Murashige, T., & Skoog, F. (1962). A revised medium for rapid growth and bioassays with tobacco tissue. *Physiologia Plantarum*, *15*, 493–497. doi: 10.1111/j.1399-3054.1962.tb08052.x.

Samalova, M., Brzobohaty, B., & Moore, I. (2005). pOp6/LhGR: A stringently regulated and highly responsive dexamethasone-inducible gene expression system for tobacco. *The Plant Journal: For Cell and Molecular Biology*, *41*, 919–935. doi: 10.1111/j.1365-313X.2005.02341.x.

Sukumaran, N. P., Weiser, C. J., & Quamme, H. (1972). Use of fluid fluorocarbons to study freezing in plant-tissues. *Plant Physiology*, *50*, 632–+. doi: 10.1104/pp.50.5.632.

Schurholz, A.-K., Lopez-Salmeron, V., Li, Z., Forner, J., Wenzl, C., Gaillochet, C., ... Wolf, S. (2018). A comprehensive tool set for inducible, cell type-specific, gene expression in *Arabidopsis*. *Plant Physiology*, *178*, 40–53. doi: 10.1104/pp.18.00463.

Rutherford, S., Brandizzi, F., Townley, H., Craft, J., Wang, Y., Jepson, I., ... Moore, I. (2005). Improved transcriptional activators and their use in mis-expression traps in *Arabidopsis*. *The Plant Journal: For Cell and Molecular Biology*, *43*, 769–788. doi: 10.1111/j.1365-313X.2005.02486.x.

Wielopolska, A., Townley, H., Moore, I., Waterhouse, P., & Helliwell, C. (2005). A high-throughput inducible RNAi vector for plants. *Plant Biotechnology Journal*, *3*, 583–590. doi: 10.1111/j.1467-7652.2005.00149.x.

BMC Plant Biology

RESEARCH

Open Access

The steroid-inducible pOp6/LhGR gene expression system is fast, sensitive and does not cause plant growth defects in rice (*Oryza sativa*)

Marketa Samalova[1*] and Ian Moore[2^]

Abstract

Inducible systems for transgene expression activated by a chemical inducer or an inducer of non-plant origin are desirable tools for both basic plant research and biotechnology. Although, the technology has been widely exploited in dicotyledonous model plants such as *Arabidopsis*, it has not been optimised for use with the monocotyledonous model species, namely rice. We have adapted the dexamethasone-inducible pOp6/LhGR system for rice and the results indicated that it is fast, sensitive and tightly regulated, with high levels of induction that remain stable over several generations. Most importantly, we have shown that the system does not cause negative growth defects in vitro or in soil grown plants. Interestingly in the process of testing, we found that another steroid, triamcinolone acetonide, is a more potent inducer in rice than dexamethasone. We present serious considerations for the construct design to avoid undesirable effects caused by the system in plants, leakiness and possible silencing, as well as simple steps to maximize translation efficiency of a gene of interest. Finally, we compare the performance of the pOp6/LhGR system with other chemically inducible systems tested in rice in terms of the properties of an ideal inducible system.

Keywords: Dexamethasone, Glucocorticoid, Chemically inducible gene expression, GVG, XVE, Promotor, Monocots

Background

Chemically inducible systems that regulate gene expression are crucial tools for basic plant biology research and biotechnology applications. They allow analysis of gene primary effects before homeostatic mechanisms start to counteract and reveal a clear correlation between induction of a transgene and occurrence of an altered phenotype. Their applications include expression of gene products that interfere with regeneration, growth or reproduction; regulation and expression at different stages of plant development; conditional genetic complementation, co-suppression and overexpression studies. However, adaption of existing inducible systems developed in model dicotyledonous plants to other species including monocotyledonou plant rice and important crop plants, has not been easily achieved.

The systems typically contain two transcription units. The first unit employs a constitutive or tissue-specific promoter to express a chemical-responsive transcription factor, the second unit consists of multiple copies of the transcription factor binding site linked to a minimal plant promoter, which is used to express the target gene. The pOp6/LhGR system [9, 48] comprises of a transcription activator LhGR which is a fusion between a high-affinity DNA-binding mutant of *Escherichia coli lac* repressor, *lacI*^{His17}, transcription-activation-domain-II of Gal4 from

*Correspondence: marketa.samalova@sci.muni.cz
[1] Department of Experimental Biology, Masaryk University, Brno, Czech Republic
Full list of author information is available at the end of the article
Ian Moore passed away on 31st August 2018. His contributions as an author are listed in the Author Contributions section.

Saccharomyces cerevisiae and the ligand-binding domain (LBD) of the rat glucocorticoid receptor (GR). The pOp6 is a chimeric promoter that consists of six copies of *lac* operators (*lacOp*) cloned upstream of a minimal cauliflower mosaic virus (*CaMV*) 35S promoter (−50 to +8) and is apparently silent when introduced into plants. The principle of the system is that in the absence of the steroid ligand, dexamethasone (Dex), the transcription factor is trapped in an inactive complex via interaction of the GR LBD and heat-shock protein HSP90. Upon induction with Dex, this complex is disrupted and the LhGR activator binds to the pOp6 promotor and induces expression of the target gene of interest.

The most optimal systems developed to date include dexamethasone-inducible GVG (Gal4-VP16-GR [4];) and pOp6/LhGR [9, 48], estrogen-inducible XVE (LexA-VP16-ER [66];), ecdysone agonist-inducible VGE (VP16-Gal4-EcR [24, 38];) and ethanol-inducible *alc* systems (alcR [6, 44, 47];). Their characteristics and components were compared in detail by Moore et al., [30] and potential applications in plant biotechnology were reviewed by Corrado and Karali, [10].

Several attempts have been made to develop an inducible system for gene manipulation in rice. The XVE system was tested by Sreekala et al., [55] and Okuzaki et al., [35] but the use remains very limited due to the lack of systemic movement of the estradiol inducer [7, 15]. Two other steroid-inducible systems have been tested but the GVG and a modular gene expression system [59] derived from the pOp6/LhGR system met with a mixed success in rice, as they caused severe growth and developmental defects of the plants [37, 59].

An easier and more common strategy exploited in rice is the use of conditional promotors that can be activated by heat [22, 42, 56], pathogens [14, 41] or wounding [41], oxidative [62] and other stresses [32]. Other crops promoters include induction by heat in maize [11] and potato [25], by light in tomato [57] or, cold in barely [12], wheat [28] and sweet potato [16]. Often the conditional expression is combined with the Cre-lox technology [11, 12, 22, 25, 28] or an alternative site-specific recombinase system [62] to generate marker-free genetically modified plants.

Adaptation of the breakthrough CRISPR/Cas9 technology to plants [20] including rice [65] allows genome editing and creates a powerful tool for engineering knockdown, knockout or chimeric plants. This genome editing system was combined with a heat-shock-inducible promoter to generate heritable mutations in rice [34] and a virus-inducible system was developed that confers resistance to Gemini viruses in model plants *Arabidopsis* and tobacco [19]. Recently, the technology was integrated with the estradiol-inducible XVE-based cell-type-specific system [54, 66] to create an inducible genome editing (IGE) system in *Arabidopsis* that enables efficient generation of target gene knockouts in desired cell types at different developmental stages [60].

Over the years we and others have made considerable efforts to develop the dexamethasone-inducible transcription activation system, pOp6/LhGR, as a tool for the growing demands on modern gene technologies. It is a widely used system for which a comprehensive library of cell-type specific activator lines was created in *Arabidopsis* [52]; the system was combined with artificial microRNA (amiRNA) to knockdown multigene expression [13, 50] and hairpin RNAi molecules to silence gene expression [27, 61]. Apart from *Arabidopis* [9] and tobacco [48] the system was tested in various other species including citrus plant [45] and *Medicago truncatula* [27] and most recently in rice [59]. However, the specific modifications made to the original version of the pOp6/LhGR system caused undesirable effects in plants.

This report describes the functionality of the pOp6/LhGR system in rice, its stability over several generations, time course and dose response characteristics; optimization of induction by various steroids as inducers and methods of systemic and localised applications that do not have any detrimental effects in rice even after prolonged induction.

Results

Evidence that the pOp6/LhGR system is functional in rice

To adopt the pOp6/LhGR system for rice, first we chose a binary pVec8-overexpression vector [23] in which we placed the LhGR2 activator sequence that incorporates the *Arabidopsis* codon-optimized *GAL4* sequence [46] under the control of a maize ubiquitin promoter that contains an intron (*pZmUbi*). The inclusion of an intron is well known to greatly increase expression efficiency in monocots, but similar effects have been reported in dicots and other eukaryotes [43]. Secondly, we checked in the literature [29, 53] that none of the sequences of the pOpIn2 bidirectional reporter cassette [49] including the *lacOp*, minimal promoters and tobacco mosaic virus (*TMV*) omega (Ω) translation enhancers have been reported to be toxic or non-functional in monocots and cloned it into the activator construct to create pVecLhGR2 as depicted in Fig. 1 and Supp. Figure 1. For simplicity of testing the regulated expression of the pOp6/LhGR in rice, we used the *uidA* (encoding β-glucuronidase; GUS) and the yellow fluorescent protein (*YFP*) as the genes of interest.

To create stable transgenic rice lines, we used a protocol for *Agrobacterium*-mediated transformation of calli induced from seeds of *Oryza sativa* spp. *japonica* cultivar Kitaake as described by [59]. We generated several

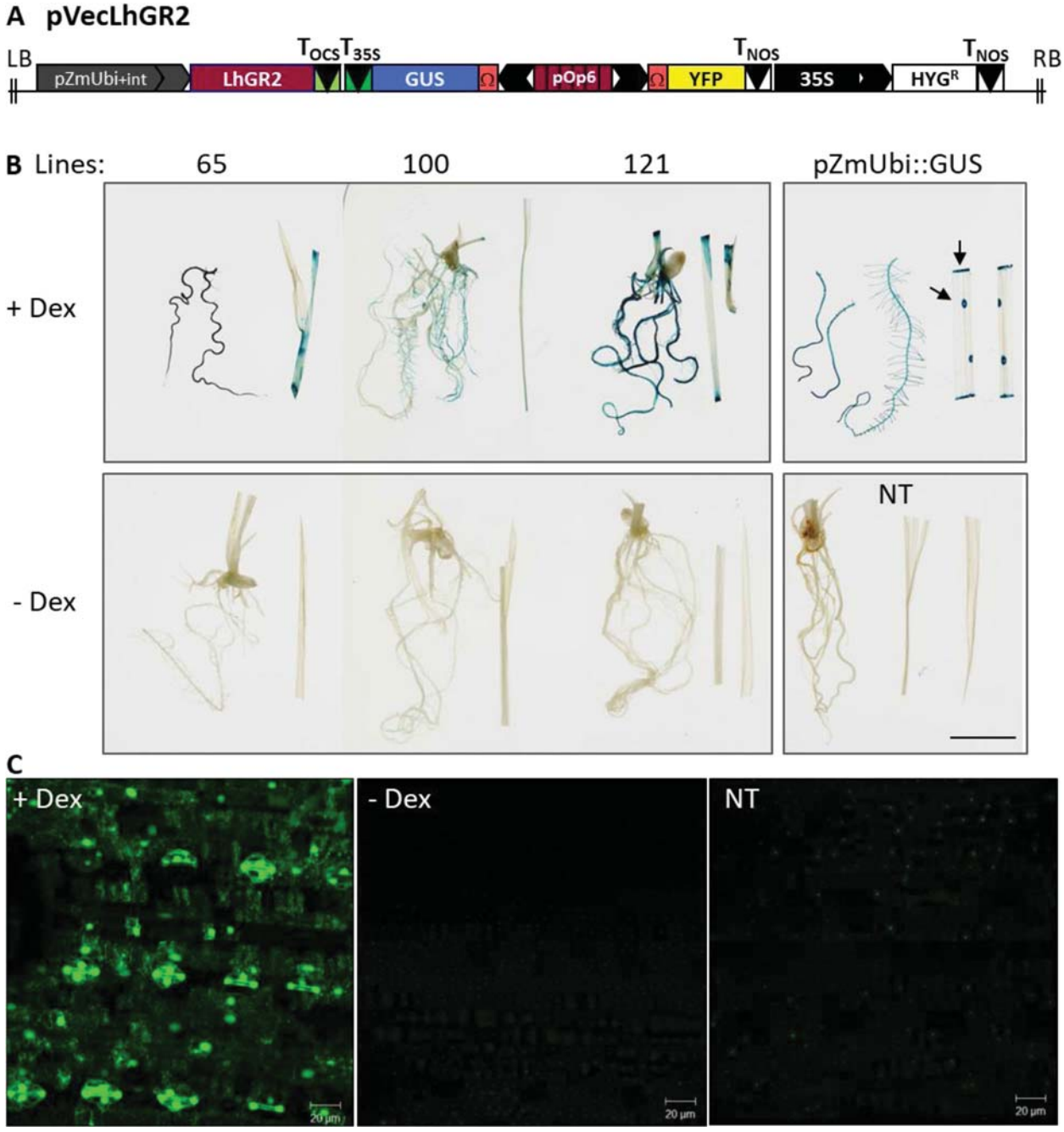

Fig. 1 The pOp6/LhGR system in rice: a proof of principle. **A** A schematic representation of the pVecLhGR2 construct that contains the *Arabidopsis* codon-optimized *GAL4* sequence [46] of the transcriptional activator LhGR2 driven by a *pZmUbi* promoter (containing an intron), a bidirectional pOp6 promotor version with two *TMV* Ω translation enhancers driving two reporter genes - *uidA* (encoding β-glucuronidase; GUS) and a yellow fluorescence protein (*YFP*), and a pCaMV35S::HYG selectable marker cassette conferring hygromycin resistance. T_{OCS}, octopine synthase terminator; T_{35S}, cauliflower mosaic virus 35S terminator; T_{NOS}, nopaline synthase terminator; LB, T-DNA left border; RB, T-DNA right border. The construct was assembled as detailed in Supplementary Fig. S1. **B** Twelve-day-old rice seedlings of three independent transgenic lines (number 65, 100 and 121) histochemically stained for GUS activity that was induced by seedling transfer onto ½ MS plates containing 30 µM Dex or control DMSO (—Dex) for 6 days. Seedlings of pZmUbi::GUS and non-transgenic (NT) were included as controls. The arrows point to an example of damaged cells/ cuts where the GUS staining substrate (5-bromo-4-chloro-3-indolyl glucuronide; X-Gluc) penetrated inside the cells. Scale bar represents 1 cm. **C** Leaves of 4-week-old plant (line 121) were painted with 30 µM Dex or control solution (—Dex) and imaged using a confocal laser scanning microscope 96 h later to detect YFP fluorescence. NT was included as a control for autofluorescence. The scale bar is 20 µm

independent transgenic lines in which the induced GUS staining was comparable to that from the constitutive promoter *pZmUbi* (Fig. 1B) and the *YFP* expression (Fig. 1C) was inducible by Dex, proving that the pOp6/LhGR system is in principle functional in rice. However, the transformation efficiency was relatively low and to induce higher levels of expression various alternate methods were tested.

Transformation efficiency and reliability of induction in subsequent generations

We tested GUS activity by histochemical staining in 120 generated putative transformants that included little plantlets with a piece of callus and some roots (Table 1). We induced them in liquid ½ MS with 30 µM Dex and stained for GUS activity 24 h later. Approximately a half of them showed visible (by eye) GUS staining in roots after 2 h and shoots after 4 h. The reaction was stopped and scored at 24 h with the following pattern: 30.8% root staining only, 9.2% shoots only, 12.5% stained shoots, roots and callus (data not shown).

One hundred and sixty-six putative primary transformants (T0) were grown to maturity and tested. The first generation of seedlings (T1) was tested for resistance to hygromycin by germinating them on ½ MS medium supplemented with the antibiotics (Table 1). Only 33 lines germinated and grew, indicating that only 20% were real transformants, of these, 8 lines (25%) showed positive GUS staining after induction with Dex. Five of the most strongly inducible lines were grown to the next generation (T2), these lines retained HYG-resistance and showed positive GUS staining upon Dex induction. Two lines (65 and 121) were tested further and showed stable inducible GUS expression in the subsequent (T3) generation (Fig. 2A).

We determined the GUS activity fluorometrically in segregating T1 and T2 progeny in roots (Fig. 2B) and shoots (Fig. 2C) of 7-day-old rice seedlings germinated and grown on ½ MS plates containing 30 µM Dex or the same concentration of DMSO (−Dex control). Interestingly, the induced GUS activity was up to 8-fold higher in roots compared to shoots and in some cases in roots it was comparable to the activity from the constitutive *pZmUbi* promoter. Perhaps a low transpiration rate in Petri dishes impaired the uptake and distribution of Dex into the shoots.

Table 1 Number of putative transformants and generated transgenic lines tested for hygromycin (HYG) resistance and induction of GUS activity in subsequent generations

Generation	No. lines tested	HYG resistant	GUS staining
T0	120	n.d.	63
T1	166	33	8
T2	5	5	5

Time course and dose response characteristics of Dex-induced GUS activity

To characterise the induction property of the pOp6/LhGR system in rice we performed time course and dose response experiments. To increase the efficiency of induction in shoots, we induced the newly developed leaves of app. 2-week old seedlings, grown in the open air, by painting the leaves with a Dex solution supplemented with 0.1% (v/v) Tween-20. Significant increase in fluorometrically determined GUS activity was detected 12 h after induction with 10 µM Dex in two independent transgenic lines (65B and 121C) and this activity reached app. a half of the *pZmUbi* constitutive promoter activity within 72 h of induction (Fig. 3A). The GUS activity was induced in plants treated with 0.01 µM Dex and while one line (65B) reached maximum levels of induction with 0.1 µM Dex, the other line (121C) had increased activity with increasing Dex concentration and reached levels similar to the constitutive *pZmUbi* promoter with 10 µM Dex after 48 h induction (Fig. 3B).

To confirm the similar characteristic of the pOp6/LhGR system in roots, we induced detached roots of 10-day old seedlings in liquid ½ MS media supplemented with increasing concentrations of Dex and performed histochemical GUS staining after specific time durations. Visible GUS staining was first detected in developing lateral roots and tips after 12 h of induction and the intensity increased throughout the root system up to 72 h tested (Fig. 3C). The maximal GUS staining intensity was detected with 1 µM Dex, the lowest concentration tested (Fig. 3D), predominantly in growing root tips after 24 h induction.

We also tested the feasibility of inducing whole seedlings (10-day old) in a liquid ½ MS medium supplemented with 10 µM Dex. Histochemical GUS staining revealed the induction after 12 h predominantly in roots and the staining pattern did not change significantly in the 48 h time-span tested (data not shown).

Optimization of induction by testing different steroids as inducers

We tried to improve the levels of induction of the pOp6/LhGR system in rice by testing different glucocorticoid derivatives (steroids) as inducers. In an attempt to reduce the surface tension at the air–liquid interface that is high in rice leaves due to epicuticular waxes preventing water vapor loss, we tested different concentrations of Tween-20 as the wetting agent rather than Silwet L-77 used previously [9, 48]. Figure 4A (i-iv) shows clear differences in

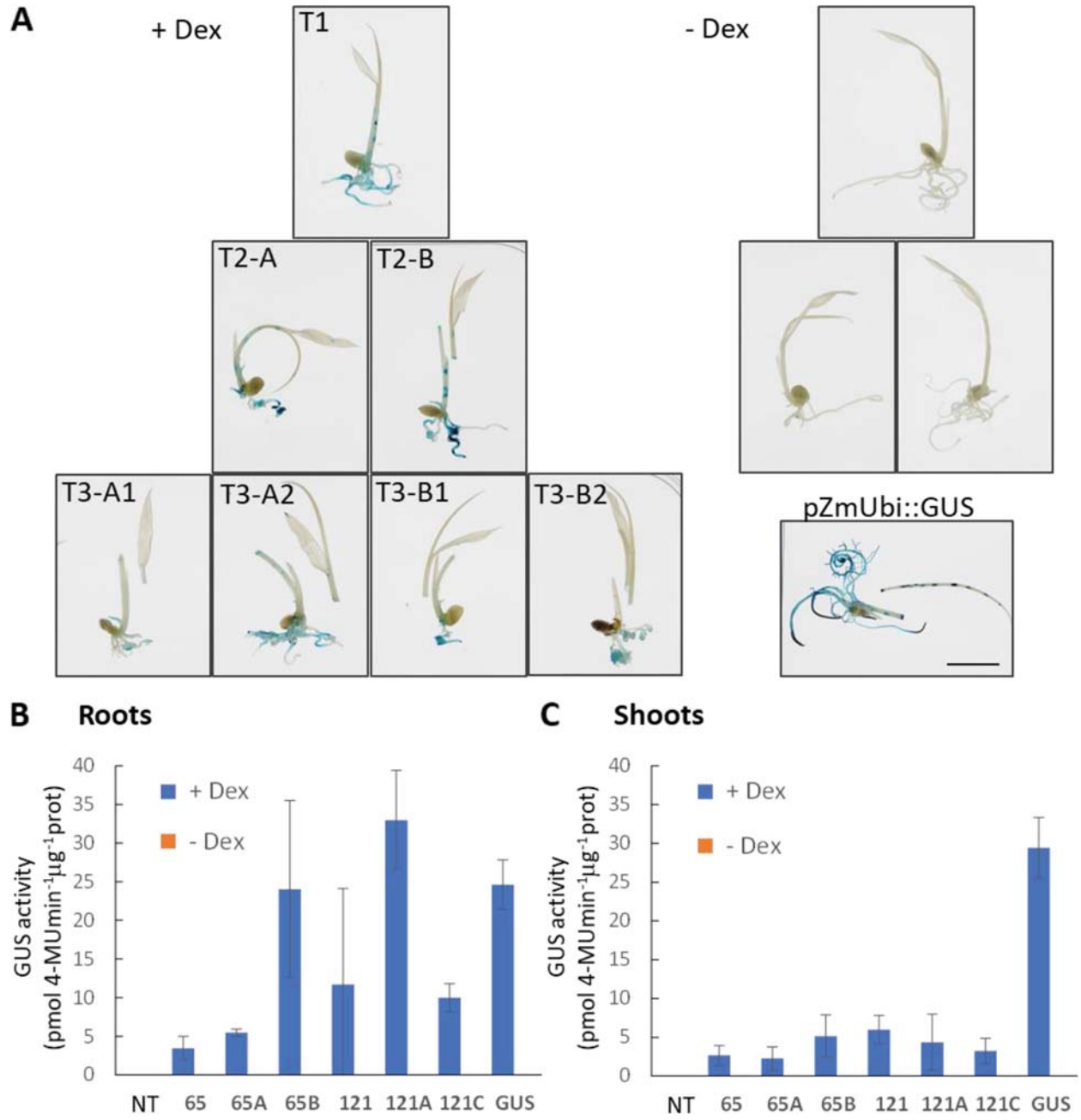

Fig. 2 Reliability of inducible expression in subsequent generations and GUS activity in rice. **A** Ten-day-old rice seedlings (line 65) of generation T1, T2 (**A** and **B**) and T3 (A1, A2 and B1, B2) histochemically stained for GUS activity induced by germinating and growing the seedlings on ½ MS plates containing 30 µM Dex or control DMSO (−Dex) for 10 days. Seedlings of pZmUbi::GUS were included as a control for the GUS staining. Scale bar represents 1 cm. **B, C** GUS activity determined fluorometrically in roots (**B**) and shoots (**C**) of 7-day-old rice seedlings (lines 65 and 121, T1 and T2) germinated and grown on ½ MS plates containing 30 µM Dex or control DMSO (−Dex) for 7 days. Seedlings of NT and pZmUbi::GUS were included as controls. The error bars represent SD

the intensity of GUS staining of the 10-day-old shoots (leaves and stems) induced with a 30 µM Dex solution supplemented with 0.1% Tween-20 compared to 0.01%. Almost no staining was visible without the addition of the surfactant apart from damaged cells.

It is known that other glucocorticoid derivatives such as triamcinolone acetonide (TA) or deoxycorticosterone (Doc) can be used as inducers to replace Dex [4]. We tested both in a 30 µM water solution supplemented with 0.1% Tween-20 (Fig. 4A v and vi) and compared GUS

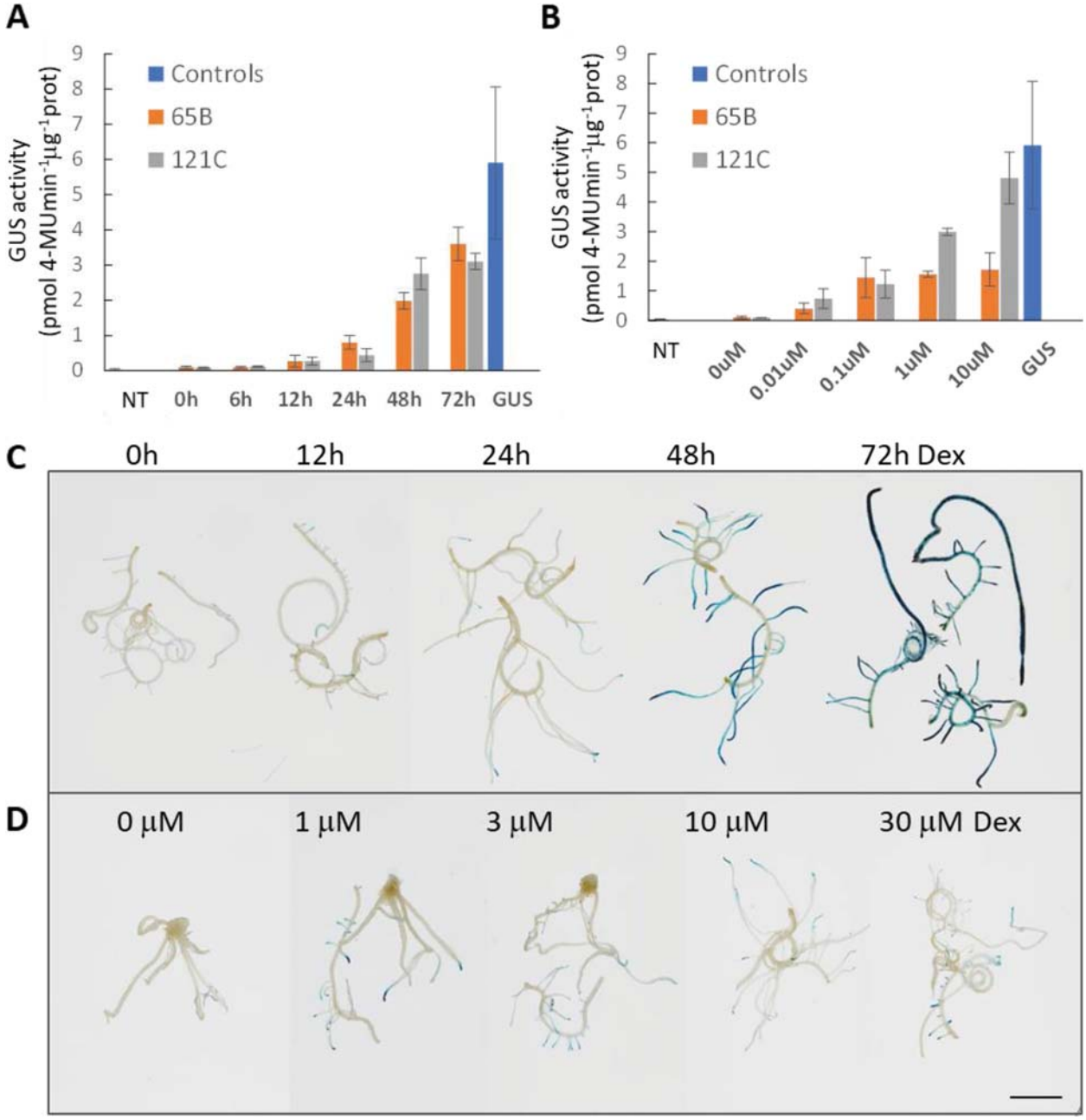

Fig. 3 Time course accumulation of induced GUS activity and dose-response of the pOp6/LhGR system in rice. GUS activity determined fluorometrically in 7-day-old rice seedlings (lines 65B and 121C) germinated on ½ MS plates (vertically placed in the incubator) and then stood up in 15 ml Falcon tubes with 2 ml water for further 5 days. The newly developed leaves were induced by painting with water supplemented with 0.1% Tween-20 and **(A)** 10 µM Dex for 0, 6, 12, 24, 48 and 72 h or **(B)** with 0, 0.01, 0.1, 1 and 10 µM Dex for 48 h. Seedlings of NT and pZmUbi::GUS were included as controls. The error bars represent SD. **C** Roots of 10-day-old seedlings (lines 65A, 121C) were induced in liquid ½ MS with 30 µM Dex for 0, 12, 24. 48 and 72 h, then histochemically stained for GUS activity. Representative images are shown. **D** Roots of 10-day-old seedlings (lines 65A, 121C) were induced in liquid ½ MS for 24 h with 0, 1, 3, 10 and 30 µM Dex, then histochemically stained for GUS activity. Representative images are shown. Scale bar represents 1 cm

staining intensities. Doc induction was negligible; however, TA induction was comparable if not higher than with Dex. To confirm this observation, we repeated the experiment on cuttings of the same leaf of 6-week-old plants that were submerged in water supplemented with 0.1% Tween-20 and 10 µM Dex or 10 µM TA for 24 h

(Fig. 4B). Depending on the efficiency of the substrate penetration, the GUS staining pattern with both inducers was comparable, but more importantly, also comparable to the staining of pZmUbi::GUS line of the same age. No GUS staining was detected without the inducers (Fig. 4B, 0.1% Tween-20).

We expanded the range of possible steroid inducers readily available and tested them in a 30 µM water solution supplemented with 0.1% Tween-20. Leaves of 5-week-old plants (Fig. 4C, lines 65A top and 121C bottom) were painted with the following steroids: betamethasone (Bet), fludrocortisone acetate (Flu), prednisone (Pre) or prednisolone (Plo) and Dex and histochemical GUS staining was carried out 24 h later. None of the new glucocorticoids reached GUS activity levels comparable to Dex in both the transgenic lines tested and the GUS staining was considerably weaker than that of the constitutive *pZmUbi* promotor activity.

Systemic and localised induction of soil-grown plants

To test the feasibility of inducing gene expression at later stages of plant development, either in a systemic or in a localized manner, Dex or the glucocorticoid TA was applied to soil-grown plants by watering (subterranean irrigation) or painting. Local induction of expression was detected after 24 h when leaves were painted with a 10 µM steroid solution supplemented with 0.1% Tween-20 (Fig. 5A). The treatment was repeated and GUS activity determined 24 h and 72 h following first application of the inducer. Interestingly, the TA treatment doubled the induced levels of GUS activity compared to Dex, and both treatments exceeded the levels of *pZmUbi* promoter activity at 72 h post induction (hpi).

Similarly, plants were watered with a 30 µM steroid solution and the treatment was repeated twice at 0 h and 24 h later. The induction triggered the reporter gene expression at the whole plant level, GUS activity was detectable in leaves 24 h after application of TA and 72 h with both Dex and TA (Fig. 5B). The induced levels again exceeded the GUS activity detected in the pZmUbi::GUS line, however, only with one of the lines tested (65B). The variability in the measurements could be due to segregating plant populations and a small sample size.

Both painting and watering experiments were repeated with a small modification of the treatment done at 2-day intervals and leaves were imaged using a confocal laser scanning microscope to observe induction of the second reporter gene, *YFP* (Fig. 5C-K). A bright YFP signal was detected 24 h after painting the leaves (Fig. 5C) but not watering the plants (Fig. 5D) with Dex. The signal became stronger at 96 hpi with both methods of treatment (Fig. 5F and G) and more cells seemed to be expressing YFP with the TA treatment than Dex (Fig. 5I and J). No signal was detected without any induction (Fig. 5E and H) as in the NT (Fig. 5K).

To summarise, higher levels of GUS activity and *YFP* expression were obtained by painting the leaves rather than watering the plants and using TA at equivalent concentrations of Dex, suggesting that TA is a more potent inducer. Thus, whole plant and single leaf phenotypes can be assessed after induction using both methods.

Long-term induction of the pOp6/LhGR system has no negative effects on rice plants

Final experiments were to determine whether there are any undesirable effects due to long term induction of the pOp6/LhGR system in rice or not. Four-week old plants were watered with either 30 µM Dex or 30 µM TA or a control solution (DMSO) at 2-day intervals for a week (Fig. 6, left) or 2 weeks and let to recover for further 6 weeks (Fig. 6, right). The images suggest that the plants grew and developed normally compared to NT plants treated with the control solution.

Discussion

A construct design: possible reasons for toxicity, leakiness and silencing

In the publication of Vlad et al. [59] the activator LhGR was codon optimized for use in rice (*rcoLhGR*) and further "domesticated" to remove all recognition sites for the Golden Gate cloning. However, severe growth defects on 10 µM Dex media were observed with all their constructs tested and in all transgenic lines. As addition of isopropyl β-D-1-thiogalactopyranoside (IPTG) to the growth media reduced the severity of the growth arrest phenotype, the authors concluded that it was a direct consequence of LhGR activity. However, in our work, we used the activator LhGR2 version that was only partially codon optimized for *Arabidopsis* to eliminate premature polyadenylation events in the Gal4 domain [46] and we

(See figure on next page.)

Fig. 4 Optimization of the pOp6/LhGR induction in rice by testing different steroid inducers. **A** Shoots of 10-day-old seedlings (lines 65A, 121C) were induced in water supplemented with either 0.01% or 0.1% Tween-20 and 30 µM steroid inducer Dex, deoxycorticosterone (Doc) or triamcinolone acetonide (TA) for 24 h, then histochemically stained for GUS activity. **B** Leaf cuttings of the same leaf of 6-week-old plants (lines 65A, 121C) were induced in water supplemented with 0.1% Tween-20 and 10 µM Dex or 10 µM TA for 24 h, then histochemically stained for GUS activity. Leaves of pZmUbi::GUS were included as controls. Representative images are shown. **C** Leaves of 5-week-old plants (lines 65A top, 121C bottom) were induced by painting with water supplemented with 0.1% Tween-20 and 30 µM steroid inducer: Dex, betamethasone (Bet), fludrocortisone acetate (Flu), prednisone (Pre) or prednisolone (Plo) for 24 h, then histochemically stained for GUS activity

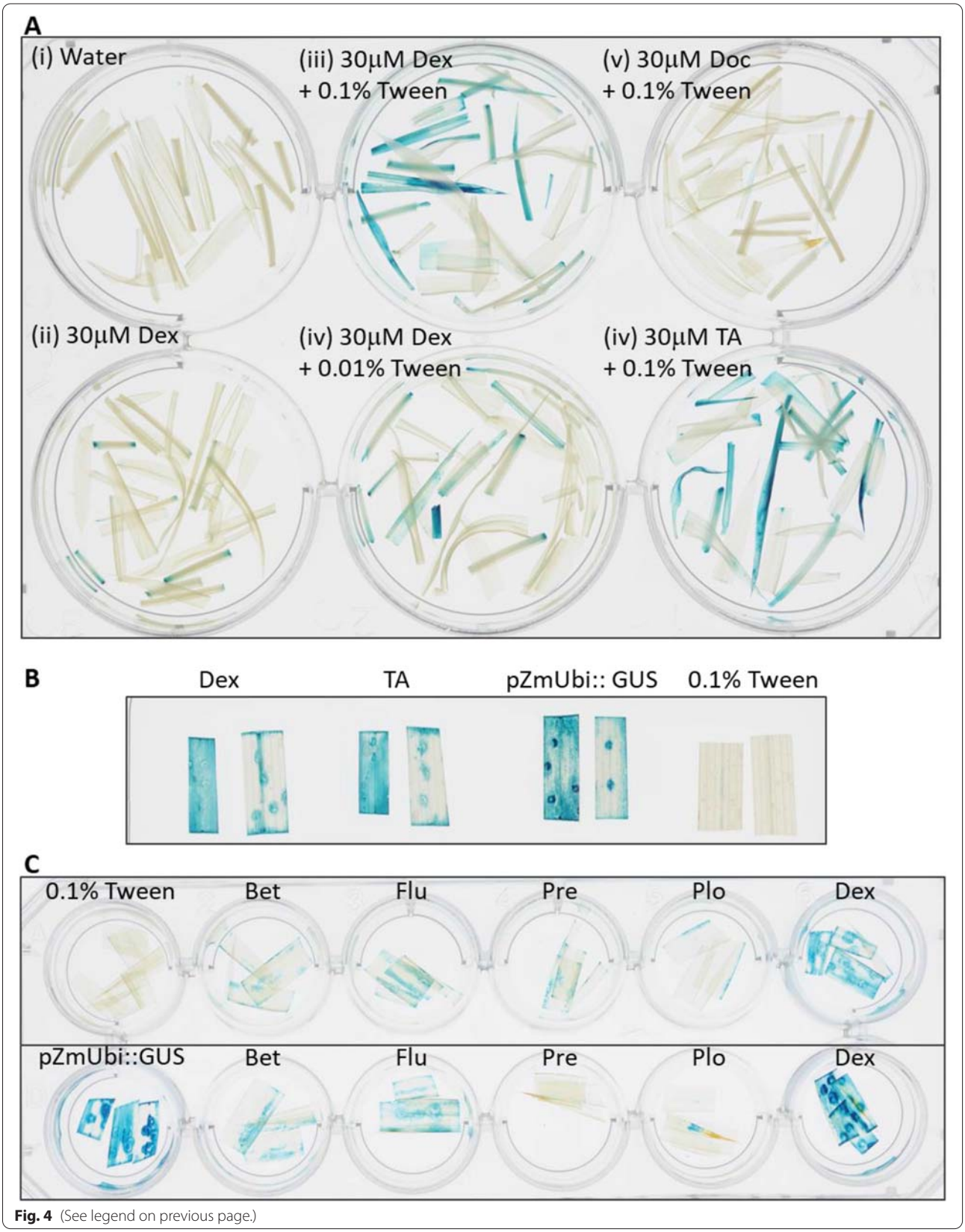

Fig. 4 (See legend on previous page.)

did not observe any undesirable growth defects. Therefore, it is possible that the rice codon optimization rendered the system too efficient and prone to non-specific off-target binding due to high rcoLhGR protein levels in the growth inhibited lines. In this regard, to optimize efficiency of an expression system it is recommended to maximize the translational efficiency of a gene of interest [30]. This can be achieved by taking some simple steps such as ensuring that the initiation codon conforms to the consensus for efficient initiation in plants [26] and including translation enhancers in the 5'UTR such as the *TMV* Ω in our study.

Similarly, the GVG synthetic transcription factor that incorporates the glucocorticoid receptor (GR) ligand binding domain was found to be detrimental when activated in rice [37] and other species including *Arabidopsis* [21], tobacco [2], *Lotus japonicus* [3]. The growth perturbations were caused probably by the GVG activator that was binding to cis-regulatory elements in the plant genome with sequence homology to *GAL4* upon Dex activation [21]. Nevertheless, the system was used successfully in a number of studies in rice [8, 33, 36, 39, 40] in which the negative effects were reduced by shortening the time of Dex exposure or selecting lines with low GVG expression levels and mild phenotype that could be used as activator lines.

Moreover, when designing a construct for an inducible system, care must be taken to ensure that enhancers in the promoter that drives the activator do not activate the target promoter (e.g. *pOp6* [30];) as such arrangement might result in transgene activation in the absence of inducer. In the pOp6/rcoLhGR constructs [59], the arrangement was not ideal, as the *pOp6* promoter was positioned directly next to the *pZmUbi* promoter driving the *rcoLhGR*. Furthermore, two other potent promoters were used on the same T-DNA; the constitutive rice actin promoter (*pOsACT*) to drive dsRed for identification of transgenic seeds, and another copy of *pOsACT* or the *CaMV 35S* promoter (for hygromycin-resistance selectable marker) that can also affect the expression of a transgene [64]. Curiously, the authors also used an intron in the reporter gene (GUS) placed again right next to the *pOp6* promoter and revealed that the presence of the intron had an enhancing effect on GUS activity levels both in the absence and presence of inducer.

Also, it must be recognized that any transgene may be susceptible to post-transcriptional gene silencing (PTGS) if transcripts accumulate to sufficient levels whether it is expressed constitutively or when induced [30]. Individual reporter genes have a gene-specific threshold of mRNA abundance that will trigger PTGS [51] and the probability of silencing of an inducible transgene locus is increased if the locus is induced [1]. In an attempt to minimize gene silencing, in our construct design we tried not to repeat the same sequence more than once, for example we used different polyadenylation signals (namely the octopine synthase terminator Tocs, nopaline synthase terminator Tnos, and T_{35S}; Fig. 1A). However, we were not able to avoid silencing as only 25% of hygromycin-resistant transgenic lines (T1) displayed GUS activity after Dex induction compared to 50% of tested transgenic calli (T0). Others described a similar decrease, for example a reporter gene (GUSPlus) was expressed in 84% of rice calli but only in 25–68% of adult plants [63]; and with the XVE system only 50% of calli derived from inducible T1 seeds showed detectable GFP signal [35].

pOp6/LhGR compared with other systems: is there an ideal inducible system for rice?

The development of chemical-inducible systems for tight control of plant gene expression is a challenging task. There are a number of properties that are required for an ideal system, such as low basal expression level, high inducibility, specificity and dynamic range of response with respect to the inducer. Also, fast response and induction by various methods is desirable. An ideal system should work in several plant species and should not cause any adverse physiological effects in plants by itself or its inducer. The inducer is further required to show high specificity for the transgene, high efficiency at low concentrations and must not be found in target plants.

The pOp6/LhGR system described here is fast, first GUS activity was detected in painted leaves (Fig. 3A) and visible GUS staining in growing root tips (Fig. 3C) after 12 h of induction and increased up to 72 h tested. Similarly, with the rcoLhGR activator, 6 h of induction was sufficient to induce high levels of GUS activity in transgenic calli and reached maximum levels at 24-96 h depending on the construct (maximum levels of activity were reached after 24 h in lines containing constructs

(See figure on next page.)

Fig. 5 Expression characteristics of the pOp6/LhGR system induced in soil-grown plants by painting and watering. Four-week-old rice plants grown in soil were induced either with TA or Dex by **(A)** painting with 10 µM solution supplemented with 0.1% Tween-20 or **(B)** watering with 30 µM solutions. The treatment was repeated twice at 0 h and 24 h later. Leaves were sampled and GUS activity determined 24 h and 72 h following first application of the inducer. NT and pZmUbi::GUS plants were used as controls. Three plants from segregating populations were used for each treatment. The error bars represent SD. **C-K** Four-week-old plants (line 121C) were induced as above except the treatment was repeated 48 h after first induction. Leaves were imaged using a confocal laser scanning microscope at 24 h and 96 h post-induction, YFP signal in green, chlorophyll autofluorescence in red. Scale bar is 20 µm

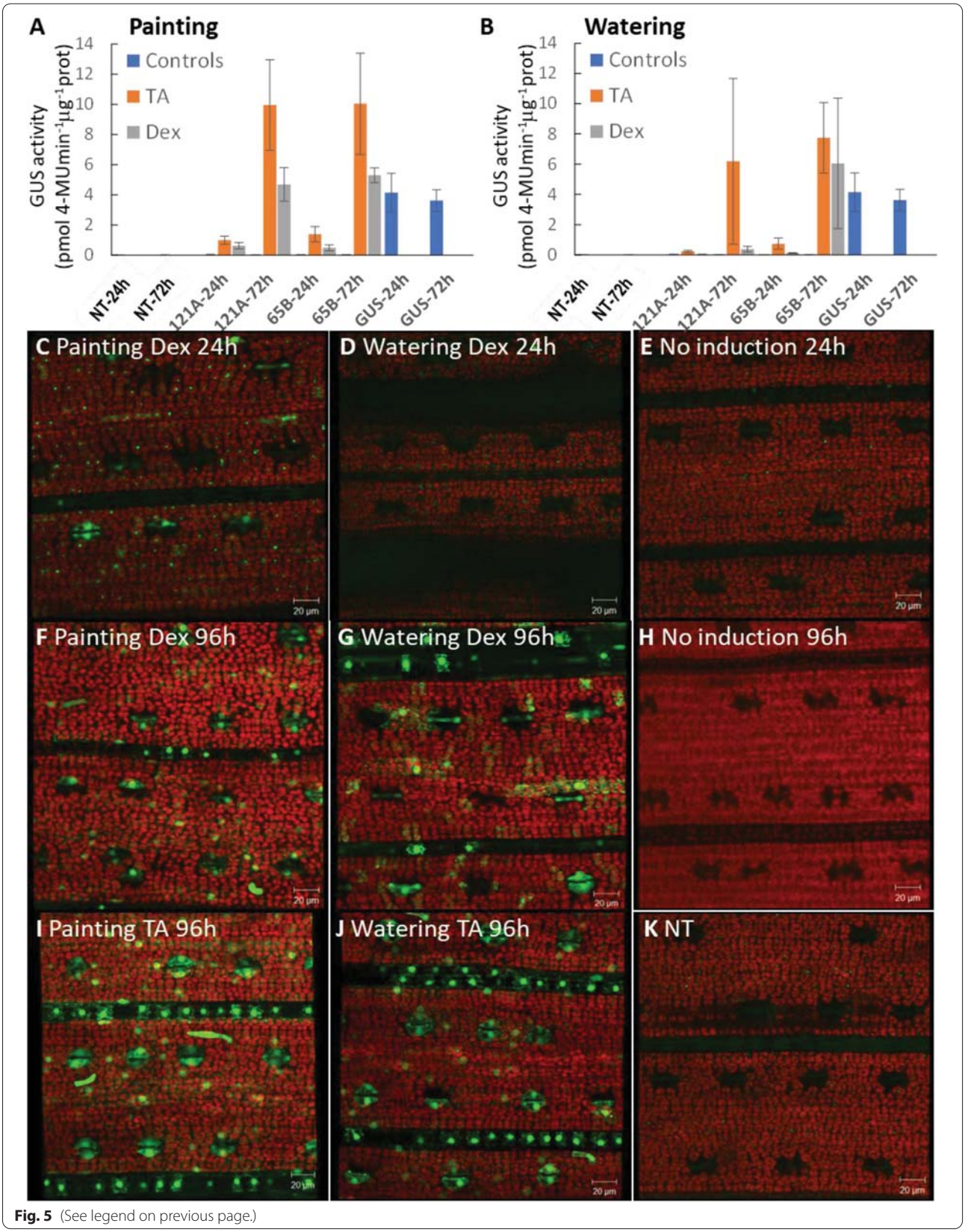

Fig. 5 (See legend on previous page.)

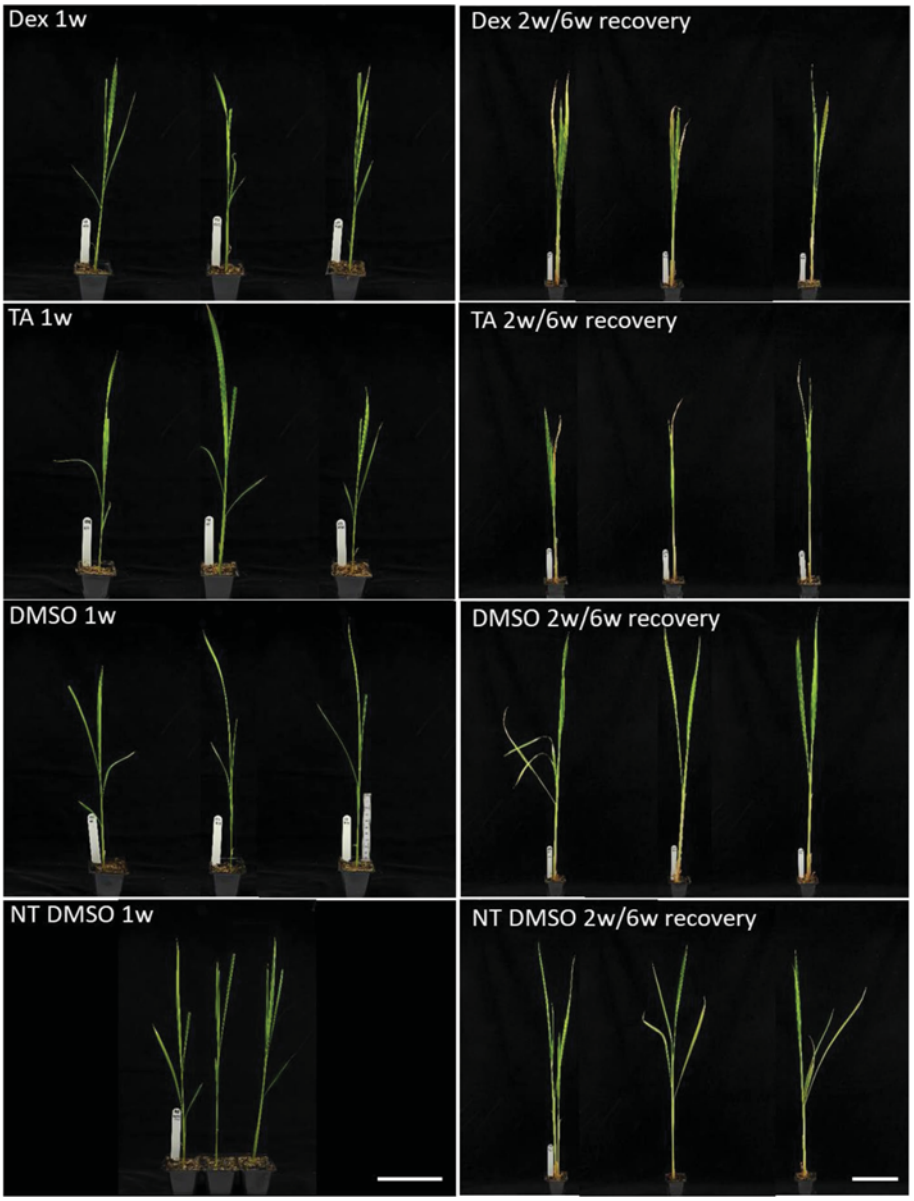

Fig. 6 Long-term effect of the pOp6/LhGR system induction on mature rice plants. Four-week-old plants (65B and 121A) were watered with 30 µM Dex or 30 µM TA or a control solution containing DMSO (600 ml per a tray of 8 plants) at 2-day intervals for a week (left) or 2 weeks and let to recover for further 6 weeks (right). NT plants treated with the DMSO solution were used as controls. Scale bar represents 10 cm. Representative images are shown

with introns in the reporter gene but required 4 days of induction in the intron-less versions) [59]. On the other hand, the GVG system tested in rice [37] required 4 days for the activity to be detected and 2 weeks of induction for GUS activities to reach levels comparable to those conferred by the strong *CaMV 35S* promoter. With the XVE system, a GFP signal was detected in rice calli 48 h after induction (with 1 µM 17-β-estradiol) and reached maximum (with treatment at 25 µM) in 8 days. However, in calli and leaves of transgenic lines the GFP signals were weaker than those in the leaves of p35S::GFP line, only in roots the signals were similar with 17-β-estradiol treatment at > 10 µM [35].

The pOp6/LhGR system is very sensitive, 0.01 µM Dex was sufficient to induce GUS activity in painted leaves (Fig. 3B) and in roots of in vitro grown seedlings of the pOp6/rcoLhGR [59]. Interestingly, in some lines maximum levels of induction were reached with 0.1 µM

Dex, while others required 10 µM Dex to reach levels similar to the constitutive *pZmUbi* promoter (Fig. 3B). This makes the pOp6/LhGR system ten-times more sensitive than the GVG system that required minimum of 0.1 µM Dex for induction and 1–10 µM for maximum.

The pOp6/LhGR system is tightly regulated and strong, the average fold induction was app. 500 in shoots of plants induced in vitro (Fig. 2C) or in soil by Dex, however, reached 1000-fold induction when plants were treated with TA (Fig. 5). In roots the magnitude of Dex-induction reached at least 1000- to 6000-fold (Fig. 2B), similar to the values reported for the GVG system [37]. Both the pOp6/LhGR and the pOp6/rcoLhGR systems used the same line that constitutively expressed a synthetic GUS variant from *Staphylococcus* (GUSPlus) under the control of the *pZmUbi* promoter as a positive control. The GUSPlus was reported to be ten-fold more active than the enzyme encoded by *E. coli uidA* that was used in the inducible constructs [5, 18], suggesting that activation of the pOp6 promoter by the activators is very effective.

The pOp6/LhGR system is inducible by various methods in vitro and in soil-grown plants. Painting the leaves with an inducer solution supplemented with 0.1% Tween-20 (to help the inducer to penetrate through the protective wax layer) proved to be more effective than subterranean irrigation (watering). It is worth to note that using these methods of application, TA proved to be almost twice as more an efficient inducer than Dex (Fig. 5). This could be due to the nature of the inducer as Dex could be more rapidly metabolized or compartmentalized than TA [4]. Ouwerkerk et al. [37] reported that Dex was taken up efficiently by roots of mature plants in hydroponics and induced GUS activity throughout the whole plant body.

The major limitation and possible reasons for low levels of target gene induction in rice leaves using the XVE system is the inefficient uptake of estradiol from hydroponics. Interestingly, cut leaf segments placed in liquid MS media with 10 µM estradiol showed detectable GFP fluorescence in whole leaf segments within 48 h [35] and similar activation was confirmed by PCR in another study [15]. Also, spraying of leaves with the inducer was another effective method of induction [15]. The limiting factor therefore seems to be the estradiol uptake that is depending on the roots. The inducer might have been trapped by XVE expressed in roots or diffused and attenuated in leaves. Interestingly, activation by soaking transgenic seeds [7] with estradiol solution induced highly efficient site-specific recombination in germinating embryos, resulting in high-level expression of target gene or RNAi cassette in intact rice plants.

The pOp6/LhGR system is not toxic in rice and does not cause any undesirable negative developmental growth effects even at higher concentration of Dex (up to 30 µM tested) and after prolonged exposure of the plants (Fig. 6). However, for the long-term induction through soil, DMSO should be avoided and ethanol should be used as a solvent for the inducers to prevent accumulation of DMSO in the soil over several weeks of watering [30, 49]. Very unexpected were the findings of Vlad et al. [59] that the pOp6/rcoLhGR transgenic plants manifested severe developmental perturbations when grown on concentrations > 0.1 µM Dex. The direct cause of these growth defects is not known, but the authors suggested that the rice genome contains sequences with high similarity to the *lacOp* sequence, suggesting non-specific activation of endogenous genes by Dex induction. Although, the *pOp* promoter was not activated by endogenous factors in maize [30, 53] it is possible that the rice-codon optimization rendered the system too efficient. The off-target effects can be minimized by quenching with IPTG that acts as an effective antagonist for the LacI DNA binding domain in LhGR [9].

The GVG system has been shown to generate growth defects in rice [37] and other species [2, 3, 21] but the reason for this is not clear as each domain of the molecule has been used successfully in other expression systems. However, one possibility is that GVG requires higher expression levels to achieve full promoter activation, resulting perhaps in squelching or non-specific binding to *CCG(N11) CGG* sequences in the genome [30]. Apparently, the GVG level was not limiting for target-gene activation [4], therefore, selection of plants with a mild GVG phenotype in combination with optimized induction conditions was recommended for the system applications. Although, the XVE system had no effect on growth, all tested lines including controls grown in hydroponics presented a different root pattern with oestradiol treatment so the system does not appear to be suitable for root morphology studies [35].

Conclusions

Chemically inducible gene expression systems that are able to control temporal and spatial expression of a given gene are invaluable research tools for plant biologists. Our results demonstrate that it is possible to adapt the technology developed originally for dicotyledonous species to monocots by careful considerations of the construct design, application methods and purpose of the usage. We have shown that the pOp6/LhGR system has reasonable induction characteristics and, in many ways, outperforms other systems tested in rice, but most importantly it is not detrimental to the plant growth. However, the inducible gene expression system described

here is a complex system derived from components of non-plant origin and, although, it has the great potential to be combined further with other technologies such as CRISPR/Cas9, it would be worth to investigate the cell response and signalling pathways in plants triggered by the system itself.

Methods

Construct preparation and usage

The pOp6/LhGR system facilitates overexpression of transgenes or suppression of endogenous gene expression in a space-temporal manner that would not be otherwise feasible especially for non-viable phenotypes. However, to minimise the potential for off-targets binding to cis-regulatory elements in the plant genome, and to avoid interference with expression of endogenous genes, the chimeric LhGR transcription factor and the cognate pOp6 promoter must derive from sequences of heterologous plant origin. To prepare the pVecLhGR2 construct (Fig. 1A, Fig. S1), first, the LhGR2 and the octopine synthase terminator (Tocs) sequences were amplified by polymerase chain reaction (PCR) using vector pOpIn2 [49] as the template. The two PCR fragments, LhGR2 (forward primer P1: 5′-AAAAAGGTACCA TGGCTAGTGAAGCTCGAAAAACAAAG-3′; reverse primer P2: 5′- GCATATCTCATTAAAGCAGGACTC TAGTTCACTCCTTCTTAGGGTTAGGTGGAGTATC-3′) and Tocs (forward primer P3: 5′-TACTCCACCTAA CCCTAAGAAGGAGTGAACTAGAGTCCTGCTTTA ATGAGATATGC-3′; reverse primer P4: 5′- AAAAAG GTACCCTAAGGCGCGCCGTTGTCG CAAAATTCG CCCTGGACCC −3′) were joined together by overlapping PCR with primers P1 and P4 and cloned into the unique *Kpn*I site of the binary rice overexpression vector pVec8-*Kpn*IOX [23]. Secondly, an *Asc*I fragment containing the bidirectional pOp6 operator array together with *TMV* Ω translation enhancer sequences driving expression of YFP and GUS (including 35S terminator sequence) reporters of the pOpIn2YFP vector (generated by M. Kalde, I. Moore lab) was cloned into a unique *Asc*I site created in the previous cloning step. The correct orientation of the fragment and the LhGR2 in the final pVecLhGR2 vector was confirmed by sequencing.

Plant material and growth conditions

Seeds of *Oryza sativa* spp. *japonica* cultivar Kitaake were obtained from the International Rice Research Institute, Los Banos, Philippines and kindly provided by Peng Wang (Chinese Academy of Sciences, Shanghai, China). To generate stable transgenic rice lines, we used *Agrobacterium*-mediated transformation of *Oryza sativa spp. japonica* cultivar Kitaake. Calli were induced from dehulled mature seeds before co-cultivation with *A. tumefaciens* strain EHA105 transformed with the pVecLhGR2 construct. Callus transformation and seedling regeneration were performed at 28 °C according to a protocol modified from Toki et al., [58] as described by [59]. Independent pVecLhGR2 lines were tested together with positive *pZmUbi*::*GUS* [59] and negative non-transgenic (NT) controls. Soil-grown plants were cultivated in a greenhouse at 28–30 °C with a 16 h/8 h photoperiod.

Methods of steroid induction – in vitro, painting and watering

Dexamethasone (Dex) was prepared as a 30 mM stock solution in dimethyl sulfoxide (DMSO) and stored at − 20 °C. Similarly, we prepared stock solutions of betamethasone (Bet), deoxycorticosterone (Doc), fludrocortisone acetate (Flu), prednisone (Pre), prednisolone (Plo) and triamcinolone acetonide (TA), all purchased from Sigma-Aldrich. For each treatment, either a glucocorticoid (induction) or the equivalent volume of DMSO (control) was added to obtain desired concentration.

Detailed step-by-step protocols for transgene induction using the Dex-inducible pOp6/LhGR system in *Arabidopsis* and other plant species including rice are described in [49]. Briefly, for application in vitro, seedlings were grown on half strength Murashige and Skoog [31] medium (½ MS medium) supplemented with 15 g/l sucrose. Dex was added to the medium after autoclaving to obtain final working concentration, typically 30 µM Dex. Seedlings were either germinated and grown on the plates for 7–10 days, or transferred on the inducing plates after 6 days of germination or submerged in the liquid medium for up to 72 h. Shoots and leaf cuttings were also induced by submersion in distilled water supplemented with 0.1% Tween-20 and a glucocorticoid inducer (10–30 µM) for 24 h.

For induction of soil grown plants, 4-week-old rice plants were either watered with 50 ml of 30 µM Dex or 30 µM TA or newly developed leaves (3rd leaf) were painted on both sides with 10 µM Dex or 10 µM TA solution supplemented with 0.1% Tween-20. The treatments were repeated at 2-day intervals for 1 or 2 weeks.

Analysis of ß- glucuronidase (GUS) reporter activity

Histochemical GUS staining and fluorometric GUS assay was performed according to Jefferson [17] at 37 °C. Extracts were prepared from ground snap-frozen samples; the protein content was determined spectrophotometrically using Bio-Rad Protein Assay (Bio-Rad laboratories). The fluorogenic reaction was carried out in 96 well-plates using protein extraction buffer supplemented with 4-methylumbelliferyl ß-D-glucuronide (4-MUG) as a substrate. A standard curve of 4-MU was used to calculate the amount of 4-MU/unit of time.

Activity was calculated from three technical replicates and expressed in pmoles 4-MU/min /μg protein.

Detection of YFP fluorescence

The YFP signal was detected using a Zeiss LSM 510 Meta confocal laser-scanning microscope with 514-nm excitation from an Argon laser and a BP535-590IR emission filter.

Abbreviations

Dex: Dexamethasone; LhGR: Chimeric transcription factor; pOp6: Inducible promoter based on the *lac* operators; *lacOp*: *Lac* operators; *CaMV*: Cauliflower mosaic virus; *pZmUbi*: Maize ubiquitin promoter containing an intron; *TMV*: Tobacco mosaic virus; *Ω*: Omega translation enhancers; *uidA*: Gene encoding β-glucuronidase or GUS; YFP: Yellow fluorescent protein; HYG: Hygromycin phosphotransferase; ½ MS: Half strength Murashige and Skoog medium; DMSO: Dimethyl sulfoxide; TA: Triamcinolone acetonide; 4-MU: 4-methyl umbelliferone; 4-MUG: 4-methylumbelliferyl ß-D-glucuronide; *rco*: Rice codon optimized; IPTG: Isopropyl β-D-1-thiogalactopyranoside.

Supplementary Information

The online version contains supplementary material available at https://doi.org/10.1186/s12870-021-03241-w.

Additional file 1: Supplementary Figure S1. Cloning strategy for preparation of the pVecLhGR2 construct.

Acknowledgements

I would like to dedicate this publication to my colleague and friend Ian Moore, and his beloved family, without whom science is much less fun. I want to thank to Peng Wang (Chinese Academy of Sciences, Shanghai, China) for the control pZmUbi::GUS line and the rice transformation protocol; to Chul Min Kim (University of Oxford) for the pVec8-*Kpn*IOX vector and to Monika Kalde (University of Oxford) for the pOpIn2YFP vector. I am grateful to Molly Dewey for her suggested word changes.

Significance statement

The non-monocot codon-optimized version of the dexamethasone inducible pOp6/LhGR system does not cause severe developmental perturbations in the monocotyledonous model species rice plants.

Authors' contributions

MS: Conceptualization; Investigation; Writing IM: Conceptualization; Supervision; Funding. The author(s) read and approved the final manuscript.

Funding

Not applicable.

Availability of data and materials

All data generated or analysed during this study are included in this published article.

Declarations

Ethics approval and consent to participate

Not applicable.

Consent for publication

Not applicable.

Competing interests

No conflicts of interest declared.

Author details

[1]Department of Experimental Biology, Masaryk University, Brno, Czech Republic. [2]Department of Plant Sciences, Oxford University, Oxford, UK.

Received: 1 June 2021 Accepted: 28 September 2021
Published online: 09 October 2021

References

1. Abranches R, Shultz RW, Thompson WF, Allen GC. Matrix attachment regions and regulated transcription increase and stabilize transgene expression. Plant Biotechnol J. 2005;3:535–43.
2. Amirsadeghi S, McDonald AE, Vanlerberghe CC. A glucocorticoid-inducible gene expression system can cause growth defects in tobacco. Planta. 2009;226:453–63.
3. Andersen SU, Cvitanich C, Hougaard BK, Roussis A, Gronlund M, Jensen DB, et al. The glucocorticoid-inducible GVG system causes severe growth defects in both root and shoot of the model legume *Lotus japonicus*. Mol Plant-Microbe Interact. 2003;16:1069–76.
4. Aoyama T, Chua N-H. A glucocorticoid-mediated transcriptional induction system in transgenic plants. Plant J. 1997;11:605–12.
5. Broothaerts W, Mitchell HJ, Weir B, Kaines S, Smith LMA, Yang W, et al. Gene transfer to plants by diverse species of bacteria. Nature. 2005;433:629–33.
6. Caddick MX, Greenland AJ, Jepson I, Krause K-P, Qu N, Riddell KV, et al. An ethanol inducible gene switch for plants used to manipulate carbon metabolism. Nat Biotechnol. 1998;16:177–80.
7. Chen ZJ, Cheng QQ, Hu CQ, Guo XR, Chen ZQ, Lin Y, et al. A chemical-induced, seed-soaking sctivation procedure for regulated gene expression in rice. Front Plant Sci. 2017;8:1447.
8. Chern M, Bai W, Chen X, Canlas PE, Ronald PC. Reduced expression of glycolate oxidase leads to enhanced disease resistance in rice. Peer J. 2013;1:e28.
9. Craft J, Samalova M, Baroux C, Townley H, Martinez A, Jepson I, et al. New pOp/LhG4 vectors for stringent glucocorticoid-dependent transgene expression in *Arabidopsis*. Plant J. 2005;41:899–918.
10. Corrado G, Karali M. Inducible gene expression systems and plant biotechnology. Biotechnol Adv. 2009;27:733–43.
11. Du DX, Jin RC, Guo JJ, Zhang FD. Construction of marker-free genetically modified maize using a heat-inducible auto-excision vector. Genes. 2019;10:374.
12. Eva C, Teglas F, Zelenyanszki H, Tamas C, Juhasz A, Meszaros K, et al. Cold inducible promoter driven Cre-lox system proved to be highly efficient for marker gene excision in transgenic barley. J Biotechnol. 2018;265:15–24.
13. Goh H-H, Sloan J, Dorca-Fornell C, Fleming A. Inducible repression of multiple expansin genes leads to growth suppression during leaf development. Plant Physiol. 2012;159:1759–70.
14. Helliwell EE, Wang Q, Yang Y. Transgenic rice with inducible ethylene production exhibits broad-spectrum disease resistance to the fungal pathogens *Magnaporthe oryzae* and *Rhizoctonia solani*. Plant Biotechnol J. 2013;11:33–42.
15. Hirose T, Mizutani R, Mitsui T, Terao T. A chemically inducible gene expression system and its application to inducible gene suppression in rice. Plant Prod Sci. 2012;15:73–8.
16. Honma Y, Yamakawa T. High expression of GUS activities in sweet potato storage roots by sucrose-inducible minimal promoter. Plant Cell Rep. 2019;38:SI 1417–26.
17. Jefferson RA. Assaying chimeric genes in plants: the GUS gene fusion system. Plant Mol Biol Report. 1987;5:387–405.
18. Jefferson RA, Kilian A, Wilson KJ, Keese PK. Microbial β-glucuronidase genes, gene products and uses thereof. US Patent. 2003;391:547.
19. Ji X, Si XM, Zhang Y, Zhang HW, Zhang F, Gao CX. Conferring DNA virus resistance with high specificity in plants using virus-inducible genome-editing system. Genome Biol. 2018;19:197.
20. Jiang WZ, Zhou HB, Bi HH, Fromm M, Yang B, Weeks DP. Demonstration of CRISPR/Cas9/sgRNA-mediated targeted gene modification in *Arabidopsis*, tobacco, sorghum and rice. Nucleic Acids Res. 2013;41:e188.

21. Kang HG, Fang Y, Singh KB. A glucocorticoid-inducible transcription system causes severe growth defects in *Arabidopsis* and induces defense-related genes. Plant J. 1999;20:127–33.
22. Khattri A, Nandy S, Srivastava V. Heat-inducible Cre-lox system for marker excision in transgenic rice. J Biosci. 2011;36:37–42.
23. Kim CM, Dolan L. ROOT HAIR DEFECTIVE SIX-LIKE class I genes promote root hair development in the grass *Brachypodium distachyon*. PLoS Genet. 2016;12:e1006211.
24. Koo JC, Asurmendi S, Bick J, Woodford-Thomas T, Beachy RN. Ecdysone agonist-inducible expression of a coat protein gene from tobacco mosaic virus confers viral resistance in transgenic *Arabidopsis*. Plant J. 2004;37:439–48.
25. Kopertekh L, Krebs E, Guzmann F. Improvement of conditional Cre-lox system through application of the regulatory sequences from cowpea mosaic virus. Plant Biotechnol Rep. 2018;12:127–37.
26. Koziel MG, Carozzi NB, Desai N. Optimizing expression of transgenes with an emphasis on post-transcriptional events. Plant Mol Biol. 1996;32:392–405.
27. Liu SM, Yoder JI. Chemical induction of hairpin RNAi molecules to silence vital genes in plant roots. Sci Rep. 2016;6:37711.
28. Meszaros K, Eva C, Kiss T, Banyai J, Kiss E, Teglas F, et al. Generating marker-free transgenic wheat using minimal gene cassette and cold-inducible Cre/lox system. Plant Mol Biol Report. 2015;33:1221–31.
29. Mitsuhara I, Ugaki M, Hirochika H, Ohshima M, Murakami T, Gotoh Y, et al. Efficient promoter cassettes for enhanced expression of foreign genes in dicotyledonous and monocotyledonous plants. Plant Cell Physiol. 1996;37:49–59.
30. Moore I, Samalova M, Kurup S. Transactivated and chemically inducible gene expression in plants. Plant J. 2006;45:651–83.
31. Murashige T, Skoog F. A revised medium for rapid growth and bioassays with tobacco tissue. Physiol Plant. 1962;15:493–7.
32. Nakashima K, Tran LSP, Van Nguyen D, Fujita M, Maruyama K, Todaka D, et al. Functional analysis of a NAC-type transcription factor OsNAC6 involved in abiotic and biotic stress-responsive gene expression in rice. Plant J. 2007;51:617–30.
33. Nakayama A, Fukushima S, Goto S, Matsushita A, Shimono M, Sugano S, et al. Genome-wide identification of WRKY45-regulated genes that mediate benzothiadiazole-induced defense responses in rice. BMC Plant Biol. 2013;13:150.
34. Nandy S, Pathak B, Zhao S, Srivastava V. Heat-shock-inducible CRISPR/Cas9 system generates heritable mutations in rice. Plant Direct. 2019;3:UNSP145.
35. Okuzaki A, Konagaya K-I, Nanasato Y, Tsuda M, Tabei Y. Estrogen-inducible GFP expression patterns in rice (*Oryza sativa* L.). Plant Cell Rep. 2011;30:529–38.
36. Onodera H, Shingu S, Ohnuma M, Horie T, Kihira M, Kusano H, et al. Establishment of a conditional TALEN system using the translational enhancer dMac3 and an inducible promoter activated by glucocorticoid treatment to increase the frequency of targeted mutagenesis in plants. PLoS One. 2018;13:e0208959.
37. Ouwerkerk PBF, de Kam RJ, Hodge JHC, Meijer AH. Glucocorticoid-inducible gene expression in rice. Planta. 2001;213:370–8.
38. Padidam M, Gore M, Lu DL, Smirnova O. Chemical-inducible, ecdysone receptor-based gene expression system for plants. Transgenic Res. 2003;12:101–9.
39. Park C-J, Canlas PE, Ronald PC. Establishment of glucocorticoid-mediated transcriptional induction of the rice Xa21 pattern recognition receptor. J Plant Biol. 2012;55:43–9.
40. Qu S, Jeon J-S, Ouwerkerk PBF, Bellizzi M, Leach J, Ronald P, et al. Construction and application of efficient ac-ds transposon tagging vectors in rice. J Integr Plant Biol. 2009;51:982–92.
41. Quilis J, Lopez-Garcia B, Meynard D, Guiderdoni E, San SB. Inducible expression of a fusion gene encoding two proteinase inhibitors leads to insect and pathogen resistance in transgenic rice. Plant Biotechnol J. 2014;12:367–77.
42. Rerksiri W, Zhang X, Xiong H, Chen X. Expression and promoter analysis of six heat stress-inducible genes in rice. Sci World J. 2013;2013:397–401.
43. Rose AB. The effect of intron location on intron-mediated enhancement of gene expression in *Arabidopsis*. Plant J. 2004;40:744–51.
44. Roslan HA, Salter MG, Wood CD, White MRH, Croft KP, Robson F, et al. Characterization of the ethanol-inducible *alc* gene-expression system in *Arabidopsis thaliana*. Plant J. 2001;28:225–35.
45. Rossignol P, Orbovic V, Irish VF. A dexamethasone-inducible gene expression system is active in citrus plants. Sci Hortic. 2014;172:47–53.
46. Rutherford S, Brandizzi F, Townley H, Craft J, Wang Y, Jepson I, et al. Improved transcriptional activators and their use in mis-expression traps in *Arabidopsis*. Plant J. 2005;43:769–88.
47. Salter MG, Paine JA, Riddell KV, Jepson I, Greenland AJ, Caddick M, et al. Characterisation of the ethanol-inducible alc gene expression system for transgenic plants. Plant J. 1998;16:127–32.
48. Samalova M, Brzobohaty B, Moore I. pOp6/LhGR: a stringently regulated and highly responsive dexamethasone-inducible gene expression system for tobacco. Plant J. 2005;41:919–35.
49. Samalova M, Kirchhelle C, Moore I. Universal methods for transgene induction using the dexamethasone-inducible transcription activation system pOp6/LhGR in *Arabidopsis* and other plant species. Curr Protoc Plant Biol. 2019;4:e20089.
50. Samalova M, Elsayad K, Melnikava A, Peaucelle A, Gahurova E, Gumulec J, Spyroglou I, Zemlyanskaya EV, Ubogoeva EV, Hejatko J. Expansin-controlled cell wall stiffness regulates root growth in *Arabidopsis*. bioRxiv 2020;2020.06.25.170969.
51. Schubert D, Lechtenberg B, Forsbach A, Gils M, Bahadur S, Schmidt R. Silencing in *Arabidopsis* T-DNA transformants: the predominant role of a gene specific RNA sensing mechanism versus position effects. Plant Cell. 2004;16:2561–72.
52. Schurholz AK, Lopez-Salmeron V, Li ZN, Forner J, Wenzl C, Gaillochet C, et al. A comprehensive toolkit for inducible, cell type-specific gene expression in *Arabidopsis*. Plant Physiol. 2018;178:40–53.
53. Segal G, Song R, Messing J. A new opaque variant of maize by a single dominant RNA-interference-inducing transgene. Genetics. 2003;165:387–97.
54. Siligato R, Wang X, Yadav SR, Lehesranta S, Ma GJ, Ursache R, et al. Multisite gateway-compatible cell type-specific gene-inducible system for plants. Plant Physiol. 2016;170:627–41.
55. Sreekala C, Wu L, Gu K, Wang D, Tian D, Yin Z. Excision of a selectable marker in transgenic rice (*Oryza sativa* L.) using a chemically regulated Cre/loxP system. Plant Cell Rep. 2005;24:86–94.
56. Sun F, Qi W, Qian X, Wang Q, Yang M, Dong X, et al. Investigating the role of *OsPDCD5*, a homolog of the mammalian *PDCD5*, in programmed cell death by inducible expression in rice. Plant Mol Biol Report. 2012;30:87–98.
57. Timerbaev V, Dolgov S. Functional characterization of a strong promoter of the early light-inducible protein gene from tomato. Planta. 2019;250:1307–23.
58. Toki S, Hara N, Ono K, Onodera H, Tagiri A, Oka S, et al. Early infection of scutellum tissue with agrobacterium allows high-speed transformation of rice. Plant J. 2006;47:969–76.
59. Vlad D, Abu-Jamous B, Wang P, Langdale J. A modular steroid-inducible gene expression system for use in rice. BMC Plant Biol. 2019;19:426.
60. Wang X, Ye L, Lyu M, Ursache R, Loytynoja A, Mahonen AP. Aa inducible genome editing system for plants. Nat Plants. 2020;6:766–72.
61. Wielopolska A, Townley H, Moore I, Waterhouse P, Helliwell C. A high-throughput inducible RNAi vector for plants. Plant Biotechnol J. 2005;3:583–90.
62. Woo HJ, Qin Y, Park SY, Park SK, Cho YG, Shin KS, et al. Development of selectable marker-free transgenic rice plants with enhanced seed tocopherol content through FLP/FRT-mediated spontaneous auto-excision. PLoS One. 2015;10:e0132667.
63. Wu CY, Li XJ, Yuan WY, Chen GX, Kilian A, Li J, et al. Development of enhancer trap lines for functional analysis of the rice genome. Plant J. 2003;35:418–27.
64. Yoo SY, Bomblies K, Yoo SK, Yang JW, Choi MS, Lee JS, et al. The 35S promoter used in a selectable marker gene of a plant transformation vector affects the expression of the transgene. Planta. 2005;221:523–30.
65. Zhang H, Zhang JS, Wei PL, Zhang BT, Gou F, Feng ZY, et al. The CRISPR/Cas9 system produces specific and homozygous targeted gene editing in rice in one generation. Plant Biotechnol J. 2014;12:797–807.
66. Zuo J, Niu Q-W, Chua N-H. An estrogen receptor-based transactivator XVE mediates highly inducible gene expression in transgenic plants. Plant J. 2000;24:265–73.

Publisher's Note

Traffic 2006; **7:** 1701–1723
Blackwell Munksgaard

doi: 10.1111/j.1600-0854.2006.00502.x

Ratiometric Fluorescence-Imaging Assays of Plant Membrane Traffic Using Polyproteins

Marketa Samalova, Mark Fricker and Ian Moore*

Department of Plant Sciences, University of Oxford, South Parks Road, Oxford OX1 3RB, UK
**Corresponding author: Ian Moore, ian.moore@plants.ox.ac.uk*

Fluorescent protein markers are widely used to report plant membrane traffic; however, effective protocols to quantify fluorescence or marker expression are lacking. Here the 20 residue self-cleaving 2A peptide from Foot and Mouth Disease Virus was used to construct polyproteins that expressed a trafficked marker in fixed stoichiometry with a reference protein in a different cellular compartment. Various pairs of compartments were simultaneously targeted. Together with a bespoke image analysis tool, these constructs allowed biosynthetic membrane traffic to be assayed with markedly improved sensitivity, dynamic range and statistical significance using protocols compatible with the common plant transfection and transgenic systems. As marker and effector expression could be monitored in populations or individual cells, saturation phenomena could be avoided and stochastic or epigenetic influences could be controlled. Surprisingly, mutational analysis of the ratiometric assay constructs revealed that the 2A peptide was dispensable for efficient cleavage of polyproteins carrying a single internal signal peptide, whereas the signal peptide was essential. In contrast, a construct bearing two signal peptide/anchors required 2A for efficient separation and stability, but 2A caused the amino-terminal moiety of such fusions to be mis-sorted to the vacuole. A model to account for the behaviour of 2A in these and other studies in plants is proposed.

Key words: *Arabidopsis*, confocal, Golgi, green fluorescent protein, mRFP1, *Nicotiana*, reticulum, secretion, translocation, yellow fluorescent protein

Received 11 May 2006, revised and accepted for publication 27 September 2006

In recent years, studies of membrane traffic and endomembrane organization in plant cells have made increasing use of fluorescent proteins to visualize endomembrane organelles (1–5). Green fluorescent protein (GFP) has also been used to assay biosynthetic traffic to the apoplast or vacuole in plants (3,6–19). As GFP fails to accumulate in a fluorescent form in either destination owing to low pH and proteolysis (3,6,7,17,18), perturbation of anterograde traffic is readily visualized by the accumulation of fluorescence in upstream compartments such as endoplasmic reticulum (ER), Golgi apparatus or prevacuolar compartments (PVC). This strategy is effective in transformed mutant *Arabidopsis* seedlings (5,16) but has been used most frequently in transient expression, either in protoplasts or transfected leaf epidermis, to investigate the effect of genetically dominant derivatives of putative membrane trafficking proteins (3,6,12,13–15,19). Despite its popularity, there are still significant limitations to the use of these markers, particularly in quantitative studies.

To provide reliable data in such assays, it is important to keep transfection rates sufficiently low to prevent perturbation or saturation of trafficking process (3,6,9,10,18,20). However, the stochastic nature of the transfection process inevitably leads to wide cell-to-cell variation in marker expression. This significantly complicates sampling strategies and the interpretation of observations. Problems become acute if high-magnification imaging is required to visualize changes in marker distribution or organelle morphology. They are exacerbated further when the protein under investigation cannot be visibly tagged or when transfection rates are low. In these circumstances, analyses often rely on subjective scoring of individual transfected cells in the population (3,6,12–14).

Besides morphological information, the accumulation of GFP reporters in fluorescent form in upstream compartments potentially provides quantitative data about perturbation of trafficking processes (1,3). The fluorescence of a secreted GFP marker (secGFP) can be quantified from low-magnification confocal images of transfected tobacco leaf epidermis (1,3) and has been used to estimate the effect of dominant inhibitory Rab GTPases on biosynthetic membrane traffic (3). However, the stochasticity of transient expression in individual fields of view coupled with variable sampling of 3D space limits the ability of this approach to resolve differences in marker accumulation between treatments. Sampling errors are exacerbated at higher magnification and are compounded in vacuolated plant cells by the 3D organization of the cytoplasm into a thin, curved cortical layer connected by dynamic transvacuolar strands (1). Similar considerations significantly complicate the acquisition of quantitative fluorescence data from complex non-planar organs such as the roots of transgenic plants or from lower efficiency transient expression systems such as the commonly used *Arabidopsis* protoplast transfection systems (13–15,19).

A solution to these limitations is to infer the expression efficiency of the trafficked marker by providing a stoichiometric baseline-reference that can be measured

simultaneously in either transfected protoplasts, single cells or whole tissues over a broad range of magnifications. This approach corrects for variability in marker expression and imaging efficiency while providing a means to normalize between experiments in an analogous manner to ratio imaging techniques used, for example, for physiological ion measurements (1). Here we evaluate various strategies to achieve stoichiometric co-expression of appropriate trafficked and reference fluorescent protein markers.

One strategy exploits the 2A peptide from Foot and Mouth Disease Virus (FMDV) to generate 'self-cleaving' polyproteins (21). The FMDV 2A peptide (hereafter referred to simply as 2A) is a 20 amino acid peptide that promotes separation of the 2A and 2B viral translation products from a polyprotein. The peptide retains its activity when translocated into other polypeptide contexts (21–26). Current models suggest that 2A acts as an esterase within the ribosome to hydrolyze the link between the nascent polypeptide and the t-RNA in the ribosome P-site prior to formation of the terminal Gly-Pro bond of the 2A sequence (21). Translation can continue after hydrolysis, so sequences upstream and downstream of 2A thus emerge as distinct polypeptides in a fixed stoichiometry (21–26). Previous studies have shown that 2A can be used to generate polyproteins in plants (22–26) and have suggested that differential targeting of cleavage products to endomembrane and cytosolic compartments may be possible (27–30).

Here we show that ratiometric trafficking markers based on the 2A peptide can target proteins to distinct cellular compartments to provide versatile and accurate quantitative trafficking assays in plants. Surprisingly, however, we found that the 2A sequence was required only when both halves of the fusion were translocated across the ER and that in these cases, 2A caused the upstream moiety to be sorted to the vacuole. Furthermore, in contrast to expectations from the literature, we show that the 2A sequence in a range of different fluorescent protein fusions does not efficiently promote disruption of the polypeptide backbone during translation on plant ribosomes. We propose an alternative model to account for the role of 2A in promoting the translocation of two separate polypeptides across the ER membrane during translation of a single open reading frame (ORF). We suggest how previous observations can be reconciled with these findings and discuss their implications for the use of 2A technology in plant cells.

Results

Strategies for quantitative transient co-expression of independent markers

We evaluated three strategies to achieve stoichiometric co-expression of two fluorescent proteins. Constructs were expressed using the high-efficiency *Agrobacterium*-mediated transfection of tobacco leaf abaxial epidermal cells (3,31), which has been used widely in plant membrane trafficking studies with fluorescent protein reporters (3,6–9,11,12). Furthermore, we have previously used this method to establish quantitative imaging protocols for assaying membrane traffic as reported by a secGFP marker (3). In the first approach, leaves were co-inoculated with separate GFP-HDEL and yellow-fluorescent-protein-(YFP)-HDEL strains (Figure 1A and B), which target each fluorescent protein to the ER. However, individual epidermal cells expressed each marker independently, such that the fluorescence intensity of one marker in an individual cell did not predict the expression efficiency of the other (Figure 2A and B). This was confirmed by the low correlation observed in scatter plots of pixel intensities for the GFP and YFP channels (Figure 2C). Thus co-inoculation is not a generally applicable strategy for ratiometry.

In the second approach, we constructed a transfer DNA (T-DNA) in which GFP-HDEL and YFP-HDEL were each transcribed divergently from the same CaMV 35S enhancer elements (GH–YH, Figure 1C). This improved the overlap visible between signals from individual cells (Figure 2D and E) and increased the degree of correlation on a pixel-by-pixel basis in the scatter plot (Figure 2F). We used a quantification procedure (3) to calculate the mean GFP and YFP pixel intensities in nine random low-magnification images such as the one in Figure 2D and asked whether the YFP signal could be used to normalize for image-to-image variation in the GFP signal. The mean coefficient of variance (standard deviation divided by the mean, expressed as a percentage) for the GFP signal in four independent experiments was approximately halved by normalization to YFP, representing a significant improvement in data quality (Figure 2M, GH–YH). Nevertheless, it was clear that considerable variation still existed in the relative expression levels of each marker in individual cells, seriously limiting the predictive value of the single T-DNA approach for analysis of single cells.

In the third approach, we took advantage of the of the 'self-cleaving' FMDV 2A peptide (21,22,27) to link YFP and ER-targeted GFP-HDEL in a single construct, Y_m-2A-GH (Figure 1G; the legend to Figure 1 explains the nomenclature used for this and other 2A constructs). Following transfection with this construct, there was a close correlation between the YFP and GFP signals for individual cells over a wide range of intensities (Figure 2G and H). The YFP accumulated in the cytoplasm and nucleoplasm, while GFP was confined to the ER and nuclear envelope (Figure 2H; see also Figure 3A–C), consistent with cleavage between the two fluorescent proteins and localization according to the ER targeting and retention sequences on the GFP moiety. The improved correlation between GFP and YFP intensities was confirmed by the scatter plot of individual pixel intensities in Figure 2I and by *z*-projections of higher magnification images of the cortical cytoplasm (Figure 2J–L). GFP and YFP signals substantially co-localized as the ER and cytoplasm are not readily resolved even at this level of

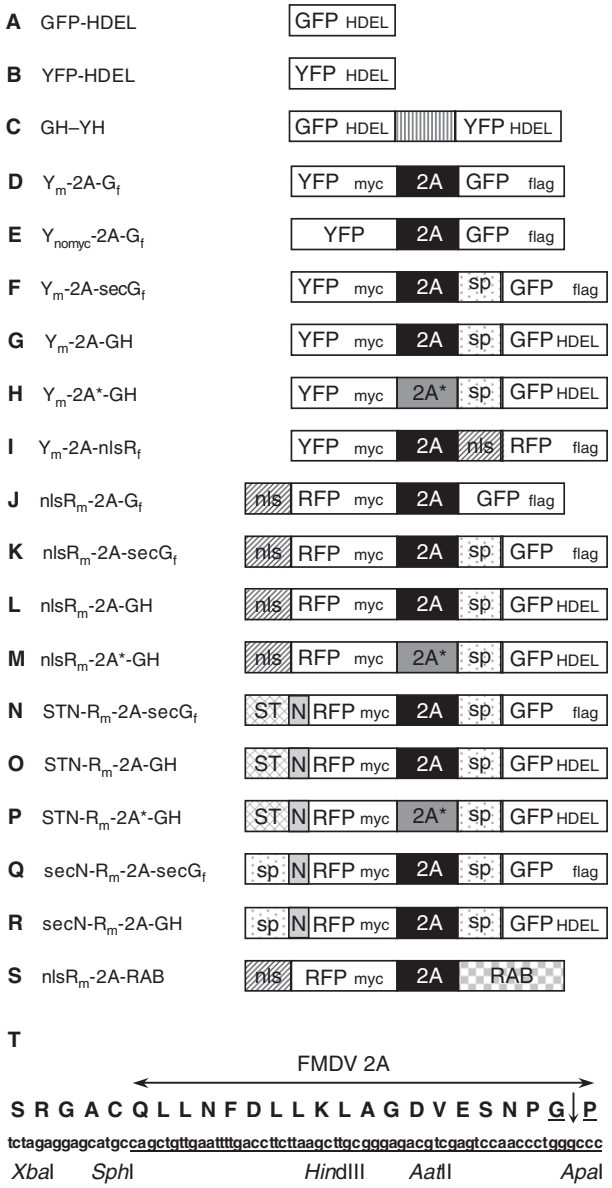

Figure 1: Schematic representation of constructs. (A–S) The components of each construct described in this paper are named and illustrated according to the following scheme: G or GFP, green fluorescent protein (mGFP5); Y or YFP, yellow fluorescent protein; R or RFP, red fluorescent protein (mRFP1); sp, signal peptide; sec, secreted form of a fluorescent protein; H or HDEL, presence of an ER retrieval signal in addition to signal peptide; nls, nuclear localization signal; ST, Golgi-targeting signal from rat sialyl transferase; N, engineered *N*-glycosylation site (6); Rab, *Arabidopsis* Rab GTPase *At*RAB-D2[a] either wild type or mutant forms; $_{m}$ or myc, c-myc epitope tag; $_{nomyc}$, c-myc epitope tag is missing; $_{f}$ or flag, FLAG epitope tag; 2A, FMDV 2A peptide; 2A*, mutant form of the 2A peptide in which the two terminal residues [G and P, underlined in (T)] were each converted to alanine. (T) Amino acid and nucleotide sequence of the 2A peptide and upstream flanking sequence used in this study, taken from the constructs described by Halpin et al. (22); the arrow indicates the site at which 2A activity disrupts the polypeptide backbone; the underlined residues were converted to alanine in the 2A* sequence.

magnification. The mean coefficient of variance was more than halved when the ratio was calculated (Figure 2M, Y_m-2A-GH) and the improvement in the quality of the ratiometric data was manifest over a 30-fold range of *Agrobacterium* titres (from OD_{600} 0.013 to 0.40, Figure 2N). Thus, although the absolute accumulation of GFP varied approximately 10-fold, the ratio of GFP:YFP varied only 1.4-fold. The ratio was unchanged above OD_{600} 0.05 and was linear up to this point, suggesting that an OD_{600} close to 0.05 is optimal for use of constructs like Y_m-2A-GH. The coefficient of variance for the ratio data was threefold lower than that of the absolute fluorescence data for bacterial titres of 0.05 or less (Figure 2O). We concluded that, in principle, 2A constructs offered an effective strategy to produce stoichiometric levels of reference and target markers suitable for ratiometric analysis of GFP expression levels in individual cells and in cell populations, with YFP accumulation reliably predicting GFP expression efficiency in each cell.

Constructs for ratiometric assays of membrane traffic

Images of cells expressing Y_m-2A-GH indicated that the GFP moiety could be targeted to the ER while YFP remained cytosolic (Figures 2H and 3A–C). To obtain a 2A-based ratiometric fluorescent marker of biosynthetic membrane traffic, we replaced the ER-retrieval signal (HDEL) on the GFP moiety of Y_m-2A-GH with a sequence encoding the FLAG epitope tag (Figure 1F). It was expected that the GFP moiety of the new construct, Y_m-2A-$secG_f$, would be trafficked to the apoplast, perhaps with a fraction being sorted to the vacuole as reported previously for secGFP in tobacco epidermis (3). In either location, GFP accumulation and fluorescence is known to be poor (3,6,7,11). Consistent with this prediction, when expressed in plant cells, GFP accumulation from Y_m-2A-$secG_f$ was almost undetectable under conditions that revealed clear GFP fluorescence in the ER of cells expressing comparable amounts of Y_m-2A-GH as judged by YFP accumulation (compare Figure 3C and D). As described in later sections, the difference between these two extremes of GFP accumulation, normalized to the level of expression of the reference (YFP) marker, provides a quantitative ratiometric assay of GFP trafficking.

While the Y_m-2A-$secG_f$ construct successfully combined a trafficked GFP marker with a cytoplasmic YFP reference in stoichiometric quantities, we sought to extend the utility of the ratiometric approach and to test the versatility of the 2A peptide for targeting proteins to distinct endomembrane compartments. Therefore, we assembled a series of constructs in which the intended location of the reference marker was altered and YFP was replaced by red fluorescent protein (mRFP1) (32) to simplify spectral separation of the two fluorescence signals.

Targeting the reference to the nucleus provides a more convenient object for reliable semi-automated quantitative

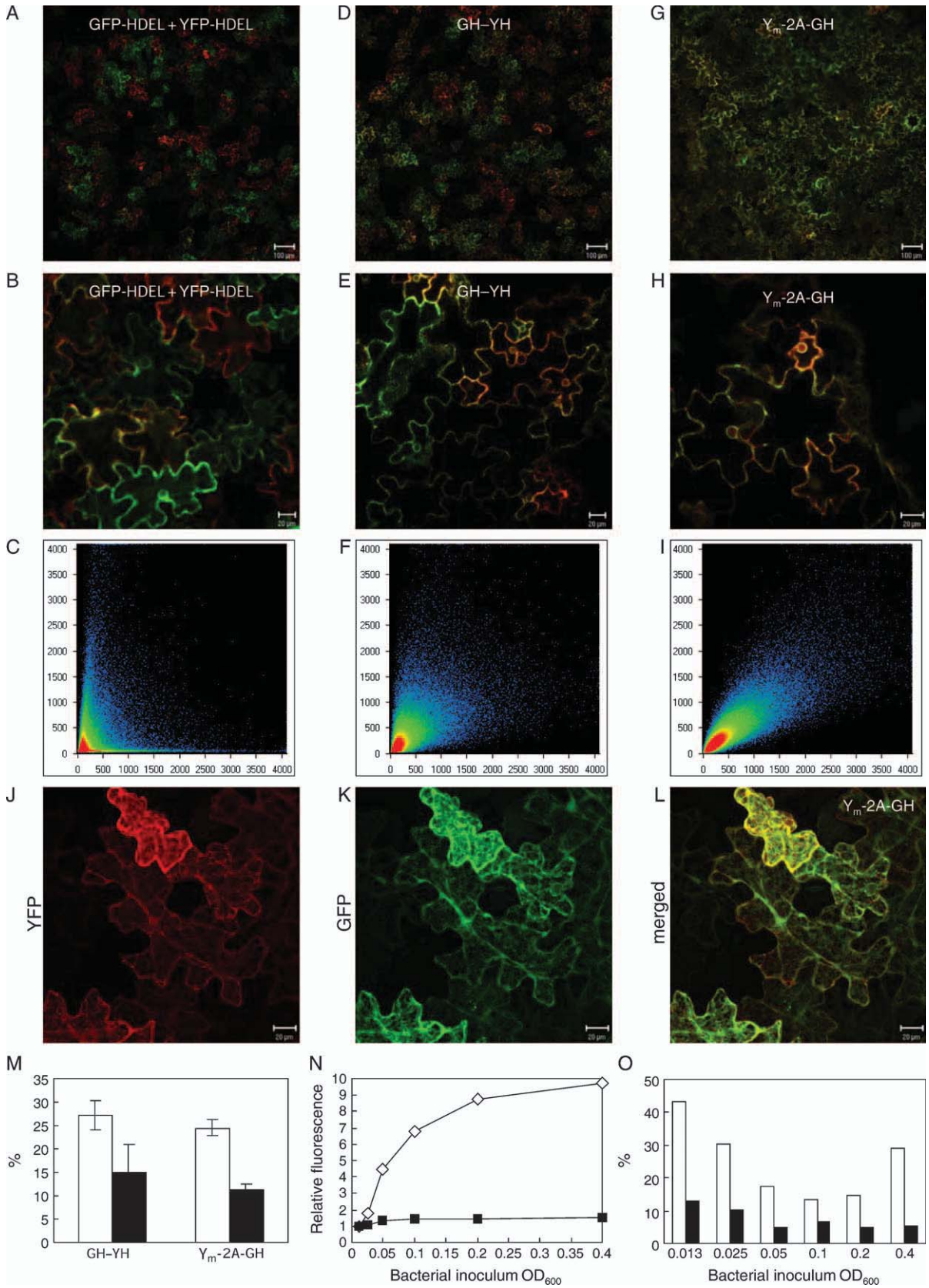
A
GFP-HDEL + YFP-HDEL
D
GH–YH
G
Ym-2A-GH
B
GFP-HDEL + YFP-HDEL
E
GH–YH
H
Ym-2A-GH
C
F
I
J
YFP
K
GFP
L
Ym-2A-GH
merged
M
%
GH–YH
Ym-2A-GH
N
Relative fluorescence
Bacterial inoculum OD600
O
%
Bacterial inoculum OD600

measurements. As shown in Figure 3E–G, nlsR$_m$-2A-GH (Figure 1L) successfully targeted mRFP1 to the nucleus via a nuclear localization signal at its amino-terminus, while GFP was targeted to the ER as before. When the ER-retrieval signal on the GFP-HDEL moiety of nlsR$_m$-2A-GH was replaced by the FLAG epitope tag to generate nlsR$_m$-2A-secG$_f$ (Figure 1K), RFP fluorescence was still detected in the nucleus, but little GFP accumulated in the endomembrane system (compare Figure 3G and H), consistent with the expected export of the secGFP$_f$ moiety from the ER.

Targeting the reference marker to the ER may provide a better quantitative (intensity) and qualitative (morphology) reference for perturbation of the early secretory pathway as it would co-localize precisely with the accumulated trafficking marker. A 2A-based polyprotein that generated an ER-localized reference marker would require both the amino-terminal (RFP) and carboxy-terminal (GFP) moieties to be translocated across the ER membrane. In such a configuration, the timing of the proposed 2A cleavage is expected to be critical. If chain separation occurs before the signal peptide of the second fluorescent protein encounters the translocation channel, this signal peptide could be inserted independently into the translocon, carboxy-terminus first, allowing translocation as normal into the ER lumen. In contrast, if the nascent GFP-HDEL or secG$_f$ moiety emerged from the ribosome before 2A-mediated separation had occurred, the signal peptide would enter the translocation channel amino-terminus first and would be expected to act as a stop-transfer signal owing to its hydrophobic nature (33–35). This would cause the GFP moiety to accumulate on the cytoplasmic face of the ER membrane where the ER-retrieval signal would not encounter the luminal retrieval receptor.

To test whether the 2A peptide was able to generate stoichiometric quantities of ER-localized reference and trafficked markers, we constructed a secreted-RFP/ER-GFP dual reporter (secN-R$_m$-2A-GH) and a Golgi-RFP/ER-GFP dual reporter (STN-R$_m$-2A-GH) (Figure 1R and O) using either a cleavable signal peptide or the Golgi-targeting signal of rat sialyl transferase (ST), as described previously (6). We also constructed plasmids in which the HDEL signal of the GFP moiety was replaced by the FLAG epitope tag to test whether ER residency of the reference GFP marker was dependent on this retrieval signal as expected. The RFP moieties of these constructs incorporated *N*-glycosylation sites to allow glycan processing to be assessed in trafficking assays (6).

When expressed in tobacco leaf epidermis, STN-R$_m$-2A-GH efficiently targeted RFP to mobile punctate structures typical of the Golgi apparatus, while GFP fluorescence appeared to be confined exclusively to the ER (Figure 3I–K). Red fluorescent protein was not observed in the ER except at the early stages of transient expression, when faint ER labelling could sometimes be detected most probably due to the transport of new protein through the ER to the Golgi (6). When the HDEL signal on the GFP moiety was replaced with the FLAG epitope tag to generate STN-R$_m$-2A-secG$_f$ (Figure 1N), GFP accumulation was dramatically reduced relative to STN-R$_m$-2A-GH (compare Figure 3K and L), consistent with secretion of secGFP$_f$. Thus, it appears that the GFP moieties were indeed translocated into the lumen of the ER where GFP-HDEL was retained by virtue of its carboxy-terminal HDEL signal while secGFP$_f$ was exported and were not simply associated with the cytoplasmic face of the ER membrane via an uncleaved signal peptide.

When secN-R$_m$-2A-GH and secN-R$_m$-2A-secG$_f$ were expressed in tobacco leaf epidermis, GFP accumulated in the ER in an HDEL-dependent fashion as expected, but RFP was unexpectedly observed to accumulate in the vacuole rather than the apoplast (Figure 3M–P). Indeed, the apoplast was evident as a dark line between adjacent cells (Figure 3M and P). It has been shown that mRFP1 is stable and fluorescent in the apoplast of tobacco epidermal cells [(3); see also Figure 4R below] so the absence of signal suggests that the RFP moiety of secN-R$_m$-2A constructs has not been transported there to any significant extent. In cells that expressed STN-R$_m$-2A-GH and STN-R$_m$-2A-secG$_f$ to comparatively high levels, RFP fluorescence was also observed in the vacuole (Figure 3I). This suggested that the RFP-2A moieties of both constructs were unexpectedly sorted to the vacuole with high efficiency after leaving the Golgi.

Figure 2: (opposite) Strategies for stoichiometric transient expression of fluorescent markers. Low (A, D, G) and higher (B, E, H) magnification confocal images of tobacco leaf epidermal cells transiently expressing a mixture of GFP-HDEL and YFP-HDEL (A and B), GH–YH (D and E) or Y$_m$-2A-GH (G and H) with the YFP channel shown in red and the GFP channel in green in a single merged image. (C, F, I) Scatter plots of pixel intensities in the GFP channel (*x* axis) and YFP channel (*y* axis) for images similar to those shown in A, D and G, respectively; colours indicate the frequency with which particular intensity combinations are observed with blue being the lowest and red the highest. (J–L) Projections in *z* of 22 1.5-μm confocal optical sections through the cortical cytoplasm of cells expressing Y$_m$-2A-GH with varying efficiency; YFP (red), GFP (green) and merged channel images are shown as indicated. Scale bars 100 μm (A, D, G), 20 μm (B, E, H and J–L). *Agrobacterium* strains carrying each constructs were infiltrated at OD$_{600}$ 0.03. (M) Coefficients of variance (*V*) for absolute (open bars) and ratiometric (shaded bars) measurements of GFP fluorescence in nine low-magnification confocal images, such as those in (D) and (G), taken from leaves expressing GH–YH or Y$_m$-2A-GH; bars show the mean value of *V* and the standard error of four experiments. (N) Absolute (open diamonds) and ratiometric (shaded squares) measurements of GFP fluorescence in epidermal cells of tobacco leaves infiltrated with *Agrobacterium* strains carrying Y$_m$-2A-GH at various titres; data are the means of two experiments. (O) Average coefficients of variance for each absolute (open bars) and ratiometric (shaded bars) measurement in (N).

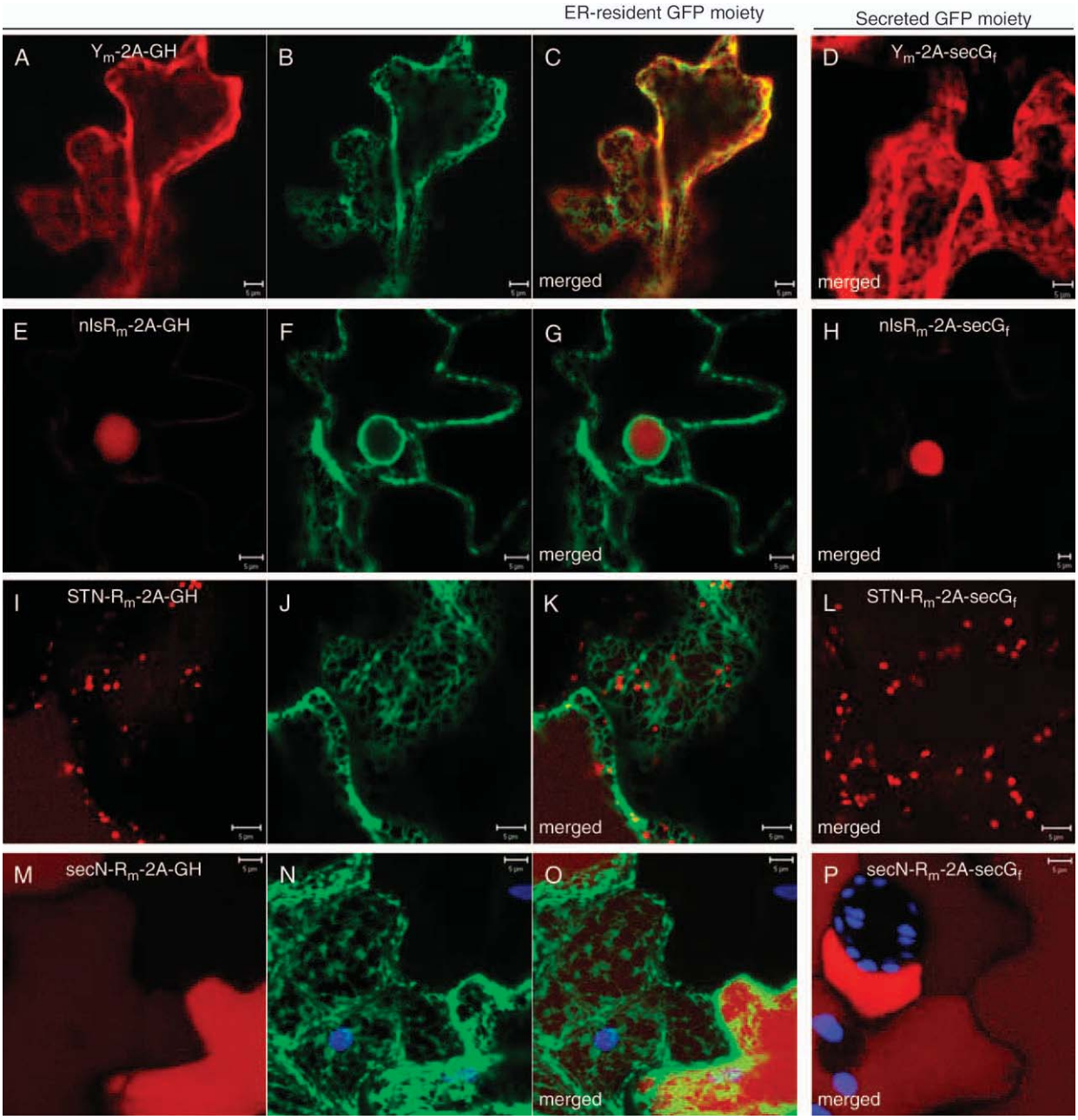

Figure 3: Targeting of translation products of 2A peptide fusions to different compartments. Confocal images of tobacco leaf epidermal cells transiently expressing (A–C) Y_m-2A-GH, (D) Y_m-2A-$secG_f$, (E–G) $nlsR_m$-2A-GH, (H) $nlsR_m$-2A-$secG_f$, (I–K) STN-R_m-2A-GH, (L) STN-R_m-2A-$secG_f$, (M–O) secN-R_m-2A-GH, (P) secN-R_m-2A-$secG_f$. YFP and RFP channels are shown in red and the GFP channel in green. Merged channel images are indicated. (M–P) Chlorophyll fluorescence is indicated in blue. Shown are single sections (A–C and E–H) and projections (D and I–P). Scale bar is 5 μm.

2A acts as a sorting determinant for the Rab-F2 PVC in plant cells

To establish whether the RFP moiety of secN-R_m-2A constructs passes through the endomembrane system *en route* to the vacuole, we sought to visualize it in transit at steady state. Therefore, leaves were infiltrated with the secN-R_m-2A-GH strain at OD_{600} 0.25, five times the usual titre and were examined by confocal microscopy 18 h after the onset of transient expression (48 h post-infiltration) when steady-state levels of RFP in transit through the endomembrane system would be at their highest (Figure 4 A–D′). Under these conditions, RFP was visible in the vacuole (Figure 4A, C′), but much of the RFP moiety was associated with the ER network marked by GFP (Figure 4 A, B and D). Red fluorescent protein was also clearly visible in distinct punctate structures that excluded the ER marker

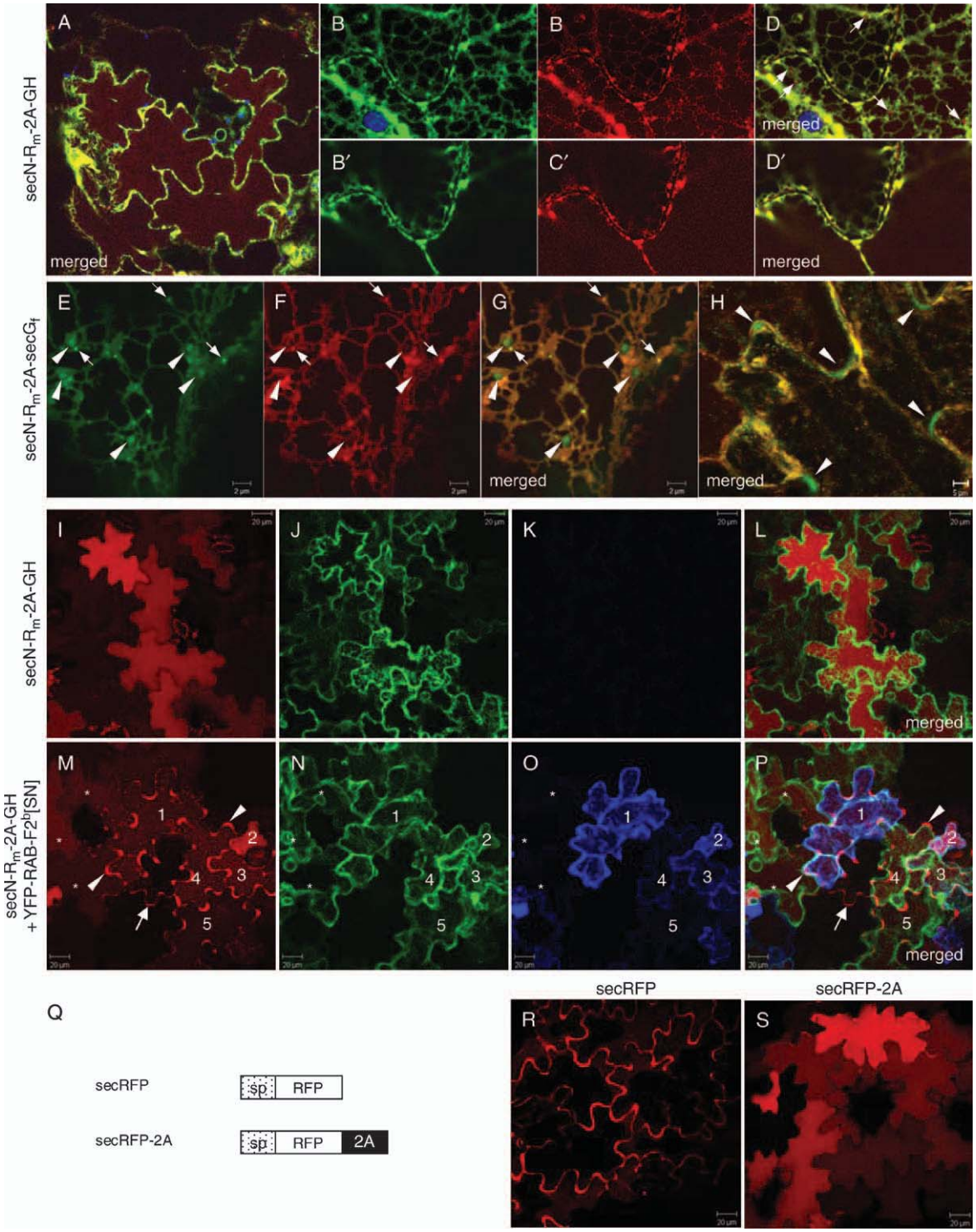

Figure 4: Legend on next page.

and probably represented intermediates on a vacuolar pathway (Figure 4D, arrows). When cells expressing secN-R_m-2A-$secG_f$ under similar conditions were imaged to reveal both RFP and GFP in transit through the endomembrane system, each labelled the ER network (Figure 4 E–H), while GFP, but not RFP, was detectable in the cell wall at these high-expression levels (Figure 4H, arrowheads). Both markers, however, labelled small bright punctate structures (arrows in Figure 4E–G). These probably represent the same punctate RFP-labelled intermediates

observed with secN-R_m-2A-GH (Figure 4D, arrows). Similar structures were previously observed with secreted and vacuolar GFP markers and identified as a PVC (3,12), suggesting that RFP may follow the same route to the vacuole. To test this possibility, we asked whether transport of the RFP moiety of secN-R_m-2A-GH to the vacuole was dependent on Rab GTPases of the Rab-F2 subclass. It has been shown that a YFP-tagged member of this subclass, *At*RAB-$F2^b$ (ARA7) of *Arabidopsis*, localizes predominantly to this PVC in tobacco leaf epidermis and that the S24N mutant of this protein (YFP-RAB-$F2^{b[S24N]}$) causes the vacuolar marker aleuGFP to be mis-sorted to the vacuole (12). The secN-R_m-2A-GH was infiltrated either alone (Figure 4I–L) or with a strain expressing YFP-RAB-$F2^{b[S24N]}$ and epidermal cells were imaged 54 h later (Figure 4M–P). In the absence of YFP-RAB-$F2^{b[S24N]}$, RFP signals were absent from the cell wall and confined to the vacuole (Figure 4I and asterisked cells in Figure 4M). However, in cells co-expressing YFP-RAB-$F2^{b[S24N]}$, strong RFP fluorescence was detected in the apoplast in addition to the vacuole.

It is notable too that RFP and GFP moieties of secN-R_m-2A-secG_f were additionally observed in punctate structures that were larger and fainter than the PVC (arrowheads in Figure 4E–G). Similar structures have previously been observed with secGFP and identified as Golgi (3). Interestingly, the secN-RFP signal in these structures relative to the ER and PVC was significantly lower than that of secGFP, suggesting that its residence time in the Golgi may be lower. It also confirms that separation of RFP and GFP moieties occurs before the Golgi. We concluded that both the RFP and GFP moieties of the secN-RFP_{myc}-2A and STN-RFP_{myc}-2A fusions were translocated across the ER membrane, but that the RFP moieties were then sorted from the Golgi to the vacuole via the conventional PVC/Rab-F2-dependent pathway rather than following the default pathway to the apoplast.

We next investigated the location of the vacuolar-sorting signal within the RFP moiety of the 2A constructs. To test whether the signal resides within the 2A peptide itself, this sequence was fused to the carboxy-terminus of secRFP (Figure 4Q), a previously described secreted RFP molecule (3), and expressed in tobacco epidermal cells. While secRFP accumulated exclusively in the apoplast without appearing in the vacuole, as reported previously (3), secRFP-2A, which carried the 2A sequence was almost exclusively vacuolar (Figure 4R and S). The 2A sequence is, therefore, sufficient for vacuolar targeting of mRFP1 in the plant endomembrane system.

2A fusions behave similarly in tobacco epidermis and Arabidopsis seedlings

We were interested in knowing whether the 2A-based markers would exhibit similar behaviour in other plant species, particularly the genetic model organism *Arabidopsis thaliana*. Therefore, all of the constructs mentioned above were used to generate stable transformants in *Arabidopsis* and the roots and leaves of T3 homozygous plants were analysed by confocal microscopy. In every case, we observed efficient separation of YFP or RFP moieties from ER-resident or secGFP in the leaves. Notably, the STN-RFP_m-2A and secN-RFP_m-2A proteins accumulated clearly in the vacuoles of leaves as observed in tobacco leaf epidermis (Figure 5). Similar behaviour was observed in roots (data not shown) with the exception of STN-RFP_m-2A-GH where RFP signals were clearly associated with the ER, particularly in meristematic and elongating cells. Thus, the 2A-based constructs behave similarly in the two most common dicot models, *Arabidopsis* and tobacco, and may, therefore, have general utility.

2A fusions involving YFP and RFP are not cleaved with equal efficiency

Confocal analysis suggested that the 2A fusions were cleaved with high efficiency as upstream and downstream moieties accumulated predominantly in distinct compartments. To investigate the efficiency of cleavage directly, protein extracts were prepared from transfected tobacco leaves or transgenic *Arabidopsis* seedlings and analysed on immunoblots using anti-GFP or anti-c-myc antisera. The Y_m-2A, nlsR_m-2A and STN-R_m-2A fusions each gave rise to bands of the expected molecular weight when probed with anti-c-myc antisera in tobacco (Figure 6A), although the

Figure 4: (on previous page) 2A acts as a vacuolar-sorting determinant in tobacco leaf epidermis. Confocal images of tobacco leaf epidermal cells transiently expressing various fluorescent proteins as indicated. (A–D′) secN-R_m-2A-GH infiltrated at OD_{600} 0.25 and examined 48 h later. RFP (red) is visible in the vacuole (A and C′) and associates with the ER network marked by GFP (green) and is also clearly visible in distinct punctate structures that excluded the ER marker (D, arrows). B′–D′ show single sections through the vacuole of cells whose cortical cytoplasm is shown in projection (B–D). Chlorophyll fluorescence is indicated in blue. (E–G) secN-R_m-2A-secG_f similarly imaged to reveal RFP and GFP in transit through the endomembrane system; each protein labels the ER network and putative PVC (arrows) and Golgi stacks (arrowheads). (H) A projection of cells expressing secN-R_m-2A-secG_f, indicating that GFP but not RFP is detectable in the cell wall (arrowheads). (I–P) secN-R_m-2A-GH infiltrated either alone (I–L) or with a strain expressing YFP-RAB-$F2^{b[S24N]}$ (M–P). In the absence of the YFP-RAB-$F2^{b[S24N]}$, RFP signal is absent from the cell wall and confined to the vacuole (I and asterisked cells in M); however, in cells co-expressing the Rab GTPase mutant (numbered 1–5 in M–P), strong RFP fluorescence is detected in the apoplast in addition to the vacuole (arrowheads). The arrow indicates RFP that has apparently diffused from cells 1, 4 and 5 into the adjoining wall between two non-infected cells. RFP is in red, GFP in green and YFP in blue. (Q) Schematic representation of secRFP and secRFP-2A constructs. (R and S) secRFP accumulates exclusively in the apoplast (R) while secRFP-2A is almost exclusively vacuolar (S). (A, B′–D′) and (E–G) are single sections; (B–D, H, I–P) and (R and S) are projections. Scale bars 20 μm (I–P and R and S), 5 μm (H) and 2 μm (E–G).

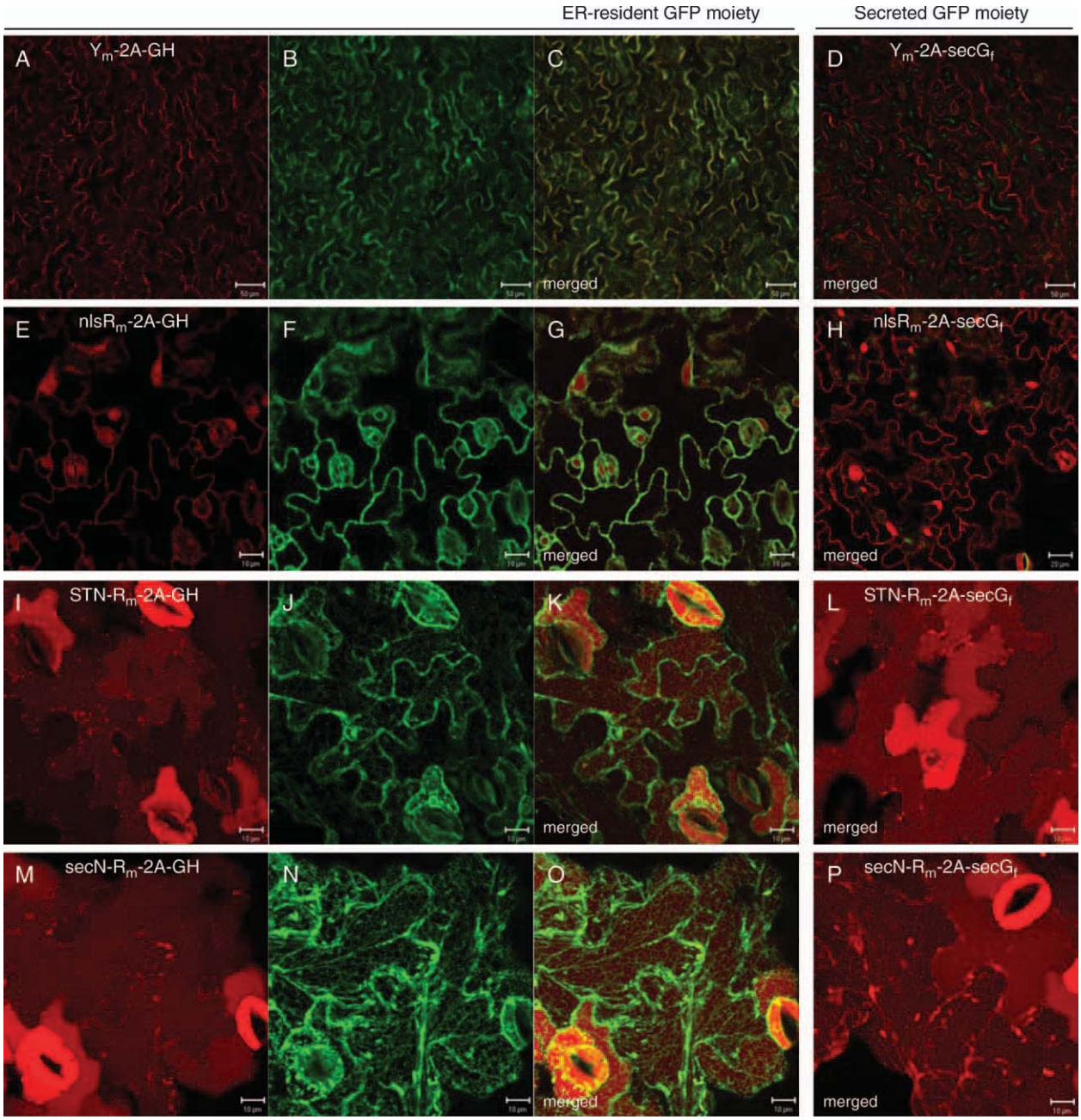

Figure 5: 2A fusions in *Arabidopsis* seedlings. Confocal microscopy of leaves of transgenic *Arabidopsis* plants expressing (A–C) Y_m-2A-GH, (D) Y_m-2A-$secG_f$, (E–G) $nlsR_m$-2A-GH, (H) $nlsR_m$-2A-$secG_f$, (I–K) STN-R_m-2A-GH, (L) STN-R_m-2A-$secG_f$, (M–O) secN-R_m-2A-GH, (P) secN-R_m-2A-$secG_f$. YFP and RFP channels are shown in red and the GFP channel in green. Merged channel images are indicated. (A–H) and (L) are single sections and while (I–K) and (M–P) are projections. Scale bars 50 μm (A–D) and 10 μm (E–P).

YFP_m-2A moiety accumulated as two bands in *Arabidopsis* (Figure 6C, lanes 2 and 3). Occasionally, a second higher band was seen, suggesting some heterogeneity of cleavage or some instability at one or other terminus of the primary cleavage product (data not shown). The same result was obtained with secN-R_m-2A-GH and secN-R_m-2A-$secG_f$ (data not shown). None of the fusions involving RFP gave rise to detectable uncleaved translation product. In contrast, a faint band corresponding to the uncleaved YFP fusions was consistently detectable with Y_m-2A-GH and Y_m-2A-$secG_f$ (Figure 6A and C, arrowheads).

We also probed the same protein extracts with anti-GFP antibodies. This revealed major bands of the expected molecular weight (29 kDa) for all constructs. Consistent with the fluorescence data, ER-resident GFP expressed from the -2A-GH constructs was more abundant than the secreted protein of the -2A-$secG_f$ constructs. Faint bands

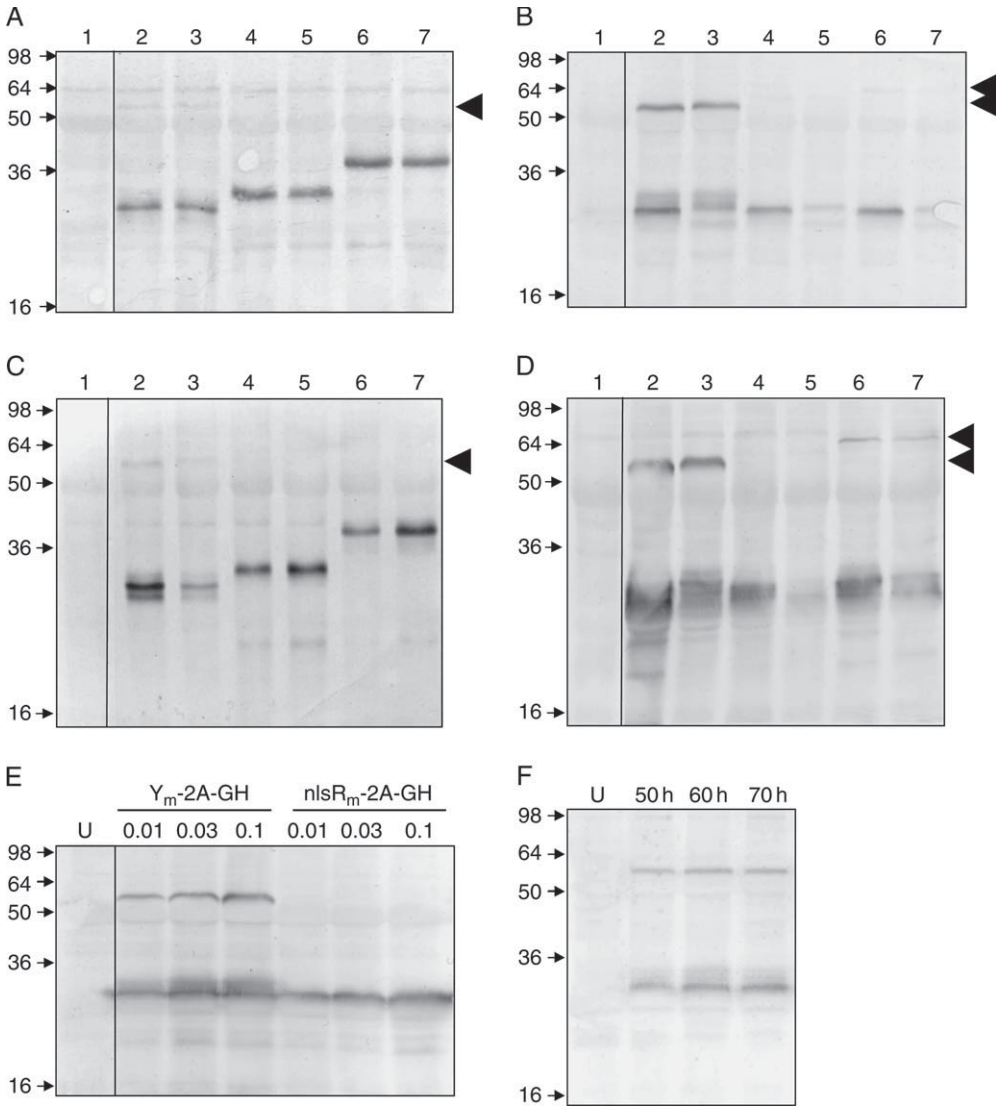

Figure 6: Immunoblot analysis of 2A fusions in transfected tobacco leaves. Immunoblot analysis using anti-c-myc antiserum (A and C) or anti-GFP/YFP antiserum (B and D) of protein extracts prepared from tobacco leaves (A and B) or *Arabidopsis* transgenic seedlings (C and D) expressing Y_m-2A-GH (lane 2), Y_m-2A-secG_f (lane 3), nlsR_m-2A-GH (lane 4), nlsR_m-2A-secG_f (lane 5), STN-R_m-2A-GH (lane 6), STN-R_m-2A-secG_f (lane 7) or non-transfected/non-transgenic plants used as a control (lane 1). Major bands of the expected mobility were detected in all cases, however, full-length, uncleaved, translation product was detected to varying extents with the YFP fusions (lower arrowheads) and mRFP1 fusions (upper arrowheads). (E) Immunoblot analysis using anti-GFP/YFP antiserum of Y_m-2A-GH and nlsR_m-2A-GH tested over a 10-fold range of *Agrobacterium* titres (OD_{600} as indicated). (F) Immunoblot analysis using anti-GFP/YFP antiserum of Y_m-2A-GH over a 20-h period from 50 to 70 h post-infiltration. Lanes labelled U (E and F) show extracts of un-infiltrated leaf. Arrows indicate the positions of markers whose molecular weight is indicated in kDa.

corresponding to the uncleaved product were detectable with the STN-R_m-2A fusions (Figure 6B and D, lanes 6 and 7, upper arrowheads), but significantly more uncleaved Y_m-2A-GH and Y_m-2A-secG_f fusion proteins were detected in both tobacco and *Arabidopsis* (Figure 6B and D, lanes 2 and 3, lower arrowheads). Even allowing for the fact that Y_m-2A fusions bear twice as many GFP epitopes as the RFP-based fusions, it is clear that a greater proportion of the YFP fusions accumulated in the uncleaved form. The ratio of full-length and cleaved translation product did not change when Y_m-2A-GH or nlsR_m-2A-GH were expressed using a 10-fold range of *Agrobacterium* titres (Figure 6E) or when Y_m-2A-GH was monitored over a 20-h period starting approximately 20 h after the onset of transient expression (50–70 h post-infiltration; Figure 6F).

Thus, it appears that the 2A fusions with RFP at their amino-termini were cleaved with greater efficiency than those with YFP at that position. It is notable that the uncleaved YFP fusions were barely detected by the c-myc

antibody so, despite the fact that c-myc occurs only once in the fusion protein whereas the anti-GFP epitopes occur twice, the c-myc epitope is apparently not recognized efficiently in the context of the full-length Y_m-2A fusions.

Ratiometric analysis of membrane traffic in cell populations

We selected nlsR-2A-secG_f and YFP-2A-secG_f to test the effectiveness of ratiometric approaches for quantifying biosynthetic membrane traffic in tobacco epidermal cells. The YFP-2A-secG_f is suitable for use with the quantification method used in Figure 2 as the cytosolic YFP and endomembrane-localized GFP signals are distributed similarly in low-magnification images of transfected cells. The incomplete cleavage of this fusion may not compromise its use in trafficking assays because the uncleaved product appeared to be transported efficiently through the endomembrane system as judged by the lack of intracellular GFP signal in confocal images (Figure 3D). We reasoned that the YFP domain on the cytoplasmic face of endomembrane compartments will experience a constant environment during transit, while the GFP moiety will encounter the same luminal/apoplastic environments as the cleaved secG_f product. Thus, the YFP and GFP fluorescence intensities from the uncleaved transmembrane molecule were expected to respond like those of the separated YFP and GFP moieties when biosynthetic trafficking is inhibited.

Y_m-2A-secG_f or Y_m-2A-GH was expressed either alone or with the dominant N121I mutant of the *Arabidopsis* Rab GTPase, *At*RAB-D2^a (ARA5; AtRab1b; At1g02130), a homologue of mammalian Rab1 (36) that is known to block ER to Golgi transport (3,6,19). The two extremes of the assay were set by the signal from the secGFP marker alone (Figure 7A) and the GFP-HDEL marker (Figure 7C). Consistent with previous observations [(3,6) and H. Betts and I. Moore, unpublished observations], absolute measurements of GFP fluorescence intensity indicated that the dominant-negative *At*RAB-D2$^{a[N121I]}$ mutant had little or no effect on the accumulation of GFP-HDEL already trapped in the ER (Figure 7D and E) but increased the accumulation of secGFP (Figure 7B and E) to 50–75% of the GFP-HDEL value (Figure 7E). When the ratiometric approach, which normalizes for expression level and imaging efficiency using the co-expressed YFP signal, was used to analyse the same images, the results differed in three notable ways (Figure 7F). First, the statistical significance of the data was improved as illustrated by the lower coefficients of variance (Figure 7G). Second, *At*RAB-D2$^{a\ [N121I]}$ caused secGFP to accumulate to levels comparable to those of ER-resident GFP-HDEL (expressed from Y_m-2A-GH), whereas the absolute expression data in Figure 7E and previous studies suggested a figure of only 50–75% of GFP-HDEL. This can be explained most simply by a previously undetected reduction in transient expression efficiency in leaf areas co-infiltrated with the *At*RAB-D2$^{a\ [N121I]}$ mutant strain. Third, the Rab mutant also caused a small but significant ($P = 0.05$) increase in the accumulation of GFP-HDEL owing most probably to escape of some GFP-HDEL molecules from the ER in cells expressing Y_m-2A-GH alone.

Ratiometric analysis of membrane traffic in individual cells

The 2A-based ratiometric approach can also be applied to individual cells imaged at high magnification where it can establish whether the accumulation or mis-localization of a trafficking marker results from inhibition of biosynthetic trafficking or from high rates of marker synthesis. For example in Figure 8A, we infer that cell 2 is presumably co-expressing the co-infiltrated dominant inhibitory *At*RAB-D2$^{a[N121I]}$ mutant as it accumulates more GFP than neighbouring cells or control cells (Figure 8B) with similar nlsRFP accumulation. This approach is potentially versatile, as it can be applied to transfected protoplasts or to specific cells of transgenic plants where the low-magnification method described above is not readily employed.

Therefore, to quantify GFP accumulation ratios in individual cells, we developed an image analysis tool that can be used in conjunction with the nlsR-2A constructs. To measure signals unambiguously from specific cells, analysis was performed on the nucleus and perinuclear region of a series of confocal sections along the *z*-axis. Starting from a position in the nucleus, a series of transects was drawn across the cytoplasm into the surrounding vacuole (see Figure 8C). The maximum GFP signal along each transect was then extracted and averaged, while the nuclear RFP intensity was automatically extracted from the 3D data set from a user-defined seed. Figure 8D shows that in cells expressing nlsR_m-2A-GH, under the imaging conditions used, there was a linear correlation ($R^2 = 0.85$) between the RFP and GFP fluorescence for RFP pixel intensities up to 150, after which GFP-HDEL signal plateaued at less than the maximum possible pixel intensity (255), suggesting saturation of the ER-retrieval mechanism at these expression levels. Similar analysis of cells expressing nlsR_m-2A-secG_f showed that little GFP accumulated in the nuclear envelope or ER over the entire range of RFP expression values (Figure 8D, shaded squares). The slopes of fitted lines indicated that GFP-HDEL accumulated in the ER 1000-fold more efficiently than secGFP_f (GFP-HDEL $= 1.2 \times$ nlsRFP; secGFP_f $= 0.0009 \times$ nlsRFP), providing a far greater dynamic range in this assay method in comparison to the low-magnification approach described hitherto (3) (Figures 2 and 7).

Ratiometric analysis of membrane traffic with quantification of effector levels

In the assays described so far, the presence or absence of the dominant inhibitory mutant in any cell could only be inferred from the value of the secGFP_f ratio. Clearly if the

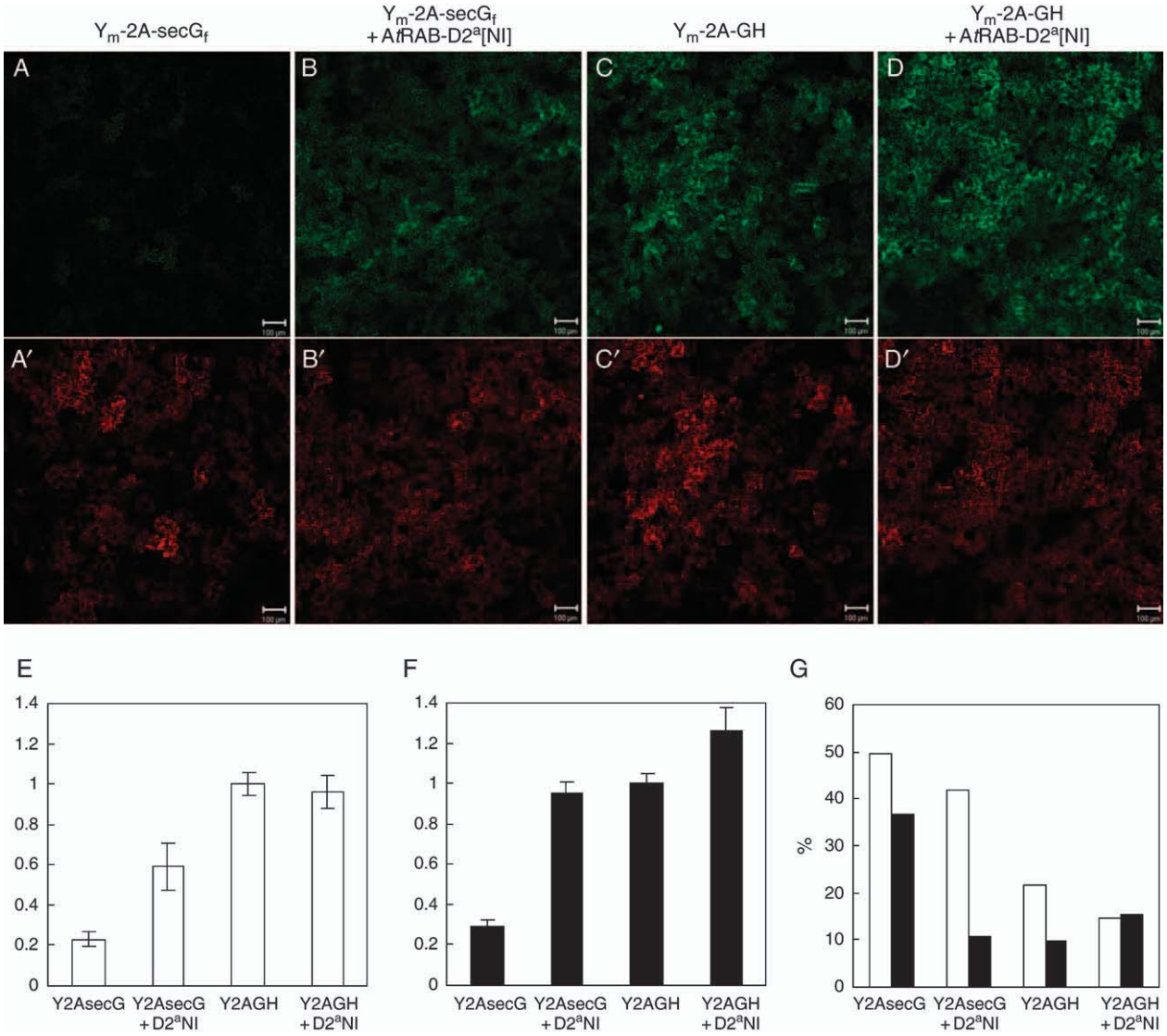

Figure 7: Absolute and ratiometric measurements of GFP trafficking in tobacco leaf epidermal cells. (A–D′) Low-magnification images of Y_m-2A-secG_f expressed alone (A and A′) or co-expressed with *At*RAB-D2$^{a[N121I]}$ (B and B′) and compared with Y_m-2A-GH expressed alone (C and C′) or co-expressed with *At*RAB-D2$^{a[N121I]}$ (D and D′). GFP channel (A–D) is green and YFP channel (A′–D′) is red. Scale bar is 100 μm. (E and F) absolute (E) and ratiometric (F) measurements of secGFP_f and GFP-HDEL accumulation in cells expressing Y_m-2A-secG_f (Y2AsecG) or Y_m-2A-GH (Y2AGH) with or without *At*RAB-D2$^{a[N121I]}$ (D2^{a}NI); means of three experiments normalized to the value for Y_m-2A-GH; error bars are SE. (G) Average coefficient of variance for absolute (open bars) and ratiometric (shaded bars) measurements of GFP accumulation; $n = 5$ except for Y2AGH + D2^{a}NI where $n = 3$. *Agrobacterium* strains were used at OD_{600} 0.05 (Y_m-2A-secG_f and Y_m-2A-GH) or 0.03 (*At*RAB-D2$^{a[N121I]}$), and images were acquired 70–74 h after infiltration.

protein can be visualized by tagging with a third fluorescent protein, its relative abundance in each cell could be determined directly and correlated with its effect on marker trafficking. Tagging *At*RAB-D2$^{a[N121I]}$ with YFP at its amino-terminus renders it inactive and apparently unstable (data not shown), but fusions to the carboxy-terminus were stable and appeared to exhibit some residual inhibitory activity. We, therefore, asked whether this low activity could be quantified using the nlsR_m-2A-secG_f trafficking assay. As shown in Figure 8E–H, accumulation of the secGFP marker was clearly dependent on the abundance of both RFP and *At*RAB-D2$^{a[N121I]}$-YFP in the same transfected cell (compare cells 1 and 2 with cell 3). Using the image analysis tool described above, the YFP, RFP and GFP signal intensities in such images were quantified in cell populations co-infected with nlsR_m-2A-secG_f and either wild-type or mutant YFP-tagged *At*RAB-D2^a. For each cell, the YFP intensity was plotted against the GFP-to-RFP ratio. To provide a standard against which to compare the relative data generated by this analysis, the secGFP signal in each cell was expressed as a percentage of the GFP signal that would be expected for nlsR_m-2A-GH

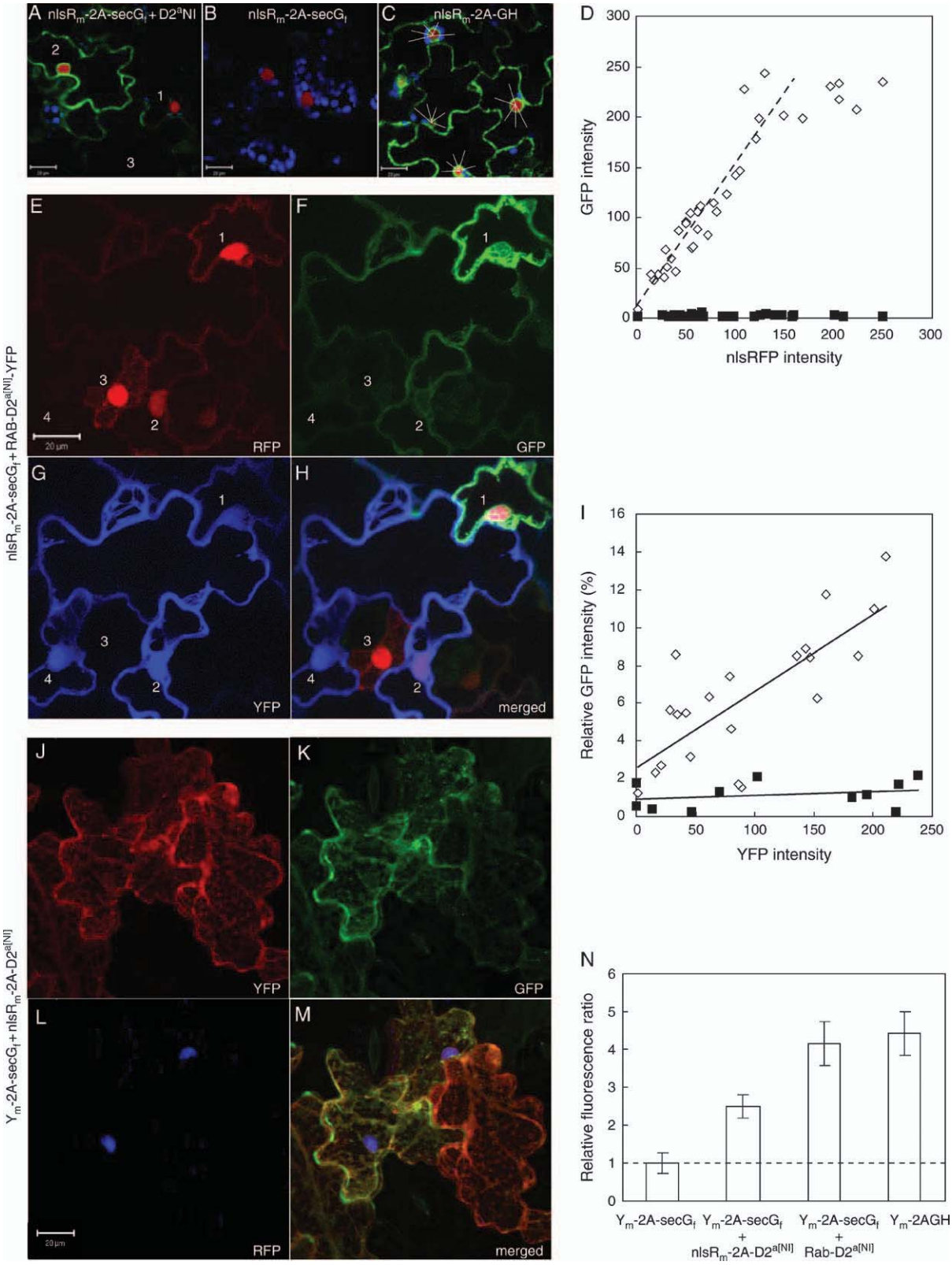

Figure 8: Legend on next page.

expressed at the same level. Thus, the RFP intensity was used to read off the expected GFP-HDEL intensity from the slope of the dotted line in Figure 8D derived from cells expressing nlsR$_m$-2A-GH in the same experiment. Wild-type *At*RAB-D2^a-YFP had no effect on secGFP$_f$ accumulation, but *At*RAB-D2$^{a[N121I]}$-YFP caused secGFP$_f$ to accumulate to approximately 10% of GFP-HDEL in the most highly expressing cells, confirming that it retained some residual inhibitory activity (Figure 8I). Note that this small increase would not be measurable using the previous low-magnification approach (Figure 7).

Use of 2A to monitor the expression level of cytoplasmic effectors

As direct tagging is likely to be problematic for many effector proteins, we next asked whether the 2A peptide could be used to provide a stoichiometric marker for the expression level of proteins such as *At*RAB-D2$^{a[N121I]}$ which exhibit little or no activity when tagged at either terminus. Linking such a protein to a fluorescent marker via the 2A peptide is predicted to leave just a single additional proline residue at the amino-terminus of the tagged protein, which may, therefore, retain functionality. Thus, we fused the *At*RAB-D2$^{a[N121I]}$ ORF downstream of the nlsRFP$_m$-2A coding sequence to generate nlsR$_m$-2A-D2$^{a[NI]}$. nlsRFP$_m$-2A was chosen because it appeared to be more efficiently cleaved than YFP$_m$-2A and should give a readily measurable signal in the nucleus of each transfected cell. This construct was then used in conjunction with Y$_m$-2A-secG$_f$ to assay GFP trafficking. When individual cells were imaged at high magnification, it was evident that high GFP-to-YFP ratios correlated with high-RFP fluorescence in the nuclei (Figure 8J–M).

In these and other membrane trafficking experiments, nlsR$_m$-2A-D2$^{a[NI]}$ typically exhibited a weaker inhibitory influence on trafficking of secreted and Golgi markers than untagged *At*RAB-D2$^{a[N121I]}$ (Figure 8N). Assays of secGFP accumulation using the low-magnification ratiometric method with Y$_m$-2A-secG$_f$ confirmed that nlsR$_m$-2A-D2$^{a[NI]}$ increased secGFP$_f$ accumulation by approximately half as much as native *At*RAB-D2$^{a[N121I]}$. This lower activity may reflect either lower expression efficiency, some sensitivity to the additional amino-terminal proline or inefficient separation of the Rab and RFP moieties leaving dysfunctional full-length protein. When immunoblots of extracts from cells expressing nlsR$_m$-2A-D2$^{a[NI]}$ and control constructs were probed with anti-c-myc antibodies, we observed that approximately 50% of the protein accumulated in the unseparated form (Figure 9A). This result was surprising given the efficient separation of the RFP and GFP moieties in the 2A fusions described above. Therefore, we further investigated the mechanism responsible for cleavage of 2A-fusion proteins.

The FMDV 2A peptide exhibits little activity at the carboxy-terminus of YFP and RFP in tobacco leaf epidermis

The cleavage efficiency of the 2A protein is known to be influenced by sequences upstream but not by sequences downstream (21). Thus, the accumulation of uncleaved 2A fusion protein in cells expressing nlsR$_m$-2A-D2$^{a[NI]}$ suggested

Figure 8: (on previous page) Use of 2A-based ratiometric markers for analysis of individual tobacco leaf epidermal cells. Single optical sections of cells from infiltrated leaves expressing (A) nlsR$_m$-2A-secG$_f$ and *At*RAB-D2$^{a\ [N121I]}$, (B) nlsR$_m$-2A-secG$_f$, only, or (C) nlsR$_m$-2A-GH; in (C) transects used for image analysis are displayed as white lines. In (A), the expression level of the marker is similar in cells 1 and 2 and similar to the control cells in (B) as indicated by the intensity of the red nuclei, however, only cell 2 accumulates secGFP (green); note that the weak GFP signal below nucleus 1 is in the adjacent cell 3; chlorophyll fluorescence is indicated in blue. (D) GFP intensity in the nuclear envelope and adjacent cytoplasm plotted against nuclear RFP intensity in individual cells expressing either nlsR$_m$-2A-secGFP$_f$ (shaded squares) or nlsR$_m$-2A-GH (open squares); each datum represents a measurement from a single cell; the dotted line through the data for nlsR$_m$-2A-GH shows the best fit ($R^2 = 0.85$) for nlsRFP values from 0 to 150 above which GFP-HDEL accumulation plateaus. (E–H) Projections of a series of optical sections from tobacco leaf epidermis expressing the ratiometric marker nlsR$_m$-2A-secG$_f$ and C-terminally tagged *At*RAB-D2$^{a[N121I]}$-YFP. Cell 1 expresses both constructs to high level as indicated by the nlsRFP signal (red) and YFP signal (blue) and accumulates high levels of secGFP$_f$ (green); cell 2 expresses less of the marker and accumulates less secGFP$_f$; cell 3 expresses only the marker and indicates the extent of secGFP$_f$ accumulation in control cells while cell 4 expresses only the YFP-tagged Rab GTPase and indicates that there is minimal bleed-through into the GFP channel under these conditions; (E–H) show the individual detection channels and merged image as indicated. (I) Quantitative analysis of secGFP$_f$ accumulation relative to the expression of YFP-tagged *At*RAB-D2^a wild type (shaded squares) and N121I mutant (open squares) in individual tobacco leaf epidermal cells; to assess the extent of secGFP$_f$ accumulation, GFP fluorescence is expressed as a percentage of the GFP fluorescence that would be expected if nlsR$_m$-2A-GH was expressed at the same level as nlsR$_m$-2A-secG$_f$ in each cell, based on its individual RFP signal and the slope of the line in (D) which was obtained from control cells expressing nlsR$_m$-2A-GH only; GFP data is corrected for bleed-through of YFP fluorescence into the GFP channel using a function determined by analysis of cells that expressed only the YFP-tagged wild-type Rab GTPase. (J–M) Projections of optical sections through the cortical cytoplasm of cells from leaf areas co-transfected with the Y$_m$-2A-secG$_f$ and nlsR$_m$-2A-D2$^{a[NI]}$ constructs; (J–M) show the individual detection channels and merged image as indicated. (N) Ratiometric measurements of secGFP$_f$ accumulation in cells expressing Y$_m$2AsecG$_f$ alone or together with nlsR$_m$-2A-D2$^{a[NI]}$ or *At*RAB-D2$^{a[N121I]}$ compared with Y$_m$2AGH. Bars indicate means of three experiments normalized to the value for Y$_m$-2A-secG$_f$; error bars are SE. Scale bars in all images are 20 μm. Infiltrations were performed with nlsR$_m$-2A-secG$_f$ and nlsR$_m$-2A-GH strains at OD$_{600}$ 0.05 (A–C), 0.04 (D and I) or 0.02 (E–H); *At*RAB-D2^a-YFP and *At*RAB-D2$^{a[N121I]}$-YFP strains at OD$_{600}$ 0.02; and *At*RAB-D2$^{a[N121I]}$ and nlsR$_m$-2A-D2$^{a[NI]}$ at OD$_{600}$ 0.03.

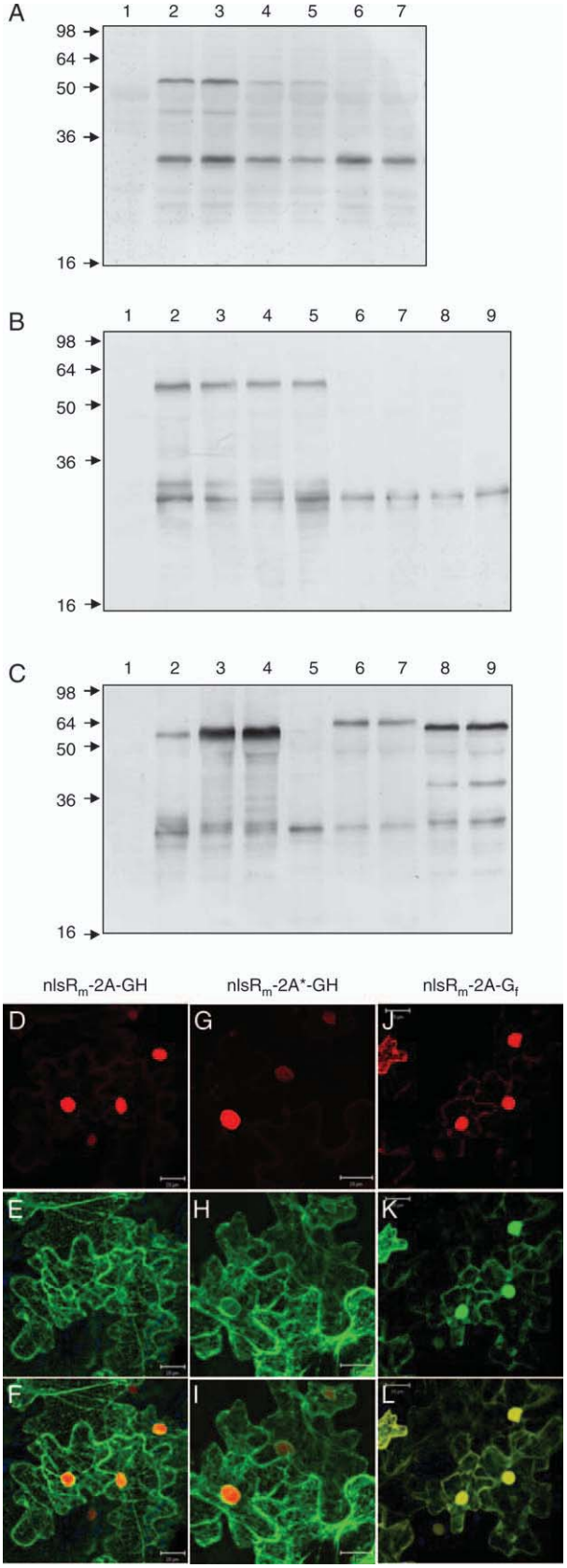

Figure 9: Analysis of fusion proteins with or without functional 2A sequences or signal peptides in tobacco epidermal cells. For each construct extracts were prepared from cells expressing two independently constructed plasmids. Arrows indicate the positions of markers and their molecular weights are given in kDa. (A) Immunoblot analysis of 2A fusions to *At*RAB-D2^a using anti-c-myc antiserum. Lanes: 1, uninfected tissue; 2 and 3, nlsR$_m$-2A-D2^a wt; 4 and 5, nlsR$_m$-2A-D2$^{a[NI]}$; 6 and 7, control nlsR$_m$-2A-GH. (B) Immunoblot analysis using anti-GFP/YFP antiserum of constructs carrying wild-type or mutant 2A sequences. Lanes: 1, uninfected tissue; 2 and 3, Y$_m$-2A*-GH; 4 and 5, Y$_m$-2A-GH; 6 and 7, nlsR$_m$-2A*-GH; 8 and 9, nlsR$_m$-2A-GH. (C) Immunoblot analysis using anti-GFP/YFP antiserum of 2A fusions with or without a signal peptide. Lanes: 1, uninfected tissue; 2, Y$_m$-2A-GH control; 3 and 4, Y$_m$-2A-G$_f$; 5, nlsR$_m$-2A-GH control; 6 and 7, nlsR$_m$-2A-G$_f$; 8 and 9, Y$_m$-2A-nlsR$_f$. (D–L) Projections of series of confocal images of tobacco leaf epidermal cells expressing nlsR$_m$-2A-GH (D–F), nlsR$_m$-2A*-GH (G–I) and nlsR$_m$-2A-G$_f$ (J–L); RFP is in red, GFP in green, chlorophyll in blue, (F, I and L) merged channels. Scale bars 20 μm.

that the apparently efficient cleavage of other nlsRFP-2A fusions may have resulted either from instability of the uncleaved fusion protein or from cleavage by a mechanism that is independent of 2A. One possibility for such a mechanism was cleavage by signal peptidase between the signal peptide and the GFP sequence of the various 2A-GH and 2A-secG$_f$ fusions.

To test these possibilities, we assembled a series of fusions that either lacked the signal peptide or carried a mutant form of the 2A sequence (here designated 2A*) in which the two terminal residues were each converted to alanine (Figure 1T, underlined). Either substitution is sufficient to prevent 2A-mediated polypeptide separation during translation *in vitro* or in mammalian cells (21,29,37). As shown in Figure 9B, Y$_m$-2A*-GH and nlsR$_m$-2A*-GH, which carried the mutant 2A sequence, gave rise to almost identical ratios of monomeric and dimeric translation products as the corresponding wild-type clones, although the mutant sequence sometimes resulted in lower quantities of expressed protein. Confocal analysis of transfected cells also indicated efficient separation of the GFP-HDEL moiety from the upstream YFP or RFP moiety of the 2A* fusions (Figure 9D–I and data not shown). Conversely, when the signal peptide was eliminated from Y$_m$-2A-GH or nlsR$_m$-2A-GH fusions, giving rise to Y$_m$-2A-G$_f$ and nlsR$_m$-2A-G$_f$, or when nlsRFP was placed downstream of Y$_m$-2A, the translation product accumulated predominantly as the uncleaved fusion (Figure 9C). Images of transfected cells confirmed that in the absence of a signal peptide, the GFP and RFP moieties of nlsR$_m$-2A-G$_f$ accumulated at the same ratio in nucleus and cytoplasm of infected cells (Figure 9J–L). Together, these results indicate that the presence of a signal peptide, but not a functional 2A sequence is critical for separation of the GFP moiety from the upstream RFP and YFP moieties in the Y$_m$-2A-GH and nlsR$_m$-2A-GH constructs. In the case of the nlsR$_m$-2A-D2^a proteins, as we do not have antibodies to detect the *At*RAB-D2^a moiety, it remains unclear

whether the monomeric nlsRFP$_{myc}$ species arose from partial 2A-mediated cleavage or instability of the Rab moiety in the fusion protein.

Given previous reports of successful separation of GFP-2A fusions in plant and animal cells and *in vitro* translation systems, we asked whether the presence of the c-myc epitope tag immediately upstream of the 2A sequence in all of our fusions influenced the results. Y$_{nomyc}$-2A-G$_f$ is identical to Y$_m$-2A-G$_f$ except for the absence of the myc sequence between the C-terminus of YFP and the 2A peptide (Figure 1D and E). As shown in Figure 10, this construct exhibited the same intracellular distribution as Y$_m$-2A-G$_f$ in transfected cells and accumulated predominantly as a dimer when analysed by immunoblot (Figure 10G). Thus, the behaviour of 2A in the constructs described here is not determined by the presence of the c-myc sequence at its amino-terminus.

The 2A sequence is required for correct assembly and targeting of STN-RFP-2A-GH translation products

The conclusion that nlsRFP$_{myc}$-2A is cleaved inefficiently in plant cells raised questions about the mechanism responsible for the correct insertion of RFP and GFP moieties into the ER during translation of STN-R$_m$-2A-GH and secN-R$_m$-2A-GH. As discussed earlier, because the upstream RFP moiety of these constructs is translocated through the ER, if cleavage did not occur the signal peptide of the GFP moiety would be expected to enter the ER translocation channel amino-terminus first where it would act as a stop-transfer signal leaving the GFP moiety, its signal-peptidase cleavage site, and its ER-retrieval signal on the cytoplasmic face of the ER membrane. In contrast, GFP appeared to be separated efficiently from the RFP moiety and to accumulate in the ER lumen (e.g. Figure 3I–P and 6B). To investigate whether 2A is indeed essential for the correct processing of STN-R$_m$-2A-GH, a derivative carrying the mutant 2A sequence was constructed. When this was expressed in tobacco leaf epidermal cells, the mutant 2A sequence caused a dramatic reduction in the accumulation of both the RFP and the GFP moieties (Figure 11A–F). When transfected cells were imaged under conditions that allowed the accumulated protein to be visualized, it was clear that some RFP was present in structures typical of the Golgi, but a significant proportion was associated with the ER which also accumulated a small quantity of GFP (Figure 11G and H). Immunoblot analysis confirmed that very little STN-R$_m$-2A*-GH translation product accumulated and that all the visibly accumulated protein was full length (Figure 11I). Thus, the presence of a wild-type 2A sequence is responsible for the efficient processing, sorting and stable accumulation of STN-R$_m$-2A-GH translation products. As discussed below, in light of the results with mutant 2A peptides in other proteins, it may be that correct processing of STN-R$_m$-2A-GH and secN-R$_m$-2A-GH constructs is dependent on a property of the 2A peptide that is unrelated to its self-cleaving activity.

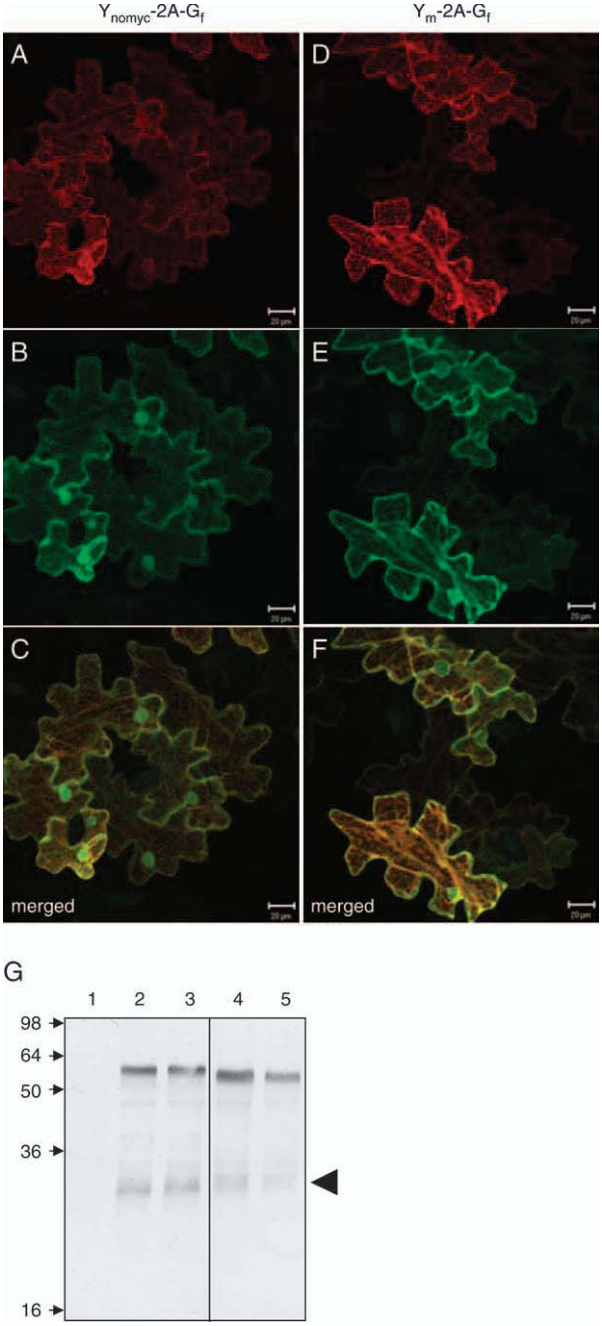

Figure 10: Confocal and immunoblot analysis of Y$_{nomyc}$-2A-G$_f$. Projections of series of confocal images of tobacco leaf epidermal cells expressing (A–C) Y$_{nomyc}$-2A-G$_f$ and (D–F) Y$_m$-2A-G$_f$; YFP is in red and GFP is in green. (G) Immunoblot analysis of transfected tobacco leaf tissues using anti-GFP/YFP antiserum. Lane 1, uninfected tissue; lanes 2 and 3, independent Y$_{nomyc}$-2A-G$_f$ constructs; lanes 4 and 5, independent Y$_m$-2A-G$_f$ constructs. The minor bands detected (arrowhead) represent the cleaved translation products. Arrows indicate the positions of markers whose molecular weight is indicated in kDa.

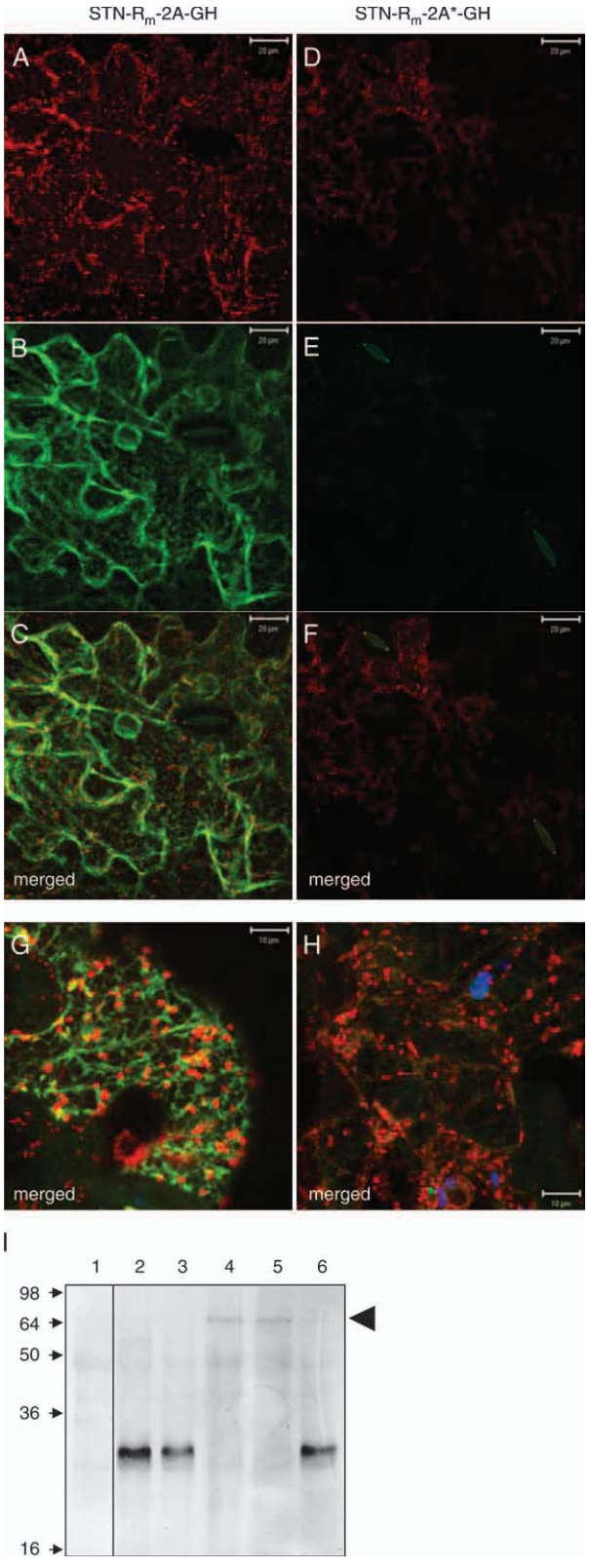

Figure 11: The 2A sequence is important for proper assembly and targeting of STN-R_m-2A-GH. Projections of series of confocal images of tobacco leaf epidermal cells expressing STN-R_m-2A-GH (A–C and G) or STN-R_m-2A*-GH (D–F and H). RFP is in red and GFP in green. (G and H) merged channels from images acquired with enhanced sensitivity allowing the translation products of STN-RFP_m-2A*-GH to be visualized (chlorophyll is in blue). Scale bars 20 μm (A–C and D–F) and 10 μm (G and H). *Agrobacterium* strains were inoculated at OD_{600} 0.06. (I) Immunoblot analysis using anti-GFP/YFP antiserum. Lane 1, uninfected tissue; lane 2, $nlsR_m$-2A-GH; lane 3, $nlsR_m$-2A*-GH; lanes 4 and 5 two independently constructed STN-R_m-2A*-GH fusions; lane 6, STN-R_m-2A-GH. The weak bands in lanes 4 and 5 (arrowhead) represent the uncleaved translation product of STN-R_m-2A*-GH. Arrows indicate the positions of markers whose molecular weight is indicated in kDa.

Discussion

The ratiometric assay described here offers greatly improved quantitative assays of biosynthetic membrane traffic in plant cells using fluorescence microscopy. We show that two polypeptides derived from a single ORF can be differentially targeted between cytoplasmic and endomembrane compartments if a signal peptide is positioned between the polypeptides. However, contrary to expectation, the use of a self-cleaving peptide such as the FMDV 2A peptide was unnecessary unless both polypeptides were translocated across the ER membrane. Furthermore, it was shown that the FMDV 2A peptide resulted in low rates of polypeptide separation in plant cells when placed downstream of mRFP1 or GFP derivatives.

Ratiometric trafficking assays using FMDV 2A fusions

Imaging protocols to quantify intracellular accumulation of secGFP in transfected tobacco leaf epidermis have been described (3), but the ratiometric constructs described here improve these assays in several ways. The ratiometric approach reduces the error associated with variable transfection rates and variable sampling of 3D space within and between experiments. It normalizes, too, for systematic variations in transfection rates between treatments. It also allows saturation phenomena to be identified and data to be collected only from cells with appropriate expression levels (see for example Figure 8D). These allow the influence of a test construct to be established with greater accuracy and statistical support. The ratiometric constructs can also be used to quantify marker expression and trafficking in individual cells using an image analysis tool developed specifically for the purpose. This quantification procedure has a far greater sensitivity, accuracy and dynamic range; with secreted and ER-resident GFP markers exhibiting a 1000-fold difference in accumulation compared with the approximately fivefold difference they exhibit in our previous protocol (3). The method is also more versatile, being applicable to transfected protoplasts that are commonly used for trafficking studies (13–15,19) and also to specific cell types of transgenic plants (3,5). The approach also allows multiple data points to be

extracted from cells in a single transfection experiment. Variability in marker expression can be positively exploited to plot accumulation against expression and it is this that provides the high dynamic range in estimated trafficking rates noted above. Importantly, nlsR$_m$-2A and Y$_m$-2A fusions behave similarly in the two commonly used model dicots, tobacco and *Arabidopsis*.

Cleavage products containing the 2A peptide are sorted from the Golgi to plant vacuoles

It is shown that the 2A sequence contains an efficient vacuolar-sorting signal for tobacco epidermal cells. Consequently, when a cleavage product bearing the 2A sequence at its carboxy-terminus was located in the endomembrane system, it was sorted to the vacuole rather than being secreted. The *Arabidopsis* endomembrane system also sorted 2A-containing proteins to the vacuole, suggesting that the sorting mechanism is conserved. This property of 2A-based proteins will restrict its suggested use for modification of plant cell wall and endomembrane metabolism (25–28,38) and can explain some previous failures of 2A-based co-expression strategies. For example, when two secreted plant defensins, linked via the FMDV 2A peptide, were expressed in *Arabidopsis* (28), the protein upstream of 2A remained intracellular, while the subunit at the carboxy-terminus was secreted. In light of our observations, it now seems likely that the amino-terminal subunit was sorted to the vacuole owing to the 2A-derived sequence at its carboxy-terminus, a conclusion that is consistent with the circumstantial evidence discussed by François et al. (28).

The secN-R$_m$-2A-GH may be useful for assaying vacuolar sorting. The secN-R$_m$-2A moiety appears to follow the same vacuolar pathway as proteins bearing sequence-specific vacuolar-sorting signals as it traffics through a PVC on a Rab-F2-dependent pathway, as described for aleuGFP (12). The GFP-HDEL signal can be used to monitor expression levels to avoid saturation of the sorting receptor, as its accumulation is unlikely to be affected by specific intervention in the vacuolar-sorting process. As mRFP1 is stable in both the vacuole and apoplast, the proportion of the protein in each location is readily observed, although diffusion of RFP in the apoplast (Figure 4P, arrow) may complicate the analysis of sorting events in individual cells.

The 2A peptide does not promote efficient cleavage at the carboxy-terminus of GFP or RFP derivatives in plant cells

Our observations indicate that in plant cells, the 2A peptide promotes minimal polypeptide separation when placed downstream of GFP and RFP derivatives. Previous reports have indicated that 2A cleavage activity can exhibit wider sequence-specific variation in plants than in animals, so these data do not necessarily contradict reports of successful 2A-mediated cleavage in plants (21,23,29,39). As FMDV is presumably optimized to function at 37°C rather than at 21°C, at which our plants were incubated, we incubated plants at 17, 21 or 30°C but saw no differences in cleavage efficiency, suggesting that temperature is not a significant factor (data not shown). YFP and mRFP1-based fusions carrying downstream signal peptides exhibited different efficiencies of polypeptide cleavage. However, this may reflect differences in the efficiency of signal peptide insertion and cleavage rather than differences in 2A-mediated cleavage, as mutation of 2A had little or no effect on any YFP-2A or RFP-2A fusion. Whatever the mechanism, as these fusions all have an identical 15-residue linkers and epitope tag sequence immediately upstream of 2A, sequences still further upstream must play important roles in determining cleavage efficiency, perhaps by formation of interfering secondary structures in the ribosome exit channel. Consistent with this, deletion of the c-myc sequence had no effect on cleavage.

Unfortunately, the inefficient cleavage of 2A-based markers with mRFP1 or YFP as the amino-terminal moiety prevented us from using 2A technology to circumvent the inherent sensitivity of *At*RAB-D2[a] to tagging of its amino-terminus, so other strategies will be needed to determine the expression levels of such proteins in individual cells. The poor activity of 2A in mediating chain separation downstream of common fluorescent proteins must also be considered if it is to be used for applications such as stoichiometric expression of FRET pairs (FRET is fluorescence resonance energy transfer).

Our conclusion that 2A works inefficiently downstream of GFP is at odds with that of El Amrani et al. (27). They reported on a construct in which an ER-targeted GFP derivative (GFP with a signal peptide and carboxy-terminal KDEL signal for retrieval to the ER) was followed by 2A and a phleomycin-resistance marker, Ble. Immunoblot analysis of transgenic cells showed that the GFP and Ble moieties were efficiently separated and that GFP was detectable in the ER. However, constructs lacking functional 2A sequences were not studied, so it is unclear whether the 2A sequence contributed to the separation of GFP and Ble moieties. Indeed, the conclusion that GFP was efficiently retained in the ER after 2A-mediated separation, which would leave the 2A sequence at the C-terminus of the GFP-KDEL moiety, is at odds with the highly conserved extreme C-terminal location of ER-retrieval signals in animals, fungi and plants (40,41). Furthermore, it was not demonstrated directly that the Ble protein was indeed cytosolic (27). The observations of El Amrani et al. are, however, compatible with an alternative interpretation that is consistent with our findings. We suggest that in most cases, the entire GFP-2A-Ble fusion was translocated intact into the ER by the signal peptide at its amino-terminus. It was then exported to the Golgi and, as retrieval to the ER was ineffective owing to the internal location of the KDEL motif, it was transported either to the cell wall by default or was sorted to the vacuole by virtue of the 2A peptide (see above). In either location, proteolysis

at the carboxy-terminus of GFP, which is known to occur in tobacco and *Arabidopsis* cells (6,9,16,17), would cause separation of GFP and Ble. Indeed, the low stability of GFP in the apoplast and vacuoles of tobacco leaf epidermis (3,6) could account for the low accumulation of the GFP moiety relative to the ER-resident GFP control (27). The weak GFP fluorescence detected in the ER may represent newly synthesized protein in transit at steady state, as observed previously (3).

The roles of 2A and signal/anchor sequences in differential targeting of polyprotein-derived polypeptides in plants

A surprising conclusion from our analysis of the ratiometric markers in plant cells is that the 2A sequence was not required for targeting and separation of proteins that accumulated on different sides of the ER membrane. It appears that the signal peptide sufficed to give efficient cleavage, presumably by signal peptidase, ensuring that the sequence at its carboxy-terminus was translocated into the ER lumen while amino-terminal moieties remained on the cytosolic side.

Similar considerations may apply when the 2A peptide is used to deliver two proteins to other organelles. Ralley et al. (24) added a chloroplast transit peptide to each of two bacterial enzymes involved in carotenoid metabolism and linked them via the 2A peptide. Both enzymes were detected in the plastids of transgenic plants. The downstream enzyme accumulated at the native molecular weight indicating that the transit peptide had been removed. However, the molecular weight of the upstream moiety could not be determined and constructs lacking a functional 2A sequence were not investigated. Consequently, it is not clear that cleavage occurred at the 2A peptide nor that the 2A sequence was essential for polypeptide separation. It remains possible that another mechanism such as transit peptide cleavage was responsible for processing the polyprotein.

In contrast to our findings with tobacco and *Arabidopsis*, in transfected mammalian cells, ER- and Golgi-targeted protein moieties located downstream of YFP-2A required the 2A peptide for translocation into or through the ER membrane (29). It is unclear whether this difference arises from some detail of the fusions used or from differences in the ability of plant and mammalian cells to act on internally positioned signal peptides.

The role of 2A during co-translational insertion of dual constructs into the ER

In contrast to constructs carrying a single internal signal peptide in which 2A contributed little to targeting or separation of the upstream and downstream moieties, a construct that carried more than one signal peptide or signal anchor sequence was dependent on a functional 2A sequence for correct targeting, efficient separation and stable accumulation (STN-R_m-2A-GH). Similarly, when maize β- and δ-zein proteins, each carrying its own signal peptide, were expressed in transgenic tobacco as a fusion protein linked by 2A, β-zein-2A and δ-zein moieties were readily detected, but when the zeins were fused directly without 2A, the fusion was highly unstable and no separation of β- and δ-zein moieties was observed (25). In each of these studies, therefore, 2A appears to promote the stable accumulation of two separate polypeptides targeted to the ER membrane or lumen. In the absence of 2A-mediated cleavage, the second signal peptide is expected to act as a stop-transfer signal preventing the downstream sequence from entering the lumen or membrane of the ER. It is unclear why the resulting fusion proteins are unstable in these cases, but it may be that the second transmembrane domain interferes with proper protein folding. We suggest two non-exclusive explanations to account for the requirement for 2A when targeting two polypeptides to the ER.

One possibility is that 2A-mediated polypeptide separation occurs during translation of some proportion of proteins. These separated molecules may then be independently inserted into the ER using their respective signal peptide or signal anchor sequences. In contrast, those translation products that are not separated during translation may be unstable, as observed for the 2A* constructs and are, therefore, not detected. This model is consistent with the observation that 2A may effect limited polypeptide separation downstream of mRFP1 derivatives. However, it also predicts that significantly less RFP should accumulate from secN-RFP_m-2A-GH and STN-RFP_m-2A-GH (two signal peptide/anchor sequences) than from nlsRFP$_m$-2A-GH (single signal peptide); yet, we have no evidence from our immunoblot or imaging analyses that this is the case (e.g. Figure 6A).

An alternative hypothesis is that some feature of the 2A peptide that is independent of its role in polypeptide separation facilitates correct insertion of the second signal peptide into the translocation channel while still part of a polyprotein. In this regard, we note that structural predictions for the 2A sequence suggest that it has an α-helical structure with a sharp type-VI reverse turn formed at its C-terminus by the PGP tripeptide. Proteins can adopt secondary structures within the exit tunnel of the ribosome and in the mouth of the Sec61/SecY translocon (33–35). Indeed, it appears that signal sequences can flip orientation within the translocation channel and have tens of seconds to achieve their preferred orientation (35,42). We suggest that this tight turn may have formed at the carboxy-terminus of 2A by the time it emerges from the ribosome exit tunnel, causing the second signal peptide to be presented to the translocon with its amino-terminus oriented towards the cytosol as normal (Figure 12C). In this orientation, rather than acting as a stop-transfer signal, the signal sequence could allow subsequent translation to translocate the remaining sequence into the ER lumen as

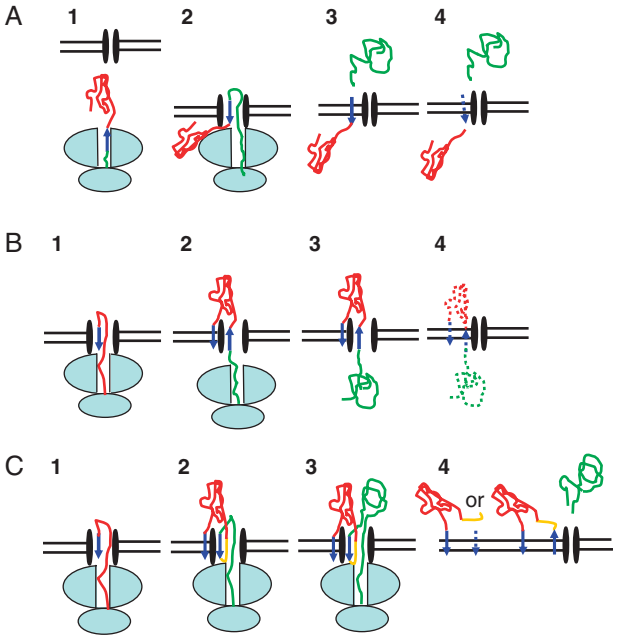

Figure 12: Schematic model for processing of various polyproteins in plant cells. (A) Polyproteins bearing a single internal signal peptide. The amino-terminal moiety (red) is translated on free ribosomes (1) which are targeted to the translocation channel (black ovals) upon emergence of the signal peptide (blue arrow) which is inserted as normal with the amino-terminus towards the cytosol (2); translation translocates the carboxy-terminal moiety (green) across the ER membrane and signal peptidase cleaves to release it (3); the signal peptide at the carboxy-terminus of the amino-terminal moiety is presumably degraded (4) as the amino-terminal moieties were observed to accumulate in the cytosol and nucleus without preferential accumulation at the ER membrane. (B) Polyproteins bearing two signal peptides or signal anchors. The signal on the amino-terminal moiety targets the ribosome to the translocation channel (1) causing translocation of the nascent chain across the membrane; the second signal peptide enters the translocon amino-terminus first and acts as a signal anchor blocking further translocation (2) and causing the carboxy-terminal moiety to accumulate on the cytoplasmic face of the membrane (3); as the signal peptidase cleavage site is on the cytoplasmic face, it cannot effect chain separation and the resulting fusion protein is unstable (4). (C) Polyproteins bearing two signal peptides or signal anchors and a wild-type 2A sequence. Step 1 proceeds as in (B) but when the 2A signal peptide enters the translocon the tight Type-VI turn at the carboxy-terminus of 2A (yellow line) helps to orient the second signal peptide with its amino-terminus towards the cytoplasm allowing translation to translocate the downstream moiety across the membrane; signal peptidase cleaves the fusion and the signal peptide at the carboxy-terminus of 2A is either degraded (as in A) or my remain attached and membrane associated if it is able to flip orientation in the translocon as nascent signal peptides can (34,42); fusions carrying the mutant 2A* sequence act as in (B) owing to disruption of the type-VI turn in the 2A sequence.

normal (Figure 12). The mutations in the PGP tripeptide of 2A that disrupt its polypeptide separation activity are also predicted to disrupt formation of the type-VI reverse turn and thus to prevent the second signal peptide from being presented in the manner envisaged here. Consequently, in the case of 2A* fusions, a second signal peptide is expected to enter the translocon amino-terminus-first, partition into the lipid bilayer and act as a stop-transfer signal. Structural and mutational analysis may help to distinguish these possible mechanisms.

Materials and Methods

Molecular cloning

Standard molecular techniques as described by Ausubel et al. (43) were followed. Firstly, several DNA fragments were generated by polymerase chain reaction (PCR) using Platinum *Pfx* DNA polymerase (Invitrogen, Carlsbad, CA, USA) using the following primers: (i) myc-2A using primers P1 + P2; (ii) 2A-GFP$_{flag}$ using primers P3 + P5; (iii) 2A-secGFP$_{flag}$ using primers P4 + P5; and (iv) 2A-GFP-HDEL using primers P4 + P6. pBINm-gfp5-ER (K. Siemering, S. Hodge, J. Haseloff, MRC Laboratory of Molecular Biology, Cambridge, UK) was used as a template for GFP fusions and pGUS-2A-GFP (22) was used as a template for 2A. Secondly, by overlapping-PCR, fragment 1 was joined to fragments 2 and 3 using primers P1 + P5 and to fragment 4 using primers P1 + P6. The PCR products were digested with *Xba*I/*Bam*HI, cloned into the same sites of pBluescript II SK+ (Stratagene, La Jolla, CA, USA) and confirmed by sequencing. YFP$_{myc}$ was amplified using primers P7 + P8 and pVKH-N-ST-YFP (11) as a template. The product was digested with *Xho*I and *Bam*HI, cloned into pBluescript and checked by sequencing. The *Xho*I/*Bam*HI fragment was re-isolated and cloned downstream of an enhanced CaMV 35S promoter in the *Sal*I–*Bam*HI sites of pVKHEn6-Ara5m-ΔGUS vector (6) replacing the previous insert to generate pVKHEn6-YFP$_{myc}$ (YFP$_{myc}$). Y$_m$-2A-G$_f$, Y$_m$-2A-secG$_f$ and Y$_m$-2A-GH were created by cloning *Xba*I/*Bam*HI fragments (isolated from the appropriate pBluescript derivatives described above) containing 2A-GFP$_{flag}$, 2A-secGFP$_{flag}$ and 2A-GFP-HDEL into *Xba*I and *Bam*HI sites of the YFP$_{myc}$ vector. Y$_{nomyc}$-2A-G$_f$ was created by cloning *Xba*I/*Bam*HI fragment containing 2A-GFP$_{flag}$ isolated from Y$_m$-2A-G$_f$ into *Spe*I and *Bam*HI sites of pVKHEn6-HAvenus (3) from which a stop codon was deleted.

The nlsRFP$_{myc}$ fragment was amplified using primers P9+P10 and mRFP1 (32) as a template. By overlapping-PCR, myc-2A fragment (see above) was added to it using primers P11 + P12. The PCR (nlsRFP$_{myc}$2A*stop*) product was digested with *Xho*I and *Bam*HI, cloned into pBluescript and checked by sequencing. nlsR$_m$-2A-secG$_f$ and nlsR$_m$-2A-GH were created by cloning *Xho*I/*Xba*I fragment containing nlsRFP$_{myc}$ (isolated from nlsRFP$_{myc}$2A*stop*) into *Sal*I and *Xba*I sites of Y$_m$-2A-secG$_f$ and Y$_m$-2A-GH vectors replacing the YFP$_{myc}$ fragment. nlsR$_m$-2A-G$_f$ was created by cloning *Xba*I/*Bam*HI fragment containing 2A-GFP$_{flag}$ isolated from Y$_m$-2A-G$_f$ into the same sites of nlsR$_m$-2A-GH and/or nlsR$_m$-2A-secG$_f$ vectors replacing the 2A-GFP-HDEL and/or 2A-secGFP$_{flag}$ fragments.

The STN fragment was amplified using primers P13 + P14 and pVKH-N-ST-YFP (11) as a template. N-RFP$_{myc}$ fragment was amplified using primers P15 + P16 (and nlsRFP$_{myc}$2A*stop* as a template). The two fragments were joined together by overlapping PCR using primers P13 + P16, the product (STN-RFP$_{myc}$) was digested with *Bam*HI and *Xba*I, cloned into pBluescript and checked by sequencing. STN-R$_m$-2A-secG$_f$ and STN-R$_m$-2A-GH were created by cloning *Spe*I/*Xba*I fragment containing STN-RFP$_{myc}$ (isolated from pBluescript) into the same sites of Y$_m$-2A-secG$_f$ and Y$_m$-2A-GH vectors, respectively, replacing the YFP$_{myc}$ fragment. secN-R$_m$-2A-secG$_f$ and secN-R$_m$-2A-GH were created by cloning *Sal*I/*Bam*HI fragment containing N-RFP$_{myc}$-2A-secG$_f$ and N-RFP$_{myc}$-2A-GH isolated from the STN-RFP$_{myc}$-2A clones (see above) into the same sites of pVKH-N-secYFP (11) vector replacing the N-secYFP fragment.

In the mutant 2A sequence 2A*, the 2A amino acid sequence PGP (5′-CCT GGG CCC-3′) was altered to PAA (5′-CCT GCA GCT-3′) creating a *Pst*I restriction site using primers P1 + P18 in PCR. GFP-HDEL was then amplified using primers P17 + P6 and the two fragments were joined together using

primers P1 + P6. The PCR product (myc-2A*-GFP-HDEL) was digested with *Xba*I and *Bam*HI, cloned into pBluescript and checked by sequencing. Y_m-2A*-GH, nlsR_m-2A*-GH and STN-R_m-2A*-GH were created by cloning *Xba*I/*Bam*HI fragment containing 2A*-GFP-HDEL (isolated from pBluescript) into the same sites of Y_m-2A-GH, nlsR_m-2A-GH and STN-R_m-2A-GH, respectively, replacing the 2A-GFP-HDEL fragments. YFP_{myc}-2A-*Asc*I fragment was generated by PCR using primers P7 + P19, the product was digested with *Xho*I and *Bam*HI, cloned into pBluescript and checked by sequencing. *Acs*I-nlsRFP_{flag} fragment was generated by PCR using primers P20 + P21, the product was digested with *Acs*I and *Bam*HI and cloned into the same sites of YFP_{myc}-2A-*Asc*I in pBluescript. YFP_{myc}-2A-nlsRFP_{flag} was cut out from the pBluescript vector above using *Spe*I and *Bam*HI and cloned into the same sites of Y_m-2A-GH vector replacing the YFP_{myc}-2A-GFP-HDEL fragment.

The RAB-D2[a] fragments were generated by PCR using primers P22 + P23 and corresponding wild-type and N121I-mutant *At*RAB-D2[a] (ARA5; AtRab1b; At1g02130) cDNA sequences as template (6). To create 2A-RabD[2a] fusions, these PCR products were used together with Y_m-2A-GH as a template in overlapping-PCR using primers P24 + P23. The final PCR product (2A-RabD[2a]) was digested with *Xba*I and *Bam*HI, cloned into pK18 (44) and checked by sequencing. The nlsR_m-2A-RabD[2a] clones were created by cloning *Xba*I/*Bam*HI fragments containing the 2A-RabD[2a] fusions (isolated from pK18 derivatives) into the same sites of nlsR_m-2A-secG_f and/or nlsR_m-2A-GH replacing the 2A-secGFP_{flag} and/or 2A-GFP-HDEL fragments.

To make secRFP-2A, RFP and 2A sequences were amplified using primers P25 + P26 and P27 + P12, respectively, and secN-R_m-2A-GH as a template. The two fragments were joined together by overlapping PCR using primers P25 + P12, the product (RFP-2A) was digested with *Bam*HI and *Xho*I, cloned into pBluescript and checked by sequencing. secRFP-2A was created by cloning a *Sal*I/*Bam*HI fragment containing RFP-2A (isolated from pBluescript) into the same sites of secN-R_m-2A-GH vector replacing the N-R_m-2A-GH fragment.

List of primers

P1: GAGCAGAAACTTATCTCTGAGGAGGATTTGTCTAGAGGAGCATGCCAGCTGTTG
P2: GGGCCCAGGGTTGGACTCGACG
P3: TCGAGTCCAACCCTGGGCCCATGAGTAAAGGAGAAGAACTTTTCA
P4: TCGAGTCCAACCCTGGGCCCATGAAGACTAATCTTTTTCTCTTTCTCATC
P5: TTTTGGATCCTTACTTATCGTCATCATCCTTATAATCTTTGTATAGTTCATCCATGCCATGTG
P6: TTTTGGATCCTTAAAGCTCATCATGTTTGTATAGTTCATCCATGCCATGTG
P7: AAAACTCGAGACTAGTGGAGGGGTCGACCATGAGCAAGGGCGAGGAGCTG
P8: GGCGGATCCTATCTAGACAAATCCTCCTCAGAGATAAGTTTCTGCTCGGCGGCGGTCACGAAC
P9: ATGGCTCCTAAGAAAAAGAGAAAGGTTGGAGCTGGAATGGCCTCCTCCGAGGACGTC
P10: CAAATCCTCCTCAGAGATAAGTTTCTGCTCGGCGCCGGTGGAGTGGCGGCCC
P11: AAAAGGATCCCTCGAGCCACCATGGCTCCTAAGAAAAAGAGAAAGGT
P12: AAAAGGATCCCTAGGGCCCAGGGTTGGACTCGACG
P13: AAAAGGATCCACTAGTCCACAATGATTCATACCAACTTGAAGAAAAAG
P14: GATGACGTCCTCGGAGGAGGCCATAGTCGAGCCGGTAACGGTTCCATTTG AAACAAGTTC
P15: GGCTCGACTATGGCCTCCTCCGAGGACGTCATC
P16: AAAATCTAGACAAATCCTCCTCAGAGATAAGTTTCTGC
P17: AGTCCAACCCTGCAGCTATGAAGACTAATCTTTTTCTCTTTCTCATC
P18: AGATTAGTCTTCATAGCTGCAGGGTTGGACTCGACGTCTCCCG
P19: AAAGGATCCTTGAGCTCCGGTCGACGGCGCGCCGGGCCCAGGGTTGGACTCGACG
P20: AAAAGGCGCGCCGATGGCTCCTAAGAAAAAGAGAAAG
P21: TTTGGATCCTACTTATCGTCATCATCCTTATAATCGGCGCCGGTGGAGTGGCGG
P22: GTCGAGTCCAACCCTGGGCCCATGAATCCTGAGTACGACTATCTTTTC
P23: ATCTAGGATCCTCAAGTTGAGCAGCAGCCGTTCTTCTGTGCC
P24: AAATCTAGAGGAGCATGCCAGCTGTTGAATTTTG
P25: AAAACTCGAGACTAGTGTCGACCATGGCCTCCTCCGAGGACGTCATCAAG
P26: CAACAGCTGGCATGCTCCTCTAGAGGCGCCGGTGGAGTGGCGGCCC
P27: GGGCCGCCACTCCACCGGCGCCTCTAGAGGAGCATGCCAGCTGTTG

Plant material and Agrobacterium tumefaciens-mediated transient expression

Transient expression or co-expression of the constructs in tobacco (*Nicotiana tabacum*, cv Petit Havana) leaf epidermal cells was performed as described in Batoko et al. (6) and modified according to Zheng et al. (3). Unless otherwise stated, the bacterial OD_{600} used for infiltration of the lower epidermis was 0.05–0.06 for the fluorescent 2A markers and 0.015–0.03 for the Rab constructs.

Arabidopsis thaliana (ecotype Columbia-0) transgenic lines expressing the fluorescent 2A markers were generated by *Agrobacterium*-mediated transformation using the vacuum infiltration method described by Bechtold et al. (45). Transgenic plants were selected on Murashige and Skoog (MS) medium (46) (SIGMA-Aldrich, Poole, UK) containing 15 μg/ml hygromycin (Calbiochem, San Diego, CA, USA). Plants were grown either on the MS medium or in soil at 20–22°C under 16-h photoperiod.

Protein extraction and immunoblot analysis

Proteins were extracted from tobacco leaf samples (52–60 h after *Agrobacterium* infiltration) or whole *Arabidopsis* seedlings (approximately 100 mg of fresh tissue) by homogenization in two volumes of the extraction buffer: 50 mM sodium citrate, pH 5.5, 150 mM NaCl, 5% SDS (w/v), 0.01% BSA (w/v), 2% β-mercaptoethanol and 17 μl protease inhibitor cocktail (Sigma) per 1 ml of the buffer. The homogenate was boiled for 10 min and cleared by centrifugation at 4°C. The supernatant was transferred to a microcentrifuge tube and stored on ice. Aliquots were frozen in liquid N_2 and stored at −80°C until used. Before loading, 5–10 μl of a sample was mixed with a 1–2 μl loading dye and heated to 55–60°C for 5 min. SeeBlue Plus2 (Invitrogen) was used as a pre-stained marker to identify the size of the proteins. Protein samples were first separated on a 12% polyacrylamide gel, electrotransferred onto a polyvinylidene fluoride membrane, blocked and detected as described in Batoko et al. (6). Antisera to full-length GFP (Molecular Probes, Leiden, The Netherlands) or anti-c-myc (Covance, Berkeley, CA, USA) were used at 1/1000 dilution to probe the membrane overnight at 4°C. Alkaline phosphatase-conjugated secondary antibodies (anti-rabbit IgG or anti-mouse IgG; Sigma) were used at 1/10 000 dilution for 1-h incubation at room temperature.

Sampling and confocal imaging

Unless otherwise stated, 52–60 h after tobacco leaf infiltration with *Agrobacterium* strains, lower epidermis was analysed with a Zeiss LSM 510 META laser-scanning microscope (Carl Zeiss Ltd., Welwyn Garden City, Herts, UK) as described in Zheng et al. (3). Detector gains were set to avoid saturation in the brightest samples in the experiment and amplifier offset was set to minimize pixels with a value of 0 in the vacuoles of the dimmest samples. For quantification of fluorescence intensities at low magnification, the average GFP and YFP pixel intensity was measured in at least nine images of each sample using the Histogram function of the Zeiss AIM software version 3.0 or 3.2. Background fluorescence was similarly estimated from nine images of un-infiltrated areas of the leaf.

For simultaneous imaging of mGFP5, mRFP1 and YFP in tobacco leaf epidermis, two different triple-track line-sequential imaging configurations

were used. For the images in Figure 8E–H, we used a HFT458/543 primary dichroic mirror to reflect excitation wavelengths; a NFT635vis secondary dichroic mirror to split emission between channel 1 (long wavelength) and channels 2 and 3 and a NFT515 dichroic mirror to split emission between channels 2 (short wavelength) and channel 3; mGFP5 emission was detected in channel 2 using a BP475-525 filter, YFP in channel 3 using BP535-590IR filter and mRFP1 in channel 1 using the 592–635 nm range of the META detector; in track 1 mRFP1 was detected using 543-nm excitation from a HeNe laser with channel 1 active, in track 2 YFP was detected using 514-nm excitation from an Argon laser with channel 3 active and in track 3 mGFP5 was detected using 405-nm excitation from a blue diode laser with channel 2 active. For the images in Figure 4I–P and for the quantitative analysis presented in Figure 8D and I, we used a NT80/20 mirror to reflect excitation wavelengths; a NFT545 secondary dichroic mirror to split emission between channel 1 (long wavelength) and channels 2 and 3, and a NFT515 dichroic mirror to split emission between channels 2 (short wavelength) and channel 3; mGFP5 emission was detected in channel 2 using a BP500/20IR filter, YFP in channel 3 using BP535-590IR filter and mRFP1 in channel 1 using the 581–635 nm range of the META detector; in track 1 mRFP1 was detected using 543-nm excitation from a HeNe laser with channel 1 active, in track 2 YFP was detected using 514 nm line of an Argon laser with channel 3 active and in track 3 mGFP5 was detected using the 458 nm line of an Argon laser with channel 2 active. Scatter plots with colour-coded frequencies were generated using the default parameters in the co-localization function of Zeiss AIM software version 3.2.

Ratiometric analysis of single cells using nlsR$_m$-2A-secG$_f$ and nlsR$_m$-2A-GH

For quantitative analysis, the imaging parameters were set to avoid saturation in the brightest cells in an initial survey of the transfected population. The 3D image stacks were collected with pixel spacing of $0.3 \times 0.3 \times 2$ or $0.22 \times 0.22 \times 1$ μm in *x*, *y* and *z*, respectively, and imported into the Matlab environment (The MathWorks, Natick, MA, USA). Images were spatially averaged with a $3 \times 3 \times 5$ kernel in *x*, *y* and *z*, respectively, and then visualized as a maximum brightness projection. The location of the brightest pixel in *z* was also recorded. In the nuclear region, this value typically corresponds to the mid-plane of the nucleus where the brightest intensities occur. The average RFP and YFP signals were measured from the nucleus of selected cells using at least three manually defined seed pixels. The seed pixel was also used as an anchor point in *x*, *y* and *z* for transects with a 3×3 spatially averaged kernel from a single *z*-plane to manually defined end-points in the adjacent vacuole. Each transect thus spanned the nuclear envelope and a thin layer of cytoplasm adjacent to the nucleus. The level of ER-localized GFP was estimated from the average of the brightest features along each transect. Analysis was confined to cells whose nuclei exhibited nuclear RFP fluorescence in the range 90–240 (8-bit data) to ensure sufficient marker expression for quantification of secGFP accumulation while avoiding saturation. Similarly, cells exhibiting YFP values above 240 were not considered in the analysis. A bleed-through correction for YFP emission in the GFP detection channel was determined from cells expressing the *At*RAB-D2^a-YFP fusion at various intensities, in the absence of the ratiometric nlsR$_m$-2A-secG$_f$ fusion, that is, cells with nuclear nlsRFP pixel intensity at near background levels.

The GFP-HDEL signal was measured using the same approach from cells transfected with nlsR$_m$-2A-GH, as this approximates the maximum signal possible for a probe that is retained in the ER. To bring this signal into the same range as the test constructs, images were acquired using twofold lower 458-nm excitation intensity (for the GFP-HDEL signal) and twofold-higher 543-nm excitation intensity (for the mRFP1 signal). As fluorescence brightness scales linearly with changes in laser intensity, the corresponding ratio was multiplied by a factor of 4. As both the secG$_f$ and the GFP-HDEL signals were corrected for the overall expression level from their corresponding nlsRFP signal, it was possible to express the effect of the Rab constructs on secG$_f$ accumulation as a fraction of the maximum GFP-HDEL signal.

Acknowledgments

We are grateful to Dr Claire Halpin, University of Dundee, for providing a cloned 2A sequence and for helpful discussions; to Dr Martin Ryan, University of St. Andrews for sharing information prior to publication; to Dr Julia Legen, University of Oxford, for providing secN-R$_m$-2A-secG$_f$ and secN-R$_m$-2A-GH; to three undergraduate students, Mariana Morales (for help with constructing the *At*RAB-D2^a-YFP fusions), Robert Langford (for early studies with the single T-DNA approach), and Jennifer Robertson (for help with early stages of 2A plasmid construction and ratiometric imaging); to Pauline White and Caroline O'Brien for technical assistance; to Dr Dan Bebber, University of Oxford, for advice on statistical analysis and to Dr J. Perez-Gomez, University of Oxford, for helpful comments on the manuscript. This work was supported by BBSRC grant 43/C13425 to I. M. and M.D.F.

References

1. Fricker MD, Runions J, Moore I. Quantitative fluorescence microscopy: from art to science. Annu Rev Plant Biol 2006;57:79–107.
2. Brandizzi F, Irons SL, Johansen J, Kotzer A, Neumann U. GFP is the way to glow: bioimaging of the plant endomembrane system. J Microsc 2004;214:138–158.
3. Zheng HQ, Camacho L, Wee E, Henri BA, Legend J, Leaver CJ, Malho R, Hussey PJ, Moore I. A Rab-E GTPase mutant acts downstream of the Rab-D subclass in biosynthetic membrane traffic to the plasma membrane in tobacco leaf epidermis. Plant Cell 2005;17:2020–2036.
4. Matsushima R, Kondo M, Nishimura M, Hara-Nishimura I. A novel ER-derived compartment, the ER body, selectively accumulates a β-glucosidase with an ER retention signal in *Arabidopsis*. Plant J 2003;33:493–502.
5. Tamura K, Shimada T, Kondo M, Nishimura M, Hara-Nishimura I. KATAMARI1/MURUS3 is a novel Golgi membrane protein that is required for endomembrane organization in *Arabidopsis*. Plant Cell 2005;17:1764–1776.
6. Batoko H, Zheng HQ, Hawes C, Moore I. A Rab1 GTPase is required for transport between the endoplasmic reticulum and Golgi apparatus for normal Golgi movement in plants. Plant Cell 2000;12:2201–2217.
7. Boevnik P, Martin B, Oparka K, Cruz SS, Hawes C. Transport of virally expressed green fluorescent protein through the secretory pathway in tobacco leaves is inhibited by cold shock and brefeldin A. Planta 1999;208:392–400.
8. DaSilva LLP, Snapp EL, Denecke J, Lippincott-Schwartz J, Hawes C, Brandizzi F. Endoplasmic reticulum export sites and Golgi bodies behave as single mobile secretory units in plant cells. Plant Cell 2004; 16:1753–1771.
9. DaSilva LLP, Taylor JP, Hadlington JL, Hanton SL, Snowden CJ, Fox SJ, Foresti O, Brandizzi F, Denecke J. Receptor salvage from the prevacuolar compartment is essential for efficient vacuolar protein targeting. Plant Cell 2005;17:132–148.
10. Flückiger R, De Caroli M, Piro G, Dalessandro G, Neuhaus J-M, Di Sansebastiano G-P. Vacuolar system distribution in *Arabidopsis* tissues, visualized using GFP fusion proteins. J Exp Bot 2003;54: 1577–1584.
11. Geelen D, Leyman B, Batoko H, Di Sansabastiano GP, Moore I, Blatt MR. The abscisic acid-related SNARE homolog NtSyr1 contributes to secretion and growth: evidence from competition with its cytosolic domain. Plant Cell 2002;14:387–406.
12. Kotzer AM, Brandizzi F, Neumann U, Paris N, Moore I, Hawes C. AtRabF2b (Ara7) acts on the vacuolar trafficking pathway in tobacco leaf epidermal cells. J Cell Sci 2004;117:6377–6389.

13. Lee GJ, Sohn EJ, Lee MH, Hwang I. The *Arabidopsis* Rab5 homologs Rha1 and Ara7 localize to the prevacuolar compartment. Plant Cell Physiol 2004;45:1211–1220.
14. Sohn EJ, Kim ES, Zhao M, Kim SJ, Kim H, Kim YW, Lee YJ, Hillmer S, Sohn U, Jiang LW, Hwang IW. Rha1, an *Arabidopsis* Rab5 homolog, plays a critical role in the vacuolar trafficking of soluble cargo proteins. Plant Cell 2003;15:1057–1070.
15. Takeuchi M, Ueda T, Sato K, Abe H, Nagata T, Nakano A. A dominant–negative mutant of Sar1 GTPase inhibits protein transport from the endoplasmic reticulum to the Golgi apparatus in tobacco and *Arabidopsis* cultured cells. Plant J 2000;23:517–525.
16. Zheng HQ, Kunst L, Hawes C, Moore I. A GFP-based assay reveals a role for RHD3 in transport between the endoplasmic reticulum and Golgi apparatus. Plant J 2004;37:398–414.
17. Tamura K, Shimada T, Ono E, Tanaka Y, Nagatani A, Higashi S, Watanabe M, Nishimura M, Hara-Nishimura I. Why green fluorescence fusion proteins have not been observed in the vacuoles of higher plants. Plant J 2003;35:545–555.
18. Di Sansebastiano GP, Paris N, Marc-Martin S, Neuhaus J-M. Specific accumulation of GFP in a non-acidic vacuolar compartment via a C-terminal propeptide-mediated sorting pathway. Plant J 1998;15:449–457.
19. Park M, Kin SJ, Vitale A, Hwang I. Identification of the protein storage vacuole and protein targeting to the vacuole in leaf cells of three plant species. Plant Physiol 2004;134:625–639.
20. Frigerio L, de Virgilio M, Prada A, Faoro F, Vitale A. Sorting of phaseolin to the vacuole is saturable and requires a short c-terminal peptide. Plant Cell 1998;101:1031–1042.
21. Ryan MD, Donnelly M, Lewis A, Mehrotra AP, Wilkie J, Gani D. A model for nonstoichiometric, cotranslational protein scission in eukaryotic ribosomes. Bioorg Chem 1999;27:55–79.
22. Halpin C, Cooke SE, Barakate A, El Amrani A, Ryan MD. Self-processing 2A-polyproteins – a system for co-ordinate expression of multiple proteins in transgenic plants. Plant J 1999;17:453–459.
23. Ma CL, Mitra A. Expressing multiple genes in a single open reading frame with the 2A region of foot-and-mouth disease virus as a linker. Mol Breed 2002;9:191–199.
24. Ralley L, Enfissi EMA, Misawa N, Schuch W, Bramley PM, Fraser PD. Metabolic engineering of ketocarotenoid formation in higher plants. Plant J 2004;39:477–486.
25. Randall J, Sutton D, Ghoshroy S, Bagga S, Kemp JD. Co-ordinate expression of β− and δ−zeins in transgenic tobacco. Plant Sci 2004; 167:367–372.
26. Yasuda H, Tada Y, Hayashi Y, Jomori T, Takaiwa F. Expression of the small peptide GLP-1 in transgenic plants. Transgenic Res 2005;14: 677–684.
27. El Amrani A, Barakate A, Askari BM, Li X, Roberts AC, Ryan MD, Halpin C. Coordinate expression and independent subcellular targeting of multiple proteins from a single transgene. Plant Physiol 2004;135: 16–24.
28. François IEJA, Van Hemelrijck W, Aerts AM, Wouters PFJ, Proost P, Broekaert WF, Cammue BPA. Processing in *Arabidopsis thaliana* of a heterologous polyprotein resulting in differential targeting of the individual plant defensins. Plant Sci 2004;166:113–121.
29. De Felipe P, Ryan MD. Targeting of proteins derived from self-processing polyproteins containing multiple signal sequences. Traffic 2004;5:616–626.
30. De Felipe P, Hughes LE, Ryan MD, Brown JD. Co-translational, intraribosomal cleavage of polypeptides by the foot-and-mouth disease virus 2A peptide. J Biol Chem 2003;278:11441–11448.
31. Rossi L, Escudero J, Hohn B, Tinland B. Efficient and sensitive assay for T-DNA-dependent transient gene expression. Plant Mol Biol Rep 1993;11:220–229.
32. Campbell RE, Tour O, Palmer AE, Steinbach PA, Baird GS, Zacharias DA, Tsien RY. A monomeric red fluorescent protein. Proc Natl Acad Sci U S A 2002;99:7877–7882.
33. Higy M, Junne T, Spiess M. Topogenesis of membrane proteins at the endoplasmic reticulum. Biochemistry 2004;43:12716–12722.
34. White SH, von Heijne G. The machinery of membrane protein assembly. Curr Opin Struct Biol 2004;14:397–404.
35. White SH, von Heijne G. Transmembrane helices before, during, and after insertion. Curr Opin Struct Biol 2005;15:378–386.
36. Tisdale EJ, Bourne JR, Khosravifar R, Der CJ, Balch WE. GTP-binding mutants of Rab1 and Rab2 are potent inhibitors of vesicular transport from the endoplasmic-reticulum to the Golgi-complex. J Cell Biol 1992;119:749–761.
37. Szymczak AL, Workman CJ, Wang Y, Vignali KM, Dilioglou S, Vanin EF, Vignali DAA. Correction of multi-gene deficiency *in vivo* using a single ''self-cleaving'' 2A peptide-based retroviral vector. Nat Biotechnol 2004;22:589–594.
38. Halpin C. Gene stacking in transgenic plants-the challenge for 21st century plant biotechnology. Plant Biotechnol J 2005;3:141–155.
39. Lengler J, Holzmüller H, Salmons B, Günzburg WH, Renner M. FMDV-2A sequence and protein arrangement contribute to functionality of CYP2B1-reporter fusion protein. Anal Biochem 2005;343: 116–124.
40. Denecke J, De Rycke R, Botterman J. Plant and mammalian sorting signals for protein retention in the endoplasmic reticulum contain a conserved epitope. EMBO J 1992;11:2345–2355.
41. Munro S, Pelham HBR. A C-terminal signal prevents secretion of luminal ER proteins. Cell 1987;48:899–907.
42. Goder V, Junne T, Spiess M. Sec61p contributes to signal sequence orientation according to the positive-inside rule. Mol Biol Cell 2004; 15:1470–1478.
43. Ausubel F, Brent R, Kingston RE, Moore JG, Seidman JG, Smith JA, Struhl JG. Current Protocols in Molecular Biology. New York: John Wiley; 1999.
44. Pridmore RD. New and versatile cloning vectors with kanamycin-resistance marker. Gene 1987;56:309–312.
45. Bechtold N, Ellis J, Pelletier G. *In planta* agrobacterium-mediated gene-transfer by infiltration of adult *Arabidopsis thaliana* plants. CR Acad Sci, Paris, Life Science 1993;316:1194–1199.
46. Murashige T, Skoog F. A revised medium for rapid growth and bioassays with tobacco tissue. Physiol Plant 1962;15:493–497.

Genetic evidence that the higher plant Rab-D1 and Rab-D2 GTPases exhibit distinct but overlapping interactions in the early secretory pathway

Hazel Pinheiro[1,*], Marketa Samalova[1], Niko Geldner[2,3], Joanne Chory[3], Alberto Martinez[4] and Ian Moore[1,‡]

[1]Department of Plant Sciences, University of Oxford, South Parks Road, Oxford OX1 3RB, UK
[2]Department of Plant Molecular Biology, Biophore, UNIL-Sorge, University of Lausanne, 1015 Lausanne, Switzerland
[3]The Salk Institute, PBIO-C, 10010 North Torrey Pines Road, La Jolla, CA 92036, USA
[4]Syngenta, Jealott's Hill Research Station, Bracknell, Berkshire RG42 6ET, UK

*Neé Hazel Betts
‡Author for correspondence (ian.moore@plants.ox.ac.uk)

Accepted 3 August 2009
Journal of Cell Science 122, 3749-3758 Published by The Company of Biologists 2009
doi:10.1242/jcs.050625

Summary

GTPases of the Rab1 subclass are essential for membrane traffic between the endoplasmic reticulum (ER) and Golgi complex in animals, fungi and plants. Rab1-related proteins in higher plants are unusual because sequence comparisons divide them into two putative subclasses, Rab-D1 and Rab-D2, that are conserved in monocots and dicots. We tested the hypothesis that the Rab-D1 and Rab-D2 proteins of *Arabidopsis* represent functionally distinct groups. RAB-D1 and RAB-D2a each targeted fluorescent proteins to the same punctate structures associated with the Golgi stacks and *trans*-Golgi-network. Dominant-inhibitory N121I mutants of each protein inhibited traffic of diverse cargo proteins at the ER but they appeared to act via distinct biochemical pathways as biosynthetic traffic in cells expressing either of the N121I mutants could be restored by coexpressing the wild-type form of the same subclass but not the other subclass. The same interaction was observed in transgenic seedlings expressing RAB-D1 [N121I]. Insertional mutants confirmed that the three *Arabidopsis* Rab-D2 genes were extensively redundant and collectively performed an essential function that could not be provided by *RAB-D1*, which was non-essential. However, plants lacking *RAB-D1*, *RAB-D2b* and *RAB-D2c* were short and bushy with low fertility, indicating that the Rab-D1 and Rab-D2 subclasses have overlapping functions.

Supplementary material available online at
http://jcs.biologists.org/cgi/content/full/122/20/3749/DC1

Key words: AtRab1b, ARA5, Ypt1, Rab GTPases, pOp6/LhGR

Introduction

Membrane traffic in eukaryotes is dependent on accurate targeting of transport vesicles between the diverse membrane-bound compartments of the biosynthetic and endocytic pathways. One of the key regulatory protein families is the Rab family of small GTPases, which contribute variously to the specification of membrane identity, the accuracy of vesicle targeting and the recruitment of molecular motors to membranes (Olkkonen and Stenmark, 1997; Behnia and Munro, 2005; Grosshans et al., 2006; Markgraf et al., 2007; Woollard and Moore, 2008). Rab GTPases undergo a regulated cycle between GDP- and GTP-bound forms and in so doing they cycle on and off particular endomembranes where they participate in specific membrane trafficking events (Olkkonen and Stenmark, 1997; Markgraf et al., 2007; Woollard and Moore, 2008).

Genomic data have shown that yeasts, animals and plants have each elaborated distinct sets of Rab proteins. *Arabidopsis* and mammals each have roughly 60 Rab GTPases compared to the six to ten that are found in yeasts, but it is striking that 80% of the predicted mammalian Rab GTPase subclasses are missing in *Arabidopsis* (Pereira-Leal and Seabra, 2001; Rutherford and Moore, 2002; Vernoud et al., 2003; Woollard and Moore, 2008). The diversity of the Rab GTPases family in mammals relative to that of yeasts appears to reflect the greater complexity and diversity of membrane trafficking events that occur in the diverse cell types of mammals (Bock et al., 2001; Pereira-Leal and Seabra, 2001). The situation is less clear in angiosperms, where phylogenetic analysis shows that all 57 *Arabidopsis* RAB sequences fall into just eight clades (RAB-A to RAB-H). Each of these clades is clearly related to one of the six Rab subclasses that are common to all three kingdoms or to mammalian Rab2 and Rab18 (Rutherford and Moore, 2002; Vernoud et al., 2003). Nevertheless, analysis of specificity-determining regions of Rab GTPases (Moore et al., 1995; Pereira-Leal and Seabra, 2000) predicts that several of the eight plant Rab clades might contain functionally distinct proteins (Pereira-Leal and Seabra, 2001; Rutherford and Moore, 2002), leading to the proposal that *Arabidopsis* could have as many as 18 distinct functional Rab subclasses. If so, it would mean that the Rab GTPase family has undergone distinct adaptive radiations in mammalian and angiosperm lineages and that many Rab subclasses in *Arabidopsis* are plant-specific (Rutherford and Moore, 2002). So far, however, there has been little experimental testing of these phylogenetic predictions. It has been shown that proteins of the Rab5-related Rab-F1 (ARA6) and Rab-F2 subclasses (ARA7 and RHA1) localise to different but overlapping populations of prevacuolar or endosomal compartments (Ueda et al., 2004) even though they share an exchange factor (Goh et al., 2007).

Here, we have investigated the Rab1-related proteins of *Arabidopsis*. The Rab1 subclass is one of the most highly conserved in eukaryotes and members of this subclass have been shown to act in early stages of biosynthetic traffic to or through the Golgi complex in yeasts, animals and plants (Plutner et al., 1991; Tisdale

et al., 1992; Pind et al., 1994; Jedd et al., 1995; Batoko et al., 2000; Alvarez et al., 2003; Zheng et al., 2005). Animal Rab1 and its budding-yeast homologue, Ypt1p, are known to interact with similar regulatory and effector proteins (such as Uso1p/p115 and the TRAPP complex) to promote the targeting of COPII vesicles to the *cis*-Golgi (Beard et al., 2005; Grosshans et al., 2006; Markgraf et al., 2007; Cai et al., 2008). Rab1/Ypt1 proteins of higher plants are unusual, however, because sequence comparisons suggest that they can be divided into two distinct clades, Rab-D1 and Rab-D2, that could represent distinct functional subclasses (Pereira-Leal and Seabra, 2001; Rutherford and Moore, 2002; Vernoud et al., 2003) (supplementary material Fig. S1).

In *Arabidopsis*, the Rab-D1 subclass is represented by a single gene, *RAB-D1* (also known as *RABD1*, *At3g11730*, *ATFP8*), whereas the Rab-D2 subclass is represented by three genes, *RAB-D2a*, *RAB-D2b* and *RAB-D2c* (*RABD2A*, *At1g02130*, *ARA5*, *Rab1b*; *RABD2B*, *At5g47200*; and *RABD2C*, *At4g17530*, respectively) which are predicted to be extensively redundant (Biermann et al., 1996; Rutherford and Moore, 2002) (supplementary material Fig. S1). Several reports have shown that a dominant-negative mutant of *Arabidopsis* RAB-D2a inhibits traffic between the ER and Golgi in plant cells (Batoko et al., 2000; Saint-Jore et al., 2002; Park et al., 2004; Zheng et al., 2005; Samalova et al., 2006). By contrast, the higher plant Rab-D1 subclass has not been investigated. Here, by use of protein tagging, dominant-negative mutants and loss of function mutants we provide evidence that the *Arabidopsis* Rab-D1 and Rab-D2 proteins do indeed represent distinct functional groups that act in transport between the endoplasmic reticulum (ER) and Golgi complex via distinct interactions.

Results

Tagged *Arabidopsis* RAB-D1 and RAB-D2a colocalise on Golgi and TGN

We first investigated the membrane targeting signals in RAB-D proteins in tobacco leaf epidermal cells where yellow fluorescent protein (YFP)-tagged RAB-D2a (ARA5; AtRab1b) has been localised to Golgi-associated punctate structures (Zheng et al., 2005). Similarly, in cells that exhibited the lowest detectable accumulation of YFP:RAB-D1, the fusion protein was observed in the cytoplasm and on mobile punctate structures that were often closely associated with the mobile Golgi stacks (Fig. 1A; supplementary material Fig. S2A,B). In cells exhibiting higher expression levels, YFP:RAB-D1 accumulated in the cytoplasm, indicating that targeting to the punctate structures was saturable (not shown). No labelling of the ER network was observed (supplementary material Fig. S2C). GFP:RAB-D2a colocalised with YFP:RAB-D2a and YFP:RAB-D1, indicating that both proteins target the same mobile punctate structures (Fig. 1B; supplementary material Fig. S2D,E).

The identity of the structures that did not associate with Golgi stacks was unclear but it has been suggested that they might represent ER-export sites (Zheng et al., 2005). To investigate their identity in *Arabidopsis*, we used YFP-tagged forms of RAB-D1 and RAB-D2a from the Wave collection (Wave 25y and Wave 29y respectively) (Geldner et al., 2009). As in tobacco leaf epidermis, in leaf and root tip epidermis of *Arabidopsis*, YFP:RAB-D1 and YFP:RAB-D2a labelled punctate structures, some of which colocalised with Golgi stacks while others were distinct from, but often close to, the Golgi (Fig. 1C,D; supplementary material Fig. S3A,B). Surprisingly, treatment of root tips with the drug brefeldin A (BFA) caused a portion of the YFP:RAB-D1 and YFP:RAB-D2a signal to accumulate in the core of the BFA-bodies (Fig. 1E; supplementary material Fig. S3C). These

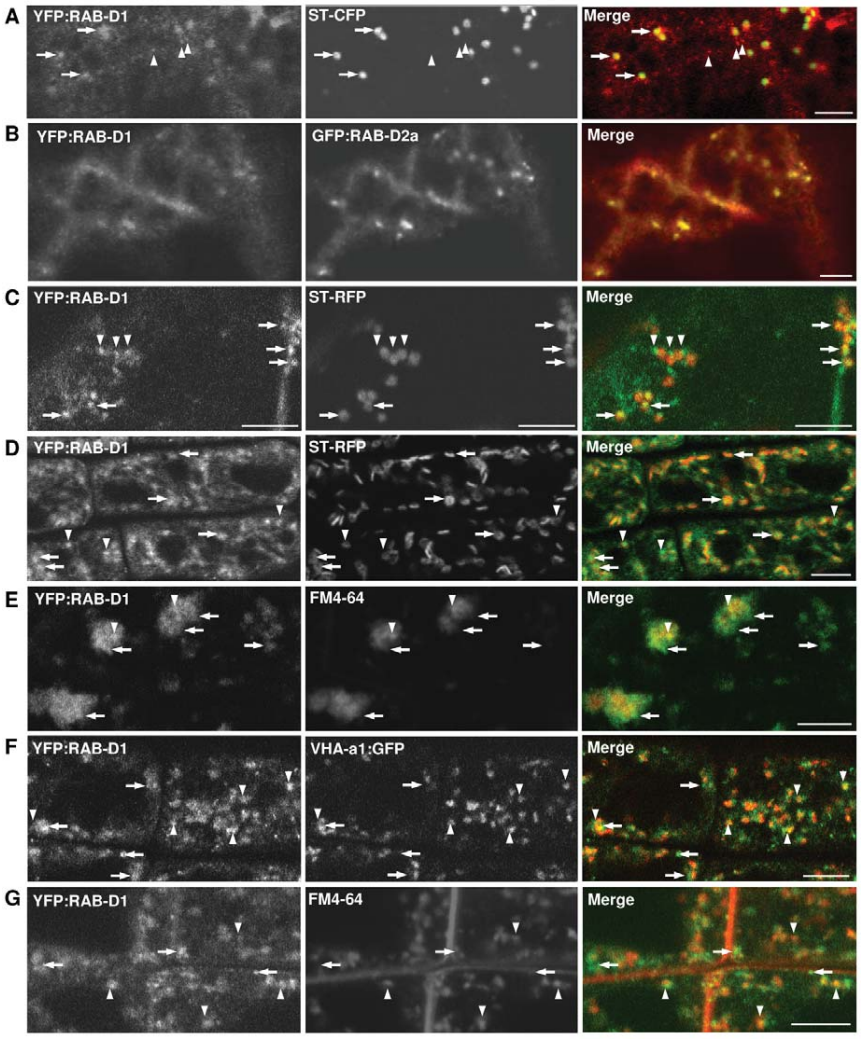

Fig. 1. Localisation of YFP:RAB-D1. Confocal laser scanning microscope (CLSM) images of tobacco (A,B) or *Arabidopsis* (C-G) cells coexpressing YFP:RAB-D1 (green) with various markers (red). (A,B) YFP:RAB-D1 in tobacco leaf abaxial epidermis coexpressing either the Golgi marker ST-CFP (A) or GFP:RAB-D2a (B). (C) *Arabidopsis* leaf abaxial epidermis coexpressing the Golgi marker ST-RFP. (D-G) Localisation of YFP:RAB-D1 in *Arabidopsis* root tips together with the Golgi marker ST-RFP (D), the TGN marker VHA-a1:GFP (F), or the endosomal dye FM4-64 (E,G). Root tips in E were treated with brefeldin A. Arrows indicate YFP:RAB-D1-labelled punctate structures that associate with Golgi stacks. Arrowheads show structures that associate with the TGN. Scale bars: 5 μm.

bodies are aggregations of *trans*-Golgi-network (TGN) and endosomal compartments with Golgi stacks clustered at their periphery (Grebe et al., 2003; Dettmer et al., 2006; Richter et al., 2007; Teh and Moore, 2007). This suggested that a portion of the YFP:RAB-D1 and YFP:RAB-D2a signal localised to the TGN or endosomes in addition to Golgi stacks.

Introduction of VHA-a1:GFP, a marker of the TGN in *Arabidopsis* (Dettmer et al., 2006), confirmed that some of the structures labelled by YFP:RAB-D1 and YFP:RAB-D2a colocalised with the TGN (Fig. 1F; supplementary material Fig. S3D). The TGN also acts as an early endosome in *Arabidopsis*, accumulating the endocytic dye FM4-64 shortly after it is taken up into root-tip cells (Dettmer et al., 2006; Chow et al., 2008). Consistent with this, FM4-64 also accumulated in a subset of the compartments labelled with YFP:RAB-D1 and YFP:RAB-D2a (Fig. 1G; supplementary material Fig. S3E). Similar observations have been made with RAB-D2b using independent markers of the Golgi and the TGN in *Arabidopsis* (N.G. and J.C., unpublished). We concluded that proteins of the *Arabidopsis* Rab-D1 and Rab-D2 subclasses target YFP to both the Golgi stack and the TGN.

Dominant-negative RAB-D1 inhibits traffic between the ER and Golgi complex

To investigate the pathways in which the Rab-D1 subclass acts, we adopted a dominant mutant approach based on well-characterised amino acid substitutions in small GTPases (Olkkonen and Stenmark, 1997). We generated RAB-D1 [S22N], which is expected to promote the inactive GDP-bound state, and RAB-D1 [N121I], which is expected to promote the nucleotide free state. Each of these substitutions in Rab GTPases can generate a dominant-negative mutant owing to the titration of interactors (such as nucleotide-exchange factors) in a non-functional complex (Tisdale et al., 1992; Jedd et al., 1995; Jones et al., 1995; Olkkonnen and Stenmark, 1997; Goh et al., 2007). We also generated RAB-D1 [Q67L], which is predicted to be GTPase-deficient and thus to promote the active state (Olkkonnen and Stenmark, 1997; Richardson et al., 1998).

To establish whether the RAB-D1 mutants interfered with secretory traffic in plant cells, they were coexpressed with the secreted GFP marker (secGFP) using *Agrobacterium*-mediated transient expression in tobacco leaf epidermis, in which the function of RAB-D2a in biosynthetic traffic has been extensively characterised (Batoko et al., 2000; Saint-Jore et al., 2002; Zheng et al., 2005; Samalova et al., 2006; Duarte et al., 2008). In this assay, inhibiting the traffic of secGFP to the apoplast (where GFP fluorescence is not favoured) results in the accumulation of fluorescent GFP molecules within endomembrane compartments and this increased fluorescence signal can be imaged and quantified (Zheng et al., 2004; Zheng et al., 2005; Samalova et al., 2006). Quantitative confocal microscopy of transfected epidermal cells revealed that expression of RAB-D1 [N121I] but not wild-type RAB-D1 [S22N] or RAB-D1 [Q67L] resulted in marked intracellular accumulation of secGFP (Fig. 2A,B). In this respect RAB-D1 behaved like yeast Ypt1p and mammalian RAB1A or RAB1B where the equivalent N-to-I mutants are also more inhibitory than the corresponding S-to-N mutants and the Q-to-L mutant forms are not inhibitory (Tisdale et al., 1992; Pind et al., 1994; Richardson et al., 1998; Yoo et al., 1999; Alvarez et al., 2003). RAB-D1 [N121I] was selected for further work and compared with the corresponding mutant of RAB-D2a, which has been used to characterise RAB-D2a-dependent trafficking (Batoko et al., 2000; Saint-Jore et al., 2002; Park et al., 2004; Zheng et al., 2005; Duarte et al., 2008).

In the presence of either RAB-D1 or RAB-D2a N121I mutants, secGFP accumulated in a polygonal and planar network (Fig. 2C) typical of the ER in the presence of RAB-D2a [N121I] (Batoko et al., 2000; Samalova et al., 2006). Similarly, the Golgi marker N-ST-RFP co-accumulated with a coexpressed ER marker, GFP-HDEL, indicating that RAB-D1 [N121I] interfered with traffic between the ER and Golgi (Fig. 2D) as reported previously for RAB-D2a [N121I] (Batoko et al., 2000; Samalova et al., 2006). Both mutants also inhibited trafficking of diverse other fluorescently tagged cargo molecules at the ER (Fig. 3). These molecules included integral and glycosylphosphatidylinositol (GPI)-anchored plasma membrane proteins [the H^+-ATPase PMA4-GFP and HIPL1-GFP, respectively (Lefebvre et al., 2004; Borner et al., 2005)] and markers of the vacuole lumen and tonoplast [aleu-GFP and BobTIP-GFP, respectively (Kotzer et al., 2004)] all of which accumulated in the ER (Fig. 3A-D). Similarly, both mutants promoted the accumulation of zein-GFP (Fig. 3E), which follows a recently described vacuolar pathway for degradation of proteins that misfold in the ER (Foresti et al., 2008).

Finally, we investigated the effect of each mutant on the COPII-vesicle-coat component AtSEC24, which normally distributes between the cytoplasm and Golgi-associated ER-export sites (ERES) (Fig. 3F,G) (Stefano et al., 2006). Both mutants caused YFP-SEC24 to accumulate in a large number of dots, which were apparently smaller and brighter than ERES and did not associate with residual Golgi stacks (Fig. 3F,G). Thus, both RAB-D1 [N121I] and RAB-D2a [N121I] inhibit traffic of diverse biosynthetic trafficking markers at the ER.

These studies also showed that RAB-D1 [N121I] and RAB-D2a [N121I] each inhibited an essential cellular function because two weeks after infiltration of tobacco leaves, areas expressing either protein developed necrotic lesions (supplementary material Fig. S4). These lesions appeared earlier and were more extensive as the titre of *Agrobacterium* in the transfection was increased.

RAB-D1 and RAB-D2a act in ER-Golgi traffic via different interactors

Dominant-negative Rab GTPase mutants inhibit membrane trafficking by titration of an essential interacting partner such as a nucleotide exchange factor (Jones et al., 1995; Olkkonnen and Stenmark, 1997; Walch-Solimena et al., 1997; Cool et al., 1999; Goh et al., 2007). If this interactor has additional activities that are independent of its interaction with the mutated Rab GTPase, the effects of the dominant-negative mutant might not reflect the true activity of the Rab GTPase. Therefore, to establish whether inhibition of secretory traffic by RAB-D1 [N121I] can be attributed to loss of Rab-D1 function, we asked whether trafficking could be restored by coexpression of wild-type RAB-D1 to compete with the N121I mutant. This approach has been used previously with dominant-negative mutants of RAB-D2a and RAB-F2b (Batoko et al., 2000; Kotzer et al., 2004). For these experiments, we again used the quantitative secGFP accumulation assay in tobacco leaf epidermis (Zheng et al., 2005). Using this quantitative method we were able to confirm the previous observation (Batoko et al., 2000) that inhibition of ER-Golgi traffic by RAB-D2a [N121I] could be restored by coexpression of wild-type RAB-D2a but not by coexpression of RAB-E1d (At5g03520; AtRAB-E1d) which is a member of a different but closely related *Arabidopsis* Rab subclass that is implicated in post-Golgi secretory traffic (Zheng et al., 2005)

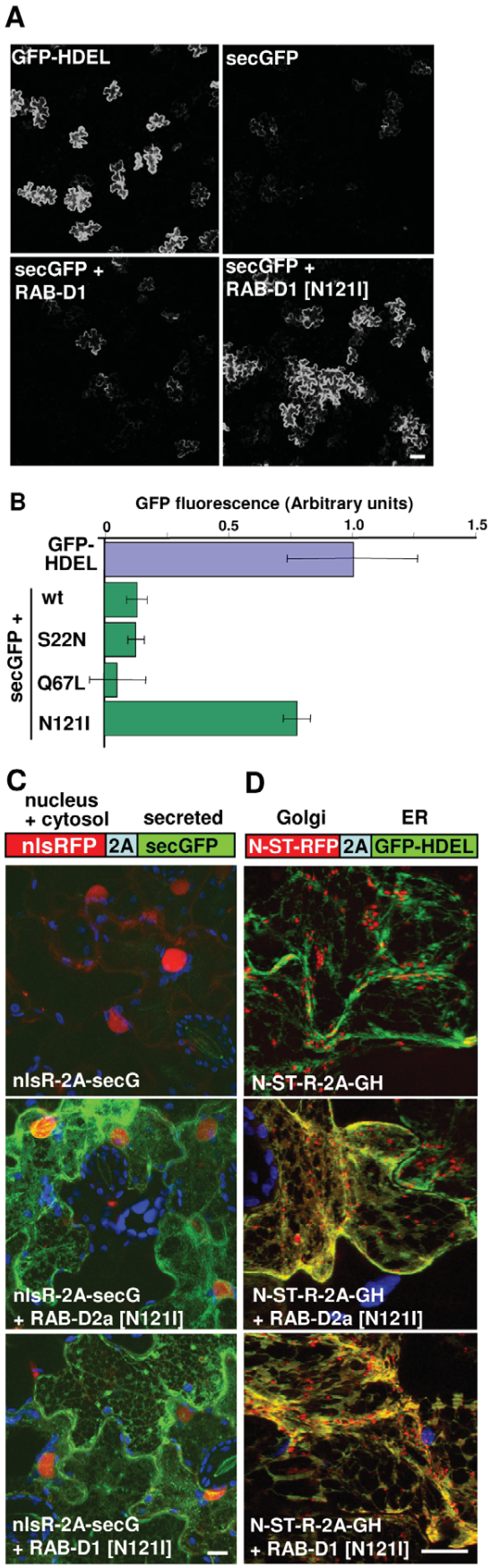

Fig. 2. RAB-D1 [N121I] inhibits secretory traffic between the ER and Golgi. (A) Confocal images of tobacco leaf epidermal cells expressing the ER luminal marker GFP-HDEL or the secreted GFP marker secGFP either alone or together with wild-type or the N121I mutant forms of RAB-D1. (B) Quantification of the effect of RAB-D1 and the indicated mutants on the intracellular accumulation of secGFP (green bars). The fluorescence signal from the ER-lumenal marker GFP-HDEL (blue bar) was set to 1 and that for secGFP alone to 0. Error bars represent standard deviation of each sample. (C,D) Use of ratiometric fluorescent polyproteins to localise secreted and Golgi markers in the presence of RAB-D1 [N121I] and RAB-D2a [N121I]. (C) nlsR-2A-secG expresses secGFP (green) and a nuclear-targeted RFP (red) in fixed stoichiometry as a polyprotein linked by the self-cleaving 2A polypeptide (Samalova et al., 2006). Transfected cells are marked by red nuclei but do not accumulate GFP, which is secreted to the cell wall (top). In the presence of RAB-D1 [N121I] (bottom) or RAB-D2a [N121I] (centre), cells expressing similar quantities of the marker have similarly bright RFP signals in their nuclei, but now secGFP accumulates in a polygonal and planar ER network. (D) N-ST-R-2A-GH expresses the Golgi marker N-ST-RFP (red) in fixed stochiometry with the ER-marker GFP-HDEL (green), which indicates the relative expression level in each cell. In the presence of RAB-D1 [N121I] and RAB-D2a [N121I], the Golgi marker accumulates in the ER where it colocalises with GFP. In C and D, chlorophyll is blue. Scale bars:100 μm in A; 10 μm in C and D.

(Fig. 4A, grey bars). Similarly, inhibition of secGFP trafficking by RAB-D1 [N121I] was substantially restored by coexpression of wild-type RAB-D1 but not RAB-E1d (Fig. 4B, grey bars). It is unlikely that the rescue phenomenon resulted from co-suppression at high expression levels because doubling the titre of bacteria expressing either of the dominant-negative mutants resulted in increased rather than reduced secGFP accumulation. Immunoblot analysis with an anti-Rab-D2 serum confirmed that *Arabidopsis* RAB-D2a was expressed in the rescued samples (Fig. 4C, lane c). We concluded that wild-type RAB-D1 and RAB-D2 proteins each act in membrane traffic between the ER and Golgi.

As RAB-D1 and RAB-D2a both act in traffic between the ER and Golgi complex we were interested to know whether they interact with the same partners. Therefore, we asked whether wild-type RAB-D1 was able to rescue membrane traffic in cells inhibited by dominant-negative RAB-D2a [N121I] and vice versa. Strikingly, in reciprocal rescue experiments we found that neither wild-type protein was able to rescue traffic inhibited by the mutant form of the other protein (Fig. 4A,B, black bars), arguing that RAB-D1 [N121I] and RAB-D2a [N121I] mutants each inhibited membrane traffic between ER and Golgi by titrating different interactors. Although *Arabidopsis* RAB-D2a was unable to rescue traffic inhibited by RAB-D1 [N121I], immunoblot analysis with an anti-Rab-D2 serum confirmed that it was expressed (Fig. 4C, lane e).

To establish whether dominant-negative mutants of the Rab-D1 subclass exhibit the same selective interactions in whole *Arabidopsis* plants, we expressed RAB-D1 and RAB-D1 [N121I] in seedlings using the dexamethasone-inducible pOp6/LhGR promoter system (Craft et al., 2005). When germinated on dexamethasone-containing medium, seedlings expressing RAB-D1 [N121I], but not those expressing wild-type RAB-D1, were severely dwarfed and died after prolonged exposure to dexamethasone (Fig. 5A). To test the ability of Rab-D1 and Rab-D2 proteins to suppress the dwarfing caused by RAB-D1 [N121I], plants from a homozygous RAB-D1 [N121I] line with an intermediate dwarf phenotype were crossed with plants expressing wild-type RAB-D1 or RAB-D2a from the same inducible promoter system. F1 progeny were germinated on medium with or without dexamethasone. As shown in Fig. 5B,C, seedlings from the crosses with the inducible RAB-D1 lines exhibited a wild-type growth

phenotype, whereas those from four separate crosses with inducible RAB-D2a lines continued to show the dwarf phenotype.

To rule out the possibility that the apparent restoration of growth by RAB-D1 resulted from co-suppression of the RAB-D1 [N121I] transgene in the F1 seedlings, we performed reverse-transcriptase-PCR (RT-PCR) on the rescued plants and confirmed that mRNA from the RAB-D1 [N121I] transgene was still abundant (Fig. 5D). This also confirmed that the endogenous RAB-D1 transcript was expressed under all conditions, thus excluding the possibility that the dwarf phenotype associated with expression of RAB-D1 [N121I] resulted from co-suppression of the endogenous transcript. Finally, RT-PCR analysis of seedlings from a cross with an inducible RAB-D2a line confirmed that the RAB-D2a transcript was still expressed 18 days after germination on inductive medium, despite the dwarf phenotype exhibited by the seedlings (supplementary material Fig. S5).

The Rab-D2 subclass is essential in *Arabidopsis* but the Rab-D1 subclass is not

The behaviour of dominant-negative mutants had suggested that *Arabidopsis* Rab-D1 and Rab-D2 proteins perform distinct functions in ER-Golgi traffic, so we next used loss-of-function mutants to look at whether each subclass was essential in *Arabidopsis*. T-DNA insertion mutants were obtained for RAB-D1 and each of the three RAB-D2 proteins, RAB-D2a, RAB-D2b and RAB-D2c (supplementary material Fig. S6A). In each case, RT-PCR showed that transcripts were absent in the homozygous mutant lines (Fig. 5A,B). Immunoblot analysis of double-mutant combinations with anti-Rab-D2 antibodies confirmed that each insertion allele prevented protein accumulation from the three loci in this subclass (Fig. 6C).

Plants homozygous for insertions in the three Rab-D2 genes were fertile and phenotypically normal under greenhouse conditions, as were the three double mutants (*rab-D2a rab-D2b*, *rab-D2a rab-D2c* and *rab-D2b rab-D2c*) (Fig. 6D,E). By contrast, however, we were unable to recover triple mutants that lacked all three RAB-D2 proteins. Thus, plants with the *rab-D2a rab-D2b rab-D2c/+* genotype developed normally (Fig. 6D; supplementary material Fig. S6B, aabbCc)

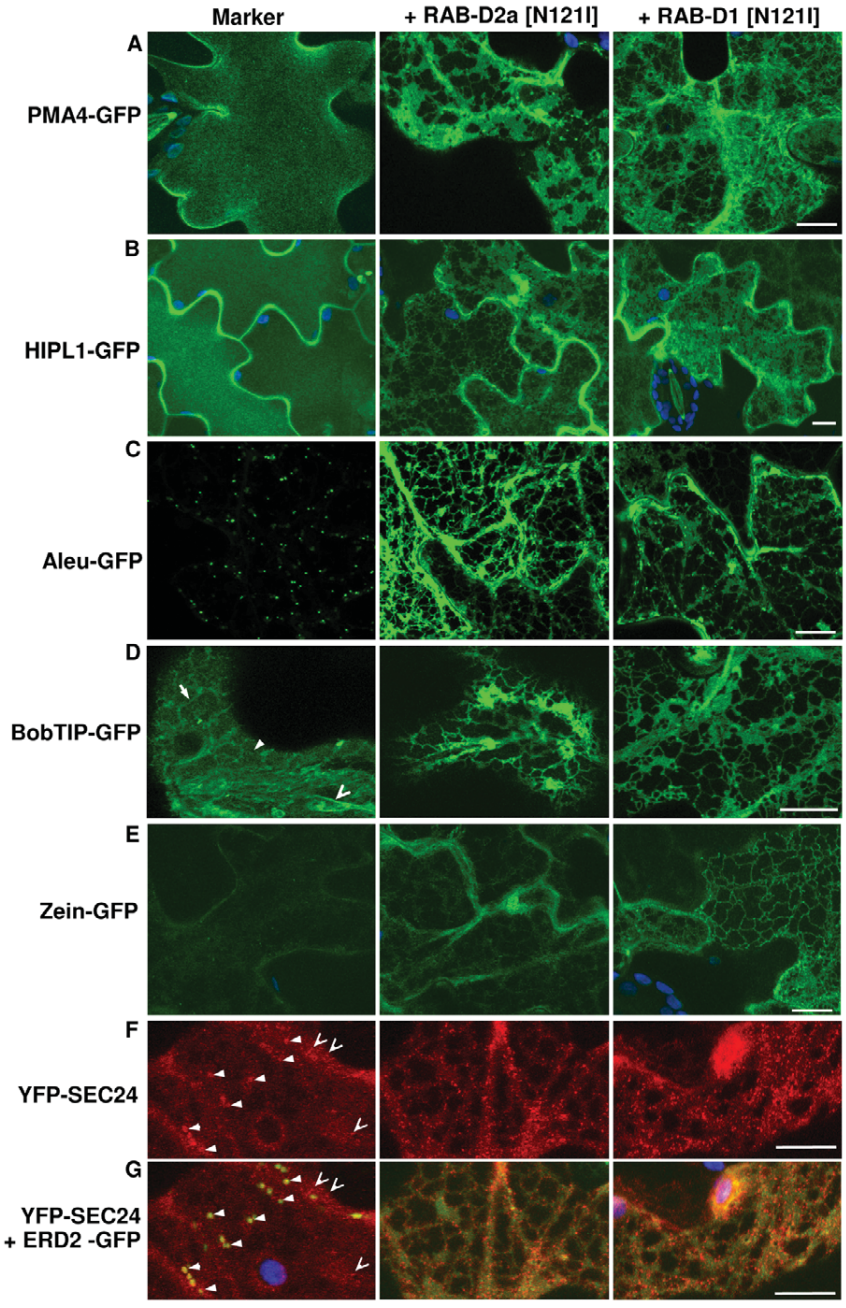

Fig. 3. Inhibition of plasma membrane and vacuolar traffic by RAB-D1 [N121I] and RAB-D2a [N121I]. Projections in *z* of series of confocal images from the cortical cytoplasm of transfected tobacco leaf epidermal cells expressing diverse fluorescent markers based on GFP (green) or YFP (red) in the absence (left) or presence of RAB-D1 [N121I] and RAB-D2a [N121I] (right and centre, respectively); chlorophyll, blue. (A,B) The H^+-ATPase marker PMA4-GFP and the GPI-anchored protein marker HIPL1-GFP each accumulate at the plasma membrane in control cells but are trapped in the ER in the presence of RAB-D1 [N121I] or RAB-D2a [N121I]. (C) The vacuolar luminal marker aleu-GFP is usually visible only in punctate prevacuolar compartments en route to the vacuole (left) but is trapped in the ER in the presence of RAB-D1 [N121I] or RAB-D2a [N121I]. (D) In control cells (left), the tonoplast marker BobTIP-GFP is visible over the surface of the tonoplast underlying the cortical cytoplasm (solid arrowhead) and around transvacuolar strands (open arrowhead) with a faint signal from newly synthesised proteins in the ER (arrow); the marker is confined to the ER in the presence of RAB-D1 [N121I] or RAB-D2a [N121I]. (E) The misfolded ER-protein zein-GFP is faintly visible in control cells (left) but accumulates in the presence of RAB-D1 [N121I] and RAB-D2a [N121I]. (F,G) The COPII vesicle coat component YFP-SEC24 (red) accumulates on Golgi-associated ERES (solid arrowheads) and on additional independent punctate structures (open arrowheads), which are more numerous and pronounced in the presence of RAB-D1 [N121I] or RAB-D2a [N121I]. (G) The same cells as F, showing the coexpressed Golgi marker ERD2-GFP (green), which colcalises with ERES in control cells but accumulates in the ER in the presence of RAB-D1 [N121I] or RAB-D2a [N121I]; arrowheads as in F. Scale bars: 10 μm.

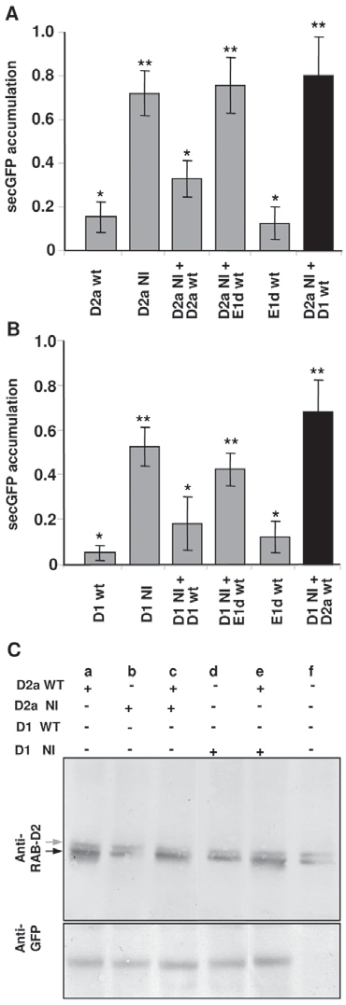

Fig. 4. RAB-D1 and RAB-D2a act in ER-Golgi traffic via independent interactions. (A,B) Quantitation of secGFP accumulation (arbitrary units) in tobacco leaf epidermal cells expressing secGFP together with wild-type (wt) or N121I mutant forms (NI) of RAB-D1 (D1), RAB-D2a (D2a) or RAB8-E1d (E1d) alone or in combination as indicated. Error bars represent s.e.m. Values that are not significantly different ($P \geq 0.05$) are marked by an asterisk. Values with one asterisk are significantly different from values with two asterisks ($P \leq 0.05$). (A) Restoration of traffic inhibited by RAB-D2a [N121I]. (B) Restoration of traffic inhibited by RAB-D1 [N121I]. (C) Immunoblot analysis of tobacco leaves transiently expressing wild-type or mutant forms of RAB-D1 or RAB-D2a (as in A and B) using an anti-RAB-D2 antibody (see Materials and Methods). In uninfected plants (f) this antibody recognises two bands, most probably tobacco RAB-D proteins, the lower of which (black arrow) co-migrates with transiently expressed *Arabidopsis* RAB-D2a (lanes a, c and e). Note that the RAB-D2a [N121] mutant is not significantly overexpressed under these conditions and that it accumulates less efficiently than the wild type, consistent with previous observations that small GTPases are unstable in the nucleotide-free state when not bound to the exchange factor (Okkonen and Stenmark, 1997; Cool et al., 1999).

but exhibited approximately 25% ovule abortion. In 1626 PCR-genotyped progeny we recovered only *rab-D2c*/+ heterozygotes or wild types. Similarly, plants with the *rab-D2a rab-D2b*/+ *rab-D2c* genotype also developed normally (Fig. 6D; supplementary material Fig. S6B, aaBbcc) but exhibited approximately 25% ovule abortion and yielded no homozygous mutants amongst 1418 PCR-genotyped progeny. Thus, the *Arabidopsis* Rab-D2 subclass performs an essential function that cannot be provided by *RAB-D1*. Furthermore, this data confirms that all three members of the Rab-D2 subclass are extensively redundant because all three double mutant combinations were viable.

In contrast to the Rab-D2 subclass, however, the Rab-D1 subclass appeared to be dispensable in *Arabidopsis* as we were able to recover healthy fertile plants that were homozygous for either of two independent T-DNA insertions in *RAB-D1* (supplementary material Fig. S6A), which is the only representative of this subclass in *Arabidopsis* (Pereira-Leal and Seabra, 2001; Rutherford and Moore, 2002; Vernoud et al., 2003) (Fig. 6A,E, ddAABBCC).

The Rab-D1 and Rab-D2 subclasses have overlapping function in *Arabidopsis*

The viability of the *rab-D1* insertion alleles in *Arabidopsis* contrasted with the lethal phenotype associated with the expression of its dominant-negative mutant in seedlings. Thus the dominant-negative RAB-D1 [N121I] mutant must inhibit a function for which RAB-D1 is not essential, presumably by titrating a factor that performs an essential function with another protein. To investigate the possibility that these other proteins are members of the essential Rab-D2 subclass, we generated Rab-D2 mutants in a *rab-D1* background. Plants homozygous for *rab-D1-1* and insertions in single *RAB-D2* loci were phenotypically normal (data not shown). Strikingly however, plants homozygous for insertions in *RAB-D1* as well as *RAB-D2b* and *RAB-D2c*, which are the two most abundant members of the Rab-D2 subclass (Fig. 6C), exhibited a stunted bushy growth phenotype and very low fertility (Fig. 6E, ddAAbbcc). Transformation of these plants (ddAAbbcc) with a *RAB-D1* cDNA under control of the CaMV 35S promoter complemented the bushy growth phenotype and infertility in 11 of 19 primary transformants (supplementary material Fig. S7A). This confirmed that both phenotypes resulted from the loss of Rab-D1 function in this background. As these phenotypes were not seen in the single *rab-D1* mutant or in the *rab-D2b rab-D2c* double mutant (Fig. 6E, DDAAbbcc), the functions of *RAB-D1* and these *RAB-D2* genes must overlap. Furthermore, these data show that in the absence of RAB-D1, RAB-D2a alone is insufficient for normal development. The bushy phenotype of these plants arose in part because the upper region of the primary inflorescence stem became necrotic a few millimetres below the apex (see Fig. 6E, inset). Notably, the same phenotype was observed in inflorescences of *Arabidopsis* plants expressing the dominant-negative RAB-D2a [N121I] mutant (supplementary material Fig. S7B).

Discussion

Higher plants are unusual in that their Rab1/Ypt1-related proteins can be divided into two clades, Rab-D1 and Rab-D2, that might represent subclasses with distinct functions in membrane trafficking (Pereira-Leal and Seabra, 2001; Rutherford and Moore, 2002; Vernoud et al., 2003). Here, we show that the single *Arabidopsis* Rab-D1 protein, RAB-D1, targets YFP to the same Golgi-associated punctate compartments as RAB-D2a and that, like RAB-D2a, it acts in membrane traffic between the ER and Golgi, consistent with the activities of other Rab1/Ypt1-related proteins. However, based on the behaviour of dominant-negative RAB-D1 and RAB-D2a mutants in reciprocal rescue experiments, we propose that Rab-D1 and Rab-D2 proteins act in ER-Golgi traffic via distinct biochemical interactions. Thus, the inhibition of membrane traffic by dominant-negative RAB-D1 in tobacco leaf epidermis or *Arabidopsis* seedlings could be substantially restored by coexpressing wild-type

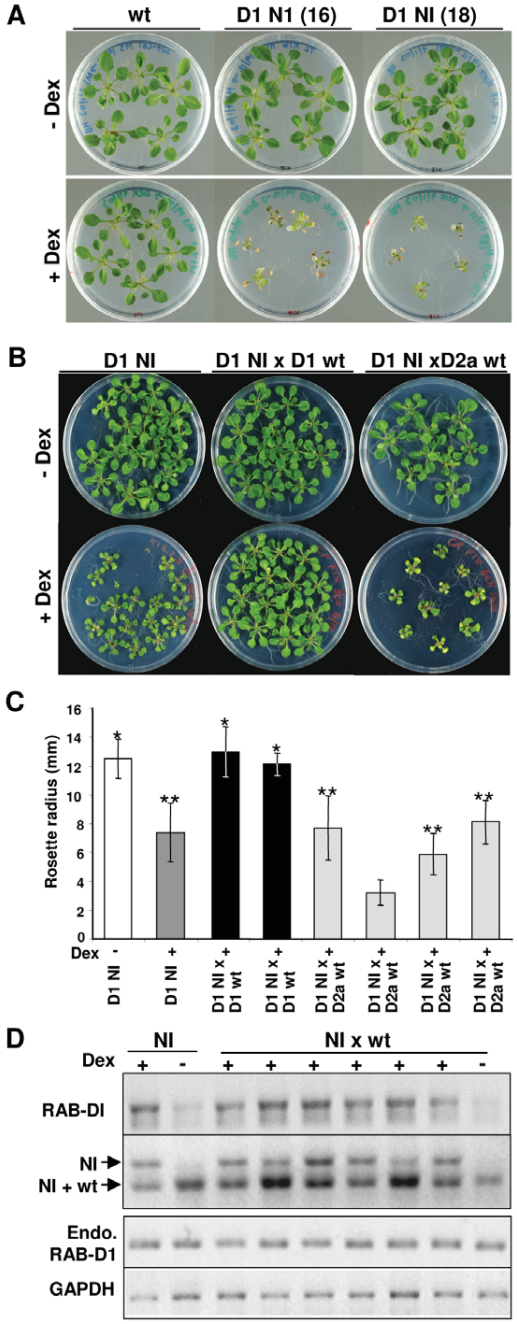

Fig. 5. RAB-D1 [N121I] inhibits *Arabidopsis* growth and cannot be rescued by RAB-D2a. (A) Seedlings exhibiting inducible expression of RAB-D1 [N121I] (D1 NI) but not wild type (wt) grown in the presence (+Dex) or absence (–Dex) of the inducer dexamethasone. Seedlings are shown from one wild-type and two N121I lines in which inducible expression of the transgene was confirmed by RNA gel blot (not shown). (B) As in A, but with seedlings expressing RAB-D1 [N121I] alone (D1 NI) compared with the F1 progeny of a cross to lines expressing wild-type RAB-D1 or RAB-D2a from the same inducible promoter system. (C) Quantitative analysis of rosette diameter in 18-day-old plants expressing RAB-D1 [N121I] only (D1 NI) in the presence (+) or absence (–) of dexamethasone (dark grey and white bars, respectively) or in the F1 progeny of crosses to lines expressing wild-type RAB-D1 (black bars) or RAB-D2a (pale grey bars). Each black and pale grey bar represents F1 progeny from an independent cross. Sets of data whose means are not significantly different ($P<0.001$) from D1 NI in either the absence or presence of dexamethasone are marked by single and double asterisks respectively. (D) RT-PCR analysis of transcript accumulation from the RAB-D1 wild-type and N121I mutant transgenes in the parental N121I line (NI) and the F1 progeny from crosses between lines carrying each transgene (NI×wt) in the presence (+) or absence (–) of dexamethasone (Dex). The upper panel shows total RAB-D1 transcript accumulation. The second panel shows RT-PCR products digested with *Hin*dIII to distinguish transcripts from the transgenes expressing the N121I and wild-type sequences; the upper band is characteristic for the mutant sequence and shows that the mutant is transcribed in the rescued plants that exhibit normal growth rates. The third panel shows that transcripts from the endogenous (Endo.) *RAB-D1* locus are unaffected by expression of the transgenes. The lower panel shows transcripts for GAPDH, which served as a loading control. RNA was extracted after 18 days of growth.

RAB-D1 but not wild-type RAB-D2a. Similarly, inhibition of ER-Golgi traffic by dominant-negative RAB-D2a could be restored by coexpression of wild-type RAB-D2a but not of RAB-D1.

Because the dominant-negative mutants are likely to act by competitive titration of essential cofactors, we propose that RAB-D1 and RAB-D2 preferentially interact with and titrate different factors. When overexpressed, the cognate wild-type protein can compete with the dominant-negative mutant and restore the missing function, whereas the incorrect partner either cannot compete with the dominant-negative mutant or cannot fulfil the same function if it does interact.

These observations support the phylogenetic prediction that the plant Rab-D1 and Rab-D2 clades have acquired distinct functions in membrane traffic (Pereira-Leal and Seabra, 2001; Rutherford and Moore, 2002). Further support is provided by insertional mutants that demonstrated: (i) that all three members of the *Arabidopsis* Rab-D2 subclass are extensively redundant; and (ii) that the Rab-D2 subclass performs an essential function that cannot be provided by *RAB-D1*. Attempts to investigate whether the inability of *RAB-D1* to substitute for Rab-D2 function arises from differences in the coding sequences or in expression patterns were unsuccessful because RAB-D2 cDNAs did not complement the triple RAB-D2 mutant when expressed from their own promoter (data not shown). In contrast to Rab-D2, the Rab-D1 subclass is apparently dispensable for normal development. Nevertheless these two putative subclasses exhibit some overlap of function because *Arabidopsis* plants lacking the two most highly expressed members of the Rab-D2 subclass (RAB-D2b and RAB-D2c) were phenotypically wild type but were stunted and highly infertile when *RAB-D1* was also disrupted. Consistent with this, the expression of dominant-negative RAB-D2a [N121I] phenocopied the *rab-D1 rab-D2b rab-D2c* plants with respect to the stunting of growth and the necrosis of the apical region of the stem. This is the region of the stem that exhibits the highest rate of elongation (Fukaki et al., 1996), which might not be sustainable when Rab-D1 and Rab-D2 function is compromised by the dominant-negative mutant.

The overlap in function between Rab-D1 and Rab-D2 subclasses might account for the contradictory observations regarding the lethality of RAB-D1 dominant-negative and loss-of-function mutants: whereas *rab-D1* plants were apparently normal and fertile, expression of dominant-negative RAB-D1 [N121I] resulted in severe growth defects and eventually in cell death in both *Arabidopsis* and tobacco. Thus, the dominant-negative mutant must inhibit activities in which Rab-D1 is not essential. Nevertheless, the membrane trafficking and cell viability phenotypes caused by dominant-negative RAB-D1 can be rescued specifically by coexpression with wild-type RAB-D1, suggesting that this protein can fulfil the essential functions that are inhibited by the mutant.

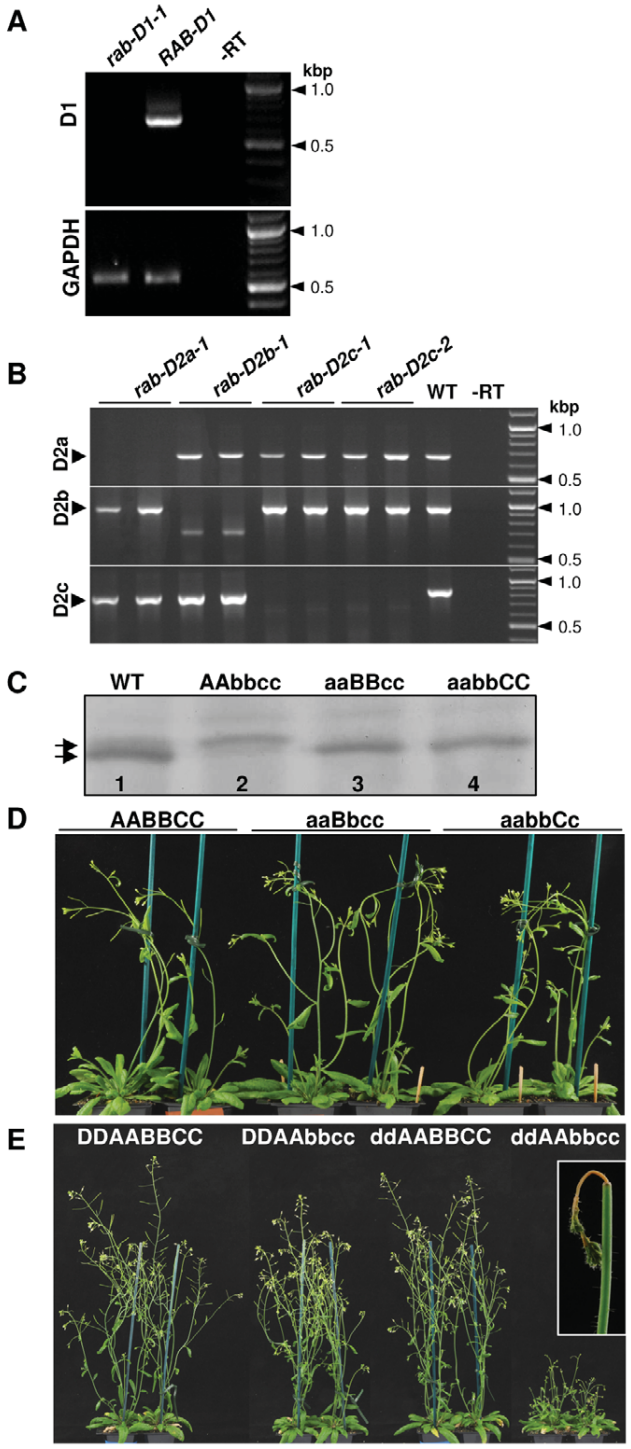

Fig. 6. Phenotypes of insertional mutants in the Rab-D1 and Rab-D2 subclasses. (A,B) RT-PCR analysis of Rab-D1 and Rab-D2 transcript abundance in plants carrying insertion mutants in individual genes or in wild-type plants (WT). –RT indicates PCR without reverse transcription on RNA isolated from wild-type plants. Transcripts for GAPDH served as a loading control. (C-E) Genotypes are indicated by the letters D, A, B and C denoting *RAB-D1*, *RAB-D2a*, *RAB-D2b* and *RAB-D2c*, respectively. Lower case letters (d, a, b, c) denote a mutant allele. (C) Immunoblot analysis of protein extracts from whole seedlings and T-DNA insertion mutants using a peptide antibody that recognises a conserved epitope in the Rab-D2 subclass. Extracts were prepared from wild-type plants and three double mutant genotypes that retained only a single wild-type *RAB-D2* locus: lane 2, genotype AAbbcc retains only *RAB-D2a*; lane 3, genotype aaBBcc, retains only *RAB-D2b*; lane 4, genotype aabbCC retains only *RAB-D2c*. In the wild type (lane 1), the antibody recognises two RAB-D2-specific bands (arrows), with the upper band corresponding to RAB-D2a and the stronger lower band corresponding to RAB-D2b and RAB-D2c. (D) Phenotype of wild-type plants (AABBCC) or plants carrying a single wild-type copy of a single Rab-D2 gene, either RAB-D2b (aaBbcc) or RAB-D2c (aabbCc). (E) Phenotype of wild-type plants (DDAABBCC) or plants carrying mutations either in RAB-D1 (ddAABBCC) or in RAB-D2b and RAB-D2c (DDAAbbcc), or in all three loci (ddAAbbcc).

A simple resolution to this apparent paradox is suggested by the overlap in function between Rab-D1 and Rab-D2 proteins discussed above. Thus, even though proteins of the Rab-D2 subclass might be unable to compete with the dominant-negative RAB-D1 [N121I] mutant they might nevertheless be able to interact productively with the usual partners of RAB-D1 when RAB-D1 is simply missing (*rab-D1* T-DNA alleles). This interpretation is consistent with biochemical data that show that small GTPase mutants of the NI class (equivalent to N116I of Ras) bind tightly to essential regulators such as nucleotide exchange factors (Jones et al., 1995; Olkkonen and Stenmark, 1997; Walch-Solimena et al., 1997; Goh et al., 2007) to the extent that their dominant-inhibitory effect is not always alleviated by coexpression of the wild-type protein (Tisdale et al., 1992; Pind et al., 1994; Jones et al., 1995; Yoo et al., 1999). The interpretation is also consistent with the previous proposal that Rab-D1 and Rab-D2 proteins interact preferentially with different interactors and that each interaction contributes an essential function. In support of this, when the two most highly expressed Rab-D2 loci, *RAB-D2b* and *RAB-D2c*, were disrupted along with *RAB-D1*, the single remaining Rab-D2 gene (*RAB-D2a*) is apparently insufficient to fulfil Rab-D1 function (these 'ddAAbbcc' plants were stunted and infertile) even though it can evidently fulfil all essential Rab-D2-specific functions (*rab-D2b rab-D2c* plants, 'DDAAbbcc' were healthy and fertile but triple mutants in the Rab-D2 subclass were not viable).

We cannot rule out the alternative explanations that dominant-negative RAB-D1 [N121I] titrates an essential factor that does not normally interact with wild-type RAB-D1, or that the titrated factor has additional functions that are required for cell viability independently of RAB-D1. Indeed the fact that wild-type RAB-D1 does not completely restore trafficking when coexpressed with RAB-D1 [N121I] in tobacco leaf epidermis could be interpreted as evidence of this. It is also possible that, in this context, restoration is partial simply because of the stochasticity of transient coexpression of wild-type and mutant forms of the Rab protein in individual epidermal cells with this system (Samalova et al., 2006).

Cellular functions of Rab-D1 and Rab-D2 subclasses

Rab1 in mammalian cells is associated principally with *cis*-Golgi membranes and ER-Golgi intermediates, consistent with its function in the early stages of biosynthetic traffic (Saraste et al., 1995). In plant cells, however, we found that Rab-D1 and Rab-D2 proteins targeted YFP to the TGN as well as the Golgi stack, suggesting that they might function on late as well as early Golgi compartments. There is evidence that Ypt1 function is required in yeast for efficient recycling of membrane proteins from the post-Golgi endosome via the Golgi (Lafourcade et al., 2004) and it has been suggested that the *Arabidopsis* TGN is homologous to the yeast post-Golgi endosome (Chow et al., 2008). The TRAPP complex that acts as an exchange factor for Ypt1 functions across the whole Golgi (Sacher et al., 2008) and in rat liver, Rab1a has been associated with transcytotic vesicles as well as ER-Golgi intermediates (Jin et al.,

1996). The strong accumulation of plant Rab1-homologues at *trans*- rather than *cis*-Golgi membranes might perhaps reflect the fact that most of the material secreted by plants cells originates within the Golgi rather than the ER (Staehelin and Moore, 1995). As a result, there might be more active recycling within the Golgi and between the Golgi and plasma membrane than between the Golgi and ER.

Whereas the genetic evidence suggests distinct roles for the Rab-D1 and Rab-D2 subclasses in ER-Golgi traffic, the cellular and biochemical basis of this difference is unclear. We do not have any evidence that Rab-D1 and Rab-D2 proteins have spatially distinct functions because proteins of each subclass targeted fluorescent proteins to the same Golgi-associated structures. The two subclasses could potentially act either in parallel biosynthetic pathways between ER and Golgi, in opposing pathways in ER-Golgi cycling, or at different points on a single pathway. In yeast, Ypt1p is required for the selective packaging of GPI-anchored cargo at the ER (Morsomme and Reizman, 2002). The observation that dominant-negative mutants of both RAB-D1 and RAB-D2a acted similarly on the trafficking and distribution of the GPI-anchored fusion protein HIPL1-GFP, the heterologous artificial secretory protein secGFP, and the COPII-vesicle component YFP-SEC24 argues that both proteins are required for the default pathway. This is supported by the observation that both types of mutant also inhibited trafficking of luminal and membrane markers of the vacuole as well as a marker of a newly described vacuolar degradation pathway (Foresti et al., 2008).

Mammalian Rab1 and yeast Ypt1p have been implicated in distinct trafficking steps at the Golgi: targeting of ER-derived COPII vesicles to the *cis*-face and a subsequent intra-Golgi transport step in which the ArfGEF GBF1 is implicated (Plutner et al., 1991; Jedd et al., 1995; Alvarez et al., 2003; Cai et al., 2008). Ypt1 is also required for retrograde transport between Golgi and ER in yeast and for endocytic recycling from the post-Golgi-endosome to the Golgi complex (Lafourcade et al., 2004; Kamena et al., 2008). One possibility is that in plants, Rab-D1 and Rab-D2 proteins have become specialised to act preferentially in one or other of these processes. Confocal microscopy did not reveal consistent differences between the effects of RAB-D1 and RAB-D2a N121I mutants on any of the markers we analysed, but such differences might not be resolvable by these methods or might be confounded by secondary effects. The identification of RAB-D1 and RAB-D2a interactors could allow this hypothesis to be tested experimentally.

Materials and Methods

Plant material

Arabidopsis plants expressing YFP fusions to RAB-D1 and RAB-D2a, lines WAVE 25y and 29y, respectively, were generated as part of the WAVE collection (http://www.unil.ch/dbmv/page52928_en.html#2). The T-DNA insertion alleles described here correspond to the following stocks: *rab-D1-1*, SALK_033433; *rab-D1-2* SALK_054734; *rab-D2a-1*, SALK_099495; *rab-D2b-1*, TMRI 151_C11; *rab-D2c-1*, SALK_034873; *rab-D2c-2*, SALK_054626. SAIL (Syngenta Arabidopsis Insertion Library) lines were obtained from TMRI (Torrey Mesa Research Institute, San Diego, CA). SALK Institute Genomic Analysis Laboratory (SIGnAL) lines were obtained from NASC or ABRC (Arabidopsis Biological Resource Center). Other plant materials and bacterial strains are described in the relevant sections below.

Molecular cloning

Molecular cloning was performed according to standard protocols as described previously (Batoko et al., 2000; Craft et al., 2005). The RAB-D1 cDNA sequence was amplified using primers P1 and P2 to introduce *Bam*HI and *Sal*I sites upstream and a *Bam*HI site downstream of the coding sequence. The S22N, Q67L and N121I mutations were introduced by overlapping PCR (Batoko et al., 2000) using primers P1 and P2 together with primers P3 and P4, P5 and P6, or P7 and P8, respectively. These mutagenic primer pairs also contained silent mutations that introduced an *Acc*I site into the S22N mutant, a *Pvu*II site into the Q71L mutant and a *Hin*fI site into the N121I mutant and disrupted a *Hin*dIII site in the N121I mutant. All RAB-D1 sequences were introduced as *Sal*I and *Bam*HI fragments into the expression vector pVKH18-En6-GUS (Batoko et al., 2000) for Agrobacterium-mediated transient expression in tobacco leaf epidermis and for complementation of T-DNA insertion mutants in *Arabidopsis*. The same fragments were inserted into the *Sal*I and *Bam*HI sites of pV-TOP (Craft et al., 2005) for dexamethasone-inducible expression via the pOp/LhGR system in the *Arabidopsis* driver line 4C-S5/7 (Craft et al., 2005) and of pVKHEn6-HAvenus (Zheng et al., 2005) to generate N-terminal fusions to the Venus variant of YFP. The RAB-D2a and RAB-D2a [N121I] cDNA sequences were inserted into pV-TOP and pVKHEn6-HAvenus as *Xho*I-*Bam*HI fragments from pBluescript SK+ derivatives described previously (Batoko et al., 2000) and introduced into the *Arabidopsis* driver line 4C-S5/7 (Craft et al., 2005). The GFP fusion to RAB-D2a was a kind gift of Ulla Neumann and Chris Hawes (Oxford Brookes University, Oxford, UK).

Growth and RT-PCR analysis of dexamethasone-inducible Rab-D expression in *Arabidopsis*

Seedlings were germinated and grown on medium supplemented with 20 μM dexamethasone or with an equivalent volume of DMSO as described (Craft et al., 2005). RT-PCR was performed on individual F1 seedlings of crosses between lines expressing RAB-D1 or RAB-D1 [N121I] from pV-TOP in the *Arabidopsis* driver line 4C-S5/7 (Craft et al., 2005) and on seedlings of the parental generation. Total *At*RabD1 transcript was amplified from total RNA as described previously (Craft et al., 2005) using the intron-spanning primers P9 and P10 and digested with *Hin*dIII to reveal the 350 bp fragment specific to transcripts of the RAB-D1 [N121I] transgene. Endogenous *At*RabD1 transcript was amplified using the intron-spanning primers P9 and P11.

RT-PCR of knock-out lines

RNA extracted from 100 mg of leaves of 12-day-old seedlings homozygous for T-DNA insertion mutants using the Qiagen RNeasy Kit (Qiagen, Crawley, UK) was analysed by RT-PCR. RT reactions were performed as follows: a mixture of 0.5 μl 10x diluted deoxyribonuclease I (DNaseI, Invitrogen), 0.9 μl 10x DNase I buffer, 0.5 μl RNase inhibitor (RNasin, Promega), 2.1 μl RNase-free water and 5 μl of sample RNA (2.5 μg diluted to 5 μl) was left for 15 minutes at room temperature. EDTA (1 μl of 25 mM) was added and reactions were incubated at 65°C for 10 minutes. Primer P12 (1 μl of 100 mM) and 1 μl of a mix of dNTPs at 10 mM was added and the reaction was left for a further 5 minutes at 65°C. On ice, 2 μl of 0.1M DTT, 4 μl 5× First Strand buffer (Invitrogen) and 1 μl RNasin was added and the reaction was incubated at 42°C for 2 minutes. SuperScript II RNase H-RT (1 μl) from Invitrogen was added and the tubes were incubated at 42°C for 1 hour and then at 70°C for 15 minutes. Final cDNA was diluted five- to tenfold and 1 μl was used for initial PCR reactions. PCR was performed using the following primers: P9 + P11 primers to amplify the *At*RabD1 sequence; P13 + P14 to amplify the RAB-D2a sequence; P15 + P16 to amplify the RAB-D2b sequence; P17 + P18 to amplify the RAB-D2c sequence; and P19 + P20 primers to amplify the GAPDH sequence. Amplification was performed at 94°C for 5 minutes, followed by 25 cycles of 94°C for 30 seconds, 58°C for 30 seconds and 72°C for 130 seconds, and finally at 72°C for 10 minutes. Products were analysed by agarose gel electrophoresis in the presence of ethidium bromide and imaged under UV illumination.

Genotyping T-DNA insertion mutants

The following primers were used to identify wild-type and insertion alleles: T-DNA *rab-D1-1*, P2 + P21; WT *rab-D1-1*, P2 + P7; T-DNA *rab-D1-2*, P9 + P21; WT *rab-D1-2*, P2 + P9; T-DNA *rab-D2a*, P21 + P22; WT *rab-D2a*, P22 + P23; T-DNA *rab-D2b*, P24 + P25; WT *rab-D2b*, P25 + P26; T-DNA *rab-D2c-1* and *rab-D2c-2*, P21 + P27; WT *rab-D2c-1* and *rab-D2c-2*, P27 + P28. PCR was performed with Taq polymerase using 50 mM Tris-HCl pH 9.1, 14 mM $(NH_4)_2SO_4$ and 2.5 mM $MgCl_2$ buffer with the following cycle: 94°C for 5 minutes; then 30-35 cycles of 94°C for 30 seconds, 55°C for 30 seconds and 72°C for 130 seconds; and finally 72°C for 10 minutes. Plants carrying a single remaining wild-type Rab-D2 allele were maintained as heterozygotes and were all genotyped by PCR in each generation and following Agrobacterium-mediated transformation by floral dip.

Tobacco leaf infiltrations and confocal microscopy

The quantitative secGFP accumulation assay in tobacco leaf epidermis and detection of fluorescent proteins by confocal microscopy was as described by Zheng and colleagues (Zheng et al., 2005). Ratiometric imaging constructs and simultaneous imaging of GFP with mRFP1 or YFP were as described by Samalova and colleagues (Samalova et al., 2006).

Immunoblot analysis

Protein isolation and blotting was performed as described by Samalova and colleagues (Samalova et al., 2006). Proteins were extracted from tobacco leaf samples 48 hours after Agrobacterium infiltration. OD 0.03 and 0.01 was used for the RAB-D and ST-GFP Agrobacterium cultures, respectively. Affinity-purified polyclonal antibody for RAB-D2 was raised in rabbits against the peptide antigen acetyl-NARPPTVQIRGQPVAQKNGC-amide (Cambridge Research Biochemicals, Cambridge, UK). Full-length GFP antibody was obtained from Molecular Probes (Leiden, The Netherlands). Each was used at 1/1000 dilution to probe the membrane overnight at 4°C. Alkaline-phosphatase-conjugated secondary antibodies (anti-rabbit IgG; Sigma) were used at 1/10,000 dilution for 1-hour incubation at room temperature.

List of oligonucleotides

Oligonucleotides were synthesised by MWG-Biotech (Germany) or Sigma-Genosys (Cambridge, UK). See supplementary material Table S1.

This work was supported by BBSRC research grant BBS/B/03904 to I.M. and by a BBSRC CASE studentship to H.P. The Wave lines were generated with support from an HFSP fellowship and the Swiss National Science Foundation to N.G. and from the HHMI, USDA and NIH to J.C. We thank Ulla Neumann and Chris Hawes for *Agrobacterium* strains expressing GFP:RAB-D2a, YFP-SEC24 and ERD2-GFP; Allessandro Vitale (CNR_IGV, Portici, Italy) and Michele Bellucci (Istituto di Genetica Vegetale-Sezione di Perugia, Perugia, Italy) for zein-GFP; and Paul Dupree (University of Cambridge, Cambridge, UK) for HIPL1-GFP. John Baker for photography, and Caroline O'Brien for technical assistance. We thank the Torrey Mesa Research Institute and SALK Institute Genomic Analysis Laboratory for the T-DNA insertion lines from the SAIL and SIGnAL collections, some of which were obtained from the Nottingham Arabidopsis Stock Centre, UK, or the Arabidopsis Biological Resource Centre, Columbus, OH. Deposited in PMC for release after 12 months.

References

Alvarez, C., Garcia-Mata, R., Brandon, E. and Sztul, E. (2003). COPI recruitment is modulated by a Rab1b-dependent mechanism. *Mol. Biol. Cell* **14**, 2116-2127.

Batoko, H., Zheng, H. Q., Hawes, C. and Moore, I. (2000). A Rab1 GTPase is required for transport between the endoplasmic reticulum and Golgi apparatus and for normal Golgi movement in plants. *Plant Cell* **12**, 2201-2217.

Beard, M., Satoh, A., Shorter, J. and Warren, G. (2005). A cryptic Rab1-binding site in the p115 tethering protein. *J. Biol. Chem.* **280**, 25840-25848.

Behnia, R. and Munro, S. (2005). Organelle identity and the signposts for membrane traffic. *Nature* **438**, 597-604.

Biermann, B., Randall, S. K. and Crowell, D. N. (1996). Identification and isoprenylation of plant GTP-binding proteins. *Plant Mol. Biol.* **31**, 1021-1028.

Bock, J. B., Matern, H. T., Peden, A. A. and Scheller, R. H. (2001). A genomic perspective on membrane compartment organization. *Nature* **409**, 839-841.

Borner, G. H. H., Sherrier, D. J., Weimar, T., Michaelson, L. V., Hawkins, N. D., MacAskill, A., Napier, J. A., Beale, M. H., Lilley, K. S. and Dupree, P. (2005). Analysis of detergent-resistant membranes in Arabidopsis. evidence for plasma membrane lipid rafts. *Plant Physiol.* **137**, 104-116.

Cai, Y., Chin, H. F., Lazarova, D., Menon, S., Fu, C., Cai, H., Sclafani, A., Rodgers, D. W., De La Cruz, E. M., Ferro-Novick, S. et al. (2008). The structural basis for activation of the Rab Ypt1p by the TRAPP membrane-tethering complexes. *Cell* **133**, 1202-1213.

Chow, C. M., Neto, H., Foucart, C. and Moore, I. (2008). Rab-A2 and -A3 GTPases define a trans-Golgi endosomal membrane domain in Arabidopsis that contributes substantially to the cell plate. *Plant Cell* **20**, 101-123.

Cool, R. H., Schmidt, G., Lenzen, C. U., Prinz, H., Vogt, D. and Wittinghofer, A. (1999). The Ras mutant D119N is both dominant negative and activated. *Mol. Cell. Biol.* **19**, 6297-6305.

Craft, J., Samalova, M., Baroux, C., Townley, H., Martinez, A., Jepson, I., Tsiantis, M. and Moore, I. (2005). New pOp/LhG4 vectors for stringent glucocorticoid-dependent transgene expression in Arabidopsis. *Plant J.* **41**, 899-918.

Dettmer, J., Hong-Hermesdorf, A., Stierhof, Y. D. and Schumacher, K. (2006). Vacuolar H+-ATPase activity is required for endocytic and secretory trafficking in Arabidopsis. *Plant Cell* **18**, 715-730.

Duarte, P., Pissarra, J. and Moore, I. (2008). Processing and trafficking of a single isoform of the aspartic proteinase cardosin A on the vacuolar pathway. *Planta* **227**, 1255-1268.

Foresti, O., De Marchis, F., de Virgilio, M., Klein, E., Arcioni, S., Belluci, M. and Vitale, A. (2008). Protein domains involved in assembly in the endoplasmic reticulum promote vacuolar delivery when sused to secretorey GFP, indicating a quality control pathway for degradation in the plant vacuole. *Mol. Plant* **1**, 1067-1076.

Fukaki, H., Fujisawa, H. and Tasaka, M. (1996). Gravitropic response of inflorescence stems in Arabidopsis thaliana. *Plant Physiol.* **110**, 933-943.

Geldner, N., Dénervaud-Tendon, V., Hyman, D. L., Mayer, U., Stierhof, Y. D. and Chory, J. (2009). Rapid, combinatorial analysis of membrane compartments in intact plants with a multicolor marker set. *Plant J.* **59**, 169-178.

Goh, T., Uchida, W., Arakawa, S., Ito, E., Dainobu, T., Ebine, K., Takeuchi, M., Sato, K., Ueda, T. and Nakano, A. (2007). VPS9a, the common activator for two distinct types of Rab5 GTPases, is essential for the development of Arabidopsis thaliana. *Plant Cell* **19**, 3504-3515.

Grebe, M., Xu, J., Mobius, W., Ueda, T., Nakano, A., Geuze, H. J., Rook, M. B. and Scheres, B. (2003). Arabidopsis sterol endocytosis involves actin-mediated trafficking via ARA6-positive early endosomes. *Curr. Biol.* **13**, 1378-1387.

Grosshans, B. L., Ortiz, D. and Novick, P. (2006). Rabs and their effectors: achieving specificity in membrane traffic. *Proc. Natl. Acad. Sci. USA* **103**, 11821-11827.

Jedd, G., Richardson, C., Litt, R. and Segev, N. (1995). The Ypt1 GTPase is essential for the first 2 steps of the yeast secretory pathway. *J. Cell Biol.* **131**, 583-590.

Jin, M., Saucan, L., Farquhar, M. G. and Palade, G. E. (1996). Rab1a and multiple other Rab proteins are associated with the transcytotic pathway in rat liver. *J. Biol. Chem.* **271**, 30105-30113.

Jones, S., Litt, R. J., Richardson, C. J. and Segev, N. (1995). Requirement of nucleotide exchange factor for Ypt1 GTPase mediated protein-transport. *J. Cell Biol.* **130**, 1051-1061.

Kamena, F., Diefenbacher, M., Kilchert, C., Schwarz, H. and Spang, A. (2008). Ypt1p is essential for retrograde Golgi-ER transport and for Golgi maintenance in S. cerevisiae. *J. Cell Sci.* **121**, 1293-1302.

Kotzer, A. M., Brandizzi, F., Neumann, U., Paris, N., Moore, I. and Hawes, C. (2004). *At*RabF2b (Ara7) acts on the vacuolar trafficking pathway in tobacco leaf epidermal cells. *J. Cell Sci.* **117**, 6377-6389.

Lafourcade, C., Galan, J. M., Gloor, Y., Haguenauer-Tsapis, R. and Peter, M. (2004). The GTPase-activating enzyme Gyp1p is required for recycling of internalised membrane material by inactivation of the Rab/Ytp GTPase Ypt1p. *Mol. Cell. Biol.* **24**, 3815-3826.

Lefebvre, B., Batoko, H., Duby, G. and Boutry, M. (2004). Targeting of a *Nicotiana plumbaginifolia* H^+-ATPase to the plasma membrane is not by default and requires cytosolic structural determinants. *Plant Cell* **16**, 1772-1789.

Markgraf, D. F., Peplowska, K. and Ungerman, C. (2007). Rab cascades and tethering factors in the endomembrane system. *FEBS Lett.* **581**, 2125-2130.

Moore, I., Schell, J. and Palme, K. (1995). Subclass-specific sequence motifs identified in Rab GTPases. *Trends Biochem Sci.* **20**, 10-12.

Morsomme, P. and Riezman, H. (2002). The Rab GTPase Ypt1p and tethering factors couple protein sorting at the ER to vesicle targeting to the Golgi apparatus. *Dev. Cell* **2**, 307-317.

Olkkonen, V. M. and Stenmark, H. (1997). Role of rab GTPases in membrane traffic. In *International Review of Cytology: A Survey of Cell Biology*, vol. 176 (ed. K. W. Jeon), pp. 1-85. New York: Academic Press.

Park, M., Kim, S. J., Vitale, A. and Hwang, I. (2004). Identification of the protein storage vacuole and protein targeting to the vacuole in leaf cells of three plant species. *Plant Physiol.* **134**, 625-639.

Pereira-Leal, J. B. and Seabra, M. C. (2000). The mammalian Rab family of small GTPases: Definition of family and subfamily sequence motifs suggests a mechanism for functional specificity in the Ras superfamily. *J. Mol. Biol.* **301**, 1077-1087.

Pereira-Leal, J. B. and Seabra, M. C. (2001). Evolution of the Rab family of small GTP-binding proteins. *J. Mol. Biol.* **313**, 889-901.

Pind, S. N., Nuoffer, C., McCaffery, J. M., Plutner, H., Davidson, H. W., Farquhar, M. G. and Balch, W. E. (1994). Rab1 and Ca2+ are required for the fusion of carrier vesicles mediating endoplasmic-reticulum to Golgi transport. *J. Cell Biol.* **125**, 239-252.

Plutner, H., Cox, A. D., Pind, S., Khosravi-Far, R., Bourne, J. R., Schwaninger, R., Der, C. J. and Balch, W. E. (1991). Rab1B regulates vesicular transport between the endoplasmic reticulum and successive Golgi compartments. *J. Cell Biol.* **115**, 31-43.

Richardson, C. J., Jones, S., Litt, R. J. and Segev, N. (1998). GTP hydrolysis is not important for Ypt1 GTPase function in vesicular transport. *Mol. Cell. Biol.* **18**, 827-838.

Richter, S., Geldner, N., Schrader, J., Wolters, H., Stierhof, Y. D., Rios, G., Koncz, C., Robinson, D. G. and Jürgens, G. (2007). Functional diversification of closely related ARF-GEFs in protein secretion and recycling. *Nature* **448**, 488-492.

Rutherford, S. and Moore, I. (2002). The Arabidopsis Rab GTPase family: another enigma variation. *Curr. Opin. Plant Biol.* **5**, 518-528.

Sacher, M., Kim, Y. G., Lavie, A., Oh, B. H. and Segev, N. (2008). The TRAPP complex: insights into its architecture and function. *Traffic* **9**, 2023-2042.

Saint-Jore, C. M., Evins, J., Batoko, H., Brandizzi, F., Moore, I. and Hawes, C. (2002). Redistribution of membrane proteins between the Golgi apparatus and endoplasmic reticulum in plants is reversible and not dependent on cytoskeletal networks. *Plant J.* **29**, 661-678.

Samalova, M., Fricker, M. and Moore, I. (2006). Ratiometric fluorescence-imaging assays of plant membrane traffic using polyproteins. *Traffic* **7**, 1701-1723.

Saraste, J., Lahtinen, U. and Goud, B. (1995). Localization of the small GTP-binding protein rab1p to early compartments of the secretory pathway. *J. Cell Sci.* **108**, 1541-1552.

Staehelin, L. A. and Moore, I. (1995). The plant Golgi apparatus-Structure, functional organization and trafficking mechanisms. *Annu. Rev. Plant Physiol. Mol. Biol.* **46**, 261-288.

Stefano, G., Renna, L., Chatre, L., Hanton, S. L., Moreau, P., Hawes, C. and Brandizzi, F. (2006). In tobacco leaf epidermal cells, the integrity of protein export from the endoplasmic reticulum and of ER export sites depends on active COPI machinery. *Plant J.* **46**, 95-110.

Teh, O. K. and Moore, I. (2007). An ARF-GEF acting at the Golgi and in selective endocytosis in polarized plant cells. *Nature* **448**, 493-496.

Tisdale, E. J., Bourne, J. R., Khosravifar, R., Der, C. J. and Balch, W. E. (1992). GTPbinding mutants of Rab1 and Rab2 are potent inhibitors of vesicular transport from the endoplasmic-reticulum to the Golgi-complex. *J. Cell Biol.* **119**, 749-761.

Ueda, T., Uemura, T., Sato, M. H. and Nakano, A. (2004). Functional differentiation of endosomes in Arabidopsis cells. *Plant J.* **4**, 783-789.

Vernoud, V., Horton, A. C., Yang, Z. and Nielsen, E. (2003). Analysis of the small GTPase gene superfamily of Arabidopsis. *Plant Physiol.* **131**, 1191-1208.

Walch-Solimena, C., Collins, R. N. and Novick, P. J. (1997). Sec2p mediates nucleotide exchange on Sec4p and is involved in polarized delivery of post-Golgi vesicles. *J. Cell Biol.* **137**, 1495-1509.

Woollard, A. A. D. and Moore, I. (2008). The functions of Rab GTPases in plant membrane traffic. *Curr. Opin. Plant Biol.* **11**, 610-619.

Yoo, J. S., Grabowski, R., Xing, L., Trepte, H. H., Schmitt, H. D. and Gallwitz, D. (1999). Functional implications of genetic interactions between genes encoding small GTPases involved in vesicular transport in yeast. *Mol. Gen. Genet.* **261**, 80-91.

Zheng, H., Kunst, L., Hawes, C. and Moore, I. (2004). A GFP-based assay reveals a role for RHD3 in transport between the endoplasmic reticulum and Golgi apparatus. *Plant J.* **37**, 398-414.

Zheng, H. Q., Camacho, L., Wee, E., Henri, B. A., Legen, J., Leaver, C. J., Malho, R., Hussey, P. J. and Moore, I. (2005). A Rab-E GTPase mutant acts downstream of the Rab-D subclass in biosynthetic membrane traffic to the plasma membrane in tobacco leaf epidermis. *Plant Cell* **17**, 2020-2036.

FUNGAL BIOLOGY REVIEWS 25 (2011) 181–188

Opinion Article

The rise and rise of emerging infectious fungi challenges food security and ecosystem health

Sarah GURR[a,*], *Marketa SAMALOVA*[a], *Matthew FISHER*[b]

[a]*Department of Plant Sciences, University of Oxford, OX1 3RB, UK*
[b]*Imperial College, School of Public Health, St Mary's Campus, London W2 1PG, UK*

ARTICLE INFO

Article history:
Received 7 October 2011
Received in revised form
13 October 2011
Accepted 13 October 2011

Keywords:
Disease triangle
Emerging infectious disease
Epidemics
Food security
Fungi
Oomycete
Policy
Public awareness
Species extinction

ABSTRACT

This article highlights some of the more notable persistent fungal diseases of our times. It draws attention to the emergence of new fungal pathotypes infecting food staple crops, due largely to modern agricultural practices, and to nascent fungal diseases decimating frog populations worldwide and killing hibernating bats in Northern USA. We invoke use of the basic disease triangle concept to highlight the "missing" data, with regards to pathogen and host biology and to the various environmental parameters which may dictate disease spread. Given these data "voids" we comment on the implementation of policy. We conclude with a series of recommendations for improved disease surveillance and reporting, the need for greater public awareness of these issues and a call for greater funding for fungal research. In so doing, we have exploited *Magnaporthe oryzae* and *Batrachochytrium dendrobatidis* as exemplar emerging infectious fungi. Our aim is to highlight the impact of emerging and emergent fungi on food security and, more broadly, ecosystem health.

1. Introduction

The global, social, economic and, indeed, potential impact of fungi is huge. Thus far, it has been estimated that we have identified only about 0.2–6 % of fungi predicted as extant in our biosphere (Hibbett *et al.*, 2011). Of these, a select few are highly exploited, as edible mushrooms and in food production, or as producers of industrial enzymes and pharmaceuticals. Less obviously, fungi are intrinsic to recycling organic matter and promoting plant growth. For example, the arbuscular mycorrhizal glomeromycete fungal symbionts are present in 90 % of land plants (Maillet *et al.*, 2011; Parniske, 2008) and are fundamental to plant health. Conversely, pathogenic fungi challenge food security by decimating our harvests, causing widespread malnutrition and starvation (Royal Society Report, 2009; Pennisi, 2010; Skamnioti and Gurr, 2009), they threaten extinction of wildlife, such as species of amphibians (Fisher *et al.*, 2009) and bats (Blehert *et al.*, 2009) whilst human pathogenic fungi cause debilitating disease or acute or fatal infections, particularly in immunocompromised patients (Butler *et al.*, 2009).

* *Corresponding author*.
E-mail address: sarah.gurr@plants.ox.ac.uk (S. Gurr).
1749-4613/$ – see front matter
doi:10.1016/j.fbr.2011.10.004

2. The complement of fungi and one oomycete under discussion

We review, albeit briefly, our state of knowledge with regards to three specific diseases of three significant staple food crops, notably rice blast, wheat stem rust and late blight of potato, the so-called "green pathogens". These are, respectively the Ascomycete *Magnaporthe oryzae* (*Mo*, Wilson and Talbot, 2009); Basidiomycete *Puccinia graminis* (*Pg*, Leonard and Szabo, 2005) and Oomycete *Phytophthora infestans* (*Pi*, Fry, 2008; Haas *et al.*, 2009). To this "cauldron of curses" we add the Ascomycete *Geomyces destructans* (*Gd*) (Gargas *et al.*, 2009; Frick *et al.*, 2010), causing white nose syndrome of hibernating bats in USA and the Chytridiomycete *Batrachochytrium dendrobatidis* (*Bd*) causing amphibian chytridiomycosis and affecting over 450 amphibian species (Longcore *et al.*, 1999; Fisher *et al.*, 2009; Kilpatrick *et al.*, 2010), the so-called "red pathogens" (Table 1).

Table 1 – Emerging or persistent fungal (oomycete) diseases, and their respective threat levels. These threat levels are assessed by the disease impact of recent emergence of new virulent races in the green pathogens, as, for example, with *P. infestans* US-8 and Blue 13 (Fry (2008) and Haas *et al.*, 2009); *P. graminis* (Leonard and Szabo, 2005). Early accounts of the green pathogens exist, disease being identifiable by the host symptoms described, as, for example, in during the 1845 Irish potato famine (Haas *et al.*, 2009); with *M. oryzae*, first described in 17th century as "rice fever" (Skamnioti and Gurr, 2009); *P. graminis*, identified from descriptions made in 690 BC (Leonard and Szabo (2005)). New races are, as yet, unknown in the red pathogens. The dates of emergence of the red pathogens are recorded in Table 1, with, for example, *G. destructans* first documented in a photograph taken near Albany New York (Blehert *et al.*, 2009) and *B. dendrobatidis* described in 1998 (Fisher *et al.*, 2009) but recognised later in a *Xenopus laevis* museum specimen preserved in 1938. It is not known, at this stage, as to whether these red pathogens have caused earlier epidemics (designated as ?)

	Emerging?	Persistent but with epidemics?	Threat Level posed by new races
P. infestans	No	Yes (1845 onwards)	High, new races (US-8, Blue 13)
M. oryzae	No	Yes (17thC)	High
P. graminis	No	Yes (690 BC)	High (Ug 99)
G. destructans	Yes (2006)	?	High New races?
B. dendrobatidis	Yes (1998)	? (1938)	High New races?

3. Can we quantify the disease burden inflicted by these microbes?

"Armed and dangerous" – fungi which threaten food security

With regards to wheat, rice and potatoes – these staple crops rank respectively first, second and eighth in terms of the area of global agricultural harvested (millions of hectares) but with potatoes moving up to fourth position due to its production (millions of tonnes) (FAO, 2008). We highlight the disease burden on potatoes for the very particular reason that this crop remains relatively stable in terms of world price fluctuation as there is little international trade in this commodity, due to transport problems. This is in sharp contrast to the fluctuating prices of wheat and rice as evidenced by the huge rise in price of these crops in 2008 and to a lesser extent in 2010, caused partly by climate fluctuations, rampant price speculation and competition for grain for food and fuel (web@foodsecurity.ac.uk). So, what is the cost of disease in terms of loss of crops? Oerke (2006) records that pests and pathogens cause global losses of around 27 % for wheat, 37 % for rice and 40 % for potatoes – this is despite the use of current crop protection practices. Of the various pests and pathogens it is the fungi (and the oomycete *P. infestans*) which cause the most significant losses.

"Active and deadly" – fungi which challenge wild species

While pathogens are not normally recognised as posing a threat of extinction to their hosts owing to density-dependent limitations on the transmission of infection (Anderson, 1979), two phyla of fungi have driven wildlife species extinct and a third threatens future populations. Both the chytrid *Bd* (Crawford *et al.*, 2010) and microsporidian fungi in the genus *Steinhausia* (Cunningham and Daszak, 1998) have been recognised as the aetiological agents that have eradicated their host species; for the former this may number hundreds of species. Concomitantly, the rapidly emerging infection of bats, white nose syndrome (WNS) caused by *G. destructans* is predicted to have a similarly severe impact on affected species (Frick *et al.*, 2010) and the "fungal-like" oomycetes are now known to be widely destructive in vertebrate and invertebrate species; for instance crayfish plague caused by *Aphanomyces astaci* (Alderman *et al.*, 1999). There is now a growing body of evidence that fungi may outrank better-recognised classes of pathogen (bacterial and viral) in the destructive impact that they have on wildlife species while leaving us questioning what underlies this emergent phenomenon.

4. Are these diseases emerging or persistent?

The criteria used to describe emerging infectious diseases (EIDs) are well-defined in human, livestock and wildlife disease but have been used rarely to describe plant disease. There is with one particular exception, that is by Anderson *et al.* (2004), who undertook the first (and only) meta-analysis of EIDs in crops and wild plants. We have exploited their EID descriptors of an increase in disease incidence due to changed geography and/or host range; altered virulence or

pathogenicity: newly evolved, recognised or discovered species (Table 1). These are robust markers, based on loss or crops or creatures, awareness of epidemics and meta-analyses (Anderson *et al.*, 2004). We must, however, be wary of more fragile markers, such as sensationalistic press headlines (for example, "Fungus suspect in frog deaths", "Scientists mash potato blight"), be aware that human disease attracts more attention than disease on wild animal species or crops, and not be overly influenced by the number of articles published on the various pathogens (Table 2). It is clear, however, that the three crop pathogens are endemic and persistent, but with the capacity to evolve novel virulent races, whilst *Bd* and *Gd* are novel emerging diseases which also carry the threat of genesis of new races (Table 1).

5. The disease triangle: evaluating the drivers of emerging and persistent disease

We invoke use of the disease triangle (Fig. 1), a concept much used in the study of plant disease, to assess the "knowns" and "unknowns" of the afore-mentioned green and red pathogens.

The pathogen

It is clear that we know considerably more about the sexual and asexual life-cycles of the green plant pathogens than about the red fungi (Table 3). All have sequenced genomes but analysis of gene number, amount of repetitive DNA and SNP frequency lags behind in *Bd* and *Gd*. By contrast, these facts are known in *Mo*, *Pg* and *Pi*; this difference reflects the relatively recent origin of these red pathogens and perhaps a lack of industry-sponsored research into their genetics. The 'green' data is alarming, in particular with regards to the amount of repetitive DNA in the *Pi* genome (74 %) and the high frequency of SNPs. Such data sends us a clear marker that emergence of further virulent

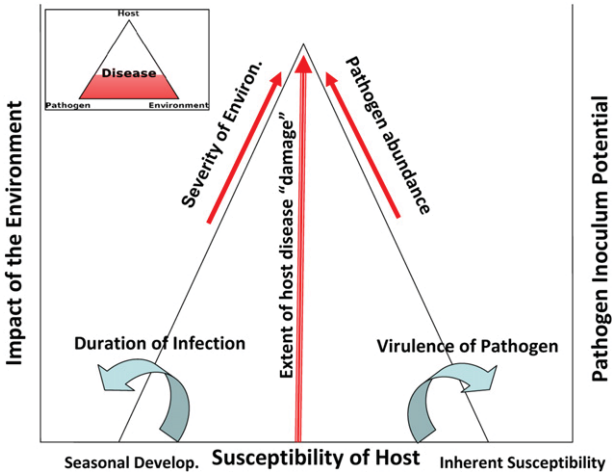

Fig. 1 – The disease triangle elaborated (with basic disease triangle inset), adapted from Scholthof (2007).

isolates (such as the recent naissance of Blue 13) and the emergence of resistance to fungicides, is not only ongoing, but further evolution is imminent. For *Bd* it is well known that the presence of infection does not necessarily signal decline and recent work on *Bd*'s population genomics has shown the existence of both hypo- as well as hypervirulent lineages likely drives aspects of this pattern. This shows that further evolution of the panzootic may occur if lineages are able to outcross, or if they are introduced into naïve host populations and species (Farrer *et al.*, in

Table 2 – Emerging infectious diseases (EISs), as evidenced by the fragile marker of the publication record. The descriptors given in column one were used to trawl the Google scholar data-base, for complete years 2005–2010. The total numbers of articles is recorded and expressed as a percentage published over this 5 y period. Inset in this column is the figure derived from adding the word "epidemiology" to the initial descriptor

Google Scholar *key words*	2005–2010	Total article no.	% Published over past 5 y
Late blight of Potato	3 650	31,500	11.6% 12.7%
Rice blast	20,700	160,000	12.9% 23.0%
Wheat stem rust	6 100	85,600	7.1% 13.8%
White nose fungus bats	2 480	17,900	13.9% 22.3%
Batrachochytrium dendrobatidis	998	2 200	45% 46.3%

Red for animal pathogens.
Green for plant pathogens.

Table 3 – The disease triangle; pathogen life-cycle characteristics of asexual and sexual reproduction (highlighting the missing data for the red pathogens as ?), clonality and genome structure, including estimates of repetitive DNA and Single Nucleotide Polymorphism (SNP) frequencies. Ascomycete (Asco.) *G. destructans* (*Gd*) – www.broadinstitute.org/genome/Geomyces_destructans; Chytridiomycete (Chytrid.) *B. dendrobatidis* (*Bd*) – www.broadinstitute.org/genome/batrachochytrium_dendrobatidis; Ascomycete (Asco.) *M. oryzae* (*Mo*), Dean *et al.*, 2005; Oomycete (Oomyc.) *P. infestans* (*Pi*), Haas *et al.*, 2009: Basidiomycete (Basidio.) *P. graminis* (*Pg*), www.broadinstitute.org/annotation/genome/puccinia

Pathogen	*Gd* Ascomycete	*Bd* Chytridio-mycete	*Mo* Ascomycete	*Pg* Basidio-mycete	*Pi* Oomycete
Asexual *and* Sexual life-cycle Spore "forms"	Yes ? 1 plus arthro-spores plus others?	Yes ? 2? Diploid?	Yes Yes 2	Yes Yes 5	Yes Yes 3 Diploid
Clonal	Yes?	Yes	Yes	Yes	Yes
Genome size (Broad Inst.) gene no.	30.65 Mb 9,075	23.7 Mb 8,794	41.7 Mb 12,841	88.6 Mb 20,567	228.5 Mb 18,179
Repetitive DNA SNP frequency	? ?	? 1 per 1.2 Kb	9.7% 1 per 2.3 Kb	80%? > 1 per Kb	74% 1 per 426 bp

review). While far less is currently known about *Gd*, it has been shown that several bat species in Europe are affected by the pathogen however do not manifest acute clinical symptoms (Puechmaille *et al.*, 2010; Wibbelt *et al.*, 2010). While this may signal the existence of different lineages of *Gd*, the necessary population genetic analyses have yet to be undertaken.

The host

The comparison between red pathogens infecting wild species and green pathogens infecting domesticated crop cultivars is a rather artificial one. Table 4 highlights our more advanced knowledge about the host range of *Mo*, *Pg* and *Pi*, as well as their respective invasion and feeding strategies. It underscores our over-reliance on having bred single dominant race specific resistance genes into modern cultivars. By contrast, we have only recently been able to describe the host range of *Bd* and *Gd*. Strikingly, both species appear to affect a wide range of amphibian and bat species, respectively, showing that broad-host ranges are perhaps the norm across red fungal pathosystems. This contrasts with the green pathogens, where host/pathogen interactions can be specific in the extreme (as, for example, in the biotroph *Pg*). Such an observation suggests that host/pathogen interactions are fundamentally different when comparing between reds and green pathogenic fungi. However, data is still lacking on the exact nature of the infection process for both *Bd* and *Gd* beyond a basic description of the genes differentially regulated during infection (Ribas *et al.*, 2009: Rosenblum *et al.*, 2008), and this area of research will likely reveal novel host/pathogen interactions such as novel classes of effectors and host ligands (Kale *et al.*, 2010; Haldar *et al.*, 2006).

The environment

Table 5 summarises our current state of knowledge with regards to geographic spread of these pathogens, that is by "natural" dispersal or resulting from trade and transport. It highlights the significance of man in the global dissemination of pathogens, with *P. graminis* alone being spread not only by seed but by natural dispersal over large distances as aeciospores (Brown and Hovmoller, 2002). The missing data again concerns *Bd* and *Gd*, where the data for both alternate hosts and the extremes of survival of the two fungi is only just becoming known. However, it is increasingly clear that, for *Bd*, the global trade in amphibians is a fundamental driver of pathogen spread, with multiple introductions owing to human movement of infected hosts, being demonstrated (Walker *et al.*, 2008; Cunningham *et al.*, 2005). Thus for both reds and greens, it appears that anthropogenic dispersal processes underpin the emergence of disease worldwide.

Whilst the basic disease triangle (inset Fig. 1) highlights the missing data, it remains somewhat of a naïve concept. A more sophisticated and realistic model (Fig. 1), adapted from Scholthof (2007) takes into account: i) the pathogen inoculum potential, its virulence status and abundance; ii) the seasonal development of the host, its inherent susceptibility, duration of infection and accounts for the amount of host damage; and iii) the basic environmental parameters, alongside more quantitative data on the relationship between the environment, its impact on disease and vectors of infection. We do not have this complete data-set for any of the aforementioned pathogens and thus accurate modelling of epidemics and disease forecasting, while being a highly desirable aim, is currently impossible.

6. Policy to prevent spread of disease?

Taking into account our inability to predict disease epidemics accurately, do we have adequate data to inform and influence policy to prevent the spread of disease? In an ideal world policy should be based on robust evidence, followed by

Table 4 – The disease triangle: host range, infection strategy and host immune status. Much is known regarding infection and feeding structures formation in the green pathogens and concerning deployment of R genes in crops. The infection strategies of the red pathogens and the immune status of their respective hosts are less clear

	Wild spp.		Domesticated cultivars		
1° host	Bat	Amphibian	Rice	Wheat	Potato
Pathogen	*G. destructans*	*B. dendrobatidis*	*M. oryzae*	*P. graminis*	*P. infestans*
Host range	7 spp. hibernating bats	> 450 amphibian spp.	Rice; *Mg* spp. complex on 50 grass spp.	*Pgt* – 28 spp; *Pg* on 365 cereal grass spp.	Solanaceae
Infection strategy	Superficial? Invasive?	Superficial?	Invasive	Invasive	Invasive
Host immune Status	Suppressed in hibernation	Suppressed by infection ?	Race-specific R (RSR) Ephemeral	RSR ephemeral Temp. sensitive	RSR ephemeral

Table 5 – The disease triangle: the environment, geographic spread (continents) and dispersal of pathogens, reservoirs of infection and pathogen growth and survival parameters. This highlights the missing data with regards to *Gd*. The growth temperatures of the green pathogens reflect differences in night and day temperatures

Pathogen	*G. destructans*	*B. dendro-batidis*	*M. oryzae*	*P. graminis*	*P. infestans*
Geographic spread	US, Canada (EU)	six continents	6	6	6
Long distance dispersal (DD)	No	No	No	Yes '000s km	No
Short DD, via..	Yes contact	Yes contact	Yes 1–5 m	Yes 1–5 m	Yes > 1 m
Trade/Transport	Yes	Yes	Yes	Yes	Yes
Alternate hosts / infection Reservoirs	Soil sapro phyte	Bullfrogs plus tol erant spp	Grasses	Barberry / Mahonia spp.	Solan aceae
T °C - Growth Survival	2 to 14 °C ?	18 to 20 1 to 30	18 to 24 4 to 35	15 to 24 (–10) to 35	8 to 20 (–5) to 28

implementation and improvement based on an iterative evaluation process. The reality is more bleak – policy is often imposed in ignorance of the full facts and without sufficient data gathered to inform improvements. To understand why policy fails here we must realise that we, as scientists, are driven by academic purity, prestige and the need for high impact publications. By contrast, policy makers are driven by the desire for re-election or reappointment, the need to satisfy the public and by various economic or social realities. Take, for example, the 2001 UK disease outbreak of Foot and Mouth Virus. The policy of contiguous pre-emptive culling led to the slaughter of 6,268,769 farm animals (Thompson *et al.*, 2002), at a cost of £3 and £5 billion to the public sector and private sectors, respectively (Bourn, 2002) and an elevated level of psychological morbidity amongst farmers and rural workers (Peck, 2005). This controversial cull policy was recently challenged by new evidence that cattle afflicted with the virus are only infectious for a brief period (Charleston *et al.*, 2011). This knowledge, coupled with the broader use of diagnostic tools which reveal virus infection in the field before clinical signs appear, could have vastly reduced the costs, both human and animal, associated with controlling the epizootic (Charleston *et al.*, 2011).

We illustrate these various points with two particular case studies.

The rice blast fungus, M. oryzae

Rice currently feeds half of the world's population. With the numbers of mouths predicted to rise by 33 % over the next 40 y, and with 86 % of these new peoples clustered in developing countries, rice will gain yet greater significance as an essential prerequisite for a healthy world.

The rice blast fungus is extant in some 85 countries world wide (Kato, 2001) where it causes between 10 and 30 % loss of harvest. Given the vast acres of genetically uniform rice planted, we have somewhat skewed the "arms race" in favour of the emergence of new virulent pathogen isolates and/or emergence of resistance to fungicides by setting the scene for strong directional selection on pathogen virulence. This is well-illustrated by accounting for the inoculum potential of this fungus. With up to 20,000 conidia emanating from a single leaf lesion per night, over a period of 20 nights, multiplied by the number of lesions and individual leaves per rice plant, and taking into account the polycyclic nature of the disease, the count totals up to an estimated 10^{11} spores per acre of rice in a single growing season (Barksdale and Asai, 1961). Given the abundance of transposons within the *M. oryzae* genome, coupled with the SNP frequency (Talbot, N.J., pers. comm.), blast clearly has the capacity to generate the combinatorial mutational background upon which natural selection, aided by huge effective population sizes, will act: we have clearly biased the arms race to jeopardise the longevity of host resistance.

The world rice blast population structure has been determined by seed spread and by our deployment of disease resistant rice cultivars (Tharreau *et al.*, 2009). For example, rice plants carrying the blast resistance gene Pi33 have been widely planted but yet the resistance of these plants has only been assessed against a limited number of blast isolates (Berruyer *et al.*, 2003). This highlights two particular needs i) the urgency of a co-ordinated international effort to assess the virulence status of major blast lineages and to effect robust pathogenicity assays across all rice and ii) greater deployment of broad spectrum R genes as well as a globally co-operative programme to pyramid R genes and to unmask useful QTLs for all agronomic rice cultivars (Skamnioti and Gurr, 2009).

7. Forecasting plagues of rice in tomorrows world

Ideally, plant disease forecasting systems would be based on robust epidemiological models incorporating statistically-weighted parameters described in the more sophisticated disease triangle model (Fig. 1). Notably all environmental factors (and not just meteorological measurements) acting in concert with host resistance status, the virulence of the pathogen, the stochastic effects of severe weather, CO_2, ozone and wind speed. However, the complex mathematical relationship between all environmental conditions and the disease cycle remains unknown and current forecasting systems for *M. oryzae* remain weather-based and somewhat naive. Regression analyses, describing the relationship between disease severity and meteorological conditions, has given us empirical and explanatory simulation models – as, for example, the rice blast epidemiological simulation model (BLASTSIM) Calvero *et al.* (1996) or the model described by Mukherjee *et al.* (2010). A support vector machine-based method has also been developed (Kaundel *et al.*, 2006); also see: www.imtech.res.in/raghava/rbpred/ but it is still based upon an input of meteorological parameters only (minimum and maximum temperatures and relative humidity levels, rainfall and number of rainy days per week). In essence, we must realise the complexity of the data to be gathered and the need for logistic models to inform us of imminent blast epidemics, particularly in the light of extreme weather and with the demographic movement of the pathogen and its predicted host "hops" (Skamnioti and Gurr, 2009).

The amphibian fungus, B. dendrobatidis

The realisation that *Bd* was simultaneously emerging on at least three continents (Australasia, America and Europe), had driven multiple host species extinct and is affecting the healthy functional of multiple ecosystems (Colon-Gaud *et al.*, 2009) has catalysed a wave of research of activity with over 2400 publications since its discovery. Population genetics (James *et al.*, 2009) and genomics (Farrer *et al.*, in review) have shown that a single lineage, currently named *Bd* GPL (*Bd* Global Panzootic Lineage) has evolved hypervirulence and is the driving force underpinning the panzootic. Two genomes of the globally emerging lineage have been sequenced and reveal many clues to virulence of *Bd* GPL. Comparative genomics has shown that fungalysin metallopeptidases, serine proteases and chitin binding module domains are amplified in *Bd* compared to other free living chytrids and are likely involved in virulence (Rosenblum *et al.*, 2008; Joneson *et al.*, in press). Approximately 17 % of *Bd*'s genes

are predicted to be secreted suggesting that the secretome of *Bd* is important in the host/pathogen interaction. A highly expanded group of genes that share some homology with the Crinkler family of secreted proteins found in the *Phytophthora* genus and, while their function is not confirmed, their presence suggests that effectors may play a role in the virulence of *Bd*. Therefore, it is clear that *Bd* contains a sophisticated arsenal of proteins involved in virulence and these likely underpin the severity of the infection once the pathogen attacks naive populations and species.

Bd's virulence has been widely manifested as some of the most dramatic disease-driven declines ever witnessed, leading to an international race to establish *ext situ* captive breeding programs (such as the international zoo amphibian ark project http://www.amphibianark.org/) and efforts to manage the further spread of the pathogen by establishing it as an OIE notifiable infection. However, efforts to proactively wipe out the infection in the wild have met with little success (http://www.nature.com/news/2010/100609) and underscores a crucial point: once an infectious horse has bolted, we may recover the horse but not its pathogen. For instance, escaped non-native North American bullfrogs established *Bd* infected populations in the United Kingdom. While bullfrog populations were summarily eradicated, their legacy of infection was not and *Bd* is now on the road to becoming an endemic infection in British amphibians (Cunningham *et al.*, 2005). From the point of view of containing wildlife diseases, the onus is prevent emergence in the first place. This requires not only a degree of insight into the biogeography of fungal species (thus allowing some attempts for us to predict the infections of tomorrow), but also adoption of a precautionary principle: all species (plant, animal and protist) may present a risk of infection to naive regions and thus need to be treated as "non-biosecure".

It is clear that we need to target control of all fungal pathogens, both red and green. To effect this we need to unmask environmentally benign chemistries, preferably those which target chemistries and structures absent from plant and animal cells (such as the fungal cell wall) and which have preventative, curative and eradicant – (antisporulant) activity. Recent success has been reported by amphibian biologists where the probiotic use of fungicidal bacteria can lessen pathogenicity (Harris *et al.*, 2009). The hunt is on.

8. Disease surveillance

We must establish an international collation for global surveillance of all EIDs. With regards to plant EIDs current FAO mandates are to report pest and pathogens to IPPC (International Plant Protection Convention). However, we lack protocols to standardise testing and impose quarantine status. We must, in particular standardise seed treatment protocols and boost funding for diagnostics. We recommend that disease reports are made by recognised FAO co-ordinators who, in turn are alerted to disease by such recognised authorities as BSPP (British Society for Plant Pathology), EPPO (European and Mediterranean Plant Pathology Organisation) NAPPO (North American Plant Pathology Organisation) and APS (American Phytopathological Society) and that greater use is made of ProMed (http://www.fas.org/promed) in the recording of plant disease.

Biosecurity for notifiable diseases of animals is coordinated by the World Organisation for Animal Health (also known as the OIE) and, while traditionally focused on diseases of veterinary animals, has more recently embraced the 'One Health' model. In essence, One Health recognises that human, animal and environmental health are intrinsically linked and that control of EIDs requires a broad interdisciplinary collaboration between diverse areas of research (epidemiology, molecular biology and genetics, sociobiology) and policy (international strategy and education). In the case of *Bd*, the fungus is now listed as an OIE notifiable pathogen and international trade in infected amphibians is known to be key to the spread of infection (Fisher *et al.*, 2009; Walker *et al.*, 2008). A global mapping project exists to identify infected regions enabling the prioritisation of conservation efforts and ring-fencing uninfected areas (www.bd-maps.net). The amphibian biodiversity hotspot on the island of Madagascar remains uninfected and keeping this status quo remains a key concern. However, even the best-intentioned biosecurity programs remain fallible and chytridiomycosis has emerged on New Zealand, despite the best efforts to protect the archipelago from disease introductions. It is clear that prevention is better than control in the fight against the threat of novel EIDs however, given our global model of free-trade, at what cost does effective quarantine mean to our economies?

9. Pathogens, policy and society

The economic cost, scientific breakthroughs, policy dialogue and sociological consequences of controlling nascent EIDs need to be discussed more widely. We, as scientists, must realise the need not only for high impact publications but of the need to disseminate our findings more widely and in a manner accessible to the general public. We must discourage the use of sensationalistic headlines and raise public awareness to the threat of fungal foes and the realities of control. For instance, would the public accept cessation of the majority of trade in pet and horticultural exotics in order to maintain a healthier ecosystem? We do not yet know the answer to this question. We must inform and influence policy, highlighting, in particular the need for better funding for fungal research and the need for a robust BioSecurity code of practice. It is sobering to think that as fungal biologists our funding to study disease is so very modest, yet the impact of infection is such a prominent player in food security (Skamnioti and Gurr, 2009), wild species extinctions (Fisher *et al.*, 2009) and forest health (Stenlid *et al.*, 2011).

Finally, we ask – do EIDs really represent a "cauldron of curses"? We respond thus, having hugely corrupted the chant of the witches around the cauldron in Macbeth.

> "*Eye of newt, and toe of frog,*
> *Wing of bat, and molded log,*
> *Rusted wheat, and late blight cast,*
> *Lesions long, of rice stem blast,–*
> *For a charm of powerful trouble,*
> *Like a hell-broth boil and bubble.*"
>
> *Apologies to William Shakespeare; in homage to John Taylor (2011) FBR 25 3–13.*

Acknowledgements

Thanks are due to Nick Read for encouraging us to write this article and to Gill Petrokofsky (Oxford) for her advice on "policy". We acknowledge support from BBSRC, NERC and the John Fell Fund (Oxford).

REFERENCES

Alderman, D.J., Holdich, D., Reeve, I., 1999. Signal crayfish as vectors in crayfish plague in Britain. Aquaculture 86, 3–6.

Anderson, P.K., Cunningham, A.A., Patel, N.G., Morales, F.J., Epstein, P.R., Daszak, P., 2004. Emerging infectious diseases of plants: pathogen pollution, climate change and agrotechnology drivers. Trends Evol. Ecol. 19, 535–544.

Anderson, R.M., 1979. Parasite pathogenicity and the depression of host population equilibria. Nature 279, 150–152.

Barksdale, T.H., Asai, G.N., 1961. Diurnal spore release of *Pyricularia oryzae* (*Magnaporthe oryzae*) from rice leaves. Phytopathology 51, 313–317.

Berruyer, R., Adreit, H., Milazzo, J., Gaillard, S., Berger, A., Dioh, W., Lebrun, M.H., Tharreau, D., 2003. Identification and fine mapping of Pi33, the rice resistance gene corresponding to the *Magnaporthe grisea* avirulence gene ACE1. Theor. Appl. Genet. 107, 1139–1147.

Blehert, D.S., Hicks, A.C., Behr, M., Meteyer, C.U., Berlowski-Zier, B.M., Buckles, E.L., Coleman, J.T.H., Darling, S.R., Gargas, A., Niver, R., Okoniewski, J.C., Rudd, R.J., Stone, W.B., 2009. Bat white-nose syndrome: an emerging fungal pathogen? Science 323, 227.

Bourn, J., 2002. National Audit Office Report.

Brown, J.K.M., Hovmoller, M.S., 2002. Aerial dispersal of pathogens on the global and continental scales and its impact on plant disease. Science 297, 537–541.

Butler, G., Rasmussen, M.D., Lin, M.F., Santos, M.A.S., Sakthikumar, S., Munro, C.A., Rheinbay, E., Grabherr, M., Forche, A., Reedy, J.L., Agrafioti, I., Arnaud, M.B., Bates, S., Brown, A.J.P., Brunke, S., Costanzo, M.C., Fitzpatrick, D.A., de Groot, P.W.J., Harris, D., Hoyer, L.L., Hube, B., Klis, F.M., Kodira, C., Lennard, N., Logue, M.E., Martin, R., Neiman, A.M., Quail, E.N.M.A., Quinn, J., Santos, M.C., Schmitzberger, F.F., Sherlock, G., Shah, P., Silverstein, K.A.T., Skrzypek, M.S., Soll, D., Staggs, R., Stansfield, I., Stumpf, M.P.H., Sudbery, P.E., Srikantha, T., Zeng, Q., Berman, J., Berriman, M., Heitman, J., Gow, N.A.R., Lorenz, M.C., Birren, B.W., Kellis, M., Cuomo, C.A., 2009. Evolution of pathogenicity and sexual reproduction in eight Candida genomes. Nature 459, 657–662.

Calvero, S.B., Coakley, S.M., Teng, P.S., 1996. Development of empirical forecasting models for rice blast based on weather factors. Plant Pathol. 45, 667–678.

Charleston, B., Bankowski, B.M., Gubbins, S., Chase-Topping, M.E., Schley, D., Howey, R., Barnett, P.V., Gibson, D., Juleff, N.D., Woolhouse, M.E.J., 2011. Relationship between clinical signs and transmission of an infectious disease and the implications for control. Science 332, 726–729.

Colon-Gaud, C., Whiles, M.R., Kilham, S.S., Lips, K.R., Pringle, C.M., Connelly, S., Peterson, S.D., 2009. Assessing ecological responses to catastrophic amphibian declines: patterns of macroinvertebrate production and food web structure in upland Panamanian streams. Limnol. Oceanogr. 54, 331–343.

Crawford, A.J., Lips, K.R., Bermingham, E., 2010. Epidemic disease decimates amphibian abundance, species diversity, and evolutionary history in the highlands of central Panama. Proc. Nat. Acad. Sci. U.S.A. 107, 13777–13782.

Cunningham, A.A., Daszak, P., 1998. Extinction of a species of land snail due to infection with a microsporidian parasite. Conserv. Biol. 12, 1139–1141.

Cunningham, A.A., Garner, T.W.J., Anguilar-Sanchez, V., Banks, B., Foster, J., Sainsbury, A.W., Perkins, M., Walker, S.F., Hyatt, A.D., Fisher, M.C., 2005. The emergence of amphibian chytridiomycosis in Britain. Vet. Rec. 157, 386–387.

Dean, R.A., Talbot, N.J., Ebbole, D.J., Farman, M.L., Mitchell, T.K., Orbach, M.J., Thon, M., Kulkarni, R., Xu, J.-R., Pan, H., Read, N.D., Lee, Y.-H., Carbone, I., Brown, D., Oh, Y.Y., Donofrie, N., Jeong, J.S., Soanes, D.M., Djonovic, S., Kolomiers, E., Rehmeyer, C., Li, W., Harding, M., Kim, S., Lebrun, M.-H., Bohnert, H., Coughlan, S., Butler, J., Calvo, S., Ma, L.-J., Nicol, R., Purcell, S., Nusbaum, C., Galagan, J.E., Birren, B.W., 2005. The genome sequence of the rice blast fungus *Magnaporthe grisea*. Nature 434, 980–986.

FAO, 2008. FAOSTAT UN FAO statistics database.

Farrer, R.A., Weinert, L.A., Bielby, J., Garner, T.W.J., Balloux, F., Clare, F., Bosch, J., Cunningham, A.A., Weldon, C., du Preez, L.H., Anderson, L., Kosakovsky Pond, S.L., Shahar-Golan, R., Henk, D.A., Fisher, M.C. Multiple emergences of amphibian chytridiomycosis include a globalised hypervirulent lineage. Proc. Nat. Acad. Sci. U.S.A., in review.

Fisher, M.C., Garner, T.W.J., Walker, S.F., 2009. The global emergence of *Batrachochytrium dendrobatidis* and amphibian chytridiomycosis in space, time and host. Annu. Rev. Microbiol. 63, 291–310.

Frick, W.F., Pollock, J.F., Hicks, A.C., Langwig, K.E., Reynolds, D.S., Turner, G.G., Butchkoski, C.M., Kunz, T.H., 2010. An emerging disease causes regional population collapse of a common North American bat species. Science 329, 679–682.

Fry, W., 2008. *Phytophthora infestans*: the plant (and R gene) destroyer. Mol. Plant Pathol. 9, 385–402.

Gargas, A., Trest, M.T., Christensen, M., Volk, T.J., Blehert, D.S., 2009. *Geomyces destructans* sp nov associated with bat white-nose syndrome. Mycotaxon 108, 147–154.

Haas, B.J., Kamoun, S., Zody, M.C., Jiang, R.H.Y., Handsaker, R.E., Canol.M., Grabherr, M., Kodira, C.D., Raffaele, S., Torto-Alalibo, T., Bozkurt, T.O., Ah-Fong, A.M.V., Alvarado, L., Anderson, V.L., Armstrong, M.R., Avrova, A., Baxter, L., Beynon, J., Boevink, P.C., Bollmann, S.R., Bos, J.I.B., Bulone, V., Cai, G., Cakir, C., Carrington, J.C., Chawner, M., Conti, L., Costanzo, S., Ewan, R., Fahlgren, N., Fischbach, M.A., Fugelstad, J., Gilroy, M.E., Gnerre, S., Green, P.J., Grenville-Briggs, L.J., Griffith, J., Grünwald, N.J., Horn, K., Horner, N.R., Hu, C.-H., Huitema, E., Jeong, D.-H., Jones, A.M.E., Jones., J.D.G., Jones, R.W., Karlsson, E.K., Kunjeti, S.G., Lamour, K., Liu, Z., Ma, L., MacLean, D., Chibucos, M.C., McDonald, H., McWalters, J., Meijer, H.J.G., Morgan, W., Morris, P.F., Munro, C.A., O'Neill, K., Ospina-Giraldo, M., Pinzón, A., Pritchard, L., Ramsahoye, B., Ren, Q., Restrepo, S., Roy, S., Sadanandom, A., Savidor, A., Schornack, S., Schwartz, D.C., Schumann, U.D., Schwessinger, B., Seyer, L., Sharpe, T., Silvar, C., Song, J., Studholme, D.J., Sykes, S., Thines, M., Van de Vondervoort, P.J.I., Phuntumart, V., Wawra, S., Weide, R., Win, J., Young, C., Zhou, S., Fry, W., Meyers, B.C., Van West, P., Ristaino, J., Govers, F., Birch, P.R.J., Whisson, S.C., Judelson, H.S., Nusbaum, C., 2009. Genome sequence and analysis of the Irish potato famine pathogen *Phytophthora infestans*. Nature 461, 393–398.

Haldar, K., Kamoun, S., Hiller, N.L., Bhattacharje, S., Van Ooij, C., 2006. Common infection strategies of pathogenic eukaryotes. Nat. Rev. Microbiol. 12, 922–931.

Harris, R.N., Brucker, R.M., Walke, J.B., Becker, M.H., Schwantes, C.R., Flaherty, D.C., Lam, B.A., Woodhams, D.C., Briggs, C.J., Vredenburg, V.T., Minbiole, K.P.C., 2009. Skin microbes on frogs prevent morbidity and mortality caused by a lethal skin fungus. ISME J. 3, 818–824.

Hibbett, D.S., Ohman, A., Glotzer, D., Nuhn, M., Kirk, P.M., Nilsson, R.H., 2011. Progress in molecular and morphological taxon discovery in fungi and options for formal classification of environmental sequences. Fungal Biol. Rev. 25, 38–47.

James, T.Y., Litvintseva, A., Vilgalys, R., Morgan, J.A., Taylor, J.W., Fisher, M.C., Berger, L., Weldon, C., Du Preez, L.H., Longcore, J., 2009. Rapid expansion of an emerging fungal disease into declining and healthy amphibian populations. PLoS Pathog. 5, e1000458.

Joneson, S., Stajich, J.E., Shiu, S.-H., Rosenblum, E.B. Genomic transition to pathogenicity in chytrid fungi. PLoS Pathog. in press.

Kale, S.D., Gu, B., Capelluto, D.G.S., Dou, D., Feldman, E., Rumore, A., Arredondo, F.D., Hanlon, R., Fudal, I., Rouxel, T., Lawrence, C.B., Shan, W., Tyler, B.M., 2010. External lipid PI3P mediates entry of eukaryotic pathogen effectors into plant and animal host cells. Cell 142, 284–295.

Kato, H., 2001. Rice blast disease. Pesticide Outlook 12, 23–25.

Kaundel, R., Kapoor, A.S., Raghava, G.P.S., 2006. Machine learning techniques in disease forecasting: a case study on rice blast prediction. BMC Bioinformatics 7, 485.

Kilpatrick, A.M., Briggs, C.J., Daszak, P., 2010. The ecology and impact of chytridiomycosis, an emerging disease of amphibians. Trends Ecol. Evol. 25, 109–118.

Leonard, K.J., Szabo, L.J., 2005. Pathogen profile: stem rust of small grains and grasses caused by *Puccinia graminis*. Mol. Plant Pathol. 6, 99–111.

Longcore, J.E., Pessier, A.P., Nichols, D.K., 1999. *Batrachochytrium dendrobatidis* gen et sp *nov*, a chytrid pathogenic to amphibians. Mycologia 91, 219–227.

Maillet, F., Poinsot, V., Andre, O., Puech-Pages, V., Haouy, A., Gueunier, M., Cromer, L., Giraudet, D., Formey, D., Niebel, A., Martinez, E.A., Driguez, H., Becard, G., Denarie, 2011. Fungal lipochitooligosaccharide symbiotic signals in arbuscular mycorrhiza. Nature 469, 58–63.

Mukherjee, A.K., Mohapatra, N.K., Nayak, P., 2010. Estimation of area under the disease progress curves in a rice-blast pathosystem from two data points. Eur. J. Plant Pathol. 127, 33–39.

Oerke, E.-C., 2006. Crop losses to pests. J. Agric. Sci. 144, 31–43.

Parniske, M., 2008. Arbuscular mycorrhiza: the mother of plant root endosymbioses. Nat. Rev. Microbiol. 6, 763–775.

Peck, D.F., 2005. Foot and mouth outbreak: lessons for mental health services. Adv. Psychiatr. Treat. 11, 270–276.

Pennisi, E., 2010. Armed and dangerous. Science 327, 804–805.

Puechmaille, S.J., Verdeyroux, P., Fuller, H., Ar Gouilh, M., Bekaert, M., Teeling, E.C., 2010. White-nose syndrome fungus (*Geomyces destructans*) in bat, France. Emerg. Infect. Dis. 16, 290–293.

Royal Society Report, 2009. Reaping the Benefits: Science and the Sustainable Intensification of Global Agriculture. The Royal Society, London.

Ribas, L., Li, M.-S., Doddington, B.J., Robert, J., Seidel, J.A., Kroll, S., Zimmerman, L.B., Grassly, N.C., Garner, T.W.J., Fisher, M.C., 2009. Expression profiling the temperature-dependent amphibian response to infection by *Batrachochytrium dendrobatidis*. PloS One 4, e8408.

Rosenblum, E.B., Stajich, J.E., Maddox, N., Eisen, M.B., 2008. Global gene-expression profiles for life stages of the deadly amphibian pathogen *Batrachochytrium dendrobatidis*. Proc. Nat. Acad. Sci. U.S.A. 105, 17034–17039.

Stenlid, J., Oliva, J., Boberg, J.A., Hopkins, A.J.M., 2011. Emerging diseases in European forest ecosystems and responses in society. Forests 2, 486–504.

Scholthof, K.B., 2007. The disease triangle: pathogens, the environment and society. Nat. Rev. Microbiol. 5, 152–156.

Skamnioti, P., Gurr, S.J., 2009. Against the grain: safeguarding rice from rice blast disease. Trends Biotechnol. 27, 141–150.

Tharreau, D., Fudal, I., Andriantsimialona, D., Santoso, D., Utami, D., Fournier, E., LeBrun, M.-H., Notteghem, J.-L., 2009. World population structure and migration of the rice blast fungus *Magnaporthe oryzae*. In: Wang, G.L., Valent, B. (Eds.), Advances in Genetics, Genomics and Control of Rice Blast Disease. Springer, Dordrecht, pp. 209–215.

Thompson, D., Muriel, P., Russell, D., Osborne, P., Bromley, A., Rowland, M., Creigh-Tyte, S., Brown, C., 2002. Economic costs of the foot and mouth disease outbreak in the United Kingdom in 2001. Rev. Sci. Tech. Off. Int. Epiz. 21, 675–687.

Walker, S.F., Bosch, B., James, T.Y., Litvintseva, A.P., Oliver Valls, J.A., Piña, S., García, G., Abadie Rosa, G., Cunningham, A.A., Hole, S., Griffiths, R., Fisher, M.C., 2008. Invasive pathogens threaten species recovery programs. Curr. Biol. 18, R853–R854.

Wibbelt, G., Kurth, A., Hellmann, D., Weishaar, M., Barlow, A., Veith, M., Prüger, J., Görföl, T., Grosche, L., Bontadina, F., Zöphel, U., Seidl, H.-P., Cryan, P.M., Blehert, S.D., 2010. White-nose syndrome fungus (*Geomyces destructans*) in bats, Europe. Emerg. Infect. Dis. 16, 1237–1242.

Wilson, R.A., Talbot, N.J., 2009. Under pressure: investigating the biology of plant infection by *Magnaporthe oryzae*. Nat. Rev. Microbiol. 7, 185–195.

New Phytologist

Research

Nitric oxide generated by the rice blast fungus *Magnaporthe oryzae* drives plant infection

Marketa Samalova*, Jasper Johnson*, Mary Illes, Steven Kelly, Mark Fricker and Sarah Gurr

Department of Plant Sciences, University of Oxford, South Parks Road, Oxford, OX1 3RB, UK

Author for correspondence:
Sarah Gurr
Tel: +44 1865 275813
Email: sarah.gurr@plants.ox.ac.uk

Received: *20 June 2012*
Accepted: *31 August 2012*

New Phytologist (2013) **197:** 207–222
doi: 10.1111/j.1469-8137.2012.04368.x

Key words: DAR-4M-AM, fluorescent nitric oxide assay, germling development, nitrate and nitrite reductase, nitric oxide synthase-like, NO scavenger, plant–pathogen interaction.

Summary

- Plant-derived nitric oxide (NO) triggers defence, priming the onset of the hypersensitive response and restricting pathogen ingress during incompatibility. However, little is known about the role of pathogen-produced NO during pre-infection development and infection. We sought evidence for NO production by the rice blast fungus during early infection.
- NO production was measured using fluorescence of DAR-4M and the role of NO assessed using NO scavengers. The synthesis of NO was investigated by targeted knockout of genes potentially involved in NO synthesis, including nitric oxide synthase-like genes (*NOL2* and *NOL3*) and nitrate (*NIA1)* and nitrite reductase (*NII1*), generating single and double Δ*nia1*Δ*nii1*, Δ*nia1*Δ*nol3*, and Δ*nol2*Δ*nol3* mutants.
- We demonstrate that *Magnaporthe oryzae* generates NO during germination and in early development. Removal of NO delays germling development and reduces disease lesion numbers. NO is not generated by the candidate proteins tested, nor by other arginine-dependent NO systems, by polyamine oxidase activity or non-enzymatically by low pH. Furthermore, we show that, while *NIA1* and *NII1* are essential for nitrate assimilation, *NIA1*, *NII1*, *NOL2* and *NOL3* are all dispensable for pathogenicity.
- Development of *M. oryzae* and initiation of infection are critically dependent on fungal NO synthesis, but its mode of generation remains obscure.

Introduction

Nitric oxide (NO) is a free radical gas that can diffuse rapidly through biological membranes, allowing it to act as a transient, local, intra- and intercellular signalling molecule (Ignarro *et al.*, 1987; Palmer *et al.*, 1987). In mammals it is a pivotal messenger in the immune, nervous and cardiovascular systems (Anbar, 1995; Grisham *et al.*, 1999; Pfeiffer *et al.*, 1999; Lundberg *et al.*, 2008), while in plants it has been implicated in several processes, including germination and leaf and lateral root development, but has been most extensively studied in abiotic stress responses and plant immunity (Besson-Bard *et al.*, 2008; Wilson *et al.*, 2008; Moreau *et al.*, 2010; Gupta *et al.*, 2011). Indeed, there is considerable evidence that plant-derived NO is important in initiating plant responses to pathogens or elicitors (Delledonne *et al.*, 1998, 2001; Conrath *et al.*, 2004; Van Baarlen *et al.*, 2004; Zeier *et al.*, 2004; Prats *et al.*, 2005; Zaninotto *et al.*, 2006; Floryszak-Wieczorek *et al.*, 2007). Evidence is also emerging that NO is an important regulatory molecule in fungi, including plant pathogens, although there are few papers published, and these are spread over a wide range of different species and developmental stages. Thus, NO influences germination in *Colletotrichum coccodes* (Wang & Higgins, 2005), conidiation in *Coniothyrium minitans* (Gong *et al.*, 2007) and sporangiophore development in *Phycomyces blakesleeanus* (Maier *et al.*, 2001), and affects the formation of the appressorium in the obligate biotrophic powdery mildew fungus *Blumeria graminis* (Prats *et al.*, 2008).

This presents an interesting challenge: fungi may use NO as a signalling molecule to control development, but, concurrently, NO may prime the host plant and activate defence. Interestingly, some degree of cross-talk between plant host and fungal NO signalling systems has been reported in the necrotrophic fungus *Botrytis cinerea* (Turrion-Gomez & Benito, 2011), suggesting the non-cell autonomous activity of NO provides potential for complex interplay in species interactions.

Most data in fungal systems are derived from NO measurements *in vivo* or through exogenous application of mammalian nitric oxide synthase (NOS) inhibitors, NO scavengers or NO donors (Gong *et al.*, 2007; (Conrath *et al.*, 2004; Prats *et al.*, 2008; Turrion-Gomez & Benito, 2011). However, the mechanism of NO synthesis has not yet been described in fungi, and, thus far, it is unclear from analysis of published genomes that sequences homologous to the canonical mammalian nitric oxide synthesis (mNOS) enzymes are present. By analogy with plants, where there is similar controversy regarding the mechanism of NO synthesis, there may be a number of different routes for NO formation, including both oxidative and reductive pathways.

*These authors contributed equally to this work.

The dominant oxidative NO-synthesis pathway in mammals is through oxidation of L-arginine to give NO and citrulline, using NADPH and O_2, by varying isoforms of mNOS, although evidence is also emerging for a reductive pathway from nitrite under low oxygen tensions (Lundberg *et al.*, 2008). Structurally, mNOSs operate as homodimers with an N-terminal oxygenase with binding sites for L-arginine, haem and BH_4 (tetrahydrobiopterin), linked, by a short calmodulin binding hinge that confers calcium sensitivity, to a C-terminal reductase domain with binding sites for flavin adenine dinucleotide (FAD), flavin mononucleotide (FMN) and NADPH, which shows some similarity to cytochrome p450 reductases (Alderton *et al.*, 2001; Gorren & Mayer, 2007).

A similar mammalian-like NOS activity in plants was reported initially, but has not been substantiated, as the original putative NOS candidate, Arabidopsis AtNOA1 (Guo *et al.*, 2003), was subsequently shown to be indirectly associated with NO production, and not directly involved in NO synthesis (Moreau *et al.*, 2008). Indeed, there are no genes in higher plant genomes with significant homology to the canonical mNOS enzymes. Nevertheless, there are several lines of indirect evidence that L-arginine-dependent NO generation can occur in plants, particularly in peroxisomes and plastids, even if it is not generated by mNOS activity (Corpas *et al.*, 2004, 2009; Gas *et al.*, 2009). A key diagnostic feature of these pathways is sensitivity to arginine-substrate analogues, such as L-N^G-nitroarginine methyl ester (L-NAME).

In addition, a range of other oxidative, reductive and non-enzymatic NO-synthesis pathways have been proposed for plants, but with no clear consensus on their relative importance (Moreau *et al.*, 2010; Gupta *et al.*, 2011). For example, other potential oxidative NO-producing systems, in addition to those exploiting L-arginine, may use polyamines (Tun *et al.*, 2006; Wimalasekera *et al.*, 2011) or hydroxylamine (Rumer *et al.*, 2009) as substrates. Meanwhile, the best-characterized reductive pathway involves NO formation from the reduction of nitrite by cytosolic nitrate reductase (Yamasaki *et al.*, 1999; Yamasaki, 2000; Rockel *et al.*, 2002). In particular, analysis of single and double nitrate reductase (NR) mutants in Arabidopsis reveals that nitrate reductase 1 (NIA1) alone is the source of NO during ABA signalling (Bright *et al.*, 2006). Conversely, antisense nitrite reductase (NiR) tobacco (*Nicotiana tabacum*) plants show increased levels of nitrite and consequently increased levels of NO production (Morot-Gaudry-Talarmain *et al.*, 2002). There is also evidence for NO production by a distinct plasma-membrane bound nitrite–NO reductase (NiNOR) activity (Stohr & Stremlau, 2006), the mitochondrial electron transport chain under anoxia (Planchet *et al.*, 2005), or nonenzymatic reduction of nitrite during apoplastic acidification to pH 3–4 which can be enhanced by phenolics (Bethke *et al.*, 2004) or reductants, such as ascorbate or glutathione (Yamasaki, 2000).

The situation in fungi is even more ambiguous than in plants as a consequence of the paucity of papers published to date. On the oxidative side, mNOS or NOS-like sequences have been alluded to in *Aspergillus oryzae* (Gorren & Mayer, 2007), *Aspergillus* spp. and *Glomerella graminicola* (Turrion-Gomez & Benito, 2011). On the reductive side, nitrate reductase and nitrite reductase genes are present in all filamentous fungal genomes analysed thus far, but their potential role in NO synthesis has not, hitherto, been addressed in fungi. The molecular identity of the other potential NO-synthesis pathways in fungi is unknown.

Here, we report evidence for production of NO by germinating conidia and during early development in the hemibiotrophic ascomycete *Magnaporthe oryzae* using fluorescent probes. This fungus is a devastating pathogen of rice (*Oryza sativa*) (Fisher *et al.*, 2012) that attacks through formation of an appressorium, which develops within a few hours of germination at the tip of the germ tube distal from the conidium. The melanized appressorium allows the build-up of sufficient turgor pressure to drive entry into the host via a penetration peg (Bourett & Howard, 1990; Wilson & Talbot, 2009). This elaborate process is triggered by perception of host-derived cues, including a hard, hydrophobic surface, cutin monomers and low levels of nutrients (Ebbole, 2007; Skamnioti & Gurr, 2009; Wilson & Talbot, 2009), and is co-ordinated with cell-cycle progression and programmed cell death of cells in the conidium and germ tube (Veneault-Fourrey *et al.*, 2006). The early stages of infection-related development, including formation of melanized appressoria, can be initiated on artificial hard hydrophobic surfaces, greatly facilitating chemical and genetic dissection of signal cascades involved in germling differentiation (Wilson & Talbot, 2009).

We demonstrate a regulatory role for NO during germination and appressorium formation, using DAR-4M fluorescence measurements and NO scavengers. Notably, NO scavengers delayed germination and early development on artificial surfaces and dramatically reduced lesion formation on barley (*Hordeum vulgare*). We tested likely NO-generating enzymes, by creating knockout strains of candidate genes. We revealed that neither nitrate nor nitrite reductase is responsible for NO generation, and that both are dispensable for pathogenicity on rice and barley. Likewise, knockout of candidate members of the most closely related mNOS-like gene family does not affect NO production or produce an obvious defect in pathogenicity. We show that NO is not produced by other arginine-dependent systems or polyamine oxidases in *M. oryzae*. We conclude that nitric oxide is a critical signalling molecule in early development and has a major impact on plant–pathogen interactions, but its mode of synthesis is unresolved.

Materials and Methods

Fungal strains and growth conditions

Wild-type rice-pathogenic *Magnaporthe oryzae* (*M. grisea* (T.T. Herbert) M.E. Barr) strain Guy11 and NHEJ Δ*ku70* and mutant strains were cultured at 24°C, 14 h : 10 h, light: dark cycle. Strain maintenance and medium composition were as described by Talbot *et al.* (1993).

Growth and biomass assays

Plate growth assays assessed radial colony growth on complete medium (CM) or minimal medium (MM in the presence/absence of 300 mM potassium chlorate), inoculated with 20 µl of

2.5×10^5 conidia ml^{-1} harvested from 10-d-old cultures and incubated at 24°C for 10–14 d.

Fungal biomass was determined using 20 µl of inoculum (as above) in 20 ml of MM, dark-incubated at 24°C, and shaken at 150 rpm for 14 d. The cultures were filtered onto pre-dried, weighed glass microfibre papers (Whatman), oven-dried at 80°C and weighed. There was a minimum of three biological replicates per experiment, and two-tailed pairwise Student's *t*-test was used to assess the statistical significance of differences in growth.

Mutant strain generation

Guy11 and Δ*ku70* strains were used in DNA-mediated protoplast transformation (Talbot *et al.*, 1993). Putative transformants were selected on MM supplemented with 300 µg ml^{-1} hygromycin B (Calbiochem, Merck, Darmstadt, Germany) or defined complex medium (DCM) with 60 µg ml^{-1} Bialophos (Goldbio, St Louis, MO, USA), and subjected to PCR to confirm the presence of the antibiotic resistance marker, its correct site of integration, and native gene replacement and to Southern blot analysis (in Supporting Information Methods S1, S2) to confirm single targeted gene replacement (Fig. S5). PCR primers used to generate mutant strains are detailed in Table S2. Standard techniques (Ausubel *et al.*, 1999) were used to prepare constructs; details of the generation of single Δ*nia1*, Δ*nii1*, Δ*nol2*, Δ*nol3* and double Δ*nia1*Δ*nii1*, Δ*nol2*Δ*nol3*, Δ*nia1*Δ*nol3* strains are given in Methods S1.

Quantitative real-time RT-PCR transcript profiling

RNA was extracted from Guy11 harvested at 0, 0.5, 1, 2, 5, and 12 hours post inoculation (hpi) from detached barley epidermal peels (Skamnioti & Gurr, 2007). First-strand cDNA was synthesized from total RNA using the RETROscript First Strand kit (Ambion, Applied Biosystems, Paisley, UK). RT-PCR was performed on cDNAs, with primers summarized in Table S3, for nitric oxide synthase-like 1 (*NOL1*) (P24 and P25), *NOL2* (P26 and P27), *NOL3* (P28 and P29) and *NOL4* (P30 and P31). The transcript abundance of *NOL* genes, relative to constitutively expressed normalizer genes, *β-tubulin* (MGG_00604, P32 and P33) or *ElongationFactor-1α* (MGG_03641, P34 and P35), was quantified, using the Pfaffl method (Pfaffl, 2001), taking account of primer efficiencies, and calibrated to expression at 1 hpi.

Real-time quantification was performed in MicroAmp Optical 96-Well Reaction Plates using the 7300 Real-Time PCR System (Applied Biosystems). PCR conditions were: 50°C for 2 min, one cycle; 95°C for 10 min, one cycle; 15 s at 95°C, followed by 1 min at 60°C, 40 cycles. Reactions with no cDNA monitored for the presence of primer dimers and no reverse transcriptase controls were included for each cDNA sample. PCRs were carried out in triplicate and mean values determined.

Confocal microscopy

Spores of Guy11 (50 µl; 2.5×10^5 ml^{-1}) were inoculated onto hydrophobic glass slides and germinated in the presence of 2 µM DAR-4M-AM. Samples were viewed using the C-Apochromat × 40/1.2 water immersion lens of a Zeiss LSM 510 Meta microscope, with excitation at 543 nm from a HeNe laser attenuated to 6 µW at the objective, and emission at 590 ± 25nm. Simultaneous non-confocal transmission 4-D (*x,y,z,t*) images were collected with a pixel spacing of 0.23 µm × 0.23 µm × 3 µm as *z*-stacks of 9–12 optical sections, repeated at 60 s intervals, for up to 120 time-points. Images were smoothed with a 3 × 3 × 3 kernel and displayed as maximum projections along the *z*-axis over time for fluorescence signals and minimum projections for the simultaneous (nonconfocal) transmission images. Images were analysed using a custom software suite written in MatLab (The Mathworks, Natick, MA, USA), available from MF.

Fluorescent plate reader assay

NO production was measured using the NO-sensitive fluorescent dyes DAR-4M (non-cell permeable) and DAR-4M-AM (cell permeable) in a FLUOstar Galaxy (BMG Labtech, Aylesbury, UK) fluorescence plate reader using NUNC 96-well optical bottom plates (Thermo Fisher Scientific, Langenselbold, Germany).

Conidia were harvested from 10-d cultures, washed via centrifugation and re-suspended in demineralized water three times (to remove extracellular esterases). 1 mM DAR-4M (AM) stock in dimethyl sulphoxide (DMSO) were diluted to 2 µM DAR-4M (AM) in 10 mM HEPES, pH 7, on ice. Suspensions were dark-incubated for 30 min at room temperature to allow dye loading, washed twice and re-suspended in 10 mM HEPES, pH 7, and the spore concentration was adjusted to 2.5×10^5 spores ml^{-1}. Two hundred microlitres of conidia suspension was inoculated into each well and fluorescence (λ_{ex} = 544 nm; λ_{em} = 590 nm) was recorded for 12–16 h at 20°C, unless otherwise stated. Each experiment contained a minimum of three biological replicates and was replicated independently on at least three separate occasions. 4,4,5,5-Tetramethylimidazoline -l-oxyl3-oxide (PTIO) or carboxy-PTIO (cPTIO) was added, as described in the figure legends. A significant instantaneous drop in fluorescence was observed with increasing concentrations of PTIO, caused by an absorption or quenching effect of PTIO on the DAR-4M triazole (DAR-4M-T) fluorescence signal (Fig. S1a). The quench magnitude was estimated from the instantaneous drop at the start of each experiment, or by adding PTIO at the end of the time-course (Fig. S1b). The concentration-dependent quench response was fitted with a mono-exponential curve (Fig. S1c), inverted and used as a concentration-dependent PTIO correction factor.

Pathogenicity and infection-related morphogenesis assays

Germling and appressorium development was assessed at 1, 2, 4, 8 and 16 hpi by following differentiation on hydrophobic glass cover-slips (Gerhard Menzel, Glasbearbeitungswerk GmbH & Co., Braunschweig, Germany). One hundred and twenty germlings were counted in three independent experiments.

Cuticle penetration was assessed by scoring the frequency with which appressoria formed penetration pegs and intracellular infection hyphae on onion epidermis, after incubation at 24 hpi

at 24°C. One hundred germlings were counted in three independent experiments.

Detached leaf and whole-plant barley (*Hordeum vulgare* L.) and rice (*Oryza sativa* L.) leaf infection assays are detailed in Methods S3. To test the effect of NO scavenger PTIO on host lesion development, 2.5×10^5 spores ml^{-1} were re-suspended in 0, 250 or 500 μM PTIO, with the addition of 0.2% (w/v) gelatine, and spray-inoculated onto cut barley leaves.

Iterative hidden Markov model searches

Iterative hidden Markov model searches were performed in the search for NOL sequences (Kelly, 2011). The protein family (PFAM) (Finn *et al.*, 2010) seed domain for nitric oxide synthase (PF02898) was converted to a hidden Markov model (HMM) and used to search 937 fully sequenced genomes (Table S1), using the HMMER program (Eddy, 1998). The hits were filtered based on an e-value threshold of 1×10^{-10} and aligned using MAFFT (Katoh *et al.*, 2005). Columns that contained > 50% gaps were removed to prevent species-specific or clade-specific amino acid insertions biasing the models (Collingridge & Kelly, 2012). The gap-parsed alignments were re-parsed for > 95% identity to other sequence within the alignment, to prevent biasing of HMM towards any particular group of organisms, which may be overrepresented as a result of the presence of paralogues or uneven taxon sampling. The gap- and identity-parsed alignment was used to generate the HMM for the next search, being terminated when no further hits passing the *e*-value threshold were identified. The final sets were clustered on the basis of all pairwise BLAST similarity scores using DENDROBLAST (S. Kelly & P. K. Maini, unpublished). Hidden Markov model searches were performed using either *M. oryzae* nitrate reductase (MGG_06062) or nitrite reductase (MGG_00634) sequences and aligned as described.

Phylogenetic tree inference

Sequences were aligned using MERGEALIGN-91 (Collingridge & Kelly, 2012) and trees constructed using a 100 bootstrap maximum likelihood, inferred with RAXML (Stamatakis, 2006), employing the LG model of sequence evolution (Le & Gascuel, 2008) and CAT rate heterogeneity (fixed number of rate categories). Fifty per cent majority-rule consensus trees were calculated from the 100 bootstrap replicates using the python module dendropy (Sukumaran & Holder, 2010).

Results and Discussion

NO is produced during germling development in *M. oryzae*

A number of different techniques are available to monitor NO production (Wardman, 2007; Vandelle & Delledonne, 2008; Nagano, 2009; Mur *et al.*, 2011), although measurements are challenging as NO is active at low concentrations, has a high diffusion coefficient, and exists transiently in the cell environment before it reacts to give NO_2, N_2O_3, N_2O_4, N_2O, HNO, peroxynitrite or GSNO (Brown *et al.*, 2009; Baudouin, 2011). We chose to use *in vivo* fluorescent assays to measure intracellular synthesis rates in *M. oryzae* as these are highly sensitive to NO and can be imaged at the cellular level. A range of fluorescent probes developed by Nagano and co-workers react with N_2O_3, an auto-oxidation product of NO, to give a fluorescent triazole product (Kojima *et al.*, 1998, 1999, 2001). Of the commercially available probes, DAR-4M is reported to have greater specificity for NO, improved photostability, reduced pH sensitivity, and lower cytotoxicity in comparison to the earlier fluorescein-based probes (Kojima *et al.*, 2001; Lacza *et al.*, 2005, 2006), and was selected for use in *M. oryzae*.

Conidia were left to germinate on a hydrophobic coverslip for 0.5 h post inoculation to ensure that they were adherent, loaded with DAR-4M as the membrane-permeant acetoxymethyl (AM) ester derivative, and imaged using 4-D (*x,y,z,t*) confocal microscopy at different stages of development (Fig. 1a–f). Fluorescent DAR-4M-T increased steadily over 2 hpi during germination of the apical cell, but reached a peak and then declined in the mid and basal cell (Fig. 1c,e). Furthermore, if the DAR-4M-AM loading solution was replaced by perfusion, there was a relatively rapid partial loss of signal over 5 min from cells and background, and the subsequent rate of fluorescence increase was reduced (Fig. 1c,e). At later stages of development, during appressorium formation (Fig. 1b), signal loss was also observed from the apical cell cytoplasm, which was matched, to some degree, by increased labelling in the cell walls (Fig. 1d,f). Perfusion also reduced the signal from all three cells and the cell wall (Fig. 1 d,f). We infer that either the DAR-4M-T is sufficiently membrane-permeant to diffuse out of the cells, or that it is actively transported by an unknown plasma-membrane xenobiotic detoxification system in *M. oryzae*. The overall increase in fluorescence is consistent with NO production in developing conidia of *M. oryzae*. It is, however,

Fig. 1 Measurement of NO production during germination of *Magnaporthe oryzae* using DAR-4M. 4-D (*x,y,z,t*) confocal imaging revealed an increase in cytoplasmic fluorescence in DAR-4M-AM loaded spores (sp) during germination (a, c) and appressorium formation (b, d). Selected images are shown in hours post-inoculation (hpi) from a time-series collected at 2-min intervals. bc, basal cell; mc, medial cell; ac, apical cell; gt, germ tube; ap, appressorium. Bar, 10 μm. (e) Fluorescence intensity of conidium cells increased, notably in the apical cell, and showed some transfer to the wall (f), particularly during appressorium formation, with consequential clearing of the cytoplasm (d, f). Washout of the loading medium produced a rapid decrease in signal from germlings and medium (c–f). Error bars in (e) and (f) are derived, respectively, from an average over five and nine tracked cells/germlings. (g) Spores germinated in 96-well plates showing *c*. 60% formed appressoria. Bar, 20 μm. (h) Triple-washed spores were loaded with DAR-4M-AM in 10 mM HEPES, pH 7.0, for 30 min, washed with buffer and germinated in 96-well plates. Loaded spores showed a slight transient stimulation in fluorescence over the first 120 min, followed by an almost linear increase when compared with controls without dye added. (i) A reduction of *c*. 30% of the average DAR-4M fluorescent signal was found, after subtraction of the control, after 16 h of incubation. The diamond symbols indicate mean and SD of 21 replicate traces at selected time-points. (j) Addition of 100 μM of the NO donor detanonoate at the end of the experiment produced a substantial increase in fluorescence, demonstrating that there was still excess unreacted dye present.

challenging to make quantitative measurements of NO production as the dynamics of fluorophore localization are more complex.

To allow high-throughput measurements with multiple treatment conditions over an extended time-course, the DAR-4M fluorescence assay was adapted to a 96-well plate format. Conidia were competent to germinate in optical-bottom well plates and the majority (*c.* 60%) formed melanized appressoria (Fig. 1g), although the germ tubes were typically slightly longer than those grown on inductive glass coverslips (compare Fig. 1g with Fig. 1b). None of the commercially available 96-well plates

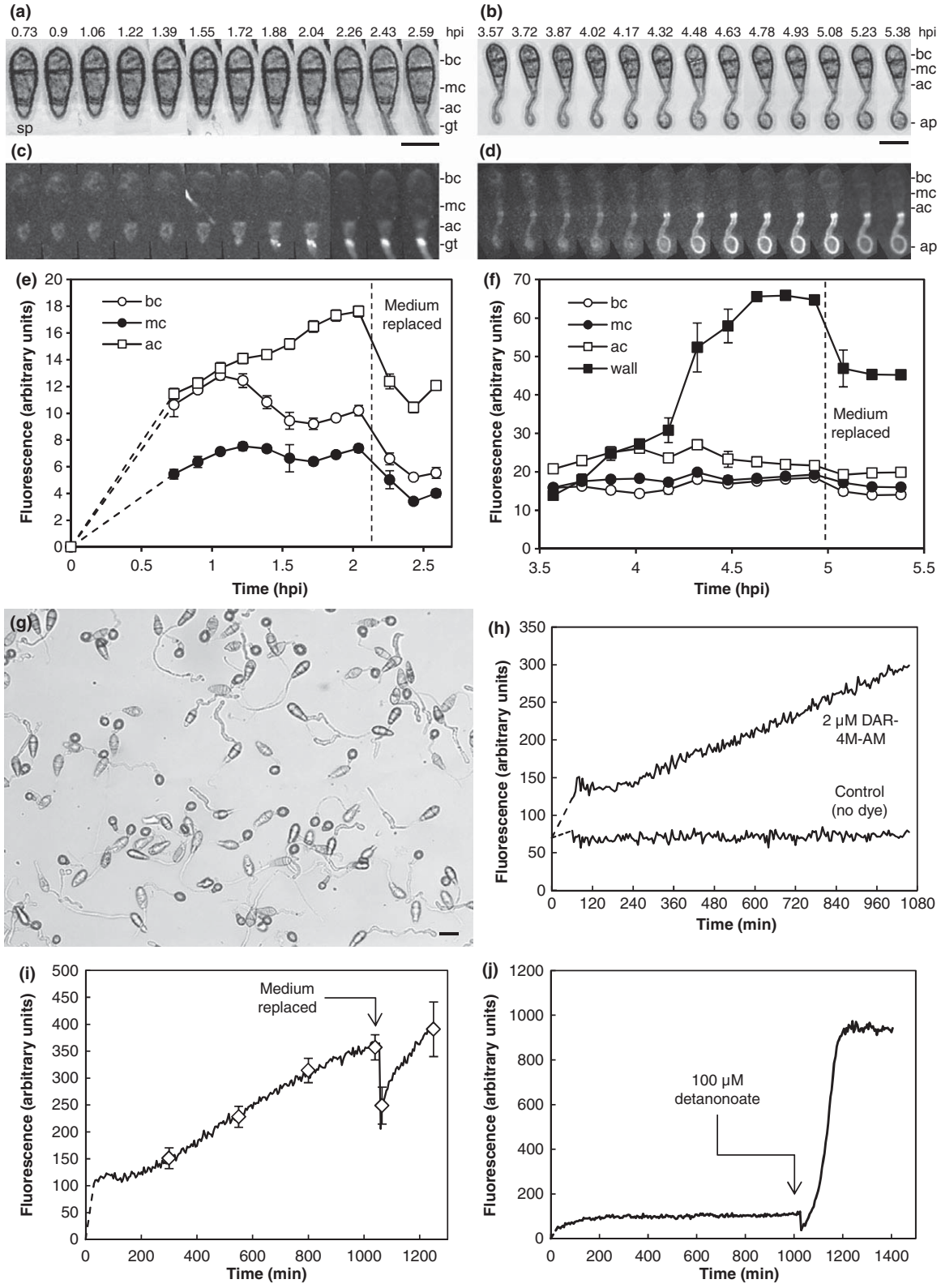

screened were fully inductive for *M. oryzae*; nevertheless, sufficient germlings progressed through to the appressorial stage to allow measurements of NO formation during early development. The first measurement, taken 30–60 min after the start of loading with DAR-4M-AM, reflected the time required to wash out excess DAR-4M-AM and set up the plate. The fluorescence showed a small initial peak, then a plateau relative to the control without dye, over the first 180 min, then increased almost linearly for the next 16 h (Fig. 1h).

The transient response observed in the first few hours is somewhat unexpected, as formation of triazole is irreversible, so the fluorescence signal should only increase (or remain constant) over time, rather than decrease. However, consistent with the observation of a decrease in signal following perfusion in the confocal imaging, we hypothesized that the fluorescent product might be released from the conidia into the medium where the detection efficiency for dye was lower compared with that in the germling adhered to the base of the well. External release of the triazole was confirmed in the plate reader system, as replacement of the buffer caused a *c.* 30% decrease in fluorescence (Fig. 1i). We confirmed that there was still an excess of active dye present in the germlings at the end of the experiment through the addition of the NO donor detanonoate ((Z)-1-[2-(2-Aminoethyl)-N-(2-ammonioethyl)amino]diazen-1-ium-1,2-diolate, 3,3-Bis(aminoethyl)-1-hydroxy-2-oxo-1-triazene, 2,2′-(Hydroxynitrosohydrazino)bisethanamine) at 16 h (Fig. 1j).

NO scavengers have a complex effect on fluorescent NO measurements

The increase in fluorescence is consistent with the production of NO during germination and early development in *M. oryzae*. However, DAR-4M and other diamine probes can react with other molecules, such as dehydroascorbate (Nagata *et al.*, 1999; Zhang *et al.*, 2002; Ye *et al.*, 2008), so increased fluorescence cannot be unequivocally attributed to NO production without additional supporting evidence. We therefore used the NO scavengers PTIO and cPTIO (Akaike *et al.*, 1993) to deplete levels of NO by oxidizing it to NO_2 (Eqn 1). PTIO is more lipophilic than cPTIO and might be expected to permeate the plasma membrane more readily, while cPTIO is regarded as being more reactive (Akaike *et al.*, 1993; Nakatsubo *et al.*, 1998). At low scavenger concentrations, the rate of NO_2 formation by (c)PTIO does not immediately consume all available NO, leading to a situation where both NO and NO_2 are present at comparable concentrations and are able to react to form N_2O_3 (Eqn 2). As N_2O_3 is the substrate for the diamine probes (Eqn 3), this gives a characteristic stimulation of triazole fluorescence at low PTIO concentrations (Nakatsubo *et al.*, 1998; Vitecek *et al.*, 2008; Mur *et al.*, 2011). At higher PTIO concentrations, all NO is rapidly converted to NO_2 and the decrease in fluorescence expected for an NO scavenger is observed.

$$PTIO + {}^{\bullet}NO \rightarrow PTI + {}^{\bullet}NO_2 \qquad \text{Eqn 1}$$

$$ {}^{\bullet}NO_2 + {}^{\bullet}NO \rightarrow N_2O_3 \qquad \text{Eqn 2}$$

$$DAR\text{-}4M + N_2O_3 \rightarrow DAR\text{-}4M\text{-}T + HNO_2 + H_2O \qquad \text{Eqn 3}$$

When conidia loaded with DAR-4M-AM were exposed to increasing concentrations of (c)PTIO, increases in fluorescence were observed with a maximum around 5 μM for PTIO (Fig. 2a) or cPTIO (Fig. 2b), consistent with Eqns (1)–(3). Higher (c)PTIO concentrations caused a decrease in fluorescence (Fig. 2a,b) once the data were corrected for absorption or quenching on the DAR-4M-T fluorescence signal (see Materials and Methods; Fig. S1). The varying impact of PTIO was summarized by integrating the area of the curve between the control in the absence of PTIO and increasing concentrations of PTIO over the first 8 h. PTIO and cPTIO gave *c.* 60% and 30% stimulation at 5 μM compared with controls, and *c.* 60% inhibition at 250 μM. There was a component of the increase in fluorescence that was not inhibited by PTIO, even at high concentrations, which may therefore be attributable to reaction with other molecules, such as the fungal antioxidant erythroascorbate (e.g. Georgiou & Petropoulou, 2001; Baroja-Mazo *et al.*, 2005), leading to a fluorescence product (Zhang *et al.*, 2002). The difference between the maximum fluorescence observed and the inhibition with 250 μM PTIO was regarded as the PTIO-sensitive component of the fluorescence signal that is most likely to be specific for NO. This PTIO-sensitive component rose to a peak around 1 hpi that was maintained for *c.* 4 h before declining towards the baseline (Fig. 2d).

To determine whether NO produced within the cells was detectable externally, we repeated the PTIO titration in the presence of cell-impermeant fluorophore DAR-4M (Fig. 2e). A small stimulation of fluorescence was observed at PTIO concentrations up to 5–10 μM over the first 3–4 h in the quench-corrected data, while higher concentrations gave the expected reduction in fluorescence. The overall response tended towards a plateau at 6h in the absence of PTIO (Fig. 2e), whereas signal from DAR-4M released internally from hydrolysis of DAR-4M-AM continued to show an increase throughout the time series (Fig. 2a,b). The absolute magnitude of the fluorescent signal from external DAR-4M was 3–4-fold higher than that observed for internal DAR-4M (compare Fig. 2a, b with Fig. 2e). The external PTIO-sensitive component increased more slowly, reaching a peak at around 5 hpi before declining (Fig. 2f).

The most parsimonious explanation for the distinctive fluorescence profiles observed in response to PTIO would be by stimulation of N_2O_3 production, as predicted, at low concentrations of PTIO, when stoichiometric amounts of NO_2 are likely to be produced, followed by inhibition at higher PTIO concentrations. Taken together, these measurements can be used as a diagnostic indicator for NO production, rather than reaction with other biomolecules, as the PTIO-sensitive component is most likely to be specific for NO. We infer, therefore, that germinating spores produce NO. We found a stronger stimulation response and at lower concentrations with PTIO compared with cPTIO. As the former is more hydrophobic, this would be consistent with an internal source of NO. However, the absolute magnitude of the fluorescence signal is greater in the presence of a cell-impermeant form of the dye, suggesting that considerable amounts of NO either diffuse out of the germling or

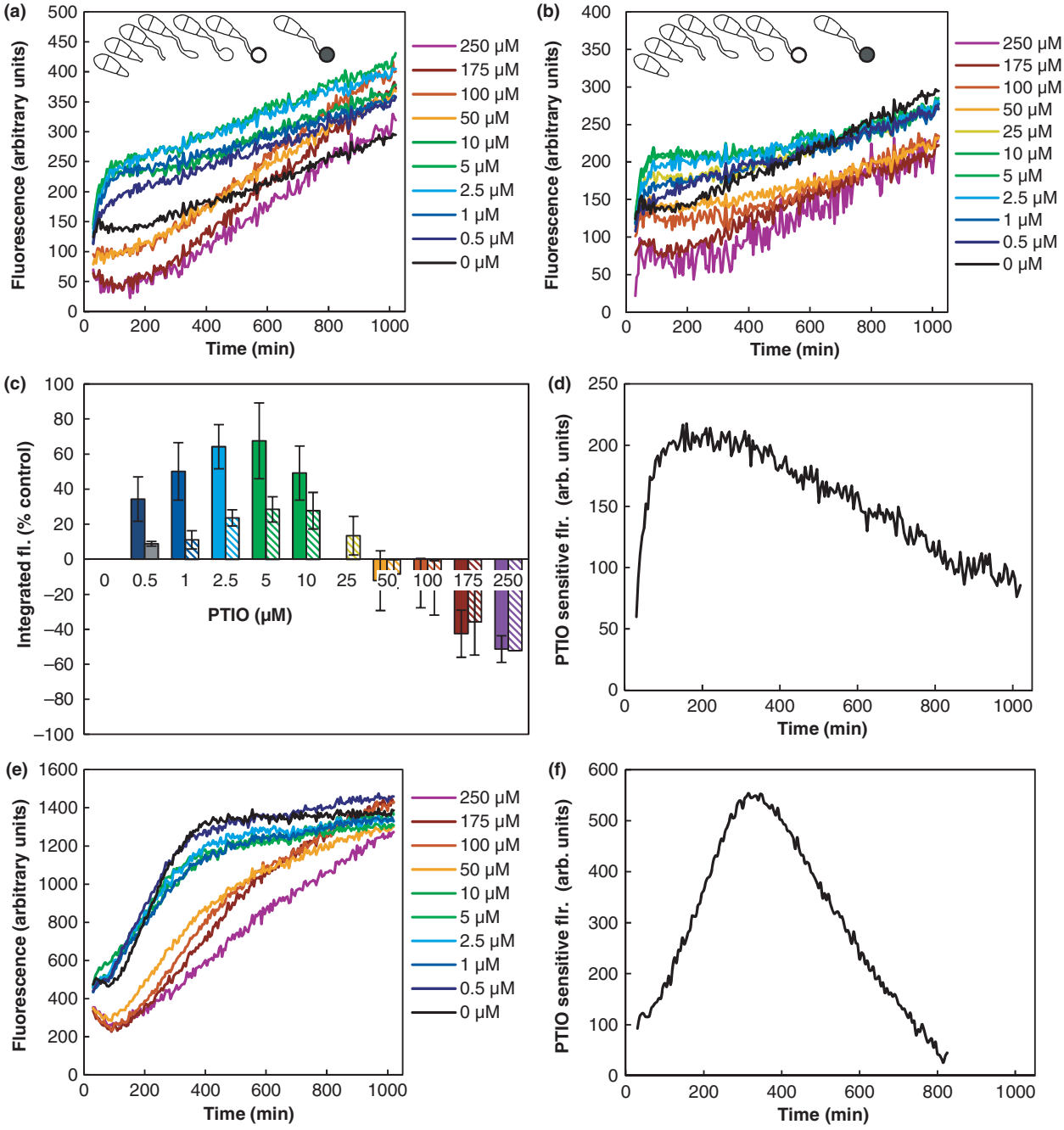

Fig. 2 Effect of NO scavengers on DAR-4M fluorescence profiles during development of *Magnaporthe oryzae*. Spores loaded with DAR-4M-AM were allowed to germinate in the presence of increasing concentrations of the NO scavenger PTIO (a) or cPTIO (b). Inset cartoons depict the stages of germling morphogenesis. At low PTIO concentrations there was a stimulation in fluorescence above the control with no PTIO added, while at PTIO concentrations above 10 µM, there was a decrease in the rate of fluorescence increase. Data have been corrected for concentration-dependent quenching by PTIO. (c) The difference in the integrated fluorescence (fl.) over the first 8 h compared with the absence of PTIO (solid) or cPTIO (dashed) confirmed the stimulation of fluorescence at low (c) PTIO concentrations, followed by an inhibition at concentrations above 50 µM. Results are shown as mean ± SEM ($n = 4$) expressed as a percentage of the control signal. (d) The PTIO-dependent fluorescence was determined from the difference between the maximum stimulation and maximum inhibition as the most reliable indicator of NO-dependent signal. (e) Response of the cell-impermeant DAR-4M to increasing concentrations of PTIO also showed a slight stimulation at low PTIO concentrations followed by inhibition at higher concentrations. In addition, the overall level of fluorescence tended towards a plateau value after 6–8 h. The PTIO-sensitive component showed a peak around 5 hpi (f).

are synthesized externally. Interestingly, intracellular NO detection continues to increase during development, while external detection tends to plateau around the time at which melanized appressoria appear.

NO scavengers delay early development in *M. oryzae*

To investigate the significance of NO production by *M. oryzae* during early development, we quantified the impact of the NO

New Phytologist

scavenger PTIO on germination, germ tube elongation and appressorium formation on a surface inductive to formation of fully melanized appressoria in wild-type *M. oryzae*. Typically, *c.* 60% of untreated spores germinated by 1 hpi, and nearly 100% by 2 hpi (Fig. 3a). Under normal conditions, germ tube elongation proceeded rapidly over the next 2–3 h, with *c.* 50% of germlings starting to form appressoria within 4 hpi, which became fully melanized by 8 hpi (Fig. 3a). The addition of 10 μM PTIO was sufficient to cause a 60% reduction in germ tube emergence at 1 hpi, but by 4 hpi, the developmental profile of these germlings had almost recovered to the control, untreated levels. Increasing concentrations of PTIO caused longer delays in germination and slowed progression through the developmental pathway. Thus, while 95% of spores had germinated at 8 hpi in the presence of 200 μM PTIO, only 10% had formed melanized appressoria (Fig. 3a). If the primary mode of action of PTIO is to deplete NO, we infer that endogenous NO is required as part of the normal developmental sequence, possibly to initiate germination in contact with an inductive surface and/or to co-ordinate subsequent development between the different germling cell types.

Depletion of NO produced by *M. oryzae* abolishes pathogenicity on barley

We asked whether the delay in germination and development observed with NO scavengers on an artificial surfaces was manifest *in vivo* during *M. oryzae* infection of a susceptible host and would reduce the level of infection in this compatible plant–pathogen interaction. Spores were sprayed onto barley leaves in the presence and absence of 250 and 500 μM PTIO, and the number of lesions scored after 5 d. There was a significant reduction in the number of lesions in the presence of PTIO (Fig. 3b,c), so providing evidence that pathogen-derived NO plays an important role in the infection process and is required for successful host colonization. By contrast, the literature has focussed largely on the impact of PTIO in plant-derived NO signalling during incompatibility in other plant–pathogen interactions. Plant-derived NO production is known to

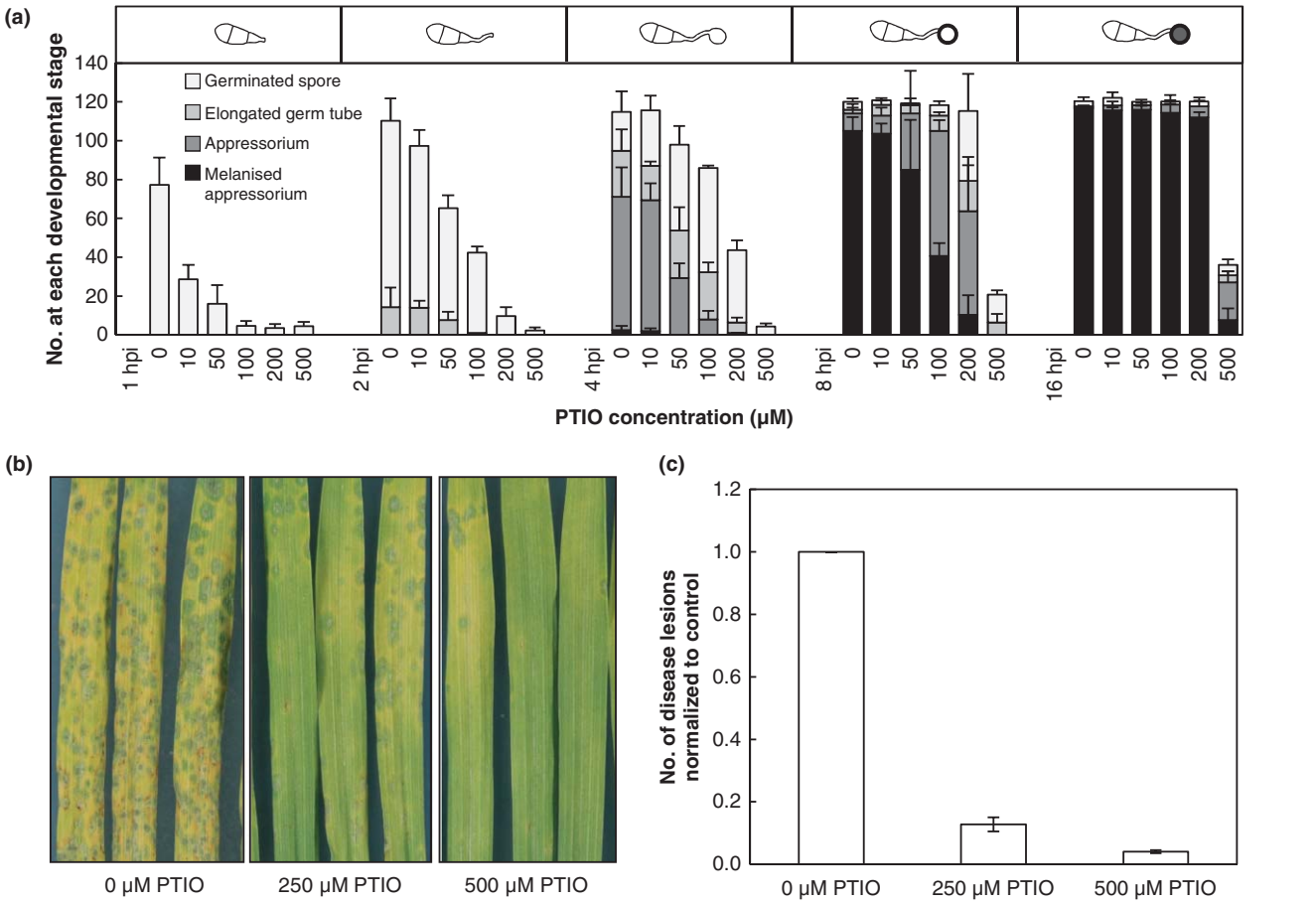

Fig. 3 Effect of the NO scavenger PTIO on *Magnaporthe oryzae* infection-related development and host lesion development. (a) Wild-type (WT) Guy11 germling morphologies at 1, 2, 4, 8 and 16 h post infection (hpi) on hydrophobic surface inductive to melanized appressorium formation in WT strain, following exposure to various concentrations of PTIO in 10 mM HEPES, pH7 (with inset cartoons depicting stages of germling morphogenesis). Bar charts show the number of germlings counted (of 120 counted in three independent experiments) at various stages of differentiation (germinated spore; elongated germ tube; appressorium formation; melanized appressorium formation) on exposure to 10, 50, 100, 200 or 500 μm PTIO. Error bars are SD. (b) Barley (*Hordeum vulgare*) cultivar Golden Promise leaves were spray-inoculated with Guy11 conidial suspensions (2.5×10^5 spores ml^{-1}) re-suspended in 0, 250 or 500 μM PTIO and incubated for 5 d for development of blast lesions. (c) The number of disease lesions was counted, for each treatment, and normalized to the control 0 μM PTIO. Results are shown as mean ± SEM ($n = 3$).

stimulate plant defence reactions during the hypersensitive response (HR) and race-specific resistance (Hong *et al.*, 2008). For example, PTIO scavenging of plant-derived NO led to increased penetration frequencies by the biotroph *Blumeria graminis* and to a reduced host response on a barley isoline manifesting HR (Prats *et al.*, 2005). Thus, production of fungal NO in the context of a compatible interaction would seem counterintuitive, as NO might be expected to prime host defence. Nevertheless, Prats *et al.* (2008) demonstrated a pivotal role for a transient burst of NO in appressorium maturation in *B. graminis*, that is, during pathogen development before host penetration, but probably at a stage that is too early to prime defence. This interplay between a biotrophic pathogen, showing extreme host specificity, differs markedly from the exchange between the necrotroph *Botrytis cinerea* and its broad range of hosts, where HR plays a critical role in fungal infection (Govrin & Levine, 2000). Here, NO facilitates fungal infection, but is also required for plant defence. Indeed, Floryszak-Wieczorek *et al.* (2007) recorded a strong and immediate host NO burst by a resistant plant cultivar upon challenge with *B. cinerea*, but a weak and slower burst in a susceptible cultivar upon infection. Clearly, the role of plant-derived NO is complex and varies with host response, while the role of pathogen-derived NO is important to infection-related development.

Genetic approaches to characterizing the mechanism of NO production in *M. oryzae*

A number of different pathways have been invoked for NO production in animals and plants, including NOS (Gorren & Mayer, 2007), NOS-like enzymes (Corpas *et al.*, 2009), nitrate reductase (Rockel *et al.*, 2002), NiNOR (Stohr & Stremlau, 2006) and polyamine oxidases (Tun *et al.*, 2006; Yamasaki & Cohen, 2006). We therefore set out to systematically test for the presence of each of these systems in *M. oryzae*.

NOS and NOS-like enzymes as potential generators of fungal NO

To determine whether fungi have homologues of the canonical metazoan nitric oxide synthase gene, we performed an iterative hidden Markov model search (Eddy, 1998; S. Kelly, unpublished) with PFAM seed alignment of the nitric oxide synthase domain (PF02898) passed 385 times over 937 completed metazoan, plant, fungal, eubacterial and archaebacterial genomes (Table S1; *e*-value cut-off of 1×10^{-10}). These sequences were clustered based on their pairwise BLAST similarity scores (DendroBLAST; Fig. S2) and analysed for the presence of domains necessary for NO production. This revealed six clusters of sequences (Fig. 4a).

In addition to NOS sequences identified in the green alga *Ostreococcus* sp. (Foresi *et al.*, 2010), the slime mould *Physarum polycephalum* (Werner-Felmayer *et al.*, 1994; Golderer *et al.*, 2001; Messner *et al.*, 2009) and possibly *Aspergillus oryzae* (acc XP-001825673), we identified three further sequences in the ascomycetes *Colletotrichum graminicola* (acc 10854T0) and *Mycosphaerella graminicola* (acc 42401 and 28714, short sequence). These fungi formed a strongly supported group separate from the amoeba and metazoan, but within the NOS cluster (Fig. S3). Interestingly, the *M. graminicola* sequence (42401) and *A. oryzae* sequence carry a reduced complement of residues characteristic of the arginine binding pocket in the mNOS oxygenase domain (Fig. 4b). The presence of this sequence in this monophyletic subgroup of fungi suggests that their common ancestor acquired this by lateral gene transfer. However, the tree is insufficiently resolved to identify the donor organism.

The iterative search revealed that there are no sequences in the *M. oryzae* genome that contain an NOS oxygenase domain (Fig. 4b), although multiple groups of sequences contain the reductase-associated domains found in canonical NOS proteins (Fig. S2). However, all these groups, with one exception, contain multiple members that have been functionally characterized in metazoa, yeast or both, and shown not to be NOSs (Fig. 4a, Fig. S2). It is highly unlikely that *M. oryzae* sequences lying in these groups are NOS.

The only group that does not have functionally characterized homologues in metazoa or amoebazoa contains a domain structure that could be consistent with NO synthesis. This fungal-specific group is composed of proteins, labelled as putative bifunctional p450: NADPH-P450 reductases, each of which contains an N-terminal cytochrome p450 domain and FAD, NAD and flavodoxin binding domains. Members represent the best candidates for oxidative production of NO in *M. oryzae* by an NOS-like mechanism. Within the fungal NOL cluster, we refer to the genes as *NOL1* (MGG_01925), *NOL2* (MGG_05401), *NOL3* (MGG_07953) and *NOL4* (MGG_10879).

Selection of candidate *NOL* genes

Of the four *NOL* genes, qRT-PCR, normalized, independently, against *β-tubulin* and *ElongationFactor-1α* (Fig. 4c,d), suggested that the *NOL2* transcript was 4–5 times more abundant at 0.5–1 hpi (germination) compared with 0 hpi, and *NOL3* showed a 24–28-fold uplift in transcript activity at 12 hpi, coincident with mature appressorium formation and initiation of host infection. These two genes were targeted as the most likely candidates for NOS activity in *M. oryzae*. To test for NOS activity directly, we expressed *NOL3* by heterologous expression in *Escherichia coli* and *Pichea pastoris*. However, we were not able to purify the protein further. Crude cell extracts did not show NOS enzymatic activity by ultrasensitive colorimetric NOS assay (Oxford Biomedical Research Inc., Rochester Hills, MI, USA), with L-arginine as the substrate (data not shown). Furthermore, attempts to isolate interacting partners that might provide a canonical substrate binding site by yeast two-hybrid assay did not yield positive results, even after extensive optimization (data not shown). At this stage, therefore, the evidence that these are potential NOS enzymes is limited to sequence data.

Nitrate and nitrite reductases as potential generators of fungal NO

Given the relatively weak sequence homology of the *NOL* genes, we considered nitrate and nitrite reductases as potential sources

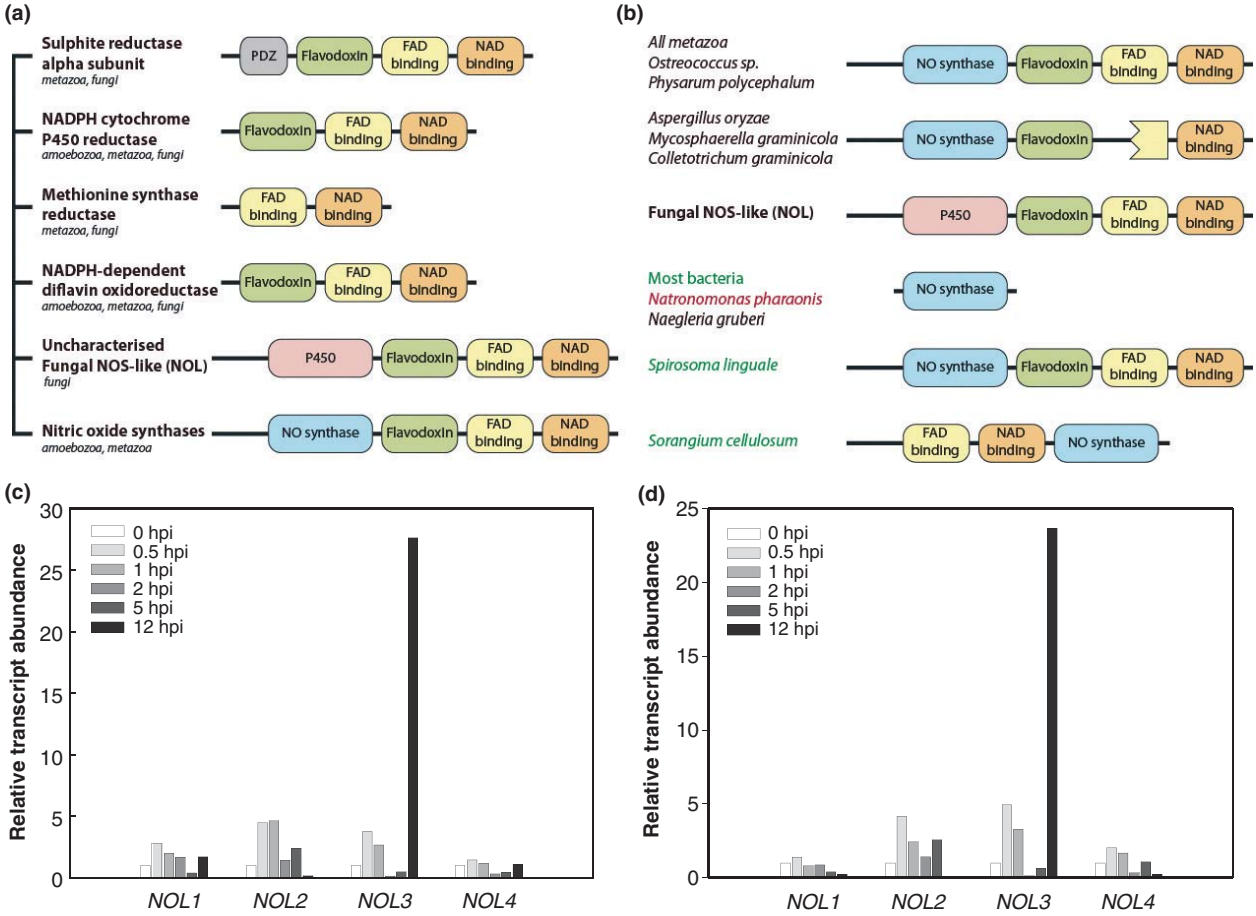

Fig. 4 NOS and NOS-like domain architecture and *Magnaporthe oryzae NOL* gene transcript profiles. (a) Cartoon representations of domain architecture of proteins with sequences related to mNOSs, with names ascribed to five of the profiles following functional characterization of family members. Of these groups, the putative bifunctional p450 reductases, herein named fungal NOS-like NOLs, lie closest to the mNOS (see also Supporting Information Fig. S2). (b) Domain architecture of fungal NOS-like NOLs as compared with metazoan sequences, the green alga *Ostreacoccus* sp., slime mould *Physarum polycephalum* and the sequences from the filamentous fungi *Aspergillus oryzae*, *Mycosphaerella graminicola* and *Colletotrichum graminicola.* Represented are the bacterial domains and the unusual architecture of the bacterial species *Spirosoma linguale* and *Sorangium cellulosum*. (c, d) Relative level of expression of *NOL* genes in *M. oryzea* germlings, from conidia through to the formation of melanized appressoria over a 12-h time-course of infection on barley (*Hordeum vulgare*) cultivar Golden Promise. Expression was quantified by qRT-PCR and is relative to constitutively expressed *β-TUB* (c) and *Elongation Factor-1a* (d). Reactions were conducted in triplicate and the data subjected to Pfaffl analysis, comparing expression values with those in the ungerminated spores (0 hpi). Relative transcript abundance is normalized to 1 at 0 hpi for each gene.

of NO, by analogy with the plant systems. The domain architecture of nitrate reductase includes binding domains for a molybdenum cofactor, cytochrome b5, FAD and NAD(P)H (Campbell & Kinghorn, 1990) and is closely conserved in all fungal sequences (Fig. S4a). This was revealed using the fungal sequences listed in Table S1, by hidden Markov model search (Eddy, 1998; S. Kelly, unpublished), using acc. MGG_06062, clustered by BLAST similarity scores (DENDROBLAST) and by domain analysis. Likewise, there is a high degree of architectural conservation for nitrite reductase proteins (using acc. MGG_00634), with all members containing cysteine, FeS-siroheme, nitrite/sulphite reductase and ferrodoxin-like domains (Fig. S4b). *Magnaporthe oryzae* carries single copies of nitrate reductase (MGG_06062; *NIA1)* and nitrite reductase (MGG_00634; *NII1*), which were therefore selected as targets for gene knockout.

Analysis of mutants deficient in nitrate reductase, nitrite reductase and nitric oxide synthase-like enzymes

To test whether nitrate reductase, nitrite reductase or the two most abundant NOLs might contribute to NO production in *M. oryzae*, single (Δ*nia1*, Δ*nii1*, Δ*nol2*, and Δ*nol3*) and double (Δ*nia1*Δ*nii1*, Δ*nia1*Δ*nol3*, and Δ*nol2*Δ*nol3*) knockouts were constructed by homologous recombination in Δ*ku70* background NHEJ strain, derived from *M. oryzae* Guy 11 (Wilson & Talbot, 2009). All knockouts were verified by PCR analysis with internal and flanking primers, and Southern blot analysis confirmed a single targeted replacement event (Fig. S5).

Plate growth assays revealed no differences in growth morphology or colony diameter among strains Guy11, Δ*ku70,* Δ*nia1*, Δ*nii1,* Δ*nia1*Δ*nii1*, Δ*nol2*, Δ*nol3*, Δ*nol2*Δ*nol3,* and Δ*nia1*Δ*nol3*

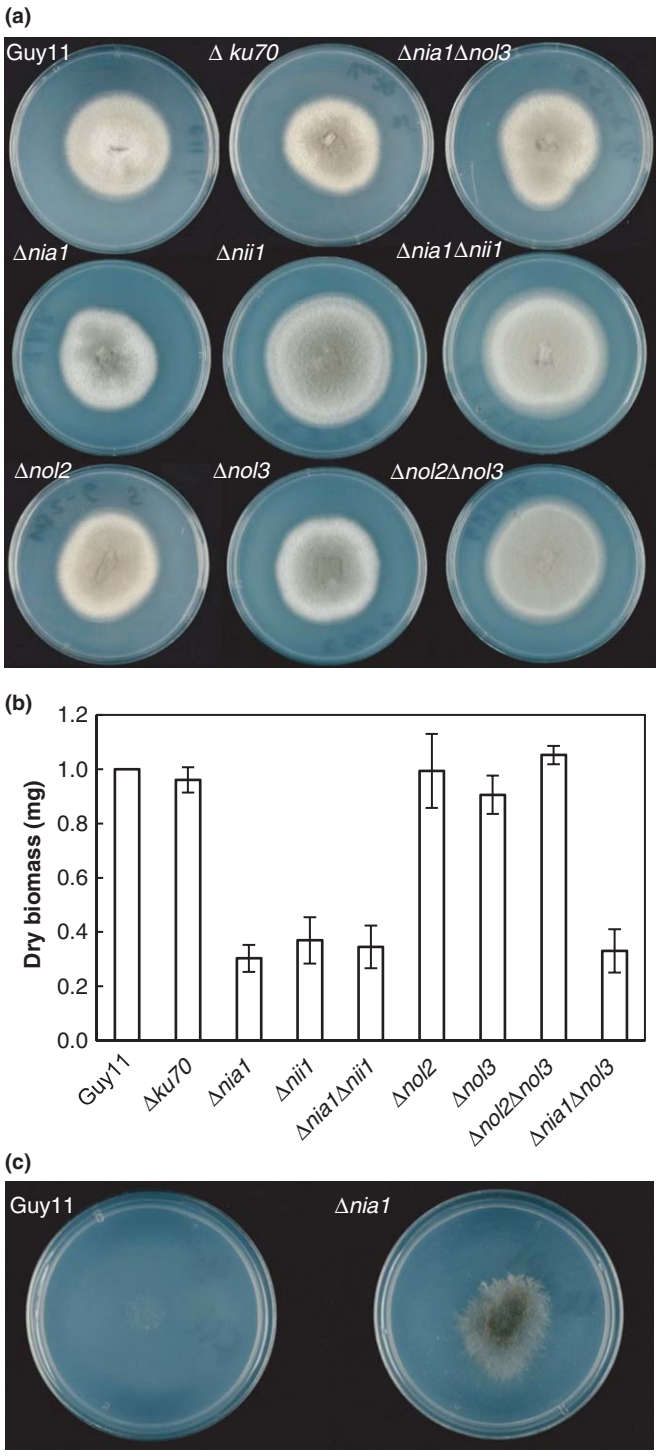

Fig. 5 Wild-type (WT) and mutant *Magnaporthe oryzae* strain growth on solid media (radial growth) and in liquid media (biomass). (a) WT Guy11, Δ*ku70*, Δ*nia1*, Δ*nii1*, Δ*nia1*Δ*nii1*, Δ*nol2*, Δ*nol3*, Δ*nol2*Δ*nol3* and Δ*nia1*Δ*nol3* grown on complete medium at 24°C for 10 d. (b) Biomass (mg dry weight) of Guy11, Δ*ku70*, Δ*nia1*, Δ*nii1*, Δ*nia1*Δ*nii1*, Δ*nol2*, Δ*nol3*, Δ*nol2*Δ*nol3* and Δ*nia1*Δ*nol3* grown in liquid minimal medium (70.6 mM $NaNO_3$) shaken at 150 rpm at 24°C for 14 d; data were normalized to WT Guy 11. The experiment was replicated three times; results are shown as mean ± SEM. (c) WT Guy11 and Δ*nia1* grown on minimal medium supplemented with 300 mM potassium chlorate at 24°C for 14 d.

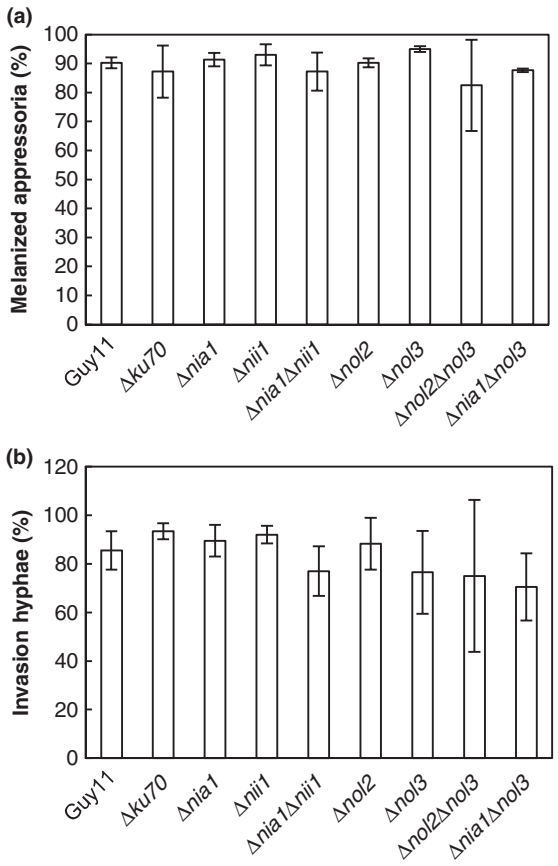

Fig. 6 Wild-type (WT) and mutant *Magnaporthe oryzae* strain germling infection-related development and invasion hypha formation. (a) WT Guy11, Δ*ku70,* Δ*nia1*, Δ*nii1*, Δ*nia1*Δ*nii1*, Δ*nol2*, Δ*nol3*, Δ*nol2*Δ*nol3* and Δ*nia1*Δ*nol3* strain development of melanized appressoria at 8 hpi, following inoculation of conidia onto hydrophobic surface inductive to melanized appressorium formation in the WT strain. (b) Invasion hypha formation, elaborated from penetration pegs, for strains WT Guy11, Δ*ku70,* Δ*nia1*, Δ*nii1*, Δ*nia1*Δ*nii1*, Δ*nol2*, Δ*nol3*, Δ*nol2*Δ*nol3* and Δ*nia1*Δ*nol3* on onion epidermal peels at 24 hpi. Both experiments were replicated three times; results are shown as mean ± SD.

on CM (Fig. 5a). On MM (containing 70.6 mM sodium nitrate) the strains showed differential growth. This was quantified by biomass determination in liquid medium and showed a significant reduction in growth of Δ*nia1*, Δ*nii1,* Δ*nia1*Δ*nii1* and Δ*nia1*Δ*nol3* as compared with the wild type (Fig. 5b), as these strains were unable to use nitrate as the sole nitrogen source in the absence of NR. By contrast, only the NR-deficient strain Δ*nia1* survived exposure to 300 mM chlorate (Fig. 5c), which is metabolized to toxic chlorite in strains with functional NR (Cove, 1976).

If the gene knockout mutants impact on NO production, we might expect them to phenocopy the effects of PTIO on germination, early development and pathogenicity. However, all strains formed melanized appressoria on glass slides within 8 hpi (Fig. 6a), and were able to initiate penetration pegs, form invasive hyphae on onion epidermis (Fig. 6b), and make lesions in a cut leaf assay on both barley and rice susceptible to wild-type *M. oryzae* infection, with similar frequencies to the parental strains (Fig. 7).

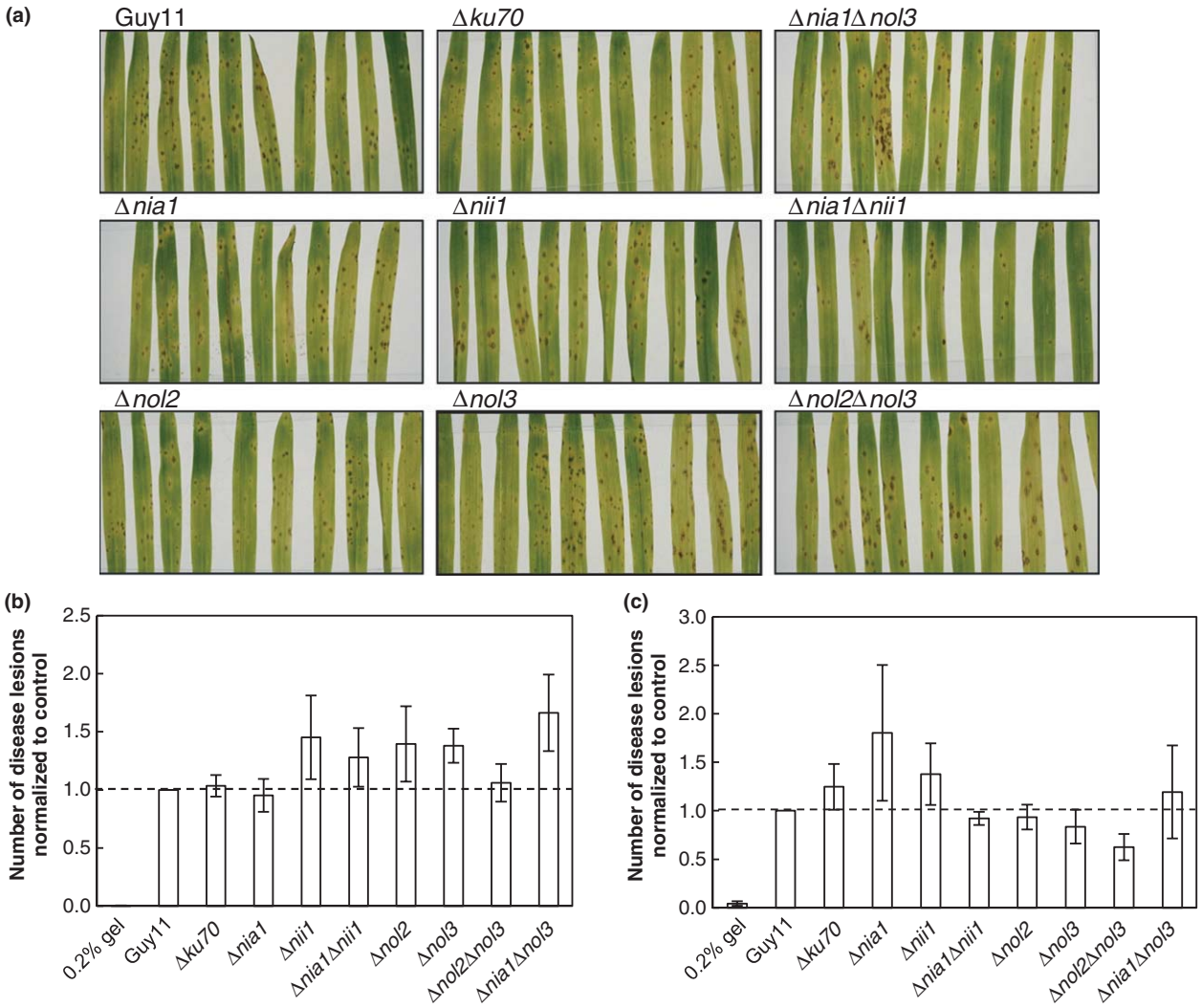

Fig. 7 Pathogenicity assays for wild-type (WT) and mutant *Magnaporthe oryzae* strains on barley and rice. (a) Barley (*Hordeum vulgare*) cultivar Golden Promise leaves were spray-inoculated with Guy11, Δ*ku70*, Δ*nia1*, Δ*nii1*, Δ*nia1*Δ*nii1*, Δ*nol2*, Δ*nol3*, Δ*nol2*Δ*nol3* and Δ*nia1*Δ*nol3* conidial suspensions (2.5×10^5 spores ml^{-1}) and incubated for 5 d for development of blast lesions. Negative control includes leaves sprayed with 0.2% gelatine (gel) only. (b, c) The number of developed lesions on barley and rice (*Oryza sativa*), respectively, was counted and normalized to Guy 11. The experiment was replicated ten times for barley and four times on detached rice leaves and twice on whole rice plants; results are shown as mean ± SEM.

Some variation was noted in the detached rice leaf bioassay (Fig. 7c), so assays were repeated on intact plants, revealing no statistically significant differences between lesion numbers in wild-type and mutant strains (Δ*nol2*Δ*nol3* $P = 0.021$; others $P > 0.2$; data not shown).

There was no significant difference in NO production in the mutants compared with the wild type, as determined by the concentration-dependent PTIO profile of triazole formation. All mutants produced NO with the characteristic stimulation at low concentrations of PTIO and inhibition at high concentrations (Fig. 8). Finally, we were not able to detect any inhibition in triazole formation with L-NAME in Guy11 or the Δ*nia1* and Δ*nii1* backgrounds (Fig. 9), or any difference in response compared with the inactive stereoisomer D-NAME up to 500 μM in Guy11. If anything, at higher (mM) concentrations, both compounds stimulated fluorescence from DAR-4M.

We infer that none of these putative NO-synthesizing enzymes are individually responsible for the observed NO production in *M. oryzae* strain Guy11. Furthermore, the absence of any strong phenotype in the double knockouts tested and in the presence of the general NOS inhibitor L-NAME further indicates the lack of functional redundancy in NO production between these pathways.

To test for the presence of polyamine oxidase activity that might produce NO (Tun *et al.*, 2006; Wimalasekera *et al.*, 2011), we analysed NO production in the presence of the polyamines spermine and spermidine (Fig. 10), but did not observe any increase in triazole fluorescence. In mammalian systems, the mNOS isozymes are stimulated by the substrate arginine and inhibited by arginine substrate analogues, such as L-NMMA and inhibitor 1400W (Garvey *et al.*, 1997) which compete for the arginine binding site. We found no evidence for inhibition of NO production by L-NMMA, D-NMMA and 1400W or with the

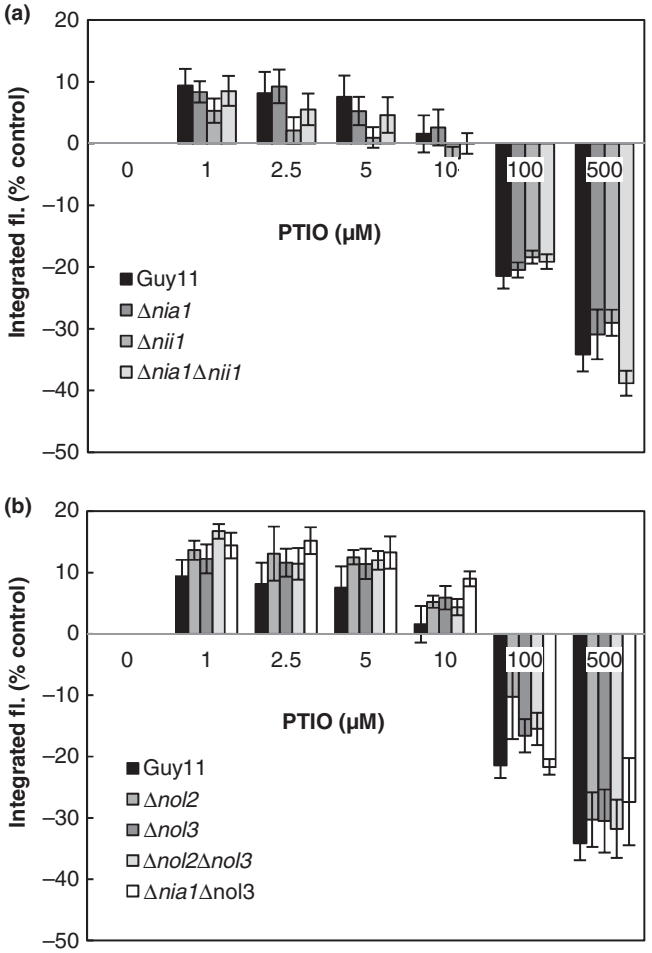

Fig. 8 Response profile of DAR-4M fluorescence to PTIO in wild-type and mutant strains. The difference in the integrated fluorescence over the first 8 h compared with the absence of PTIO expressed as a percentage of the control value was similar for (a) Guy11 ($n = 23$), Δ*nia1* ($n = 6$), Δ*nii1* ($n = 6$) and Δ*nia1*Δ*nii1* ($n = 6$), or (b) Guy11 ($n = 11$), Δ*nol2* ($n = 5$), Δ*nol3* ($n = 5$), Δ*nol2*Δ*nol3* ($n = 5$) and Δ*nia1*Δ*nol3* ($n = 5$). In all cases, the characteristic bi-phasic response to increasing PTIO concentrations suggested that all strains were producing NO to similar levels during development. Results are shown as mean ± SEM.

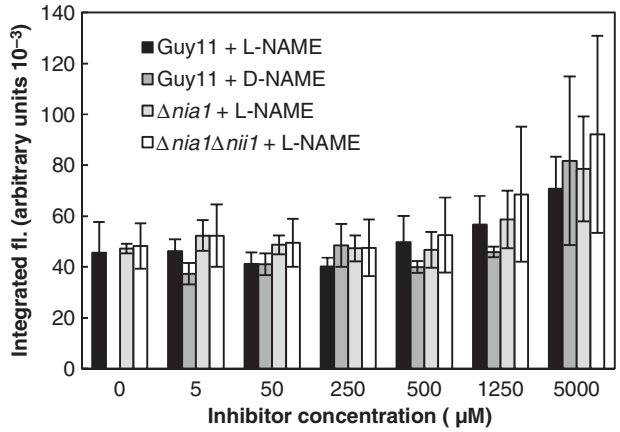

Fig. 9 Effect of the mammalian NOS inhibitor L-NAME on total levels of NO production. The fluorescence intensity from DAR-4M-AM loaded spores was integrated over 12 h as a measure of NO production. Levels of DAR-4M fluorescence were insensitive to concentrations of L-NAME below mM levels, but showed a slight and variable stimulation at higher concentrations. This pattern of fluorescence was similar with the inactive D-isomer, or in knockouts of Δ*nia1*, and Δ*nia1*Δ*nii1*. Results are shown as mean ± SEM ($n = 3$).

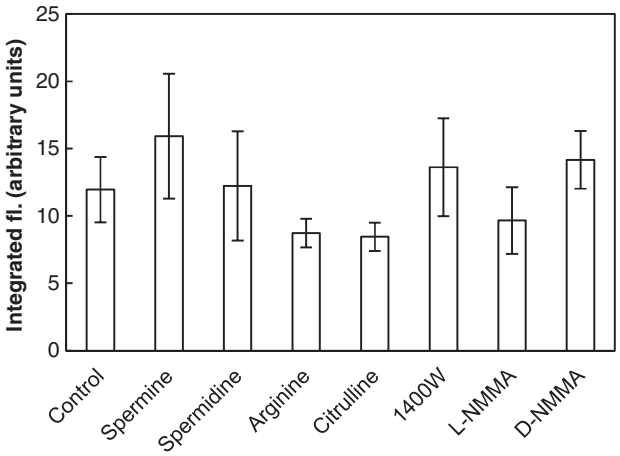

Fig. 10 Effect of polyamines and NOS inhibitors on total levels of NO production. The fluorescence intensity from DAR-4M-AM loaded WT spores was integrated over 12 h as a measure of NO production. Level of DAR-4M fluorescence showed no significant change in response to addition of 1 mM of the polyamines spermine and spermidine, the mammalian NOS substrate arginine, and the end-product citrulline, or the mammalian NOS inhibitors 1400W, L-NNMA and its inactive stereoisomer, D-NMMA. Results are shown as mean ± SEM ($n = 3$).

mNOS reaction product citrulline (Fig. 10), similar to the results obtained with L-NAME (Fig. 9). Finally, we do not consider that nonenzymatic NO production, akin to plant apoplastic NO synthesis (Bethke *et al.*, 2004), is significant, as our measurements were conducted in medium buffered at pH 7.

Conclusions

In summary, NO is produced by *M. oryzae* during germination and early development, and is critically required to progress through to appressorium formation. Thus, removal of NO by NO scavengers slows down development on artificial surfaces and abolishes infection *in vivo*. The *in vivo* fluorescent assays provide some evidence that NO diffuses out of the germlings, at least until the formation of melanized appressoria. It is possible that the role of NO is to co-ordinate behaviour between different cells in the conidium which go on to have very different fates, as a non-cell autonomous signal. We have not investigated signalling events downstream from NO, but the targets are unlikely to include soluble guanylyl cyclase (sGS), as in mammals, as fungal genomes lack these sequences (Schaap, 2005). In other systems there is the potential for extensive chemical modification, particularly by S-nitrosylation or tyrosine nitration (Mur *et al.*, 2006). These pathways are inextricably linked to the dynamics of other reactive oxygen species (ROS) (Winterbourn, 2008; Moreau *et al.*, 2010). It is likely that there will be a complex spatial and temporal interplay between NO and ROS signalling systems, such as *M. oryzae*

plasma-membrane NADPH oxidases (Egan *et al.*, 2007), which are known to be critical determinants of infection.

Despite the importance of NO identified here, the synthesis pathway in *M. oryzae* is not clear. We found no evidence for NO production by reductive nitrate reductase or nitrite reductase pathways or oxidative NOS-like enzymes, arginine-dependent NO systems, polyamine oxidases, or by low pH, that is nonenzymatically. While investigations on NO in fungi are at an early stage, this cautions against uncritical adoption of an NO-signalling paradigm from either animal or plant systems. Indeed, phylogenetic comparisons provide limited support for canonical NOS or NOS-like enzymes across all fungi, with the possible exception of a few sequences that appear to reflect horizontal gene transfer events. The mechanism by which fungi generate NO remains elusive.

Acknowledgements

This work was funded by a BBSRC award to S.G. and M.F. to support M.S. (BB/G00207x/1) and studentship funding for J.J. and M.I. We are grateful to Luis Mur (Aberystwyth) who provided impetus for this work, Mick Kershaw (Exeter) for help with rice pathogenicity assays and Nick Talbot (Exeter) for his sage advice.

References

Akaike T, Yoshida M, Miyamoto Y, Sato K, Kohno M, Sasamoto K, Miyazaki K, Ueda S, Maeda H. 1993. Antagonistic action of imidazolineoxyl N-oxides against endothelium-derived relaxing factor/•NO through a radical reaction. *Biochemistry* **32**: 827–832.

Alderton WK, Cooper CE, Knowles RG. 2001. Nitric oxide synthases: structure, function and inhibition. *Biochemical Journal* **357**: 593–615.

Anbar M. 1995. Nitric-oxide – a synchronizing chemical messenger. *Experientia* **51**: 545–550.

Ausubel FM, Brent R, Kingston RE, Moore DD, Seidman JG, Smith JA, Struhl K. 1999. *Short protocols in molecular biology: a compendium of methods from current protocols in molecular biology.* New York, NY, USA: John Wiley Press.

Baroja-Mazo A, del Valle P, Rua J, de Cima S, Busto F, de Arriaga D, Smirnoff N. 2005. Characterisation and biosynthesis of D-erythroascorbic acid in *Phycomyces blakesleeanus. Fungal Genetics and Biology* **42**: 390–402.

Baudouin E. 2011. The language of nitric oxide signalling. *Plant Biology* **13**: 233–242.

Besson-Bard A, Pugin A, Wendehenne D. 2008. New insights into nitric oxide signaling in plants. *Annual Review of Plant Biology* **59**: 21–39.

Bethke PC, Badger MR, Jones RL. 2004. Apoplastic synthesis of nitric oxide by plant tissues. *Plant Cell* **16**: 332–341.

Bourett TM, Howard RJ. 1990. *In vitro* development of penetration structures in the rice blast fungus *Magnaporthe grisea. Canadian Journal of Botany* **68**: 329–342.

Bright J, Desikan R, Hancock JT, Weir IS, Neill SJ. 2006. ABA-induced NO generation and stomatal closure in *Arabidopsis* are dependent on H_2O_2 synthesis. *Plant Journal* **45**: 113–122.

Brown AJP, Haynes K, Quinn J. 2009. Nitrosative and oxidative stress responses in fungal pathogenicity. *Current Opinion in Microbiology* **12**: 384–391.

Campbell WH, Kinghorn JR. 1990. Functional domains of assimilatory nitrate reductases and nitrite reductases. *Trends in Biochemical Sciences* **15**: 315–319.

Collingridge PW, Kelly S. 2012. MergeAlign: improving multiple sequence alignment performance by dynamic reconstruction of consensus multiple sequence alignments. *BMC Bioinformatics* **13**: 117–125.

Conrath U, Amoroso G, Kohle H, Sultemeyer DF. 2004. Non-invasive online detection of nitric oxide from plants and some other organisms by mass spectrometry. *Plant Journal* **38**: 1015–1022.

Corpas FJ, Barroso JB, Carreras A, Quiros M, Leon AM, Romero-Puertas MC, Esteban FJ, Valderrama R, Palma JM, Sandalio LM, *et al.* 2004. Cellular and subcellular localization of endogenous nitric oxide in young and senescent pea plants. *Plant Physiology* **136**: 2722–2733.

Corpas FJ, Palma JM, del Rio LA, Barroso JB. 2009. Evidence supporting the existence of L-arginine-dependent nitric oxide synthase activity in plants. *New Phytologist* **184**: 9–14.

Cove DJ. 1976. Chlorate toxicity in *Aspergillus nidulans*: The selection and characterisation of chlorate resistant mutants. *Heredity* **36**: 191–203.

Delledonne M, Xia YJ, Dixon RA, Lamb C. 1998. Nitric oxide functions as a signal in plant disease resistance. *Nature* **394**: 585–588.

Delledonne M, Zeier J, Marocco A, Lamb C. 2001. Signal interactions between nitric oxide and reactive oxygen intermediates in the plant hypersensitive disease resistance response. *Proceedings of the National Academy of Sciences, USA* **98**: 13454–13459.

Ebbole DJ. 2007. *Magnaporthe* as a model for understanding host-pathogen interactions. *Annual Review of Phytopathology* **45**: 437–456.

Eddy SR. 1998. Profile hidden Markov models. *Bioinformatics* **14**: 755–763.

Egan MJ, Wang ZY, Jones MA, Smirnoff N, Talbot NJ. 2007. Generation of reactive oxygen species by fungal NADPH oxidases is required for rice blast disease. *Proceedings of the National Academy of Sciences, USA* **104**: 11772–11777.

Finn RD, Mistry J, Tate J, Coggill P, Heger A, Pollington JE, Gavin OL, Gunasekaran P, Ceric G, Forslund K, *et al.* 2010. The Pfam protein families database. *Nucleic Acids Research* **38**: D211–D222.

Fisher MC, Henk DA, Briggs CJ, Brownstein JS, Madoff LC, McCraw SL, Gurr SJ. 2012. Emerging fungal threats to animal, plant and ecosystem health. *Nature* **484**: 186–194.

Floryszak-Wieczorek J, Arasimowicz M, Milczarek G, Jelen H, Jackowiak H. 2007. An early nitric oxide burst and the following wave of secondary nitric oxide generation enhanced effective defence responses of pelargonium to a necrotrophic pathogen. *New Phytologist* **175**: 718–730.

Foresi N, Correa-Aragunde N, Parisi G, Calo G, Salerno G, Lamattina L. 2010. Characterization of a nitric oxide synthase from the plant kingdom: NO generation from the green alga *Ostreococcus tauri* is light irradiance and growth phase dependent. *Plant Cell* **22**: 3816–3830.

Garvey EP, Oplinger JA, Furfine ES, Kiff RJ, Laszlo F, Whittle BJR, Knowles RG. 1997. 1400W is a slow, tight binding, and highly selective inhibitor of inducible nitric-oxide synthase *in vitro* and *in vivo. Journal of Biological Chemistry* **272**: 959–4963.

Gas E, Flores-Perez U, Sauret-Gueto S, Rodriguez-Concepcion M. 2009. Hunting for plant nitric oxide synthase provides new evidence of a central role for plastids in nitric oxide metabolism. *Plant Cell* **21**: 18–23.

Georgiou CD, Petropoulou KP. 2001. Role of erythroascorbate and ascorbate in sclerotial differentiation in *Sclerotinia sclerotiorum. Mycological Research* **105**: 1364–1370.

Golderer G, Werner ER, Leitner S, Grobner P, Werner-Felmayer G. 2001. Nitric oxide synthase is induced in sporulation of *Physarum polycephalum. Genes & Development* **15**: 1299–1309.

Gong XY, Fu YP, Jiang DH, Li GQ, Yi XH, Peng YL. 2007. L-arginine is essential for conidiation in the filamentous fungus *Coniothyrium minitans. Fungal Genetics and Biology* **44**: 1368–1379.

Gorren ACF, Mayer B. 2007. Nitric-oxide synthase: a cytochrome P450 family foster child. *Biochimica et Biophysica Acta* **1770**: 432–445.

Govrin EM, Levine A. 2000. The hypersensitive response facilitates plant infection by the necrotrophic pathogen *Botrytis cinerea. Current Biology* **10**: 751–757.

Grisham MB, Jourd'Heuil D, Wink DA. 1999. Nitric oxide - I. Physiological chemistry of nitric oxide and its metabolites: implications in inflammation. *American Journal of Physiology Gastrointestinal and Liver Physiology* **276**: G315–G321.

Guo FQ, Okamoto M, Crawford NM. 2003. Identification of a plant nitric oxide synthase gene involved in hormonal signaling. *Science* **302**: 100–103.

Gupta KJ, Fernie AR, Kaiser WM, van Dongen JT. 2011. On the origins of nitric oxide. *Trends in Plant Science* **16**: 160–168.

Hong JK, Yun BW, Kang JG, Raja MU, Kwon E, Sorhagen K, Chu C, Wang Y, Loake GJ. 2008. Nitric oxide function and signalling in plant disease resistance. *Journal of Experimental Botany* **59**: 147–154.

Ignarro LJ, Buga GM, Wood KS, Byrns RE, Chaudhuri G. 1987. Endothelium-derived relaxing factor produced and released from artery and vein is nitric-oxide. *Proceedings of the National Academy of Sciences, USA* **84**: 9265–9269.

Katoh K, Kuma K, Miyata T, Toh H. 2005. Improvement in the accuracy of multiple sequence alignment program MAFFT. *Genome Information* **16**: 22–33.

Kelly S. 2011. Archaeal phylogenomics provides evidence in support of a methanogenic origin of the Archaea and a thaumarchaeal origin for the eukaryotes. *Philosphical Transactions Royal Society London B, Biological Sciences* **278**: 1009–1018.

Kojima H, Hirotani M, Nakatsubo N, Kikuchi K, Urano Y, Higuchi T, Hirata Y, Nagano T. 2001. Bioimaging of nitric oxide with fluorescent indicators based on the rhodamine chromophore. *Analytical Chemistry* **73**: 1967–1973.

Kojima H, Nakatsubo N, Kikuchi K, Kawahara S, Kirino Y, Nagoshi H, Hirata Y, Nagano T. 1998. Detection and imaging of nitric oxide with novel fluorescent indicators: diaminofluoresceins. *Analytical Chemistry* **70**: 2446–2453.

Kojima H, Urano Y, Kikuchi K, Higuchi T, Hirata Y, Nagano T. 1999. Fluorescent indicators for imaging nitric oxide production. *Angew Chemica* **38**: 3209–3212.

Lacza Z, Horvath EM, Pankotai E, Csordas A, Kollai M, Szabo C, Busija DW. 2005. The novel red-fluorescent probe DAR-4M measures reactive nitrogen species rather than NO. *Journal of Pharmacological and Toxicological Methods* **52**: 335–340.

Lacza Z, Pankotai E, Csordas A, Gero D, Kiss L, Horvath EM, Kollai M, Busija DW, Szabo C. 2006. Mitochondrial NO and reactive nitrogen species production: does mtNOS exist? *Nitric Oxide* **14**: 162–168.

Le SQ, Gascuel O. 2008. An improved general amino acid replacement matrix. *Molecular Biology and Evolution* **25**: 1307–1320.

Lundberg JO, Weitzberg E, Gladwin MT. 2008. The nitrate-nitrite-nitric oxide pathway in physiology and therapeutics. *Nature Review Drug Discovery* **7**: 156–167.

Maier J, Hecker R, Rockel P, Ninnemann H. 2001. Role of nitric oxide synthase in the light-induced development of sporangiophores in *Phycomyces blakesleeanus*. *Plant Physiology* **126**: 1323–1330.

Messner S, Leitner S, Bommassar C, Golderer G, Groebner P, Werner ER, Werner-Felmayer G. 2009. *Physarum* nitric oxide synthases: genomic structures and enzymology of recombinant proteins. *Biochemical Journal* **418**: 691–700.

Moreau M, Lee GI, Wang Y, Crane BR, Klessig DF. 2008. AtNOS/AtNOA1 is a functional *Arabidopsis thaliana* cGTPase and not a nitric-oxide synthase. *Journal of Biological Chemistry* **283**: 32957–32967.

Moreau M, Lindermayr C, Durner J, Klessig DF. 2010. NO synthesis and signaling in plants - where do we stand? *Physiologia Plantarum* **138**: 372–383.

Morot-Gaudry-Talarmain Y, Rockel P, Moureaux T, Quillere I, Leydecker MT, Kaiser WM, Morot-Gaudry JF. 2002. Nitrite accumulation and nitric oxide emission in relation to cellular signaling in nitrite reductase antisense tobacco. *Planta* **215**: 708–715.

Mur LAJ, Carver TLW, Prats E. 2006. NO way to live; the various roles of nitric oxide in plant-pathogen interactions. *Journal of Experimental Botany* **57**: 489–505.

Mur LAJ, Mandon J, Cristescu SM, Harren FJM, Prats E. 2011. Methods of nitric oxide detection in plants: a commentary. *Plant Science* **181**: 509–519.

Nagano T. 2009. Bioimaging probes for reactive oxygen species and reactive nitrogen species. *Journal Clinical Biochemistry Nutrition* **45**: 111–124.

Nagata N, Momose K, Ishida Y. 1999. Inhibitory effects of catecholamines and anti-oxidants on the fluorescence reaction of 4,5-diaminofluorescein, DAF-2, a novel indicator of nitric oxide. *Journal of Biochemistry* **125**: 658–661.

Nakatsubo N, Kojima H, Sakurai K, Kikuchi K, Nagoshi H, Hirata Y, Akaike T, Maeda H, Urano Y, Higuchi T, *et al.* 1998. Improved nitric oxide detection using 2,3-diaminonaphthalene and its application to the evaluation of novel nitric oxide synthase inhibitors. *Biological & Pharmaceutical Bulletin* **21**: 1247–1250.

Palmer RMJ, Ferrige AG, Moncada S. 1987. Nitric-Oxide release accounts for the biological-activity of endothelium-derivedrelaxing factor. *Nature* **327**: 524–526.

Pfaffl MW. 2001. A new mathematical model for relative quantification in real-time RT-PCR. *Nucleic Acids Research* **29**: e45.

Pfeiffer S, Mayer B, Hemmens B. 1999. Nitric oxide: chemical puzzles posed by a biological messenger. *Angewandte Chemie, International Edition* **38**: 1715–1731.

Planchet E, Gupta KJ, Sonoda M, Kaiser WM. 2005. Nitric oxide emission from tobacco leaves and cell suspensions: rate limiting factors and evidence for the involvement of mitochondrial electron transport. *Plant Journal* **41**: 732–743.

Prats E, Carver TL, Mur LA. 2008. Pathogen-derived nitric oxide influences formation of the appressorium infection structure in the phytopathogenic fungus *Blumeria graminis*. *Research in Microbiology* **159**: 476–480.

Prats E, Mur LAJ, Sanderson R, Carver TLW. 2005. Nitric oxide contributes both to papilla-based resistance and the hypersensitive response in barley attacked by *Blumeria graminis* f. sp *hordei*. *Molecular Plant Pathology* **6**: 65–78.

Rockel P, Strube F, Rockel A, Wildt J, Kaiser WM. 2002. Regulation of nitric oxide (NO) production by plant nitrate reductase *in vivo* and *in vitro*. *Journal of Experimental Botany* **53**: 103–110.

Rumer S, Gupta KJ, Kaiser WM. 2009. Plant cells oxidize hydroxylamines to NO. *Journal of Experimental Botany* **60**: 2065–2072.

Schaap P. 2005. Guanylyl cyclases across the tree of life. *Frontiers in Bioscience-Landmark* **10**: 1485–1498.

Skamnioti P, Gurr SJ. 2007. *Magnaporthe grisea* cutinase 2 mediates appressorium differentiation and host penetration and is required for full virulence. *Plant Cell* **19**: 2674–2689.

Skamnioti P, Gurr SJ. 2009. Against the grain: safeguarding rice from rice blast disease. *Trends in Biotechnology* **27**: 141–150.

Stamatakis A. 2006. RAxML-VI-HPC: maximum likelihood-based phylogenetic analyses with thousands of taxa and mixed models. *Bioinformatics* **22**: 2688–2690.

Stohr C, Stremlau S. 2006. Formation and possible roles of nitric oxide in plant roots. *Journal of Experimental Botany* **57**: 463–470.

Sukumaran J, Holder MT. 2010. DendroPy: a Python library for phylogenetic computing. *Bioinformatics* **26**: 1569–1571.

Talbot NJ, Ebbole DJ, Hamer JE. 1993. Identification and characterization of *Mpg1*, a gene involved in pathogenicity from the rice blastfungus *Magnaporthe grisea*. *Plant Cell* **5**: 1575–1590.

Tun NN, Santa-Catarina C, Begum T, Silveira V, Handro W, Floh EI, Scherer GF. 2006. Polyamines induce rapid biosynthesis of nitric oxide (NO) in *Arabidopsis thaliana* seedlings. *Plant and Cell Physiology* **47**: 346–354.

Turrion-Gomez JL, Benito EP. 2011. Flux of nitric oxide between the necrotrophic pathogen *Botrytis cinerea* and the host plant. *Molecular Plant Pathology* **12**: 606–616.

Van Baarlen P, Staats M, Van Kan JAL. 2004. Induction of programmed cell death in lily by the fungal pathogen *Botrytis elliptica*. *Molecular Plant Pathology* **5**: 559–574.

Vandelle E, Delledonne M. 2008. Methods for nitric oxide detection during plant-pathogen interactions. *Methods in Enzymology* **437**: 575–594.

Veneault-Fourrey C, Barooah M, Egan M, Wakley G, Talbot NJ. 2006. Autophagic fungal cell death is necessary for infection by the rice blast fungus. *Science* **312**: 580–583.

Vitecek J, Reinohl V, Jones RL. 2008. Measuring NO production by plant tissues and suspension cultured cells. *Molecular Plant* **1**: 270–284.

Wang J, Higgins VJ. 2005. Nitric oxide has a regulatory effect in the germination of conidia of *Colletotrichum coccodes*. *Fungal Genetics and Biology* **42**: 284–292.

Wardman P. 2007. Fluorescent and luminescent probes for measurement of oxidative and nitrosative species in cells and tissues: progress, pitfalls, and prospects. *Free Radical Biology and Medicine* **43**: 995–1022.

Werner-Felmayer G, Golderer G, Werner ER, Grobner P, Wachter H. 1994. Pteridine biosynthesis and nitric oxide synthase in *Physarum polycephalum*. *Biochemical Journal* **304**: 105–111.

Wilson ID, Neill SJ, Hancock JT. 2008. Nitric oxide synthesis and signalling in plants. *Plant, Cell & Environment* **31**: 622–631.

Wilson RA, Talbot NJ. 2009. Under pressure: investigating the biology of plant infection by *Magnaporthe oryzae*. *Nature Review Microbiology* **7**: 185–195.

Wimalasekera R, Tebartz F, Scherer GF. 2011. Polyamines, polyamine oxidases and nitric oxide in development, abiotic and biotic stresses. *Plant Sciences* **181**: 593–603.

Winterbourn CC. 2008. Reconciling the chemistry and biology of reactive oxygen species. *Nature Chemical Biology* **4**: 278–286.

Yamasaki H. 2000. Nitrite–dependent nitric oxide production pathway: implications for involvement of active nitrogen species in photoinhibition *in vivo*.. *Philosophical Transactions of the Royal Society of London. Series B: Biological Sciences* **355**: 1477–1488.

Yamasaki H, Cohen MF. 2006. NO signal at the crossroads: polyamine-induced nitric oxide synthesis in plants? *Trends in Plant Science* **11**: 522–524.
Yamasaki H, Sakihama Y, Takahashi S. 1999. An alternative pathway for nitric oxide production in plants: new features of an old enzyme. *Trends in Plant Science* **4**: 128–129.
Ye X, Rubakhin SS, Sweedler JV. 2008. Simultaneous nitric oxide and dehydroascorbic acid imaging by combining diaminofluoresceins and diaminorhodamines. *Journal Neuroscience Methods* **168**: 373–382.
Zaninotto F, La Camera S, Polverari A, Delledonne M. 2006. Cross talk between reactive nitrogen and oxygen species during the hypersensitive disease resistance response. *Plant Physiology* **141**: 379–383.
Zeier J, Delledonne M, Mishina T, Severi E, Sonoda M, Lamb C. 2004. Genetic elucidation of nitric oxide signaling in incompatible plant-pathogen interactions. *Plant Physiology* **136**: 2875–2886.
Zhang X, Kim WS, Hatcher N, Potgieter K, Moroz LL, Gillette R, Sweedler JV. 2002. Interfering with nitric oxide measurements. 4,5-Diaminofluorescein reacts with dehydroascorbic acid and ascorbic acid. *Journal of Biological Chemistry* **277**: 48472–48478.

Supporting Information

Additional supporting information may be found in the online version of this article.

Fig. S1 Correction for PTIO quenching effects on DAR-4M-T fluorescence.

Fig. S2 Cross-Kingdom phylogenetic tree of organisms carrying proteins with nitric oxide synthase domain architecture.

Fig. S3 Nitric oxide synthase clade.

Fig. S4 Phylogenetic trees of nitrate and nitrite reductase in fungi.

Fig. S5 Southern blot analysis to confirm single targeted replacement event.

Table S1 Species list of completed sequenced genomes searched for nitric oxide synthase domain PFAM02898

Table S2 PCR primers used to generate the gene knockout strains described

Table S3 Primers used to generate the qRT-PCR *NOL* transcript profiles

Methods S1 Mutant strain generation.

Methods S2 Southern blot analysis of putative transformants.

Methods S3 Pathogenicity assays.

Please note: Wiley-Blackwell are not responsible for the content or functionality of any supporting information supplied by the authors. Any queries (other than missing material) should be directed to the *New Phytologist* Central Office.

Research

New Phytologist

Robust anti-oxidant defences in the rice blast fungus *Magnaporthe oryzae* confer tolerance to the host oxidative burst

Marketa Samalova[1], Andreas J. Meyer[2], Sarah J. Gurr[1,3] and Mark D. Fricker[1]

[1]Department of Plant Sciences, University of Oxford, South Parks Road, Oxford, OX1 3RB, UK; [2]INRES, Universität Bonn, Friedrich-Ebert-Allee 144, D-53113 Bonn, Germany; [3]Biosciences, University of Exeter, Devon EX4 4QD, UK

Author for correspondence:
Mark D. Fricker
Tel: +44 (0)1865 275 015
Email: mark.fricker@plants.ox.ac.uk

Received: *7 June 2013*
Accepted: *20 August 2013*

New Phytologist (2014) **201:** 556–573
doi: 10.1111/nph.12530

Key words: confocal redox imaging, glutathione, Grx1-roGFP2, *Magnaporthe oryzae*, mitochondrial activity, monochlorobimane, reactive oxygen species (ROS), rice blast pathogen response.

Summary

- Plants respond to pathogen attack via a rapid burst of reactive oxygen species (ROS). However, ROS are also produced by fungal metabolism and are required for the development of infection structures in *Magnaporthe oryzae*.
- To obtain a better understanding of redox regulation in *M. oryzae*, we measured the amount and redox potential of glutathione (E_{GSH}), as the major cytoplasmic anti-oxidant, the rates of ROS production, and mitochondrial activity using multi-channel four-dimensional (*x,y,z,t*) confocal imaging of Grx1-roGFP2 and fluorescent reporters during spore germination, appressorium formation and infection.
- High levels of mitochondrial activity and ROS were localized to the growing germ tube and appressorium, but E_{GSH} was highly reduced and tightly regulated during development. Furthermore, germlings were extremely resistant to external H_2O_2 exposure *ex planta*. E_{GSH} remained highly reduced during successful infection of the susceptible rice cultivar CO39. By contrast, there was a dramatic reduction in the infection of resistant (IR68) rice, but the sparse hyphae that did form also maintained a similar reduced E_{GSH}.
- We conclude that *M. oryzae* has a robust anti-oxidant defence system and maintains tight control of E_{GSH} despite substantial oxidative challenge. Furthermore, the magnitude of the host oxidative burst alone does not stress the pathogen sufficiently to prevent infection in this pathosystem.

Introduction

Rice blast disease caused by *Magnaporthe oryzae* is a major global emerging infectious disease (EID) causing rice losses sufficient to feed 3–10.6% of the world's population 2000 calories a day for 1 yr (Fisher *et al.*, 2012). Infection starts with the germination of a three-celled spore on the host surface, producing a short germ tube that develops a domed infection structure, termed the appressorium (Wilson & Talbot, 2009). Development requires progression through a single cell cycle in the apical cell, followed by autophagy (Veneault-Fourrey *et al.*, 2006) and mobilization of storage reserves to fuel appressorium development (Thines *et al.*, 2000; Wang *et al.*, 2007; Patkar *et al.*, 2012a). The appressorium becomes melanized and builds up sufficient turgor pressure to drive an infection peg into the host epidermal cell (Howard *et al.*, 1991; Money & Howard, 1996; Wilson & Talbot, 2009). In a susceptible host, the infection hyphae ramify through the infected cell and then colonize adjacent cells through plasmodesmata (Kankanala *et al.*, 2007). In resistant varieties, infection is halted at the penetration stage or during early colonization, and is associated with a hypersensitive response (HR) (Torres, 2010; Heller & Tudzynski, 2011).

Plants respond to infection by the rapid production of reactive oxygen species (ROS) using membrane-bound NADPH oxidases (Marino *et al.*, 2012), or secreted peroxidases and amine oxidases (Bolwell *et al.*, 2002), as part of the general pathogen-associated molecular pattern (PAMP)-triggered immunity (PTI) or more specific effector-triggered immunity (ETI) responses (Yoshioka *et al.*, 2009; Torres, 2010; Heller & Tudzynski, 2011; Thomma *et al.*, 2011; Tudzynski *et al.*, 2012). ROS produce cross-linked plant wall polymers to form a barrier to penetration, attack the pathogen directly or act as diffusible signals in the plant to up-regulate pathogenesis-related proteins (Lamb & Dixon, 1997; Shetty *et al.*, 2008; Heller & Tudzynski, 2011). In a resistant host challenged by an avirulent pathogen, the initial ROS burst is followed by a longer lasting second phase, culminating in an HR (Mur *et al.*, 2008) and programmed cell death (Levine *et al.*, 1994). In biotrophic and hemibiotrophic fungi, such as *M. oryzae*, which require living hosts, the first phase of ROS production still occurs, but the second phase is suppressed in susceptible hosts, probably through the secretion of effectors through the biotrophic interfacial complex (Valent & Khang, 2010), which re-programme the metabolic pathways involved in host ROS production (Parker *et al.*, 2009).

Fungi require effective anti-oxidant defence systems to operate in such an environment in which oxidative stress is endemic. An abundant array of anti-oxidant genes exists in the *M. grisea* genome (Dean *et al.*, 2005; Egan & Talbot, 2008; Morel *et al.*, 2008), although less is known about the low-molecular-weight anti-oxidants in fungi more generally (Georgiou & Petropoulou, 2001; Patsoukis & Georgiou, 2004). Nevertheless, the need to detoxify host ROS can be inferred from fungal mutants that lack critical anti-oxidant enzymes, or from treatments that manipulate ROS levels during infection. Thus, *Magnaporthe* mutants in glutathione peroxidase, Hyr1, are less tolerant to ROS and produce smaller lesions on susceptible plants (Huang *et al.*, 2011). Likewise, several redox-sensitive transcription factors, such as MoAP1 (Guo *et al.*, 2011) and MoSwi6 (Qi *et al.*, 2012), and the defence suppressor Des1 (Chi *et al.*, 2009) increase resistance to external H_2O_2, with mutants showing reduced pathogenicity and pleiotropic changes in gene expression, including decreases in extracellular peroxidases. Conversely, the reduction of external ROS levels during infection through the addition of exogenous catalase (Tanabe *et al.*, 2009) or the NADPH oxidase inhibitor diphenylene iodonium (DPI) (Chi *et al.*, 2009) promotes increased infection of compatible and incompatible strains, or particular H_2O_2-sensitive mutants.

Nevertheless, the significance of other putative anti-oxidant defences is less clear. Thus, the deletion of the major secreted *M. oryzae* catalase-peroxidase, CPXB, increases sensitivity to exogenous H_2O_2, but does not affect overall pathogenicity (Tanabe *et al.*, 2011). Likewise, mutants lacking the large subunit catalase, catB, are less pathogenic, but through changes in normal fungal wall strengthening rather than by detoxification of host-derived H_2O_2 (Skamnioti *et al.*, 2007). Furthermore, expression data from transcriptome profiling show that the genes most highly up-regulated in *M. oryzae* during infection are related to nutrient limitation rather than oxidative stress (Mathioni *et al.*, 2011). This echoes results for the necrotrophic fungus *Botrytis cinerea*, in which the redox-sensitive AP1 transcription factor homologue, Bap1, is critical for ROS resistance *in vitro*, but deletion mutants do not show reduced virulence, and the suite of downstream target genes regulated by Bap1 is not highly expressed *in planta* (Temme & Tudzynski, 2009). The authors concluded that *B. cinerea* does not suffer H_2O_2 stress *in planta*, in contrast with conventional expectations of the role of the oxidative burst in restricting infection (Temme & Tudzynski, 2009), but actually exploits the host HR as part of its necrotrophic habit (Govrin & Levine, 2000).

The interplay between ROS and anti-oxidant defences is further complicated, as ROS are produced by normal cell metabolism and act as signalling intermediates associated with key transitions in microbial development, including differentiation, sexual reproduction, conidiation, spore germination, secondary metabolism and apoptosis (Hansberg & Aguirre, 1990; Aguirre *et al.*, 2005; D'Autreaux & Toledano, 2007; Gessler *et al.*, 2007; Takemoto *et al.*, 2007; Egan & Talbot, 2008; Scott & Eaton, 2008; Shetty *et al.*, 2008; Aguirre & Lambeth, 2010; Heller & Tudzynski, 2011; Tudzynski *et al.*, 2012). Indeed, Hansberg and Aguirre originally proposed that microbial cell differentiation might be triggered by transient oxidation that initiates a shift between developmental states (Hansberg & Aguirre, 1990; Aguirre *et al.*, 2005). ROS production is well documented during pre-penetration in *M. oryzae*, whereas scavenging external ROS reduces infection rates, all consistent with a role for ROS in the developmental programme (Egan *et al.*, 2007; Ryder *et al.*, 2013).

The major cytoplasmic anti-oxidant that mitigates oxidative stress in eukaryotes is glutathione (Belozerskaya & Gessler, 2007; Gessler *et al.*, 2007; Meyer, 2008). However, little is known about the glutathione concentrations and dynamics in filamentous fungi. Tools are now available to quantify both the amount of glutathione *in vivo* (Fricker *et al.*, 2000; Meyer & Fricker, 2000, 2008; Fricker & Meyer, 2001; Meyer *et al.*, 2001) and the electrochemical potential of the reduced glutathione:oxidized glutathione (GSH:GSSG) redox couple (E_{GSH}) using transgenic redox green fluorescent protein (GFP)-based reporters (Dooley *et al.*, 2004; Schwarzlander *et al.*, 2008; Meyer & Dick, 2010). In particular, Grx1-roGFP2 includes a glutaredoxin (Grx) subunit to improve the response kinetics (Gutscher *et al.*, 2008) and is known to function correctly in fungi (Heller *et al.*, 2012). Notably, the difference in the mid-point potential between the Grx1-roGFP redox couple and the GSH:GSSG redox couple makes Grx1-roGFP exquisitely sensitive to small changes in the degree of glutathione oxidation from the highly reduced level typically found *in vivo* (Meyer & Dick, 2010). Thus, in this article, we use multi-parameter live-cell confocal imaging and a range of fluorescent reporters to determine, first, whether there is physiological evidence for the redox control of early development in *M. oryzae* mediated by changes in E_{GSH}; second, what is the relative level of endogenous ROS production during development; third, what is the capacity of the glutathione anti-oxidant system to deal with an imposed oxidative burst, as might be encountered during host infection; and fourth, what impact is exerted by the actual host oxidative burst on E_{GSH} *in vivo* during susceptible and resistant interactions.

Materials and Methods

Fungal strains and growth conditions

Wild-type *Magnaporthe oryzae* strain Guy11 and transgenic Grx1-roGFP2 strain were cultured at 24°C under a 14 h : 10 h light : dark cycle according to Talbot *et al.* (1993). Spores were scraped from 10-d-old cultures, filtered through two layers of miracloth (Calbiochem, San Diego, CA, USA), washed with sterile demineralized water (dH_2O), pelleted by centrifugation (4000 ***g***, 5 min) and resuspended in dH_2O at a spore concentration of *c.* 5×10^5 ml^{-1}.

Cloning and generation of pRP27::Grx1:roGFP2 strains

Standard molecular techniques and cloning (Ausubel *et al.*, 1999) were used to prepare the pRP27::Grx1:roGFP2 construct. A set of transformation vectors was created based on pUCAP (van Engelen *et al.*, 1995), which carries pUC19 MCS and unique *Asc*I and *Pac*I sites.

The bialophos resistance marker (GenBank AF013602) was removed as a *Sal*I fragment from pGEMTEasy-BAR vector (Samalova *et al.*, 2013), blunt-ended and cloned into the pUCAP *Sac*I site, and digested with *Ecl*136II to re-create the *Sal*I sites and generate pUCAP-BAR. The polyadenylation signal pATrpC was amplified from pMJK142.2 (kindly provided by Professor N. Talbot, Exeter, UK) using P1 and P2 primers (Table 1), digested with *BamH*I and *Kpn*I, and cloned into the same restriction sites of the pUCAP-BAR vector, creating pUCAP-pATrpC/BAR, and confirmed by sequencing. The *M. oryzae* promoter RP27 (Czymmek *et al.*, 2002) was amplified from Guy11 genomic DNA using P3 and P4 primers (Table 1). Grx1-roGFP2 was amplified from pBinCM-GRX1-roGFP2 (Gutscher *et al.*, 2008) using P5 and P6 primers (Table 1). The two fragments were fused by overlapping PCR using primers P3 and P6. The PCR product was digested with *Asc*I and *Bam*HI, and cloned into the same restriction sites of pUCAP-pATrpC/BAR. The final pUCAP-pRP27::Grx1:roGFP2 vectors were confirmed by sequencing, and digested with *Pac*I, before transformation into *M. oryzae*.

DNA-mediated protoplast transformation (Talbot *et al.*, 1993) was used to generate putative transformants that were selected on defined complex medium supplemented with 60 μg ml^{-1} bialophos (Goldbio, St Louis, MO, USA). They were subjected to PCR using P6 and P7 primers (Table 1) to confirm the presence of Grx1-roGFP2. The most fluorescent line was chosen for this study.

Leaf sheath assays

Rice cultivar CO39 (susceptible) and IR68 (resistant; Gilbert *et al.*, 2006; Hubbart *et al.*, 2007) were grown at 24°C, 80% humidity in a 14 h light cycle. Leaf sheaths of 2–3-wk-old plants were inoculated with 20–40 μl of conidial suspension (5×10^5 spores ml^{-1}) and placed onto water agar (2% w/v) in the growth chamber. Leaf sheaths were mounted using double-sided tape, sliced open with a razor blade and imaged by confocal microscopy.

Confocal imaging

Time series were collected at 30–120-s intervals for 15–45 min, as *z*-stacks of 5–10 sections taken at 0.67–3-μm intervals apart, using a Zeiss 40× 1.2 NA PlanApo water-immersion lens. Pixel sizes were 0.22–0.44 μm in *x* and *y*. Pinhole settings were adjusted individually for each channel to give an estimated optical section thickness of 2–3 μm (*c.* 2–3 Airy units) for each of the wavelength combinations. This provided some degree of optical sectioning, but with sufficient signal-to-noise to allow long-term physiological measurements with low laser intensities. Laser power was measured from the defocused beam using a Newport 1815-C power meter (Newport Corp., Irvine, CA, USA). Values ranged from 1.3 to 7.3 μW. Non-confocal bright-field images were collected simultaneously with a transmission detector.

Coverslips were placed in a perfusion chamber mounted on a Zeiss LSM510META confocal microscope and Grx1-roGFP2 (emission, 505–530 nm) was imaged with 405- and 488-nm excitation in multi-track mode with line switching. Autofluorescence was measured in parallel (excitation, 405 nm; emission, 435–485 nm).

Table 1 List of primers (5′–3′)

P1:	AAAAGGATCCGCGGCCGCTACGTAATTTAAATACTTAACGTTACTGAAATCATCAAACAG
P2:	AAAAGGTACCGGCCCTAGGGGCCAGATGTGGAGTGGGCGCTTACACAG
P3:	AAAAGGCGCGCCATAAATGTAGGTATTACCTGTACATTTTATTTATTC
P4:	CATTTTGAAGATTGGGTTCCTACGAAAGC
P5:	CGCCTAACAGATCTTGGCTTTCGTAGGAACCCAATCTTCAAAATGGCTCAAGAGTTTGTGAACTGC
P6:	AAAAGGATCCTTACTTGTACAGCTCGTCCATGCCG
P7:	AAAAACCATGGCTCAAGAGTTTGTGAACTGC

Dual-excitation confocal ratiometric analysis

Image time series were imported into a custom MatLab (The MathWorks, Natick, MA, USA) program (available on request from M.D.F.). *z*-stacks were averaged in *x*, *y* and *z* using a $3 \times 3 \times 3$ or $5 \times 5 \times 3$ kernel. The *z*-position of the brightest pixel in a maximum *z*-projection of the main channel of interest was used to extract the corresponding *z*-pixel for each of the other wavelengths to give the average intensity from all channels in a volume around the same, bright pixel in *x*, *y* and *z*. The resultant image is termed an optimum plane projection. The average background intensity was measured adjacent to the spores on coverslips, or in the vacuole for *in planta* experiments, and subtracted. The autofluorescence bleed-through contribution into the Grx1-roGFP2$_{405}$ channel was measured from Guy11 spores, and the corresponding scaling factor was used to subtract autofluorescence from the Grx1-roGFP2$_{405}$ image. Ratio images were calculated on a pixel-by-pixel basis as I_{405}/I_{488}. Pixels with intensity values < 2 standard deviation units above background, within 10% of saturation, or where the local coefficient of variance (CV) in a 3×3 neighbourhood was above 20%, were masked.

For pseudo-colour display, the masked ratio was coded by hue on a spectral colour scale ranging from blue (most reduced) to red (most oxidized), with the limits set by the *in situ* calibration. Individual germlings were segmented using Otsu's method (Otsu, 1979) and the extracted images were rotated to give a montage of selected time points for display.

Quantitative measurements were calculated as the ratio of the mean intensity from each channel from the regions of interest. *In situ* calibration was performed using 10 mM dithiothreitol (DTT) for 5 min, followed by 100 mM H_2O_2 for 5 min, to drive Grx1-roGFP2 to a highly reduced and highly oxidized form, respectively. The degree of oxidation ($OxD_{Grx1\text{-}roGFP2}$) and pH-corrected GRx1-roGFP redox potential ($E_{Grx1\text{-}roGFP2}$) were calculated according to Schwarzlander *et al.* (2008), assuming a mid-point potential ($E^{\circ}_{Grx1\text{-}roGFP2}$) of −280 mV (Dooley *et al.*, 2004; Hanson

et al., 2004; Gutscher *et al.*, 2008; Morgan *et al.*, 2011, 2013) and a cytoplasmic pH of pH 7.6 (Parton *et al.*, 1997; Hesse *et al.*, 2002).

For population studies, a Gaussian mixture model (GMM) with two to four components was fitted to the pixel intensities at each wavelength, with the contribution of each pixel weighted by the average intensity. Contour maps from the GMM were overlaid on two-dimensional histograms generated from the weighted pixel intensities. The intensity value of the Gaussian peak at each wavelength was used to calculate the ratio, and hence degree of Grx1-roGFP2 oxidation, $E_{Grx1\text{-}roGFP2}$ and E_{GSH}, respectively, for each component.

Estimation of cytosolic glutathione concentrations in spores of *M. oryzae*

The available glutathione pool was labelled *in situ* following conjugation to 100 μM monochlorobimane (MCB) to give a fluorescent glutathione–bimane (GSB) conjugate (excitation, 405 nm; emission, 435–485 nm) according to Fricker *et al.* (2000), Fricker & Meyer (2001), Meyer *et al.* (2001) and Meyer & Fricker (2002). Calibration solutions were made by reacting 10 mM monobromobimane with an excess of GSH. As GSB was transported into the vacuole, estimation of the initial cytosolic GSH concentration required correction for the cytoplasmic : vacuolar volume ratio. GSB signals from overlapping vacuoles were separated using a three-dimensional watershed and the regional maximum intensity for each vacuole was determined. Each vacuolar volume was estimated as the number of pixels above the 50% threshold between this local maximum and the background (White *et al.*, 1996; Errington *et al.*, 1997).

The cytoplasmic volume was the difference in volume between the vacuole volume and the total volume of the spore compartment, estimated after labelling the cell wall with 15 μM propidium iodide (PI; excitation, 543 nm; emission, 585–6150 nm). Three-dimensional *z*-stacks were rotated in *x, y* and tilted in *z* to align the long axis of the spore with the *x*-axis. The median wall outline was segmented from the maximum z-projection, filled and the volume was measured assuming radial symmetry from the cylinder of rotation about the *x*-axis.

Measurement of ROS levels and mitochondrial activity

Spores were labelled with 0.2–2.5 μM 2′,7′-dichlorodihydrofluorescein diacetate (H_2DCFDA) (excitation, 488 nm; emission, 500–530 nm) or CellROX Deep Red (CRDR, 2.5 μM) simultaneously with tetramethyl rhodamine methyl ester (TMRM, 100 nM) for mitochondria, and Grx1-roGFP2 for GSH redox potential, using quadruple excitation with paired line switching at 405 and 633 nm, and 488 and 543 nm. Emission wavelengths were 435–485, 500–530 and 657–721 nm for wall autofluorescence, oxidized Grx1-roGFP2 and CRDR, respectively, and 500–530 nm and 561–603 nm for reduced Grx1-roGFP2 and TMRM, respectively. A non-confocal, bright-field transmission image was collected in parallel.

Results and Discussion

Grx1-roGFP2 reports E_{GSH} in *M. oryzae*

To measure the electrochemical potential of the GSH:GSSG redox couple (E_{GSH}) *in vivo*, Grx1-roGFP2 (Gutscher *et al.*, 2008; Heller *et al.*, 2012) was expressed from the ribosomal protein RP27 promoter in *M. oryzae* and visualized using confocal ratio imaging (Meyer & Fricker, 2008; Schwarzlander *et al.*, 2008; Morgan *et al.*, 2011). Spores expressing Grx1-roGFP2 showed normal rates of germ tube extension, swelling and appressorium development (e.g. Fig. 1e), and were fully pathogenic on barley and rice (data not shown). Fluorescence was observed in the cytoplasm and, to a lesser extent, vacuoles (Fig. 1a–d, Supporting Information Video S1). Excitation at 405 nm increased with probe oxidation, but also caused autofluorescence bleed-through into the Grx1-roGFP2$_{405}$ channel, typically around the site of germ tube emergence and the appressorium wall. To correct the Grx1-roGFP2$_{405}$ images, autofluorescence images were collected at 435–485 nm (Fig. 1f), scaled by an empirically determined bleed-through correction factor and subtracted. Localization of Grx1-roGFP2 in vacuoles was not expected, but parallels other cytoplasmically expressed fluorescent proteins in *M. oryzae* germlings, such as mCherry (data not shown, see also Czymmek *et al.*, 2002), and may reflect high levels of autophagy. Nevertheless, the Grx1-roGFP2 signal in both cytoplasmic and vacuolar compartments responded to *in situ* calibration (Fig. 1g,h). Changes in the Grx1-roGFP2 spectrum were visualized as pseudo-colour-coded ratio images, scaled to the minimum and maximum of these calibration values (Fig. 1i).

Grx1-roGFP2 responses were rapid, with oxidation by H_2O_2 within 1–2 min, and reversible, with spontaneous recovery to a reduced state after washout (Fig. 1j–l), and reduction with subsequent exposure to DTT (Fig. 1j–l). Although H_2O_2 caused bleaching of the probe (Fig. 1j,k), the ratio corrected for the changes in intensity (Fig. 1l), giving a dynamic range around four, similar to previous reports with the wavelength combinations used here (Gutscher *et al.*, 2008). It is notable that *M. oryzae* was very resistant to imposed oxidative loads, with 100 mM H_2O_2 needed to drive Grx1-roGFP2 to an oxidized state *in vivo*. Using this calibration, the degree of oxidation of cytoplasmic Grx1-roGFP2 ($OxD_{Grx1\text{-}roGFP2}$) was 10–12% in all three germling cells (Fig. 1m). Interestingly, vacuolar Grx1-roGFP2 still responded to calibration, with the same dynamic range, giving a value equivalent to 50–60% oxidation (Fig. 1d,k,l). $OxD_{Grx1\text{-}roGFP2}$ was converted to the redox potential ($E_{Grx1\text{-}roGFP}$) (Gutscher *et al.*, 2008; Schwarzlander *et al.*, 2008; Meyer & Dick, 2010) using a consensus mid-point potential ($E^{o\prime}_{Grx1\text{-}roGFP2}$) of −280 mV (Dooley *et al.*, 2004) and a cytoplasmic pH of pH 7.6, as measured in filamentous fungi (Parton *et al.*, 1997; Hesse *et al.*, 2002). With these assumptions, 10% oxidation of Grx1-roGFP2 equates to $E_{Grx1\text{-}roGFP2}$ of −316 mV. Assuming that $E_{Grx1\text{-}roGFP2}$ equilibrates with E_{GSH} (Morgan *et al.*, 2011), this requires tight regulation of GSSG at submicromolar concentrations (Meyer & Dick, 2010; Morgan *et al.*, 2013). Thus, we infer that Grx1-roGFP2 provides a rapid and highly sensitive readout *of* E_{GSH} in

M. oryzae, similar to previous reports for the necrotrophic fungus *B. cinerea* (Heller *et al.*, 2012). Nevertheless, high-resolution imaging is also required to separate signals from cytoplasm and vacuole.

The glutathione pool shows only slight shifts in the degree of oxidation during development

To determine whether there were shifts in glutathione oxidation associated with developmental transitions (Hansberg & Aguirre, 1990), we quantified $OxD_{Grx1\text{-}roGFP2}$ at different developmental stages, classified as: spores (0–0.5 h post-inoculation, hpi), germination (0.5–1 hpi), germ tube growth (1–2 hpi), germ tube swelling (2–3 hpi), appressorium formation (3–5 hpi) and appressorial melanization (5–8 hpi).

A highly reduced cytoplasmic Grx1-roGFP2 signal (< 5% oxidized) was measured during germination in all three spore cells (Fig. 2i), becoming slightly more oxidized (8–12%) as the germ tube developed at 1–2 hpi (Fig. 2a,b,i, see also Fig. 1). Ratios from the mid and basal cells were progressively dominated by the oxidized Grx1-roGFP2 vacuolar signal once appressoria started to form at 5 hpi (Fig. 2c,d,i), making it difficult to extract a clean cytoplasmic value. Absolute fluorescence intensities were also reduced from the basal and mid cells *c.* 8 hpi (Fig. 2e,f), and disappeared following isolation and autophagic cell death at 24 hpi (Fig. 2g,h). At this stage, the apical cell was more vacuolate, but the cytoplasmic probe was still responsive to calibration. The appressorium itself showed a highly reduced cytoplasmic Grx1-roGFP2 signal throughout development, with a characteristic ring of more oxidized vacuoles around the periphery (Fig. 2f,h,i). However, Grx1-roGFP2 in the melanizing appressorium (Fig. 2f) was protected from H_2O_2 calibration, with slower responses at 8 hpi and complete insensitivity to 100 mM H_2O_2 at 24 hpi (Fig. 2 h).

We infer that *M. oryzae* maintains a highly reduced cytoplasmic E_{GSH} during early development, and there was only very limited evidence that E_{GSH} increases during appressorium formation, indicative of a glutathione-mediated redox-associated developmental switch (Hansberg & Aguirre, 1990).

There are high levels of endogenous ROS production during development

In the absence of a host, E_{GSH} reflects the rate of detoxification of endogenous metabolic ROS. Previous measurements of ROS levels in *M. oryzae* have used the relatively non-specific probe

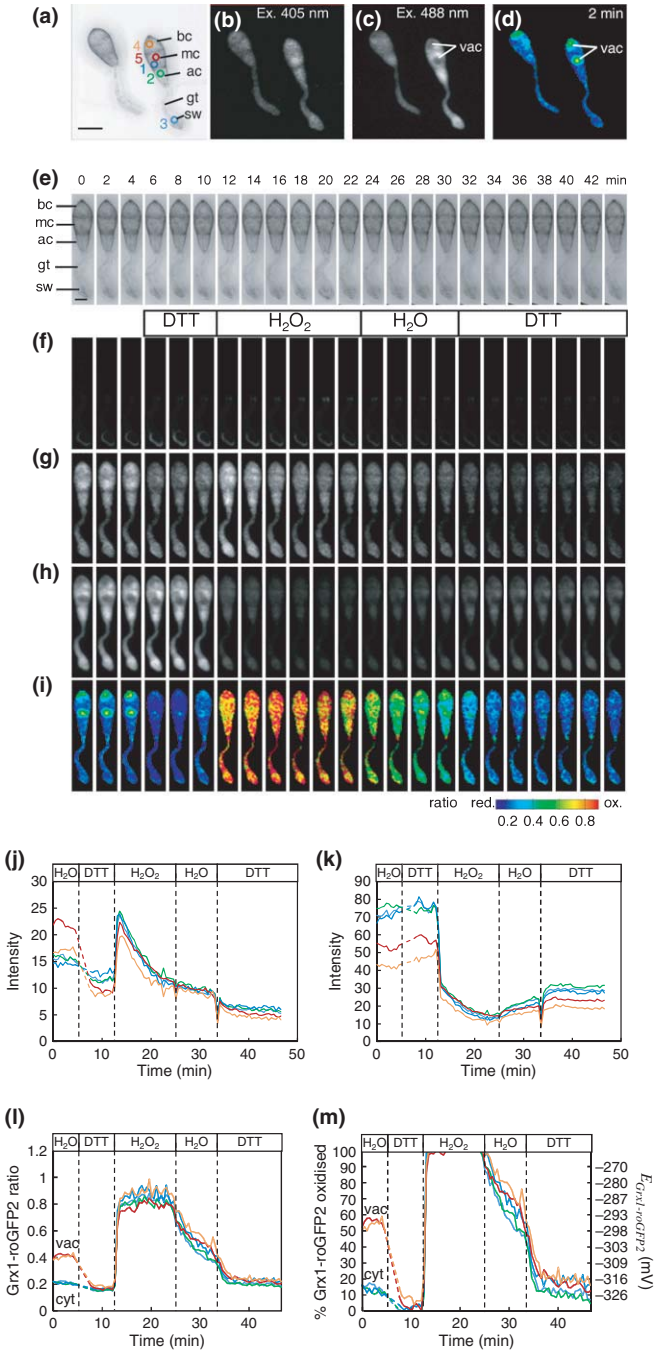

Fig. 1 Measurement of the redox potential of the glutathione pool in *Magnaporthe oryzae* germlings using recombinant Grx1-roGFP2. Germinating spores of *M. oryzae* (a, e) expressing Grx1-roGFP2 from the RP27 promoter were sequentially imaged with excitation at 405 nm (b, g) and 488 nm (c, h) as z-stacks with 2-μm spacing at 60-s time intervals, and analysed as optimum plane projections (g, h) after smoothing with a 3 × 3 averaging filter and correction for bleed-through from autofluorescence (f) in the 405-nm channel. Grx1-roGFP2 was located predominantly in the cytoplasm of the basal cell (bc), mid cell (mc) and apical cell (ac), including the germ tube (gt) and swelling germ tube tip (sw). Fluorescence was also observed in the vacuole (vac), particularly in the basal and mid cells. The degree of oxidation of Grx1-roGFP2 was visualized from the pseudo-colour-coded ratio (d, i), following calibration with 10 mM dithiothreitol (DTT) to reduce the internal pool, and 100 mM H_2O_2 to oxidize it (f–i). Although the cytoplasm showed a uniform low ratio, Grx1-roGFP2 ratios from the vacuoles indicated that the probe was more oxidized, but still capable of responding to calibration (i). To quantify the responses, the average fluorescence from regions of interest in (a) were measured for excitation at 405 nm (j) and 488 nm (k), with the corresponding ratio (l) and conversion to the degree of oxidation of the GRx1-roGFP probe ($OxD_{Grx1\text{-}roGFP2}$) (m). The corresponding redox potential ($E_{Grx1\text{-}roGFP2}$) was calculated using $E^{o\prime}_{Grx1\text{-}roGFP2} = -280$ mV and a cytoplasmic pH of pH 7.6 (m). Assuming that the Grx1-roGFP redox couple is in equilibrium with the GSH:GSSG redox couple, E_{GSH} is equal to $E_{Grx1\text{-}roGFP2}$. Bar, 10 μm. See Supporting Information Video S1 for a movie of the complete time series.

H_2DCFDA (Egan *et al.*, 2007; Kim *et al.*, 2009; Guo *et al.*, 2011; Huang *et al.*, 2011). H_2DCFDA is membrane permeant, but trapped intracellularly following the cleavage of the di-acetate groups by intracellular esterases, where oxidation gives fluorescent 2′,7′-dichlorofluorescein (DCF). Nevertheless, it is not clear to which ROS the probe responds, as intrinsic reaction rates with H_2O_2 and superoxide are low, and the probe is likely to be oxidized by more reactive species or through the action of peroxidases or haem proteins (Halliwell & Whiteman, 2004; Rhee *et al.*, 2010).

DCF fluorescence accumulated mainly in the cytoplasm in all three cells at all stages of germling development (Fig. 3b,d, see also Video S2). The greatest increase in fluorescence was observed in the mid cell (Fig. 3e,f), at about twice the rate in the other cells. Significant DCF also accumulated in the appressorium wall (Fig. 3d,f, see also Video S2). These data are similar to previous reports of DCF staining in conidia and in septal cell walls before germination, followed by labelling in germ tubes and a burst during appressorium formation, which might reflect the activity of the Nox1 NADPH oxidase (Egan *et al.*, 2007; Ryder *et al.*, 2013). However, this would also imply that there was sufficient de-esterified H_2DCF in the apoplast to react with externally produced ROS.

Washout of the labelling medium led to rapid loss of the wall-associated label, consistent with free dye in the apoplast (Fig. 3d, f). However, there was also substantial loss of cytoplasmic fluorescence in all three cell types, together with some recovery in the appressorial wall (Fig. 3d,f). We infer that DCF is either very membrane permeant in *M. oryzae*, or there is an additional plasma membrane xenobiotic detoxification system, which would also explain the inverse kinetics of cytoplasmic and wall signals during washout (Fig. 3d,f). Previously, we have reported a similar phenomenon for the NO reporter diaminorhodamine-4M (DAR-4M) in *M. oryzae* (Samalova *et al.*, 2013). Indeed, *Magnaporthe* is well endowed with potential transporters, with 50 members of the ATP-binding cassette (ABC) transporter family and 251 members of the major facilitator superfamily (MFS)

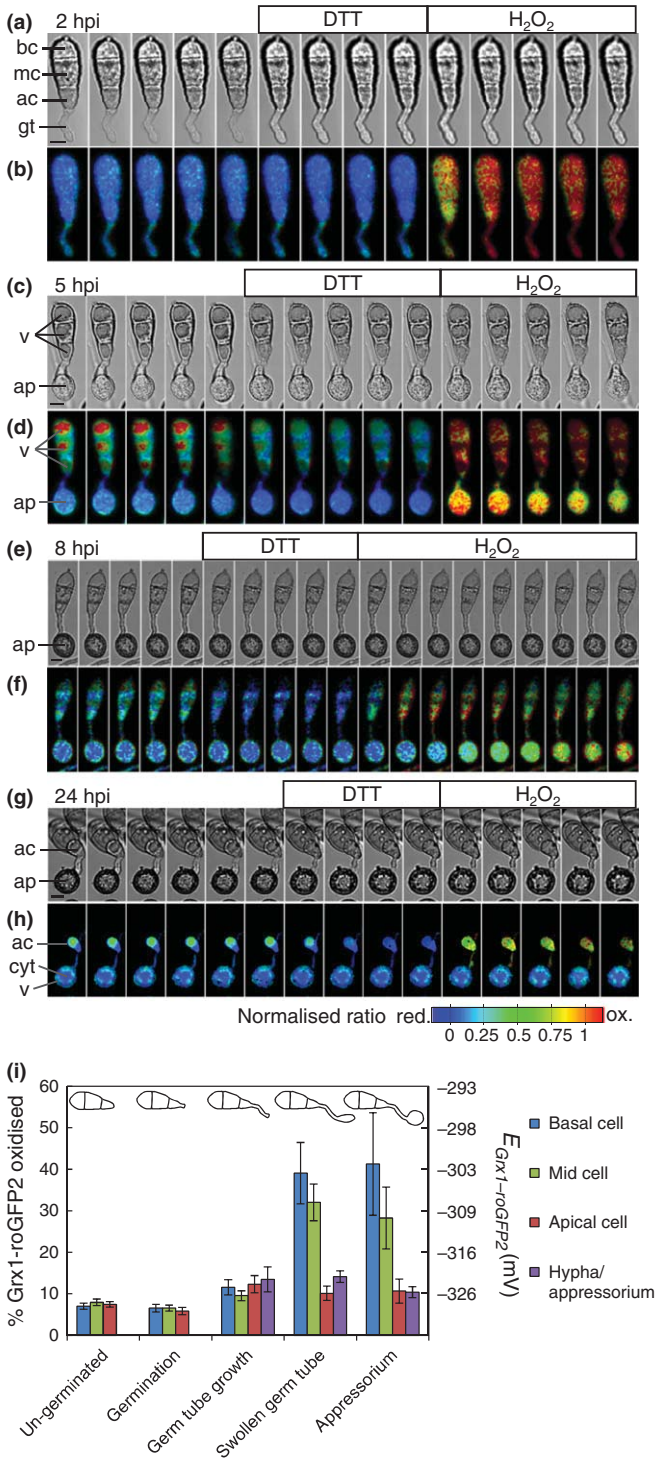

Fig. 2 Glutathione redox potential during development in different cell types of *Magnaporthe oryzae*. The degree of oxidation of Grx1-roGFP ($OxD_{Grx1\text{-}roGFP2}$) was calculated for each cell type in spores and developing germlings, following calibration with dithiothreitol (DTT) and H_2O_2. $OxD_{Grx1\text{-}roGFP2}$ was low in un-germinated and germinating spores, with average values of *c.* 6% ($n = 15$) and 4% ($n = 12$), respectively), in each cell type (i), but rose slightly to *c.* 8–12% during germ tube growth (a, b, i, $n = 10$). This corresponds to a shift of only a few millivolts (mV) in redox potential (i). Around 3–5 h post-inoculation (hpi), when germ tubes began to swell and form appressoria, the signal from the basal cell (bc) and mid cell (mc) was dominated by the vacuole, with a corresponding higher resting level of oxidation (c, d, i, $n = 13$), that prevented the measurement of a true cytoplasmic ratio. At 8 hpi, the appressorium only responded slowly to the calibration solutions, even with extended incubation (e, f, $n = 9$). Signals from the basal cell and mid cell were weak (f), and much more oxidized (i). By 24 hpi, when the appressorium was melanized (g), there was essentially no signal from the basal or mid cell, whereas the apical cell started to become vacuolated. Grx1-roGFP2 in the cytoplasm in the appressorium remained highly reduced (*c.* 8% oxidized), but was *c.* 40% oxidized in the small ring of vacuoles around the periphery (h). The signal in the apical cell still responded to calibration (h). However, Grx1-roGFP2 in the appressorium was effectively insulated from the calibration solutions at this developmental stage (h). Fluorescent images are shown as optimum plane projections of each z-stack (a–f) or every other z-stack (g, h), following smoothing with a $3 \times 3 \times 3$ spatial average and autofluorescence correction, from a multi-channel (x,y,z,t) four-dimensional image series collected at 60-s intervals. The bright-field image was a minimum projection of the non-confocal transmission images collected in parallel. ac, apical cell; ap, appressorium; cyt, cytoplasm; gt, germ tube; v, vacuole. Results are presented as mean ± SEM. Bars, 5 μm.

New Phytologist

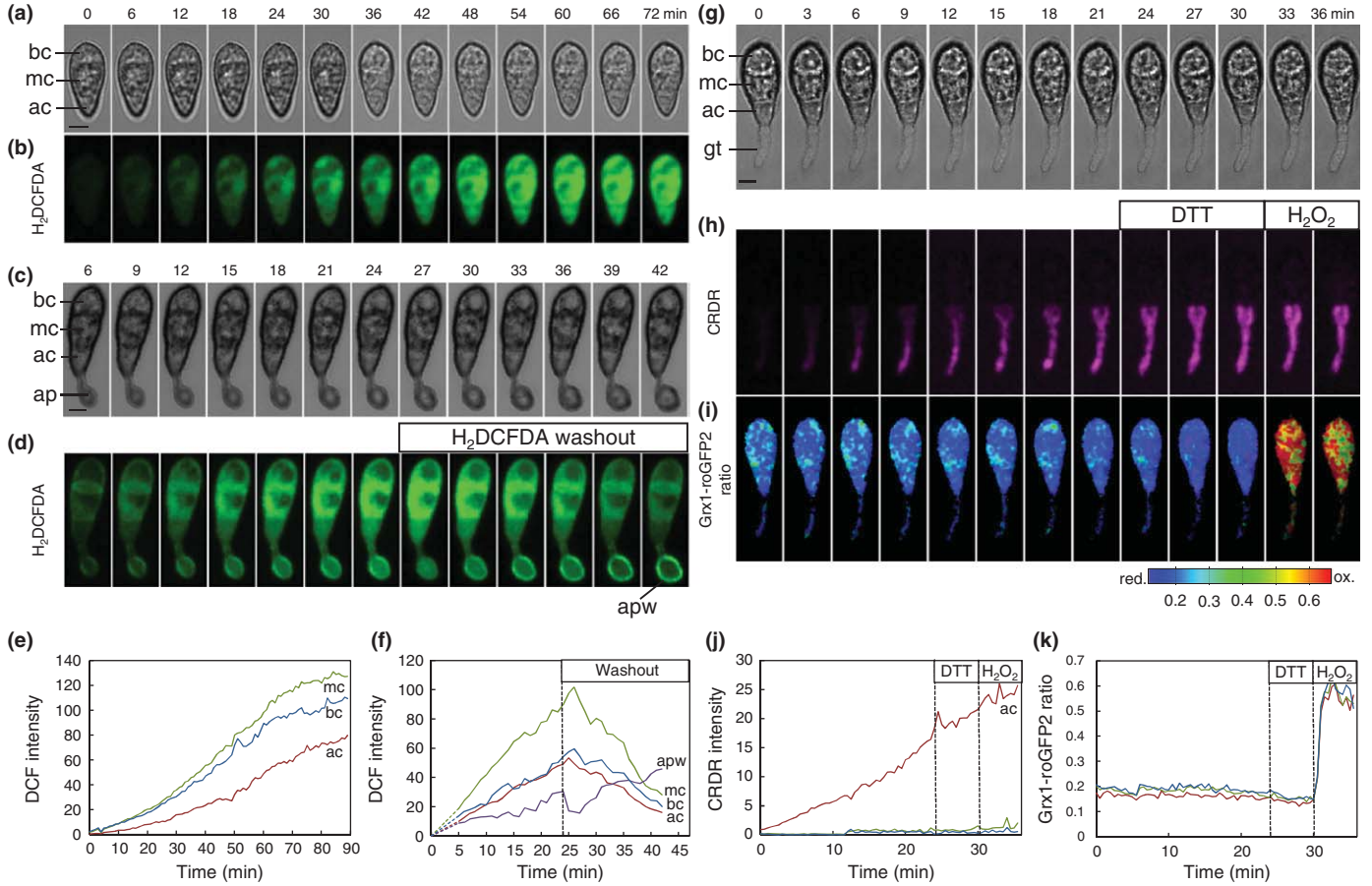

Fig. 3 Endogenous reactive oxygen species (ROS) production during development in *Magnaporthe oryzae*. Germlings of *M. oryzae* were labelled with 2′,7′-dichlorodihydrofluorescein diacetate (H_2DCFDA), as a non-specific reporter for ROS, at different stages of development. Fluorescent signals increased in all three cell types during germination (a, b, e) and appressorium formation (c, d, f), with signal also appearing in the appressorium cell wall (apw) (d, f). In the continuous presence of dye in the medium, labelling rates showed some sigmoidicity during germination (e), but were approximately linear at subsequent time points (f), with the highest rate in the mid cell (mc). However, replacement of the dye loading solution led to rapid loss of signal from the appressorium cell wall, followed by the apical cell (ac) with a delay of *c*. 1 min, and then the mid (mc) and basal (bc) cells after 2–3 min (d, f). CellROX Deep Red (CRDR) was used as an alternative ROS sensor as it can be used in conjunction with Grx1-roGFP2 (g–k). CRDR showed strong labelling of punctate tubular structures in the apical cell (g, h) that increased linearly over time (j), with only weak diffuse signal from the other cells in the germling (h, j). The ratio from Grx1-roGFP2 was close to a fully reduced state (i, k). Fluorescence images are shown as maximum (b,d) or optimum plane (h,i) z-projections, following smoothing with a 3 × 3 × 3 spatial average, of every third (a–d) or sixth (g–i) z-stack from multi-channel four-dimensional (*x*,*y*,*z*,*t*) images collected at 60- or 30-s intervals, respectively. Bright-field images are mid-sections from the non-confocal transmission images collected in parallel. Bars, 5 μm. See Video S2 for a movie of the complete time series.

(Coleman & Mylonakis, 2009). Furthermore, several of these transporters are up-regulated during appressorium formation (Oh *et al.*, 2008), under stress treatments or *in planta* (Mathioni *et al.*, 2011), and are required for pathogenicity (Urban *et al.*, 1999; Sun *et al.*, 2006; Patkar *et al.*, 2012b), possibly to protect against the buildup of peroxides and oxidative damage (Sun *et al.*, 2006).

Given our concerns over H_2DCFDA localization and specificity, we also examined the more sensitive, specific and photostable long-wavelength ROS probe CRDR. CRDR showed a time-dependent increase in fluorescence in *M. oryzae* spores, but, by contrast with H_2DCFDA, CRDR labelled discrete punctate structures, predominantly in the apical cell (Fig 3h,j). Despite this apparent asymmetric ROS production, simultaneous imaging with Grx1-roGFP2 showed a consistent low ratio in all three cell types (Fig. 3k). We speculate that CRDR might highlight mitochondrial ROS production, and probably reacts with superoxide rather than H_2O_2, given the lack of response to H_2O_2 addition (Fig. 3k).

Mitochondria show different activity in each germling cell type during development

To investigate whether the increase in CRDR fluorescence principally reflects the high level of ROS produced by mitochondrial activity (Schwarzlander & Finkemeier, 2013), we tested whether the punctate CRDR structures co-localized with active mitochondria, identified by potential-dependent accumulation of TMRM, and whether the mitochondria were differentially active in the different spore cells. In addition, we examined whether there were any changes in mitochondrial ROS production associated with developmental switches, particularly as mitochondria are involved

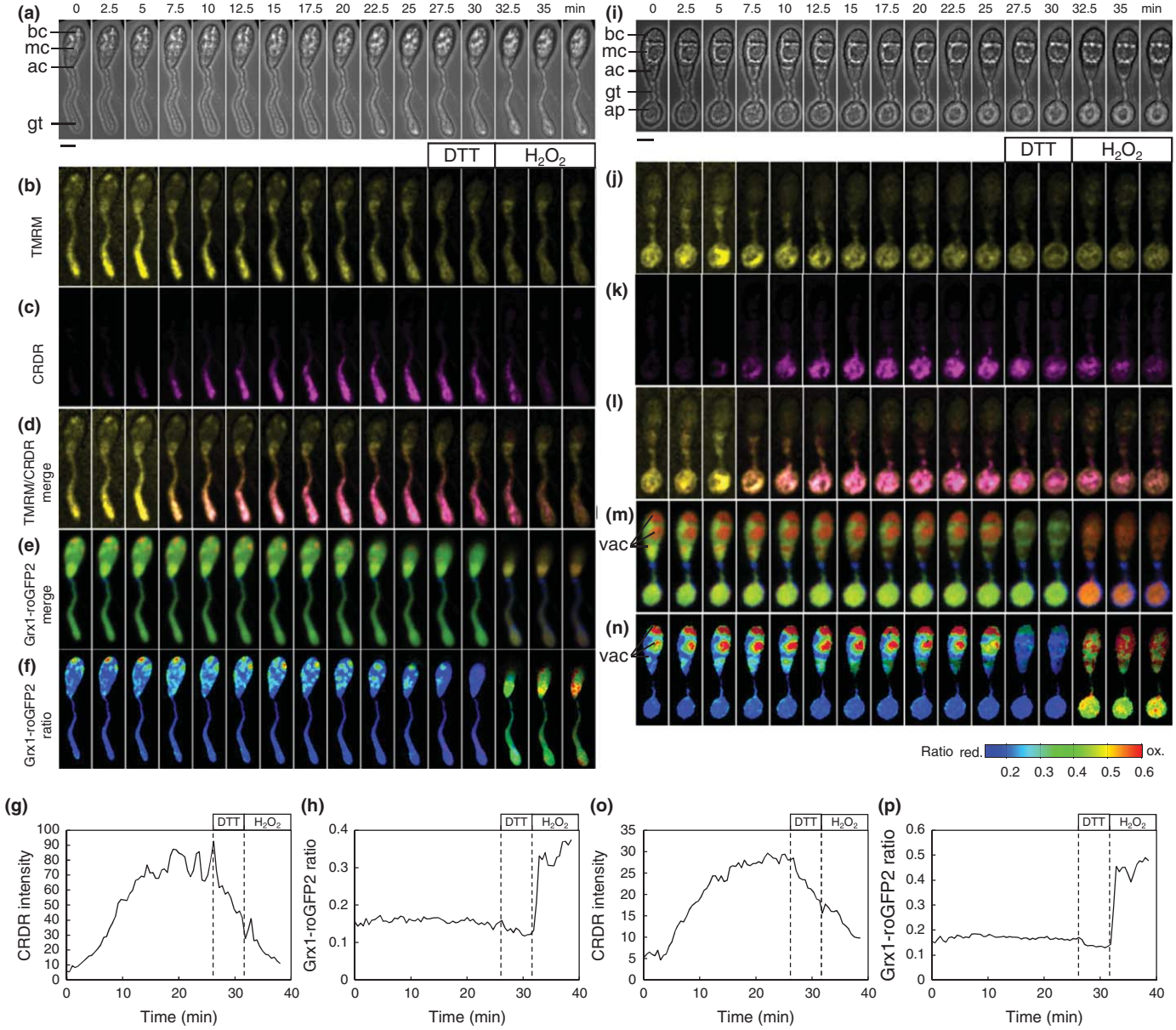

Fig. 4 Simultaneous measurement of reactive oxygen species (ROS), mitochondrial membrane potential and glutathione redox potential in germlings of *Magnaporthe oryzae*. Mitochondrial activity was measured using membrane potential partitioning of tetramethyl rhodamine methyl ester (TMRM) (excitation, 543 nm; emission, 561–603 nm) during germ tube growth (a, b) or appressorium formation (i, j). ROS were visualized in parallel with CellROX Deep Red (CRDR; excitation, 633 nm; emission, 657–721 nm) (c, k). Levels of ROS increased linearly in the cytoplasm of all three cells to a low level, but much more pronounced accumulation was observed in punctate structures in the apical cell and growing germ tube (b, g) or the appressorium (j,o). The punctate structures labelled by CRDR overlapped with the TMRM signal (d, l), from which we infer that CRDR predominantly reports mitochondrial ROS in this system. Cells also expressed Grx1-roGFP2, colour coded as Grx1-roGFP2$_{405}$ in red, Grx1-roGFP2$_{488}$ in green and autofluorescence in blue (e, m). The redox potential of the glutathione pool was measured simultaneously using ratio imaging (excitation, 405 nm, 488 nm; emission, 500–525 nm) following autofluorescence bleed-through correction (f, n), and showed a consistently reduced cytoplasmic redox potential during germ tube swelling (f, h) and appressorial formation (n, p). During the Grx1-roGFP2 calibration, the CRDR signal was also lost (g, o). Fluorescent images are shown as optimum plane projections of every fifth *z*-stack, following smoothing with a 3 × 3 × 3 spatial average, autofluorescence correction and low signal masking, from a multi-channel (*x*,*y*,*z*,*t*) four-dimensional image series collected at 30-s intervals. The bright-field image was a maximum brightness projection of the non-confocal transmission images collected in parallel. ac, apical cell; ap, appressorium; bc, basal cell; mc, mid cell; gt, germ tube. Bars, 5 μm. See Videos S3 and S4 for movies of the complete time series.

in autophagic cell death (Scherz-Shouval & Elazar, 2011), which forms part of the developmental programme in *M. oryzae* (Veneault-Fourrey *et al.*, 2006; Talbot & Kershaw, 2009).

TMRM labelling revealed highly motile tubular mitochondria, particularly in the apical cell during germ tube growth (Fig. 4b) and appressorium formation (Fig. 4j). In parallel, CRDR showed a time-dependent increase in punctate fluorescence in swelling germ tubes (Fig. 4c, see also Video S3) and developing appressoria (Fig. 4k, see also Video S4), which overlapped the TMRM signal (Fig. 4d,l). Lower levels of TMRM and CRDR

New Phytologist

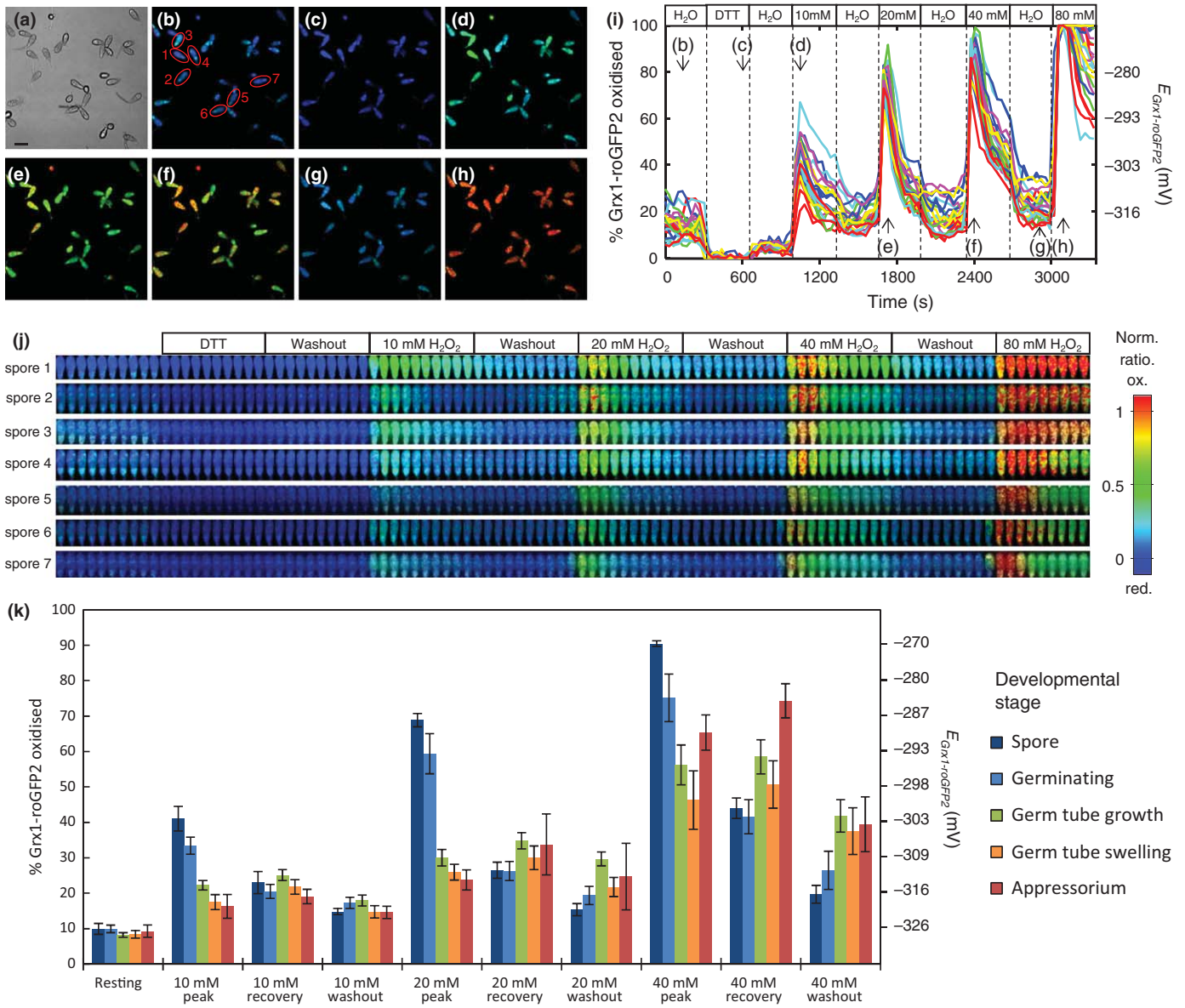

Fig. 5 Response of the redox potential of the glutathione pool to transient oxidative stress in germlings of *Magnaporthe oryzae*. The response to oxidative bursts was measured from the apical cell in populations of developing germlings at 2 h post-inoculation (hpi) (a) during transient exposure to increasing concentrations of H_2O_2. Cytoplasmic Grx1-roGFP2 was *c.* 10% oxidized in resting cells (b), although there was some variation between germlings (i), possibly reflecting the difficulty in unambiguously selecting cytoplasmic regions of interest in low magnification images. Dithiothreitol (DTT) was used initially to reduce the total glutathione pool and set the calibration minimum (c) and significantly reduced the variation in resting level after washout (i). A 5-min exposure to 10 mM H_2O_2 elicited strong transient oxidation of Grx1-roGFP2 to a peak at *c.* 35% (d), which recovered to a varying extent, even during continued exposure to H_2O_2 (i). Recovery was improved following washout of the H_2O_2 to *c.* 20% (i). The kinetics showed considerable variation between individual germlings in the duration of the response, and the extent of the recovery (i). A representative set of germling images, outlined in (b), is shown in (j), ordered with increasing tolerance to H_2O_2 shocks. Subsequent shocks with 20 mM (e) and 40 mM (f) gave more pronounced initial peaks, but the germlings were still able to recover to a considerable extent, even in the continued presence of H_2O_2 (i–k). Thus, following washout at the end of the pulse series (g), before the final calibration with 80 mM H_2O_2 (h), the level of Grx1-roGFP2 oxidation averaged *c.* 25%, or a shift in $E_{Grx1\text{-}roGFP2}$ from −326 to −312 mV for the experiment shown here (i–k). Germ tubes continued to grow following 10 and 20 mM shocks, but slowed or ceased to elongate at 40 mM and above. To determine whether there was any variation in response with development, germlings were grouped by developmental stage from five separate experiments and $OxD_{Grx1\text{-}roGFP2}$ was measured at the peak, recovery and washout phases during the pulse sequence (k). The corresponding values for $E_{Grx1\text{-}roGFP2}$, and hence E_{GSH}, are given assuming $E^{o\prime}_{Grx1\text{-}roGFP2} = -280$ mV and a cytoplasmic pH of pH 7.6. Both the initial peak and the recovery were most marked in spores and during germination, whereas transients in more advanced stages were less dramatic, but also showed less spontaneous recovery (k). Results are shown as mean ± SEM for: $n = 7$, spores; $n = 11$, germinating 1 hpi; $n = 36$, long germ tubes 2 hpi; $n = 24$, swollen germ tube 3 hpi; $n = 11$, appressorium 5 hpi. Bar, 20 μm.

accumulation were observed in the other cells throughout development (e.g. Fig. 4b–d,j–l, see also Fig. 3 h), even after extended periods of incubation. We infer that the mitochondria in these cells are in a different metabolic state, possibly geared towards the synthesis of metabolic intermediates (e.g. Patkar *et al.*, 2012a), rather than ATP production.

The Grx1-roGFP2 signal measured in parallel from the swelling germ tube apical tip (Fig. 4e,f,h, see also Video S3) and developing appressorium (Fig. 4m,n,p, see also Video S4) showed the expected reduced profile in the cytoplasm and a more oxidized signal in punctate vacuoles. However, there was no evidence for any substantial changes in $E_{Grx1\text{-}roGFP2}$ that might reflect a burst of ROS production (Fig. 4 h,p) during these and more than 30 other time series spanning 2–5 hpi when appressoria develop. Interestingly, the internal CRDR signal was also lost rapidly during the calibration sequence in these cells. We infer, as with DAR-4M and DCF, that CRDR can be rapidly expelled by *M. oryzae*.

The apparent compartmentalization of mitochondrial activity and ROS production was unexpected if the three cells of the spore have direct cytoplasmic continuity, as has been argued previously from transmission electron microscopy (TEM) images for *M. oryzae* conidia, which show open septal pores (Money & Howard, 1996; Soundararajan *et al.*, 2004). Equally, differential turgor pressures in adjacent cells have been interpreted as evidence for the regulation of pore opening and closure to permit the transfer of materials between cells (Money & Howard, 1996). We found evidence using fluorescence recovery after photobleaching (FRAP) of Grx1-roGFP2 that spore cells were functionally isolated during germination and hyphal growth, but allowed communication during appressorium formation (Fig. S1). Furthermore, TEM images (Methods S1) showed occlusion of some septal pores by Woronin bodies (Fig. S2). These data are consistent with regulated septal conductivity during early development, with an increased probability of opening when transfer of reserves to the developing appressorium is required.

It is clear that there are differential rates of endogenous ROS production in each cell of germlings of *M. oryzae* during early development. However, at this stage, we do not have strong evidence for oxidative shifts during developmental transitions from either ROS measurements or changes in $E_{Grx1\text{-}roGFP2}$. Equally, quantitative interpretation of ROS levels and localization are challenging, as the signal represents a dynamic balance between dye uptake, intracellular hydrolysis, ROS production, reaction rates and subsequent probe sequestration (Fricker *et al.*, 2001; Halliwell & Whiteman, 2004; Meyer & Fricker, 2008). It is also possible that the glutathione pool may not be the most sensitive marker for redox events involved in signalling (Patsoukis & Georgiou, 2004; Belozerskaya & Gessler, 2007; Winterbourn,

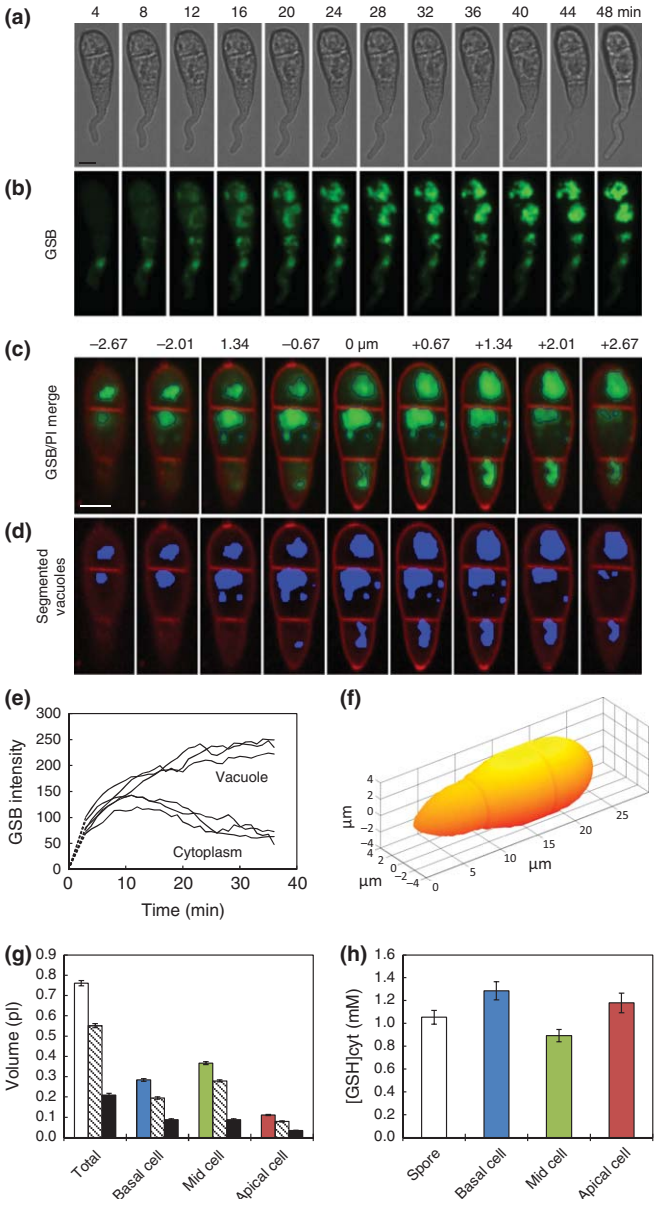

Fig. 6 Estimation of cytoplasmic GSH concentrations in *Magnaporthe oryzae* using *in vivo* imaging. Germinating spores of *M. oryzae* (a) were labelled with monochlorobimane (MCB), which reacts with GSH in the presence of a glutathione transferase to give fluorescent glutathione-bimane (GSB). GSB was imaged with four-dimensional (x,y,z,t) confocal microscopy (excitation, 405 nm; emission, 435–485 nm). The GSB signal increased in the cytoplasm during the initial reaction, but was transferred to the vacuole over time, possibly by a tonoplast GSX-conjugate pump. Maximum projections are shown in (b) for a subset of the time points in a typical experiment. Similar kinetics were observed from regions of interest from the basal, mid and germinating apical cell for both cytoplasmic and vacuolar areas (e). Labelling reached a plateau after *c.*30 min, with the majority of the signal in the vacuole. See Video S5 for a movie of the complete time series. The original cytoplasmic concentration of GSH was calculated from the total fluorescence in each compartment, corrected by the relative volume. To measure the total vacuolar volume and vacuolar GSB, individual vacuoles were separated using a three-dimensional watershed algorithm and then segmented using a local 50% intensity threshold above background for each vacuole (c, d). The total cell volume was calculated automatically from the outline of a maximum projection of the propidium iodide (PI)-stained cell wall, assuming that the spore was rotationally symmetric about the long axis (f). See Video S6 for example movies of the segmented vacuole images. The total spore volume was *c.* 0.76 ± 0.01 pl (mean ± SEM, $n = 81$), split in the ratio 37% : 48% : 15% basal : mid : apical (g). All three cells had a similar high cytoplasmic volume, *c.* 70% of the total cell volume (g) (open/coloured bars, total; hatched bars, cytoplasm; black bars, vacuole). The measured GSB intensities in the different compartments were calibrated against GSB standards, and the initial GSB cytoplasmic concentration was then calculated using the cytoplasmic and vacuolar volumes. The average was just over 1 mM (h), with slightly lower concentrations in the mid cell (h).

2008; Winterbourn & Hampton, 2008), with more reactive targets, such as thioredoxin and peroxiredoxins, being responsible for the initiation of developmental responses (D'Autreaux & Toledano, 2007; Meyer, 2008; Heller & Tudzynski, 2011). Indeed, it has been proposed in yeast that the primary function of cytosolic GSH is to drive extra-mitochondrial iron–sulfur cluster maturation, and GSH only acts as a back up to thioredoxin in redox homeostasis (Kumar *et al.*, 2011; Toledano *et al.*, 2013). The development of probes for these other redox couples is underway (Meyer & Dick, 2010) and would greatly facilitate physiological measurements in parallel with Grx1-roGFP2 to test such hypotheses. Likewise, the solution to understanding the spatial and temporal dynamics of ROS production would benefit from the further development of specific, transgenic ratio probes for the different ROS species, such as HyPer (Belousov *et al.*, 2006) or roGFP2-Orp1 (Gutscher *et al.*, 2009; Meyer & Dick, 2010).

M. oryzae can tolerate extreme oxidative stress

Whilst the maintenance of a highly reduced cytoplasm is required for normal cell physiology, one of the major defences in plants and animals to pathogen attack is through pronounced localized production of ROS to high levels, often within a few hours of inoculation (Xu *et al.*, 2009). We therefore tested how well *M. oryzae* might handle transient exposure to increasing concentrations of H_2O_2 to mimic attack by a host-derived oxidative burst.

In five extended time-series experiments, with a total of 89 germlings classified into different developmental stages, cells initially showed a rapid transient oxidation of Grx1-roGFP2 in response to short (5 min) exposure to increasing concentrations of H_2O_2, which returned to a more reduced state, even in the continued presence of the oxidant. A typical experiment is shown in Fig. 5 for a field of developing germlings (Fig. 5a). The average ratio for each apical cell is shown in Fig. 5(i). Ratio images are shown at low resolution for all cells at rest (Fig. 5b), following DTT (Fig. 5c), at the peak of each of the H_2O_2 exposures (Fig. 5d–f,h) and for the penultimate recovery (Fig. 5g). More detailed time-series images are shown for specific germlings to highlight the variability in response (Fig. 5j). Each increasing concentration of H_2O_2 gave a marked transient oxidation of Grx1-roGFP2 in these germlings, which rapidly returned towards resting levels, even in the continued presence of H_2O_2. The peak responses in other experiments were not as strong, but were captured in the average peak response for multiple cells and replicates (Fig. 5k). Washout of the H_2O_2 allowed $OxD_{Grx1\text{-}roGFP2}$ to return to near resting levels, even with treatments up to 40 mM H_2O_2 (Fig. 5i–k). Germ tube growth continued with 10 and 20 mM H_2O_2 shocks, but showed a reduction or ceased completely with 40–80 mM H_2O_2.

Within this overall pattern, there was variability in response at different developmental stages, most notably the rate of spontaneous recovery (Fig. 5i,j). During germination (0–1 hpi) and germ tube growth (2–3 hpi), the apical spore cell showed the greatest excursions in response to H_2O_2, but also the most rapid recovery (Fig. 5k). Developing appressoria (3–5 hpi) did not respond as strongly to oxidative stress, but also showed a lower subsequent rate of reduction of Grx1-roGFP2 (Fig. 5k). As noted previously, after *c.* 8 hpi, melanized appressoria were essentially insensitive to shocks of even 100 mM H_2O_2 (Fig. 2).

We infer that germlings of *M. oryzae* are able to withstand an aggressive imposed oxidative burst of H_2O_2, with transient excursions rapidly brought down to a new steady state. Germ tube growth continued in short-term exposures to 10–20 mM H_2O_2, whilst the melanizing appressorium was impervious to much higher H_2O_2 concentrations. The difference in $E^{o'pH}_{Grx1-roGFP2}$ and $E^{o'pH}_{GSH}$ makes Grx1-roGFP2 particularly sensitive to subtle shifts in E_{GSH}, with submicromolar cytoplasmic concentrations of GSSG, even with millimolar concentrations of exogenous H_2O_2. In addition to the rapid reduction of GSSG by glutathione reductase, it is possible that GSSG is sequestered in the vacuole to maintain tight control of cytoplasmic E_{GSH}, as has recently been documented for yeast (Morgan *et al.*, 2013).

Fig. 7 Redox relationships during infection of susceptible CO39 rice leaf sheaths with *Magnaporthe oryzae* expressing Grx1-roGFP2. Spores expressing Grx1-roGFP2 were inoculated on rice cultivar CO39 and three-dimensional (*x,y,z*) images were collected with dual-excitation confocal ratio imaging of Grx1-roGFP2 with excitation at 405 nm (c, i, o, s) or 488 nm (d, j, p, t) and emission at 500–530 nm, and additional wall autofluorescence (with either excitation at 405 nm, emission at 435–485 nm or excitation at 543 nm, emission at 656–615 nm). Bright-field images (a, g, m) were collected in parallel with a non-confocal transmission detector. Fluorescence channels were merged and colour coded as $Grx1\text{-}roGFP2_{405}$ in red, $Grx1\text{-}roGFP2_{488}$ in green and autofluorescence in blue (b, h, n, v), particularly to map the level of oxidative host response, visible as a red/purple colour in the cell walls. *In situ* calibration was not possible, but occasionally dying hyphae with oxidized Grx1-roGFP2 were observed (a–e). The ratio image (e) and pixel population statistics, fitted with a two-component Gaussian mixture model (GMM), confirmed that the dynamic range of the probe measured during infection was comparable with that observed for spores germinated on coverslips and imaged in parallel (f). During the early stages of infection, *c.* 16 h post-inoculation (hpi) (g), Grx1-roGFP2 signals from the cytoplasm in the appressorium (ap) and invasion hyphae (ih), and vacuoles (vac) in the appressorium and apical cell (ac) could be distinguished (h–j), and reported different degrees of oxidation in the ratio image (k) and population statistics, fitted with a four-component GMM (l). At 24 hpi (m), the majority of the signal could be attributed to cytoplasmic Grx1-roGFP2 in the invasion hyphae (n–p), although there was some host wall fluorescence arising from the host response with a very different broad spectrum (n, q). Cytoplasmic Grx1-roGFP2 was highly reduced in both the appressorium and invasion hyphae (q), and clearly separated from the autofluorescence in the pixel distributions (r). By 48 hpi, microscopic lesions were beginning to form as hyphae spread to multiple adjacent cells (s–w). Levels of vacuolation increased, particularly in the centre of the colony (v and w), but the cytoplasmic and vacuolar Grx1-roGFP2 signals were well separated using a two-component GMM (u). Two-component GMM models were also fitted to the cytoplasm and vacuoles in the centre and periphery of the colony separately, which showed a very slight increase in $E_{Grx1\text{-}roGFP2}$, but a more substantial increase in the vacuoles (*x*, mean ± SEM, $n = 17$). Images are presented as optimum plane projections of three-dimensional (*x,y,z*) stacks collected at 3-μm intervals. bc, basal cell; cyt, cytoplasm; gt, germ tube; mc, mid cell; sp, spore. Bars, 10 μm. See Video S7 for movies of 16- and 24-hpi time points, and Video S8 for the 48-hpi time point.

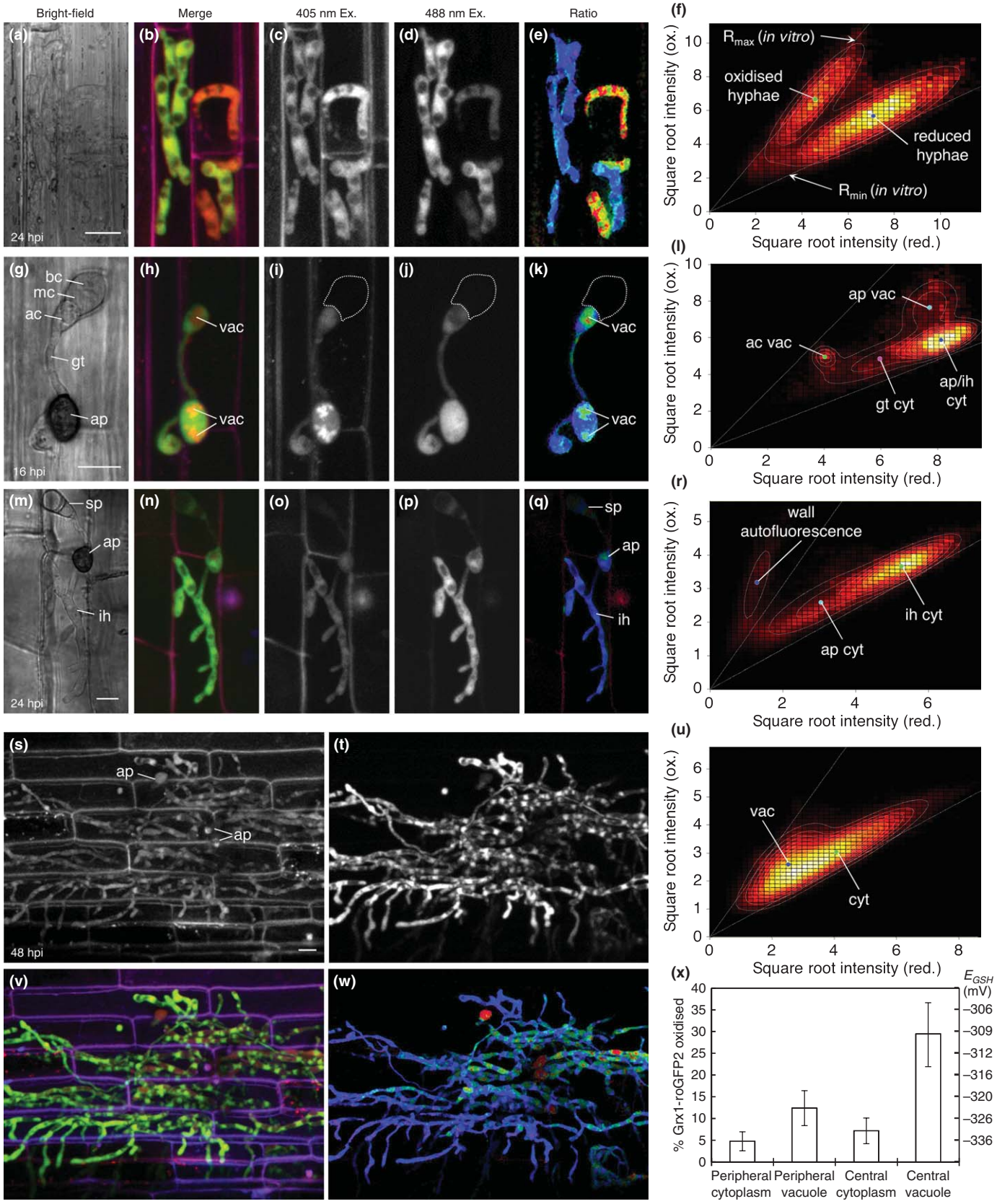

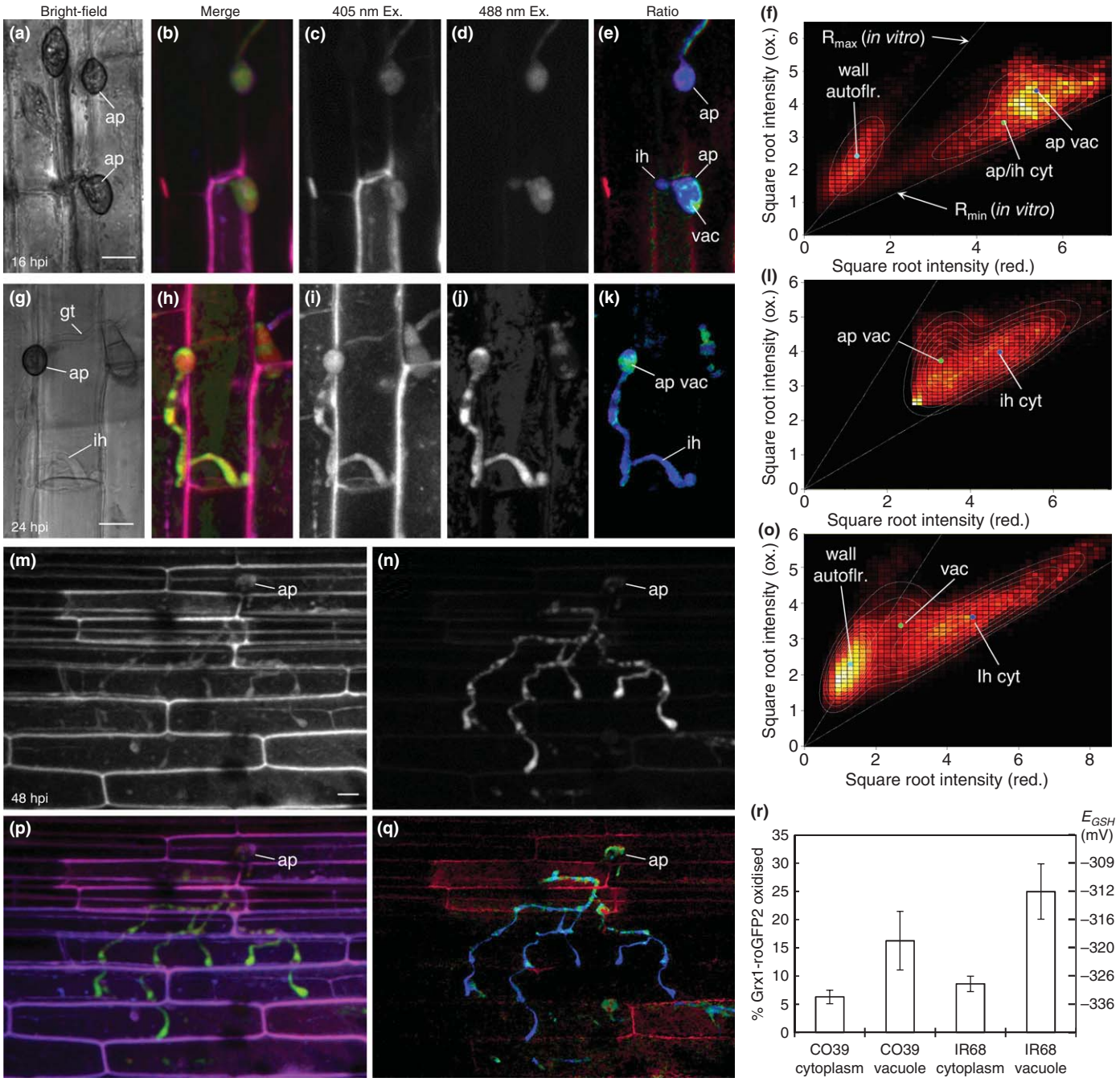

Fig. 8 Redox relationships during infection of resistant IR68 rice leaf sheaths with *Magnaporthe oryzae* expressing Grx1-roGFP2. The majority of spores failed to form penetration pegs on the resistant IR68 rice variety. However, occasionally successful penetration was observed followed by limited intracellular development. At 16 h post-inoculation (hpi) (a), there was considerable wall autofluorescence in infected cells, particularly with excitation at 405 nm (b–d), although the Grx1-roGFP2 signal remained reduced in the appressorium and invasion hyphae (e). Bright-field images (a, g) were collected in parallel with a non-confocal transmission detector. Fluorescence channels were merged and colour coded as Grx1-roGFP2$_{405}$ in red, Grx1-roGFP2$_{488}$ in green and autofluorescence in blue (b, h, p), particularly to map the level of the oxidative host response, visible as a red/purple colour in the cell walls. It was possible to separate out the wall autofluorescence and cytoplasmic and vacuolar signals with a three-component Gaussian mixture model (GMM) (f). At 24 hpi, rare intracellular growth was observed, with relatively thin, un-branched and vacuolated hyphae (g) and considerable localized wall autofluorescence, particularly with excitation at 405 nm (h–j). Cytoplasmic Grx1-roGFP remained fully reduced (k, l). At 48 hpi, there was occasional spindly growth through multiple cells with little or no branching (m–q). Fluorescent signals were relatively weak (m, n) and there were high levels of wall autofluorescence (p). Nevertheless, the ratio still showed a reduced signal through much of the cytoplasm (q). A three-component GMM fitted to the pixel distributions confirmed that cytoplasmic Grx1-roGFP2 remained reduced (o), and comparisons showed that the degree of cytoplasmic oxidation was only marginally higher in the resistant IR68 (mean ± SEM, $n = 10$) than in the susceptible CO39 (mean ± SEM, $n = 17$) cultivar (r). Images are presented as optimum plane projections of three-dimensional (x,y,z) stacks collected at 3-μm intervals. ap, appressorium; cyt, cytoplasm; ih, invasion hyphae; vac, vacuole. Bars, 10 μm. See Video S9 for a movie of 16- and 24-hpi time points, and Video S10 for the 48-hpi time point.

GSH levels are at millimolar concentrations in *M. oryzae*

Given the variable levels of endogenous ROS observed, the highly reduced E_{GSH} and the ability to tolerate substantial external bursts of H_2O_2, we sought to measure the absolute cytoplasmic concentration of glutathione to determine whether *M. oryzae* has a particularly high anti-oxidant capacity compared with non-pathogenic fungi and other organisms. Total levels of GSH were measured following *in situ* reaction with MCB to give a fluorescent GSB conjugate (Fricker *et al.*, 2000; Meyer & Fricker, 2000, 2008; Fricker & Meyer, 2001; Meyer *et al.*, 2001). MCB requires a glutathione transferase to react at an appreciable rate *in vivo*, and thus preferentially labels the existing cytoplasmic GSH pool, together with any GSSG that can be re-reduced by glutathione reductase (Fricker *et al.*, 2000; Meyer & Fricker, 2000; Fricker & Meyer, 2001; Meyer *et al.*, 2001). GSB was formed in the cytoplasm initially, and subsequently sequestered in the vacuoles over *c.* 30 min (Fig. 6a,b, see also Video S5), with similar kinetics in all three cells of the spore (Fig. 6e). This matches the xenobiotic detoxification pathways in plant and animal systems, where GSB is exported from the cytoplasm by glutathione-S-conjugate pumps (Coleman *et al.*, 1997; Fricker & Meyer, 2001). To measure the original cytoplasmic GSH concentration, the total GSB was corrected for the relative volume of the cytoplasmic and vacuolar compartments. The volume of the numerous vacuoles was determined from segmentation of the bimane images (Fig. 6c,d, see also Video S6), whereas the total cell volume was estimated from a maximum projection of the PI-stained cell wall, assuming that the spore was rotationally symmetric about the long axis (Fig. 6f). The cytoplasmic volume was calculated as the difference between the total cell and vacuolar volumes (Fig. 6g). At this stage of development, all three cells in the spore were densely cytoplasmic, at *c.* 70% of the total cell volume. Using the estimated cytoplasmic and vacuolar volumes, the total GSH concentration ranged from 1.29 ± 0.08 mM in the basal cell to 0.89 ± 0.05 mM in the mid cell, $n = 81$ (Fig. 6 h).

These GSH concentrations are comparable with those of aerial plant tissues, but at the low end for root tissues, yeast and mammalian cells (Meister & Anderson, 1983; Meyer, 2008; Noctor *et al.*, 2012). Thus, it appears that anti-oxidant defences in *M. oryzae* are not based on a massive constitutive GSH pool; the highly reduced E_{GSH} must be based on either rapid re-reduction of any GSSG produced or rapid removal of GSSG, or both (Morgan *et al.*, 2013).

M. oryzae does not appear to experience oxidative stress *in vivo*

Having determined the amount of GSH, and the capacity of *M. oryzae* to withstand imposed oxidative stress, we asked what happens to E_{GSH} during infection. On susceptible hosts, *M. oryzae* formed appressoria and penetration pegs within 16 hpi (Fig. 7g, see also Video S7), which developed to form swollen, branched infection hyphae by 24 hpi (Fig. 7m, see also Video S7). Over the next 24 h, *M. oryzae* colonized and spread through neighbouring cells to form small, microscopic lesions by 48 hpi (Fig. 7s, see also Video S8).

The quantification of E_{GSH} in hyphae ramifying in three dimensions was challenging, as single-point measurements did not capture the potential variation throughout the colony. Estimates were further complicated by vacuolar Grx1-roGFP2 signals, and high levels of host autofluorescence. Thus, we developed a pixel population approach to quantify $OxD_{Grx1\text{-}roGFP2}$ within the entire network structure. The fluorescence signal at both excitation wavelengths of Grx1-roGFP2 was fitted with a Gaussian mixture model (GMM) comprising two to four components (Fig. 7f,l,r,u), reflecting different cytoplasmic, vacuolar or autofluorescence signals in different regions of the colony. Ratios were compared with *in situ* calibration of germinating spores imaged under the same conditions. It was not possible to perform a comparable *in planta* calibration, because of the strong reaction of the plant tissue to the high H_2O_2 concentrations needed to calibrate Grx1-roGFP2 within intracellular fungal hyphae (data not shown). Occasionally, however, cells containing dying hyphae were observed, which provided an internal control for oxidized Grx1-roGFP2 (Fig. 7a–f), and confirmed the applicability of the *ex planta* calibration.

Cytoplasmic E_{GSH} was highly reduced throughout the infection process when quantified by ratio imaging (Fig. 7k,q,w, see also Videos S7, S8) or Gaussian modelling (Fig. 7 l,r,u). Both approaches highlighted the more oxidized signal from the numerous vacuoles present, particularly at later stages of infection (Fig. 7w). There were increasing levels of host wall fluorescence visible as a red/purple colour, resulting from the overlap between the autofluorescence channel, coded in blue, and bleed-through into the $GRx1\text{-}roGFP2_{405}$ channel, coded in red (Fig. 7h,n,v), indicative of a host ROS response. Around 48 hpi, the centre of the lesion showed some cell necrosis (Fig. 7v,w), a slightly higher average cytoplasmic redox potential compared with hyphae from the expanding colony margin, and an increased number of vacuoles with oxidized Grx1-roGFP2 (Fig. 7x). In general, Grx1-roGFP2 reported a highly reduced E_{GSH} throughout, with no evidence for shifts during early penetration events at *c.* 16–24 hpi, or during subsequent internal colonization.

In a resistant IR68 cultivar, cell penetration and intracellular development of *M. oryzae* were dramatically reduced with few successful penetration events and much higher levels of host wall autofluorescence or cell death, consistent with a strong oxidative host defence response (Fig. 8b,h,p, see also Videos S9, S10). Nevertheless, spores, germ tubes and the numerous appressoria unable to form infection pegs still maintained a reduced cytoplasmic GSH pool (see upper appressorium in Fig. 8e), with no evidence for extensive oxidation of Grx1-roGFP2 in the ratio images (Fig. 8e, see also Videos S9, S10) or GMM (Fig. 8f). When sparse intracellular hyphae did form, they were thinner than in the susceptible interaction, more vacuolated, and appeared to migrate between cells with little or no intracellular branching (Fig. 8 h,p). Nevertheless, the cytoplasmic E_{GSH} of these hyphae remained as highly reduced as in the susceptible plants (Fig. 8e,k,i,q, see also Videos S9, S10).

This represents something of a conundrum – at a physiological level, it is not obvious that ROS toxicity plays a dominant role in host resistance to rice blast as, under normal circumstances, *M. oryzae* has sufficient anti-oxidant defences to deal with both endogenous and exogenous ROS production and tightly regulates E_{GSH} with submicromolar levels of oxidized GSSG present. Equally, fungal mutants that have compromised anti-oxidant pathways suffer decreased pathogenicity. This parallels the results reported for the necrotroph *B. cinerea* (Temme & Tudzynski, 2009), in which the key redox-sensitive regulatory transcription factor, Bap1, was required for tolerance to exogenous H_2O_2 *ex planta*, but the corresponding Bap1 target genes were not induced during infection, with the clear implication that the fungus was not experiencing oxidative stress *in planta*. Furthermore, Bap1 was not essential for pathogenesis (Temme & Tudzynski, 2009), similar to results for the deletion of AP1 homologues in the human pathogen *Aspergillus fumigatus* (Lessing *et al.*, 2007) and the plant pathogen *Cochliobolus heterotrophus* (Lev *et al.*, 2005). The situation in *M. oryzae* is not identical, as deletion of the homologous gene, *MoAP1*, causes a reduction in pathogenicity, but during later intracellular infection and hyphal growth, rather than during appressorium formation and host penetration. MoAP1 has a wide range of targets, but reduced secretion of peroxidases and laccases might provide the strongest mechanistic link to ROS tolerance (Guo *et al.*, 2010, 2011). Similarly, deletion of *AP1* homologues in *Ustilago maydis* (Molina & Kahmann, 2007) and *Alternaria alternata* (Lin *et al.*, 2009, 2011; Yang *et al.*, 2009) also affects both H_2O_2 tolerance and pathogenicity.

The overall picture emerging is that *M. oryzae* tightly regulates E_{GSH} and has sufficient anti-oxidant capacity to handle even a strong host response, with the consequence that ROS toxicity alone is not sufficient to kill the pathogen. We infer that a distinction needs to be drawn between the presence of a high oxidative load during the host response, and the extent that a fungus actually experiences oxidative stress *in planta*, which cannot necessarily be inferred from *ex planta* responses to oxidative stress, but requires *in vivo* measurements.

Acknowledgements

Funding was provided by the Biotechnology and Biological Sciences Research Council (BBSRC) (BB/G00207X/1) to S.J.G. and M.D.F. We would like to thank Sarah Rodgers for the TEM images and Ian Moore for reading the manuscript.

References

Aguirre J, Lambeth JD. 2010. Nox enzymes from fungus to fly to fish and what they tell us about Nox function in mammals. *Free Radical Biology and Medicine* **49**: 1342–1353.

Aguirre J, Rios-Momberg M, Hewitt D, Hansberg W. 2005. Reactive oxygen species and development in microbial eukaryotes. *Trends in Microbiology* **13**: 111–118.

Ausubel FM, Brent R, Kingston RE, Moore DD, Seidman JG, Smith JA, Struhl K. 1999. *Short protocols in molecular biology: a compendium of methods from current protocols in molecular biology*. Chichester, UK: John Wiley.

Belousov VV, Fradkov AF, Lukyanov KA, Staroverov DB, Shakhbazov KS, Terskikh AV, Lukyanov S. 2006. Genetically encoded fluorescent indicator for intracellular hydrogen peroxide. *Nature Methods* **3**: 281–286.

Belozerskaya TA, Gessler NN. 2007. Reactive oxygen species and the strategy of antioxidant defense in fungi: a review. *Applied Biochemistry and Microbiology* **43**: 506–515.

Bolwell GP, Bindschedler LV, Blee KA, Butt VS, Davies DR, Gardner SL, Gerrish C, Minibayeva F. 2002. The apoplastic oxidative burst in response to biotic stress in plants: a three-component system. *Journal of Experimental Botany* **53**: 1367–1376.

Chi M-H, Park S-Y, Kim S, Lee Y-H. 2009. A novel pathogenicity gene is required in the rice blast fungus to suppress the basal defenses of the host. *PLoS Pathogens* **5**: e1000401.

Coleman JJ, Mylonakis E. 2009. Efflux in fungi: la piece de resistance. *PLoS Pathogens* **5**: e1000486.

Coleman JOD, BlakeKalff MMA, Davies TGE. 1997. Detoxification of xenobiotics by plants: chemical modification and vacuolar compartmentation. *Trends in Plant Science* **2**: 144–151.

Czymmek KJ, Bourett TM, Sweigard JA, Carroll A, Howard RJ. 2002. Utility of cytoplasmic fluorescent proteins for live-cell imaging of *Magnaporthe grisea* in planta. *Mycologia* **94**: 280–289.

D'Autreaux B, Toledano MB. 2007. ROS as signalling molecules: mechanisms that generate specificity in ROS homeostasis. *Nature Reviews in Molecular and Cellular Biology* **8**: 813–824.

Dean RA, Talbot NJ, Ebbole DJ, Farman ML, Mitchell TK, Orbach MJ, Thon M, Kulkarni R, Xu JR, Pan HQ *et al.* 2005. The genome sequence of the rice blast fungus *Magnaporthe grisea*. *Nature (London)* **434**: 980–986.

Dooley CT, Dore TM, Hanson GT, Jackson WC, Remington SJ, Tsien RY. 2004. Imaging dynamic redox changes in mammalian cells with green fluorescent protein indicators. *Journal of Biological Chemistry* **279**: 22284–22293.

Egan MJ, Talbot NJ. 2008. Genomes, free radicals and plant cell invasion: recent developments in plant pathogenic fungi. *Current Opinion in Plant Biology* **11**: 367–372.

Egan MJ, Wang ZY, Jones MA, Smirnoff N, Talbot NJ. 2007. Generation of reactive oxygen species by fungal NADPH oxidases is required for rice blast disease. *Proceedings of the National Academy of Sciences, USA* **104**: 11772–11777.

van Engelen FA, Molthoff JW, Conner AJ, Nap JP, Pereira A, Stiekema WJ. 1995. pBINPLUS: an improved plant transformation vector based on pBIN19. *Transgenic Research* **4**: 288–290.

Errington RJ, Fricker MD, Wood JL, Hall AC, White NS. 1997. Four-dimensional imaging of living chondrocytes in cartilage using confocal microscopy: a pragmatic approach. *American Journal of Physiology-Cell Physiology* **41**: C1040–C1051.

Fisher MC, Henk DA, Briggs CJ, Brownstein JS, Madoff LC, McCraw SL, Gurr SJ. 2012. Emerging fungal threats to animal, plant and ecosystem health. *Nature (London)* **484**: 186–194.

Fricker MD, May M, Meyer AJ, Sheard N, White NS. 2000. Measurement of glutathione levels in intact roots of *Arabidopsis*. *Journal of Microscopy* **198**: 162–173.

Fricker MD, Meyer AJ. 2001. Confocal imaging of metabolism *in vivo*: pitfalls and possibilities. *Journal of Experimental Botany* **52**: 631–640.

Fricker MD, Parsons A, Tlalka M, Blancaflor E, Gilroy S, Meyer A, Plieth C. 2001. Fluorescent probes for living plant cells. In: Hawes C, Satiat-Jeunemaitre B, eds. *Plant cell biology: a practical approach*. Oxford, UK: OUP, 35–84.

Georgiou CD, Petropoulou KP. 2001. Role of erythroascorbate and ascorbate in sclerotial differentiation in *Sclerotinia sclerotiorum*. *Mycological Research* **105**: 1364–1370.

Gessler NN, Aver'yanov AA, Belozerskaya TA. 2007. Reactive oxygen species in regulation of fungal development. *Biochemistry-Moscow* **72**: 1091–1109.

Gilbert MJ, Thornton CR, Wakley GE, Talbot NJ. 2006. A P-type ATPase required for rice blast disease and induction of host resistance. *Nature (London)* **440**: 535–539.

Govrin EM, Levine A. 2000. The hypersensitive response facilitates plant infection by the necrotrophic pathogen Botrytis cinerea. *Current Biology* **10**: 751–757.

Guo M, Chen Y, Du Y, Dong YH, Guo W, Zhai S, Zhang HF, Dong SM, Zhang ZG, Wang YC *et al.* 2011. The bZIP transcription factor MoAP1 mediates the oxidative stress response and is critical for pathogenicity of the rice blast fungus *Magnaporthe oryzae*. *PLoS Pathogens* **7**: e1001302.

Guo M, Guo W, Chen Y, Dong S, Zhang X, Zhang H, Song W, Wang W, Wang Q, Lv R *et al.* 2010. The basic leucine zipper transcription factor Moatf1 mediates oxidative stress responses and is necessary for full virulence of the rice blast fungus *Magnaporthe oryzae*. *Molecular Plant–Microbe Interactions* **23**: 1053–1068.

Gutscher M, Pauleau AL, Marty L, Brach T, Wabnitz GH, Samstag Y, Meyer AJ, Dick TP. 2008. Real-time imaging of the intracellular glutathione redox potential. *Nature Methods* **5**: 553–559.

Gutscher M, Sobotta MC, Wabnitz GH, Ballikaya S, Meyer AJ, Samstag Y, Dick TP. 2009. Proximity-based protein thiol oxidation by H_2O_2-scavenging peroxidases. *Journal of Biological Chemistry* **284**: 31532–31540.

Halliwell B, Whiteman M. 2004. Measuring reactive species and oxidative damage *in vivo* and in cell culture: how should you do it and what do the results mean? *British Journal of Pharmacology* **142**: 231–255.

Hansberg W, Aguirre J. 1990. Hyperoxidant states cause microbial cell-differentiation by cell isolation from dioxygen. *Journal of Theoretical Biology* **142**: 201–221.

Hanson GT, Aggeler R, Oglesbee D, Cannon M, Capaldi RA, Tsien RY, Remington SJ. 2004. Investigating mitochondrial redox potential with redox-sensitive green fluorescent protein indicators. *Journal of Biological Chemistry* **279**: 13044–13053.

Heller J, Meyer AJ, Tudzynski P. 2012. Redox-sensitive GFP2: use of the genetically encoded biosensor of the redox status in the filamentous fungus *Botrytis cinerea*. *Molecular Plant Pathology* **13**: 935–947.

Heller J, Tudzynski P. 2011. Reactive oxygen species in phytopathogenic fungi: signaling, development, and disease. *Annual Review of Phytopathology* **49**: 369–390.

Hesse SJA, Ruijter GJG, Dijkema C, Visser J. 2002. Intracellular pH homeostasis in the filamentous fungus *Aspergillus niger*. *European Journal of Biochemistry* **269**: 3485–3494.

Howard RJ, Ferrari MA, Roach DH, Money NP. 1991. Penetration of hard substrates by a fungus employing enormous turgor pressures. *Proceedings of the National Academy of Sciences, USA* **88**: 11281–11284.

Huang K, Czymmek KJ, Caplan JL, Sweigard JA, Donofrio NM. 2011. HYR1-mediated detoxification of reactive oxygen species is required for full virulence in the rice blast fungus. *PLoS Pathogens* **7**: e1001335.

Hubbart S, Peng S, Horton P, Chen Y, Murchie EH. 2007. Trends in leaf photosynthesis in historical rice varieties developed in the Philippines since 1966. *Journal of Experimental Botany* **58**: 3429–3438.

Kankanala P, Czymmek K, Valent B. 2007. Roles for rice membrane dynamics and plasmodesmata during biotrophic invasion by the blast fungus. *Plant Cell* **19**: 706–724.

Kim K-H, Willger SD, Park S-W, Puttikamonkul S, Grahl N, Cho Y, Mukhopadhyay B, Cramer RA Jr, Lawrence CB. 2009. TmpL, a transmembrane protein required for intracellular redox homeostasis and virulence in a plant and an animal fungal pathogen. *Plos Pathogens* **5**: e1000653.

Kumar C, Igbaria A, D'Autreaux B, Planson AG, Junot C, Godat E, Bachhawat AK, Delaunay-Moisan A, Toledano MB. 2011. Glutathione revisited: a vital function in iron metabolism and ancillary role in thiol-redox control. *EMBO Journal* **30**: 2044–2056.

Lamb C, Dixon RA. 1997. The oxidative burst in plant disease resistance. *Annual Review of Plant Physiology and Plant Molecular Biology* **48**: 251–275.

Lessing F, Kniemeyer O, Wozniok I, Loeffler J, Kurzai O, Haertl A, Brakhage AA. 2007. The *Aspergillus fumigatus* transcriptional regulator AfYap1 represents the major regulator for defense against reactive oxygen intermediates but is dispensable for pathogenicity in an intranasal mouse infection model. *Eukaryotic Cell* **6**: 2290–2302.

Lev S, Hadar R, Amedeo P, Baker SE, Yoder OC, Horwitz BA. 2005. Activation of an AP1-like transcription factor of the maize pathogen *Cochliobolus heterostrophus* in response to oxidative stress and plant signals. *Eukaryotic Cell* **4**: 443–454.

Levine A, Tenhaken R, Dixon R, Lamb C. 1994. H_2O_2 from the oxidative burst orchestrates the plant hypersensitive disease resistance response. *Cell* **79**: 583–593.

Lin CH, Yang SL, Chung KR. 2009. The YAP1 homolog-mediated oxidative stress tolerance is crucial for pathogenicity of the necrotrophic fungus *Alternaria alternata* in citrus. *Molecular Plant–Microbe Interactions* **22**: 942–952.

Lin C-H, Yang SL, Chung K-R. 2011. Cellular responses required for oxidative stress tolerance, colonization, and lesion formation by the necrotrophic fungus *Alternaria alternata* in citrus. *Current Microbiology* **62**: 807–815.

Marino D, Dunand C, Puppo A, Pauly N. 2012. A burst of plant NADPH oxidases. *Trends in Plant Science* **17**: 9–15.

Mathioni SM, Belo A, Rizzo CJ, Dean RA, Donofrio NM. 2011. Transcriptome profiling of the rice blast fungus during invasive plant infection and *in vitro* stresses. *BMC Genomics* **12**: 49.

Meister A, Anderson ME. 1983. Glutathione. *Annual Review of Biochemistry* **52**: 711–760.

Meyer AJ. 2008. The integration of glutathione homeostasis and redox signaling. *Journal of Plant Physiology* **165**: 1390–1403.

Meyer AJ, Dick TP. 2010. Fluorescent protein-based redox probes. *Antioxidants & Redox Signaling* **13**: 621–650.

Meyer AJ, Fricker MD. 2000. Direct measurement of glutathione in epidermal cells of intact *Arabidopsis* roots by two-photon laser scanning microscopy. *Journal of Microscopy-Oxford* **198**: 174–181.

Meyer AJ, Fricker MD. 2002. Control of demand-driven biosynthesis of glutathione in green *Arabidopsis* suspension culture cells. *Plant Physiology* **130**: 1927–1937.

Meyer AJ, Fricker MD 2008. Imaging thiol-based redox processes in live cells. In: Hell R, Dahl C, Knaff D, Leustek T, eds. *Sulfur metabolism in phototrophic organism. Advances in photosynthesis and respiration, vol 27*. Dordrecht, Netherlands: Springer, 483–501.

Meyer AJ, May MJ, Fricker M. 2001. Quantitative *in vivo* measurement of glutathione in *Arabidopsis* cells. *Plant Journal* **27**: 67–78.

Molina L, Kahmann R. 2007. An *Ustilago maydis* gene involved in H_2O_2 detoxification is required for virulence. *Plant Cell* **19**: 2293–2309.

Money NP, Howard RJ. 1996. Confirmation of a link between fungal pigmentation, turgor pressure, and pathogenicity using a new method of turgor measurement. *Fungal Genetics and Biology* **20**: 217–227.

Morel M, Kohler A, Martin F, Gelhaye E, Rouhier N. 2008. Comparison of the thiol-dependent antioxidant systems in the ectomycorrhizal *Laccaria bicolor* and the saprotrophic *Phanerochaete chrysosporium*. *New Phytologist* **180**: 391–407.

Morgan B, Ezeriņa D, Amoako TNE, Riemer J, Seedorf M, Dick TP. 2013. Multiple glutathione disulfide removal pathways mediate cytosolic redox homeostasis. *Nature Chemical Biology* **9**: 119–125.

Morgan B, Sobotta MC, Dick TP. 2011. Measuring EGSH and H_2O_2 with roGFP2-based redox probes. *Free Radical Biology and Medicine* **51**: 1943–1951.

Mur LAJ, Kenton P, Lloyd AJ, Ougham H, Prats E. 2008. The hypersensitive response; the centenary is upon us but how much do we know? *Journal of Experimental Botany* **59**: 501–520.

Noctor G, Mhamdi A, Chaouch S, Han Y, Neukermans J, Marquez-Garcia B, Queval G, Foyer CH. 2012. Glutathione in plants: an integrated overview. *Plant, Cell & Environment* **35**: 454–484.

Oh Y, Donofrio N, Pan HQ, Coughlan S, Brown DE, Meng SW, Mitchell T, Dean RA. 2008. Transcriptome analysis reveals new insight into appressorium formation and function in the rice blast fungus *Magnaporthe oryzae*. *Genome Biology* **9**: R85.

Otsu N. 1979. Threshold selection method from gray-level histograms. *IEEE Transactions on Systems Man and Cybernetics* **9**: 62–66.

Parker D, Beckmann M, Zubair H, Enot DP, Caracuel-Rios Z, Overy DP, Snowdon S, Talbot NJ, Draper J. 2009. Metabolomic analysis reveals a common pattern of metabolic re-programming during invasion of three host plant species by *Magnaporthe grisea*. *Plant Journal* **59**: 723–737.

Parton RM, Fischer S, Malho R, Papasouliotis O, Jelitto TC, Leonard T, Read ND. 1997. Pronounced cytoplasmic pH gradients are not required for tip growth in plant and fungal cells. *Journal of Cell Science* **110**: 1187–1198.

Patkar RN, Ramos-Pamplona M, Gupta AP, Fan Y, Naqvi NI. 2012a. Mitochondrial beta-oxidation regulates organellar integrity and is necessary for

conidial germination and invasive growth in *Magnaporthe oryzae*. *Molecular Microbiology* **86**: 1345–1363.

Patkar RN, Xue YK, Shui GH, Wenk MR, Naqvi NI. 2012b. Abc3-mediated efflux of an endogenous digoxin-like steroidal glycoside by *Magnaporthe oryzae* is necessary for host invasion during blast disease. *PLoS Pathogens* **8**: e1002888.

Patsoukis N, Georgiou CD. 2004. Determination of the thiol redox state of organisms: new oxidative stress indicators. *Analytical and Bioanalytical Chemistry* **378**: 1783–1792.

Qi ZQ, Wang Q, Dou XY, Wang W, Zhao Q, Lv RL, Zhang HF, Zheng XB, Wang P, Zhang ZG. 2012. MoSwi6, an APSES family transcription factor, interacts with MoMps1 and is required for hyphal and conidial morphogenesis, appressorial function and pathogenicity of *Magnaporthe oryzae*. *Molecular Plant Pathology* **13**: 677–689.

Rhee SG, Chang TS, Jeong W, Kang D. 2010. Methods for detection and measurement of hydrogen peroxide inside and outside of cells. *Molecules and Cells* **29**: 539–549.

Ryder LS, Dagdas YF, Mentlak TA, Kershaw MJ, Thornton CR, Schuster M, Chen J, Wang Z, Talbot NJ. 2013. NADPH oxidases regulate septin-mediated cytoskeletal remodeling during plant infection by the rice blast fungus. *Proceedings of the National Academy of Sciences, USA* **110**: 3179–3184.

Samalova M, Johnson J, Illes M, Kelly S, Fricker M, Gurr S. 2013. Nitric oxide generated by the rice blast fungus *Magnaporthe oryzae* drives plant infection. *New Phytologist* **197**: 207–222.

Scherz-Shouval R, Elazar Z. 2011. Regulation of autophagy by ROS: physiology and pathology. *Trends in Biochemical Sciences* **36**: 30–38.

Schwarzlander M, Finkemeier I. 2013. Mitochondrial energy and redox signaling in plants. *Antioxidants & Redox Signaling* **18**: 2122–2144.

Schwarzlander M, Fricker MD, Muller C, Marty L, Brach T, Novak J, Sweetlove LJ, Hell R, Meyer AJ. 2008. Confocal imaging of glutathione redox potential in living plant cells. *Journal of Microscopy* **231**: 299–316.

Scott B, Eaton CJ. 2008. Role of reactive oxygen species in fungal cellular differentiations. *Current Opinion in Microbiology* **11**: 488–493.

Shetty NP, Jorgensen HJL, Jensen JD, Collinge DB, Shetty HS. 2008. Roles of reactive oxygen species in interactions between plants and pathogens. *European Journal of Plant Pathology* **121**: 267–280.

Skamnioti P, Henderson C, Zhang ZG, Robinson Z, Gurr SJ. 2007. A novel role for catalase B in the maintenance of fungal cell-wall integrity during host invasion in the rice blast fungus *Magnaporthe grisea*. *Molecular Plant–Microbe Interactions* **20**: 568–580.

Soundararajan S, Jedd G, Li X, Ramos-Pamplona M, Chua NH, Naqvi NI. 2004. Woronin body function in *Magnaporthe grisea* is essential for efficient pathogenesis and for survival during nitrogen starvation stress. *Plant Cell* **16**: 1564–1574.

Sun CB, Suresh A, Deng YZ, Naqvi NI. 2006. A multidrug resistance transporter in *Magnaporthe* is required for host penetration and for survival during oxidative stress. *Plant Cell* **18**: 3686–3705.

Takemoto D, Tanaka A, Scott B. 2007. NADPH oxidases in fungi: diverse roles of reactive oxygen species in fungal cellular differentiation. *Fungal Genetics and Biology* **44**: 1065–1076.

Talbot NJ, Ebbole DJ, Hamer JE. 1993. Identification and characterization of MGP1, a gene involved in pathogenicity from the rice blast fungus *Magnaporthe grisea*. *Plant Cell* **5**: 1575–1590.

Talbot NJ, Kershaw MJ. 2009. The emerging role of autophagy in plant pathogen attack and host defence. *Current Opinion in Plant Biology* **12**: 444–450.

Tanabe S, Ishii-Minami N, Saitoh K, Otake Y, Kaku H, Shibuya N, Nishizawa Y, Minami E. 2011. The role of catalase-peroxidase secreted by *Magnaporthe oryzae* during early infection of rice cells. *Molecular Plant–Microbe Interactions* **24**: 163–171.

Tanabe S, Nishizawa Y, Minami E. 2009. Effects of catalase on the accumulation of H_2O_2 in rice cells inoculated with rice blast fungus, *Magnaporthe oryzae*. *Physiologia Plantarum* **137**: 148–154.

Temme N, Tudzynski P. 2009. Does *Botrytis cinerea* ignore H_2O_2-induced oxidative stress during infection? Characterization of Botrytis Activator Protein 1. *Molecular Plant–Microbe Interactions* **22**: 987–998.

Thines E, Weber RWS, Talbot NJ. 2000. MAP kinase and protein kinase A-dependent mobilization of triacylglycerol and glycogen during appressorium turgor generation by *Magnaporthe grisea*. *Plant Cell* **12**: 1703–1718.

Thomma BPHJ, Nürnberger T, Joosten MHAJ. 2011. Of PAMPs and effectors: the blurred PTI–ETI dichotomy. *Plant Cell* **23**: 4–15.

Toledano MB, Delaunay-Moisan A, Outten CE, Igbaria A. 2013. Functions and cellular compartmentation of the thioredoxin and glutathione pathways in yeast. *Antioxidants & Redox Signaling* **18**: 1699–1711.

Torres MA. 2010. ROS in biotic interactions. *Physiologia Plantarum* **138**: 414–429.

Tudzynski P, Heller J, Siegmund U. 2012. Reactive oxygen species generation in fungal development and pathogenesis. *Current Opinion in Microbiology* **15**: 653–659.

Urban M, Bhargava T, Hamer JE. 1999. An ATP-driven efflux pump is a novel pathogenicity factor in rice blast disease. *European Molecular Biology Organization Journal* **18**: 512–521.

Valent B, Khang CH. 2010. Recent advances in rice blast effector research. *Current Opinion in Plant Biology* **13**: 434–441.

Veneault-Fourrey C, Barooah M, Egan M, Wakley G, Talbot NJ. 2006. Autophagic fungal cell death is necessary for infection by the rice blast fungus. *Science* **312**: 580–583.

Wang ZY, Soanes DM, Kershaw MJ, Talbot NJ. 2007. Functional analysis of lipid metabolism in *Magnaporthe grisea* reveals a requirement for peroxisomal fatty acid beta-oxidation during appressorium-mediated plant infection. *Molecular Plant–Microbe Interactions* **20**: 475–491.

White NS, Errington RJ, Fricker MD, Wood JL. 1996. Aberration control in quantitative imaging of botanical specimens by multidimensional fluorescence microscopy. *Journal of Microscopy* **181**: 99–116.

Wilson RA, Talbot NJ. 2009. Under pressure: investigating the biology of plant infection by *Magnaporthe oryzae*. *Nature Reviews Microbiology* **7**: 185–195.

Winterbourn CC. 2008. Reconciling the chemistry and biology of reactive oxygen species. *Nature Chemical Biology* **4**: 278–286.

Winterbourn CC, Hampton MB. 2008. Thiol chemistry and specificity in redox signaling. *Free Radical Biology and Medicine* **45**: 549–561.

Xu Q, Liu SY, Zou QJ, Guo XL, Dong XY, Li PW, Song DY, Chen H, Zhao YD. 2009. Microsensor *in vivo* monitoring of oxidative burst in oilseed rape (*Brassica napus* L.) leaves infected by *Sclerotinia sclerotiorum*. *Analytica Chimica Acta* **632**: 21–25.

Yang SL, Lin C-H, Chung K-R. 2009. Coordinate control of oxidative stress tolerance, vegetative growth, and fungal pathogenicity via the AP1 pathway in the rough lemon pathotype of *Alternaria alternata*. *Physiological and Molecular Plant Pathology* **74**: 100–110.

Yoshioka H, Asai S, Yoshioka M, Kobayashi M. 2009. Molecular mechanisms of generation for nitric oxide and reactive oxygen species, and role of the radical burst in plant immunity. *Molecules and Cells* **28**: 321–329.

Supporting Information

Additional supporting information may be found in the online version of this article.

Fig. S1 Functional isolation of septal compartments in developing spores in *Magnaporthe oryzae* measured using fluorescent recovery after photobleaching (FRAP) of Grx1-roGFP2.

Fig. S2 Occlusion of septal pores in developing spores in *Magnaporthe oryzae* observed using transmission electron microscopy.

Methods S1 Transmission electron microscopy of conidia from *Magnaporthe oryzae*.

Video S1 Measurement of the redox potential of the glutathione pool in *Magnaporthe oryzae* germlings using recombinant Grx1-roGFP2.

Video S2 Measurement of reactive oxygen species (ROS) using 2′,7′-dichlorodihydrofluorescein diacetate (H_2DCFDA) in developing spores and during appressorium formation in *Magnaporthe oryzae*.

Video S3 Simultaneous measurement of mitochondrial membrane potential, reactive oxygen species (ROS) and Grx1-roGFP2 ratio in a swelling germ tube of *Magnaporthe oryzae*.

Video S4 Simultaneous measurement of mitochondrial membrane potential, reactive oxygen species (ROS) and Grx1-roGFP2 ratio in a developing appressorium of *Magnaporthe oryzae*.

Video S5 Formation of glutathione-bimane and subsequent vacuolar sequestration in a developing germling of *Magnaporthe oryzae*.

Video S6 Animated three-dimensional projections of vacuolar segmentation in spores of *Magnaporthe oryzae* during the early stages of germination.

Video S7 Animated three-dimensional projections of Grx1-roGFP2 fluorescence expressed in *Magnaporthe oryzae*, and the corresponding ratio images, 16 or 24 h after inoculation on a susceptible rice variety, CO39.

Video S8 Animated three-dimensional projections of Grx1-roGFP2 fluorescence expressed in *Magnaporthe oryzae*, and the corresponding ratio images, 48 h after inoculation on a susceptible rice variety, CO39.

Video S9 Animated three-dimensional projections of Grx1-roGFP2 fluorescence expressed in *Magnaporthe oryzae*, and the corresponding ratio images, 16 or 24 h after inoculation on a resistant rice variety, IR68.

Video S10 Animated three-dimensional projections of Grx1-roGFP2 fluorescence expressed in *Magnaporthe oryzae*, and the corresponding ratio images, 48 h after inoculation on a resistant rice variety, IR68.

Please note: Wiley Blackwell are not responsible for the content or functionality of any supporting information supplied by the authors. Any queries (other than missing material) should be directed to the *New Phytologist* Central Office.

Received: 21 July 2016 | Revised: 23 August 2016 | Accepted: 24 August 2016

DOI 10.1111/cmi.12659

WILEY

RESEARCH ARTICLE

The β-1,3-glucanosyltransferases (Gels) affect the structure of the rice blast fungal cell wall during appressorium-mediated plant infection

Marketa Samalova[1] | Hugo Mélida[2,3] | Francisco Vilaplana[2] | Vincent Bulone[2,4] | Darren M. Soanes[5] | Nicholas J. Talbot[5] | Sarah J. Gurr[1,5]

[1] Department of Plant Sciences, University of Oxford, Oxford, UK

[2] Division of Glycoscience, School of Biotechnology, Royal Institute of Technology (KTH), Stockholm, Sweden

[3] Centre for Plant Biotechnology and Genomics, Universidad Politécnica de Madrid, Madrid, Spain

[4] ARC Centre of Excellence in Plant Cell Walls and School of Agriculture, Food and Wine, University of Adelaide, Urrbrae, South Australia, Australia

[5] School of Biosciences, College of Life and Environmental Sciences, University of Exeter, Exeter, UK

Correspondence
Sarah J. Gurr, School of Biosciences, College of Life and Environmental Sciences, University of Exeter, Exeter EX4 4QD, UK
Email: s.j.gurr@exeter.ac.uk

Abstract

The fungal wall is pivotal for cell shape and function, and in interfacial protection during host infection and environmental challenge. Here, we provide the first description of the carbohydrate composition and structure of the cell wall of the rice blast fungus *Magnaporthe oryzae*. We focus on the family of glucan elongation proteins (Gels) and characterize five putative β-1,3-glucan glucanosyltransferases that each carry the Glycoside Hydrolase 72 signature. We generated targeted deletion mutants of all Gel isoforms, that is, the GH72^{+}, which carry a putative carbohydrate-binding module, and the GH72^{-} Gels, without this motif. We reveal that *M. oryzae GH72^{+} GELs* are expressed in spores and during both infective and vegetative growth, but each individual Gel enzymes are dispensable for pathogenicity. Further, we demonstrated that a *Δgel1Δgel3Δgel4* null mutant has a modified cell wall in which 1,3-glucans have a higher degree of polymerization and are less branched than the wild-type strain. The mutant showed significant differences in global patterns of gene expression, a hyper-branching phenotype and no sporulation, and thus was unable to cause rice blast lesions (except via wounded tissues). We conclude that Gel proteins play significant roles in structural modification of the fungal cell wall during appressorium-mediated plant infection.

1 | INTRODUCTION

The fungal wall forms a protective barrier against adverse stresses imposed by environmental fluctuations, or during host infection. It acts as a conduit, or harbor, for hydrolytic enzymes or toxins, and is involved in adhesion to abiotic or biotic surfaces. The wall is composed of a reticulate network of stress-bearing, shape-conferring polysaccharides with noncovalently and covalently bound embedded proteins, such as glycosylphosphatidylinositol (GPI)-anchored proteins, and proteins with internal repeats (PIR: Chaffin 2008; Latge 2010). This layered wall carries distinct proportions of β-glucans (β-1,3-glucans, β-1,6-glucans, and, in some species, β-(1,3;1,4)-glucans (Fontaine et al. 2000), chitin, and proteins, which vary between species, but also with cell type within a given species (Ruiz-Herrera, Elorza, Valentin, & Sentandreu 2006; Latge 2010; Ruiz-Herrera & Ortiz-Castellanos 2010; Mélida, Sain, Stajich, & Bulone 2015). Glucans are the major components of this "generic" fungal wall, dominated by β-1,3-glucans. Linear chains of β-1,3-glucan are synthesized by a membrane-localized glucan synthase (Latge 2007; Gastebois et al. 2010a) and are extruded into the wall as polymerization proceeds. Extensive remodeling occurs, most likely in the cell wall, involving formation of β-1,6 branching points and cross links between β-glucans and chitin (Aimanianda & Latge 2010; Latge 2010). The orchestration and precise order of the cell wall biosynthetic events and remodeling remains elusive.

Of the various cell wall moieties, β-1,3-glucans make up between 40 and 50% of the wall mass *Saccharomyces cerevisiae* and *Candida albicans* (Lipke & Ovalle 1998; Klis, De Groot, & Hellingwerf 2001), and about 60–70% in filamentous fungi such as *Neurospora crassa* (Mélida et al. 2015). In *C. albicans*, *S. cerevisiae*, *Schizosaccharomyces pombe*, *Aspergillus fumigatus*, *Fusarium oxysporum*, *Neurospora crassa*, and *Tuber melanosporum*, the incorporation of nascent β-1,3-glucan molecules into the existing β-glucan network likely involves members of a conserved family, known as the Glycolipid anchored surface proteins (Gas), or Glucan elongation (Gel) proteins (Mühlschlegel &

Fonzi 1997; Popolo & Vai 1999; Mouyna et al. 2000a; Caracuel, Martinez-Rocha, Di Pietro, Madrid, & Roncero 2005; Medina-Redondo et al. 2010; Kamei et al. 2013; Sillo et al. 2013). Evidence for this comes from *S. cerevisiae Δgas1*, which shows a decrease in β-1,3-glucan content in the mutant wall, compared with the wild-type strain, coupled with a rise in β-1,3-glucan in the growth medium (Ram et al. 1998). Such data implies that Gas proteins are involved in the incorporation of β-1,3-glucan into the wall, but that they are not involved in glucan synthesis (Ram et al. 1998). An analysis of products resulting from *in vitro* incubation of recombinant Gas proteins with a reduced laminarioligosaccharide suggests a two-step transglycosylating mechanism for these enzymes. Here, Gas proteins cleave a β-1,3 glycosidic linkage in the glucan chain and subsequently reform a β-1-3 linkage between the reducing end of one released chain and the nonreducing end of side branches in existent β-glucans (Hurtado-Guerrero et al. 2009). Thus, the transglycosylating activity of Gas proteins leads to the integration of nascent β-1,3-glucan chains into the existing ß-glucan network. However, a role for Gas proteins in incorporating β-1,3-glucan into the wall has not been demonstrated *in vivo*. Thus far, the phenotype of *GAS* deletion mutants has been taken as proxy evidence in support of this model, being, specifically, loss of β-glucan to the medium, reduction in alkali-insoluble wall glucan, and induction of the cell wall integrity (CWI) pathway (Ram et al. 1998; Fonzi 1999; Carotti et al. 2004; Mouyna et al. 2005; Gastebois, Fontaine, Latge, & Mouyna 2010b).

The filamentous fungus *Magnaporthe oryzae* is the causal agent of rice blast disease (Couch & Kohn 2002). Under blast-favorable conditions, up to 30% of the annual rice crop can be lost to infection; controlling disease would constitute a major contribution to ensuring global food security (Talbot 2003). Disease is initiated when a three-celled conidium detaches from conidiophore-laden host lesions and attaches to the plant surface, by release of apical spore tip mucilage (Hamer, Howard, Chumley, & Valent 1988). Germination leads to formation of a short germ tube, which matures at its tip into an appressorium. This infection structure forms in response to host cues, such as the hard, hydrophobic leaf surface and plant cutin, as well as absence of nutrients (Skamnioti & Gurr 2007; Wilson & Talbot 2009). Autophagy then occurs in the conidium whose content is recycled into the appressorium (Veneault-Fourrey, Barooah, Egan, Wakley, & Talbot 2006), which is lined with melanin on the inner edge of the fungal wall. Turgor pressure rises within this newly sealed chamber (De Jong, McCormack, Smirnoff, & Talbot 1997), leading to the emergence of a narrow penetration peg, which pushes through the cuticle and cell wall, expands to form a primary hypha, and then differentiates into bulbous invasive hyphae. The fungus spreads rapidly through a susceptible host (Kankanala, Czymmek, & Valent 2007; Khang et al. 2010), culminating in lesions on aerial tissues, which discharge prolific numbers of conidia, thereby promoting epidemic disease spread (Skamnioti & Gurr 2009). The fungus is capable of causing disease on approximately fifty grass and sedge species. Blast disease is thus of concern with regard to its changing demographics and ability to move to new hosts (Yoshida et al. 2016), with its movement fuelled by global climate change (Bebber, Ramotowski, & Gurr 2013).

Our understanding of the mechanisms which underpin pathogenesis remain far from complete, and thus has not yet fuelled the hunt for target-specific antifungals (Skamnioti & Gurr 2009). Attractive amongst prospective targets is the fungal cell wall. However, little is known about the organization of the *M. oryzae* wall or about wall variation between cell types during plant infection. Previously, research has considered the architecture of the spore surface, revealing a multi-layered rodlet surface structure, composed of the hydrophobin Mpg1, which is important in appressorium attachment and morphogenesis (Talbot, Ebbole, & Hamer 1993; Talbot et al. 1996; Kershaw, Thornton, Wakley, & Talbot 2005). Electron micrographs by Howard and Valent (1996) and Mares et al. (2006) also showed, respectively, the layered structures of the conidium and hyphal cell, purportedly comprising β-1,3-glucans and chitin.

At present, the polysaccharide composition of the *M. oryzae* wall remains unknown. Recently, however, Fujikawa et al. (2009, 2012) revealed that it carries α-1,3-glucan moieties and that these surface-lying polymers play a role in camouflaging the fungus from recognition by the host immune system during formation of infectious hyphae.

In this report, we provide the first detailed profile of the *M. oryzae* wall carbohydrate composition and structure. We consider the roles of the Gel family of β-1,3-glucanosyltransferases in infective and vegetative fungal growth. We show that Gel proteins are expressed during infection-related development and plant infection, and a mutant defective in three Gel enzymes does not cause rice blast disease.

2 | RESULTS

2.1 | Putative Gel proteins in *M. oryzae*

A search of the *M. oryzae* genome database (http://www.broadinstitute.org) revealed five putative Glucan Elongation (Gel)/Glycolipid Anchored Surface (Gas) proteins, based on sequence similarity to *S. cerevisiae* Gas1 (Ragni, Fontaine, Gissi, Latge, & Popolo 2007). This family features an N-terminal signal peptide followed by a catalytic Glycoside Hydrolase 72 domain (GH72) (Pfam: PF03198), a linker region connecting C-terminal low complexity region with a Ser/Thr percentage of 29–40% (Sillo et al. 2013), and a putative GPI anchor (Figure 1a).

In addition to the GH72 domain, two of these proteins, named Gel3 (MGG_08370.7) and Gel4 (MGG_11861.7), carry a family 43 Carbohydrate Binding Module (CBM43 in CAZy database) also known as an X8 domain (Pfam: PF07983). The CBM43 domain is found in a subset of Gas proteins (Ragni et al. 2007) and carries eight conserved Cys residues (Cys-box). Based on previous classifications, the two proteins carrying the Cys-box belong to the $GH72^{+}$ subfamily whilst Gel1 (MGG_07331.7), Gel2 (MGG_06722.7), and Gel5 (MGG_03208.7) belong to the $GH72^{-}$ subfamily (Figure 1a).

To unmask likely evolutionary relationships of *M. oryzae GEL* genes, we used maximum likelihood (ML) analysis (Sillo et al. 2013) to compare 237 proteins belonging to 24 Pezizomycotina (e.g., *M. oryzae*, *A. fumigatus*), 25 Saccharomycotina (e.g., *S. cerevisiae*, *C. albicans*), and 2 *Schizosaccharomyces* (*S. pombe*, *S. japonicas*). Three Basidiomycota sequences were used as outgroup taxa (Figure 1b). The tree clearly distinguishes between the $GH72^{+}$ and $GH72^{-}$ subfamilies. Moreover, $GH72^{-}$ could be further divided into alpha, beta, and gamma clades, alongside a newly identified delta clade with members

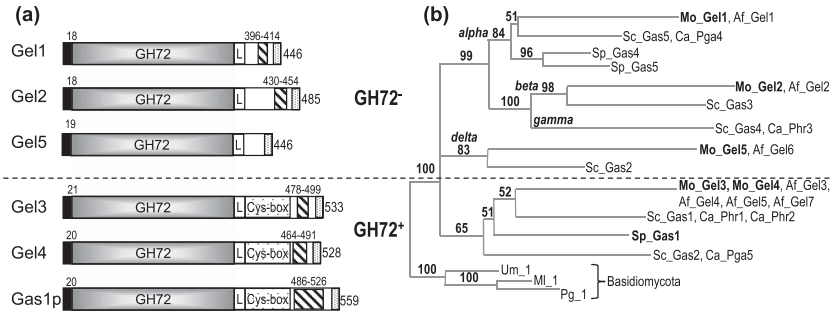

FIGURE 1 *Magnaporthe oryzae* Gel protein structure and evolutionary phylogenetic tree. (a) Schematic representation of *M. oryzae* Gel proteins compared to yeast Gas1p. The black and dotted boxes at the N- and the C-terminus are the signal peptide and the GPI-anchor, respectively. L is the putative linker that links the GH72 catalytic domain (grey) with C-terminal low complexity region enriched with Ser/Thr (striped box) and the Cys-box, cysteine-enriched module, present in GH72^{+}subfamily. Note Gas1p contains poly Ser/Thr region unlike any of the *Magnaporth*e Gels. (b) Maximum likelihood phylogenetic tree, comparing Ascomycota Gel proteins of *M. oryzae* (Mo), *Aspergillus fumigatus* (Af), *Saccharomyces cerevisiae* (Sc), *Candida albicans* (Ca) and *Schizosaccharomyces pombe* (Sp) rooted to Basidiomycota *Ustilago maydis* (Um), *Melampsora larici-populina* (Ml) and *Puccinia graminis* (Pg), clearly divides the proteins (indicated by a dash line) into two subfamilies, the GH72^{-}cluster (carrying alfa, beta, gamma and delta clades) and the GH72^{+} cluster, which contains the carbohydrate-binding module of family 43 (Cys-box). The maximum likelihood tree was adapted from Sillo et al. (2013)

carrying a truncated Cys-box (6Cys-box) or no Cys-box, as with Mo_Gel5. Most Ascomycota carry 3–7 Gel proteins, but Basidiomycota possess only one GH72^{+} *GEL*.

2.2 | *M. oryzae* GH72^{+} Gels do not complement yeast *Δgas1*

To investigate Gel3 and/or Gel4 function, we attempted complementation of yeast *Δgas1* mutant. Its phenotype is well characterized; it shows reduced growth, abnormal rounded cells, aberrant budding, increased sensitivity to Congo Red (CR) and Calcofluor White (CFW), oxidative stress, and alkaline pH (Ram, Wolters, Ten Hoopen, & Klis 1994; Ni & Snyder 2001; Serrano, Bernal, Simon, & Arino 2004; Liu, Lee, & Lee 2006; Ando, Nakamura, Murata, Takagi, & Shima 2007). We used the pYES2 heterologous expression system, exploiting the GAL1-inducible promoter in *S. cerevisiae*. Mutant cells show reduced growth without induction, when compared with the wild-type (WT) strain (Figure S1, glucose). However, the addition of galactose restored growth when the original yeast *GAS1* was expressed and cells were plated on galactose-inducing medium (SG) supplemented with CR, CFW, or SDS. *M. oryzae GEL3* did not complement *Δgas1*; *GEL4* showed partial complementation of *Δgas1* on CFW but not on other growth media. Based on this result, we decided to investigate the *M. oryzae* GH72^{+}subfamily further.

2.3 | *M. oryzae* GH72^{+} enzymes are essential for normal vegetative growth under stress conditions

The GH72 domain and Cys-box of fungal GH72^{+} enzymes have been reported to physically interact and are essential for correct folding and enzyme activity (Popolo et al. 2008; Hurtado-Guerrero et al. 2009). We thus investigated whether *M. oryzae* GH72^{+} enzymes play an essential role in wall remodeling by creating single targeted *GEL3* and *GEL4* deletion mutants and a double mutant *Δgel3Δgel4*. To complement the single mutant strains, we fused the *GEL* sequence with a fluorescent protein positioned as an N-terminal fusion following the signal peptide and expressed the gene under control of its native promoter (Experimental Procedures).

We assayed the effect of various cell wall perturbation chemistries (CR, CFW), applied cell wall and plasma membrane stresses (SDS, alkaline pH, sorbitol, and glycerol), and oxidative stress (hydrogen peroxide). Surprisingly, we observed growth reduction of *Δgel4* and *Δgel3Δgel4* mutants on minimal medium (MM; by approximately 25%), and in CM supplemented with CR (30%) or SDS (25% for *Δgel3Δgel4*; Figure S2). Interestingly, the emergent germ tubes of *Δgel3Δgel4* mutants, germinated in 0.005% (*w*/*v*) SDS, were significantly shorter than Guy11. However, approximately 50% of germlings in the mutant progressed to develop mature appressoria at 24 hpi. The *Δgel3Δgel4* showed reduced growth (by approximately 15%) under oxidative stress, but other factors did not affect growth. The complemented strain *Δgel3/GEL3:mCherry* appeared to be functional but *Δgel4/GEL4:eGFP* only partly restored WT growth.

2.4 | GH72^{+} *GEL3* and *GEL4* localize to the cell periphery but with different expression patterns in *M. oryzae*

We used complemented strains *Δgel3/GEL3:mCherry* and *Δgel4/GEL4:eGFP* to localise GH72^{+} *in vivo* by confocal laser scanning microscopy (CLSM), following germling development on hydrophobic glass slides. These surfaces support appressorium differentiation in *M. oryzae* (Wilson & Talbot 2009). *GEL3* and *GEL4* are both expressed, and their

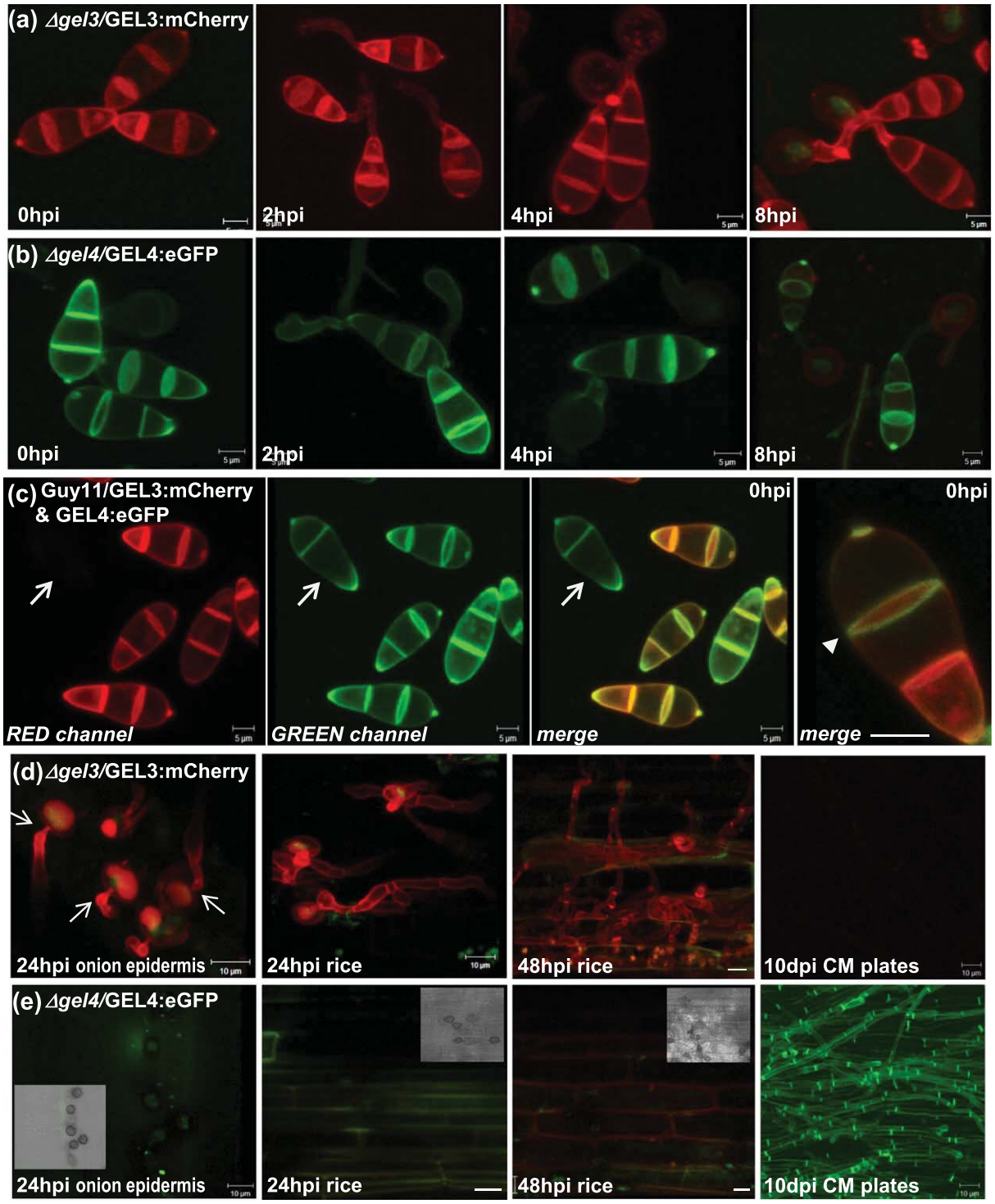

FIGURE 2 Confocal imaging of fluorescently labeled *GEL3* and *GEL4* at different stages of *Magnaporthe oryzae* development. (a) and (b) Projections of Z-stacks following spore development on hydrophobic surface (a) *Δgel3* mutant complemented with *GEL3:mCherry* fusion (b) *Δgel4* mutant complemented with *GEL4:eGFP* fusion at 0, 2, 4, and 8 hours post-inoculation (hpi). (c) Guy11 transformed with both *GEL3:mCherry* and *GEL4:eGFP* fusions at 0 hpi shown in split red and green, as well as merged channels. The arrow points to a spore that is expressing the *GEL4:eGFP* fusion only, therefore appearing invisible in the red channel. The arrow head points to differential circumferential localization of *GEL3:mCherry*, while *GEL4:eGFP* persists along the edges of the spore cell–cell boundaries. Projections of Z-stacks following expression of (d) *Δgel3/GEL3:mCherry* and (e) *Δgel4/GEL4:eGFP* during development of penetration pegs (arrows) and infection hyphae on onion peels, at 24 hpi and rice, at 24 and 48 hpi. *GEL4* is not visible at these stages; the transmitted-light micrograph insert shows that melanized appressoria with invasion hyphae are present. *GEL4* is strongly expressed in vegetative mycelia of 10-day-old cultures; *GEL3* is not. The confocal images were collected for both red and green channels to indicate the autofluorescence for the opposite fluorophore. The scale bars are 5 (a, b, c) or 10 (d, e) μm

respective protein products localise to the cell periphery of the three-celled spores and emergent germ tubes up to 4 hours post-inoculation (hpi; Figure 2a and b). Appressoria were, however, not labeled by the fusions, indeed, by 8 hpi *GEL4* expression is reduced and then

disappears completely. When *Δgel3/GEL3:mCherry* and *Δgel4/GEL4:eGFP* fusions were expressed simultaneously in Guy11, some differential labeling was observed; in extreme cases, only *GEL4* was visible but not *GEL3* (Figure 2c, arrow). *GEL3* was more highly expressed and could be tracked during germling development on onion epidermis. This "surface" supports development of penetration pegs and invasive hyphae (Chida & Sisler 1987) (Figure 2d and e). At 24 hpi, the *GEL3:mCherry* fusion highlights a large central vacuole in the appressorium and emerging penetration pegs. Labeling of the cell periphery of invasive hyphae was also clear in infected rice cells, 24 and 48 hpi (Figure 2d). *GEL3:mCherry* was not expressed visibly in vegetative hyphae. By contrast, *GEL4* is not expressed during plant infection but it is expressed in vegetative hyphae (Figure 2). Thus, *GEL3* and *GEL4* are expressed in conidia, but show differential localization during vegetative and invasive hyphal growth, with *GEL3* most strongly associated with host invasion.

2.5 | GH72$^+$ Gels are not essential for spore and appressorium development and infection

As *GEL3* and *GEL4* are both expressed during conidial development and *GEL3* is expressed during infection, we investigated the role of GH72$^+$ in pathogenicity. We followed germling and appressorium development on hydrophobic glass slides and compared the number of melanized appressoria at 8 hpi between the strains. There was no significant difference between the Guy11, single *Δgel3* and *Δgel4*, and double *Δgel3Δgel4* mutants, or the complemented strains (Figure S2e). Furthermore, we observed no difference in the development of penetration pegs and invasion hyphae on onion epidermis at 24 hpi (Figure S2f). Indeed, the mutants were fully pathogenic on barley (Figure S2g and h).

2.6 | Monosaccharide composition of *M. oryzae* cell wall polysaccharides

There has been no detailed analysis of the monosaccharide composition and specific glycosidic linkages of the WT strain Guy11 wall hitherto. We therefore investigated wall monosaccharide composition in Guy11 and compared it with *Δgel3Δgel4*, grown in CM. Total wall polysaccharides were extracted, fully hydrolyzed to their constituent monosaccharides and analyzed by GC/EI-MS. Table 1 shows only minor differences in total mannose, galactose, glucose and *N*-acetylglucosamine content between three independent double *Δgel3Δgel4* mutants and Guy11. We also observed that when Guy11 is grown in MM, the wall mannose content was reduced significantly, but was compensated by a significant increase in glucose. Growth conditions thus affect cell wall composition (Aguilar-Uscanga & Francois 2003).

TABLE 1 Total sugar analysis of the *Magnaporthe oryzae* cell walls (mol%)

	Guy11 MM		Guy11 CM		*Δgel3Δgel4*	
	AV	SEM	AV	SEM	AV	SEM
Mannose	8.5	0.1	15.0	0.1	14.3	0.1
Galactose	0.9	0.0	2.0	0.0	1.6	0.1
Glucose	85.6	0.0	75.7	0.1	77.1	0.1
N-Acetylglucosamine	5.0	0.2	7.3	0.1	7.0	0.2

2.7 | Targeted deletion of *GEL1*, *GEL2*, and *GEL5* does not affect fungal development

To investigate the role of the Gel proteins, we created null mutants of GH72$^-$ subfamily, *Δgel1*, *Δgel2*, and *Δgel5*. However, no phenotypic differences (germination, germling differentiation assays, or plate growth assays) were observed when various exogenous stresses were imposed (data not shown). Despite protracted efforts, we were unable to visualize GFP or RFP fluorescent tagged GH72$^-$ Gels during asexual spore development, penetration and hyphal infection, mycelial growth, or in sexual perithecia and ascospores (data not shown). GH72$^-$ *GEL*s appear lowly expressed, as shown by RNAseq data (Soanes, Chakrabarti, Paszkiewicz, Dawe, & Talbot 2012). To confirm this, we used qRT-PCR to profile expression, revealing only modest fold changes during spore development and early stages of plant infection of all members of *M. oryzae GEL*s (Figure S3a). The most upregulated gene was *GEL2*, which showed a threefold upregulation compared to nongerminated spores at 0 hpi, at 24 hpi, coincident with the time of invasive hypha development. qRT-PCR results also confirmed that *GEL4* (and *GEL2*) are slightly upregulated in mycelium compared to spores while *GEL3* (and *GEL1*) are downregulated, as seen by confocal microscopy. *GEL5* is weakly expressed in spores but strongly upregulated in mycelium (Figure S3b and S3c).

2.8 | A Gel-deficient mutant of *M. oryzae* is unable to cause rice blast disease

Our observations suggest that GH72$^+$ Gel proteins are important in normal mycelial growth under stress conditions. To investigate the coordinated action of the whole Gel family, we introduced deletions in GH72$^-$ genes in *Δgel3Δgel4* background to create *Δgel1Δgel3Δgel4*, *Δgel2Δgel3Δgel4*, and *Δgel5Δgel3Δgel4* triple mutants. We also created a *Δgel1Δgel2Δgel5* mutant, thereby deleting all GH72$^-$ genes. Finally, we created a double *Δgel2Δgel3* mutant, in which the GH72$^+$ and GH72$^-$ members, showing elevated expression during spore development and early infection, were deleted.

Plate growth assays showed that *Δgel1Δgel3Δgel4*, and to lesser extent, the *Δgel2Δgel3Δgel4*, were hypersensitive to exogenous stresses including plasma membrane and cell wall-acting agents, as well as to oxidative and heat stress. The treatments included CR, CRW, SDS, NaCl, glycerol, sorbitol, hydrogen peroxide, and elevated temperature (32°C). Most striking was the almost complete inhibition of growth of *Δgel1Δgel3Δgel4* on MM and CM medium supplemented with CR (Figure 3), with growth significantly reduced on CM medium but recovered upon addition of sorbitol or glycerol. The growth of *Δgel5Δgel3Δgel4* was comparable to that of its progenitor strain *Δgel3Δgel4*. *Δgel1Δgel2Δgel5* did not show any growth defects under conditions tested, suggesting that GH72$^-$ is dispensable for vegetative growth. Similar results were obtained with *Δgel2Δgel3* (data not shown).

Pathogenicity assays of single, double, and triple mutants confirmed that all strains, with the exception of *Δgel1Δgel3Δgel4* (which does not sporulate), produce melanized appressoria (Figure 4a), penetration pegs, and invasive hyphae and are all as pathogenic as Guy11

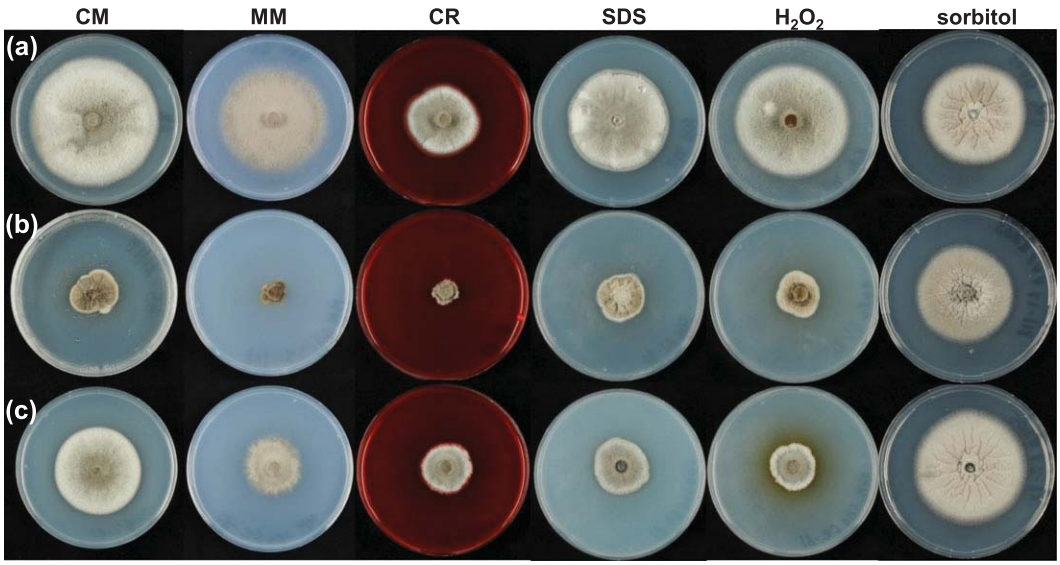

FIGURE 3 Plate growth assays of wild-type and triple mutant strains of *Magnaporthe oryzae*. (a) Guy11, (b) *Δgel1Δgel3Δgel4*, and (c) *Δgel2Δgel3Δgel4* strains grown on complete medium (CM), minimal medium (MM), CM supplemented with CR, SDS, H_2O_2, and sorbitol at 24°C for 10 days. The experiment was replicated three times with a minimum of two independent lines of each strain; representative pictures are shown

(Figure 4b). Thus, $GH72^+$ and $GH72^-$ members are both dispensable for pathogenicity, but specific isoforms are essential for spore formation and host infection (see below).

2.9 | Δgel1Δgel3Δgel4 has a hyperbranching phenotype and does not produce conidia

Δgel1Δgel3Δgel4 does not produce fully formed conidia (but occasionally round and terminally swollen hyphal tip cells only), even when plated onto an osmotic medium that supports its growth (Figure 3). Pathogenicity assays were performed with excised and inverted mycelial plugs placed onto a rice leaf. This mode of infection showed that the Guy11 strain causes significant lesion formation at 5 dpi (Figure 4c), but inverted mycelial plugs of the *Δgel1Δgel3Δgel4* mutant do not cause disease symptoms. After leaf cuticle abrasion, however, disease symptoms developed following *Δgel1Δgel3Δgel4* inoculation (Figure 4c), with invasive hyphae invading secondary cells through plasmodesmata.

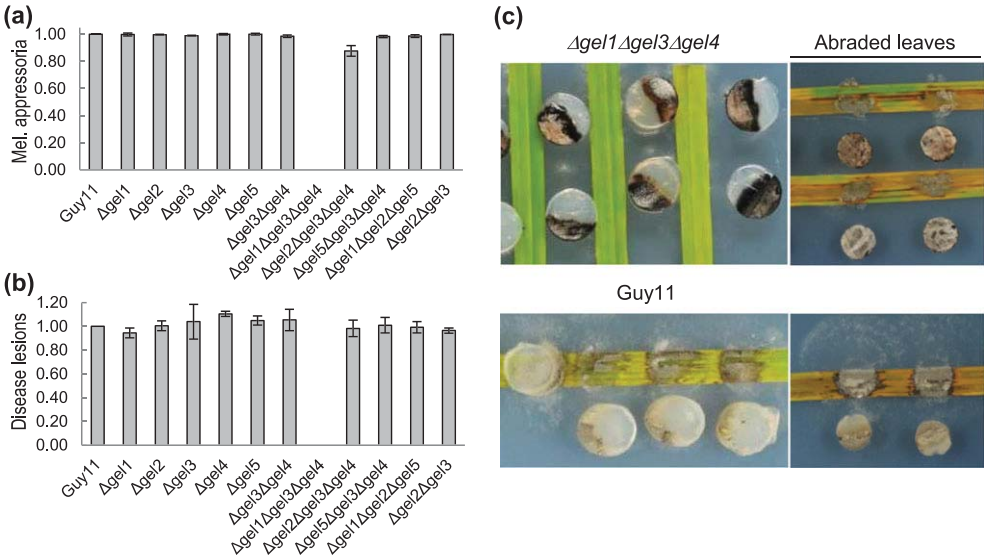

FIGURE 4 Germling infection-related development and pathogenicity assays of wild-type and mutant *Magnaporthe oryzae* strains. Guy11, *Δgel1*, *Δgel2*, *Δgel3*, *Δgel4*, *Δgel5*, *Δgel3Δgel4*, *Δgel1Δgel3Δgel4*, *Δgel2Δgel3Δgel4*, *Δgel5Δgel3Δgel4*, *Δgel1Δgel2Δgel5*, and *Δgel2Δgel3* mutants were assessed for (a) number of melanized appressoria 8 hours post-inoculation of conidial suspensions (2.5×10^{-5} spores ml^{-1}) onto a hydrophobic surface. (b) Number of lesions developed on rice (*Oryza sativa*) leaves spray-inoculated with conidial suspensions (2.5×10^{-5} spores ml^{-1}) and incubated for 5 days. Both experiments were replicated three times with a minimum of two independent lines of each strain; results were normalized to Guy11 and shown as mean ± SEM. Note that the triple *Δgel1Δgel3Δgel4* mutant does not produce spores. (c) Representative examples of Guy11 and the *Δgel1Δgel3Δgel4* mutant inoculated as mycelial plugs on rice shown 5 days later when the plugs were removed and placed next to the leaf for photography

Microscopic observation of the growing edge of *Δgel1Δgel3Δgel4* mycelium also revealed a hyperbranching phenotype (Figure 5a, CFW). In addition, there are differences in general staining intensity, perhaps due to the less branched glucans allowing greater accessibility to CFW, and greater intensity at growing tips, where the newly synthesized glucans are unlikely to have branched or be highly cross-linked.

The mutant mycelial cells are short, often round, and branch frequently (Figure 5b). Furthermore, when grown across a glass cover slip for 6 days, *Δgel1Δgel3Δgel4* formed terminal rounded tip ends, which then continued to grow and form hyphae (Figure 5c, CR).

Sensitivity to exposure to the fungal wall-degrading enzyme Glucanex was used to compare the rates of release of protoplasts by *Δgel1Δgel3Δgel4* with Guy11 from mycelial tissues (*Δgel1Δgel3Δgel4* does not sporulate). This revealed that *Δgel1Δgel3Δgel4* releases fewer protoplasts and at a slower rate than the Guy11 strain—approximately 5–10-fold fewer protoplasts than Guy11, some 180 minutes post-exposure to wall-degrading enzymes (Figure 5d). This data suggests that the altered mutant wall is more resistant to Glucanex degradation than WT—a result that attests to the unknown enzyme specificity of these members of the Gel family. *Δgel1Δgel3Δgel4* protoplasts were

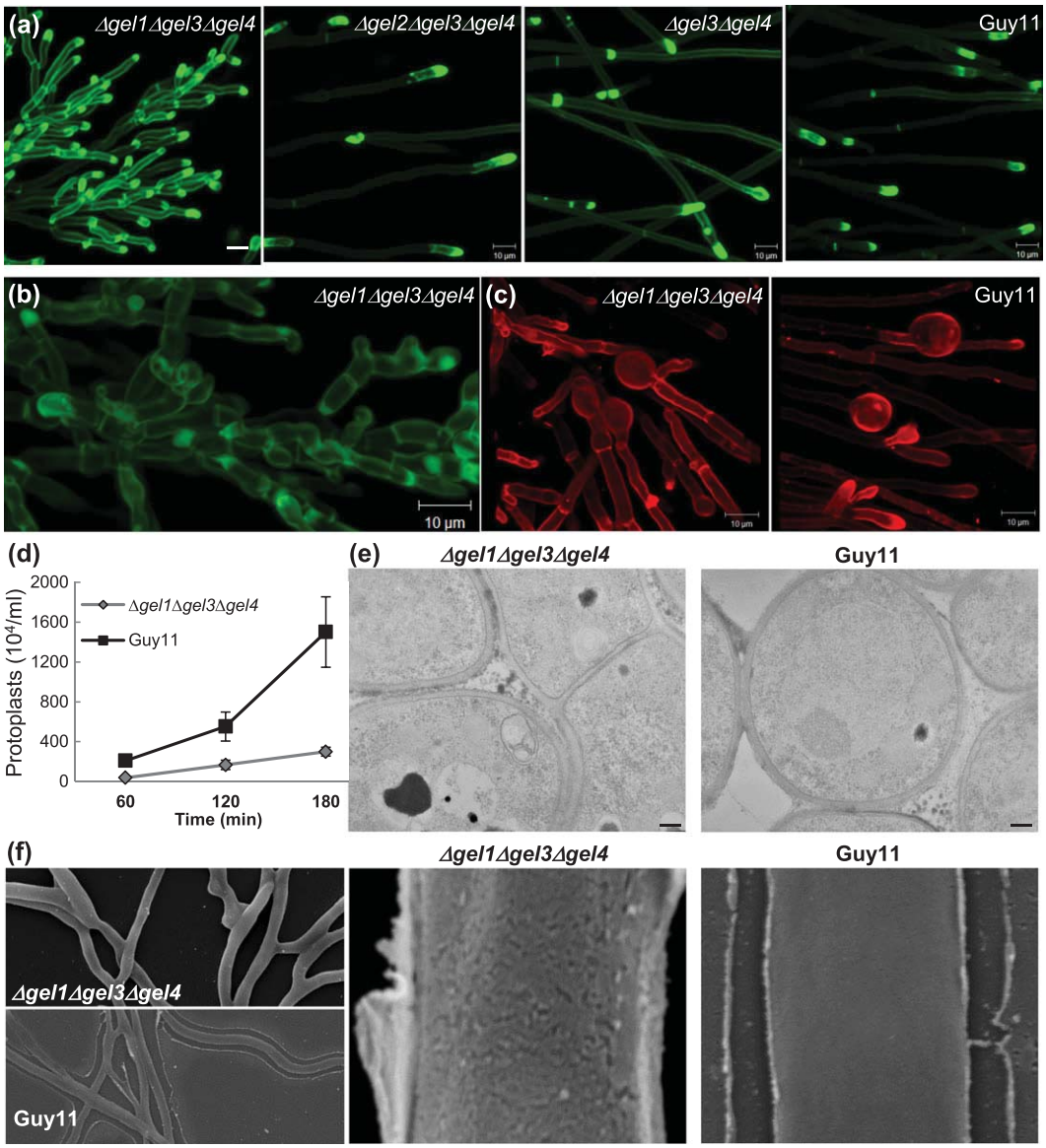

FIGURE 5 Characterization of triple *Δgel1Δgel3Δgel4* mutant phenotype by confocal microscopy, transmission electron microscopy (TEM), and scanning electron microscopy (SEM). (a) Projection of z-stack of CFW-stained growing tips of the triple *Δgel1Δgel3Δgel4* mutant showing hyperbranching phenotype compared to *Δgel2Δgel3Δgel4*, *Δgel3Δgel4*, or wild-type strain Guy11. The scale bar indicates 10 μm. (b) Higher magnification image of *Δgel1Δgel3Δgel4* mutant stained as in (a) shows very short and rounded cells with multiple branching. (c) Projection of z-stack of CR stained mycelia near colony edge (5 mm) showing swollen cells in *Δgel1Δgel3Δgel4* mutant that continue to grow, as compared with Guy11 where these are terminal cells. (d) Three-day-old Guy11 and *Δgel1Δgel3Δgel4* liquid cultures were exposed to Glucanex for up to 180 minutes post-treatment and the numbers of protoplast released counted. The experiment was repeated twice with three replica treatments per strain. (e) TEM images of mycelial cross section of *Δgel1Δgel3Δgel4* mutant and Guy11 at 20.000× magnification. The scale bar represents 200 nm. (f) SEM images of *Δgel1Δgel3Δgel4* mutant and Guy11 at 1.700× (left) and 35.000× (middle and right) magnification. The surface of the triple mutant appears rough while Guy11 is smooth but with extruded extracellular matrix

restored to full growth on CM plates, in a similar manner to Guy11 growth (data not shown).

We compared the mycelial walls of *Δgel1Δgel3Δgel4* and Guy11 by TEM (Figure 5e). This revealed no gross differences in wall thickness between the strains, with *Δgel1Δgel3Δgel4* walls being 81.1 ± 40.6 nm thick and Guy11 walls at 73.8 ± 35.2 nm (P = 0.342, n = 50). We compared cryo-SEM images of *Δgel1Δgel3Δgel4* and Guy11 mycelium near its growing edge, showing again the mutant's densely branching phenotype (Figure S4). Finally, we collected SEM images of *Δgel1Δgel3Δgel4* mutant and Guy11, revealing that the mutant surface appears stippled, whilst Guy11 is smooth but with ECM extruded from the wall—a feature absent from the triple mutant (Figure 5f).

2.10 | Monosaccharide composition and linkage analysis of *M. oryzae* cell wall polysaccharides in the triple Δgel1Δgel3Δgel4 mutant

We determined the monosaccharide composition of alkali soluble and insoluble fractions (Table 2), and specific glycosidic linkages in the *Δgel1Δgel3Δgel4* wall. Consistent with the double mutant *Δgel3Δgel4*, the triple mutant showed a greater abundance of linear 1,3-glucans (approximately 18% higher than WT). Indeed, with a decreased proportion in terminal—and 1,3,6-glycosidic linkages, the glucans are characterized by a higher degree of polymerization and a lower number of 1,6-branching points (Figure 6). In essence, 1,3-Glc*p* in *Δgel3Δgel4* (P = 0.042, n = 3) and *Δgel1Δgel3Δgel4* (P = 0.002, n = 4), and t-Glc*p* in *Δgel1Δgel3Δgel4* (P = 0.025, n = 4); all such values (of double and triple mutant variants) are thus statistically significant from Guy11.

2.11 | Transcriptional analysis of the triple *Δgel1Δgel3Δgel4* mutant strains and Guy11

The triple mutant strain *Δgel1Δgel3Δgel4* shows a nonsporulating, hyper-branching phenotype. We asked whether this altered morphology correlated with specific changes in genes expression between the mutant and wild-type strains—we thus investigated which genes were differentially expressed as compared with Guy11. We identified global patterns of gene expression in two independent *Δgel1Δgel3Δgel4* mutant strains, compared with Guy11, by RNA-Seq analysis. Three independent replicates were analyzed from each strain. Figure S5a shows the overall Euclidean distance (distance between two points in space as showing a measure of the differences between the wild type and mutant strains) between all samples. Individual replicates from each sample cluster together and expression data from the

TABLE 2 Monosaccharide composition of the alkali soluble (ASF) and insoluble (AIF) fraction in *Magnaporthe oryzae* cell walls (mol %)

	ASF				AIF			
	Guy11		*Δgel1Δgel3Δgel4*		Guy11		*Δgel1Δgel3Δgel4*	
	AV	SD	AV	SEM	AV	SD	AV	SEM
Ara	0.74	0.08	7.40	0.08	nd	nd	nd	nd
Xyl	0.13	0.02	2.30	0.14	nd	nd	nd	nd
Mannose	39.80	2.42	30.20	0.68	4.71	1.30	3.55	0.08
Galactose	6.53	0.28	10.93	0.29	1.32	0.37	1.33	0.05
Glucose	51.99	2.50	49.15	0.26	86.53	1.56	86.28	0.45
N-Acetylglucosamine	0.80	0.15	nd	nd	7.45	0.76	8.90	0.42

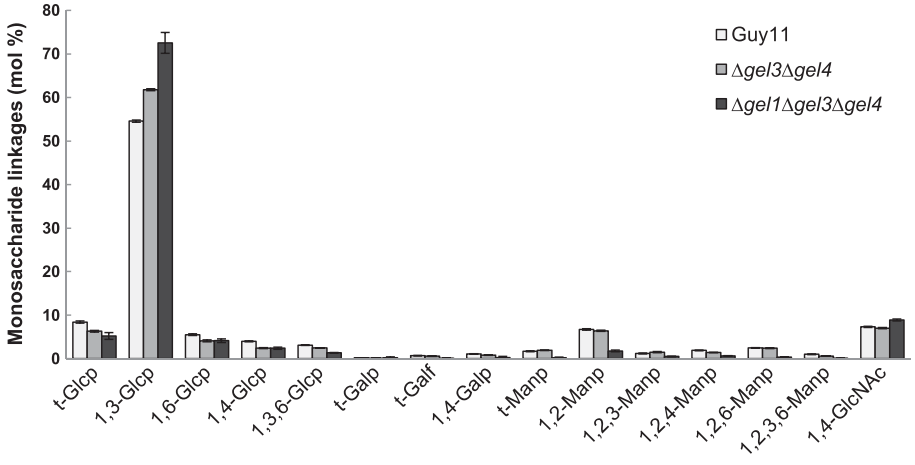

FIGURE 6 Linkage analysis of purified cell wall polysaccharides from Guy11, *Δgel3Δgel4*, and *Δgel1Δgel3Δgel4* mutant strains (GC/EI-MS). Liquid complete medium was inoculated with spores or hyphal residues (as the triple mutant does not sporulate) and shaken at 150 rpm at 24°C for 4 or 7 days. Cell wall polysaccharides were purified and analyzed as described in Section 4. The percentage of monosaccharide derivatives identified from each of the three strains was determined from four technical replicates derived from each of the three independently grown biological replicates

two individual mutants are far closer to each other than to Guy11. Based on *p*-values (adjusted for multiple testing, using Benjamini-Hochberg method) <0.01 and at least two-fold difference in expression, the two mutants share 310 genes upregulated and 235 genes downregulated, compared to Guy11 (Table S6 and S7).

GO terms that are more highly represented in genes that showed differential upregulation in *Δgel1Δgel3Δgel4* (as compared with the whole genome) are shown in Figure S5b. Of these, the most interesting are the glycoside hydrolases (GH) (GO:0016798). Nineteen GH encoding genes are upregulated, of which, 14 are predicted to be secreted (Supp Table S8). Fungal cell wall remodeling enzymes include the glucan 1,3-beta-glucosidase and chitinase, as well as the wall-building chitin synthase and polysaccharide-degrading enzymes, predicted to be extracellular, such as alpha amylase, xylanase, alpha-galactosidase, and beta-fructofuranosidase. Interestingly, *GEL2* is upregulated strongly in the mutant, possibly to compensate for the absence *GEL1*, *GEL3*, and *GEL4*. This follows a similar finding with Gel7 in *Aspergillus fumigatus* (Zhao, Li, Liang, & Sun 2014). The sole gene encoding alpha-1,3 glucan synthase (*MgAGS1*, Fujikawa et al. 2012) is also upregulated. This gene has been reported to be under the control of MAP kinase Mps1 and therefore may be induced under conditions of cell wall stress (Yoshimi et al. 2013). Other notable differences are shown in Table S9.

GO terms that are more highly represented in downregulated genes found in *Δgel1Δgel3Δgel4* are summarized in Figure S5c and listed in Table S7. They include six genes involved in cell surface signaling (GO:0007166; Kulkarni, Thon, Pan, & Dean 2005), seven genes encoding copper ion-binding proteins (GO:0005507)—two of which are involved in conidial pigment biosynthesis (Figure S7), five chitin-binding proteins (GO:0008061), and also *MGG_02246*, a homologue of *N. crassa* highly expressed conidiation-specific protein 6 (White & Yanofsky 1993). Both *GEL1* and *GEL4* are significantly downregulated in *Δgel1Δgel3Δgel4*.

Thus, many of the changes in gene expression identified in *Δgel1Δgel3Δgel4* are likely due either directly or indirectly (because of exogenously imposed wall stress), to the lessened proportion of wall ß-1,3-glucans. The elevated expression of a number of secreted proteases and certain wall-remodeling enzymes may also be in response to changes in wall composition. Indeed, in *C. albicans*, secreted protease activity influences wall function, by proteolytic cleavage of wall proteins (Schild et al. 2011). We conclude that the Gel-deficient *Δgel1Δgel3Δgel4* mutant shows significant differences in gene expression of a wide range of wall-encoding enzymes. This highlights the global effect of perturbation of the β-1,3-glucan content and the impact this structural modification has on cell wall composition and fungal virulence.

3 | DISCUSSION

During plant infection, the rice blast fungus undergoes a series of morphogenetic transitions. These include development of the appressorium and formation of invasive hyphae that colonize rice cells and propagate by pseudohyphal growth, a feature not observed in vegetative culture. In this report, we provide the first comprehensive description of the wall composition in the rice blast fungus, which is related to the developmental biology of the pathogen. In *M. oryzae*, glucosyl residues dominate, representing 75% of the monosaccharide components of the wall. The other monosaccharides occurring in the fungal wall are mannose (14%), *N*-acetylglucosamine (7%), galactose (2%), and traces of arabinose and xylose. We are aware of only one other plant-pathogenic fungus where the wall has been described in detail, that is, the necrotroph *Botrytis cinerea* (Cantu, Greve, Labavitch, & Powell 2009). The glucose component appears higher in the *B. cinerea* wall, with approximately 90% glucose and much lower amounts of galactose, mannose, and arabinose (Cantu et al. 2009). The *M. oryzae* data align well with the wall compositions described in *S. cerevisiae* (Dallies, Francois, & Paquet 1998) and C. albicans (Ene et al. 2012), whereas in A. fumigatus and *S. pombe*, galactomannans are more prevalent, but such analyses account for both the wall and ECM (Xie & Lipke 2010). It is important to note that the amounts of each the constituent monosaccharides are not absolutes as they fluctuate during growth and morphogenesis, and in response to external stress or medium composition.

As the fungal wall comprises components unique to the Kingdom Fungi, it forms an attractive target for the development of novel antifungal drugs. Indeed, towards the goal of rational design of novel antifungals, it is prescient to characterize the proteins considered to catalyze early steps in the formation of the uniquely fungal elongate and branched chains—that is the step, likely driven by Gel activity in fungi. These proteins are tethered to the plasma membrane by GPI anchors and face the wall: They are thus perfectly placed to create branch points/branches on the main backbone of the emergent chain.

We thus investigated the GH72 family of putative β-1,3-glucanosytransferases. In *M. oryzae*, 5 *GEL* genes encode the family GH72^{+} (*GEL3* and *GEL4*), the GH72^{-} (*GEL1*, *GEL2*, and *GEL5*). These proteins have been investigated in a number of fungal species, including *S. cerevisiae* (Ragni et al. 2007), *S. pombe* (Medina-Redondo et al. 2010), and the filamentous fungi *C. albicans* and *A. fumigatus* (Mouyna et al. 2000b; Mouyna et al. 2005). The Gels display β-1,3-glucanosyltransferase activity *in vitro*, although they differ in their specificity for substrate length, cleavage point, and product size. However, when we overexpressed *M. oryzae GEL3* and *GEL4* in yeast *Δgas1*, neither fully complemented the mutant phenotype (despite having both functional GH72 and CBM43 domains) suggesting a different role for these proteins in the rice blast fungus. Despite protracted effort, we were unable to express *GEL4* in heterologous expression systems in *P. pastoris* and *E. coli*. Gel3 was successfully expressed, albeit at very low levels, but its instability precluded *in vitro* enzymatic assays (data not shown). Nevertheless, detailed linkage analysis of the wall polysaccharides of *Δgel3Δgel4* revealed increased proportions of 1,3-linked glucose residues, while the proportions of terminal glucose and residues indicative of the presence of branching points (1,3,6-Glc*p*) were less abundant. These data suggest that the proteins function on the 1,3-glucan chains and might be involved in branching activity indirectly.

We localized Gel3 and Gel4 to the cell wall periphery by creating internal fusions with mCherry and GFP, and expressing them under their respective native promoters. Similar localization was reported for YFP-gas1 and gas2-GFP fusions in *S. pombe* (Medina-Redondo

et al. 2010) and Phr1-GFP fusion in C. albicans (Ragni et al. 2011). We showed spatial and temporal differences in expression between the two genes: Both are expressed in ungerminated and germinated spores, and germ tubes but do not completely co-localise. This was demonstrated in the WT strain transformed with both fusions: For example, while the Gel4-GFP localized more to the periphery of the conidial septum between the basal and middle cell, the Gel3-mCherry was uniformly dispersed within the septum. Similar observations were made in *S. pombe* where Gas1p localized as a disc to the nascent septum, whereas Gas2p remained at the septum edging during its synthesis (Medina-Redondo et al. 2010).

Single *GEL* gene deletions of all family members did not reveal any phenotypic differences from Guy11, apart from reduced growth of *Δgel4* on MM or on CM supplemented with CFW or SDS, as reported for many CW mutants (Maddi, Dettman, Fu, Seiler, & Free 2012). This finding resonates with the observation that *GEL4* is strongly expressed in mycelium. This phenotype was further enhanced in double *Δgel3Δgel4* mutant, which was also sensitive to oxidative stress. However, both $GH72^{+}$ gene mutant strains, (*Δgel3Δgel4*), as well as $GH72^{-}$ mutant, tested as *Δgel1Δgel2Δgel5* proved dispensable for pathogenicity.

From the combinatorial triple deletion strains generated in this study, *Δgel1Δgel3Δgel4* is a non-sporulating hyperbranching mutant emanating from shortened hyphal cells. The mutant does not infect intact rice leaves but it can cause lesion formation when mycelium is inoculated onto an abraded cuticle. Detailed analysis of this triple mutant strain reveals that it is more resistant to digestion by glucan-degrading enzymes than WT, as has been demonstrated previously in *N. crassa* (Kamei et al. 2013). There is, however, no obvious difference in cell wall thickness, as evidenced by TEM. The mutant strain wall appeared rougher than the WT wall, and ECM was absent from *Δgel1Δgel3Δgel4*.

Cell wall analysis revealed only minor differences in the glucose between the *Δgel1Δgel3Δgel4* mutant and WT, but galactose is significantly increased, while mannose reduced. Perhaps the most surprising is the 10-fold increase in arabinose and xylose in the triple mutant. However, these are minor components of the mutant wall suggestive of the presence of arabinoxylans. The linkage analysis further confirmed the observation made with the double *Δgel3Δgel4* mutant, that is, an increased number of 1,3-glucose linkages in the triple mutant strain.

When considered together, we have invoked the use of *GEL* gene deletions to show that the cell wall composition of *M. oryzae* differs during infection-related development, and we have described the differential contributions of the family of ß-1,3-glucan glucanosyltransferases. These enzymes play key roles in the development and structural composition of conidia and germ tubes, but do not contribute to the rigid cell wall associated with the melanin-pigmented appressorium that is formed by the fungus to bring about plant infection. Although individually dispensable for virulence of *M. oryzae*, a mutant lacking three of the *GEL*-encoding genes, *Δgel1Δgel3Δgel4*, was unable to cause rice blast disease and also showed a different developmental phenotype, with a hyper-branching hyphal phenotype and the absence of spores. This suggests that the structural integrity and flexibility of the cell wall is adversely affected by the disruption to ß-1,3-glucan glucanosyltransferase activity. This also, however, clearly has wider impacts, based on RNA-seq analysis, which revealed an effect not only on perturbed expression of genes encoding cell wall-associated enzymes, but on many membrane proteins associated with surface sensing, such as G-protein-coupled receptors. Taken together, this highlights the interplay and reliance of membrane signaling on the structural properties of the fungal wall, and how perturbation of wall characteristics can exert a profound effect on external communication by fungal cells, which affects their ability to undergo the developmental transitions required for host infection.

4 | EXPERIMENTAL PROCEDURES

4.1 | Fungal strains and growth conditions

The WT rice pathogenic *M. oryzae* strain Guy11 and mutants were cultured at 24°C, with a 14-h light 10-h dark cycle. Strain maintenance and media composition are as Talbot et al. (1993).

4.2 | Targeted deletion of *M. oryzae GELs*

To generate single targeted gene deletions *Δgel1*, *Δgel2*, *Δgel3*, *Δgel4*, *Δgel5*, *M. oryzae GEL1* (*MGG_07331*) and *GEL3* (*MGG_08370*) were replaced by a hygromycin resistance cassette (Sweigard, Chumly, Carrol, Farrall, & Valent 1997); and *GEL2* (*MGG_06722*), *GEL4* (*MGG_11861*), and *GEL5* (*MGG_03208*) by the bialophos resistance marker (GenBank AF013602). Fragments carrying approximately 1.5 kb upstream and 1.2 kb downstream of GEL-specific flanking sequences were PCR amplified using primers GELx-KO-F + pGELx-R and pAGELx-F + GELx-KO-R, respectively. Fragments were conjoined, amplified using pGELx-F + pAGELx-R primers, and carrying a selectable marker, by over-lapping PCR using GELx-KO-F + GELx-KO-R primers and the amplicon used directly for DNA-mediated protoplast transformation of Guy11 (Talbot et al. (1993). Putative transformants were selected on MM supplemented with 300 $\mu g/ml^{-1}$ hygromycin B (Calbiochem, Merck, Darmstadt, Germany) or defined complex medium (DCM) supplemented with 60 $\mu g/ml^{-1}$ Bialophos (Goldbio, St Louis, MO, USA); subjected to PCR and Southern blot analysis to confirm single targeted gene replacement, as in Samalova et al. (2013) (Figure S6). To generate double knock-outs *Δgel3Δgel4*, *Δgel3* was retransformed with *GEL4*; *Δgel2Δgel3*, *Δgel3* was retransformed with *GEL2*; *Δgel1Δgel5*, *Δgel5* was retransformed with *GEL1*.

To generate triple knock-outs *Δgel1Δgel3Δgel4*, *Δgel2Δgel3Δgel4*, *Δgel5Δgel3Δgel4*; *Δgel3Δgel4* was retransformed with *GEL1*, *GEL2*, or *GEL5*, respectively. Finally, to generate *Δgel1Δgel2Δgel5; Δgel1Δgel5* was retransformed with *GEL2*. We used a third selectable marker, a resistant allele of *M. oryzae ILV1* gene (*MGG_06868*) to sulphonylurea in pCB1532 plasmid and GAP-repair *S. cerevisiae* cloning (Oldenburg, Vo, Michaelis, & Paddon 1997), to assemble the constructs in pNEB1284 (primers detailed in Table S3). Putative transformants were selected on BDCM medium, supplemented with 100 $\mu g/ml^{-1}$ chlorimuron ethyl (Sigma Aldrich, UK), and confirmed, as above.

4.3 | Confocal imaging

Spores (2.5×10^5/ml^{-1}) of Guy11 and complemented strains were collected from 10-day old plates and inoculated in 50-µl droplets onto hydrophobic glass cover slips (0, 2, 4, 8, and 16 hpi), onion peels (24 and 48 hpi), or rice leaf sheaths (24 and 48 hpi), as in Samalova, Meyer, Gurr, and Fricker (2014). To image vegetative hyphae, a glass cover slip was coated with a thin layer of growth medium; placed by the fungal growing edge and left to overgrow for two days. The coverslip was lifted off and the edge imaged using the C-Apochromat 40×/1.2 water-corrected objective lens of a Zeiss LSM510 Meta confocal microscope at 500–530 nm, with 488-nm Argon laser for eGFP, and 543-nm HeNe laser and BP565–615 filter for mCherry.

The CFW and CR staining was performed by overgrowing Guy11 and mutants on cover slips for 2–6 days then a drop of CFW or CR, at concentration 0.5 mg/ml^{-1}, was added 1 hr prior to imaging. The samples were viewed using CLS microscope, with 405-nm excitation and LP420 filter for CFW, and 543-nm excitation and LP585 for CR.

4.4 | Plate growth assays

Radial colony growth was assessed on CM and MM. CM plates, supplemented with CR: 150 mg/L^{-1}, CFW: 40 mg/L^{-1}, 0.005% (*w*/v) SDS, 0.5 M NaCl, 1 M sorbitol, 1 M glycerol, and 5 mM H_2O_2, were inoculated with a mycelial plug of 10-day-old plates (or 21-day-old plates for *Δgel1Δgel3Δgel4* mutant) and incubated for 10 days at 24°C in dark; apart from CM, MM, and SDS plates, grown under normal light cycle conditions. Heat stress was by moving CM plates to 32°C, 3 days post-inoculation. Colony diameters were measured; assays were with minimum four technical replicates in three biologically replicated experiments.

4.5 | Pathogenicity and infection-related morphogenesis assays

Infection-related appressorium development was assessed 8 hpi, following germling differentiation on hydrophobic glass cover slips (Gerhard Menzel, Glasbearbeitungswerk GmbH & Co., Braunschweig, Germany), counting 100 germlings in 3 independent experiments. Cuticle penetration was assessed, scoring frequency of penetration pegs and intracellular infection hyphae formation on onion epidermis, after incubation at 24°C for 24 hr.

Leaf infection assays were performed on blast-susceptible, 14–21-day-old seedlings of rice (*Oryza sativa* L.) cultivar CO39 or 7-day-old seedlings of barley (*Hordeum vulgare* L.) cultivar Golden Promise, using suspension of conidia (2.5×10^5/ml^{-1}) in 0.2% (w/v) gelatine water, spray inoculated onto leaves as Samalova et al. (2013). For the *Δgel1Δgel3Δgel4* mutant and Guy11, healthy and abraded (with fine-grade Emory board) rice leaves were inoculated with inverted plugs of colony edge-growing mycelium and infection assessed 5 days later. Leaves were autoclaved in 50 ml 1 M KOH, rinsed 3× in SDW, several drops of 0.05% (w/v) aniline blue in 0.067 M K_2HPO^4 (pH 9.0) added and samples viewed by epifluorescence microscopy (Hood & Shew 1996).

4.6 | Cell wall purification, fractionation and monosaccharide linkage analysis

Samples for wall analysis were prepared by scraping spores or hyphal residues (for *Δgel1Δgel3Δgel4*) from 10-day-old plates and inoculating 150-ml liquid CM medium (without yeast extract), shaking at 150 rpm at 24°C for 4 or 7 days for the triple mutant. The cultures were washed three times with SDW and freeze-dried.

Cell wall polysaccharides were purified and fractionated into alkali soluble fraction (ASF) and alkali insoluble fraction (AIF), as Mélida, Sandoval-Sierra, Dieguez-Uribeondo, and Bulone (2013), with three modifications: (a) mechanical disruption of mycelium with a vibratory disc mill (RS400, Retsch) in 2 cycles of 30 min at 30 Hz/s; (b) alcohol-insoluble residue was treated with α-amylase to remove starch/glycogen carbohydrates; (c) no SDS-mercaptoethanol treatment.

Total carbohydrate composition analysis of the two fractions was by acid hydrolysis, derivatization of released monosaccharides to their alditol acetates, and final quantification by GC-EI-MS (Blakeney, Harris, Henry, & Stone 1983; Mélida et al. 2013). Mild acid hydrolysis by TFA (3 h, 121°C) was employed for ASF (Albersheim, Nevins, English, & Karr 1967); for AIF, Saeman two-step sulfuric hydrolysis (72% H_2SO_4, R.T., 3 h; diluted H_2SO_4, 100°C, 3 h) was applied.

Monosaccharide linkage analysis was by methylation using the CH_3I/NaOH method (Ciucanu & Kerek 1984; Mélida et al. 2013). Partially methylated alditol acetates were analyzed by GC/EI-MS. Monosaccharide linkages (mol%) were obtained from four technical replicates of each of three biological replicates.

4.7 | Protoplast release by Glucanex

Three-day-old liquid cultures of Guy11 and *Δgel1Δgel3Δgel4* mutant, prepared as for *M. oryzae* transformation, were digested with Glucanex (13 mg/ml^{-1}) for 60, 120, and 180 min, after which, 10-µl aliquots were withdrawn and protoplasts counted.

4.8 | Transmission electron microscopy

Mycelial squares (app 5 × 5 mm) were cut from the growing edge of 10-day CM plates, fixed and viewed as described in Samalova et al. (2014).

4.9 | Scanning electron microscopy

Guy11 and *Δgel1Δgel3Δgel4* strains were grown for 2–4 days over glass cover slips laid on CM plates and fixed in 2% aqueous osmium tetroxide for 2 h and sequentially dehydrated in ethanol/water mixtures (25, 50, 75, 95, and 100% ethanol (30 min each mixture)) and transferred to dry ethanol. Following critical point drying (Tousimis Autosamdri® 815), material was coated with gold/palladium (Polaron SC7640) and viewed in a JEOL 5510 SEM operating at 15 kV.

4.10 | RNA seq

RNA-seq libraries were prepared using 5 µg of total RNA isolated from 21-day-old cultures grown on CM plates with TruSeq SBS Kit v3 from

Illumina (Agilent), according to manufacturers' instructions. One hundred base paired-end reads were sequenced from mRNA libraries on Illumina HiSeq 2500 (Illumina, Inc.) and filtered by fastq-mcf programme from the ea-utils package (http://code.google.com/p/ea-utils/), applying –x 0.01, –q 20, –p 10, and –u, and mapped to *Magnaporthe oryzae* 70–15 reference genome version 8 (Dean et al. 2005), using the TopHat2 splice site-aware aligner (Kim et al. 2013). Counts of reads mapping to each gene in the genome were generated using the HTSeq-count function of the HTSeq package (Anders, Pyl, & Huber 2015). Relative gene expression was quantified and differentially expressed genes identified using DESeq (Anders & Huber 2010). Gene ontology (GO) annotation of the *M. oryzae* genome and analysis of GO categories were performed using BLAST2GO (Conesa & Götz 2008).

ACKNOWLEDGMENTS

We acknowledge BBSRC grant BB/J008923/1. We are grateful to Sarah Rodgers, Hugh Dickinson, (Oxford) Andy Foster, and George Littlejohn (Exeter) for help with various images.

REFERENCES

Aguilar-Uscanga, B., & Francois, J. M. (2003). A study of the yeast cell wall composition and structure in response to growth conditions and mode of cultivation. *Letters in Applied Microbiology*, *37*, 268–274.

Aimanianda, V., & Latge, J. P. (2010). Problems and hopes in the development of drugs targeting the fungal cell wall. *Expert Rev of Anti Infec Ther*, *8*, 359–361.

Albersheim, P., Nevins, D. J., English, P. D., & Karr, A. (1967). A method for the analysis of sugars in plant cell wall polysaccharides by gas–liquid chromatography. *Carbohydrate Res*, *5*, 340–345.

Anders, S., & Huber, W. (2010). Differential expression analysis for sequence count data. *Genome Biology*, *11*, R106.

Anders, S., Pyl, P. T., & Huber, W. (2015). HTSeq-a Python framework to work with high-throughput sequencing data. *Bioinformatics*, *31*, 166–169.

Ando, A., Nakamura, T., Murata, Y., Takagi, H., & Shima, J. (2007). Identification and classification of genes required for tolerance to freeze–thaw stress revealed by genome-wide screening of *Saccharomyces cerevisiae* deletion strains. *FEMS Yeast Research*, *7*, 244–253.

Bebber, D. P., Ramotowski, M. A. T., & Gurr, S. J. (2013). Crop pests and pathogens move polewards in a worming world. *Nat Climate Change*, *3*, 958–988.

Blakeney, A. B., Harris, P. J., Henry, R. J., & Stone, B. A. (1983). A simple and rapid preparation of alditol acetates for monosaccharide analysis. *Carbohydrate Res*, *113*, 291–299.

Cantu, D., Greve, L. C., Labavitch, J. M., & Powell, A. L. T. (2009). Characterization of the cell wall of the ubiquitous plant pathogen *Botrytis cinerea*. *Mycological Research*, *113*, 1396–1403.

Caracuel, Z., Martinez-Rocha, A. L., Di Pietro, A., Madrid, M. P., & Roncero, M. I. (2005). *Fusarium oxysporum GAS1* encodes a putative ß-1,3-glucanosyltransferase required for virulence on tomato plants. *Molecular Plant-Microbe Interactions*, *18*, 1140–1147.

Carotti, C., Ragni, E., Palomares, O., Fontaine, T., Tedeschi, G., Rodriguez, R., … Popolo, L. (2004). Characterization of recombinant forms of the yeast Gas1 protein and identification of residues essential for glucanosyltransferase activity and folding. *The FEBS Journal*, *271*, 3635–3645.

Chaffin, W. L. (2008). *Candida albicans* cell wall proteins. *Microbiology and Molecular Biology Reviews*, *72*, 495–544.

Chida, T., & Sisler, H. D. (1987). Restoration of appressorial penetration ability by melanin precursors in *Pyricularia oryzae* treated with antipenetrants and in melanin-deficient mutants. *Journal of Pesticide Science*, *12*, 49–55.

Ciucanu, I., & Kerek, F. (1984). Simple and rapid method for the permethylation of carbohydrates. *Carbohydrate Res*, *131*, 209–217.

Conesa, A., & Götz, S. (2008). Blast2GO: A comprehensive suite for functional analysis in plant genomics. *Int J Plant Genomics*, *2008*, 619832.

Couch, B. C., & Kohn, L. M. (2002). A multilocus gene genealogy concordant with host preference indicates segregation of a new species, *Magnaporthe oryzae*, from *M. grisea*. *Mycologia*, *94*, 683–693.

Dallies, N., Francois, J., & Paquet, V. (1998). A method for quantitative determination of polysaccharides in the yeast cell wall. *Application to the cell wall defective mutants of Saccharomyces cerevisiae. Yeast*, *14*, 1297–1306.

De Jong, J. C., McCormack, B. J., Smirnoff, N., & Talbot, N. J. (1997). Glycerol generates turgor in rice blast. *Nature*, *389*, 244–244.

Dean, R. A., Talbot, N. J., Ebbole, D. J., Farman, M. L., Mitchell, T. K., Orbach, M. J., … Birren, B. W. (2005). The genome sequence of the rice blast fungus *Magnaporthe grisea*. *Nature*, *434*, 980–986.

Ene, I. V., Adya, A. K., Wehmeier, S., Brand, A. C., MacCallum, D. M., Gow, N. A., & Brown, A. J. (2012). Host carbon sources modulate cell wall architecture, drug resistance and virulence in a fungal pathogen. *Cellular Microbiology*, *14*, 1319–1335.

Fontaine, T., Simenel, C., Dubreucq, G., Adam, O., Delepierre, M., Lemoine, J., … Latge, J. P. (2000). Molecular organization of the alkali-insoluble fraction of *Aspergillus fumigatus* cell wall. *The Journal of Biological Chemistry*, *275*, 27594–27607.

Fonzi, W. A. (1999). *PHR1* and *PHR2* of *Candida albicans* encode putative glycosidases required for proper cross-linking of ß-1,3- and ß-1,6-glucans. *Journal of Bacteriology*, *181*, 7070–7079.

Fujikawa, T., Kuga, Y., Yano, S., Yoshimi, A., Tachiki, T., Abe, K., & Nishimura, M. (2009). Dynamics of cell wall components of *Magnaporthe grisea* during infectious structure development. *Molecular Microbiology*, *73*, 553–570.

Fujikawa, T., Sakaguchi, A., Nishizawa, Y., Kouzai, Y., Minami, E., Yano, S., … Nishimura, M. (2012). Surface α-1,3-glucan facilitates fungal stealth infection by interfering with innate immunity in plants. *PLoS Pathogens*, *8*, 1–16.

Gastebois, A., Mouyna, I., Simenel, C., Clavaud, C., Coddeville, B., Delepierre, M., … Fontaine, T. (2010a). Characterization of a new β(1-3)-glucan branching activity of *Aspergillus fumigatus*. *J Biol Chemistry*, *285*, 2386–2396.

Gastebois, A., Fontaine, T., Latge, J. P., & Mouyna, I. (2010b). β(1-3) Glucanosyltransferase Gel4p is essential for *Aspergillus fumigatus*. *Eucaryotic Cell*, *9*, 1294–1298.

Hamer, J. E., Howard, R. J., Chumley, F. G., & Valent, B. (1988). A mechanism for surface attachment in spores of a plant pathogenic fungus. *Science*, *239*, 288–290.

Hood, M. E., & Shew, H. D. (1996). Applications of KOH-Aniline Blue fluorescence in the study of plant-fungal interactions. *Phytopathology*, *86*, 704–708.

Howard, R. J., & Valent, B. (1996). Breaking and entering: Host penetration by the fungal rice blast pathogen *Magnaporthe grisea*. *Annual Review of Microbiology*, *50*, 491–512.

Hurtado-Guerrero, R., Schuttelkopf, A. W., Mouyna, I., Ibrahim, A. F., Shepherd, S., Fontaine, T., … van Aalten, D. M. (2009). Molecular mechanisms of yeast cell wall glucan remodelling. *The Journal of Biological Chemistry*, *284*, 8461–8469.

Kamei, M., Yamashita, K., Takahashi, M., Fukumori, F., Ichiishi, A., & Fujimura, M. (2013). Deletion and expression analysis of beta-(1,3)-glucanosyltransferase genes in *Neurospora crassa*. *Fungal Genet and Biol*, *52*, 65–72.

Kankanala, P., Czymmek, K., & Valent, B. (2007). Roles for rice membrane dynamics and plasmodesmata during biotrophic invasion by the blast fungus. *Plant Cell*, *19*, 706–724.

Kershaw, M., Thornton, C. R., Wakley, G. E., & Talbot, N. J. (2005). Four conserved intramolecular disulphide linkages are required for secretion and cell wall localization of a hydrophobin during fungal morphogenesis. *Molecular Microbiology*, *56*, 117–125.

Khang, C. H., Berruyer, R., Giraldo, M. C., Kankanala, P., Park, S. Y., Czymmek, K., … Valent, B. (2010). Translocation of *Magnaporthe oryzae* effectors into rice cells and their subsequent cell-to-cell movement. *Plant Cell*, *22*, 1388–1403.

Kim, D., Pertea, G., Trapnell, C., Pimentel, H., Kelley, R., & Salzberg, S. L. (2013). TopHat2: Accurate alignment of transcriptomes in the presence of insertions, deletions and gene fusions. *Genome Biology*, *14*, R36.

Klis, F. M., De Groot, P., & Hellingwerf, K. (2001). Molecular organization of the cell wall of *Candida albicans*. *Medical Mycology*, *39*, 1–8.

Kulkarni, R. D., Thon, M. R., Pan, H., & Dean, R. A. (2005). Novel G-protein-coupled receptor-like proteins in the plant pathogenic fungus *Magnaporthe grisea*. *Genome Biology*, *6*, R24.

Latge, J. P. (2007). The cell wall: A carbohydrate armour for the fungal cell. *Molecular Microbiology*, *66*, 279–290.

Latge, J. P. (2010). Tasting the fungal cell wall. *Cellular Microbiology*, *12*, 863–872.

Lipke, P. N., & Ovalle, R. (1998). Cell wall architecture in yeast: New structure and new challenges. *Journal of Bacteriology*, *180*, 3735–3740.

Liu, Y. W., Lee, S. W., & Lee, F. J. (2006). Arl1p is involved in transport of the GPI-anchored protein Gas1p from the late Golgi to the plasma membrane. *Journal of Cell Science*, *119*, 3845–3855.

Maddi, A., Dettman, A., Fu, C., Seiler, S., & Free, S. J. (2012). WSC-1 and HAM-7 are MAK-1 MAP kinase pathway sensors required for cell wall integrity and hyphal fusion in *Neurospora crassa*. *PloS One*, *7*, .e42374

Mares, D., Romagnoli, C., Andreotti, E., Forlani, G., Guccione, S., & Vicentini, C. B. (2006). Emerging antifungal azoles and effects on *Magnaporthe grisea*. *Mycological Research*, *110*, 686–696.

Medina-Redondo, M., Arnaiz-Pita, Y., Clavaud, C., Fontaine, T., del Rey, F., Latge, J. P., & Vazquez de Aldana, C. R. (2010). β(1,3)-Glucanosyltransferase activity is essential for cell wall integrity and viability of *Schizosaccharomyces pombe*. *PloS One*, *5*, 1–13.

Mélida, H., Sandoval-Sierra, J. V., Dieguez-Uribeondo, J., & Bulone, V. (2013). Analysis of extracellular carbohydrates in oomycetes unveil the existence of three different cell wall types. *Eukaryotic Cell*, *12*, 194–203.

Mélida, H., Sain, D., Stajich, J. E., & Bulone, V. (2015). Deciphering the uniqueness of Mucoromycotina cell walls by combining biochemical and phylogenomic approaches. *Environ Microbioly*, *17*, 1649–1662.

Mouyna, I., Fontaine, T., Vai, M., Monod, M., Fonzi, W. A., Diaquin, M., … Latge, J. P. (2000a). Glycosylphosphatidylinositol-anchored glucanosyltransferases play an active role in the biosynthesis of the fungal cell wall. *The Journal of Biological Chemistry*, *275*, 14882–14889.

Mouyna, I., Monod, M., Fontaine, T., Henrissat, B., Lechenne, B., & Latge, J. P. (2000b). Identification of the catalytic residues of the first family of ß-(1,3)glucanosyltransferases identified in fungi. *The Biochemical Journal*, *347*, 741–747.

Mouyna, I., Morelle, W., Vai, M., Monod, M., Lechenne, B., Fontaine, T., … Latge, J. P. (2005). Deletion of GEL2 encoding for a ß-(1,3)-glucanosyltransferase affects morphogenesis and virulence in *Aspergillus fumigatus*. *Molecular Microbiology*, *56*, 1675–1688.

Mühlschlegel, F., & Fonzi, W. (1997). *PHR2* of *Candida albicans* encodes a functional homolog of the pH- regulated gene *PHR1* with an inverted pattern of pH-dependent expression. *Molecular and Cellular Biology*, *10*, 5960–5967.

Ni, L., & Snyder, M. (2001). A genomic study of the bipolar bud site selection pattern in *Saccharomyces cerevisiae*. *Molr Biol Cell*, *12*, 2147–2170.

Oldenburg, K. R., Vo, K. T., Michaelis, S., & Paddon, C. (1997). Recombination-mediated PCR-directed plasmid construction *in vivo* in yeast. *Nucleic Acids Research*, *25*, 451–452.

Popolo, L., & Vai, M. (1999). The Gas1 glycoprotein, a putative wall polymer cross-linker. *Biochim et Biophys Acta – General Subjects*, *1426*, 385–400.

Popolo, L., Ragni, E., Carotti, C., Palomares, O., Aardema, R., Back, J. W., … de Koster, C. G. (2008). Disulfide bond structure and domain organization of yeast ß-(1,3)-glucanosyltransferases involved in cell wall biogenesis. *The Journal of Biological Chemistry*, *283*, 18553–18565.

Ragni, E., Fontaine, T., Gissi, C., Latge, J. P., & Popolo, L. (2007). The Gas family of proteins of *Saccharomyces cerevisiae*: Characterization and evolutionary analysis. *Yeast*, *24*, 297–308.

Ragni, E., Calderon, J., Fascio, U., Sipiczki, M., Fonzi, W. A., & Popolo, L. (2011). Phr1p, a glycosylphosphatidylinositol-anchored ß (1,3)-glucanosyltransferase critical for hyphal wall formation, localizes to the apical growth sites and septa in *Candida albicans*. *Fungal Genet and Biol*, *48*, 793–805.

Ram, A. F., Wolters, A., Ten Hoopen, R., & Klis, F. M. (1994). A new approach for isolating cell wall mutants in *Saccharomyces cerevisiae* by screening for hypersensitivity to calcofluor white. *Yeast*, *10*, 1019–1030.

Ram, A. F. J., Kapteyn, J. C., Montijn, R. C., Caro, L. H. P., Douwes, J. E., Baginsky, W., … Klis, F. M. (1998). Loss of the plasma membrane-bound protein Gas1p in *Saccharomyces cerevisiae* results in the release of ß-1,3-glucan into the medium and induces a compensation mechanism to ensure cell wall integrity. *Journal of Bacteriology*, *180*, 1418–1424.

Ruiz-Herrera, J., & Ortiz-Castellanos, L. (2010). Analysis of the phylogenetic relationships and evolution of the cell walls from yeasts and fungi. *FEMS Yeast Research*, *10*, 225–243.

Ruiz-Herrera, J., Elorza, M. V., Valentin, E., & Sentandreu, R. (2006). Molecular organization of the cell wall of *Candida albicans* and its relation to pathogenicity. *FEMS Yeast Research*, *6*, 14–29.

Samalova, M., Johnson, J., Illes, M., Kelly, S., Fricker, M., & Gurr, S. (2013). Nitric oxide generated by the rice blast fungus *Magnaporthe oryzae* drives plant infection. *The New Phytologist*, *197*, 207–222.

Samalova, M., Meyer, A. J., Gurr, S. J., & Fricker, M. D. (2014). Robust anti-oxidant defence in the rice blast fungus *Magnaporthe oryzae* confer tolerance to the host oxidative burst. *The New Phytologist*, *201*, 556–573.

Schild, L., Heyken, A., de Groot, P. W., Hiller, E., Mock, M., de Koster, C., … Hube, B. (2011). Proteolytic cleavage of covalently linked cell wall proteins by *Candida albicans* Sap9 and Sap10. *Eukaryotic Cell*, *10*, 98–109.

Serrano, R., Bernal, D., Simon, E., & Arino, J. (2004). Copper and iron are the limiting factors for growth of the yeast *Saccharomyces cerevisiae* in an alkaline environment. *The Journal of Biological Chemistry*, *279*, 19698–19704.

Sillo, F., Gissi, C., Chignoli, D., Ragni, E., Popolo, L., & Balestrini, R. (2013). Expression and phylogenetic analyses of the Gel/Gas proteins of *Tuber melanosporum* provide insights into the infection and evolution of glucan remodelling enzymes in fungi. *Fungal Genet and Bioly*, *53*, 10–21.

Skamnioti, P., & Gurr, S. J. (2007). *Magnaporthe grisea* Cutinase2 mediates appressorium differentiation and host penetration and is required for full virulence. *Plant Cell*, *19*, 2674–2689.

Skamnioti, P., & Gurr, S. J. (2009). Against the grain: safeguarding rice from rice blast disease. *Trends Biotech*, *27*, 141–150.

Soanes, D. M., Chakrabarti, A., Paszkiewicz, K. H., Dawe, A. L., & Talbot, N. J. (2012). Genome-wide transcriptional profiling of appressorium development by the rice blast fungus. *PLoS Pathogens*, *8*, .e1002514

Sweigard, J., Chumly, F., Carrol, A., Farrall, L., & Valent, B. (1997). A series of vectors for fungal transformation. *Fungal Genet Newsl*, *44*, 52–55.

Talbot, N. J. (2003). On the trail of a cereal killer: exploring the biology of *Magnaporthe grisea*. *Annual Review of Microbiology*, *57*, 177–202.

Talbot, N. J., Ebbole, D. J., & Hamer, J. E. (1993). Identification and characterization of *MPG1*, a gene involved in pathogenicity from the rice blast fungus *Magnaporthe grisea*. *Plant Cell*, *5*, 1575–1590.

Talbot, N. J., Kershaw, M. J., Wakley, G. E., De Vries, O. M. H., Wessels, J. G. H., & Hamer, J. E. (1996). MPG1 encodes a fungal hydrophobin involved in surface interactions during infection-related development of *Magnaporthe grisea*. *Plant Cell*, *8*, 985–999.

Veneault-Fourrey, C., Barooah, M., Egan, M., Wakley, G., & Talbot, N. J. (2006). Autophagic fungal cell death is necessary for infection by the rice blast fungus. *Science*, *312*, 580–583.

White, B. T., & Yanofsky, C. (1993). Structural characterization and expression analysis of the *Neurospora* conidiation gene con-6. *Developmental Biology*, *160*, 254–264.

Wilson, R. A., & Talbot, N. J. (2009). Under pressure: Investigating the biology of plant infection by *Magnaporthe oryzae*. *Nature Reviews. Microbiology*, *7*, 185–195.

Xie, X., & Lipke, P. N. (2010). On the evolution of fungal and yeast cell walls. *Yeast*, *27*, 479–488.

Yoshida, K., Saunders, D. G. O., Mitsuoka, C., Natsume, S., Kosugi, S., Saitoh, H., … Terauchi, R. (2016). Host specialization of the blast fungus *Magnaporthe oryzae* is associated with dynamic gain and loss of genes linked to transposable elements. *BMC Genomics*, *17*, 370–377.

Yoshimi, A., Sano, M., Inaba, A., Kokubun, Y., Fujioka, T., Mizutani, O., … Abe, K. (2013). Functional analysis of the α-1,3-glucan synthase genes agsA and agsB in Aspergillus nidulans: agsB is the major α-1,3-glucan synthase in this fungus. *PloS One*, *8*, .e54893

Zhao, W., Li, C., Liang, J., & Sun, S. (2014). The *Aspergillus fumigatus* β-1,3-glucanosyltransferase Gel7 plays a compensatory role in maintaining cell wall integrity under stress conditions. *Glycobiol*, *24*, 418–427.

SUPPORTING INFORMATION

Additional Supporting Information may be found online in the supporting information tab for this article.

How to cite this article: Samalova, M, Mélida, H, Vilaplana, F, et al. The β-1,3-glucanosyltransferases (Gels) affect the structure of the rice blast fungal cell wall during appressorium-mediated plant infection, *Cell. Microbiol.* 2017;**19**:e12659. https://doi.org/10.1111/cmi.12659

GPI Anchored Proteins in *Aspergillus fumigatus* and Cell Wall Morphogenesis

Marketa Samalova, Paul Carr, Mike Bromley, Michael Blatzer, Maryse Moya-Nilges, Jean-Paul Latgé, and Isabelle Mouyna

Contents

Abstract Glycosylphosphatidylinositol (GPI) anchored proteins are a class of proteins attached to the extracellular leaflet of the plasma membrane via a post-translational modification, the glycolipid anchor. GPI anchored proteins are expressed in all eukaryotes, from fungi to plants and animals. They display very diverse functions ranging from enzymatic activity, signaling, cell adhesion, cell wall metabolism, and immune response. In this review, we investigated for the first time

Electronic supplementary material The online version of this chapter (https://doi.org/10.1007/82_2020_207) contains supplementary material, which is available to authorized users.

M. Samalova · M. Blatzer · J.-P. Latgé · I. Mouyna (✉)
Aspergillus Unit, Institut Pasteur, 25 Rue Du Docteur Roux, 75015 Paris, France
e-mail: isabelle.mouyna@pasteur.fr

P. Carr · M. Bromley
Division of Infection, Immunity and Respiratory Medicine, Manchester Fungal Infection Group, Faculty of Biology, Medicine and Health, University of Manchester, Manchester, UK

M. Moya-Nilges
Unité Technologie et Service Bioimagerie Ultrastructurale (UTechS UBI), Institut Pasteur, 28 Rue Du Docteur Roux, 75015 Paris, France

Current Topics in Microbiology and Immunology
https://doi.org/10.1007/82_2020_207

an exhaustive list of all the GPI anchored proteins present in the *Aspergillus fumigatus* genome. An *A. fumigatus* mutant library of all the genes that encode in silico identified GPI anchored proteins has been constructed and the phenotypic analysis of all these mutants has been characterized including their growth, conidial viability or morphology, adhesion and the ability to form biofilms. We showed the presence of different fungal categories of GPI anchored proteins in the *A. fumigatus* genome associated to their role in cell wall remodeling, adhesion, and biofilm formation.

1 Introduction

The fungal cell wall is composed of polysaccharides and glycoproteins. The main central core of this cell wall is very similar in all fungal species but the nature of the carbohydrates and the degree and type of bridges between polysaccharides vary from one species to another. Synthases responsible for the biogeneration of linear polysaccharides are transmembrane proteins acting alone or in protein complexes (Latgé et al. 2017). The neosynthesized polysaccharides are extruded through the plasma membrane via as yet, undefined mechanisms. They are modified in the periplasmic space by remodeling enzymes. Many of the cell wall associated proteins responsible for the remodeling of these polysaccharides are anchored to the plasma membrane by a **g**lycosylphosphatidyl**I**nositol (GPI) anchor and designed as GPI anchored proteins.

The role of GPI anchored proteins has been previously investigated in *Saccharomyces cerevisiae* and *Candida albicans* (Caro et al. 1997; Plaine et al. 2008). In silico analysis suggested that *C. albicans* possesses 115 putative GPI anchored proteins, almost twice the number reported for *S. cerevisiae*. Moreover, it has been shown previously that some of the GPI anchored proteins play a major enzymatic role in cell wall morphogenesis like, for example, the elongation of β-(1–3)-glucans in yeasts and molds (Popolo and Vai 1999; Mouyna et al. 2000a; Gastebois et al. 2010a), whereas in yeast, it was also mentioned that these proteins are covalently bound to the cell wall polysaccharide (Caro et al. 1997; Kapteyn et al. 2000; Frieman et al. 2002). Herein, we describe our in silico analysis to provide comprehensive role of the cohort of genes that encode GPI anchored proteins in *A. fumigatus* genome. To aid our understanding of the role of these GPI proteins in the construction of the cell wall, we have generated and characterized null mutants for all of the genes we identified in this study.

2 Identification of putative GPI anchored proteins in the *A. fumigatus* genome

The identification of putative GPI anchored proteins in the *A. fumigatus* genome (AF293; http://fungi.ensembl.org/Aspergillusfumigatus/Info/Index) has been undertaken using the prediction programs PredGPI (http://gpcr.biocomp.unibo.it/

predgpi/proteome.htm) and big PI (http://mendel.imp.ac.at/sat/gpi/gpi_server.html) (Eisenhaber et al. 2004). In total, 86 proteins have been identified and predicted as being GPI anchored (see Table 1).

3 Comparative genomic analysis

By performing BLAST analysis (https://www.yeastgenome.org/blast-fungal and https://blast.ncbi.nlm.nih.gov/Blast.cgi?PAGE=Proteins) with these proteins, we were able to show that all had orthologues in a second *A. fumigatus* isolate A1163. Orthologues of only 28 proteins (32.5%) were commons to the yeasts *S. cerevisiae* and *C. albicans* and filamentous fungi and a further 38 proteins (44%) were restricted to filamentous fungal species. Interestingly, 20 GPI anchored proteins (23.5%) were found exclusively in the genomes of the *Aspergilli* (Table 1).

4 Functions of GPI anchored proteins

Of the GPI anchored proteins that we have identified, the role of 34 proteins has been previously characterized either in *A. fumigatus* or in other fungi. In the following section, we describe their known roles.

(a) GPI anchored common to yeast and filamentous fungi acting on cell wall morphogenesis

Among the GPI anchored proteins previously described, several enzymes, *GEL*, *BGT2*, *DFG*, *SUN,* and *CRH*, have been well studied and shown to have functions associated with remodeling cell wall polysaccharides. The GPI anchors on these proteins result in them being co-localized with other cell membrane proteins that have direct roles in cell wall biogenesis and hence allow them to modify neosynthesized polysaccharides. The most extensively studied of these enzymes belong to the *GEL* family (GH72 in the CaZy database http://www.cazy.org/ which describes families of structurally related catalytic and carbohydrate-binding modules). Seven members of this family are encoded in the *A. fumigatus* genome, whereas *S. cerevisiae* (GAS) and *C. albicans* (PHR) have five members each (Rolli et al. 2011; Popolo et al. 2017). *GEL/GAS/PHR* family enzymes are responsible for the elongation of β-(1,3)-glucans, which is an essential activity given that deletion of *GEL4* in *A. fumigatus* is lethal (Hartland et al. 1996; Mouyna et al. 2000a, b; Gastebois et al. 2010a). It was recently shown that some members of this family have a dual activity that allows them not only to elongate but also to branch the neo elongated β-(1,3)-glucan (Aimanianda et al. 2017). This branching activity is only seen in enzymes that have the carbohydrate-binding module, CBM43, and loss of this motif abolishes β-(1,3)-glucan branching (Aimanianda et al. 2017).

Table 1 List of predictive GPI anchored proteins

AFUB number	AFUA.number	Gene name or function	Phenotype	Fungi	References
AFUB_018250	AFUA_2G01170	GEL1 §	no	Yeast and Filamentous	Hartland et al. (1996); Mouyna et al. (2000a, b)
AFUB_077400	AFUA_6G11390	GEL2 §	Conidia, Growth, S-D	Yeast and Filamentous	Mouyna et al. (2005)
AFUB_028470	AFUA_2G12850	GEL3	no phenotype	Yeast and Filamentous	Gastebois et al. (2010a
AFUB_022370	AFUA_2G05340	GEL4	Growth, S-D	Yeast and Filamentous	Gastebois et al. (2010a)
AFUB_084480	AFUA_8G02130	GEL5	no	Yeast and Filamentous	Gastebois et al. (2010a)
AFUB_036000	AFUA_3G13200	GEL6	no	Yeast and Filamentous	Gastebois et al. (2010a)
AFUB_078410	AFUA_6G12410	GEL7	no	Yeast and Filamentous	Gastebois et al. (2010a)
AFUB_048180	AFUA_3G00270	BGT2	no	Yeast and Filamentous	Gastebois et al. (2010b); Millet et al. (2018)
AFUB_002130	AFUA_1G01730	DFG1	no	Yeast and Filamentous	Muszkieta et al. (2019)
AFUB_017760	AFUA_2G00680	DFG2	no	Yeast and Filamentous	Muszkieta et al. (2019)
AFUB_048110	AFUA_3G00340	DFG3	Growth, S-D	Yeast and Filamentous	Muszkieta et al. (2019)
AFUB_047740	AFUA_3G00700	DFG4	no	Yeast and Filamentous	Muszkieta et al. (2019)
AFUB_101170	AFUA_4G00620	DFG5	no	Yeast and Filamentous	Muszkieta et al. (2019)
AFUB_100440	AFUA_4G02710	DFG7	no	Yeast and Filamentous	Muszkieta et al. (2019)
AFUB_013430	AFUA_1G13940	SUN2	no	Yeast and Filamentous	Gastebois et al. (2013)
AFUB_095070	AFUA_6G03230	CRH1 §	no	Yeast and Filamentous	Fang et al. (2019)
AFUB_020180	AFUA_2G03120	CRH2 §	no	Yeast and Filamentous	Fang et al. (2019)
AFUB_074470	AFUA_6G08510	CRH4	no	Yeast and Filamentous	Fang et al. (2019)
AFUB_015530	AFUA_1G16190	CRH5	no	Yeast and Filamentous	Fang et al. (2019)
AFUB_029980	AFUA_2G14360	ENG2	no	Yeast and Filamentous	Hartl et al. (2011)
AFUB_034540	AFUA_3G14680	PBL3	no	Yeast and Filamentous	Shen et al. (2004)
AFUB_052270	AFUA_5G03760	Chitinase A1	no	Yeast and Filamentous	Alcazar-Fuoli et al. (2011)
AFUB_063890	AFUA_4G06820	Ecm33 §	Conidia,virulence	Yeast and Filamentous	Chabane et al. (2006)

(continued)

Table 1 (continued)

AFUB number	AFUA.number	Gene name or function	Phenotype	Fungi	References
AFUB_076480	AFUA_6G10430	CDA6	no	Yeast and Filamentous	Mouyna et al (2020)
AFUB_092930	AFUA_6G05350	OPSB	no	Yeast and Filamentous	
AFUB_064130	AFUA_4G07040	CTSD	no	Yeast and Filamentous	Vickers et al. (2007)
AFUB_042000	AFUA_3G07050		no	Yeast and Filamentous	
AFUB_056560	AFUA_5G09020		no	Yeast and Filamentous	
AFUB_020300	AFUA_2G03230	AmylaseA	no	Filamentous fungi***	
AFUB_047500	AFUA_3G00900	Amylase	conidia, Growth,conidiation	Filamentous fungi***	
AFUB_000660	AFUA_6G14090	CFEMA	no	Filamentous Fungi	Vaknin et al. (2014)
AFUB_076620	AFUA_6G10580	CFEMB	no	Filamentous Fungi	Vaknin et al. (20201414)
AFUB_072620	AFUA_6G06690	CFEMC	no	Filamentous Fungi	Vaknin et al. (2014)
AFUB_057130	AFUA_5G09580	RODA #	Conidia,virulence	Filamentous Fungi	Aimanianda et al. (2009); Valsecchi et al. (2017a)
AFUB_016640	AFUA_1G17250	RODB #	no	Filamentous Fungi	Valsecchi et al. (2017a)
AFUB_042020	AFUA_3G07030	Glutaminase	no	Filamentous Fungi	
AFUB_081470	AFUA_8G06030	α(1-3) glucanase	no	Filamentous Fungi	
AFUB_097010	AFUA_6G00500	chitosanase	no	Filamentous Fungi	
AFUB_003980	AFUA_1G03570	PhoA §	no	Filamentous Fungi	Bernard et al. (2002)
AFUB_022180	AFUA_2G05150	AfMP2	Biofilm	Filamentous Fungi	Woo et al. (2018)
AFUB_099880	AFUA_4G03240	AFMP1	no	Filamentous Fungi	Woo et al. (2018)
AFUB_006180	AFUA_1G05790		Biofilm	Filamentous Fungi	
AFUB_087030	AFUA_7G00450		Biofilm	Filamentous Fungi	
AFUB_001030	AFUA_6G13710		no	Filamentous Fungi	
AFUB_004040	AFUA_1G03630		no	Filamentous Fungi	
AFUB_008960	AFUA_1G09510		no	Filamentous Fungi	

(continued)

Table 1 (continued)

AFUB number	AFUA.number	Gene name or function	Phenotype	Fungi	References
AFUB_009040	AFUA_1G09590		no	Filamentous Fungi	
AFUB_009100	AFUA_1G09650		no	Filamentous Fungi	
AFUB_018780	AFUA_2G01710		no	Filamentous Fungi	
AFUB_035550	AFUA_3G13640		no	Filamentous Fungi	
AFUB_036090	AFUA_3G13110		no	Filamentous Fungi	
AFUB_044890	AFUA_3G03370		no	Filamentous Fungi	
AFUB_047260	AFUA_3G01150		no	Filamentous Fungi	
AFUB_047510	AFUA_3G00880		no	Filamentous Fungi	
AFUB_050450	AFUA_5G01920		no	Filamentous Fungi	
AFUB_056330	AFUA_5G08800		no	Filamentous Fungi	
AFUB_057570	AFUA_5G09960		no	Filamentous Fungi	
AFUB_057610	AFUA_5G10010		no	Filamentous Fungi	
AFUB_069330	AFUA_4G12370		no	Filamentous Fungi	
AFUB_082130	AFUA_8G05410		no	Filamentous Fungi	
AFUB_083170	AFUA_8G04370		no	Filamentous Fungi	
AFUB_084140	AFUA_8G02450		no	Filamentous Fungi	
AFUB_085740	AFUA_8G00830		no	Filamentous Fungi	
AFUB_088990	AFUA_7G02440		no	Filamentous Fungi	
AFUB_089500	AFUA_7G03970		no	Filamentous Fungi	
AFUB_095500	AFUA_6G02800		no	Filamentous Fungi	
AFUB_010650	AFUA_1G11220		Conidia, S-D	Aspergillus	
AFUB_066710	AFUA_4G09600		conidia, conidiation	Aspergillus	
AFUB_096850	AFUA_6G00620		Conidia	Aspergillus	
AFUB_099690	AFUA_4G03360		Conidia	Aspergillus	
AFUB_018220	AFUA_2G01140		Conidia	Aspergillus	

(continued)

Table 1 (continued)

AFUB number	AFUA.number	Gene name or function	Phenotype	Fungi	References
AFUB_040120	AFUA_3G08990	CSPA	Conidia, adhesion	Aspergillus	Levdansly et al. (2010); Valsecchi et al. (2017b)
AFUB_019530	AFUA_2G02440		no	Aspergillus	
AFUB_031860	AFUA_2G16180		no	Aspergillus	
AFUB_044000	AFUA_3G03960		no	Aspergillus	
AFUB_084580	AFUA_8G02030		no	Aspergillus	
AFUB_087170	AFUA_7G00580		no	Aspergillus	
AFUB_087560	AFUA_7G00970		no	Aspergillus	
AFUB_000740	AFUA_6G14010		no	Aspergillus	
AFUB_082630	AFUA_8G04860		no	Aspergillus	
AFUB_030420	AFUA_2G14780		no	Aspergillus*	
AFUB_037960	AFUA_3G11190		no	Aspergillus*	
AFUB_089000	AFUA_7G02460		no	Aspergillus*	
AFUB_016760	AFUA_1G17390		no	Aspergillus*	
AFUB_066570	AFUA_4G09450		no	Aspergillus*	
AFUB_084830	AFUA_8G01770		Conidia, Growth, S-D	Aspergillus*	Mouyna et al. (2020) in preparation

List of the putative GPI-anchored proteins identified by the two softwares in the A. fumigatus genome including the corresponding AFUB and AFUA number (http://fungi.ensembl.org/Aspergillus_fumigatus/Info/Index), the gene name when identified, the phenotype of the mutant and their presence in the other genomes. Yeast and Filamentous: Proteins which are present in *C. albicans*, *S. cerevisiae*, *A. fumigatus* and others filamentous fungi; Filamentous Fungi: proteins present in filamentous fungi and not in the yeast genome; Filamentous Fungi***: these proteins are not present in the *S. cerevisiae* and C. albicans genome but they are present in the S. pombe and C. neoformans genome. Aspergillus: proteins only present in *Aspergillus* species; *Aspergillus**: proteins only present in few species of Aspergillus like *A. clavatus*, *A. lentulus*, *A. thermomutatus*, and the *A. turcosus* species; S-D: sensitivity to drugs. The GPI mutant library was screened for the growth on different media (Malt or Minimal medium), or Minimal medium (MM) including calcofluor white (40mg/ml), or congo red (50mg/ml) after 48h at 37°C, conidial morphology, conidial viability as described by (Millet et al. 2018), adhesion (104 conidia were incubated at 37°C on MM medium + 0.01% tween 20 on plates TPP for 24h) as described by Fontaine et al., (2010) and the ability to form biofilm on agar plates on MM medium after 22h of growth at 37° as described by (Beauvais et al., 2007). NB: no=no phenotype; S-D: higher sensitivity to drugs; Conidia: mutants which are affected in their conidia (shape, linear chains); Conidiation: mutants which are affected in conidiation. # RODA and RODB predicted to be GPI in silico but proved biochemically to be non GPI. § Proteins proved to be GPI biochemically

The GH17 family in *A. fumigatus* contains five members (*BGT1–3, SCW4 and SCW11)*; however, *BGT2* is the only member of this family that is GPI anchored. Bgt1 transfers the donor β-(1,3)-glucan on the non-reducing end of the chain (Mouyna et al. 1998), whereas Bgt2 preferentially transfers within the β-(1,3)-glucan chain (Gastebois et al. 2010b). No phenotype has been associated to the deletion of *BGT2* alone in *A. fumigatus* or its ortholog *BGL2* in the yeast *S. cerevisiae* (Cappellaro et al. 1998). However, Millet et al. (2018) and Sestak et al. (2004) showed that in *A. fumigatus* and *S. cerevisiae,* the non-GPI-members of the

GH17 family, especially Scw4, Scw11, and Bgt3 and Scw4, Scw10, and Scw11, are important for cell wall integrity. The enzymatic activity of Scw4, Scw11, and Bgt3 is still unknown but the analysis of the quintuple null mutant showed that Scw4, Scw11, and Bgt3 have antagonistic and distinct functions to Bgt2 and Bgt1.

Recently, it has been shown in *A. fumigatus* that the *DFG* family (GH76 CaZy family) is involved in the covalent binding of Galactomannan (GM) to the β-(1,3)-glucan–chitin core of the cell wall. This family contains seven members in *A. fumigatus*, all of which are GPI anchored proteins, except *DFG6* (Muszkieta et al. 2019). The single mutant Dfg3 is playing the major role in the association of the GM to the glucan core. However, the phenotype defect was enhanced in the septuple *DFG* deleted mutant, such as highly reduced growth with hyper-branched hyphae and higher sensitivity to drugs, showing that Dfgs have additional activities on structural properties of the cell wall (Muszkieta et al. 2019). In both, *S. cerevisiae* and *C. albicans*, although single knockouts of *DFG5* and *DCW1* are viable, a double knockout is synthetically lethal (Kitagaki et al. 2002; Spreghini et al. 2003). Interestingly as yeasts do not have galactomannan in their cell wall, the biochemical function of these remodeling enzymes remains to be discovered.

The *SUN* family *in A. fumigatus* (also known as the GH132 CaZy family) comprises two members, *SUN1* and *SUN2* which is the only one predicted to be GPI anchored in *A. fumigatus*. They are so called as they encode a SUN domain originally identified in the yeast proteins *SIM1*, *UTH1*, *NCA3,* and *SUN4*. The SUN domain is closely related, at the sequence level, to a β-glucosidase of *Candida wickerhamii;* however, the yeast proteins have no detectable β-glucosidase activity. The deletion of *SUN2*, which is most closely related to the uncharacterized protein YMR244W in *S. cerevisiae*, did not induce any morphological alterations. In contrast, the deletion of the *SUN1* genes in yeasts and molds has been shown to exhibit defects in septum closure (Hiller et al. 2007; Norice et al. 2007; Firon et al. 2007; Gastebois et al. 2013) However, the baker's yeast *SUN1* and their ortholog in *C. albicans SUN41/SUN42,* which encodes an exo β-(1,3)-glucanase but are not a GPI anchored protein, play a role in cell wall morphogenesis. Inactivation of *SUN1* genes and orthologs leads to a defect in the separation of daughter cells from mother cells, and simultaneous inactivation of *SUN41* and *SUN42* is lethal in the absence of osmotic protection. Like for *A. fumigatus*, cell wall defects seen in this double mutant are mainly localized in the region surrounding the septa in mother yeast cells and subapical hyphal compartments. The role taken by each SUN protein remains unknown as well as the role of the GPI anchor in the function of *A. fumigatus SUN2* in the cell.

The *CRH* (for Congo Red Hypersensitivity) GH16 CaZy family has been associated to glucan/chitin linkage in yeast *S. cerevisiae* (Rodríguez-Peña et al. 2000; Cabib et al. 2008; Blanco et al. 2012; Arroyo et al. 2016). In *A. fumigatus*, five members are present in the genome (four proteins being GPI anchored proteins). The phenotype of the quintuple mutant is very weak and not associated to congo red resistance. Congo red toxicity is pleiopropic with this molecule acting not only on cell wall biosynthesis but also in oxido-reduction pathways. Moreover, the biochemical function of the Crh proteins has not been demonstrated and there is

not a definite proof that these genes could be essential for the establishment of chitin–glucan linkages (Fang et al. 2019).

Members of the *SPS2* family (which are not assigned to a CaZy family) play an essential role in the formation of the ascospore cell wall in *S. cerevisiae* (Coluccio et al. 2004), whereas the ortholog in *A. fumigatus*, *ECM33*, is important for conidial morphogenesis and virulence (Chabane et al. 2006). However, its enzymatic function remains unknown.

Three GPI anchored proteins, CFEM (A-C), containing fungal-specific CFEM domains (Common in Fungal Extracellular Membrane) are characterized by spaced cysteine residues (Kulkarni et al. 2003). Most CFEM-containing cell wall proteins studied to date have been shown to be involved in host-pathogen interactions and virulence. In *C. albicans*, deletion of the three GPI anchored-CFEM-encoding genes in the genome (Rbt5/Rbt51/Csa1) results in an increased sensitivity to cell wall damaging agents and a reduced ability to form a biofilm (Pérez et al. 2006, 2011). In contrast, in *A. fumigatus*, (Vaknin et al. 2014) showed that these proteins, even though their respective mutants display a higher sensitivity to congo red and calcofluor white than their parental strain, did not play any role in cell wall morphogenesis or virulence.

Finally, no phenotype has been associated to the endo β-(1,3)-glucanase *ENG2* (Hartl et al. 2011) or the chitinase A1 (Alcazar-Fuoli et al. 2011) and the chitin deacetylase *CDA6* (Mouyna et al. 2020), which are the only GPI members in their respective family. However, the sequential deletion of *ENG2–5* belonging to the GH16 family altogether with *ENG1* (GH81) showed conidiogenesis defects, with linear chains of conidia unable to separate while the germination rate was not affected (Mouyna et al. 2016).

(b) GPI anchored proteins only found in filamentous fungi which are associated to cell wall structures

In addition to the GPI anchored proteins common to yeast and filamentous fungi which have been shown to be biochemically associated to cell wall construction, other GPI anchored proteins identified in silico are present only in the cell wall of filamentous fungi and are involved in adhesion and biofilm formation (Table 1).

The outer layer of the conidium is composed of melanin covered by a rodlet layer that confers hydrophobic properties to *A. fumigatus* conidia. This rodlet layer is exclusively composed of hydrophobins, which are low molecular weight proteins rich in cysteins residues. This rodlet layer masks conidial recognition by the human innate immune system (Aimanianda et al. 2009). Recently, (Valsecchi et al. 2017a) showed that seven hydrophobins (RodA–RodG) are present in the genome of *A. fumigatus*. RodA and RodB were identified as putative GPI anchored protein based on our in silico analysis. However, two lines of evidence indicate that the proteins are probably not GPI anchored: the predicted ω cleavage site which is the amino acid immediately upstream of the putative site of GPI anchor addition (the omega site) is located between Cys-residues C7 and C8, which would disrupt a conserved disulfide bridge that is important to stabilize the structure of the proteins; moreover,

it has been shown that the C-terminus of RodA extracted from conidia corresponds to that of the full-length protein (Pille et al. 2015; Valsecchi et al. 2017a).

It has been shown by Levdansky et al. (2010) that deletion of *CSPA*, a repeat rich GPI anchored protein only found in *Aspergillus* sp., is involved in reduced adhesion and increase speed of conidial germination. Moreover, Valsecchi et al. (2017b) showed that conidia of the *CSPA* mutant tended to stay grouped together in long chains and adhered also between themselves. This gene has been shown to be regulated by the Myb1 transcription factor (Valsecchi et al. 2017b).

5 Investigating the role of newly identified GPI anchored proteins in cell wall morphogenesis

Most of the previously analyzed GPI proteins were associated somehow to cell wall construction and fungal morphogenesis. These results suggested that all GPI anchored proteins may have essential functions in fungal growth some of them being undefined and this was at the basis of the study of the GPI proteins in *A.fumigatus*. In order to investigate exhaustively the role of the GPI anchored proteins, an *A. fumigatus* mutant library of all the genes identified in silico were constructed following the procedures outlined in Zhao et al. (2019) and Furukawa et al. (2020) using the oligonucleotide primers described in Supplementary Table 1 and screened for growth, conidiation, and biofilm formation.

From the screening analysis, three categories of GPI anchored protein null mutants were identified: proteins found in yeast and filamentous fungi, proteins found exclusively in filamentous fungi, and proteins found exclusively in *Aspergillus* species. Ten of the 57 new mutants (the previously published mutants are not counted) showed a distinct phenotype from the parental strain including conidial morphology, growth, sensitivity to congo red and calcofluor white, adhesion or biofilm formation (Table 1).

(a) **Proteins found in Yeast and filamentous fungi**

28 proteins are present in yeast and filamentous fungi genome, 23 being already described previously (see above) and 38 proteins are present exclusively in filamentous fungi genome.

- **Proteins with putative enzymatic functions**

Secreted proteases have always attracted attention as potential mediators of fungal invasion, conidophore development, or adhesion (Monod et al. 2002). We did not observe any distinct growth phenotype after the deletion of the aspartic proteases *CTSD* (AFUA_4G07040) (Vickers et al. 2007) and *OPSB* (AFUA_6G05350). Phospholipases (Plbs) activity which can destabilize host membranes are also considered to be virulence factors for pathogenic fungi like *C. albicans* (Leidich et al. 1998). In *A. fumigatus*, the mutant resulting from the deletion of the

phospholipase *PLB3* (AFUA_3G14680) (Shen et al. 2004) is not affected. Similarly, phosphatase plays a major role in the fungal life. In *A. fumigatus*, the acid phosphatase PhoA (AFUA_1G03570) which is specific to filamentous fungi (Bernard et al. 2002) are not directly associated to growth (data not shown). Moreover, the two genes encoding a putative chitosanase and a putative α-(1–3)-glucanase (respectively AFUA_6G00500 and AFUA_8G06030) which were predicted as GPI anchored proteins specific to filamentous fungi, do not play a role in the cell wall remodeling in *A. fumigatus* since the corresponding deleted mutant behaved like the parental strain (data not shown). However, non-GPI anchored homologs of these proteins (three for chitosanases and eight for α-(1–3)-glucanases) are present in the *A. fumigatus* genome and could be involved in compensatory mechanisms after the deletion of the GPI gene of the family.

The GPI anchored protein encoded by AFUA_3G00900, is a putative amylase. The null mutant exhibits a twofold decrease in conidiation, a slight reduction in radial growth and increased resistance to congo red (data not shown). The protein encoded by this gene belongs to the GH13 family. This CAZYme family is a large family containing various hydrolyzing and transglycosylating enzymes, mostly acting on α-(1,4)- or α-(1,6)-glycosidic linkages, which can be involved in starch degradation or in the synthesis or modification of alpha-glucan in the fungal cell wall (Morita et al. 2006; Yuan et al. 2008). In addition to AFUA_300900, four other GH13 proteins are present in the *A. fumigatus* genome: AFUA_2G03230, another GPI anchored protein specific to filamentous fungi (Table 1), AFUA_2G00710, AFUA_4G10130, and AFUA_2G13460. In contrast to AFUA_3G00900, we saw no phenotype associated with the deletion of AFUA_2G03230. The phylogenetic tree of the GH13 family of *A. fumigatus* showed two distinct groups, the first group (with AFUA_2G00710 AFUA_4G10130) associated to proteins involved in starch degradation like AmyA and AmyB in *A. niger* (Korman et al. 1990) and the second group (AFUA_3G00900, AFUA_2G03230 and AFUA_2G13460) associated to proteins with transferase activities like AgtA and AgtB in *A. niger* and Aah3 in *S. pombe* (Morita et al. 2006; van der Kaaij et al. 2007b; Yuan et al. 2008) (Fig. 1). In *A. niger*, both enzymes showed transglycosylation activity on donor substrates with alpha-(1,4)-glycosidic bonds and at least five anhydroglucose units. The enzymes, designated AgtA and AgtB, produced new alpha-(1,4)-glycosidic bonds (van der Kaaij et al. 2007b). In *S. pombe*, disruption of *AAH3* encoding a GPI anchored protein resulted in hypersensitivity toward cell wall-degrading enzymes and an aberrant cell shape, indicating that normal cell wall biosynthesis was affected (Morita et al. 2006). Disruption of *AgtA* in *A. niger* also affected cell wall stability. The protein sequence of AFUA_3G00900 and AFUA_2G13460 is very closely related to AgtA and AgtB of *A. niger* (between 50 and 60% of identity) and notably the catalytic conserved domain characteristics of transferase activities of this GH13 families (van der Kaaij et al. 2007a) suggest they may be also transferases in *A. fumigatus.*

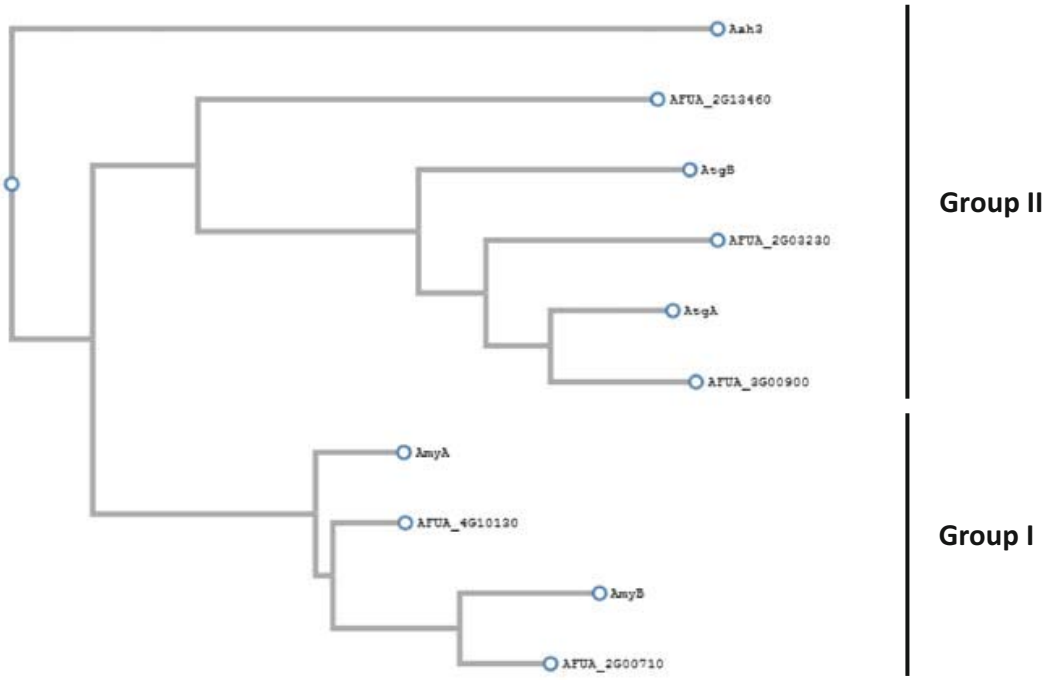

Fig. 1 Phylogeny of the GH13 family of *A. fumigatus*, AtgA-B and AmyA-B of *A. niger* and aah3 of *S. pombe*. Sequence alignment and phylogenetic reconstructions have been done using clustalW (https://www.genome.jp/tools-bin/clustalw). The tree was constructed using FastTree v2. 1.8 with default parameters

- **Proteins with unknown function**

Most of the proteins exclusively present in filamentous fungi genome display unknown functions (25 on the 38 identified).

Three null mutants corresponding to the genes (AFUA_2G05150, AFUA_7G00450, and AFUA_1G05790) showed a twofold reduced ability to form biofilm (Fig. 2a). AFUA_2G05150 is annotated as the cell wall galactomannoprotein Mp2. In contrast, the AFUA_4G03240 null mutant (also a GPI anchored protein) annotated as the galactomannoprotein Mp1 did not show any difference in biofilm formation in our study. Mp1 and Mp2 are homologous to *Penicillium marneffei* Mp1, a cell surface antigenic cell wall mannoprotein and a virulence factor (Cao et al. 1998; Woo et al. 2016). *A. fumigatus* Mp1 and Mp2 have been shown to be also immunogenic (Yuen et al. 2001; Woo et al. 2002; Chong et al. 2004). We constructed the double mutant Δ*mp*1/Δ*mp*2 but we did not observe additional decreases in biofilm formation or reduction in adhesion in comparison to the single mutant *Δmp*2 (data not shown). Recently, (Woo et al. 2018) identified two distantly others homologs in *A. fumigatus*, Mp3 and Mp4, containing also one lipid-binding domain and showed that Mp4 was involved in virulence.

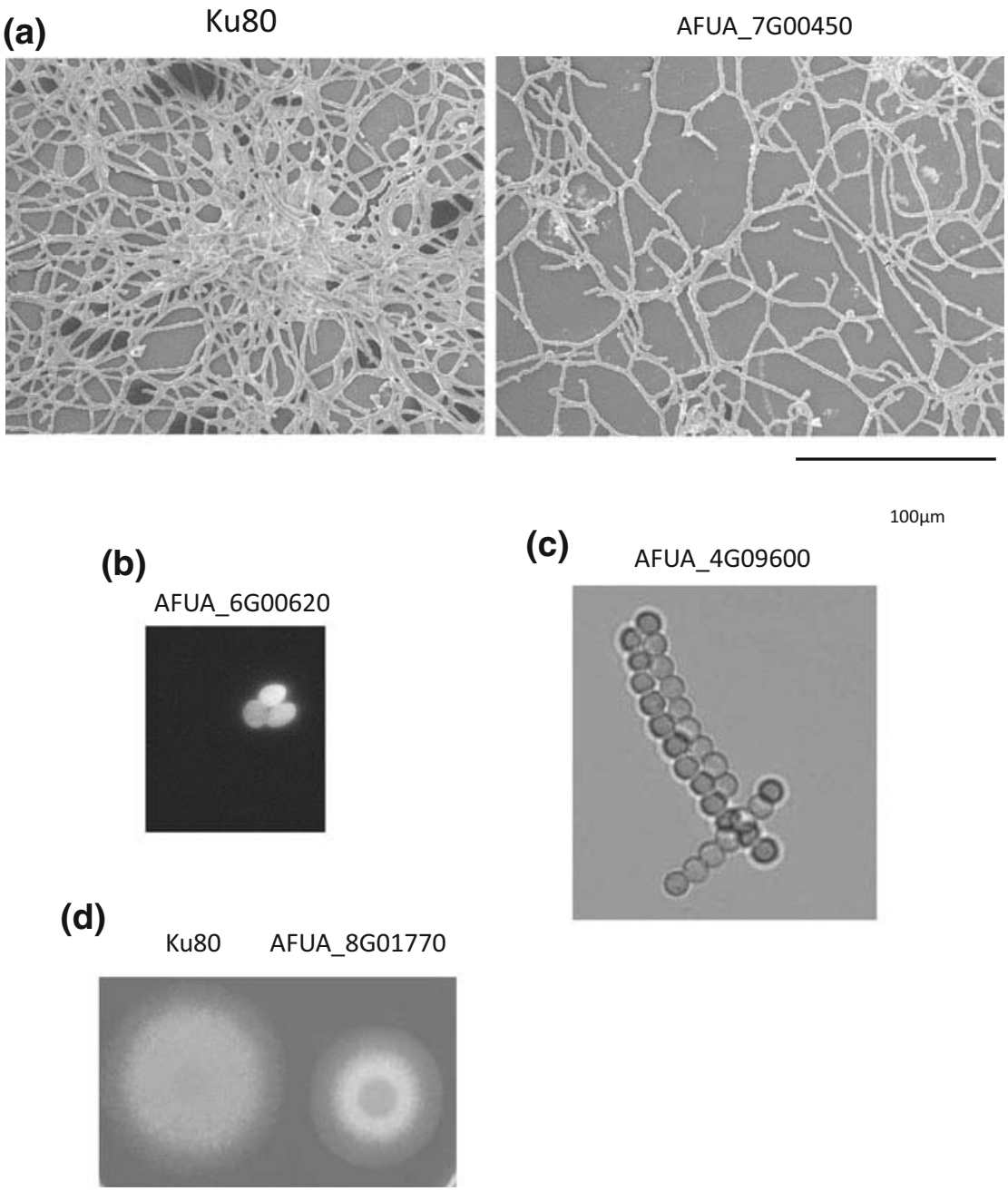

Fig. 2 Phenotype analysis of some GPI anchored protein mutants: **a** SEM of the AFUA_1G05790 deletion mutant involved in biofilm formation compared to the parental strain Ku80. **b** Light microscopy of the shape of conidia after deletion of AFUA_6G00620 gene (63x). **c** Light microscopy of the linear chains of conidia after the deletion of AFUA_4G09600 gene. **d** Growth on Malt medium of the AFUA_8G01770 deletion mutant after 48 h at 37 °C in comparison to the parental strain

(b) **Proteins found exclusively in *Aspergillus* species**

For the deletion of AFUA_2G01140, AFUA_4G03360, AFUA_6G00620, and AFUA_1G11220 which encode proteins of unknown function, we observed that the shape of 5% of the conidia were ovoids (an example is given in Fig. 2b). In the case

of AFUA_1G11220, the deletion of this gene was also associated with a twofold increase in congo red and calcofluor white sensitivity (data not shown). This modification of the morphology of the conidia and of the sensitivity to cell wall drugs suggests that the proteins encoded by these genes could be involved in the construction of the conidial cell wall.

Deletion of AFUA_4G09600, a protein containing several repetitions of amino acid motif GGPSGNDGGN and VKDAYTDDHSV also found only in *Aspergillus* sps, is correlated to a threefold reduction in conidiation compared to the parental strain (data not shown). We also observed linear chains of conidia in this mutant (Fig. 2c). This phenotype is reminiscent of the *CSPA* null mutant phenotype (Valsecchi et al. 2017b).

Six GPI proteins (AFUA_2G14780, AFUA_3G11190, AFUA_7G02460, AFUA_1G17390, AFUA_4G09450, AFUA_8G01770) are only present in the *Aspergillus* species close phylogenetically of *A. fumigatus* (*A. clavatus*, *A. lentulus*, *A. thermomutatus,* and *A. turcosus* (Table 1). No significant homology or domain has been found with any known proteins. Only the deletion of AFUA_8G01700 showed a distinct phenotype from the parental strain, reduced growth, higher sensitivity to drugs and reduced adhesion (Mouyna et al. 2020, manuscript in preparation) (Fig. 2d).

6 Discussion and Conclusion

Even if we try to dress an exhaustive list of all the GPI anchored proteins present in the *A. fumigatus* genome using different algorithms, some proteins could have been wrongly identified as GPI proteins (RodA and RodB) or missed. For example, the conidial surface protein CcpA has been shown to be GPI anchored (Voltersen et al. 2018) while it was not identified using the prediction softwares. Only few proteins have been demonstrated biochemically to be GPI anchored proteins after cleavage of the anchor by a phospholipase C releasing the protein in the Triton X-114 fraction and recognized by a cross-reacting determinant antibody. A proteomic analysis identified biochemically Gel1 and Gel2, Crh1, Crh2, Ecm33, PhoA as GPI anchored proteins (Bruneau et al. 2001). All of these proteins were identified in our bioinformatics predictions.

The localization of GPI anchored proteins has been also controversial. In the yeast *S. cerevisiae*, and *Candida* (Kapteyn et al. 2000; Frieman et al. 2002), it has been demonstrated that many GPI proteins (called GPI anchored cell wall proteins or GPI-CWPs) arrive at the plasma membrane but are then liberated. A remnant of the GPI anchor reacts with β1,6 glucan resulting in cross-linking of the GPI-CWP into the cell wall (Van der Vaart et al. 1997) suggesting that there are two terminal fates for GPI proteins—residence at the plasma membrane (GPI anchored plasma membrane proteins or GPI-PMPs) and residence at the cell wall (GPI-CWPs) (Lu et al. 1994). Moreover, based on in silico analysis of GPI anchored proteins in *S. cerevisiae*, Caro et al. (1997) proposed that a signal of two basic amino acids in the four amino acids upstream of the ω site acts to retain the protein at the plasma

membrane. In the absence of this retention signal, the proteins are mobilized to the cell wall. Using fusions of the GPI signal sequences from *S. cerevisiae* to alpha-galactosidase, (Hamada et al. 1998) found a good correlation between presence or absence of the dibasic motif and partitioning of the fusion protein to the plasma membrane or cell wall. Analysis of various point mutations in specific GPI anchor signal sequences also supported the importance of the dibasic motif in GPI anchored protein localization. In contrast, in *A. fumigatus*, the structural cell wall composition did not reveal the presence of β(1–6)glucan (Fontaine et al. 2000). Moreover, no proteins have been shown to be covalently attached to the cell wall after their release from the membrane (Bernard et al. 2002). In addition, none of the FLO, CWP or TIR family proteins identified in the *S. cerevisiae* genome (Caro et al. 1997) and predicted to be associated to the cell wall, have been found in the *A. fumigatus* genome.

The different categories of GPI anchored proteins found in *A. fumigatus* and their function are summarized in Fig. 3. The first category of proteins is highly conserved in all fungi (yeast as well as filamentous fungi) and is essential in cell wall morphogenesis. Indeed, the structural core of the cell wall between yeasts and molds is conserved. Most of them belong to multigenic families of proteins. Their analysis showed that most of the time, one or two genes in a family are responsible for the phenotype observed (Gastebois et al. 2010a; Millet et al. 2018; Muszkieta et al. 2019). Accordingly, all proteins in the same family are unlikely to have a shared function, which supports the redundancy of genes already observed in the *Aspergillus* genome. In the second category, we identified and characterized proteins present only in filamentous fungi, which are mostly involved in biofilm formation, adhesion, and virulence process. However, 60% of the proteins belonging to this category did not present any domain or identity with previously annotated

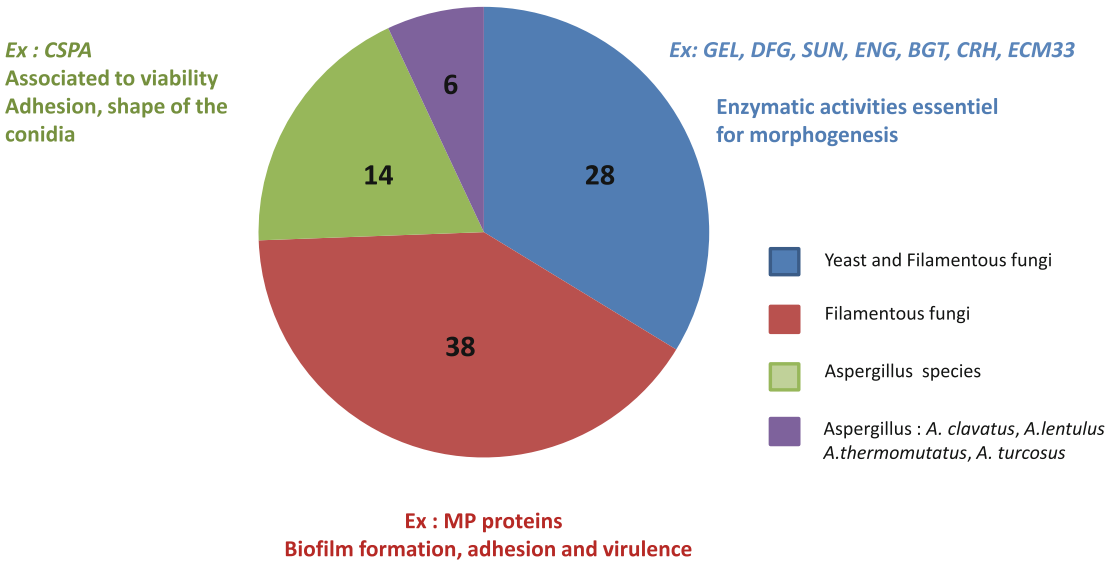

Fig. 3 Different fungal categories of GPI anchored proteins, which show an association between their putative role (cell wall remodeling, adhesion, biofilm or virulence) and their category

proteins or a distinct phenotype associated to their gene mutation. Finally, the third category of proteins is only present in *Aspergillus* species, or even in few related species of *Aspergillus*. These proteins seem to be mostly associated with the formation of the conidial stage but again their function is unknown. This review suggests that other non-GPI-bound transglycosidases are important for the remodeling of cell wall construction and remain to be discovered.

Acknowledgements This research was funded by l'Agence Nationale pour la Recherche (AfuInf ANR-16-CE92-0039), la Fondation pour la Recherche Médicale (DEQ 20150331722 LATGE Equipe FRM 2015) and the AIC (Action Incitative Ciblée) grant of Pasteur Institute. This work was also supported by the Wellcome trust grant 208396/Z/17/Z to MB.

References

Aimanianda V, Bayry J, Bozza S, Kniemeyer O, Perruccio K, Elluru SR et al (2009) Surface hydrophobin prevents immune recognition of airborne fungal spores. Nature 460:1117–1121

Aimanianda V, Simenel C, Garnaud C, Clavaud C, Tada R, Barbin L et al (2017) The dual activity responsible for the elongation and branching of β-(1,3)-glucan in the fungal cell wall. mBio 8. 8(3):e00619–17

Alcazar-Fuoli L, Clavaud C, Lamarre C, Aimanianda V, Seidl-Seiboth V, Mellado E, Latgé J-P (2011) Functional analysis of the fungal/plant class chitinase family in *Aspergillus fumigatus*. Fungal Genet Biol 48:418–429

Arroyo J, Farkaš V, Sanz AB, Cabib E (2016) Strengthening the fungal cell wall through chitin-glucan cross-links: effects on morphogenesis and cell integrity. Cell Microbiol 18:1239–1250

Beauvais A, Schmidt C, Guadagnini S, Roux P, Perret E, Henry C et al (2007) An extracellular matrix glues together the aerial-grown hyphae of *Aspergillus fumigatus*. Cell Microbiol 9:1588–1600

Bernard M, Mouyna I, Dubreucq G, Debeaupuis J-P, Fontaine T, Vorgias C et al (2002) Characterization of a cell-wall acid phosphatase (PhoAp) in *Aspergillus fumigatus*. Microbiol 148:2819–2829

Blanco N, Reidy M, Arroyo J, Cabib E (2012) Crosslinks in the cell wall of budding yeast control morphogenesis at the mother-bud neck. J Cell Sci 125:5781–5789

Bruneau JM, Magnin T, Tagat E, Legrand R, Bernard M, Diaquin M et al (2001) Proteome analysis of *Aspergillus fumigatus* identifies glycosylphosphatidylinositol-anchored proteins associated to the cell wall biosynthesis. Electrophoresis 22:2812–2823

Cabib E, Farkas V, Kosík O, Blanco N, Arroyo J, McPhie P (2008) Assembly of the yeast cell wall. Crh1p and Crh2p act as transglycosylases in vivo and in vitro. J Biol Chem 283:29859–29872

Cao L, Chan CM, Lee C, Wong SS, Yuen KY (1998) MP1 encodes an abundant and highly antigenic cell wall mannoprotein in the pathogenic fungus *Penicillium marneffei*. Infect Immun 66:966–973

Cappellaro C, Mrsa V, Tanner W (1998) New potential cell wall glucanases of *Saccharomyces cerevisiae* and their involvement in mating. J Bacteriol 180:5030–5037

Caro LH, Tettelin H, Vossen JH, Ram AF, van den Ende H, Klis FM (1997) In silicio identification of glycosyl-phosphatidylinositol-anchored plasma-membrane and cell wall proteins of *Saccharomyces cerevisiae*. Yeast 13:1477–1489

Chabane S, Sarfati J, Ibrahim-Granet O, Du C, Schmidt C, Mouyna I et al (2006) Glycosylphosphatidylinositol-anchored Ecm33p influences conidial cell wall biosynthesis in *Aspergillus fumigatus*. Appl Environ Microbiol 72:3259–3267

Chong KTK, Woo PCY, Lau SKP, Huang Y, Yuen K (2004) AFMP2 encodes a novel immunogenic protein of the antigenic mannoprotein superfamily in *Aspergillus fumigatus*. J Clin Microbiol 42:2287–2291

Coluccio A, Bogengruber E, Conrad MN, Dresser ME, Briza P, Neiman AM (2004) Morphogenetic pathway of spore wall assembly in *Saccharomyces cerevisiae*. Eukaryot Cell 3:1464–1475

Eisenhaber B, Schneider G, Wildpaner M, Eisenhaber F (2004) A sensitive predictor for potential GPI lipid modification sites in fungal protein sequences and its application to genome-wide studies for *Aspergillus nidulans*, *Candida albicans*, *Neurospora crassa*, *Saccharomyces cerevisiae* and *Schizosaccharomyces pombe*. J Mol Biol 337:243–253

Fang W, Sanz AB, Bartual SG, Wang B, Ferenbach AT, Farkaš V et al (2019) Mechanisms of redundancy and specificity of the *Aspergillus fumigatus* Crh transglycosylases. Nat Commun 10:1669

Firon A, Aubert S, Iraqui I, Guadagnini S, Goyard S, Prévost M-C et al (2007) The SUN41 and SUN42 genes are essential for cell separation in *Candida albicans*. Mol Microbiol 66:1256–1275

Fontaine T, Simenel C, Dubreucq G, Adam O, Delepierre M, Lemoine J et al (2000) Molecular organization of the alkali-insoluble fraction of aspergillus fumigatus cell wall. J Biol Chem 275:41528

Fontaine T, Beauvais A, Loussert C, Thevenard B, Fulgsang CC, Ohno N et al (2010) Cell wall alpha1-3glucans induce the aggregation of germinating conidia of *Aspergillus fumigatus*. Fungal Genet Biol 47:707–712

Frieman MB, McCaffery JM, Cormack BP (2002) Modular domain structure in the Candida glabrata adhesin Epa1p, a beta1,6 glucan-cross-linked cell wall protein. Mol Microbiol 46:479–492

Furukawa T, van Rhijn N, Fraczek M, Gsaller F, Davies E, Carr P et al (2020) The negative cofactor 2 complex is a key regulator of drug resistance in *Aspergillus fumigatus*. Nat Commun 11:427

Gastebois A, Aimanianda V, Bachellier-Bassi S, Nesseir A, Firon A, Beauvais A et al (2013) SUN proteins belong to a novel family of β-(1,3)-glucan-modifying enzymes involved in fungal morphogenesis. J Biol Chem 288:13387–13396

Gastebois A, Fontaine T, Latgé J-P, Mouyna I (2010a) beta(1-3)Glucanosyltransferase Gel4p is essential for *Aspergillus fumigatus*. Eukaryot Cell 9:1294–1298

Gastebois A, Mouyna I, Simenel C, Clavaud C, Coddeville B, Delepierre M et al (2010b) Characterization of a new beta(1-3)-glucan branching activity of *Aspergillus fumigatus*. J Biol Chem 285:2386–2396

Hamada K, Terashima H, Arisawa M, Kitada K (1998) Amino acid sequence requirement for efficient incorporation of glycosylphosphatidylinositol-associated proteins into the cell wall of *Saccharomyces cerevisiae*. J Biol Chem 273:26946–26953

Hartl L, Gastebois A, Aimanianda V, Latgé J-P (2011) Characterization of the GPI-anchored endo β-1,3-glucanase Eng2 of *Aspergillus fumigatus*. Fungal Genet Biol 48:185–191

Hartland RP, Fontaine T, Debeaupuis JP, Simenel C, Delepierre M, Latgé JP (1996) A novel beta-(1-3)-glucanosyltransferase from the cell wall of *Aspergillus fumigatus*. J Biol Chem 271:26843–26849

Hiller E, Heine S, Brunner H, Rupp S (2007) *Candida albicans* Sun41p, a putative glycosidase, is involved in morphogenesis, cell wall biogenesis, and biofilm formation. Eukaryot Cell 6:2056–2065

Kapteyn JC, Hoyer LL, Hecht JE, Müller WH, Andel A, Verkleij AJ et al (2000) The cell wall architecture of *Candida albicans* wild-type cells and cell wall-defective mutants. Mol Microbiol 35:601–611

Kitagaki H, Wu H, Shimoi H, Ito K (2002) Two homologous genes, DCW1 (YKL046c) and DFG5, are essential for cell growth and encode glycosylphosphatidylinositol (GPI)-anchored membrane proteins required for cell wall biogenesis in *Saccharomyces cerevisiae*. Mol Microbiol 46:1011–1022

Korman DR, Bayliss FT, Barnett CC, Carmona CL, Kodama KH, Royer TJ et al (1990) Cloning, characterization, and expression of two alpha-amylase genes from *Aspergillus niger* var. awamori. Curr Genet 17:203–212

Kulkarni RD, Kelkar HS, Dean RA (2003) An eight-cysteine-containing CFEM domain unique to a group of fungal membrane proteins. Trends Biochem Sci 28:118–121

Latgé J-P, Beauvais A, Chamilos G (2017) The cell wall of the human fungal pathogen *Aspergillus fumigatus*: biosynthesis, organization, immune response, and virulence. Annu Rev Microbiol 71:99–116

Leidich SD, Ibrahim AS, Fu Y, Koul A, Jessup C, Vitullo J et al (1998) Cloning and disruption of caPLB1, a phospholipase B gene involved in the pathogenicity of *Candida albicans*. J Biol Chem 273:26078–26086

Levdansky E, Kashi O, Sharon H, Shadkchan Y, Osherov N (2010) The *Aspergillus fumigatus* cspA gene encoding a repeat-rich cell wall protein is important for normal conidial cell wall architecture and interaction with host cells. Eukaryot Cell 9:1403–1415

Lu CF, Kurjan J, Lipke PN (1994) A pathway for cell wall anchorage of *Saccharomyces cerevisiae* alpha-agglutinin. Mol Cell Biol 14:4825–4833

Millet N, Latgé J-P, Mouyna I (2018) Members of glycosyl-hydrolase family 17 of *A. fumigatus* differentially affect morphogenesis. J Fungi Basel 4(1)

Monod M, Capoccia S, Léchenne B, Zaugg C, Holdom M, Jousson O (2002) Secreted proteases from pathogenic fungi. Int J Med Microbiol 292:405–419

Morita T, Tanaka N, Hosomi A, Giga-Hama Y, Takegawa K (2006) An alpha-amylase homologue, aah3, encodes a GPI-anchored membrane protein required for cell wall integrity and morphogenesis in *Schizosaccharomyces pombe*. Biosci Biotechnol Biochem 70:1454–1463

Mouyna I, Morelle W, Vai M, Monod M, Léchenne B, Fontaine T, Beauvais A, Sarfati J, Prévost MC, Henry C, Latgé JP (2005) Deletion of GEL2 encoding for a beta(1–3)glucanosyltransferase affects morphogenesis and virulence in Aspergillus fumigatus. Mol Microbiol 56:1675–1688

Mouyna I, Hartland RP, Fontaine T, Diaquin M, Simenel C, Delepierre M et al (1998) A 1,3-glucanosyltransferase isolated from the cell wall of *Aspergillus fumigatus* is a homologue of the yeast Bgl2p. Microbiology 144:3171–3180

Mouyna I, Fontaine T, Vai M, Monod M, Fonzi WA, Diaquin M et al (2000a) Glycosylphosphatidylinositol-anchored glucanosyltransferases play an active role in the biosynthesis of the fungal cell wall. J Biol Chem 275:14882–14889

Mouyna I, Monod M, Fontaine T, Henrissat B, Léchenne B, Latgé JP (2000b) Identification of the catalytic residues of the first family of beta(1-3)glucanosyltransferases identified in fungi. Biochem J 347(Pt 3):741–747

Mouyna I, Aimanianda V, Hartl L, Prevost M-C, Sismeiro O, Dillies M-A et al (2016) GH16 and GH81 family β-(1,3)-glucanases in *Aspergillus fumigatus* are essential for conidial cell wall morphogenesis. Cell Microbiol 18:1285–1293

Mouyna I, Delliere S, Beauvais A, Gravelat F, Snarr B, Lehoux M et al (2020) What are the functions of chitin deacetylases in *Aspergillus fumigatus*? Front Cell Infect Microbiol 10:28

Muszkieta L, Fontaine T, Beau R, Mouyna I, Vogt MS, Trow J et al (2019) The glycosylphosphatidylinositol-anchored DFG family is essential for the insertion of galactomannan into the β-(1,3)-glucan-chitin core of the cell wall of *Aspergillus fumigatus*. mSphere 4:e00397–19

Norice CT, Smith FJ, Solis N, Filler SG, Mitchell AP (2007) Requirement for *Candida albicans* Sun41 in biofilm formation and virulence. Eukaryot Cell 6:2046–2055

Pérez A, Pedrós B, Murgui A, Casanova M, López-Ribot JL, Martínez JP (2006) Biofilm formation by *Candida albicans* mutants for genes coding fungal proteins exhibiting the eight-cysteine-containing CFEM domain. FEMS Yeast Res 6:1074–1084

Pérez A, Ramage G, Blanes R, Murgui A, Casanova M, Martínez JP (2011) Some biological features of *Candida albicans* mutants for genes coding fungal proteins containing the CFEM domain. FEMS Yeast Res 11:273–284

Pille A, Kwan AH, Cheung I, Hampsey M, Aimanianda V, Delepierre M et al (2015) (1)H, (13)C and (15)N resonance assignments of the RodA hydrophobin from the opportunistic pathogen *Aspergillus fumigatus*. Biomol NMR Assign 9:113–118

Plaine A, Walker L, Da Costa G, Mora-Montes HM, McKinnon A, Gow NAR et al (2008) Functional analysis of *Candida albicans* GPI-anchored proteins: roles in cell wall integrity and caspofungin sensitivity. Fungal Genet Biol 45:1404–1414

Popolo L, Vai M (1999) The Gas1 glycoprotein, a putative wall polymer cross-linker. Biochim Biophys Acta 1426:385–400

Popolo L, Degani G, Camilloni C, Fonzi WA (2017) The PHR family: the role of extracellular transglycosylases in shaping *Candida albicans* cells. J Fungi 3(4)

Rodríguez-Peña JM, Cid VJ, Arroyo J, Nombela C (2000) A novel family of cell wall-related proteins regulated differently during the yeast life cycle. Mol Cell Biol 20:3245–3255

Rolli E, Ragni E, de Medina-Redondo M, Arroyo J, de Aldana CRV, Popolo L (2011) Expression, stability, and replacement of glucan-remodeling enzymes during developmental transitions in *Saccharomyces cerevisiae*. Mol Biol Cell 22:1585–1598

Sestak S, Hagen I, Tanner W, Strahl S (2004) Scw10p, a cell-wall glucanase/transglucosidase important for cell-wall stability in *Saccharomyces cerevisiae*. Microbiology 150:3197–3208

Shen D-K, Noodeh AD, Kazemi A, Grillot R, Robson G, Brugère J-F (2004) Characterisation and expression of phospholipases B from the opportunistic fungus *Aspergillus fumigatus*. FEMS Microbiol Lett 239:87–93

Spreghini E, Davis DA, Subaran R, Kim M, Mitchell AP (2003) Roles of *Candida albicans* Dfg5p and Dcw1p cell surface proteins in growth and hypha formation. Eukaryot Cell 2:746–755

Vaknin Y, Shadkchan Y, Levdansky E, Morozov M, Romano J, Osherov N (2014) The three *Aspergillus fumigatus* CFEM-domain GPI-anchored proteins (CfmA-C) affect cell-wall stability but do not play a role in fungal virulence. Fungal Genet Biol 63:55–64

Valsecchi I, Dupres V, Stephen-Victor E, Guijarro JI, Gibbons J, Beau R et al (2017a) Role of hydrophobins in *Aspergillus fumigatus*. J Fungi 4(1):2

Valsecchi I, Sarikaya-Bayram Ö, Wong Sak Hoi J, Muszkieta L, Gibbons J, Prevost MC, Mallet A, Krijnse-Locker J, Ibrahim-Granet O, Mouyna I, Carr P, Bromley M, Aimanianda V, Yu JH, Rokas A, Braus GH, Saveanu C, Bayram Ö, Latgé JP (2017b) MybA, a transcription factor involved in conidiation and conidial viability of the human pathogen Aspergillus fumigatus. Mol Microbiol 105:880–900

van der Kaaij RM, Janeček Š, van der Maarel MJEC, Dijkhuizen L (2007a) Phylogenetic and biochemical characterization of a novel cluster of intracellular fungal alpha-amylase enzymes. Microbiol 153:4003–4015

van der Kaaij RM, Yuan X-L, Franken A, Ram AFJ, Punt PJ, van der Maarel MJEC, Dijkhuizen L (2007b) Two novel, putatively cell wall-associated and glycosylphosphatidylinositol-anchored alpha-glucanotransferase enzymes of *Aspergillus niger*. Eukaryot Cell 6:1178–1188

Van der Vaart JM, te Biesebeke R, Chapman JW, Toschka HY, Klis FM, Verrips CT (1997) Comparison of cell wall proteins of *Saccharomyces cerevisiae* as anchors for cell surface expression of heterologous proteins. Appl Environ Microbiol 63:615–620

Vickers I, Reeves EP, Kavanagh KA, Doyle S (2007) Isolation, activity and immunological characterisation of a secreted aspartic protease, CtsD, from *Aspergillus fumigatus*. Protein Expr Purif 53:216–224

Voltersen V, Blango MG, Herrmann S, Schmidt F, Heinekamp T, Strassburger M et al (2018) Proteome analysis reveals the conidial surface protein CcpA essential for virulence of the pathogenic fungus *Aspergillus fumigatus*. mBio 9(5)

Woo PCY, Chan C-M, Leung ASP, Lau SKP, Che X-Y, Wong SSY et al (2002) Detection of cell wall galactomannoprotein Afmp1p in culture supernatants of *Aspergillus fumigatus* and in sera of aspergillosis patients. J Clin Microbiol 40:4382–4387

Woo PCY, Lau SKP, Lau CCY, Tung ETK, Au-Yeung RKH, Cai J-P et al (2018) Mp1p homologues as virulence factors in *Aspergillus fumigatus*. Med Mycol 56:350–360

Woo PCY, Lau SKP, Lau CCY, Tung ETK, Chong KTK, Yang F et al (2016) Mp1p is a virulence factor in *Talaromyces* (Penicillium) *marneffei*. PLoS Negl Trop Dis 10:e0004907

Yuan X-L, van der Kaaij RM, van den Hondel CAMJJ, Punt PJ, van der Maarel MJEC, Dijkhuizen L, Ram AFJ (2008) *Aspergillus niger* genome-wide analysis reveals a large number of novel alpha-glucan acting enzymes with unexpected expression profiles. Mol Genet Genomics MGG 279:545–561

Yuen KY, Chan CM, Chan KM, Woo PC, Che XY, Leung AS, Cao L (2001) Characterization of AFMP1: a novel target for serodiagnosis of aspergillosis. J Clin Microbiol 39:3830–3837

Zhao C, Fraczek MG, Dineen L, Lebedinec R, Macheleidt J, Heinekamp T et al (2019) High-throughput gene replacement in *Aspergillus fumigatus*. Curr Protoc Microbiol 54:e88

Quantitative Plant Biology

cambridge.org/qpb

Expansin-mediated developmental and adaptive responses: A matter of cell wall biomechanics?

Marketa Samalova[1,2], Evelina Gahurova[1,3] and Jan Hejatko[1,3]

[1]CEITEC - Central European Institute of Technology, Masaryk University, Brno, Czech Republic; [2]Department of Experimental Biology, Faculty of Science, Masaryk University, Brno, Czech Republic; [3]National Centre for Biotechnological Research, Faculty of Science, Masaryk University, Brno, Czech Republic

Review

Cite this article: M. Samalova et al. Expansin-mediated developmental and adaptive responses: A matter of cell wall biomechanics?. *Quantitative Plant Biology*, **3**:e11, 1–14
https://dx.doi.org/10.1017/qpb.2022.6

Received: 30 June 2021
Revised: 16 March 2022
Accepted: 29 March 2022

Keywords:
biomechanics; cell wall loosening; cell wall remodelling; development; expansin; plant.

Author for correspondence:
J. Hejatko,
E-mail: jan.hejatko@ceitec.muni.cz

Abstract

Biomechanical properties of the cell wall (CW) are important for many developmental and adaptive responses in plants. Expansins were shown to mediate pH-dependent CW enlargement via a process called CW loosening. Here, we provide a brief overview of expansin occurrence in plant and non-plant species, their structure and mode of action including the role of hormone-regulated CW acidification in the control of expansin activity. We depict the historical as well as recent CW models, discuss the role of expansins in the CW biomechanics and address the developmental importance of expansin-regulated CW loosening in cell elongation and new primordia formation. We summarise the data published so far on the role of expansins in the abiotic stress response as well as the rather scarce evidence and hypotheses on the possible mechanisms underlying expansin-mediated abiotic stress resistance. Finally, we wrap it up by highlighting possible future directions in expansin research.

1. Introduction

The primary plant cell wall (CW) is a multi-layered structure in which each layer (lamella) consists of load bearing cellulose microfibrils laterally interconnected possibly with xyloglucan and embedded into a pectin matrix (Zhang et al., 2019a; 2021a). The properties of CW are being constantly modified to allow for morphological changes that are necessary for plant growth and development both in the shoot (Gruel et al., 2016; Hamant et al., 2008; Hervieux et al., 2017; Landrein et al., 2015; Majda et al., 2017; Pien et al., 2001; Reinhardt et al., 1998; Sampathkumar et al., 2014; Takatani et al., 2020) and root (Barbez et al., 2017; Hurny et al., 2020; Mielke et al., 2021; Pacifici et al., 2018; Ramakrishna et al., 2019; Vermeer et al., 2014). Mechanical properties of the CW are regulated by a variety of agents including expansins (Cosgrove, 2000; McQueen-Mason et al., 1992), glucanases (Yoshida & Komae, 2006; Yuan et al., 2001; Zhang et al., 2019a), pectin methylesterases (Goldberg et al., 1996; Peaucelle et al., 2008; Wang et al., 2020), calcium ions (Bou Dahner et al., 2018; Wang et al., 2020) and others. While endoglucanases and other enzymes typically decrease the number of linkages between cellulose and other CW molecules (i.e., mediate CW remodelling, see the Glossary) leading to a weaker (i.e., more easily breakable) wall, α-expansins induce creep—an irreversible time-dependent CW enlargement (Cosgrove, 2016a; Park & Cosgrove, 2012a; Wang et al., 2013; Yuan et al., 2001). These types of biomechanical modifications should be distinguished. Thus, the timing and location of growth are controlled by spatial- and time-specific modification of the mechanical properties of the CW. Here we review recent contributions on the role of α-expansins in the control of biomechanical CW properties, focusing primarily on their role in plant development and abiotic stress response.

2. Expansin discovery and evolution

Expansins were discovered in plants as proteins that play a crucial role in CW loosening (McQueen-Mason et al., 1992), as they induce stress relaxation and extension in plant CWs during pH-dependent 'acid growth' (Rayle & Cleland, 1992). Since then, expansins have been

John Innes Centre
Unlocking Nature's Diversity
CAMBRIDGE UNIVERSITY PRESS

shown to be involved in many aspects of plant growth and development. Expansins are present to the best of our knowledge in all plant species, although some gene loss is observable in highly adapted aquatic species (Hepler et al., 2020). Expansins can also be found in fungi and bacteria, probably as a result of horizontal gene transfer (Georgelis et al., 2015). However, the presence of these genes in all eukaryotic microorganisms that use cellulose as a structural component of their CW suggests that expansins evolved in ancient marine microorganisms long before the evolution of land plants (Chase et al., 2020). Expansins from diverse bacteria and fungi assisting plant–microbe interactions in nature have often been utilised in industrial applications to facilitate lignocellulose degradation that is used further in the conversion of biomass into alternative fuels (Georgelis et al., 2015; Liu et al., 2015).

3. The expansin (super)family

Based on phylogenetic sequence homology, four distinct genetic subfamilies of expansins are currently recognised in vascular plants: α-expansin (EXPA), β-expansin (EXPB), expansin-like A (EXLA) and expansin-like B (EXLB) (Sampedro & Cosgrove, 2005). Two of these subfamilies, the α and β expansins have been demonstrated experimentally to induce CW loosening (Cosgrove et al., 1997; McQueen-Mason et al., 1992). EXPA is the most numerous subfamily, for example in *Arabidopsis thaliana* there are 26 *EXPA* genes, 6 *EXPB*, 3 *EXLA* and 1 *EXLB*. Apart from *Arabidopsis*, rice and poplar (Sampedro & Cosgrove, 2005), genome-wide identification and expression profile analysis of expansin gene families have recently been performed in sugarcane (Santiago et al., 2018), wheat (Han et al., 2019; Zhang et al., 2018a), potato (Chen et al., 2019), Chinese jujube (Hou et al., 2019), cotton (Lv et al., 2020) and *Brassica* species (Li et al., 2021a).

Although the main focus of this review is on EXPA, it is worth mentioning that the group of β-expansins expanded significantly in grasses (Sampedro et al., 2015). As an example, EXPB1 (also called Zea m 1) is a member of group-1 grass pollen allergens and its crystal structure has been resolved suggesting the role of EXPB1 in the local movement and stress relaxation of (arabino)xylan-cellulose networks within the wall (Yennawar et al., 2006). Detailed characterisation of EXPB1 function in extracted maize CWs revealed that the protein primarily binds glucuronoarabinoxylan, the major polysaccharide in grass CWs (Wang et al., 2016a) that is largely absent in primary CWs of dicots (Carpita, 1996; Vogel, 2008). In maize, the group is needed for pollen separation and stigma penetration (Valdivia et al., 2009).

4. Expansin structure and mode of action

4.1. Expansin structure

Expansins are modular, torpedo-shaped proteins that consist of two tightly packed, structured domains of 200–250 amino acids, connected by a short linker and preceded by a signal peptide. The *N*-terminal domain (D1) is a six-stranded double-psi (ω) β-barrel related to family 45 glycoside hydrolases (GH45), but lacks the critical catalytic Asp required for hydrolytic activity (Cosgrove, 2015; Georgelis et al., 2015; Kerff et al., 2008; Yennawar et al., 2006). The *C*-terminal domain (D2) with a β-sandwich fold is related to group-2 grass pollen allergens and resembles the carbohydrate binding module (CBM) family 63 (Chase et al., 2020; Georgelis et al., 2012). Both domains are required for full CW loosening activity (Georgelis et al., 2011; Sampedro & Cosgrove, 2005). The Expansin Engineering Database (ExED; https://exed.biocatnet.de) is a useful navigation and classification tool for expansins and their homologues and is based on newly created profile hidden Markov models of the two expansin domains (Lohoff et al., 2020).

Despite the rather long history of expansin research, many of the details of the functional and structural properties underlying the molecular mechanism of expansin action in enabling CW expansion still remain undiscovered. One of the reasons for this knowledge gap is that, unlike bacterial or fungal expansins, plant α-expansins have proven difficult to produce in the active form using heterologous expression systems (Gaete-Eastman et al., 2015). Nonetheless, computational 3D models built through comparative modelling and molecular dynamics simulations have yielded the first structural approximation of several α-expansins (Gaete-Eastman et al., 2015; Mateluna et al., 2017; Pastor et al., 2015; Valenzuela-Riffo et al., 2018; 2020) and confirmed that expansins can form a stable complex with cellulose via the flat aromatic surface of the *C*-terminal domain (Valenzuela-Riffo et al., 2018). Based on the model, the expansins also interacted with the xyloglucan XXFG ligand, but were less likely to bind the XXXG ligand; they did not interact with pectin (Valenzuela-Riffo et al., 2020), the latter being in contrast to experimental data (Nardi et al., 2013). Recently, the protein structure of several expansins was determined by the AlphaFold protein prediction algorithm (Figure 1a) proven to be highly reliable in terms of the predicted protein structure (Jumper et al., 2021; Varadi et al., 2021).

4.2. Bacterial expansins

Because of the aforementioned limitations, our knowledge of the mode of expansin action at atomic resolution is limited to bacterial expansins. Cellulose binding was demonstrated for *Bacillus subtilis* expansin EXLX1, a bacterial expansin that can loosen plant CWs. Through hydrophobic interactions of three linearly arranged, highly conserved aromatic residues (W125, W126 and Y157) in the D2 domain, EXLX1 binds tightly to crystalline cellulose rather than to linear oligosaccharides (Boraston et al., 2001; Georgelis et al., 2012; Kim et al., 2013). Molecular dynamics simulations suggest that the expansin has both a cellulose-weakening and a cellulose-binding activity that depends on substrate crystallinity (Orłowski et al., 2018). Indeed, adsorption of EXLX1 onto a cellulose film decreased the crystallinity index, disrupted hydrogen bonding, and increased the surface area of cellulose, indicating greater accessibility of the substrate to proteins (Duan et al., 2018). It is this characteristic that makes expansin and expansin-like proteins that act synergistically with cellulases during hydrolysis useful for industry, and they are often used as biological pre-treatments to disrupt and open up recalcitrant lignocellulose complexes for industrial applications (Georgelis et al., 2011; 2015; Kerff et al., 2008; Kim et al., 2009).

Other investigations of EXLX1 adsorption onto cellulose, using quartz crystal microbalance with dissipation (QCM-D), confirmed that cellobiose and xylose enhanced EXLX1 adsorption at low concentrations but inhibited it at high concentrations (Zhang et al., 2020). Monitoring real-time adsorption of endo/exo-glucanases with EXLX1 and the enzymatic hydrolysis of cellulose showed synergistic effects. This increased activity can be due to easier access of the cellulase to the cellulose chains, but other effects such as electrostatic or other physical interactions between the adsorbed EXLX1 and cellulases cannot be ruled out (Zhang et al., 2021b). However, bacterial expansins have much weaker cellulose binding and wall-loosening activity than plant α-expansins (Kerff et al.,

https://doi.org/10.1017/qpb.2022.6 Published online by Cambridge University Press

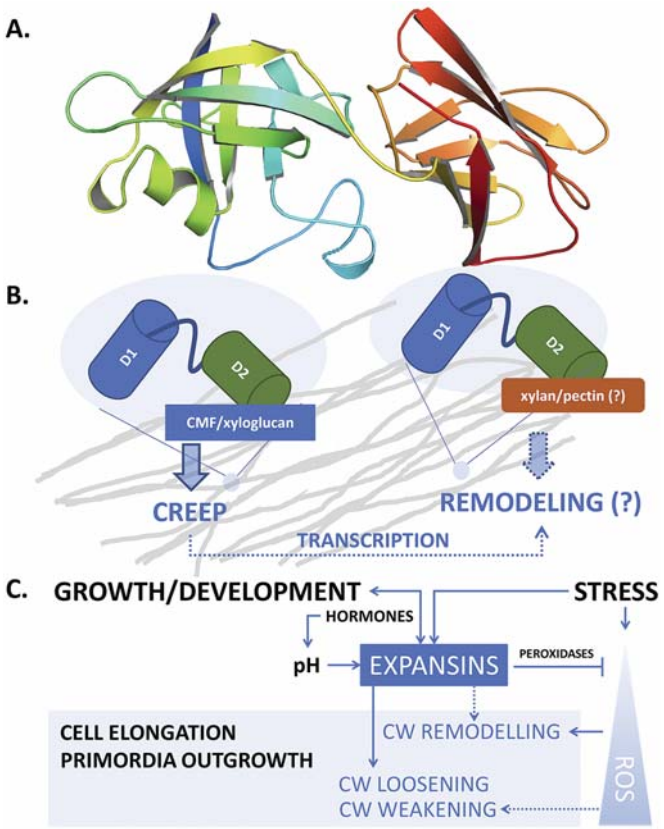

Fig. 1. (a) Structure of AtEXPA1 determined by the AlphaFold algorithm. *N*-terminal six-stranded double-psi (ω) β-barrel D1 domain related to family 45 glycoside hydrolases (GH45) (green/blue, left) and *C*-terminal β-sandwich fold D2 domain related to group-2 grass pollen allergens resembling the carbohydrate binding module (CBM) family 63 (red/orange, right); the unstructured signal peptide is not shown. (b) Upon binding the load-bearing cellulose microfibril (CMF) network laterally interconnected with possible xyloglucan contribution (grey), expansins induce CW expansion via CW creep. By interfering with CW remodelling enzymes via binding to xylan and/or pectin or through transcriptional feedback regulations in a response to changed CW biomechanics, expansins might contribute to CW remodelling, too. (c) Expansin expression and localization is regulated during plant development, ensuring expansin action in a manner that is specific to their dose and the particular developmental context. Conversely, expansin action on CW biomechanics affects plant development and growth responses by regulating cell elongation and/or primordia specification/outgrowth. Expansins are activated in response to various stresses associated with ROS production. Expansin expression might be mediated by developmental- and stress-regulated hormone production, controlling expansin activity also via spatial-specific CW acidification. Expansins could mitigate ROS effects by upregulating CW peroxidases. In turn, ROS also contribute to the regulation of CW biomechanical properties. While short-term or low-level ROS production leads to growth inhibition by inducing crosslinking of CW components, high ROS levels/long-term ROS production leads to OH°-radical formation that was hypothesised to allow restoration of cell expansion via polymer cleavage, leading to CW weakening. See the main text for a more detailed description.

2008; Kim et al., 2009), and recent results suggest that although EXLX1 is homologous with plant expansins, it possibly has distinct effects on plant CWs (Hepler & Cosgrove, 2019).

4.3. Expansin-mediated CW loosening

According to the loosening theory (Cosgrove, 2015), well-hydrated non-growing cells reach osmotic equilibrium with wall stresses counter-balancing the outward turgor pressure against the wall. In growing cells, however, walls are loosened (primarily via pH-dependent action of expansins), which means that the load-bearing part of the wall is relaxed, releasing the tensile stress and simultaneously reducing cell turgor. Consequently, water flows into the cell, expanding the wall and restoring turgor and wall stress, together driving cell growth (Cosgrove, 2015; 2018a). Importantly, cell expansion starts with CW loosening/relaxation, followed by a decrease and a subsequent increase of cell turgor, not vice versa (Cosgrove, 1993).

There is a significant body of evidence suggesting that expansins themselves are incapable of hydrolysing the polysaccharide substrate itself (Kerff et al., 2008; McQueen-Mason & Cosgrove, 1995; McQueen-Mason et al., 1992). Nevertheless, pH-dependent, expansin-mediated CW loosening promotes relaxation of the CW structure, thus contributing to CW remodelling by allowing different hydrolases to access their polysaccharide substrates (Cosgrove, 2000; 2005; Whitney et al., 2000).

4.4. Apoplast acidification is necessary for expansin-mediated cell expansion

According to the 'acid growth theory' (Hager et al., 1971; Rayle & Cleland, 1970), auxin triggers extrusion of protons (H^+) into the apoplast, which activates expansins that subsequently loosen the CW and allow growth (McQueen-Mason et al., 1992). The most important players in this process are plasma membrane P-type H^+-ATPases which pump out protons to the wall matrix, consequently leading to apoplast acidification (Takahashi et al., 2012). Later it was discovered that the transport inhibitor response1/auxin signaling F-box—auxin/indole-3-acetic acid (TIR1/AFB-Aux/IAA) auxin signalling machinery transcriptionally upregulates the SMALL AUXIN UP-RNA 19 (SAUR19) expression levels (Fendrych et al., 2016). SAUR19 inhibits the activity of TYPE 2C PROTEIN PHOSPHATASES (PP2C), thus maintaining the H^+-ATPase in an active state (Spartz et al., 2014). Pumping protons causes plasma membrane hyperpolarisation and also activates K^+ channels that (in a short term) electrically balance the H^+ efflux and (in the long term) maintain intracellular osmotic potential low, thus allowing sustained water uptake and turgor pressure forcing the CW to extend (Thiel & Weise, 1999; for review see Arsuffi & Braybrook, 2018).

Given the different effects of auxins on shoots compared with roots (for review see Du et al., 2020; Dunser & Kleine-Vehn, 2015; Li et al., 2021b), the acid growth theory seems to be more complex in roots, suggesting possible non-transcriptional regulations (Pacheco-Villalobos et al., 2016). In line with that, the non-transcriptional branch of the cytosolic TIR1/AFB pathway was demonstrated to trigger a rapid Cyclic Nucleotide-Gated Channel 14 (CNGC14)-mediated $Ca2^+$ influx and an unknown channel or transporter-mediated H^+ influx leading to apoplast alkalization inhibiting the growth (Fendrych et al., 2018; Li et al., 2021b). Recently, it was shown that the cell surface-based TRANSMEMBRANE KINASE1 (TMK1) directly binds and activates plasma membrane H^+-ATPases thus promoting CW acidification in both shoots and roots (Li et al., 2021c; Lin et al., 2021), acting antagonistically to the noncanonical TIR1/AFB pathway (Li et al., 2021b).

However, not only auxin can control apoplastic pH. Cytokinins were proposed to upregulate the expression of genes for H^+-ATPases AHA2 and AHA7, facilitating thus EXPA1-mediated induction of cell elongation in the root transition zone (Pacifici et al., 2018). Furthermore, Großeholz et al. (2021) recently proposed a new model in which brassinosteroid-mediated cell elongation response depends on the amount and activity of

https://doi.org/10.1017/qpb.2022.6 Published online by Cambridge University Press

H^+-ATPases in the plasma membrane. Also here, the K^+ antiport, this time mediated via CNGC10, is necessary to compensate for H^+ efflux, thus keeping the plasma membrane potential constant. Using microelectrode ion flux estimation measurements, Großeholz et al. (2021) demonstrated net H^+ influx in the root meristematic zone while H^+ efflux in the root transition zone. The resulting pH gradient is proposed to be instructive for the cell elongation in the root transition/elongation zone. Altogether, not only the spatiotemporal specificity of *EXPAs* expression and protein localization but also the spatial-specific control over H^+ fluxes leading to the changes in the apoplastic pH are important factors controlling the EXPA-mediated cell expansion.

5. Expansins and CW biomechanics

5.1. Historical overview of the primary CW models

Previous depictions of accepted CW models (Carpita & Gibeaut, 1993; Fry, 1989; Hayashi, 1989; Nishitani, 1998) presented cellulose microfibrils as well-spaced and non-contacting rods with xyloglucan covering most cellulose surfaces and tethering them together to form the load-bearing network. Indeed, it was confirmed that enlargement of the CW required separation of cellulose microfibrils; however, high resolution (FESEM and AFM) images from slowly extended CWs in vitro and control non-extended samples, appeared indistinguishable (Marga et al., 2005). CW can therefore extend slowly through creep but without passive reorientation of the innermost microfibrils, suggesting that the loosening agents act selectively on the cross-linking polymers between parallel microfibrils, rather than more generally on the wall matrix, increasing microfibril spacing but without reorienting them (Marga et al., 2005).

In 2008, Cavalier et al. (2008) showed that *Arabidopsis* xyloglucan-deficient (*xylosyltransferase1/xylosyltransferase2*; *xxt1/xxt2*) mutant plants were reduced in size, but otherwise seemed to develop normally. Nevertheless, stress/strain assays performed by Park and Cosgrove (2012b) showed that the *xxt1/xxt2* walls were more pliant than wild-type (WT) walls but less extensible in the creep and stress-relaxation processes mediated by α-expansin, suggesting that xyloglucan plays a CW strengthening role. Similarly, loosening agents that act on xylans and pectins elicited greater extension in creep assays of the mutant xyloglucan-deficient CWs, demonstrating that these polymers take on a larger mechanical role in the absence of xyloglucan. The results also indicated that growth reduction in *xxt1/xxt2* plants is likely due to the absence of the native target for CW loosening by α-expansins (Park & Cosgrove, 2012b).

Although xyloglucan has the ability to bind tightly to cellulose, NMR analyses of complex CWs showed that very little of the cellulose microfibril surface is actually in contact with xyloglucan (Bootten et al., 2004; Dick-Perez et al., 2011). On the other hand, pectin content is approximately 3-fold that of xyloglucan in *Arabidopsis* CWs (White et al., 2014) and makes the majority of matrix contacts with cellulose surfaces. The binding of xyloglucan is restricted to a minor component that appears to be closely intertwined with cellulose at discrete sites designated as 'biomechanical hotspots' (Cosgrove, 2014; Park & Cosgrove, 2015). Indeed, substantial wall loosening by substrate-specific endoglucanases (CXEG) was traced to the digestion of a specific component comprising <1% of the xyloglucan in the wall, indicating that only a small number of sites may control wall extensibility (Park & Cosgrove, 2012b). This picture of a few biomechanical junctions is also consistent with the low density of α-expansin binding sites in the CW (McQueen-Mason & Cosgrove, 1995).

The biomechanical '*hotspot hypothesis*' proposes that wall extensibility is controlled at discrete sites where microfibrils come into close contact with one another (Zhang et al., 2014) via a monolayer of xyloglucan binding the hydrophobic surfaces of the two microfibrils together (Cosgrove, 2018b). These may be the selective sites of CW loosening by expansins or by CXEG-type enzymes where the microfibrils slide or separate, perhaps at a rate that is influenced by the bulk viscoelasticity of the microfibril–matrix network (Park & Cosgrove, 2015). Disruption of such non-covalent bonds allows 'slippage' of carbohydrate polymers at load-bearing elements of the CW. Although the CW models assume non-covalent bonding between cellulose and hemicelluloses such as xyloglucan, *Equisetum* hetero-trans-β-glucanase (HTG) covalently attaches cellulose onto xyloglucan oligosaccharides in vitro. Interestingly, recombinant bacterial expansin EXLX1 strongly augmented the cellulose:xyloglucan endotransglucosylase activity that produces cellulose–xyloglucan covalent bonds in the CWs of structural plant tissues in vitro (Herburger et al., 2020).

The current view of the primary CW is represented by a mesoscale coarse-grained molecular dynamics model (Zhang et al., 2021a). The assembled epidermal CW is based on the supramolecular structure of cellulose and matrix polysaccharides that resembles (real) physics and tensile mechanics. The multi-layered CW has a cross-lamellate organisation in which individual layers (lamellae) of stiff cellulose microfibrils form a laterally interconnected network binding noncovalently to hemicellulose that is embedded in pectin, forming a gel-like matrix. Individual lamellar microfibrils are aligned in the same direction and appear anisotropic in terms of in-plane stress resistance; however, the complete (real) CWs, consisting of many lamellae (approx. 100) are highly isotropic. Interestingly, the simple non-covalent-bonding generated cellulose network in which fibril–fibril sliding of aligned cellulose bundles bears most of the stress despite frequent xyloglucan bridging between microfibrils, and pectin abundance. Overall, in this dynamic load-bearing network, tensile forces are transmitted primarily through direct lateral contacts between cellulose microfibrils, rather than by matrix polysaccharides. Thus, although the action of expansins and other wall-modifying proteins was not part of it, the model clearly highlights the importance of the lateral cellulose microfibrils contacts and its potential modulators (particularly expansins) in the overall transmission of in-plane tensile forces.

5.2. Expansin-mediated changes in the CW biomechanics

The CW can undergo several types of deformation that can be measured either in situ (ideally in living plant tissues) or in simplified models, most frequently using onion epidermis peels clamped in a custom-made mechanical testing device (Cosgrove, 1989; 2011; Durachko & Cosgrove, 2009; Durachko et al., 2017; Wang et al., 2020; Zhang & Cosgrove, 2017; Zhang et al., 2019a). In some cases, slightly more complex systems such as de-frosted *Arabidopsis* petioles (Park & Cosgrove, 2012a; Xin et al., 2020), cucumber and *Arabidopsis* hypocotyls (Boron et al., 2015; Cosgrove, 1989; Marga et al., 2005; Park & Cosgrove, 2012b) or wheat coleoptiles (Hepler & Cosgrove, 2019) have been used. The advantage of using onion epidermal peels is that the mechanical properties of isolated CW fragments can be measured, largely neglecting the contribution of neighbouring cells, cell size or shape that might possibly influence the results when using indentation-based (AFM) measurements

https://doi.org/10.1017/qpb.2022.6 Published online by Cambridge University Press

(Cosgrove, 2018b and references therein). However, new technologies such as non-contact, optical Brillouin spectroscopy are emerging as tools to probe biomechanical properties of CWs in developing organs at the cellular (Scarcelli et al., 2015) or tissue level (Elsayad et al., 2016; Samalova et al., 2020).

When CWs become mechanically softer/more pliant (meaning more easily deformed by out-of-plane mechanical force, see the Glossary), they do not necessarily result in wall relaxation and cell growth. On the other hand, α-expansins cause in-plane stress relaxation and prolonged enlargement of CWs, but they do not change the CW viscoelastic properties, as measured by tensile tests (Cosgrove, 2018a; Yuan et al., 2001). In other words, reducing the wall stiffness doesnot necessarily lead to CW loosening. One such observation was made by Wang et al. (2020) with pectin methylesterase (PME) that selectively softened the onion epidermal wall yet reduced expansin-mediated creep. Similarly, driselase, a potent cocktail of wall-degrading enzymes, removed cellulose microfibrils in superficial lamellae sequentially, and softened the wall (reduced its indentation-measured mechanical stiffness), yet did not induce wall loosening (Zhang et al., 2019a).

In contrast to this, expansins, despite possessing no obvious enzymatic activity, are able to induce irreversible time-dependent expansion of CWs without affecting its compliance as discussed above. Expansins cause almost immediate in vitro CW extension, allowing to extend the cell length 100 times when compared to its meristematic initials (Cosgrove, 2016b and references therein). Thus, to loosen CW, expansins probably modify noncovalent bonds in the cellulose microfibril network, laterally interconnected with a possible contribution of xyloglucans bound to the hydrophobic face of the cellulose microfibrils (Cosgrove, 2018b and references therein). The consequent fibril–fibril sliding seems to allow CW extension and in-plane stress release of the multilamellate CW structure (Zhang et al., 2019a; 2021a).

6. Involvement of expansins in various aspects of plant growth and development

6.1. Cell elongation: The more (expansin) the better?

Expansins were identified as factors that primarily enhance cell elongation. The CW fraction from the actively growing (apical) portion of cucumber hypocotyls was able to induce creep of heat-inactivated cucumber hypocotyls when measured by a constant load extensometer. The observed CW extension required acidic pH and was also seen upon application of cucumber extracts to CW isolated from actively growing tissues (hypocotyls, leaves, petioles and coleoptiles) from other plant species. The CW extracts from the basal (non-growing) hypocotyls were unable to induce cell extension of apical hypocotyl fragments. Nonetheless, even the (active) CW extracts from the apical regions were unable to induce CW extension of the basal hypocotyl fragments, suggesting maturation-associated changes in CW structure limiting susceptibility to these extension-inducing factors (McQueen-Mason et al., 1992).

Cell expansion is a developmental response that is most frequently associated with upregulation of endogenous expansins in various tissues from a number of species. These include petiole elongation associated with *RpEXPA1* upregulation and CW acidification in response to ethylene entrapment following flooding in *Rumex palustris* (Vreeburg et al., 2005), enlargement of floral organs and internodes due to overexpression of *PhEXPA1* in petunia (Zenoni et al., 2011), changes in petiole and leaf-blade size associated with up- and down-regulation of *AtEXPA10* in *Arabidopsis*, root hair-specific expression of *AtEXP7* and *AtEXP18* (Cho & Cosgrove, 2002), and *AtEXPA1*-mediated cell elongation in the *Arabidopsis* root transition zone (Pacifici et al., 2018).

However, the correlation between cell extension and expansin activity is not absolute. Only a partial correlation between the activities of LeEXP2 and LeEXP18 and cell elongation has been observed in tomato. This implies the existence of another factor, acting in concert with expansins, that may control growth under certain physiological conditions (Caderas et al., 2000). In line with that, chemically regulated expression of *CsEXP1* in tobacco suggested the existence of a specific developmental phase, when the leaf is sensitive to upregulated expansin (Sloan et al., 2009). Consistent with this, downregulating several expansins being transcriptionally active during the phase of maximal leaf-cell expansion (*AtEXPA1,3, 5* and *10*) using inducible amiRNA resulted in leaf growth repression in the latter stages of leaf development. Surprisingly, the smaller leaves had larger cells, suggesting organ and cell context-specific outputs of expansin gene expression (Goh et al., 2012). In rice seedlings with inducible *OsEXP4* expression, OsEXP4 protein levels were correlated with growth, but constitutive expression of the same gene resulted in growth retardation (Choi et al., 2003). Dose-dependent effects were observed in *Arabidopsis* (over)expressing cucumber *CsEXPA1* using a DEX-inducible system (Craft et al., 2005). While low levels of *CsEXPA1* were able to broaden leaf lamina, high levels had strong negative effects, particularly on the enlargement of fast-growing (expanding) tissues like hypocotyls or petioles (Goh et al., 2014). Finally, both overexpression of *CsEXPA1* and amiRNA-based downregulation of endogenous expansins (At*EXPA1,3, 5* and *10*) impaired hypocotyl elongation in etiolated *Arabidopsis* seedlings (Ilias et al., 2019). Overall, the action of expansins on CW enlargement seems to be specific, with regard to both dose (expression level) and the particular developmental context.

6.2. Do expansins control CW enlargement by modulating CW remodelling?

As with the examples in the previous sections, transgenic tomato lines with high levels of CsEXPA1 showed overall growth inhibition. Notably, hypocotyls from CsEXPA1 OE tomatoes were less sensitive to exogenously applied expansin in the constant-load extensometer assay (Rochange et al., 2001). The authors proposed that the observed CW tension resistance can be partly due to CW adaptation to the excessive amount of CW-loosening expansins through 'a decrease in the abundance or activity of secondary loosening agents, or stiffening of the CWs via other components (such as the de-esterification of pectins or extensin crosslinking)' (quote taken from Rochange et al., 2001).

There are several other pieces of evidence supporting a possible role for expansins as modulators of CW remodelling. Downregulation of *PhEXPA1* in petunia led to CW thickening and reduction in crystalline cellulose content, suggesting involvement of PhEXPA1 in the cellulose synthesis or deposition (Zenoni et al., 2004). Further in *PhEXPA1* OE CWs, the relative abundance of CW polymers was altered (in this case less pectin and hemicellulose, but unchanged cellulose content). Another example is overexpression of root-specific *OsEXPA8* in rice, leading to changed root architecture (longer main root, more lateral roots and root hairs), taller plants and larger leaves. The *OsEXPA8* overexpression was associated with lower (AFM-measured) CW stiffness and an increase in the polysaccharide/lignin ratio as measured using FTIR (Ma et al., 2013). The observed changes in the CW composition

https://doi.org/10.1017/qpb.2022.6 Published online by Cambridge University Press

could be achieved by changes in substrate availability due to the binding of expansins also to other CW polymers besides cellulose (Zenoni et al., 2004). In support of this mechanism, the CBM of strawberry expansin 2 (CBM-FaExp2) was shown to bind not only cellulose/xyloglucans but also other CW polymers including xylan and pectin. The presence of CBM-FaExp2 decreased the activity of CW degrading enzymes such as polygalacturonase, endoglucanase, pectinase and xylanase in an in vitro assay, probably due to CBM-FaExp2 binding to the enzyme substrates (Nardi et al., 2013). Notably, the CBM of FaEXP2 shows a high level of similarity to CBMs of AtEXPA1, AtEXPA2 and potato CBM-Pot-BG097738. Furthermore, the aromatic residues of CBM-FaExp2 are conserved in CBM-Pot-BG097738, and they were proposed to be involved in binding CW polysaccharides (Nardi et al., 2013). Thus, the CW stiffening recently observed in *Arabidopsis* lines with high levels of *AtEXPA1* (Samalova et al., 2020) could be explained by a similar mechanism, that is, interference of AtEXPA1 binding to CW components with enzyme activity mediating CW softening. Furthermore, expansin-mediated changes in the accessibility of CW-modifying enzymes were also proposed to be how EXP1-controlled fruit softening in tomato (Brummell et al., 1999). However, the role of feedback regulations leading to changes in the expression of genes for several CW remodelling proteins could also contribute to the *EXPA* overexpression-induced changes in CW composition (Ilias et al., 2019).

The role of the *C*-terminal CBM and its possible functional importance in recognising cellulose and/or other CW sugar polymers was highlighted by the work of Boron et al. (2015). The overexpression of *AtEXLA2*, a member of the expansin-like A family in *Arabidopsis* led only to a weak enlargement of etiolated hypocotyls. That was accompanied by CW thickening and decreased CW strength manifesting as higher rupture frequency (twice that of WT) under load during the creep test with a constant-load extensiometer. As AtEXLA2 is lacking the three conserved residues necessary for the CW loosening activity of the *N*-terminal D1 domain, the authors hypothesise a possible role for the *C*-terminal CBM in cellulose crystallisation and/or its affecting xyloglucan/cellulose interaction, leading to the observed defects in CW biomechanical properties. However, expansins may control CW remodelling independently of competition with CW modulating enzymes by binding to a wide spectrum of CW polymers as demonstrated for GbEXPATR in cotton. GbEXPATR represents a truncated version of its homologue GbEXPA2, lacking the *C*-terminal CBM. Interestingly, while the OE of *GbEXPA2* had no significant effects on the length of mature fibres, overproduction of GbEXPATR led to longer, finer and stronger cotton fibres, probably via a GbEXPATR-mediated delay in the onset of secondary CW formation (Li et al., 2016).

The CW acts as a sensing platform and plants use a dedicated system to control and maintain CW homeostasis that allows them to adapt to developmental changes as well as to environmental stresses. The wall composition and mechanical integrity are monitored by cell wall integrity (CWI) sensors and mechanosensitive ion channels (Hamann, 2015; Novakovic et al., 2018). CWI signalling involves the perception of mechanical and physical changes of the plant cell environment and the generation of signals that are amplified through feedback processes. Disruption of CWI results in activation of stress responses and CW modifications that might prevent the cells from further damage, including oxidative crosslinking, productions of ROS, jasmonic acid (JA), salicylic acid (SA), ethylene, lignin or callose depositions, alterations in pectin methylesterification and finally swollen root cells and root growth arrest caused by the inhibition of cellulose synthesis (Gigli-Bisceglia et al., 2020; Van der Does et al., 2017). Interestingly, one of the proposed CWI sensors (reviewed in Rui & Dinneny, 2020), the GPI-anchored COBRA (COB) localises predominantly to longitudinal CWs and controls the orientation of *Arabidopsis* root cell expansion (Schindelman et al., 2001). COB was shown to be involved in the regulation of cellulose crystallinity and microfibril orientation (Roudier et al., 2005; Schindelman et al., 2001). Considering cellulose/CW matrix interaction as the primary target of EXPAs and the aforementioned role of PhEXPA in the control of cellulose crystallinity, the role of CWI and downstream feedback regulations in mediating the CW remodelling in a response to EXPA-induced changes in CW biomechanical properties cannot be excluded. However, the molecular mechanisms perceiving mechanical forces at the CW–plasma membrane interphase and controlling CWI-initiated adaptive responses remain largely unknown as it is difficult to separate them from integrated hormonal and stress signalling (Vaahtera et al., 2019).

Taken together, apart from their role in CW loosening, expansins seem to be involved in controlling CW properties and composition by interfering with the action of CW remodelling enzymes, possibly via mechanisms that are both dependent and independent of expansin interaction with CW carbohydrates (Figure 1b).

6.3. Organ primordia specification/outgrowth

Besides their role in organ growth, expansins were shown to be involved in the initiation of new organs both in the shoot and in the root. Sephacryl beads coated with expansin purified from cucumber hypocotyls disturbed phyllotaxis by inducing new leaf primordia on the shoot apical meristem (SAM) in tomato (Fleming et al., 1997). Endogenous *LeREXP18* was shown to be expressed in new leaf primordia in tomato (Reinhardt et al., 1998). Accordingly, local microinduction of cucumber expansin *CsEXP1* in the tobacco SAM was able to induce new leaf formation and reverse the direction of new primordia appearance. Furthermore, the induction of *CsEXP1* at the leaf margin changed the leaf shape by inducing ectopic leaf lamina formation (Pien et al., 2001). More recently, a possible molecular mechanism underlying the expansin-mediated primordia induction has been elucidated by placing expansin-controlled CW loosening into a previously described framework comprising a feedback loop between CW tension and microtubule orientation in the SAM (Armezzani et al., 2018; Hamant et al., 2008; Sassi et al., 2014). Briefly, mechanical stress in the complex tissue of growing SAM affects the microtubule cytoskeleton, and that in turn controls morphogenesis (Hamant et al., 2008). In parallel, auxin affects the cortical microtubule dynamics thus enhancing microtubule isotropy; together with auxin-induced softening of the CW, this seems to be sufficient to induce new organ outgrowth (Sassi et al., 2014). However, the changes in microtubule organisation were shown to activate the transcription of genes which potentially can induce CW loosening (*PME3, XTH9* and *EXPA15*) independently of auxin accumulation and transport. Conversely, interfering with wall loosening promotes changes in microtubule organisation (Armezzani et al., 2018).

In the root, cytokinin-induced *AtEXPA1* and CW acidification were suggested to induce the elongation and differentiation of cells leaving the root apical meristem (RAM) in the root transition zone (Pacifici et al., 2018), and this is somewhat analogous to new organ primordia in the SAM. However, more recent studies seem to confirm neither cytokinin-inducible *AtEXPA1* in the

https://doi.org/10.1017/qpb.2022.6 Published online by Cambridge University Press

root transition zone nor the role of *AtEXPA1* in controlling root growth (Ramakrishna et al., 2019; Samalova et al., 2020). Instead, *AtEXPA1* seems to be involved in radial swelling of the lateral root founder cell as an important determinant of asymmetric cell division, initiating the process of lateral root (primordia) formation (Ramakrishna et al., 2019). Interestingly, also here the asymmetric swelling of the lateral root founder cell is dependent on auxin signalling and position-specific reorientation of cortical microtubules (isotropic in the position of asymmetric swelling; Vilches Barro et al., 2019). This result is another puzzle in the emerging role of mechanical interactions between pericycle and endodermis cells in lateral root formation (Vermeer et al., 2014) and more generally the role of cytoskeleton dynamics in the determination of primary CW biomechanics and cell division (reviewed in Chebli et al., 2021; Robinson, 2021).

7. Expansins under abiotic stress

The transcripts of many α-expansins are up-regulated under abiotic stress (Marowa et al., 2016; Tenhaken, 2015). Accordingly, genetic approaches have shown that enhanced expansin expression might contribute to stress tolerance to drought (Chen et al., 2016; Hao et al., 2017; Liu et al., 2019; Narayan et al., 2019; Yang et al., 2020), high salinity (Chen et al., 2017; 2018a; Hao et al., 2017; Lu et al., 2013; Yan et al., 2014; Zhang et al., 2019b), heat (Xu et al., 2007; 2014), cold (Peng et al., 2019; Zhang et al., 2018a), oxidative (Chen et al., 2018b) and heavy metal (cadmium) stress (Ren et al., 2018; Zhang et al., 2018b). Moreover, Han et al. (2012; 2015) described that overexpression of β-expansin *TaEXPB23* also enhanced tolerance to oxidative and salt stress, similar to the β-expansins *ZmEXPB6* and *ZmEXPB8* studied by Geilfus et al. (2015) and Wu et al. (2001) respectively. The changes in α-expansin gene activity under various abiotic stresses in different plants are summarised in Table 1.

The mechanism of expansin action in mediating stress resistance is still rather unclear. Investigating CW biomechanics under abiotic stresses is often challenging, so the focus has predominantly remained at the molecular level on genes involved in CW remodelling and on transcriptional and proteomic changes. Concerning changes in the composition and structure of CWs, loss of water can cause enhanced bonding among individual wall components which can impact the biosynthesis and deposition of newly formed CW polymers. This can be seen, for example, during salt stress, when sodium ions might influence pectin cross-links and disrupt microtubule stability, which consequently influence cellulose deposition (Wang et al., 2016b).

Reactive oxygen species (ROS) and peroxidases may also play an important role in the process of CW remodelling. ROS production occurs under many different stress conditions, but it is also necessary for normal growth and development (Mittler, 2017) hence their production and quenching must be tightly controlled (Castro et al., 2021 and references therein). ROS are responsible for the initial cross-linking of phenolic compounds and CWs glycoproteins resulting in stiffening. On the other hand, wall polysaccharides might be directly cleaved by hydroxyl radicals and weaken plant CWs (Fry, 1998; Müller et al., 2009; Schopfer, 2001; Schweikert et al., 2000). Tenhaken (2015) proposed a simplified model in which he suggests that plant organ growth under stress is a conflict between the two processes. According to this model, growth arrest under abiotic stresses is possibly caused by ROS- and peroxidase-induced cross-linking of glycoproteins and phenolics esterified with hemicellulose polymers, resulting in a dense network in which expansins and XTH do not have access to the xyloglucan substrate. If ROS production (stress) continues and all peroxidase substrates are depleted, ROS accumulation might lead to the formation of hydroxyl radicals, inducing the opposite effect, that is, cleavage of polymer chains. This results in CW weakening that enables further growth, comparable to growth under non-stress conditions. However, the experimental evidence for the model (Figure 1c) remains to be provided.

Interestingly, the action of expansins may result in enhancing the activity of CW-bound peroxidases in order to mitigate oxidative stress; however, the mechanism remains unknown (Han et al., 2015). The increased activity of covalently bound CW peroxidases was observed in transgenic plants over-expressing *TaEXPB23* and *Arabidopsis expb2* mutant showed a reduction in the activity and a decrease of oxidative stress tolerance (Han et al., 2015). Furthermore, expansin-mediated heat stress tolerance also seems to involve increased antioxidative capacity, photosynthesis rate and reduction of structural damage (Xu et al., 2014).

According to Wu et al. (1996; 2001)), root cell elongation is maintained at low water potential following enhanced expansin expression that enables plants to withstand drought conditions. This adaptive response, enabling roots to continue growing despite reduced turgor pressure, increases the root: shoot ratio allowing roots to explore the soil for water while limiting the water loss through leaves (Cosgrove, 2021). Furthermore, expansins were also proposed to be involved in increasing CW flexibility during the de- and rehydration processes in the resurrection plant *Craterostigma plantagineum* (Jones & McQueen-Mason, 2004).

8. Conclusions and future outlines

In contrast to the long-standing perception that considered the CW a rather static structure, passively delimiting the plant cell shape and providing mechanical support to plant bodies, the CW is a complex and highly dynamic structure, whose biomechanical properties have key consequences for a number of responses. Expansins are among the factors that allow plants to selectively change CW biomechanics, thus controlling plant growth and morphogenesis. As it is clear from our brief overview of the rich literature on the topic, there are several aspects of expansin action that are worth emphasising.

First, expansins seem to act in a manner that is dependent on both their dose and the particular developmental context. Second, CW sensitivity to expansin action seems to be actively controlled during the plant life cycle and in a location-specific fashion, and this is mediated by other factors including apoplastic pH. Third, expansins seem to control CW biomechanical properties not only by inducing creep but also by influencing CW remodelling, possibly through the modulation of substrate availability to other CW remodelling factors and/or CWI signalling. These effects might have important but different consequences for the downstream developmental regulations. It is therefore obvious that in order to comprehend the importance of expansin-regulated plant development and abiotic stress responses we will need a detailed understanding of the spatiotemporal specificity of expansin expression and its localization in living plant tissues. The existence of feedback regulatory loops between expansin activity/levels and expansin-modulated CW biomechanics might explain the dose-dependent and sometimes contradictory expansin effects. Moreover, functional redundancy among members of the expansin family is highly

https://doi.org/10.1017/qpb.2022.6 Published online by Cambridge University Press

https://doi.org/10.1017/qpb.2022.6 Published online by Cambridge University Press

Table 1. Overview of published evidence on expansin role in abiotic stress response.

Gene	Plant species	Abiotic stress	Change in gene activity and/or the stress response	References
TaEXPA2	*Nicotiana tabacum*	Drought	*Triticum aestivum EXPA2* OE enhanced tolerance, increase in seed production	Chen et al. (2016)
TaEXPA2	*Triticum aestivum*	Drought	OE enhanced tolerance, RNAi—increased sensitivity	Yang et al. (2020)
29 *EXPA*, 9 *EXLA*, 2 *EXPB*	*Camellia sinensis*	Drought	The expression levels of 16 expansins were high	Bordoloi et al. (2021)
CplEXP1, CplEXP2, CplEXP3	*Craterostigma plantagineum*	Drought	Increase in transcript levels of *Craterostigma plantagineum EXP1*	Jones and McQueen-Mason (2004)
EaEXPA1, SoEXPA1, ShEXPA1	*Erianthus arundinaceus*	Drought	High expression of *Erianthus arundinaceus EXPA1*	Narayan et al. (2019)
EaEXPA1	*Saccharum* spp. *hybrid*	Drought	OE enhanced tolerance	Narayan et al. (2021)
ZmEXP1, ZmEXP5	*Zea mays*	Drought	Increased transcript levels	Wu et al. (2001)
NtEXPA4	*Nicotiana tabacum*	Drought, salt	OE enhanced tolerance, RNAi—increased sensitivity	Chen et al., (2018a)
NtEXPA11	*Nicotiana tabacum*	Drought, salt	OE enhanced tolerance	Marowa et al. (2020)
RhEXPA4	*Arabidopsis thaliana*	Drought, salt	*Rosa hybrida EXPA4* OE enhanced tolerance	Lu et al. (2013)
AnEXPA1, AnEXPA2	*Arabidopsis thaliana*	Drought, cold	*Ammopiptanthus nanus EXPAs* OE enhanced tolerance	Liu et al. (2019)
AstEXPA1	*Nicotiana tabacum*	Drought, salt, heat, cold	*Agrostis stolonifera EXPA1* OE enhanced tolerance	Hao et al. (2017)
PttEXPA8	*Nicotiana tabacum*	Drought, salt, heat, cold, cadmium	*Populus tomentosa EXPA8* OE enhanced tolerance	Zhang et al. (2019b)
TaEXPA2	*Nicotiana tabacum*	Salt	*Triticum aestivum EXPA2* OE enhanced tolerance	Chen et al. (2017)
AtEXP2	*Arabidopsis thaliana*	Salt, osmotic stress	*exp2* increased sensitivity, *Arabidopsis thaliana EXP2* OE enhanced tolerance	Yan et al. (2014)
AsEXP1	*Agrostis scabra, Agrostis stolonifera*	Heat	The expression level of *Agrostis scabra EXP1* was highly upregulated in shoots	Xu et al. (2007)
PpEXP1	*Nicotiana tabacum*	Heat	*Poa pratensis EXP1* OE enhanced tolerance	Xu et al. (2014)
TaEXPAs	*Triticum aestivum*	Cold	Differential expression could be related to low-temperature tolerance or sensitivity	Zhang et al. (2018a)
TaEXPA8	*Arabidopsis thaliana*	Cold, drought	TaEXPA8 genes were induced by low-temperature and drought TaEXPA8 genes were induced by low-temperature and drought *Triticum aestivum EXPA8* OE enhanced low-temperature tolerance	Peng et al. (2019)
PtoEXPA12	*Nicotiana tabacum*	Cadmium	*Populus tomentosa EXPA12* OE enhanced Cd uptake and led to Cd toxicity	Zhang, et al. (2018b)
TaEXPA2	*Nicotiana tabacum*	Cadmium	*Triticum aestivum EXPA2* OE enhanced tolerance	Ren et al. (2018)
TaEXPA2 AtEXPA2	*Triticum aestivum, Arabidopsis thaliana*	H_2O_2 (oxidative stress)	The expression level of *TaEXPA2 was* upregulated, *Triticum aestivum EXPA2 OE* enhanced tolerance	Chen et al. (2018b)

Note: TaEXPA8 genes were induced by low-temperature and drought.

likely, and this may require phenotype assays of multiple mutants in expansin genes. Further, understanding the expansin structure (either using experimental or structure prediction algorithms, see Figure 1 and the text above) and binding specificity will be necessary to elucidate the possible importance of expansins in regulating CW composition by interfering with CW remodelling factors. However, it should be emphasised that most of the experimental evidence on the possible role of expansins in CW remodelling originates from overexpression studies. Thus, more detailed studies employing, for example, cell type-specific endogenous promoters will be necessary to assess the possible role of expansins in CW remodelling.

Finally, developing tools allowing in vivo assays of quantifiable CW biomechanical properties at (sub)cellular resolution will be critical. Approaches combining biology, physics and mathematical modelling are particularly salient in order to integrate the vast array of complex observations that is expected from state-of-the-art visualisation methods, molecular biology/biochemistry and genetics studies.

Glossary of used biomechanical terms

Extensibility	In general, the ability of a material to be deformed by a tensile force. Wall extensibility is the ability of the CW to increase in surface area irreversibly during growth
Cell wall stress	A force exerted on the CW divided by the wall cross-sectional area perpendicular to the force application vector
Cell wall stress relaxation	A reduction in wall stress due to rearrangement of the load-bearing polymers in the cell wall
Cell wall remodelling	Chemical modification of CW components in which linkages between cell wall polysaccharides must be undone and reformed
Cell wall loosening	A molecular process causing wall stress relaxation (Cosgrove, 2018a). In other words, CW loosening is the sum of biochemical changes underlying the physical process of wall stress relaxation by creep
Wall creep	An irreversible, time-dependent CW deformation leading to modification of non-covalent bonds between CW polymers and allowing the fibril–fibril sliding
Cell wall softening	CW modification that makes the wall more deformable to out-of-plane mechanical force measurable by, for example, indentation techniques
Cell wall weakening	A process that reduces the force or energy needed to break the wall
Cell wall stiffening	A molecular process resulting in an increase in CW stress resistance. Stiffening can decrease the cell expansion rate or halt expansion under a given turgor

Modified from: Chebli and Geitmann (2017), Cosgrove (1993; 2018a) and Zhang et al. (2019a).

Acknowledgements

We are grateful to Prof. Olivier Hamant for his kind invitation and for the opportunity to provide our view on this highly interesting and dynamically developing topic. We thank the anonymous reviewers for their constructive and helpful comments.

Financial support. This work was supported by the Ministry of Education, Youth and Sports of CR from the European Regional Development Fund Project 'Centre for Experimental Plant Biology': No. CZ.02.1.01/0.0/0.0/16_019/0000738, LTAUSA18161 and the Czech Science Foundation (19-24753S and 22-17501S).

Conflict of interest. The authors declare no conflict of interest.

Authorship contributions. M.S., E.G. and J.H. performed the literature search, conceived the review structure and wrote the manuscript. J.H. drew Figure 1.

Data availability statement. All the data discussed in the review were obtained from the referenced papers. The AtEXPA1 (AT1G69530) structural prediction was downloaded from AlphaFold Protein Structure Database (https://alphafold.ebi.ac.uk/).

References

Armezzani, A., Abad, U., Ali, O., Andres Robin, A., Vachez, L., Larrieu, A., Mellerowicz, E. J., Taconnat, L., Battu, V., Stanislas, T., Liu, M., Vernoux, T., Traas, J., & **Sassi, M.** (2018). Transcriptional induction of cell wall remodelling genes is coupled to microtubule-driven growth isotropy at the shoot apex in *Arabidopsis*. *Development*, **145**, dev162255.

Arsuffi, G., & **Braybrook, S. A.** (2018). Acid growth: An ongoing trip. *Journal of Experimental Botany*, **2**, 137–146.

Barbez, E., Dunser, K., Gaidora, A., Lendl, T., & **Busch, W.** (2017). Auxin steers root cell expansion via apoplastic pH regulation in *Arabidopsis thaliana*. *Proceedings of the National Academy of Sciences USA*, **114**, E4884–E4893.

Bootten, T. J., Harris, P. J., Melton, L. D., & **Newman, R. H.** (2004). Solid-state ^{13}C-NMR spectroscopy shows that the xyloglucans in the primary cell walls of mung bean (*Vigna radiata* L.) occur in different domains: A new model for xyloglucan–cellulose interactions in the cell wall. *Journal of Experimental Botany*, **55**, 571–583.

Boraston, A. B., Creagh, A. L., Alam, M. M., Kormos, J. M., Tomme, P., Haynes, C. A., Warren, R. A., & **Kilburn, D. G.** (2001). Binding specificity and thermodynamics of a family 9 carbohydrate-binding module from *Thermotoga maritima* xylanase 10A. *Biochemistry*, **40**, 6240–6247.

Bordoloi, K., Dihingia, P., Krishnatreya, D., & **Agarwala, N.** (2021). Genome-wide identification, characterization and expression analysis of the expansin gene family under drought stress in tea (*Camellia sinensis* L.). *Plant Science Today*, **8**, 32–44.

Boron, A. K., Van Loock, B., Suslov, D., Markakis, M. N., Verbelen, J. P., & **Vissenberg, K.** (2015). Over-expression of *AtEXLA2* alters etiolated *Arabidopsis* hypocotyl growth. *Annals of Botany*, **115**, 67–80.

Bou Dahner, F., Chen, Y., Bozorg, B., Clough, J., Jonsson, H., & **Braybrook, S. A.** (2018). Anisotropic growth is achieved through the additive mechanical effect of material anisotropy and elastic symmetry. *eLife*, **7**, e38161.

Brummell, D. A., Harpster, M. H., Civello, P. M., Palys, J. M., Bennett, A. B., & **Dunsmuir, P.** (1999). Modification of expansin protein abundance in tomato fruit alters softening and cell wall polymer metabolism during ripening. *Plant Cell*, **11**, 2203–2216.

Caderas, D., Muster, M., Vogler, H., Mandel, T., Rose, J. K. C., McQueen-Mason, S., & **Kuhlemeier, C.** (2000). Limited correlation between expansin gene expression and elongation growth rate. *Plant Physiology*, **123**, 1399–1413.

Carpita, N. C. (1996). Structure and biogenesis of the cell walls of grasses. *Annual Review Plant Physiology Plant Molecular Biology*, **47**, 445–476.

Carpita, N. C., & **Gibeaut, D. M.** (1993). Structural models of primary cell walls in flowering plants: Consistency of molecular structure with the physical properties of the walls during growth. *Plant Journal*, **3**, 1–30.

Castro, B., Citterico, M., Kimura, S., Stevens, D. M., Wrzaczek, M., & **Coaker, G.** (2021). Stress-induced reactive oxygen species compartmentalization, perception and signalling. *Nature Plants*, **7**, 403–412.

Cavalier, D. M., Lerouxel, O., Neumetzler, L., Yamauchi, K., Reinecke, A., Freshour, G., Zabotina, O. A., Hahn, M. G., Burgert, I., Pauly, M., Raikhel, N. V., & **Keegstra, K.** (2008). Disrupting two*Arabidopsis thaliana* xylosyl-

transferase genes results in plants deficient in xyloglucan, a major primary cell wall component. *Plant Cell*, **20**, 1519–1537.

Chase, W. R., **Zhaxybayeva, O.**, **Rocha, J.**, **Cosgrove, D. J.**, & **Shapiro, L. R.** (2020). Global cellulose biomass, horizontal gene transfers and domain fusions drive microbial expansin evolution. *New Phytologist*, **226**, 921–938.

Chebli, Y., **Bidhendi, A. J.**, **Kapoor, K.**, & **Geitmann, A.** (2021). Cytoskeletal regulation of primary plant cell wall assembly. *Current Biology*, **31**, R681–R695.

Chebli, Y., & **Geitmann, A.** (2017). Cellular growth in plants requires regulation of cell wall biochemistry. *Current Opinion in Cell Biology*, **44**, 28–35.

Chen, L., **Zou, W.**, **Fei, C.**, **Wu, G.**, **Li, X.**, **Lin, H.**, & **Xi, D.** (2018a). α-Expansin *EXPA4* positively regulates abiotic stress tolerance but negatively regulates pathogen resistance in *Nicotiana tabacum*. *Plant and Cell Physiology*, **59**, 2317–2330.

Chen, Y., **Han, Y.**, **Kong, X.**, **Kang, H.**, **Ren, Y.**, & **Wang, W.** (2017). Ectopic expression of wheat expansin gene *TaEXPA2* improved the salt tolerance of transgenic tobacco by regulating Na+/K+ and antioxidant competence. *Physiologia Plantarum*, **159**, 161–177.

Chen, Y., **Han, Y.**, **Meng, Z.**, **Zhou, S.**, **Xiangzhu, K.**, & **Wei, W.** (2016). Overexpression of the wheat expansin gene *TaEXPA2* improved seed production and drought tolerance in transgenic tobacco plants. *PLoS One*, **11**, 1–24.

Chen, Y., **Ren, Y.**, **Zhang, G.**, **An, J.**, **Yang, J.**, **Wang, Y.**, & **Wang, W.** (2018b). Overexpression of the wheat expansin gene *TaEXPA2* improves oxidative stress tolerance in transgenic *Arabidopsis plants*. *Plant Physiology and Biochemistry*, **124**, 190–198.

Chen, Y., **Zhang, B.**, **Li, C.**, **Lei, C.**, **Kong, C.**, **Yang, Y.**, & **Gong, M.** (2019). A comprehensive expression analysis of the expansin gene family in potato (*Solanum tuberosum*) discloses stress-responsive expansin-like B genes for drought and heat tolerances. *PLoS One*, **14**, e0219837.

Cho, H. T., & **Cosgrove, D. J.** (2002). Regulation of root hair initiation and expansin gene expression in *Arabidopsis*. *Plant Cell*, **14**, 3237–3253.

Choi, D. S., **Lee, Y.**, **Cho, H. T.**, & **Kende, H.** (2003). Regulation of expansin gene expression affects growth and development in transgenic rice plants. *Plant Cell*, **15**, 1386–1398.

Cosgrove, D. J. (1989). Characterization of long-term extension of isolated cell-walls from growing cucumber hypocotyls. *Planta*, **177**, 121–130.

Cosgrove, D. J. (1993). Wall extensibility: Its nature, measurement and relationship to plant cell growth. *New Phytologist*, **124**, 1–23.

Cosgrove, D. J. (2000). Loosening of plant cell walls by expansins. *Nature*, **407**, 321–326.

Cosgrove, D. J. (2005). Growth of the plant cell wall. *Nature Reviews Molecular Cell Biology*, **6**, 850–861.

Cosgrove, D. J. (2011). Measuring *in vitro* extensibility of growing plant cell walls. *Methods in Molecular Biology*, **715**, 291–303.

Cosgrove, D. J. (2014). Re-constructing our models of cellulose and primary cell wall assembly. *Current Opinion in Plant Biology*, **22**, 122–131.

Cosgrove, D. J. (2015). Plant expansins: Diversity and interactions with plant cell walls. *Current Opinion in Plant Biology*, **25**, 162–172.

Cosgrove, D. J. (2016a). Plant cell wall extensibility: Connecting plant cell growth with cell wall structure, mechanics, and the action of wall modifying enzymes. *Journal of Experimental Botany*, **67**, 463–476.

Cosgrove, D. J. (2016b). Catalysts of plant cell wall loosening. *F1000Research*, **5**, 119.

Cosgrove, D. J. (2018a). Diffuse growth of plant cell walls. *Plant Physiology*, **176**, 16–27.

Cosgrove, D. J. (2018b). Nanoscale structure, mechanics and growth of epidermal cell walls. *Current Opinion Plant Biology*, **46**, 77–86.

Cosgrove, D. J. (2021). Expanding wheat yields with expansin. *New Phytologist*, **230**, 403–405.

Cosgrove, D. J., **Bedinger, P.**, & **Durachko, D. M.** (1997). Group I allergens of grass pollen as cell wall-loosening agents. *Proceedings of the National Academy of Sciences USA*, **94**, 6559–6564.

Craft, J., **Samalova, M.**, **Baroux, C.**, **Townley, H.**, **Martinez, A.**, **Jepson, I.**, **Tsiantis, M.**, & **Moore, I.** (2005). New pOp/LhG4 vectors for stringent glucocorticoid-dependent transgene expression in *Arabidopsis*. *Plant Journal*, **41**, 899–918.

Dick-Perez, M., **Zhang, Y.**, **Hayes, J.**, **Salazar, A.**, **Zabotina, O. A.**, & **Hong, M.** (2011). Structure and interactions of plant cell-wall polysaccharides by two- and three-dimensional magic-angle-spinning solid-state NMR. *Biochemistry*, **50**, 989–1000.

Du, M., **Spalding, E. P.**, & **Gray, W. M.** (2020). Rapid auxin-mediated cell expansion. *Annual Review of Plant Biology*, **71**, 379–402.

Duan, Y. H., **Ma, Y. Y.**, **Zhao, X. D.**, **Huang, R. L.**, **Su, R. X.**, **Qi, W.**, & **He, Z. M.** (2018). Real-time adsorption and action of expansin on cellulose. *Biotechnology for Biofuels*, **11**, 317–329.

Dunser, K., & **Kleine-Vehn, J.** (2015). Differential growth regulation in plants – The acid growth balloon theory. *Current Opinion in Plant Biology*, **28**, 55–59.

Durachko, D., **Park, Y. B.**, **Zhang, T.**, & **Cosgrove, D. J.** (2017). Biomechanical characterization of onion epidermal cell walls. *Bio-Protocol*, **7**, e2662. https://doi.org/10.21769/BioProtoc.22662

Durachko, D. M., & **Cosgrove, D. J.** (2009). Measuring plant cell wall extension (creep) induced by acidic pH and by alpha-expansin. *Journal of Visualized Experiments*, **25**, e1263.

Elsayad, K., **Werner, S.**, **Gallemí, M.**, **Kong, J.**, **Sanchez Guajardo, E. R.**, **Zhang, L.**, **Jaillais, Y.**, **Greb, T.**, & **Belkhadir, Y.** (2016). Mapping the subcellular mechanical properties of live cells in tissues with fluorescence emission–Brillouin imaging. *Science Signaling*, **9**, rs5.

Fendrych, M., **Akhmanova, M.**, **Merrin, J.**, **Glanc, M.**, **Hagihara, S.**, **Takahashi, K.**, **Uchida, N.**, **Torii, K. U.**, & **Friml, J.** (2018). Rapid and reversible root growth inhibition by TIR1 auxin signalling. *Nature Plants*, **4**, 453–459.

Fendrych, M., **Leung, J.**, & **Friml, J.** (2016). Tir1/AFB-aux/IAA auxin perception mediates rapid cell wall acidification and growth of *Arabidopsis* hypocotyls. *eLife*, **5**, 1–19.

Fleming, A. J., **McQueen-Mason, S.**, **Mandel, T.**, & **Kuhlemeier, C.** (1997). Induction of leaf primordia by the cell wall protein expansin. *Science*, **276**, 1415–1418.

Fry, S. C. (1989). The structure and functions of xyloglucan. *Journal of Experimental Botany*, **40**, 1–12.

Fry, S. C. (1998). Oxidative scission of plant cell wall polysaccharides by ascorbate-induced hydroxyl radicals. *Biochemical Journal*, **332**, 507–515.

Gaete-Eastman, C., **Morales-Quintana, L.**, **Herrera, R.**, & **Moya-Leon, M. A.** (2015). *In-silico* analysis of structure and binding site feature of expansin protein from mountain papaya fruit (VpEXPA2), through molecular modelling, docking and dynamics simulation studies. *Journal of Molecular Modeling*, **21**, 1–12.

Geilfus, C., **Ober, D.**, **Eichacker, L. A.**, **Mühling, K. H.**, & **Zörb, C.** (2015). Down-regulation of *ZmEXPB6* (*Zea mays*β-Expansin 6) protein is correlated with salt-mediated growth reduction in the leaves of *Z. mays* L.. *Journal of Biological Chemistry*, **290**, 11235–11245.

Georgelis, N., **Nikolaidis, N.**, & **Cosgrove, D. J.** (2015). Bacterial expansins and related proteins from the world of microbes. *Applied Microbiology and Biotechnology*, **99**, 3807–3823.

Georgelis, N., **Tabuchi, A.**, **Nikolaidis, N.**, & **Cosgrove, D. J.** (2011). Structure-function analysis of the bacterial expansin EXLX1. *Journal of Biological Chemistry*, **286**, 16814–16823.

Georgelis, N., **Yennawar, N. H.**, & **Cosgrove, D. J.** (2012). Structural basis for entropy-driven cellulose binding by a type-a cellulose-binding module (CBM) and bacterial expansin. *Proceedings of the National Academy of Sciences*, **109**, 14830–14835.

Gigli-Bisceglia, N., **Engelsdorf, T.**, & **Hamann, T.** (2020). Plant cell wall integrity maintenance in model plants and crop species-relevant cell wall components and underlying guiding principles. *Cellular and Molecular Life Sciences*, **77**, 2049–2077.

Goh, H. H., **Sloan, J.**, **Dorca-Fornell, C.**, & **Fleming, A.** (2012). Inducible repression of multiple expansin genes leads to growth suppression during leaf development. *Plant Physiology*, **159**, 1759–1770.

Goh, H. H., **Sloan, J.**, **Malinowski, R.**, & **Fleming, A.** (2014). Variable expansin expression in *Arabidopsis* leads to different growth responses. *Journal of Plant Physiology*, **171**, 329–339.

Goldberg, R., **Morvan, C.**, **Jauneau, A.**, & **Jarvis, M. C.** (1996). Methylesterificatin, de-esterification and gelation of pectins in the primary cell wall. *Progress in Biotechnology*, **14**, 151–172.

Großeholz, R., **Wanke, F.**, **Glöckner, N.**, **Rausch, L.**, **Rohr, L.**, **Scholl, S.**, **Scacchi, E.**, **Spazierer, A.-J.**, **Shabala, L.**, **Shabala, S.**, **Schumacher, K.**,

https://doi.org/10.1017/qpb.2022.6 Published online by Cambridge University Press

Kummer, U., & **Harter, K.** (2021). *Computational modeling and quantitative cell physiology reveal central parameters for the brassinosteroid-regulated cell growth of the Arabidopsis root*. *bioRxiv* 2021.04.13.439595.

Gruel, J., **Landrein, B.**, **Tarr, P.**, **Schuster, C.**, **Refahi, Y.**, **Sampathkumar, A.**, **Hamant, O.**, **Meyerowitz, E. M.**, & **Jonsson, H.** (2016). An epidermis-driven mechanism positions and scales stem cell niches in plants. *Science Advances*, **2**, e1500989.

Hager, A., **Menzel, H.**, & **Krauss, A.** (1971). Experiments and hypothesis concerning the primary action of auxin in elongation growth. *Planta*, **100**, 47–75.

Hamann, T. (2015). The plant cell wall integrity maintenance mechanism-concepts for organization and mode of action. *Plant Cell Physiology*, **56**, 215–223.

Hamant, O., **Heisler, M. G.**, **Jonsson, H.**, **Krupinski, P.**, **Uyttewaal, M.**, **Bokov, P.**, **Corson, F.**, **Sahlin, P.**, **Boudaoud, A.**, **Meyerowitz, E. M.**, **Couder, Y.**, & **Traas, J.** (2008). Developmental patterning by mechanical signals in *Arabidopsis*. *Science*, **322**, 1650–1655.

Han, Y., **Chen, Y.**, **Yin, S.**, **Zhang, M.**, & **Wang, W.** (2015). Over-expression of *TaEXPB23*, a wheat expansin gene, improves oxidative stress tolerance in transgenic tobacco plants. *Journal of Plant Physiology*, **173**, 62–71.

Han, Y. Y., **Li, A. X.**, **Li, F.**, **Zhao, M. R.**, & **Wang, W.** (2012). Characterization of a wheat (*Triticum aestivum* L.) expansin gene, *TaEXPB23*, involved in the abiotic stress response and phytohormone regulation. *Plant Physiology and Biochemistry*, **54**, 49–58.

Han, Z., **Liu, Y.**, **Deng, X.**, **Liu, D.**, **Liu, Y.**, **Hu, Y.**, & **Yan, Y.** (2019). Genome-wide identification and expression analysis of expansin gene family in common wheat (*Triticum aestivum L.*). *BMC Genomics*, **20**, 101.

Hao, Z., **Qian, X.**, **Xiao, X.**, **Huabo, L.**, **Junkai, Z.**, & **Jichen, X.** (2017). Transgenic tobacco plants expressing grass *AstEXPA1* gene show improved performance to several stresses. *Plant Biotechnology Reports*, **11**, 331–337.

Hayashi, T. (1989). Xyloglucans in the primary cell wall. *Annual Review of Plant Physiology and Plant Molecular Biology*, **40**, 139–168.

Hepler, N. K., **Bowman, A.**, **Carey, R. E.**, & **Cosgrove, D. J.** (2020). Expansin gene loss is a common occurrence during adaptation to an aquatic environment. *Plant Journal*, **101**, 666–680.

Hepler, N. K., & **Cosgrove, D. J.** (2019). Directed *in vitro* evolution of bacterial expansin BsEXLX1 for higher cellulose binding and its consequences for plant cell wall-loosening activities. *FEBS Letters*, **593**, 2545–2555.

Herburger, K., **Frankova, L.**, **Picmanova, M.**, **Loh, J. W.**, **Valenzuela-Ortega, M.**, **Meulewaeter, F.**, **Hudson, A. D.**, **French, C. E.**, & **Fry, S. C.** (2020). Hetero-trans-β-glucanase produces cellulose–xyloglucan covalent bonds in the cell walls of structural plant tissues and is stimulated by expansin. *Molecular Plant*, **13**, 1047–1062.

Hervieux, N., **Tsugawa, S.**, **Fruleux, A.**, **Dumond, M.**, **Routier-Kierzkowska, A. L.**, **Komatsuzaki, T.**, **Boudaoud, A.**, **Larkin, J. C.**, **Smith, R. S.**, **Li, C. B.**, & **Hamant, O.** (2017). Mechanical shielding of rapidly growing cells buffers growth heterogeneity and contributes to organ shape reproducibility. *Current Biology*, **27**, 3468–3479.

Hou, L., **Zhang, Z. Y.**, **Dou, S. H.**, **Zhang, Y. D.**, **Pang, X. M.**, & **Li, Y. Y.** (2019). Genome-wide identification, characterization, and expression analysis of the expansin gene family in Chinese jujube (*Ziziphus jujube* Mill.). *Planta*, **249**, 815–829.

Hurny, A., **Cuesta, C.**, **Cavallari, N.**, **Otvos, K.**, **Duclercq, J.**, **Dokladal, L.**, **Montesinos, J. C.**, **Gallemi, M.**, **Semeradova, H.**, **Rauter, T.**, **Stenzel, I.**, **Persiau, G.**, **Benade, F.**, **Bhalearo, R.**, **Sykorova, E.**, **Gorzsas, A.**, **Sechet, J.**, **Mouille, G.**, **Heilmann, I.**, ... **Benkova, E.** (2020). Synergistic on auxin and cytokinin 1 positively regulates growth and attenuates soil pathogen resistance. *Nature Communications*, **11**, 2170.

Ilias, I. A., **Negishi, K.**, **Yasue, K.**, **Jomura, N.**, **Morohashi, K.**, **Baharum, S. N.**, & **Goh, H. H.** (2019). Transcriptome-wide effects of expansin gene manipulation in etiolated *Arabidopsis* seedling. *Journal of Plant Research*, **132**, 159–172.

Jones, L., & **McQueen-Mason, S.** (2004). A role for expansins in dehydration and rehydration of the resurrection plant *Craterostigma plantagineum*. *FEBS Letters*, **559**, 61–65.

Jumper, J., **Evans, R.**, **Pritzel, A.**, **Green, T.**, **Figurnov, M.**, **Ronneberger, O.**, **Tunyasuvunakool, K.**, **Bates, R.**, **Zidek, A.**, **Potapenko, A.**, **Bridgland, A.**, **Meyer, C.**, **Kohl, S. A. A.**, **Ballard, A. J.**, **Cowie, A.**, **Romera-Paredes, B.**, **Nikolov, S.**, **Jain, R.**, **Adler, J.**, ... **Hassabis, D.** (2021). Highly accurate protein structure prediction with AlphaFold. *Nature*, **596**, 583–589.

Kerff, F., **Amoroso, A.**, **Herman, R.**, **Sauvage, E.**, **Petrella, S.**, **Filée, P.**, **Charlier, P.**, **Joris, B.**, **Tabuchi, A.**, **Nikolaidis, N.**, & **Cosgrove, D. J.** (2008). Crystal structure and activity of *Bacillus subtilis* YoaJ (EXLX1), a bacterial expansin that promotes root colonization. *Proceedings of the National Academy of Sciences USA*, **105**, 16876–16881.

Kim, E. S., **Lee, H. J.**, **Bang, W. G.**, **Choi, I. G.**, & **Kim, K. H.** (2009). Functional characterization of a bacterial expansin from *Bacillus subtilis* for enhanced enzymatic hydrolysis of cellulose. *Biotechnology and Bioengineering*, **102**, 1342–1353.

Kim, I. J., **Ko, H. J.**, **Kim, T. W.**, **Nam, K. H.**, **Choi, I. G.**, & **Kim, K. H.** (2013). Binding characteristics of a bacterial expansin (BsEXLX1) for various types of pretreated lignocellulose. *Applied Microbiology and Biotechnology*, **97**, 5381–5388.

Landrein, B., **Kiss, A.**, **Sassi, M.**, **Chauvet, A.**, **Das, P.**, **Cortizo, M.**, **Laufs, P.**, **Takeda, S.**, **Aida, M.**, **Traas, J.**, **Vernoux, T.**, **Boudaoud, A.**, & **Hamant, O.** (2015). Mechanical stress contributes to the expression of the *STM* homeobox gene in *Arabidopsis* shoot meristems. *eLife*, **4**, e07811.

Li, K., **Ma, B.**, **Shen, J.**, **Zhao, S.**, **Ma, X.**, **Wang, Z.**, **Fan, Y.**, **Tang, Q.**, & **Wei, D.** (2021b). The evolution of the expansin gene family in *brassica* species. *Plant Physiology and Biochemistry*, **167**, 630–638.

Li, L., **Gallei, M.**, & **Friml, F.** (2021a). *Bending to auxin: Fast acid growth for tropisms*. Trends in Plant Science.

Li, L., **Verstraeten, I.**, **Roosjen, M.**, **Takahashi, K.**, **Rodriguez, L.**, **Merrin, J.**, **Chen, J.**, **Shabala, L.**, **Smet, W.**, **Ren, H.**, **Vanneste, S.**, **Shabala, S.**, **De Rybel, B.**, **Weijers, D.**, **Kinoshita, T.**, **Gray, W. M.**, & **Friml, J.** (2021c). Cell surface and intracellular auxin signalling for H^+ fluxes in root growth. *Nature*, **599**, 273–277.

Li, Y., **Tu, L.**, **Pettolino, F. A.**, **Ji, S.**, **Hao, J.**, **Yuan, D.**, **Deng, F.**, **Tan, J.**, **Hu, H.**, **Wang, Q.**, **Llewellyn, D. J.**, & **Zhang, X.** (2016). *GbEXPATR*, a species-specific expansin, enhances cotton fibre elongation through cell wall restructuring. *Plant Biotechnology Journal*, **14**, 951–963.

Lin, W., **Zhou, X.**, **Tang, W.**, **Takahashi, K.**, **Pan, X.**, **Dai, J.**, **Ren, H.**, **Zhu, X.**, **Pan, S.**, **Zheng, H.**, **Gray, W. M.**, **Xu, T.**, **Kinoshita, T.**, & **Yang, Z.** (2021). TMK-based cell-surface auxin signalling activates cell-wall acidification. *Nature*, **599**, 278–282.

Liu, X., **Ma, Y.**, & **Zhang, M.** (2015). Research advances in expansins and expansion-like proteins involved in lignocellulose degradation. *Biotechnology Letters*, **37**, 1541–1551.

Liu, Y., **Zhang, L.**, **Hao, W.**, **Zhang, L.**, **Liu, Y.**, & **Chen, L.** (2019). Expression of two α-type expansins from *Ammopiptanthus nanus* in *Arabidopsis thaliana* enhance tolerance to cold and drought stresses. *International Journal of Molecular Sciences*, **20**, 5255.

Lohoff, C., **Buchholz, P. C. F.**, **Le Roes-Hill, M.**, & **Pleiss, J.** (2020). The Expansin engineering database: A navigation and classification tool for expansins and homologues. *Proteins*, **89**, 149–162.

Lu, P., **Kang, M.**, **Jiang, X.**, **Dai, F.**, **Gao, J.**, & **Zhang, C.** (2013). *RhEXPA4*, a rose expansin gene, modulates leaf growth and confers drought and salt tolerance to *Arabidopsis*. *Planta*, **237**, 1547–1559.

Lv, L.-M., **Zuo, D.-Y.**, **Wang, X.-F.**, **Cheng, H.-L.**, **Zhang, Y.-P.**, **Wang, Q.-L.**, **Song, G.-L.**, & **Ma, Z.-Y.** (2020). Genome-wide identification of the expansin gene family reveals that *expansin* genes are involved in fibre cell growth in cotton. *BMC Plant Biology*, **20**, 223–236.

Ma, N., **Wang, Y.**, **Qiu, S.**, **Kang, Z.**, **Che, S.**, **Wang, G.**, & **Huang, J.** (2013). Overexpression of *OsEXPA8*, a root-specific gene, improves rice growth and root system architecture by facilitating cell extension. *PLoS One*, **8**, e75997.

Majda, M., **Grones, P.**, **Sintorn, I. M.**, **Vain, T.**, **Milani, P.**, **Krupinski, P.**, **Zagorska-Marek, B.**, **Viotti, C.**, **Jonsson, H.**, **Mellerowicz, E. J.**, **Hamant, O.**, & **Robert, S.** (2017). Mechanochemical polarization of contiguous cell walls shapes plant pavement cells. *Developmental Cell*, **43**, 290–304.

Marga, F., **Grandbois, M.**, **Cosgrove, D. J.**, & **Tobias, I.** (2005). Cell wall extension results in the coordinate separation of parallel microfibrils: Evi-

https://doi.org/10.1017/qpb.2022.6 Published online by Cambridge University Press

dence from scanning electron microscopy and atomic force microscopy. *Plant Journal*, **43**, 181–190.

Marowa, P., **Ding, A.**, & **Kong, Y.** (2016). Expansins: Roles in plant growth and potential applications in crop improvement. *Plant Cell Reports*, **35**, 949–965.

Marowa, P., **Ding, A.**, **Xu, Z.**, & **Kong, Y.** (2020). Overexpression of *NtEXPA11* modulates plant growth and development and enhances stress tolerance in tobacco. *Plant Physiology and Biochemistry*, **151**, 477–485.

Mateluna, P., **Valenzuela-Riffo, F.**, **Morales-Quintana, L.**, **Herrera, R.**, & **Ramos, P.** (2017). Transcriptional and computational study of expansins differentially expressed in the response to inclination in radiata pine. *Plant Physiology and Biochemistry*, **115**, 12–24.

McQueen-Mason, S., **Durachko, D. M.**, & **Cosgrove, D. J.** (1992). Two endogenous proteins that induce cell wall extension in plants. *Plant Cell*, **4**, 1425–1433.

McQueen-Mason, S. J., & **Cosgrove, D. J.** (1995). Expansin mode of action on cell walls. Analysis of wall hydrolysis, stress relaxation, and binding. *Plant Physiology*, **107**, 87–100.

Mielke, S., **Zimmer, M.**, **Meena, M. K.**, **Dreos, R.**, **Stellmach, H.**, **Hause, B.**, **Voiniciuc, C.**, & **Gasperini, D.** (2021). Jasmonate biosynthesis arising from altered cell walls is prompted by turgor-driven mechanical compression. *Science Advances*, **7**, eabf0356.

Mittler, R. (2017). ROS are good. *Trends in Plant Sciences*, **22**, 11–19.

Müller, K., **Linkies, A.**, **Vreeburg, R. A.**, **Fry, S. C.**, **Krieger-Liszkay, A.**, & **Leubner-Metzger, G.** (2009). In vivo cell wall loosening by hydroxyl radicals during cress seed germination and elongation growth. *Plant Physiology*, **150**, 1855–1865.

Narayan, J. A., **Chakravarthi, M.**, **Nerkar, G.**, **Manoj, V. M.**, **Dharshini, S.**, **Subramonian, N.**, **Premachandran, M. N.**, **Kumar, R. A.**, **Surendar, K. K.**, **Hemaprabha, G.**, **Ram, B.**, & **Appunu, C.** (2021). Overexpression of expansin *EaEXPA1*, a cell wall loosening protein enhances drought tolerance in sugarcane. *Industrial Crops and Products*, **159**, 113035.

Narayan, J. A., **Dharshini, S.**, **Manoj, V. M.**, **Padmanabhan, T. S. S.**, **Kadirvelu, K.**, **Suresha, G. S.**, **Subramonian, N.**, **Ram, B.**, **Premachandran, M. N.**, & **Appunu, C.** (2019). Isolation and characterization of water-deficit stress-responsive α-expansin 1 (*EXPA1*) gene from *Saccharum* complex. *3 Biotech*, **9**, 186.

Nardi, C., **Escudero, C.**, **Villarreal, N.**, **Martinez, G.**, & **Civello, P. M.** (2013). The carbohydrate-binding module of Fragaria x ananassa expansin 2 (CBM-FaExp2) binds to cell wall polysaccharides and decreases cell wall enzyme activities "*in vitro*". *Journal of Plant Research*, **126**, 151–159.

Nishitani, K. (1998). Construction and restructuring of the cellulose–xyloglucan framework in the apoplast as mediated by the xyloglucan related protein family—A hypothetical scheme. *Journal of Plant Research*, **111**, 159–166.

Novakovic, L., **Guo, T.**, **Bacic, A.**, **Sampathkumar, A.**, & **Johnson, K. L.** (2018). Hitting the wall—Sensing and signaling pathways involved in plant cell wall remodeling in response to abiotic stress. *Plants*, **7**, 89.

Orłowski, A., **Artzi, L.**, **Cazade, P. A.**, **Gunnoo, M.**, **Bayer, E. A.**, & **Thompson, D.** (2018). On the distinct binding modes of expansin and carbohydrate-binding module proteins on crystalline and nanofibrous cellulose: Implications for cellulose degradation by designer cellulosomes. *Journal of the Chemical Society Faraday Transactions*, **20**, 8278–8293.

Pacheco-Villalobos, D., **Diaz-Moreno, S. M.**, **van der Schuren, A.**, **Tamaki, T.**, **Kang, Y. H.**, **Gujas, B.**, **Novak, O.**, **Jaspert, N.**, **Li, Z.**, **Wolf, S.**, **Oecking, C.**, **Ljung, K.**, **Bulone, V.**, & **Hardtke, C. S.** (2016). The effects of high steady state auxin levels on root cell elongation in *Brachypodium*. *Plant Cell*, **28**, 1009–1024.

Pacifici, E., **Di Mambro, R.**, **Dello Ioio, R.**, **Costantino, P.**, & **Sabatini, S.** (2018). Acidic cell elongation drives cell differentiation in the *Arabidopsis* root. *EMBO Journal*, **37**, e99134.

Park, Y. B., & **Cosgrove, D. J.** (2012a). A revised architecture of primary cell walls based on biomechanical changes induced by substrate-specific endoglucanases. *Plant Physiology*, **158**, 1933–1943.

Park, Y. B., & **Cosgrove, D. J.** (2012b). Changes in cell wall biomechanical properties in the xyloglucan-deficient *xxt1/xxt2* mutant of *Arabidopsis*. *Plant Physiology*, **158**, 465–475.

Park, Y. B., & **Cosgrove, D. J.** (2015). Xyloglucan and its interactions with other components of the growing cell wall. *Plant Cell Physiology*, **56**, 180–194.

Pastor, N., **Davila, S.**, **Perez-Rueda, E.**, & **Segovia, L.** (2015). Electrostatic analysis of bacterial expansins. *Proteins*, **83**, 215–223.

Peaucelle, A., **Louvet, R.**, **Johansen, J. N.**, **Hofte, H.**, **Laufs, P.**, **Pelloux, J.**, & **Mouille, G.** (2008). *Arabidopsis* phyllotaxis is controlled by the methylesterification status of cell-wall pectins. *Current Biology*, **18**, 1943–1948.

Peng, L., **Xu, Y.**, **Wang, X.**, **Feng, X.**, **Zhao, Q.**, **Feng, S.**, **Zhao, Z.**, **Hu, B.**, & **Li, F.** (2019). Overexpression of paralogues of the wheat expansin gene *TaEXPA8* improves low-temperature tolerance in *Arabidopsis*. *Plant Biology*, **21**, 1119–1131.

Pien, S., **Wyrzykowska, J.**, **McQueen-Mason, S.**, **Smart, C.**, & **Fleming, A.** (2001). Local expression of expansin induces the entire process of leaf development and modifies leaf shape. *Proceedings of the National Academy of Sciences USA*, **98**, 11812–11817.

Ramakrishna, P., **Ruiz Duarte, P.**, **Rance, G. A.**, **Schubert, M.**, **Vordermaier, V.**, **Vu, L. D.**, **Murphy, E.**, **Vilches Barro, A.**, **Swarup, K.**, **Moirangthem, K.**, **Jorgensen, B.**, **van de Cotte, B.**, **Goh, T.**, **Lin, Z.**, **Vobeta, U.**, **Beeckman, T.**, **Bennett, M. J.**, **Gevaert, K.**, **Maizel, A.**, & **De Smet, I.** (2019). EXPANSIN A1-mediated radial swelling of pericycle cells positions anticlinal cell divisions during lateral root initiation. *Proceedings of the National Academy of Sciences USA*, **116**, 8597–8602.

Rayle, D. L., & **Cleland, R.** (1970). Enhancement of wall loosening and elongation by acid solutions. *Plant Physiology*, **46**, 250–253.

Rayle, D. L., & **Cleland, R. E.** (1992). The acid growth theory of auxin-induced cell elongation is alive and well. *Plant Physiology*, **99**, 1271–1274.

Reinhardt, D., **Wittwer, F.**, **Mandel, T.**, & **Kuhlemeier, C.** (1998). Localized upregulation of a new expansin gene predicts the site of leaf formation in the tomato meristem. *Plant Cell*, **10**, 1427–1437.

Ren, Y., **Chen, Y.**, **An, J.**, **Zhao, Z.**, **Zhang, Z.**, **Wang, Y.**, & **Wang, W.** (2018). Wheat expansin gene *TaEXPA2* is involved in conferring plant tolerance to cd toxicity. *Plant Science*, **270**, 245–256.

Robinson, R. (2021). Mechanobiology of cell division in plant growth. *New Phytologist*, **231**, 559–564.

Rochange, S. F., **Wenzel, C. L.**, & **McQueen-Mason, S. J.** (2001). Impaired growth in transgenic plants over-expressing an expansin isoform. *Plant Molecular Biology*, **46**, 581–589.

Roudier, F., **Fernandez, A. G.**, **Fujita, M.**, **Himmelspach, R.**, **Borner, G. H. H.**, **Schindelman, G.**, **Song, S.**, **Baskin, T. I.**, **Dupree, P.**, **Wasteneys, G. O.**, & **Benfey, P. N.** (2005). COBRA, an *Arabidopsis* extracellular glycosyl-phosphatidyl inositol-anchored protein, specifically controls highly anisotropic expansion through its involvement in cellulose microfibril orientation. *Plant Cell*, **17**, 1749–1763.

Rui, Y., & **Dinneny, J. R.** (2020). A wall with integrity: Surveillance and maintenance of the plant cell wall under stress. *New Phytologist*, **225**, 1428–1439.

Samalova, M., **Elsayad, K.**, **Melnikava, A.**, **Peaucelle, A.**, **Gahurova, E.**, **Gumulec, J.**, **Spyroglou, I.**, **Zemlyanskaya, E. V.**, **Ubogoeva, E. V.**, & **Hejatko, J.** (2020). *Expansin-controlled cell wall stiffness regulates root growth in Arabidopsis*. *bioRxiv*, 2020.2006.2025.170969.

Sampathkumar, A., **Yan, A.**, **Krupinski, P.**, & **Meyerowitz, E. M.** (2014). Physical forces regulate plant development and morphogenesis. *Current Biology*, **24**, 475–483.

Sampedro, J., & **Cosgrove, D. J.** (2005). The expansin superfamily. *Genome Biology*, **6**, 242.

Sampedro, J., **Guttman, M.**, **Li, L. C.**, & **Cosgrove, D. J.** (2015). Evolutionary divergence of beta-expansin structure and function in grasses parallels emergence of distinctive primary cell wall traits. *Plant Journal*, **81**, 108–120.

Santiago, T. R., **Pereira, V. M.**, **de Souza, W. R.**, **Steindorff, A. S.**, **Cunha, B. A. D. B.**, **Gaspar, M.**, **Favaro, L. C. L.**, **Formighieri, E. F.**, **Kobayashi, A. K.**, & **Molinari, H. B. C.** (2018). Genome-wide identification, characterization and expression profile analysis of expansins gene family in sugarcane (*Saccharum spp.*) *PLoS One*, **13**, e0191081.

Sassi, M., **Ali, O.**, **Boudon, F.**, **Cloarec, G.**, **Abad, U.**, **Cellier, C.**, **Chen, X.**, **Gilles, B.**, **Milani, P.**, **Friml, J.**, **Vernoux, T.**, **Godin, C.**, **Hamant, O.**, & **Traas, J.** (2014). An auxin-mediated shift toward growth isotropy promotes

https://doi.org/10.1017/qpb.2022.6 Published online by Cambridge University Press

organ formation at the shoot meristem in *Arabidopsis*. *Current Biology*, **24**, 2335–2342.

Scarcelli, G., **Polacheck, W. J.**, **Nia, H. T.**, **Patel, K.**, **Grodzinsky, A. J.**, **Kamm, R. D.**, & **Yun, S. H.** (2015). Noncontact three-dimensional mapping of intracellular hydromechanical properties by Brillouin microscopy. *Nature Methods*, **12**, 1132–1134.

Schindelman, G., **Morikami, A.**, **Jung, J.**, **Baskin, T. I.**, **Carpita, N. C.**, **Derbyshire, P.**, **McCann, M., C .**, & **Benfey, P. N.** (2001). COBRA encodes a putative GPI-anchored protein, which is polarly localized and necessary for oriented cell expansion in *Arabidopsis*. *Genes Development*, **15**, 1115–1127.

Schopfer, P. (2001). Hydroxyl radical-induced cell-wall loosening in vitro and in vivo: Implications for the control of elongation growth. *Plant Journal*, **28**, 679–688.

Schweikert, C., **Liszkay, A.**, & **Schopfer, P.** (2000). Scission of polysaccharides by peroxidase-generated hydroxyl radicals. *Phytochemistry*, **53**, 565–570.

Sloan, J., **Backhaus, A.**, **Malinowski, R.**, **McQueen-Mason, S.**, & **Fleming, A. J.** (2009). Phased control of expansin activity during leaf development identifies a sensitivity window for expansin-mediated induction of leaf growth. *Plant Physiology*, **151**, 1844–1854.

Spartz, A. K., **Ren, H.**, **Park, M. Y.**, **Grandt, K. N.**, **Lee, S. H.**, **Murphy, A. S.**, **Sussman, M. R.**, **Overvoorde, P. J.**, & **Gray, W. M.** (2014). SAUR inhibition of PP2C-D phosphatases activates plasma membrane H^+-ATPases to promote cell expansion in *Arabidopsis*. *Plant Cell*, **26**, 2129–2142.

Takahashi, K., **Hayashi, K.**, & **Kinoshita, T.** (2012). Auxin activates the plasma membrane H^+-ATPase by phosphorylation during hypocotyl elongation in *Arabidopsis*. *Plant Physiology*, **159**, 632–641.

Takatani, S., **Verger, S.**, **Okamoto, T.**, **Takahashi, T.**, **Hamant, O.**, & **Motose, H.** (2020). Microtubule response to tensile stress is curbed by NEK6 to buffer growth variation in the *Arabidopsis* hypocotyl. *Current Biology*, **30**, 1491–1503.

Tenhaken, R. (2015). Cell wall remodeling under abiotic stress. *Frontiers in Plant Science*, **5**, 771.

Thiel, G., & **Weise, R.** (1999). Auxin augments conductance of K^+ inward rectifier in maize coleoptile protoplasts. *Planta*, **208**, 38–45.

Vaahtera, L., **Schulz, J.**, & **Hamann, T.** (2019). Cell wall integrity maintenance during plant development and interaction with the environment. *Nature Plants*, **5**, 924–932.

Valdivia, E., **Stephenson, A. G.**, **Durachko, D. M.**, & **Cosgrove, D. J.** (2009). Class B β-expansins are needed for pollen separation and stigma penetration. *Sex Plant Reproduction*, **22**, 141–152.

Valenzuela-Riffo, F., **Gaete-Eastman, C.**, **Stappung, Y.**, **Lizana, R.**, **Herrera, R.**, **Moya-Leon, M. A.**, & **Morales-Quintana, L.** (2020). Comparative *in silico* study of the differences in the structure and ligand interaction properties of three alpha-expansin proteins from *Fragaria chiloensis* fruit. *Journal of Biomolecular Structure and Dynamics*, **37**, 3245–3258.

Valenzuela-Riffo, F., **Ramos, P.**, & **Morales-Quintana, L.** (2018). Computational study of FaEXPA1, a strawberry alpha expansin protein, through molecular modeling and molecular dynamics simulation studies. *Computational Biology and Chemistry*, **76**, 79–86.

Van der Does, D., **Boutrot, F.**, **Engelsdorf, T.**, **Rhodes, J.**, **McKenna, J. F.**, **Vernhettes, S.**, **Koevoets, I.**, **Tintor, N.**, **Veerabagu, M.**, **Miedes, E.**, **Segonzac, C.**, **Roux, M.**, **Breda, A. S.**, **Hardtke, C.S.**, **Molina, A.**, **Rep, M.**, **Testerink, C.**, **Mouille, G.**, **Höfte, H.**, **Hamann, T.**, & **Zipfel, C.** (2017). The *Arabidopsis* leucine-rich repeat receptor kinase MIK2/LRR-KISS connects cell wall integrity sensing, root growth and response to abiotic and biotic stresses *public library of science genetics*, **13**, e1006832.

Varadi, M., **Anyango, S.**, **Deshpande, M.**, **Nair, S.**, **Natassia, C.**, **Yordanova, G.**, **Yuan, D.**, **Stroe, O.**, **Wood, G.**, **Laydon, A.**, **Zidek, A.**, **Green, T.**, **Tunyasuvunakool, K.**, **Petersen, S.**, **Jumper, J.**, **Clancy, E.**, **Green, R.**, **Vora, A.**, **Lutfi, M.**, . . . **Velankar, S.** (2021). AlphaFold protein structure database: Massively expanding the structural coverage of protein-sequence space with high-accuracy models. *Nucleic Acids Research*, **50**, D439–D444.

Vermeer, J. E., **von Wangenheim, D.**, **Barberon, M.**, **Lee, Y.**, **Stelzer, E. H.**, **Maizel, A.**, & **Geldner, N.** (2014). A spatial accommodation by neighboring cells is required for organ initiation in *Arabidopsis*. *Science*, **343**, 178–183.

Vilches Barro, A., **Stöckle, D.**, **Thellmann, M.**, **Ruiz-Duarte, P.**, **Bald, L.**, **Louveaux, M.**, **von Born, P.**, **Denninger, P.**, **Goh, T.**, **Fukaki, H.**, **Vermeer, J. E. M.**, & **Maizel, A.** (2019). Cytoskeleton dynamics are necessary for early events of lateral root initiation in *Arabidopsis*. *Current Biology*, **29**, 2443–2454.

Vogel, J. (2008). Unique aspects of the grass cell wall. *Current Opinion Plant Biology*, **11**, 301–307.

Vreeburg, R. A., **Benschop, J. J.**, **Peeters, A. J.**, **Colmer, T. D.**, **Ammerlaan, A. H.**, **Staal, M.**, **Elzenga, T. M.**, **Staals, R. H.**, **Darley, C. P.**, **McQueen-Mason, S. J.**, & **Voesenek, L. A.** (2005). Ethylene regulates fast apoplastic acidification and expansin a transcription during submergence-induced petiole elongation in *Rumex palustris*. *Plant Journal*, **43**, 597–610.

Wang, T., **Chen, Y.**, **Tabuchi, A.**, **Cosgrove, D. J.**, & **Hong, M.** (2016a). The target of β-expansin EXPB1 in maize cell walls from binding and solid-state NMR studies. *Plant Physiology*, **172**, 2107–2119.

Wang, T., **McFarlane, H. E.**, & **Persson, S.** (2016b). The impact of abiotic factors on cellulose synthesis. *Journal of Experimental Botany*, **67**, 543–552.

Wang, T., **Park, Y. B.**, **Caporini, M. A.**, **Rosay, M.**, **Zhong, L.**, **Cosgrove, D. J.**, & **Hong, M.** (2013). Sensitivity-enhanced solid-state NMR detection of expansin's target in plant cell walls. *Proceedings of the National Academy of Sciences USA*, **110**, 16444–16449.

Wang, X., **Wilson, L.**, & **Cosgrove, D. J.** (2020). Pectin methylesterase selectively softens the onion epidermal wall yet reduces acid-induced creep. *Journal of Experimental Botany*, **71**, 2629–2640.

White, P. B., **Wang, T.**, **Park, Y. B.**, **Cosgrove, D. J.**, & **Hong, M.** (2014). Water–polysaccharide interactions in the primary cell wall of *Arabidopsis thaliana* from polarization transfer solid-state NMR. *Journal of American Chemical Society*, **136**, 10399–10409.

Whitney, S. E. C., **Gidley, M. J.**, & **McQueen-Mason, S. J.** (2000). Probing expansin action using cellulose/hemicellulose composites. *Plant Journal*, **22**, 327–334.

Wu, Y., **Sharp, R. E.**, **Durachko, D. M.**, & **Cosgrove, D. J.** (1996). Growth maintenance of the maize primary root at low water potentials involves increases in cell-wall extension properties, expansin activity, and wall susceptibility to expansins. *Plant Physiology*, **111**, 765–772.

Wu, Y., **Thorne, E. T.**, **Sharp, R. E.**, & **Cosgrove, D. J.** (2001). Modification of expansin transcript levels in the maize primary root at low water potentials. *Plant Physiology*, **126**, 1471–1479.

Xin, X., **Lei, L.**, **Zheng, Y.**, **Zhang, T.**, **Pingali, S. V.**, **O'Neill, H.**, **Cosgrove, D. J.**, **Li, S.**, & **Gu, Y.** (2020). Cellulose synthase interactive1- and microtubule-dependent cell wall architecture is required for acid growth in *Arabidopsis* hypocotyls. *Journal of Experimental Botany*, **71**, 2982–2994.

Xu, J., **Tian, J.**, **Belanger, F. C.**, & **Huang, B.** (2007). Identification and characterization of an expansin gene *AsEXP1* associated with heat tolerance in C3 *Agrostis* grass species. *Journal of Experimental Botany*, **58**, 3789–3796.

Xu, Q., **Xu, X.**, **Shi, Y.**, **Xu, J.**, & **Huang, B.** (2014). Transgenic tobacco plants overexpressing a grass *Ppexp1* gene exhibit enhanced tolerance to heat stress. *PLoS One*, **9**, e100792.

Yan, A., **Wu, M.**, **Yan, L.**, **Hu, R.**, **Ali, I.**, & **Gan, Y.** (2014). *AtEXP2* is involved in seed germination and abiotic stress response in *Arabidopsis*, *PLoS One*, **9**, e85208.

Yang, J., **Zhang, G.**, **An, J.**, **Li, Q.**, **Chen, Y.**, **Zhao, X.**, **Wu, J.**, **Wang, Y.**, **Hao, Q.**, **Wang, W.**, & **Wang, W.** (2020). Expansin gene *TaEXPA2* positively regulates drought tolerance in transgenic wheat (*Triticum aestivum* L.). *Plant Science*, **298**, 110596.

Yennawar, N. H., **Li, L. C.**, **Dudzinski, D. M.**, **Tabuchi, A.**, & **Cosgrove, D. J.** (2006). Crystal structure and activities of EXPB1 (Zea m 1), a beta-expansin and group-1 pollen allergen from maize. *Proceedings of the National Academy of Sciences USA*, **103**, 14664–14671.

Yoshida, K., & **Komae, K.** (2006). Dynamic coordination of cytoskeletal and cell wall systems during plant cell morphogenesis. *Plant Cell Physiology*, **47**, 1541–1554.

Yuan, S., **Wu, Y.**, & **Cosgrove, D. J.** (2001). A fungal endoglucanase with plant cell wall extension activity. *Plant Physiology*, **127**, 324–333.

Zenoni, S., **Fasoli, M.**, **Tornielli, G. B.**, **Dal Santo, S.**, **Sanson, A.**, **de Groot, P.**, **Sordo, S.**, **Citterio, S.**, **Monti, F.**, & **Pezzotti, M.** (2011). Overexpression of *PhEXPA1* increases cell size, modifies cell wall polymer composition and affects the timing of axillary meristem development in *Petunia hybrida*. *New Phytologist*, **191**, 662–677.

https://doi.org/10.1017/qpb.2022.6 Published online by Cambridge University Press

Zenoni, S., **Reale, L.**, **Tornielli, G. B.**, **Lanfaloni, L.**, **Porceddu, A.**, **Ferrarini, A.**, **Moretti, C.**, **Zamboni, A.**, **Speghini, A.**, **Ferranti, F.**, & **Pezzotti, M.** (2004). Downregulation of the *Petunia hybrida* alpha-expansin gene *PhEXP1* reduces the amount of crystalline cellulose in cell walls and leads to phenotypic changes in petal limbs. *Plant Cell*, **16**, 295–308.

Zhang, H., **Ding, Y.**, **Zhi, J.**, **Li, X.**, **Liu, H.**, & **Xu, J.** (2018b). Over-expression of the poplar expansin gene *PtoEXPA12* in tobacco plants enhanced cadmium accumulation. *International Journal of Biological Macromolecules*, **116**, 676–682.

Zhang, H., **Liu, H.**, **Yang, R.**, **Xu, X.**, **Liu, X.**, & **Xu, J.** (2019b). Over-expression of *PttEXPA8* gene showed various resistances to diverse stresses. *International Journal of Biological Macromolecules*, **130**, 50–57.

Zhang, J.-F., **Xu, Y.-Q.**, **Dong, J.-M.**, **Peng, L.-N.**, **Feng, X.**, **Wang, X.**, **Li, F.**, **Miao, Y.**, **Yao, S.-K.**, **Zhao, Q.-Q.**, **Feng, S.-S.**, **Hu, B.-Z.**, & **Li, F.-L.** (2018a). Genome-wide identification of wheat (*Triticum aestivum*) expansins and expansin expression analysis in cold-tolerant and cold-sensitive wheat cultivars. *PLoS One*, **13**, e0195138.

Zhang, P., **Ma, Y.**, **Cui, M.**, **Wang, J.**, **Huang, R.**, **Su, R.**, **Qi, W.**, **He, Z.**, & **Thielemans, W.** (2020). Effect of sugars on the real-time adsorption of expansin on cellulose. *Biomacromolecules*, **21**, 1776–1784.

Zhang, P., **Su, R.**, **Duan, Y.**, **Cui, M.**, **Huang, R.**, **Qi, W.**, **He, Z.**, & **Thielemans, W.** (2021b). Synergy between endo/exo-glucanases and expansin enhances enzyme adsorption and cellulose conversion. *Carbohydrate Polymers*, **253**, 117287.

Zhang, T., & **Cosgrove, D. J.** (2017). Preparation of onion epidermal cell walls for imaging by atomic force microscopy (AFM). *Bio-Protocol*, **7**, e2647.

Zhang, T., **Mahgsoudy-Louyeh, S.**, **Tittmann, B.**, & **Cosgrove, D. J.** (2014). Visualization of the nanoscale pattern of recently-deposited cellulose microfibrils and matrix materials in never-dried primary walls of the onion epidermis. *Cellulose*, **21**, 853–862.

Zhang, T., **Tang, H.**, **Vavylonis, D.**, & **Cosgrove, D. J.** (2019a). Disentangling loosening from softening: Insights into primary cell wall structure. *Plant Journal*, **100**, 1101–1117.

Zhang, Y., **Yu, J.**, **Wang, X.**, **Durachko, D. M.**, **Zhang, S.**, & **Cosgrove, D. J.** (2021a). Molecular insights into the complex mechanics of plant epidermal cell walls. *Science*, **372**, 706–711.

https://doi.org/10.1017/qpb.2022.6 Published online by Cambridge University Press